Tailor-Made Tetraphenylmethanes: From Surface Decoration to 3D Organic Polymers

Inauguraldissertation

zur

Erlangung der Würde eines Doktors der Philosophie

vorgelegt der

Philosophisch - Naturwissenschaftlichen Fakultät

der Universität Basel

von

Marcin Lindner

aus Polen

Basel, 2017

Genehmigt von der Philosophisch-Naturwissenschaftlichen Fakultät

Auf Antrag von Prof. Dr. Marcel Mayor und Prof. Dr. Oliver Wenger

Basel, 13.12.2016

Prof. Dr. Jörg Schibler

Dekan

Dedicated to:

My Parents

Acknowledgments

First of all, I would like to gratefully acknowledge Prof. Dr. Marcel Mayor for giving me the opportunity to be a part of his research group and who opened the door for me to the scientific world of very fascinating and intriguing projects, precious hints and invaluable discussions.
I really appreciate the last four years I spent here, as I know it made me whom I am. Moreover, I would like to thank Dr. Michal Valášek, from whom I was happy to gain the experience, profiting from his scientific excellence as well as his practical skills.

Furthermore, many thanks to all the current and former members of Prof. Dr. Mayor Group. At first I would like to thank my friends from the lab: Dr. hab. Alfred Błaszczyk, Dr. Alexandrina Schramm, Jasmin Santoro and Adam Gorczyński, moreover Dr. Sylvie Drayβ, Mario Lehmann-Alvarez, Ina Bodoki, Dr. Almudena Gallego-Gonzales, Kevin Weiland, Rajesh Mannacherry, Manuel Hellstern and Dr. Michal Juríček. I appreciate scientific discussions and personal conversations during my stay in Mayor Group, both in Basel and Karlsruhe.

I am very thankful to Dr. Lukas Gerhard and Dr. Viliam Kolivoška for their readiness to explain all of the physical issues related to the measurements of molecules, which constitute also part of this thesis. Dr. Olaf Fuhr for conducted X-ray analyses. Moreover, I want to say thank to the technical staff from Institute of Nanotechnology, namely Hagen Sparrenberger and Sven Stahl.

I thank Dr. Michal Valášek, Adam Gorczyński, Kevin Weiland and John Ddungu for proofreading this thesis.

Finally, I would like to thank my family, my mother Ewa, my father Tadeusz, my friends Adam Gorczyński, Monika and Piotr Lewandowicz, Dawid Sekula, Karolina Korpik and Sylwia Sekula-Neuner for the constant support from Poland during my PhD studies and last but not least to Marta for her love.

Abstract

Chapter 1 represents brief introduction into the field of molecular electronics, its main scientific branches and aspects related to both, chemistry and physics which are highlighted within this work. Beyond omnipresent analytical toolkit, great deal of effort is put to magnify an application of tetraphenylmethane based tripodal structures, discussing structural features, which warranted strong contact of the adsorbate to the metal surface. Furthermore, solid background about history of tetraphenylmethane is given. Its syntheses, as well as ways of their applications are covered, ranging from dendrimer compounds, ending up at organic frameworks.

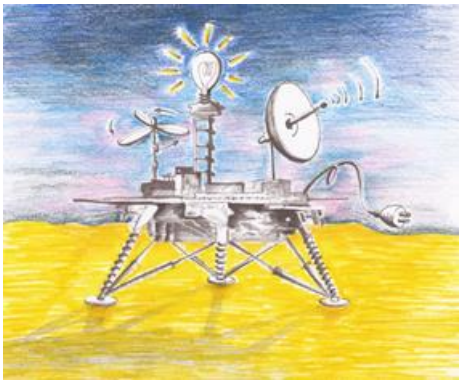

Chapter 2 described the concept of molecular tripods, terminated directly in a a *para* and *meta* position of tetragonal stands by the sulfur anchoring groups, molecular design and synthesis of target molecules. Moreover, molecular design and the synthesis of funcional molecules addressed for the surface deposition and charge transport inspection were presented.

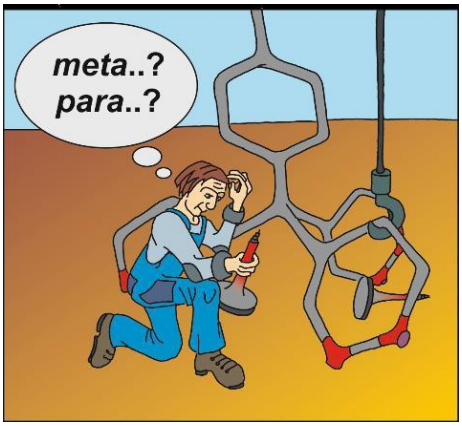

Chapter 3 presents physical investigations of a short tripodal nanoobjects, importance of anchoring groups and their position as well as phenomenon arising from their surface deposition. Indeed, oligoarylenes deocrated platforms are widely explored in terms of charge transport properties.

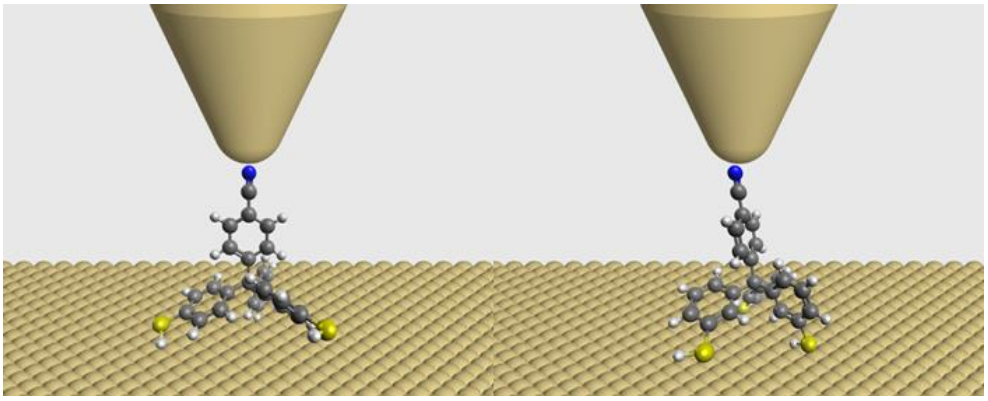

Chapter 4 shows molecular design and synthetic patways towards chmically tuned tetragonal, bidente monomer, appropiate for self-polymerisation. Moreover, the light is shed on its identification and properties.

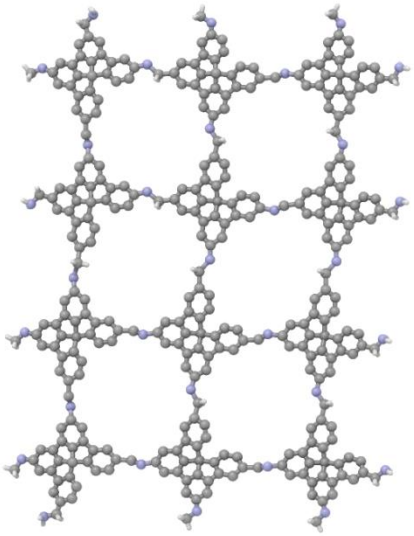

Table of Contents

List of Abbreviations

Å	Angstrom
AcCl	Acetyl chloride
AFM	Atomic force microscopy
aq.	Aqueous
BET	Braunauer-Emmer-Teller
BJ	Break junction
Boc	*tert*-butyloxycarbonyl
$(Bpin)_2$	Bis(pinacolato)diboron
br	Broad
Brine	Saturated aqueous NaCl solution
C	Celsius
calcd.	Calculated
CBS	Corey-Bakshi-Shibata
CT	Charge Transport
d	Doublet
dba	Dibenzylideneacetone
DCM	Dichloromethane
DMAc	*N*,*N*-Dimethylacetamide
DMF	Dimethylformamide
DMSO	Dimethyl sulfoxide
DNA	Deoxyribonucleic acid
dppf	1,1′-Bis(diphenylphosphino)ferrocene
DSC	Differential scanning calorimetry
EA	Elemental analysis
EI	Electron impact
Eq.	Equivalents
ESI	Electron spray ionization
Et	Ethyl
Et_2O	Diethyl ether
EtOAc	Ethyl acetate
EtOH	Ethanol
fcc	Face-centered cubic

FT IR	Fourier transform infrared spectroscopy
GCMS	Gas chromatography - mass spectrometry
hcp	Hexagonal close packed
HDT	Hexadecanethiol
HOMO	Highest occupied molecular orbital
HOPG	Highly oriented pyrolytic graphite
HR-ESI-MS	High-resolution electron spray ionization mass spectrometry
i-Pr	Isopropyl
K	Kelvin
LUMO	Lowest occupied molecular orbital
m	Multiplet
m/z	Mass per charge
MAS	Magic angle spinning
MCBJ	Mechanically controllable break junction
Me	Methyl
MeOH	Methanol
m.p.	Melting point
MO	Molecular orbital
MS	Mass spectrometry
NBS	*N*-bromosuccinimide
NIS	*N*-iodosuccinimide
n-BuLi	*n*-Butyllithium
NEXAFS	Near Edge X-Ray Absorption Fine Structure
NLO	Non-linear optical
NMR	Nuclear magnetic resonance
ODT	Octadecanethiol
OTf	Trifluoromethanesulfonate (triflate)
PG	Protecting group
Ph	Phenyl
Ppm	Parts per million
q	Quartet
r.t.	Room temperature
s	Singlet
SAM	Self-assembled monolayer

SBU	Secondary building block
S_E	Electrophilic substitution
SEM	Scanning electron microscopy
SPM	Scanning probe microscopy
SPS	Spatially resolved sensing spectroscopy
S-Phos	2-Dicyclohexylphosphino-2′,6′-dimethoxybiphenyl
STM	Scanning tunneling microscopy
t	Triplet
TADDOL	*α,α,α´,α´*-Tetraaryl-1,3-dioxolan-4,5-dimethanol
TBAB	Tetrabutylammonium bromide
TBME	Tertiary butyl methyl ether
tert-Bu	Tertiary butyl
TEM	Transmission electron microscopy
TFA	Trifluoroacetic acid
Tf_2O	Trifluoromethanesulfonic anhydride
THF	Tetrahydrofuran
TLC	Thin layer chromatography
TMS	Trimethylsilyl
ToF	Time of flight
TPM	Tetraphenylmethane
Tr	Trityl
UHV	Ultra-high vacuum
UPS	Ultraviolet photoemission spectroscopy
UV/vis	Ultraviolet/visible spectroscopy
X-Phos	2-Dicyclohexylphosphino-2′,4′,6′-triisopropylbiphenyl
X-ray	X-ray spectroscopy
Xantphos	4,5-Bis-9,9-dimethylxanthene
XPS	X-ray photoelectron spectroscopy

1 Introduction

*Chapter **I** was created to throw light onto the inception of molecular electronics, its conceptual base, main directions, the most powerful and prevalent physical tools, nature of molecules and their functionalities compatible with available techniques handled for nanotechnology. Afterwards we focused our attention on the broadly presented history of tetraphenylmethane, which becomes the main motif of this work, exposing its structural privilege, path of modifications. A broad array of applications was emphasized ranging from compounds served for surface decoration, branched architectures and omnipresent supramolecular chemistry.*

1.1 Molecular Electronics

The goal of this introductory chapter is to clearly elucidate the background of molecular electronics, showing the current interest of the scientific community and further motivations stemmed from the development of the broad analytical tools and wide array of available chemicals. Moreover, fundamentals of the physical methods relaying on immobilization of molecules onto metal electrodes, and the nature of the contacts are underlain.

Since a few decades the concept of unimolecular electronics[1] has enduringly assumed downsizing of conventional electronic devices (Figure **1**). However, its technological progress is also supported by commercial requirements which were expressed in Moore's empirical law. [2,3] Accordingly, the minimum distance between the components in integrated circuits is supposed to shrink by a factor two every two years. Hence, the speed of the digital circuit has to be improved at least by a factor of two. Furthermore, following the "design rule" by means of inorganic materials would be rather complicated and expensive because the cost of integration increases exponentially.

Quantum mechanics and thermodynamics set a fundamental limit for downsizing standard silicon circuits. Thus, there are even more important points which support the foregoing statement, indicating the advantage of molecular electronics. The smaller size of the molecules and higher density of packing may lower the cost. Subsequently, the time needed for an operation in transistors is reduced, well-organized structures exhibit better switching and sensing abilities, while geometry, conformational flexibility, variety of synthetic attributes lead to govern new electronic functions in common solid state devices.

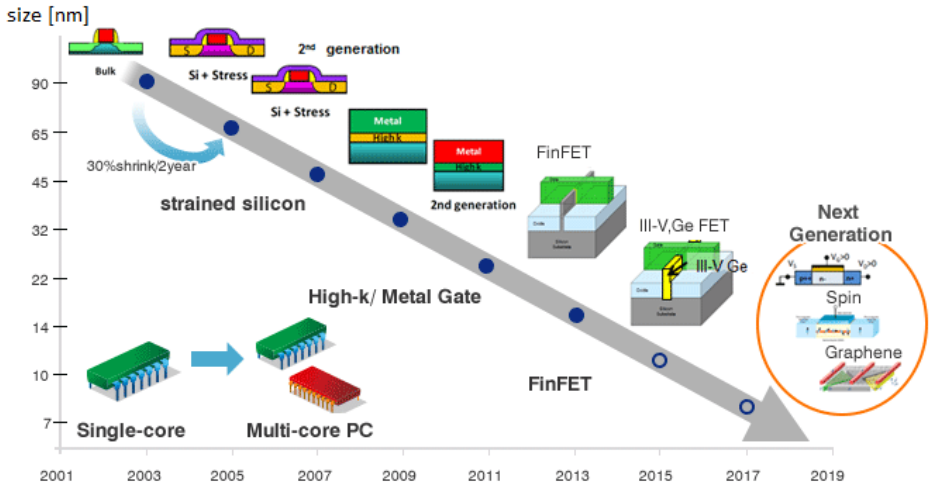

Figure 1 The Evolution in semiconductor devices as a function of size [nm] with time. The graph underscores the progress in miniaturization of electronic circuits from conventional silicon chips to the prospective, based on graphene.

Despite the fact that silicon-based materials have given invaluable input into development of technologies used in broadly known devices, they possess certain limitations. Namely, in badly insulated silicon layers with a thickness of three atoms, charge leakage has occurred, while the quantum tunneling effect is induced by a“14 nm resolution limit”.[4,5] In order to circumvent these difficulties, organic molecules may be examined as a silicon chip equivalent. The famous thesis presented at *Caltec* in 1959 by Richard Feynman who delivered a passionate speech, stating “There is plenty of room at the bottom”[6] found a great reflection in single-molecule devices and self-assembled nano objects dedicated to tunable electronic features.[7] The so-called “bottom-up” approach led to a reduction in the size of traditional devices to the nanometer scale, being opposed to the “top-down” approach where macroscopic systems and components are decreased in size. However, a lot of effort has been put in understanding the fundamentals of electron transport through the molecules, which is essential for the development and exploration of possible electronic components. To get more insight into these principles two major conditions have to be fulfilled. First of all, integration of functional building blocks into electronic circuits and their enclosing by the macroscopic electrodes, that ensures strong contact-giving anchoring groups, which are suitable for specific type of electrodes. Thereby, high measurement accuracy, electrical conductance of the functional core molecules and the effect of anchoring groups on electron transport

through individual molecules gives a warranty to achieve the control over the electronic properties of single-molecule devices. [8] Currently, a broad array of molecular resistors, wires, rectifiers, capacitors, switches, and field-effect transistors/gates have been reported. Nonetheless Kuhn and Möbius[9] placed the cornerstone of molecular electronics with early experimental contributions and later from the theoretical view point, Aviram and Ratner,[10] went on to wire molecules and explore their potential use as electronic devices, rectifiers, paving the way for further performance of novel logic gates or sensing entities.[11,12,13] Rapid progress became possible due to scanning probe microscopy (SPM) development (1982) and nanolithography enabling the study of electrical properties of single molecules.[14,15,16,17]

Current methods and approaches employed to characterize the behavior of single molecules in metal-molecule-metal junctions [18] are varied. (Figure **2**) The most common measurements on single molecular junctions are based on either the electrochemical break junction[19,20,21] or the mechanically controlled break junction (MCBJ) as well as on the scanning tunneling microscopy (STM) [15,22,23] electrochemical depositions and others.

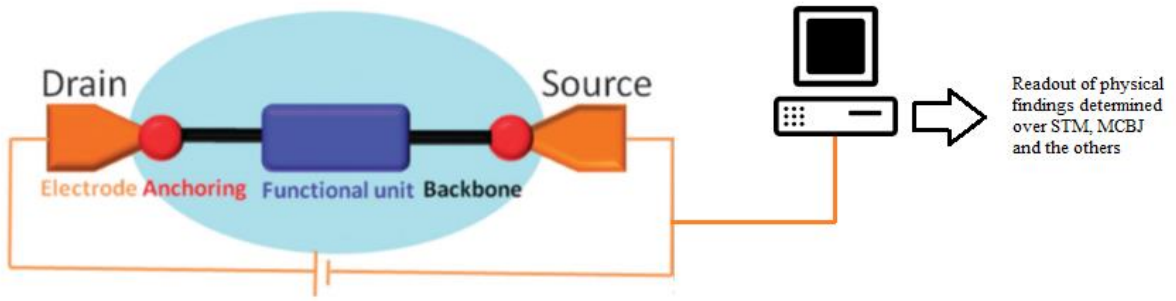

Figure 2 Illustration of commonly applied experimental setup in molecular electronics.

1.1.1 Image and Contact to Metal Electrodes

Physical measurements are indispensable for continued performance of molecular electronics. Therefore, to fully introduce the area of molecular electronics, two important physical techniques have to be discussed. Primarily, scanning probe microscopy (SPM) with particular attention to scanning tunneling microscopy (STM) as well as mechanically controllable break junctions (MCBJ) techniques, both in solid state and in solution will be outlined as an inherent analytical toolkit.

1.1.1.1 .Scanning Probe Microscopy

Fundamental studies describing the first surface analysis of molecular structures at the atomic level were carried out by Binning and Rohrer who designed and fabricated the first STM.[24] The crowning moment in the efforts of principal investigators were greatly appreciated in 1986 by awarding the Nobel Prize in Physics.[25] This milestone in molecular electronics has been further improved giving an open field for engineering and research striving for higher atomic resolution. In general, SPM characteristic boil down to the surface projection through its scanning by means of a metallic tip, controlling the interaction between the tip and surface. SPM techniques are distinguished among two of the most common branches. One of them is AFM, where van der Waals forces between the cantilever and substrate positioned on the surface are involved. The second is the STM where the tunneling current between the metallic tip and substrate occurs without any physical contact. [26,27,28,29,30]

The general working concept of STM-assumes the usage of a sample (mainly conductive metal species like Ag, Au or Cu, graphene or dichalcogenides layers like MoS_2 are employed, where inorganic or organic molecules are immobilized depending on chemical affinity, usually under UHV conditions) and a sharp probe tip (approaching the surface) typically made of tungsten by electrochemical etching, either platinum-iridium alloy (mechanical shearing) or gold. The precise vertical and lateral positioning of the tip requires a piezoelectric scanning unit (control vertical and lateral movement of the tip), a *x*,*y*-scanner, coarse sample-to-tip control, a vibration isolation system (initially magnetic levitation, nowadays mechanical spring and gas spring have prevented STM against vibrations, needed due to the precise control over the tip position regarding to the surface) and a computer (Figure **3**).[31] Basically, the tip is mounted to the *piezodrive* which comprises three perpendicular piezoelectric transducers. Subsequently these elements are broadened or shortened, while a voltage ramp is applied to the *x* and *y* piezo tubes respectively to force the tip to scan the *xy* plane. Tip and sample are brought into a distance of less than one nanometer by a rough positioner so that a tunneling current is evoked through an applied bias voltage between tip and the sample. Electrons are moved from the occupied state of the tip into empty state of the samples ($V > 0$) or vice versa ($V < 0$). This tunneling current depends exponentially on the width of the tunneling barrier that is the distance between tip and sample. Typically, reduction of the tip-sample separation to 1 Å results in an increase of the tunneling current by about one order of magnitude. This way, a STM is able to detect height

variations in the range of picometers. A high gain current amplifier converts tunneling current (typically pA to nA) to a voltage that is referred to the standard value.

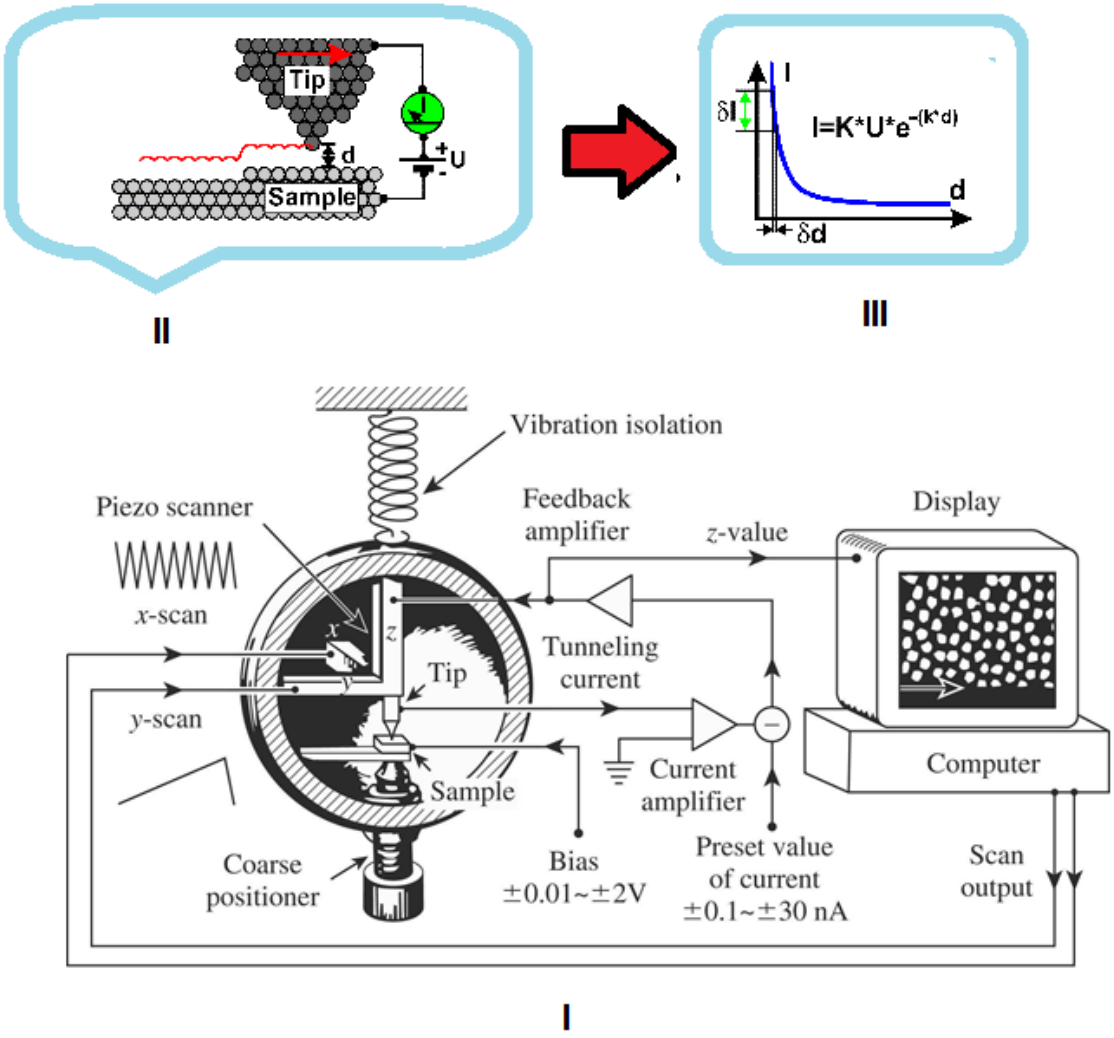

Figure 3 Common assembly of STM (**I**) where constant tunnelling current (restrained by a *z* piezo tube) is triggered by bias voltage between the tip and the sample, the *z*-value represents in fact the topography across the sample deposited on the surface. (**II**) Tunnelling is shown by **d** as a distance gap where electrons flow between sample and the tip. (**III**) Physical expression of the tunnelling and the distance **d**, increase of the gap accompanies exponential decay (**k** and **K** are constants, **U** is the tunneling bias).

When the tip passes over the *xy* plane, the changes in the height and density of the state are reflected in current changes and the tunneling-current surface is represented as contour plot (local density of state as a function of energy within the sample), combined, integrated and displayed on the computer, generating a three dimensional picture of the surface.

Alternatively, the distance between tip and sample, that is the voltage applied to the z piezo is controlled by a feed-back loop that keeps the absolute value of the tunneling current constant (constant height modes). In this mode, the tip scans a contour of constant density of states above the surface and the position of the tip reflects the topography of the sample. Besides its capability of imaging the sample, the STM tip can also be used to manipulate and to contact the sample in a controlled way. In this way, electronic properties such as the conductance of single molecules can be studied with spatial resolution. Hence, STM found several applications in catalysis, optoelectronics, stereoelectronics, and nanolithography.

1.1.1.2 Mechanically Controllable Break Junction

Investigation of charge transport (CT) through the molecules at the nanoscale has still remained a challenge. The bloom of the MCBJ was initiated by Moreland and Elkin (1985) who proved the phenomena of electron tunneling within using a thin wire of Sn-Nb attached to a flexible glass beam,[32,33] while in the very early stage of conductance measurements, Muller and Ruitenbeek established metallic nanojunctions(1989).[34,35,36] However, the prime experiment utilized a simple organic molecule (1,4-benzenedithiol, 1997)[37,38] fixed into two electrodes, allowing the formation of molecular junctions by opening/closing of the nanogap. The molecules are immobilized by drop-casting using a liquid cell filled with non-conductive solvent and target, which also forms a junction right away during the gap opening/closing process.

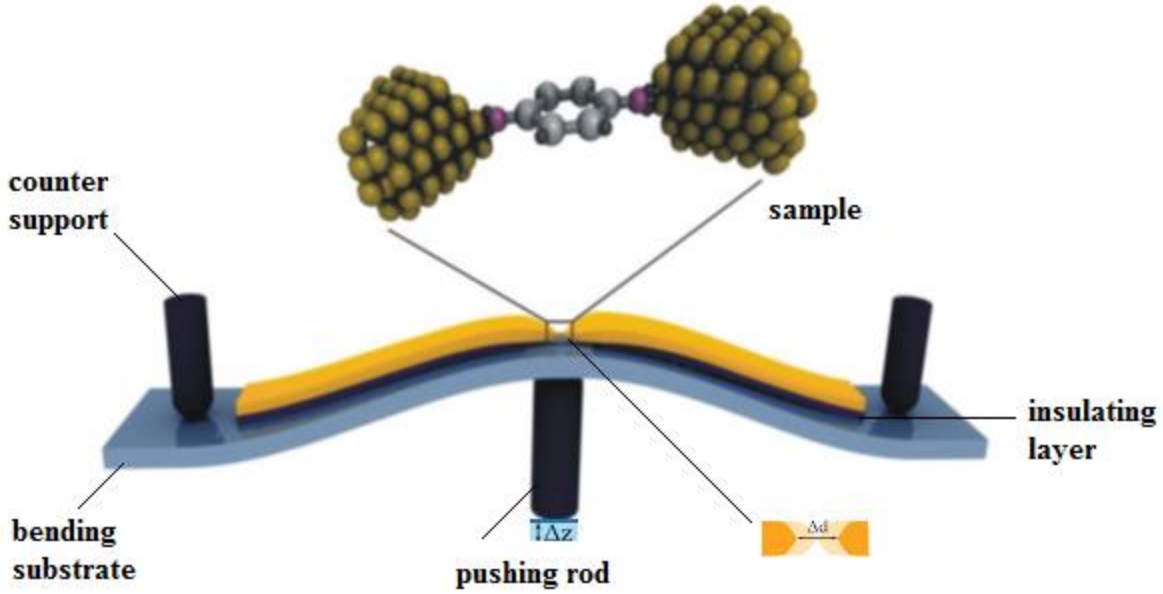

Figure 4 Illustration presents typical MCBJ setup; displacement ratio between Δ*d* (horizontal movement of nanogap) and Δ*z* (vertical movement of the pushing rod) allows precise control of the gap range [pm].

Standard MCBJ consists of two nano-spaced electrodes (made of lithography or fabricated from thin metal wire attached to the substrate and suspended middle part). Between them, flexible polyimide substrate is pushed from the top by two stable rods (counter support) and movable rod right above. Next (mechanical actuator, usually piezoelectric transducer or stepper motor) proceeds selective bounding of the substrate during opening/closing of the gap among the electrodes. Consecutively, displacement of the pushing rod exerts rapture of the metal wire, resulting in a well-controlled nanometer gap. Upon opening of the nanogap, the pushing rod is stimulated to move down, simultaneously triggering the nanogap closing. A voltage is applied between the two electrodes and the conductance of the junction is monitored as function of the displacement of the pushing rod (conductance–displacement curve). Metallic nanocontacts typically exhibit characteristic conductance steps in multiples of $G_0 = 2e^2/h$ (where G_0 conductance of the last gold atom before the wire breaks) before the contact breaks and the conductance drops to the tunneling conductance. This allows the distance between the two electrodes to be defined. Eventually a molecule still bridges the junction after breaking the metal contact. This is reflected in a conductance which is lower

than 1 G_0 but higher than the typical tunneling conductance (Figure **4**). [39,40,41,42] As break junction measurements do not allow imaging of the sample, the nature of the junction is inferred from a statistical approach: Repetition of the described process leads to various different junction configurations and thus to different conductance–displacement curves. Typical conductance values of the deposited molecule result in a higher probability for this particular conductance value and appear as a conductance peak in a 1D histogram or as a conductance plateau in a 2d histogram. This situation is exemplified in Figure **5**. Histogram **I** depicts the measurement of ODT, where **A1** represents low conductance, while **A2** corresponds to the conductance of two molecules in the junction, sharped and well specified. Taking into account the broad shape of histogram, it attributes to the variety of molecular conformations appearing during the measurement. In terms of 2D histogram the ellipsoid region features the distance information.

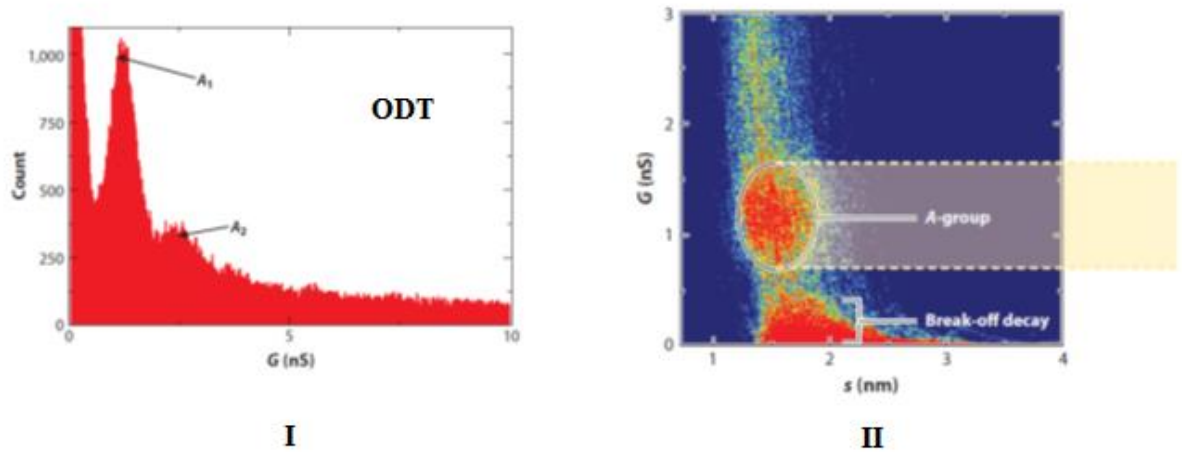

Figure 5 Conductance histograms obtained for octanedithiol (ODT).[43]

Certainly, the resistance of the MCBJ setup against vibrations is considered an advantage of this method. Indeed, the number of created junctions considerably enhances the statistical analysis, reducing the risk of faults. Nevertheless, drawbacks arise from the unidentified shape of the electrodes most likely because of the breaking process itself. Up to now MCBJ is excluded from industrial applications.

1.1.1.3 STM break junction

In 2003 Xu and Tao showed the first successful formation of single molecule junctions by means of the STM-BJ technique.[15] Essentially, the sample is immobilized on the gold surface being in or out of contact with the tip of the STM.

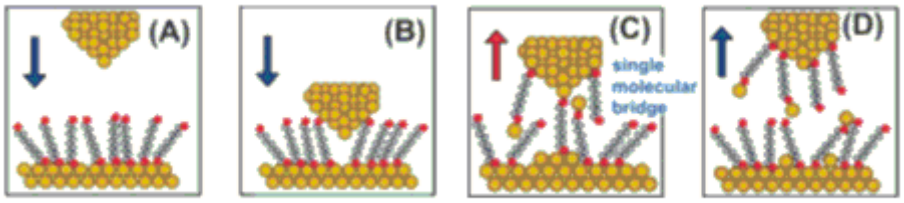

Figure 6 Schematic representation of STM-BJ experiment demonstrating at the first step the contact separation between the metal surface and STM tip (A), contact formation (B), formation of molecular junction (C) and its rupture (D).

Inertness of the gold substrate in conjunction with well-defined metal thickness is required to identify an accurate molecular resistance. Hence, conductive features of molecules may be estimated by accumulating attitudes of high resolution images with spatially resolved sensing spectroscopy (SPS). The experiment boils down to the formation and breakage of the junction among STM tip and sampled metal electrode. The illustration of the experiments is depicted on Figure **6**. As was already mentioned, in the first stage of the common STM-BJ measurement a molecule equipped with chemically tuned anchoring group creates a robust contact being adsorbed on the gold surface. While a tunneling current (active feedback) is applied to control the STM tip position over the molecular adlayer. Later on, the active feedback is switched off to enable inception of the BJ cycle. Therefore, a piezoelectric transducer is used to perform a controlled STM tip movement along the x-y plane until an assumed, ultimate current value is obtained, evidencing a stable metal-metal contact. At this value the tip leaves the substrate. Through this operation the sample is placed into the nanogap constructed by the tip and substrate. Subsequently, the tip is lifted and the junction is fractured, leading the cycle to the end. High accuracy of statistical analysis needed to carry out hundreds of thousands of cycles. Measurements may be done by using an electrochemical setup (conductive cantilever is employed).

1.1.1.4 Nature of the metal-molecule bonding

A molecule can exhibit various conductance values, [44] and its interface with the electrodes, which is usually determined by chemical anchoring groups, can have a large influence on its electrical properties. [45] For instance, transistor-type devices from the same molecule may display fundamentally different transport characteristics. [46,47] The organization of the molecules within the junction is usually based on some sort of self-assembly using chemisorption or physisorption methods to form monomolecular layers between both

electrodes. In many cases, either self-assembled monolayers (SAMs) [48] or Langmuir-Blodgett films (LB) [49,50] provide the order at the molecular level inside the junction. Preparation of self-assembled monolayers (SAMs) on a solid surface by the tight covalent bonding of organic molecules is a powerful way to accomplish interface functionalization. The anchoring group, responsible for the direct contact between metal and the functional molecule, needs to be considered in terms of its mechanical stability and also regarding its electronic transparency (week or strong coupling). An ideal molecular anchoring group is expected to provide well-defined and reproducible binding, sufficient strong anchoring between a molecule and metal surfaces, and should maintain sufficient electron density of states close to the Fermi level to pass an electron or hole through the molecule (electronically transparent nature with relatively high conductance). Furthermore, in order to design tailor-made functional devices, it must be possible to achieve well-ordered molecular orientations.

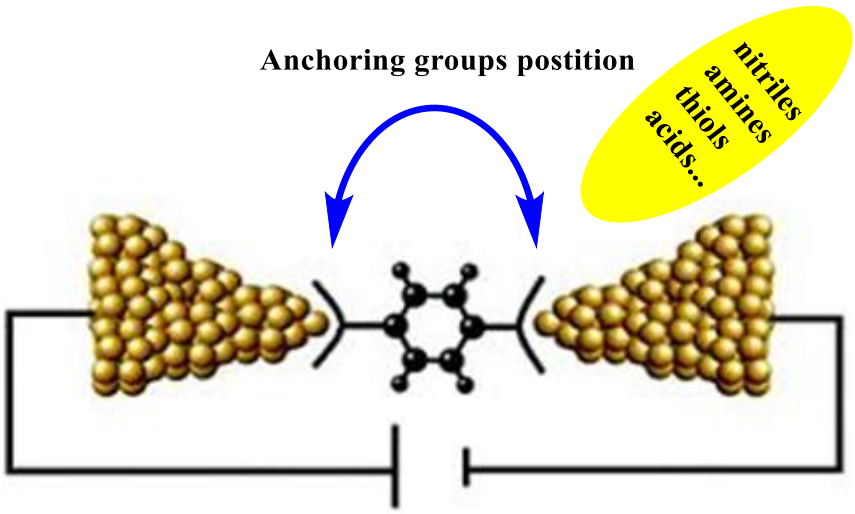

Figure 7 Concept of anchoring groups over conductance measurements. Functional groups are applied to terminate organic molecules ensuring appropriate contact between an electrodes and analyzed species.

So far, many anchoring groups, including thiols (-SH) [51,52,53,54,] amines (-NH_2)[21,51,,55], phosphines [56], pyridines [15,57,58,59,60], selenols (-SeH) [61,62,63,64], fullerenes [65,66,67], isocyanides (-NC) [55,68,69], nitriles (-CN) [70,71], nitro (-NO_2) [71], isothiocyanides (-NCS) [72], methyl sulfide (-SCH_3)[56], dithiocarbamates (-NCS_2) [73], carbodithiolates (-CS_2H) [74,75], hydroxyl (-OH)[76], *N*-heterocyclic carbenes [77,78], and carboxylic acids (-COOH) [51,79] have been investigated and used to form electronic devices, and also the influence of anchoring groups on single molecule conductance has been examined (Figure **6**). Different anchoring groups possess

different coupling strengths and contact geometries, which significantly affect the charge transport properties of the molecular junctions[80]. Nevertheless, these anchoring groups have been explored most frequently when attached to non-highly conjugated core structures (e.g. saturated alkanes), [51,55,81] that are showing significantly poor conductivity, rather than in highly conjugated systems [82,83] which are more promising candidates for molecular electronic wires, which is evident from a few studies of comparison of anchoring groups in conjugated systems. [58,69,71,76] In saturated structures, the resistance from the core molecule is higher and thus the anchoring effect is reduced. While organic π-conjugated systems are capable of more efficient charge transport along the molecular backbone due to the electron delocalization. This fundamental phenomenon is induced by the difference in the energy gap between the lowest unoccupied molecular orbital (LUMO) and highest occupied molecular orbital (HOMO) that is smaller (~3 eV) than the HOMO-LUMO gap of saturated molecules (~7 eV), increasing electron transport properties through the conjugated molecule. [23] Conductance of a conjugated system depends on several factors and not only the length of the conjugated system and its anchoring groups have a large influence on the conductance of the molecule, but also other factors like e.g. the topological connection (*ortho*-, *meta*- or *para*-) or the torsion angle between subunits are important. [84,85,86,87]

1.2 Tetraphenylmethane.

The aim of this chapter is to provide a concise background of tetraphenylmethane (TPM) chemistry. Apart from the structural properties and geometry of the core units, a brief overview based on the preparation method starting from the initial approach and its evolution within modifications of TPM units will be given. Moreover, the most prominent derivatizations will be shown discussing its substitution abilities toward highly reactive precursors dedicated for widely spread cross-coupling reactions, giving an excess to the variety of applications.

1.2.1 Tetraphenylmethane: structure and historical synthetic approaches

TPM consists of a central sp^3-hybridised carbon atom linked fourfold with aromatic phenyl rings affording a specific tetragonal core structure through molecular rigidity with high symmetry. Crystallographic study of TPM single crystals led to determine the right configuration assigning it to the $P42_1c$ space group. While the distances between **C1**/**C2** and **C2**/**C3** were founded as 1.49Å and 1.37Å respectively.[88] (**Figure 8**)

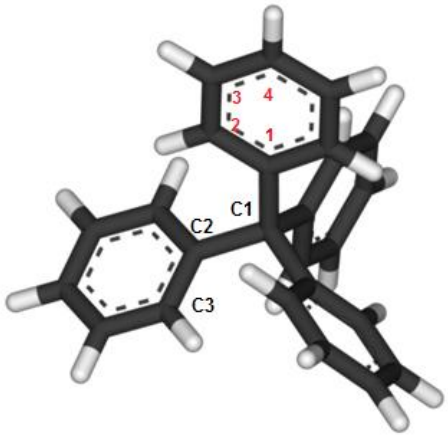

Figure 8 Model of a single tetraphenylmethane molecule.

The first successful synthesis of TPM was reported by Gomberg[89] in 1898. The preparation method relayed on substitution of bromotriphenylmethane (**1**) with phenylhydrazine. Tetrahedral product **2** was consecutively oxidized obtaining diaza-derivative (**3**). Subsequently, it thermal cleavage with simultaneous liberating of nitrogen let to provide TPM (**4**) in 2-5% yield. Fife years later Ullmann and Münzhuber[90] significantly improved the synthetic route involving trityl chloride **5** as a starting material profiting from its usefulness toward Friedel-Crafts reaction. The reaction with aniline at 200^{o}C, followed by diazotation of 4-tritylaniline **6** and its subsequent reduction allowed to obtain TPM (Scheme **1**). Through

several years, the overall yield was elevated to 93%.[91] Owing to TPM susceptibility towards electrophilic substitution (S_E2) in the *para* (4) position of each aromatic ring, symmetric derivatives have become one of the most prevalence tetrahedral scaffolds paving the way for their further modification throughout abundance of functional groups. Highly useful and explored aromatic bromides and iodides were obtained by aforementioned electrophilic substitution applying iodine[92,93] or bromine. [94,95,96]

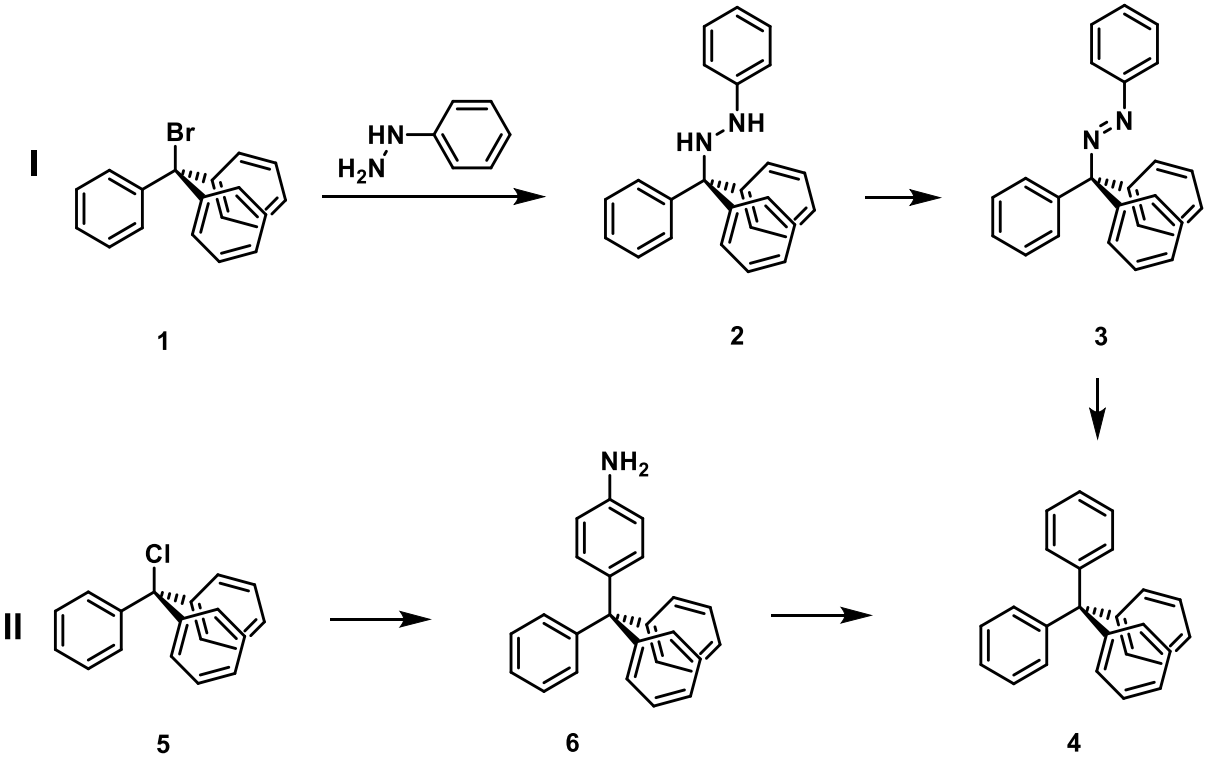

Scheme 1 Illustration of the pristine strategies of TPM synthesis, (**I**) Gomberg protocol, (**II**) Ullmann methodology

Besides halogenated products, Bernhardt demonstrated synthesis of tetrakis(4-nitrophenyl)methane which was subsequently reduced to *exo*-amine entity (**A**)[97] capable of several other transformation. Bearing in a mind how powerful halogenated building blocks are, bromo-terminated TPM was converted to cyano derivatives (**B**).[96] Its further hydrolysis allows to attain ubiquitous carboxylic acids that have warranted versatile non-planar scaffold particularly appealing for supramolecular chemistry. Moreover TPM draws up the attention of cross-coupling reactions driven by palladium chemistry. It is worthy to notice the synthesis of the very first vinyl terminated moieties as an intriguing candidate for its polymerization (**C**).[98] Stille coupling with tributyl(vinyl)stannane gave an opportunity to prepare the desired

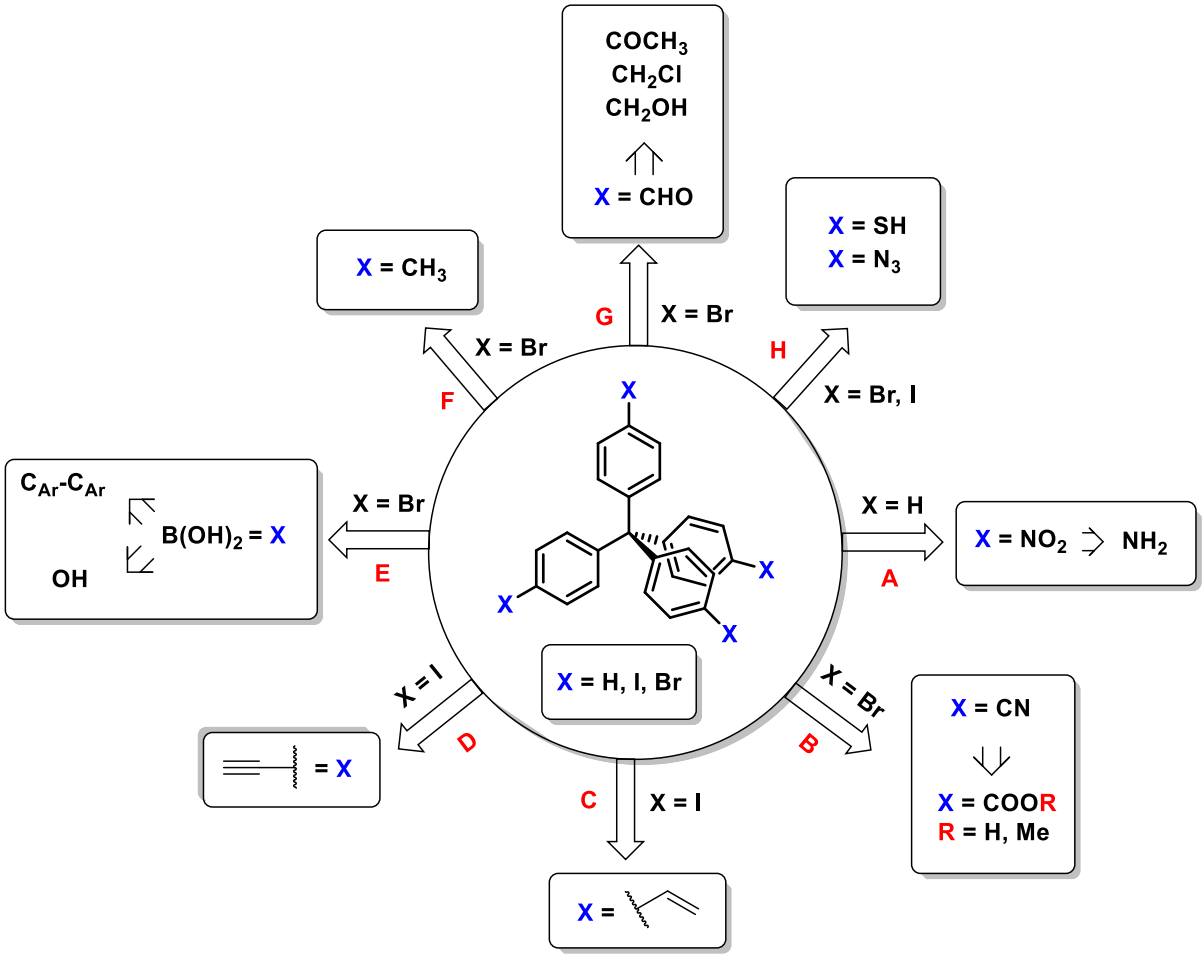

Figure 9 Library of functionalities issued on the early stage of TPM chemistry.

cross-linking agent. Furthermore, extension of molecular arms was realized owing to Sonogashira coupling, enabling formation of "tripodophrins". Easley available trimethylsilyl acetylene led to linking the tetrahedral moiety with electron-rich porphyrin building blocks (**D**) dedicated for nanofabrication experiments.[99,100] Other process involved organometallic agents (lithiation, Grignard reaction) which were highly efficacious towards formation of molecular constructions. Taking an advantage of rapid halogen-metal exchange reaction Wilson and Griffin performed synthesis of a boronic acid (**E**)[95] as a resourceful functional group prominent for Suzuki cross-coupling reaction.[101] These were elongated yielding bi or-terphenyl molecular arms. On the other hand, Wuest demonstrated an efficient synthetic approach to the formation of several molecular building blocks based on phenol, toluene, benzylic alcohol (chloride), ketone, aldehyde and isocyanate termini creating a library of modular cores (**F, G**). [102,91,103] Notably, thiolated and azide terminated ligands were very

recently reported as well (**H**), tackling a new challenge of supramolecular chemistry (Figure **9**). [104,105]

1.2.2 Applications of Tetraphenylmethane

The three dimensionality of TPM together with its easy functionalization of protruded symmetrical aromatic rings offer a wide range of modifications, tuned chemically properties of synthesized materials. By means of modern chemical tools TPM found great variety of applications represented by rigid molecular platforms, metal and covalent organic frameworks (**MOFs**, **COFs**), dendrimers and hyperbranched oligo- and polymers (**HBPs**), [106] supramolecular architectures, porous organic polymers (**POPs**), hyper cross-linked polymers (**HCPs**).

1.2.2.1 Rigid self-assembled molecular platforms

Among helming amounts of molecular devices their major part suffers from unwanted neighboring interactions, which unfavorably suppress or diminish expected effects. A solution that may tackle these problems is embodied in the bulky carbonated scaffolds affecting molecular repulsion. Thereupon, TPMs size and structural arrangements fostering the tetrahedral synthon to act as a tripodal foot,[107] organizing and controlling the spatial arrangement of molecules in self-assembled monolayers (SAMs) on flat substrates was investigated. For that purpose, three of the four phenyl units are usually decorated with anchor groups interacting with the substrate while the fourth one is expected to protrude from the surface and might be further substituted. SAMs of tetraphenylmethane model compounds exposing three functional groups comprising sulfur atoms (e.g. by $–CH_2SH$, -SAc, -SR, and –SH) to profit from their chemisorption on gold substrates were already reported. [108,109,110,111,112,113,114] Depending on the type of the substrate (silver, titanium oxide, indium-tin oxide), alternative anchor groups have been considered (selenium, pyridine, benzyl amine, alkyl ester, phosphonate, tertiary ammonium salts).[64,115,116,117,118,119,120] In order to provide binding on graphene surfaces by π-π stacking, tetraphenylmethane based model compounds functionalized with three “pyrene-feet” were investigated.[121,122] Structure stabilization by van der Waals forces in monolayers, and efficient packing in SAMs, have been reported for backbones consisting of C_3 tetrahedral symmetric units, equipped with C cores.[108,110,123] Due to the multifaceted properties, several structural impacts and broad applicability of these platforms will be described in detail in this work.

1.2.2.2 Metal and covalent organic frameworks (MOFs, COFs)

Concept of reticular chemistry gained momentum throughout rational design and synthesis of self-assembled objects at the atomic level. Inorganic and organic building blocks, the influence of their bonding features and geometry of selected spacers triggered the fascination and the considerable breakthrough reflected in the synthesis and directional amplifications of multi-pronged metal and covalent organic frameworks. Since Omar Yaghi[124,125] reported the very first original papers demonstrating TPM involved, well-established formation of three dimensional topologies for MOFs and COFs (Figure **10**), great numbers of crystalline porous materials dedicated for gas storage, molecular recognition, catalysis, and drug delivery applications have been presented. Because of their paramount importance both types of polymeric materials will be discussed in separate paragraphs.

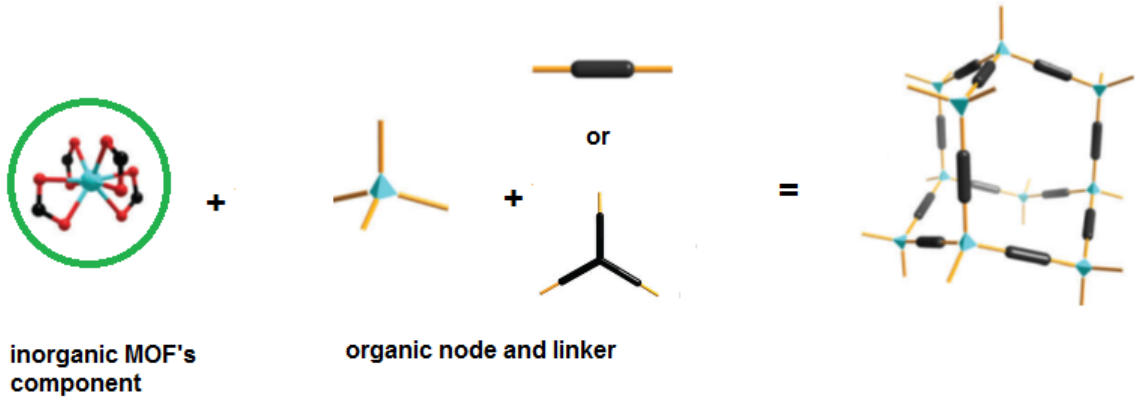

Figure 10 Graphical presentation of basic elements typically used to build up MOFs (metal cation is applied as inorganic component) and COFs spanning solely organic, light filaments.

1.2.2.3 Dendrimers and Light emitting materials

Over the last few decades many research groups sought for highly conjugated materials, exhibiting excellent optical properties with simultaneously discouraged crystallization tendency. Despite numerous coupled aromatic hydrocarbon backbones, previously designed molecules tend to self-associate, suppressing fluorescence intensity because of π-π stacking interactions. Stilbene bridged TPM exhibited a great relation between features of selected "small molecules" and structurally well-defined conjugated materials, comparing charge transport properties with morphology of explored molecules. Orientation of diverse TPMs terminated by stilbene and rods led to restrict intramolecular π-stacking effects preventing formation of unwanted excimers.[126,127,128,129,130,131,132] A series of size-

distinguished dendrons typified by DSC technique revealed a length-dependence increase of glass transition temperatures instead of melting transition temperatures. Investigating mono-vinylated species by optical methods, excimer sites were evidenced as an attribute of stilbene arms self-interaction. While measurement of elongated stilbene units displayed opposite effect elevating their film forming properties. Moreover, similar approach was proposed in oxadiazole-containing TPM cores confined by different peripheral donor/acceptor substituents pointed both in *para*- and *meta*- of electroactive components.[133] These steric reasons were taken in account to prevent molecular packing and increase quantum efficiency impacted by strong π-π* excitation of fluorine brunches.[134] These blue light emitters upon their photo-and electroluminescence survey (PL, EL), together with oxidation potential characterized by cyclic voltammetry (CV) have suggested their utility for optoelectronic applications. Hole transporters were resulted by tetrakis(triaryl)amine ingredient spanned to TPM displaying thermal and radical stability as an candidate for EL devices.[135,136] Almost the same concept was employed for construction of non-linear optical devices (NLO) exploring tolane based π-system with ionic acceptors mastering their maximal blue transparency.[137]

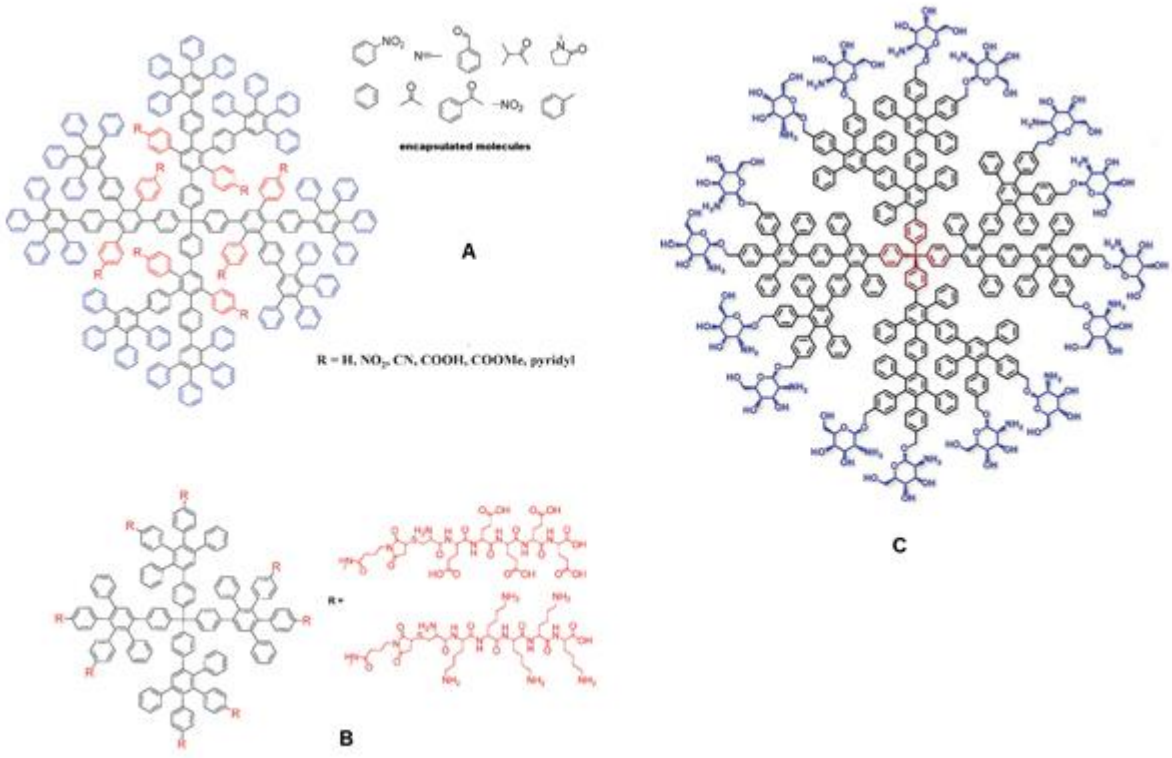

Figure 11 Prominent cores of TPM-consist dendrimers exemplified by diffrent peripheral groups.

Noteworthy, a brilliant example engaging a tetragonal TPM node was reported by Müllen. Orthogonal assembly of the triphenylene overbranched dendritic structure rules out fused rings aggregation and its fluorescence quenching, causing a rise of quantum yield with a growth of dendritic emitter's generation. [138] These motifs were examined as a specific chemical chamber and accomplished selective molecules binding. Tunable properties were adjusted through the side groups of the dendrimers (Figure **9**). [139,140] Among several tested groups, notable polar frames (**A**) were more prone to encapsulate and shuttle polar molecules (carboxylic acids interacted by hydrogen bonding with proflavin hydrochloride, while nitrile group interacted with a pinacyanol dye).[141] So affinity of deployed units give an application for molecular recognition (explosive detection, volatile organic compounds) enhanced by electron-rich species.[142] The other family of half-fluorinated, Janus type dendrimers exhibit nanofiber formation,[143] binding a specific protein (streptavidin),[144,145] whereas presence of poly(L-lysine) termini reinforced hydrophilicity, stimulating α-helical alignment (**B**),[146,147,148] and a blended approach led to reach surface amphiphilicity implementing it for drug delivery applications.[149] Furthermore, bio functions of TPM were extended owing glucosamine entities making their as a center that may contact enzymes (**C**).

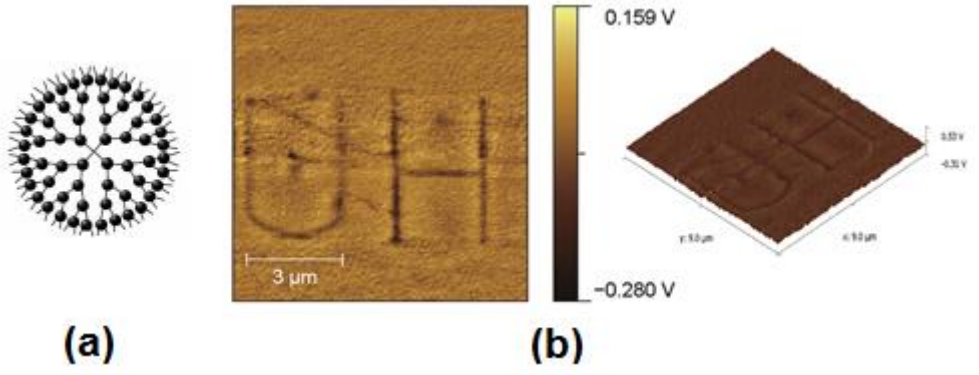

Figure 12 Graphical illustration of radical complexation (**a**) as well as electronanopattering (**b**) process fabricated by means of Yamamoto's dendrimers. [150,151]

It's worthy to note other classes of organic hybrid architecture constructed on repeating phenazomethine, ensuring radical complexation with $SnCl_2$. Spherical structures doped by a carbazole moiety have provided a source of hole transporting and photo-cross linking

material. Hence its electropolymerization, dendrimers are considered as promising photopatternable hole-transporting objects (Figure **12**).

1.2.2.4 Supramolecular architectures - molecular tectonics

Naturally occurring phenomena have recently gained considerable attention throughout imitation of bio-features in the artificial systems. Widely-known donor-acceptor interactions driven by hydrogen bounding affected by amines, alcohols etc. imply directionally specific arrangement of supramolecular components attributed also by structural factors as angle between donor-acceptor bonds. Those non-covalent associations in conjunction with firm, tetragonal skeletons have fixed a well-packed three-dimensional lattice. Seminal work devised by Wuest showed pyridone-composed 3D framework stabilized by small carboxylic acid guests even upon guest molecule removal. At this circumstance a sequence of hydrogen bonded stitches was produced (Figure **13**).[92,152,153,154]

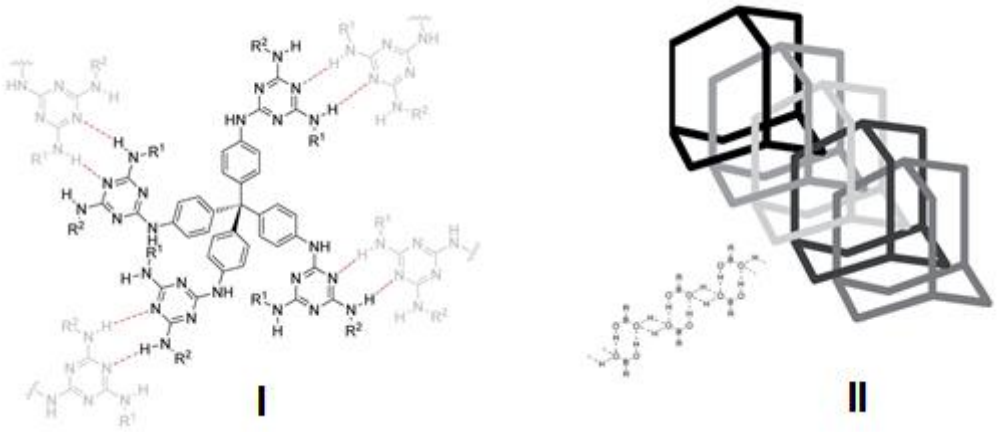

Figure 13 Hydrogen bonded model with triaminotriazene exploited as donor-acceptor unit (**I**) view of boronic acid mediated diamond structure (**II**).

A zeolite assembled aggregate mediated by diaminotriazene offers outstanding access to a hydrogen-bond intertwined network, which in spite of the weak nature of the hydrogen bond (~ 7 kcal/mol) may even surpass covalent bonds due to a strengthening synergic effect. Extensive aniline studies reveal significant diminishing of hydrogen bond numbers per tecton ranging from 8-20 for triazene ending up on 3-8 for the aniline based assembly. Furthermore there have been other reported diamondal structures stabilized by boronic acids,[155] isothiocyanates,[156] phenols[157] and phosphonic acids[158] comprising sticky sites, building up 3D porous hydrogen bonded system. Very recently, the first chiral tecton based on TPM core

modified by *S*-(α)-methylbenzyl amine or alcohol, capable of *CBS*-assisted asymmetric reduction of 1,4-diacetylbenzene, was reported. [159]

1.2.2.5 Porous Organic Polymers (POPs)

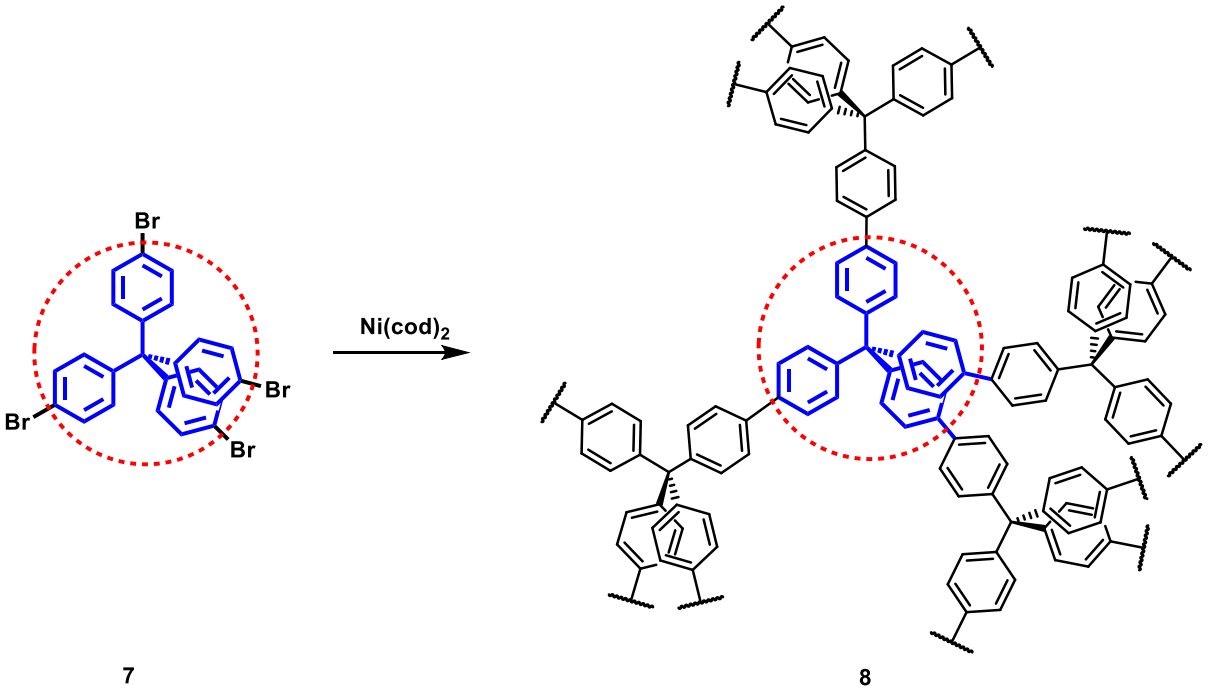

Figure 14 Pioneering Wang [160] co-polymerization of **7**

Several factors have impacted the formation of diamonded POPs. The selection of appropriate chemical tools is considered as the most crucial, emphasizing importance of Sonogashira and metathesis reactions. However since Wang (Figure **14**) subjected tetrakis(bromophenyl)methane **7** to a Yamamoto *homo-coupling* reaction, conducted by $Ni(cod)_2$, reaching beautiful micro porosity of **8**, several other approaches have been elaborated and intensively studied. Omnipresent acetylene pitches were rapidly explored in 3D materials, permitting linear as well as star-shape linkers, forcing dynamic development of gas storage materials. [161,162] Beyond Sonogashira reactions, also Glaser-homo-coupling[163] and "clickable" products were implemented.[164] Well-established synthetic protocols gave a boost to expand properties of those textures. As is depicted in Figure **15**, engaged polymers improve methane[165] and carbon dioxide capture[166] (**A**) and trigger its further conversion to carbonates (compelling the reaction with epoxides).[167] Whereas change of classical morphology to a tubular one by structural variation of connectors was also noted (**B**). [168]

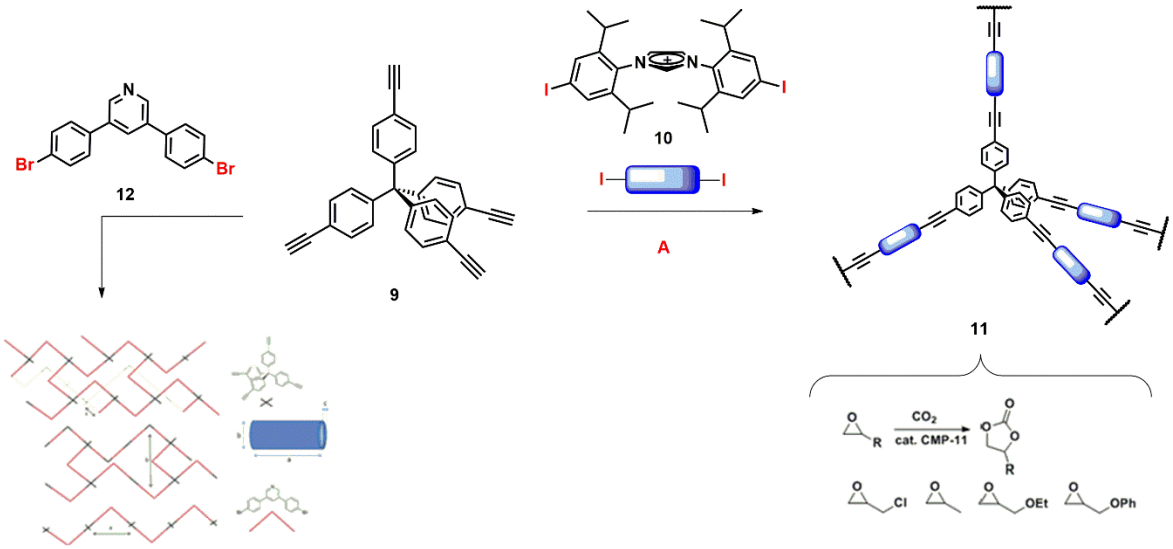

Figure 15 Products of Sonogashira coupling between iodo or bromo terminated components **10**, **12** and fourfold ethynylated species **9** yield polymeric structures, having found an application in catalysis (**A**) and materials chemistry(**B**).

1.2.2.6 Hypercross-linked polymers. (HCPs)

Other classes of materials possessing very intriguing properties are HCPs defined as non-crystalline but highly porous units. Regarding their application, bridging units may be designed and adjusted. Fields of interests were covered by a family of size-dependent diimides. Seminal work dealing with new n-type semiconductors suitable for optoelectronic devices showed the open area with respect to extended π-electron systems comprising polyimides.[169] It was found that to the enormous affinity of porous tetrahedral polyimides to reversibly uptake CO_2 arises from π- π electron rich heteroaromatic linkage, pyrometallic (**I**), [170] naphthalene (**II**) [171,172] and perylene (**III**) [173] fragments are particularly appealing to store common gases (Figure **16**). Their contribution evoked narrow pore size distribution, high thermal and chemical stability as well as catalytic usefulness.[174]

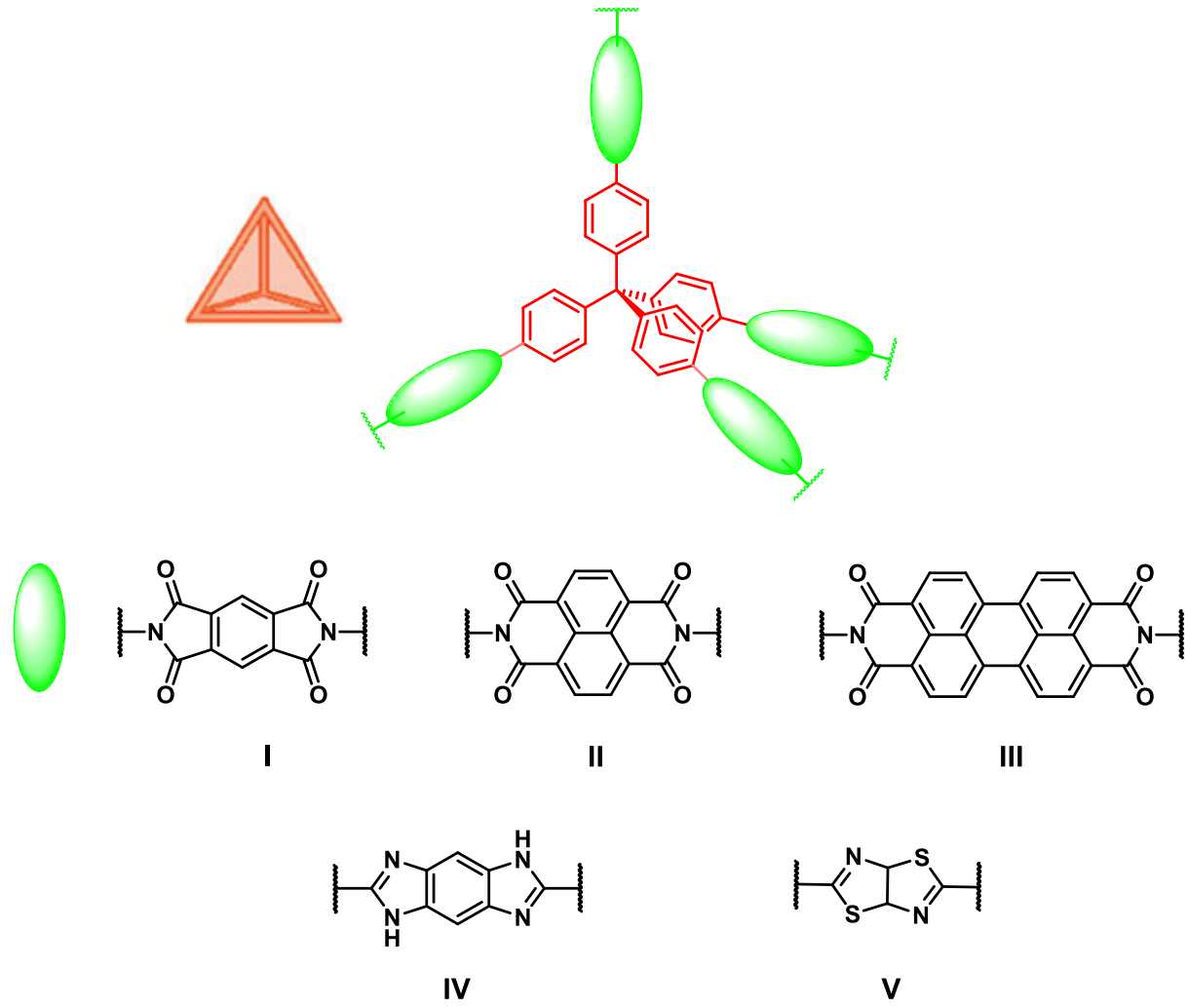

Figure 16 Illustration of polyimides tetrahedral structures displayed linkers **I-V** interspersed in TPM cores let to affect desired features.

Notably benzobisimidazole **IV** and thiazolothiazole **V** were adopted as imide analogous being eligible to achieve similar chemical and physical advantages. [175,176] Apart from the envisaged porosity of other cross linking materials,[177,178,179,180] several active ingredients were exploited to hone broad spectrum of heterogeneous organic transformations (Figure 17 **I**). Herein, intensively studied light harvesting Ru and Ir complexes were incorporated into TPM scaffolds accelerating photoredoxaza-Henry reactions,[181] and a Jørgensen-Hayashi catalyst with (L)-proline fused to the polymer handling it for asymmetric Michael additions, reaching a compromise between reaction yield and high enantioselectivity. [182] TADDOL-constructed chiral catalysts were also enclosed into three dimensional TPM platforms, assisting zinc constrained asymmetric reduction of aldehydes (Figure **17**, **II**). [183,184] It was reported that

norbonene-2,5-diene embedded into porous HCPs, performed asymmetric enone 1,4-additions to arylboronic acids, as reported by Cui.[185]

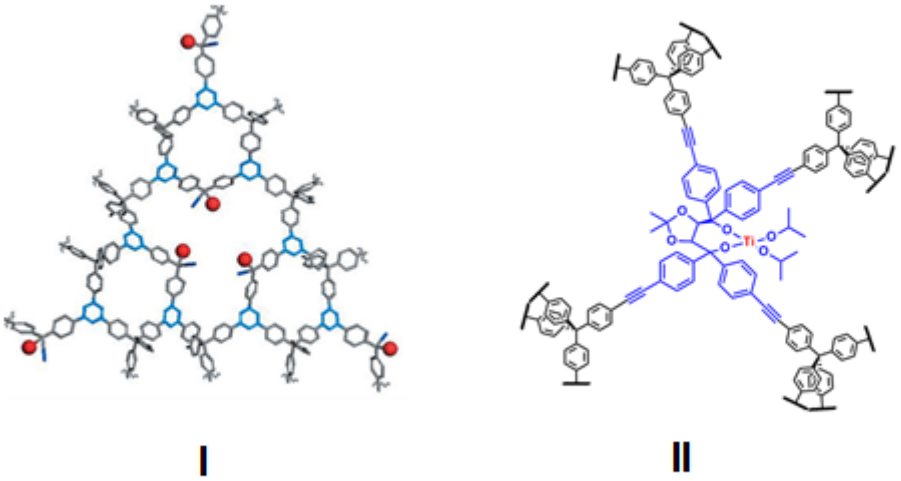

Figure 17 Schematic representation of chiral heterogeneous catalysts marked as red bowls ((L)-proline), whereas TADDOL's pocket is clearly shown.

1.3 Self-assembled monolayers - tripodal aromatic platforms.

Flat delocalized π-systems have the tendency to spread with the entire π-surface over the substrate driven by *van-der-Waals* interactions. While delocalized π-systems are the ideal model compounds of numerous electronic and optical applications, a more perpendicular arrangement with the surface would be desired to profit from their properties. In optical experiments the quenching of molecular excited states is reduced by a perpendicular arrangement and in electronic applications a perpendicular arrangement is required to separate the π-system from the substrate and to profit from the entire dimension of the molecule. While for most optical set-ups the perpendicular arrangement is the only prerequisite, in electronic applications also the contact point of the molecule with the substrate, which defines the coupling between molecule and electrode (substrate), must be controlled.

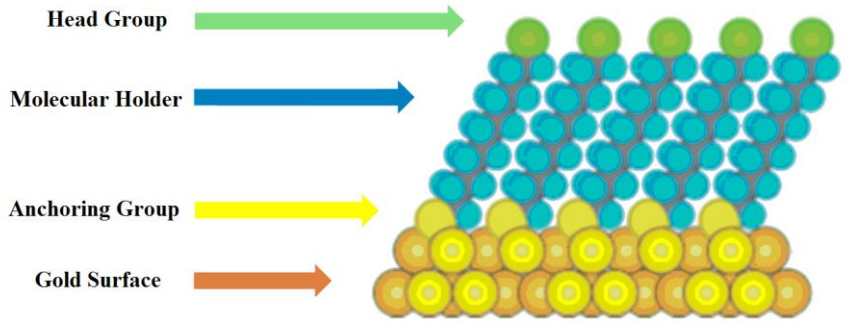

Figure 18 The general view of SAM relies of alkenothiols assembled on the gold surface.

One of the most important class of SAMs is based on the strong chemisorption of organosulfur compounds (thiols, disulfides), and related moieties on coinage metals, particularly Au (111), Ag, Cu as well as Pt, Hg, GaAs (100) and InP (100) surfaces. [48] Most frequently used for anchoring of organic molecules are gold surfaces. Figure **18** displays an illustration of SAMs created on the gold surface. Owing to aforementioned elements, surface properties can be adjusted by their chemical tuning. Moreover physical parameters are matched by the choice of the spacers determining their thickness, affecting conductivity and optical features. There are several reasons why gold surfaces are so popular. One of them is that gold can form atomically flat surfaces suitable for STM techniques. Another reason is that gold is a reasonable inert material not prone to impurities by reaction with oxygen and can be handled at ambient conditions while it can still be efficient and selectively modified

by organosulfur compounds. The Au-S bond forms a good molecular junction between adsorbates and gold electrodes, providing reasonable electrical conductivity and rapid interfacial electron transfer. Since the early stages of molecular electronics, most studies deal with molecules attached to the gold surface through one thiol (SH) group. [186] While the details of the adsorption mechanism are still under debate, it is widely believed that the hydrogen of the thiol group is eliminated in contact with gold and that a covalent Au-S bond is formed [48,187] This bond possesses a dissociation energy around 2.1 eV with the nominal strength of Au-S bonds (~ 50 kcal·mol^{-1}), which is large enough to ensure the thermal stability of thiol monolayers up to 80 °C[188]. Furthermore, it is stronger than the Au-Au bond with the dissociation energy around 0.8 eV, [189] which can lead to the removal of small gold clusters by desorbing thiols. The versatility of the thiol anchoring guarantees a dense coverage of both flat and rough gold surfaces. Substrate atoms on bare Au(111) surfaces compact slightly, forming a reconstruction with both face-centered-cubic (*fcc*) and hexagonal close-packed (*hcp*) zones and a (22 × √3) unit cell relative to the Au(111) lattice, referred to as the herringbone reconstruction. When sulfur containing molecules (e.g. thiol, disulfide) bind to Au(111) the formation of Au-S bonds removes the reconstruction, a phenomenon observed in STM experiments. This ability to remove the reconstruction can be used as a qualitative descriptor of molecular-substrate bond strengths. For instance, sulfides (R-S-R) have weaker molecule-substrate bonds than thiols; however, SAMs of sulfides nonetheless lift the Au(111) herringbone reconstruction .[190] On the Au(111) surface thiols can bind to three sites, the so-called top, bridge, and hollow site. In these configurations, the sulfur atom of the thiol is bound to one, two, and three gold atoms, respectively.[191] Furthermore, the high reactivity of the thiol group not only guarantees a robust functionalization of gold electrodes; it can also lead to complication during the self-assembly process. The intermolecular linking of bifunctional dithiols due to disulfide formation in the presence of trace amounts of oxygen may cause multilayer formation [192] and, in electrical measurements, the probing of oligomers. To address that problem the in-situ formation of thiols from thioacetates with a deprotection agent can reduce the risk of multilayer formation significantly.[186,193] Although thiol monolayers have received considerable interest in the scientific community, the stability of these SAMs and the poor tolerability of Au in CMOS technology, reduces considerably the application potential. In particular these organic films exhibit only moderate stability under ambient conditions and decompose at elevated temperatures. One of the drawbacks of the gold-thiol protocol is also that the adsorbates possess inclined configurations. With increasing complexity of the SAM constituents another drawback of densely packed SAMs, is the close

contact of component molecules, which causes significant steric and/or electrostatic interaction. To circumvent these problems, researchers have explored several strategies for generating thermally and chemically stable SAMs. A popular strategy to circumvent this problem has been preparation of mixed SAMs composed of alkenothiols of specific chain length and longer thiols carrying a functional unit. Although this approach is efficient for molecules that form tightly packed monolayers, it is not convenient for the positioning and control of individual molecules. Alternative approaches have been suggested, such as increasing the free volume of molecules in the self-assembled monolayers by integrated bulky spacer group or employing large molecular multipods or platforms (Figure **19**). This architecture provides more space for sterically demanding functional tail groups and has, potentially, the additional advantage of a more stable connection by multiple sulfur-gold interactions.

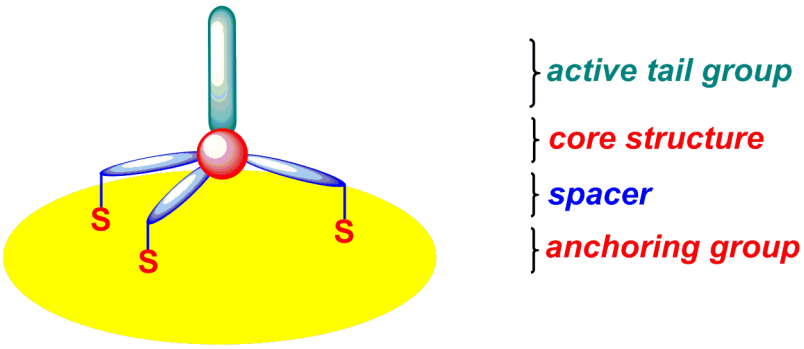

Figure 19 Schematic drawing of a molecule attached to the surface *via* a tripodal structure.

In order to also control the molecule's spatial arrangement rigid molecular architectures with multiple anchor groups are particularly appealing. Thus, the motivation for employing multipodal structures was to make a strong contact and to enforce an orientation of the molecules at a fixed distance from the surface.[194] For the multipodal systems, the minimum number of the anchoring groups that would guarantee stable arrangement of the molecular structures on the surface is three and they should not be in a line. The basic platform that fulfils this criterion is a tripod, which is common structure in chemistry. The chemical structures containing sp^3 hybridized core carbon and silicon atoms themselves represent a tripod with the fourth bond positioned perpendicular to the surface. The remaining three substituents of the tetrahedral core should be as rigid as possible to form stable contact to the surface. Consequently, these legs usually contain rigid aromatic units or phenyleneethylene species if greater length is desired. So far, a number of C_3-symmetric tripods incorporate a

carbon atom (e.g. tetraphenylmethanes), [60,64,111,195,110] a silicon atom (e.g. tetraphenylsilanes),[196,197,198,199,123,200] or adamantane [112,201,202,203,204,205,206] as the branching unit decorated with three identical sulfur-containing termini (thiol, thioacetate, sulfides), selenol-containing termini or pyridine have been described and chemisorbed on gold surfaces. In these molecular tripods forming stable and perpendicular chemisorption of molecules, however, little or no attention has been paid to maintaining the functionality of anchored molecules to obtain a strong and defined electronic coupling with a gold electrode, which yields fast electron transfer. We note that tripodal adsorbates reported so far adopted non-π-conjugated aliphatic thiol groups, such as benzylthiol and adamantylthiol anchors. While some synthetic papers focused mainly on the concept, [196,197,198,199,201] initial studies revealed an increased stability of the tripodal contact [111,195] and surface analysis by scanning probe methods,[110,204,205] or X-ray absorption techniques [203,207,208] displayed an enlarged separation due to the increased footprint of the tripod. Further evidences for a perpendicular arrangement of separated molecules were obtained by optical[110,209] and electrochemical [200,206,208] analysis of the samples. In addition, taking into account well-defined alignment of the multipodal platforms on the surface, several groups have got more insight into its possible applications as a tip for scanning probe microscopy,[196,210] a crosslinker for the creation of an arrays of gold nanoparticles, and to anchor several active tail-molecules as complex ligands, [123,200] fullerenes, [198,199,109] rotaxanes,[119] pseudorotaxanes and artificial molecular rotors [113,114,211,212] to the surface. Although the most commonly used immobilization chemistry on gold electrodes is the formation of covalent bonds between thiols and gold substrates, also a few examples even profit from the interaction of delocalized π-systems with the flat substrate to arrange a subunit perpendicular to the surface like e.g. the triazatriangulenium platforms from Herges and coworkers [213] or the tris(4-pyridyl-*p*-phenyl)methyl platform from Aso and coworkers.[60] While several of these multipods enable a perpendicular arrangement of rod-type molecular structures, the electronic coupling of the rod's π-system to the metal states is limited due to the multipodal architectures comprising sp^3 hybridized atoms. This electronic decoupling of the functional subunit is on the one hand desired to profit from the subunit's optical properties but on the other hand it represents a considerable handicap for molecular electronic applications.

1.3.3 Aromatic tripodal adsorbates

The synthesis of tetraphenylmethane-based anchor with three sulfanylmethyl feet was pioneered by Aso and co-workers. [109] They designed and studied [60] fullerene-linked oligothiophene tetramer and octamer derivative bearing a tripodal rigid anchor **13** (Figure **20**), allowing such molecules to be well-organized on the metal surfaces to construct highly efficient photovoltaic cells. This strategy to employ a tetraphenylmethane tripodal rigid anchor has led to remarkable enhancement of the photocurrent generation, as compared to the reference systems with one-armed anchoring compounds, which was determined by photoelectrochemical measurements.

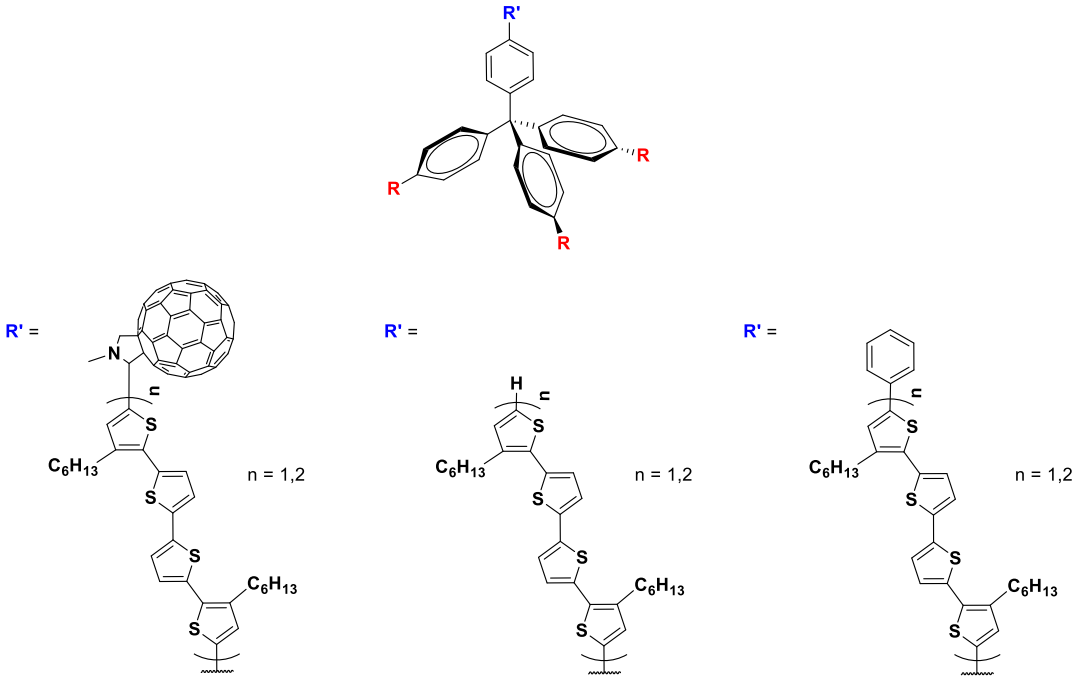

Figure 20 Functionalized tetraphenylmethane tripods **13-15**.

Further electrochemical study of SAMs of two tripodal shaped oligothiophene-bearing thiols **13** (Figure **20**) on Au(111) indicated that the packing within the SAM of shorter oligothiophene terminated tripod (n=1) is more compact than that for the longer one. [214] Both the much increased number of oligothiophene repeat units in the tail, and the higher number of C_6H_{13} side substituents causes its SAM to be less compact, and make a perfect standing of

the molecules on gold more difficult. Consequently these features were identified as unfavorable factors for charge transport through the SAM. In the case of shorter oligothiophene tail in **13**, the π-conjugated tail has an appropriate length, allowing compact packing of the molecules. A structural feature reflected in a greatly enhanced charge transport through the SAM. Organic light-emitting devices have been fabricated by using the SAM-coated Au electrode as the anode. In comparison with the bare-Au device, the electroluminescence performance of the device comprising the tripod decorated Au electrode is improved considerably reflected in reduced operating potentials, yielding much greater maximum brightness, permitting much higher currents, and better stability. Aso and co-workers have also synthetized selenium-terminated tetraphenylmethane tripods **15** bearing three selenocyanate or selenol arms as anchoring groups (Figure **20**). CV, XPS and ultraviolet photoemission spectroscopy (UPS) measurements of their monolayers on a gold surface were investigated and the results were compared with those obtained from the thiol terminated analogues **16** (Figure **20**). [64] They found that all three selenol groups of the tripod are bound to gold surface and the selenol monolayer is electrochemically more stable than the thiol one. In a comparison of the gold-sulfur and gold-selenium terminated tripodal interfaces, they found from the UPS measurements that the charge injection barrier from gold to the frontier molecular orbitals of the molecule was smaller in the gold-selenium interface, from which they expected that a large electric current could be obtained at a lower voltage in the gold-selenium interface. The Se-Au bond has a better suited electronic state to perform molecular conductance and is thus more appropriate for the molecule/electrode interface in molecular devices than the S-Au connection. These results are consistent with the trends reported recently.[63] Aso and co-workers also recently designed and synthesized the [4-(4-pyridyl)phenyl]methyl tripodal platforms **17**, **18** (Figure **21**) to realize robust single-molecule junction with a gold electrode and to achieve effective hybridization of the pyridine π orbitals with the gold electrode.[60]

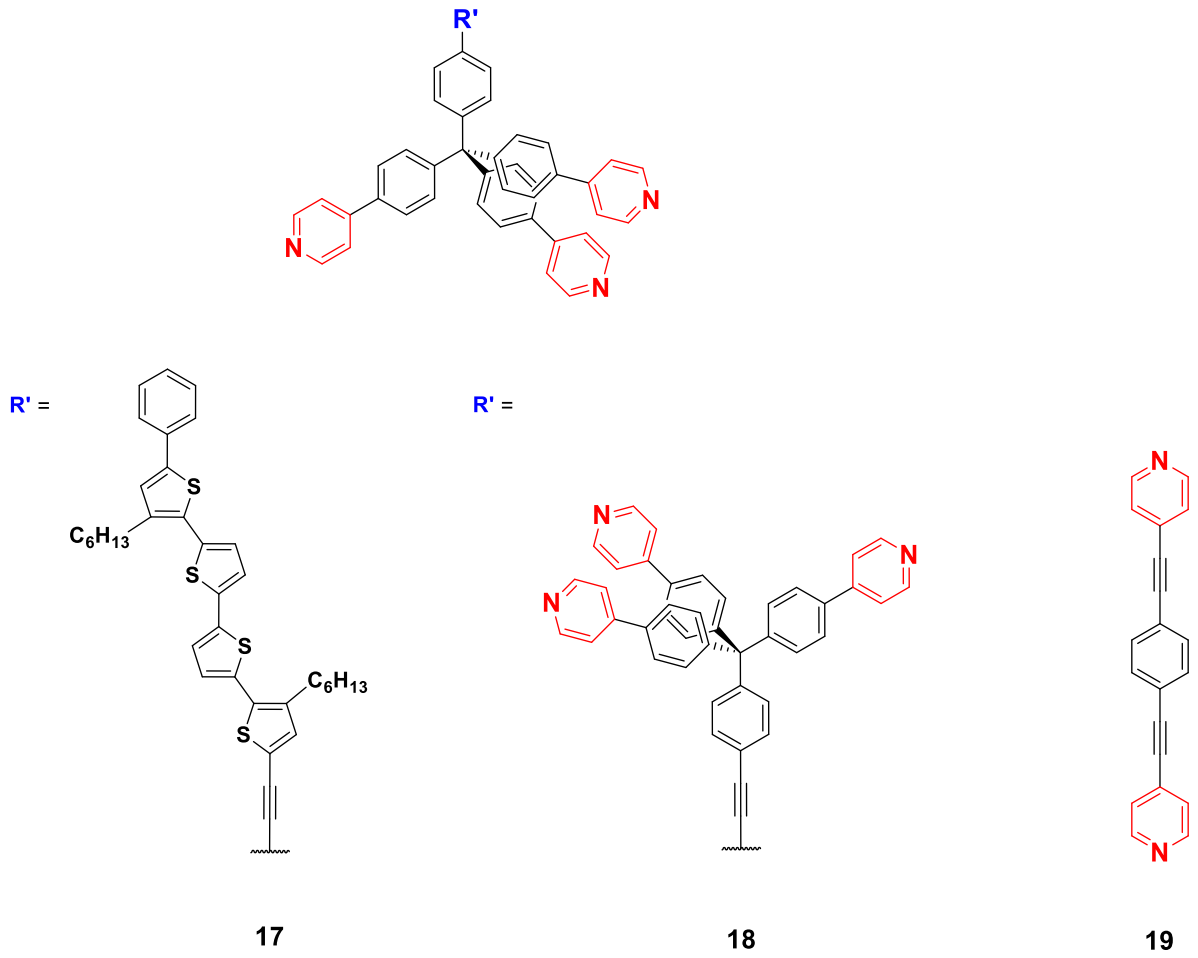

Figure 21 Structure of pyridine terminated platforms **17-19**.

SAMs of 4-pyridyl terminated tripodal **17** as well as monopodal platforms bearing both redox-active oligothiophene tail for CVs, and (triisopropylsilyl)ethynyl tail group for XPS measurements were evaluated. CVs with the redox active tripodal-modified gold electrodes displayed a reversible one-electron redox wave with the surface coverage 7.1×10^{-11} mol*cm^{-2}. This surface coverage remains at 30% of the original value after 10 scans within the range 0-0.55 V, which indicate that junctions, which are indispensable for the fabrication of molecular devices, were formed. XPS Measurements revealed that the π orbitals of the pyridines contributed to the physisorption of tripodal platform on gold. Measurements of single-molecule conductance were successfully carried out using modified STM techniques for single-molecule junctions that consisted of the tripodal anchors and diphenyl acetylene linker **18**. The obtained conductance of $5 \pm 1 \times 10^{-4}$ G_0 is substantially higher than that of previously reported shorter π-conjugated chains with monopodal pyridine anchors **19** (3.5×10^{-6} G_0, Figures **22c**, **22d**). [215] Theoretical analysis based on ab initio calculations clearly supported the experimental results and the hypothesis of π channel

conductance of the pyridine anchor moieties. The calculated results indicate an electron-transport mechanism in which the LUMO dominates the transport. In the pyridine-based tripodal anchors, the π* orbital of the pyridine part could directly interact with the gold electrode (Figures **22a**, **22b**). The pyridine-based tripodal structure is expected to form a robust junction *via* the three anchoring units, and pyridine is predicted to achieve effective π-channel electric transport.

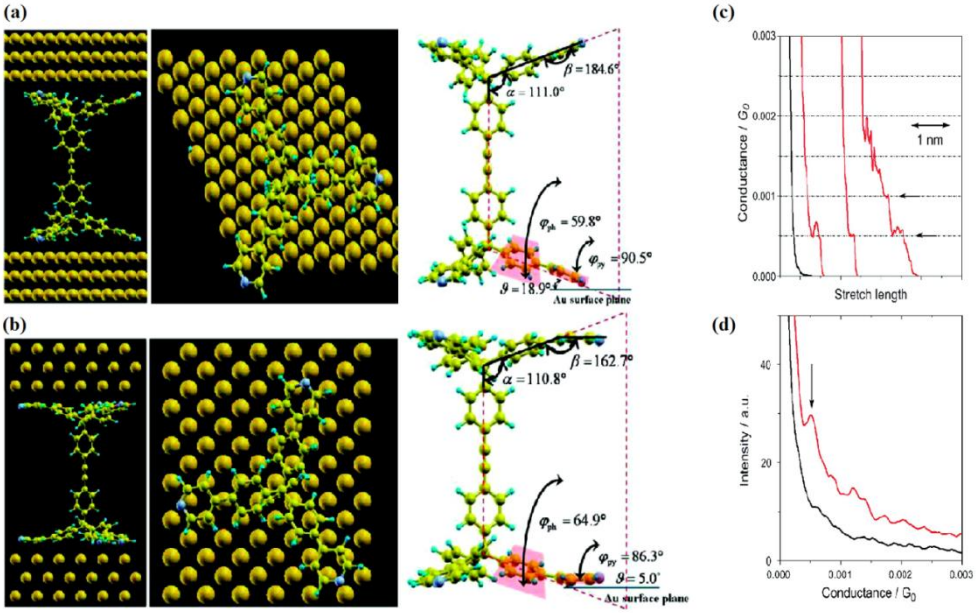

Figure 22 Structures of the junctions used for the ab initio transport calculations. (a) **18** (111) model and (b) **18** (001) model, respectively. The left panels show side views of each system, whereas the middle panels show views from the top. The right panels give the details of the parameters to identify the conformations for 3Py, such as dihedral and bending angles. (c) Conductance traces measured when breaking the Au point contacts in solutions with (red) and without (black) **18**. (d) Corresponding conductance histograms constructed without data selection from 1000 traces. Each histogram is normalized by the number of traces used to construct the histogram. The bin size is $10^{-5}G_0$.

Lindsey, Bocian and co-workers synthetized several redox-active molecules bearing a tether composed of a tripodal tetraphenylmethane with three acetylsulfanylmethyl groups **20** (Figure **23**) for surface attachment to examine the effects of spatial arrangement of the molecular structure on charge storage in SAMs.[111] The redox active molecules include ferrocene, zinc porphyrins, magnesium phthalocyanine, and triple-decker lanthanide sandwich complexes.

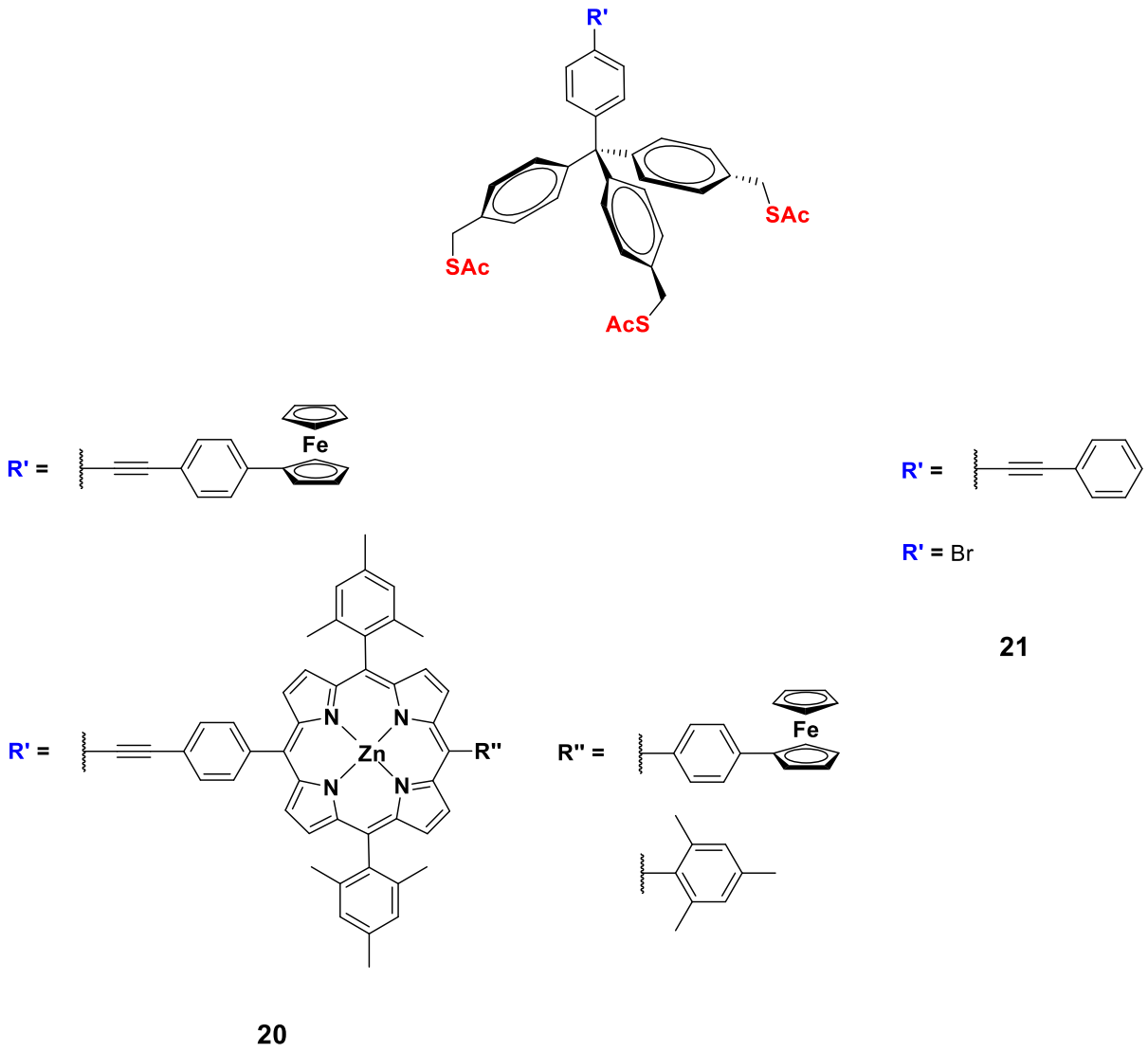

Figure 23 Red-ox active tripodal structures **20-21.**

The electrochemical characteristics of each compound were examined in solution and in SAMs on gold and indicate that the tripodal tether provides a more robust anchor to the gold surface than does a monothiolated anchoring. However, the electron-transfer and charge-dissipation characteristics of the tripodal thiolated molecules and monopodal thiolated species are generally similar. These facts that acetylsulfanylmethyl terminated tripodal tethers offers superior stability characteristics without sacrificing electrochemical performance renders these tripods attractive candidates for incorporation in molecular-based information storage media. SAMs of two tripodal thiol-terminated metalloporphyrins **20** (Zn and Cu) and three benchmark tripods were further studied by XPS and FT-IR measurements on gold substrates.[195] The benchmark molecules **21** (Figure **23**) include (1) two tripods containing a

bromo atom at the perpendicular position of the apical phenyl ring and sulfanylmethyl or acetylsulfanylmethyl feet, (2) acetylsulfanylmethylated tripod terminated in the perpendicular position with a phenylethylene unit. Together, the spectroscopic studies revealed that none of the five tripodal molecules bond to the gold surface *via* all three sulfur atoms, where the average number of bound thiol range from 1.5 to 2. This nonuniformity of binding through the different SAMs might arise from steric interaction between co-deposited molecules. As well as similar surface binding found for the *S*-acetyl protected and free thiol terminated benchmark tripods, indicating that the presence of the protecting group does not influence the binding and is probably cleaved during deposition. Furthermore, the surface binding characteristics of the SAMs are not sensitive to deposition conditions such as solvent type, deposition time, or temperature of the solvent, which was determined by IR measurements. Recently, Dong and co-workers have synthetized a self-decoupled porphyrin with a tetraphenylmethane tripodal anchor **22** (Figure **24**) and deposited it on Au(111) using different wet-chemistry methods in order to assemble a single molecule electroluminescence STM experiment (Figure **25**). [110] The rigid tripodal anchor in this molecule not only acts as a robust decoupling spacer but also controls the orientation of the porphyrin molecule in the desired up-right standing position along the tip axial direction.

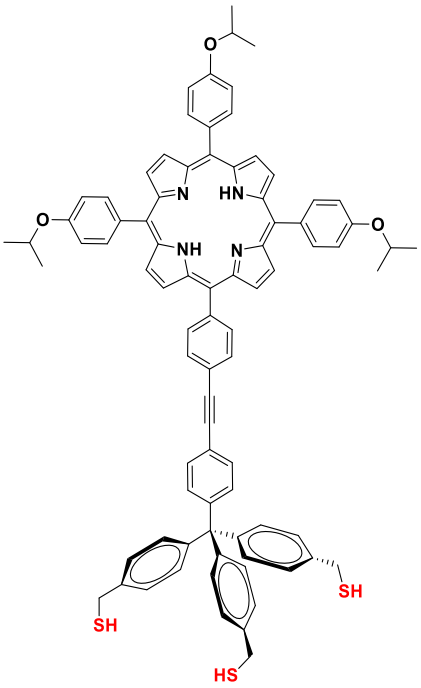

22

Figure 24 Self-decoupled porphyrin with a tetraphenylmethane scaffold **22**.

STM image has revealed formation of dispersed bright spots (~3-5 nm), fitted to the single or aggregated molecule, placed perpendicularly to the Au (111) surface. Molecular electroluminescence from single porphyrin molecules or aggregates of **22** on gold has been realized by tunneling electron excitation in the STM-junction. Moreover, the following molecule makes the tip-molecule-gold junction highly asymmetric, which enables the observation of molecular electroluminescence phenomena such as the unipolar performance. The unipolar performance of the nanoscale electroluminescence from the tripodal structure **22** suggests that the porphyrin molecule is predominantly excited by the hot electron injection, and the excited molecules then decays radiatively back to the ground state via *Frank-Condon* π^*-π transitions, producing enhanced molecular electroluminescence. These results are of interest as fundamental studies of electrically driven single-molecule light sources helping to analyze and improve the mechanisms in molecule-electrode junction in organic light-emitting diodes.

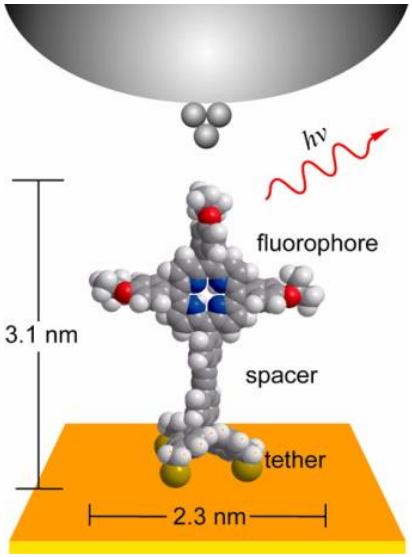

Figure 25 Schematic configuration of 22 on Au(111) and localized electrical excitation from a nanotip.

Tetraphenylmethane-based tripodal platform was also employed to immobilize oligonucleotide probes perpendicularly to the gold surface of DNA chips.[108] To realize a reliable DNA arrays for a reproducible, inexpensive, and high-throughput detection system for genetic analyses in clinical diagnostics, particular attention must be paid to form stable molecules with precise control over the spatial arrangement of oligonucleotide probes immobilized on a surface. Moreover, electrochemically controlled and potentially switchable tripodal [2]rotaxanes incorporating a viologene moiety, a crown ether, and

sulfanylmethyl-terminated extended tetraphenylmethane anchoring group **23** (Figure **26**) have been prepared and their SAMs on gold have been studied by cyclic voltammetry. [119] The thiol terminated tripodal viologens formed oriented SAMs on gold surface, and threaded crown ethers to form a hetero [2]rotaxanes with a surface coverage in the range 10^{-10}-10^{-11} mol.cm^{-2}.

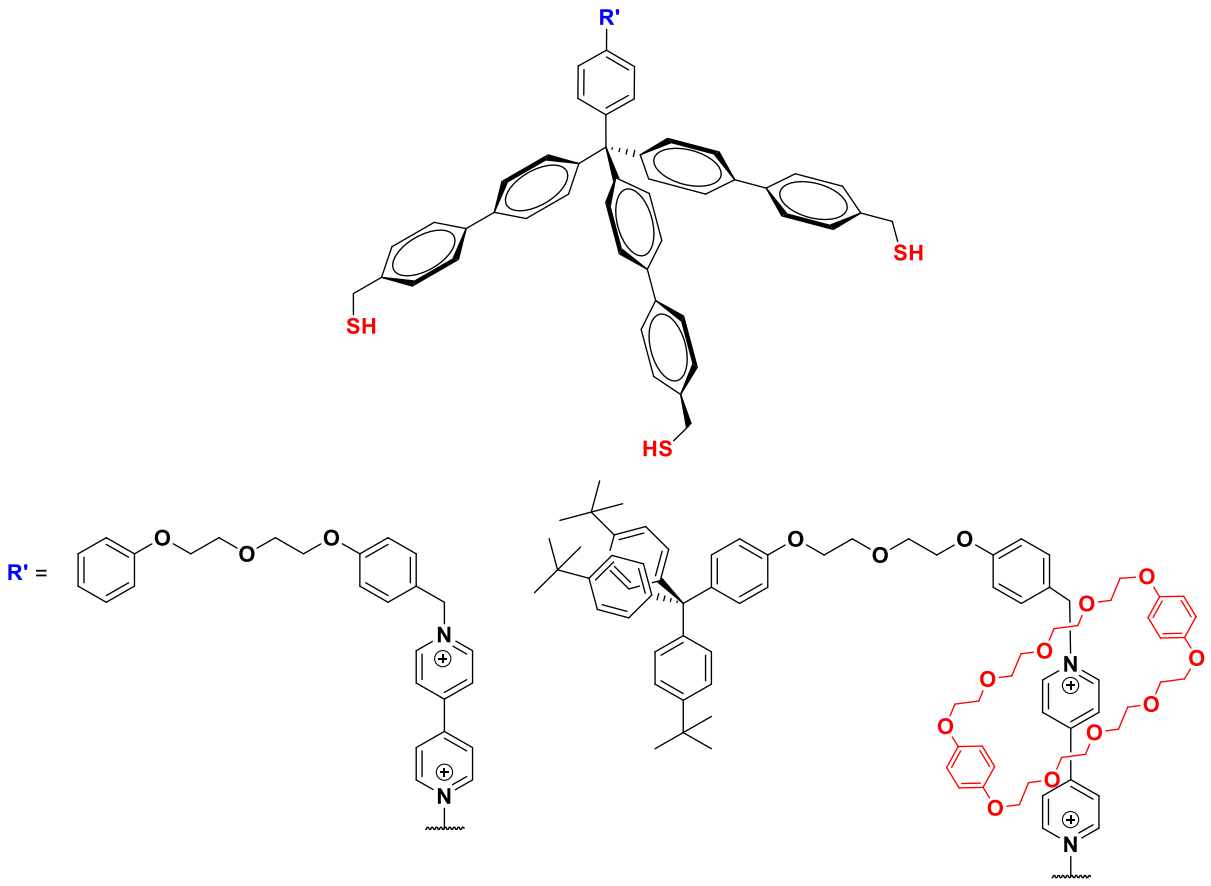

23

Figure 26 Structure of tripodal [2]rotaxanes **23**.

1.4 Covalent and coordination bonds served for *3D* organic frameworks (MOFs and COFs).

Undoubtedly, widespread linear polymers brought tremendous structural diversification offering several advantages and applications available over the whole planet. However, the challenges resulted from the consequent technological progress imposed the scientific environment to seek new materials aside from conventional polymerization methods for the novel linkage of repeating units. For many years people have asked how to store energy, how to cram unwanted products into easily accessible and disposable materials. The answer, as usual, has been inspired by the nature. Naturally occurring zeolites are tetrahedral porous aluminoslilicate solids absorbing water, binding inorganic cations, explored in catalysis and fine chemicals synthesis.[216] These were mimicked by the concept of coordination chemistry transferring it slick to the class of ever lastly growing crystalline and porous materials, based on the metal cation and organic bridging ligands.[217,218,219,220,221,222] Robson's, Moore's, Yaghi's or Zawrotko's approaches pointed out infinitive abilities of the novel coordination polymers. Furthermore, over the last three decades an overwhelming amount of work dealing with simple nets appeared, highlighting treasures of functionalities in gas separation,[223,224,225,226] alcohol adsorption,[227] luminescent behavior,[228] thin films,[229] biomedicine[230] and heterogeneous catalysis.[231] Therefore here only diamond-like structures will be profoundly discussed. Taking into account covalent bond energy and their reversible feature, organic building blocks, merged by versatile linkers, in conjunction with well-fitted geometry are pertinent to construct one, two or three dimensional multifunctional individuals. The groundwork was laid by Yaghi who is the world pioneer in the field of organic frameworks. Simple dehydration of linear 1.4-benzenediboronic acid against hexahydroxylphenylene guided formation of the first honeycomb 2D-COF. These motifs circumscribe all of the COF attributes like the nature of covalent bonding, structure and topology of the linkers and desired dimensionality, which will all be discussed here in detail.

1.4.1 3D metal organic framework based on tetraphenylmethane core structure.

This well-established class of hybrid inorganic-organic materials is composed of metal cations and organic electron donors (usually amines or carboxylates). The geometry of the desired materials is relevant to the structural features of both inorganic and organic components, so-called secondary building blocks (SBU, Figure **27**). [232,233] In principle, beyond a wide spectrum of the metals, "infinitive" numbers of ligands may be prepared, however they are rather limited to small molecules or enlarged rods, reassembling a kind of

engineering. Formation of the polymeric ensembles must be thermodynamically controlled due to several site possibilities, rooted in the cation reactivity as well as ligand flexibility, manifested through plenty of conformations that may stimulate formation of more than one type of frameworks. One of its solutions was realized through a rigid scaffold of TPM affording one type of net. Manipulation of shoulders length and the donor distinction prove to be a leading motif in all studies sacrificed for seeking new polymers, bridged by tetradentate segments with exceptional pore size distribution.

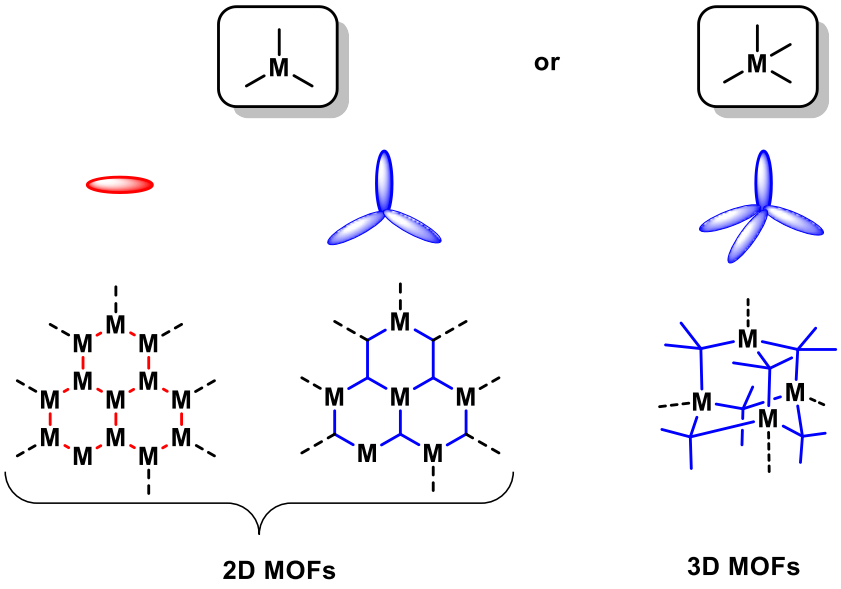

Figure 27 The Illustration shows the relationship between vacancy of selected metal ion and geometry of organic ligand enabling tunable synthesis of MOFs.

The very first adamantane-like cavities were proposed by Robinson and based on copper (I) complexation with tetrakis-(4-cyanophenyl)methane as a cornerstone of 3D-type architectures. [234,94] The carrier of the simple, symmetrically substituted tetratopic ligand was developed by Yaghi[235] who primarily demonstrated implementation of the firm tetrakis-(4-carboxyphenyl)methane assembling it with the double paddle-wheel units formed by Zn^{2+} cation forcing PtS topology essential for these classes of materials. Wherefore its zirconium(IV) MOFs (MOF 812/841) crystalized in C*2*/*c* and *I*4/*m* space groups with **itu** and **flu** topology respectively, bearing permanent porosity what jointly with great permeability may render it water absorbers (potential dehumidifiers).[125] Predictable extension of molecular struts was realized fixing to the core structure biphenyl, stilbene and phenyl-acetylene units, affording copper paddle-wheel SBUs abbreviated as $[Cu_2(O_2C\mathbf{R})_4]$(where **R** is given carboxylic acid),[236,237] representing tetragonal space groups. Unique freeze-drying

methodology reinforced the porosity, eliciting a larger surface area, increasing it up to 1725 m^2/g, providing channels for hydrogen uptake and dye inclusion. The same kind of topology is given among tetradentate pyridine moieties. [238,239] Heterocyclic species were mounted to the rigid core,[240] distinguishing them by the type of carbon-carbon bond (by the analogy to aforementioned acids). Anion-dependent and temperature resistant MOFs, built on NiX_2 and CuX_2 were obtained with the variety of shape, serving them to study morphological alteration with uniform crystals size distribution. Meanwhile, Fe (II) porous complex polymer was evaluated as prospective SCO material. The influence of the guest molecules (cyclohexane) onto SCO phenomena was deemed as molecular bracket of HS state (Figure **28**). [241] Moreover, few other ligands envisaged for MOFs synthesis and their further applications were explored including tetrazol,[242] terpyridine[243,244] and phosphonic acid. [245]

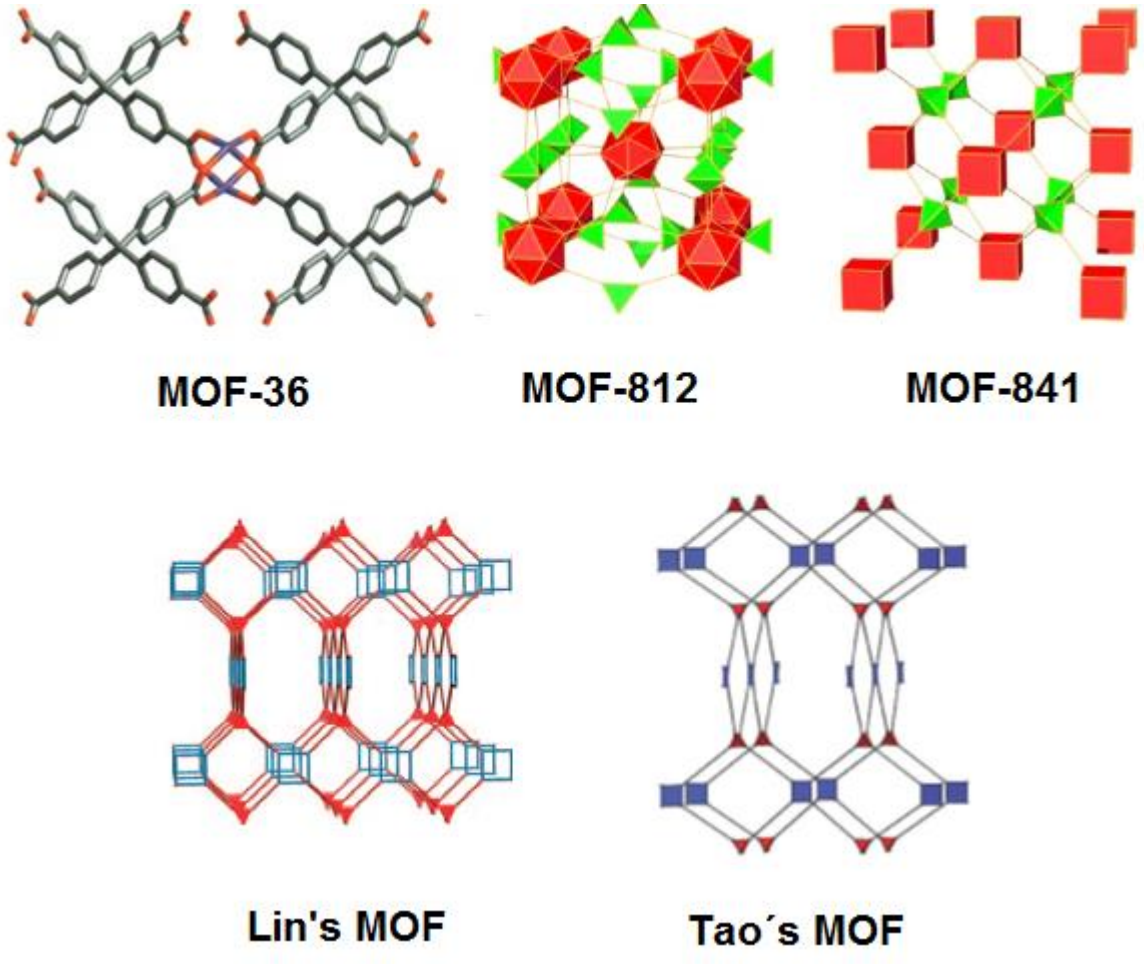

Figure 28 Illustration of the most outstanding MOFs engaged tetratopic ligands emerging as paddle-wheel units in MOF-36, zirconium coordination polymers (MOF-812/841), pyridine represented ligands (Lin's and Tao's MOFs).

1.4.2 COF: type of bonding, synthesis, structural variations and its applications.

Pivotal drawbacks of MOFs are lack of self-healing features, low stability of coordination bonds, vulnerability to harsh conditions (typically structure collapse), and lower chemical and thermal durability. They way to omit this inconvenience is delineated by organic chemistry which proposes a broad assortment of dynamic covalent bonds that have reversible and irreversible nature. However, a great deal of effort has been put to show ability of common functional groups toward regular and well structurally defined polymers. Among many others, boroxine and boronic esters have become one of the most precious linkers, created by self-condensation of boronic acids or their co-condensation with catechols either with silanol, that produce borosilicates. In consecutive steps, trimerisation of aromatic nitriles was used to form highly robust triazene-based COFs, with enormous stability and a significant for conjugation degree (Figure **29**). The tremendous development of imines and their derivatives found reflection in the chemistry of COFs as well. Similarly, condensations of aldehyde and imine moieties allow to obtain a family of Schiff-base consisting polymers, with prospective self-healing properties.[246] In order to facilitate an access to the properties that are tuned in COFs, the library of the connectors was established mutually with the choice and synthesis of building blocks, guaranteeing their rigidity. These have affected a highly predictable geometry of performing ensembles. Thus, the length and width of organic skeletons, physical and chemical robustness and conformational stability turn out to have a decisive impact in the choice of the ingredients. The most prevalent units are pointed out in Figure **30** evidencing their direct influence onto COF shape due to the numbers of possible combinations. Depending on linkage, geometry and final structure, different preparation methods were applied. Moreover the equilibrium, being the driving force of all thermodynamic transformations, helps to assemble organic frameworks. Therefore, particular synthetic protocols have to be deployed to rule out linear products or other unwanted processes. Hence, solvothermal synthesis was carried out in a sealed pyrex tube which is considered as a suitable tool to overcome solubility problems, reaction rate, prompting the growth of crystals, preventing a left-side shift of the equilibrium.

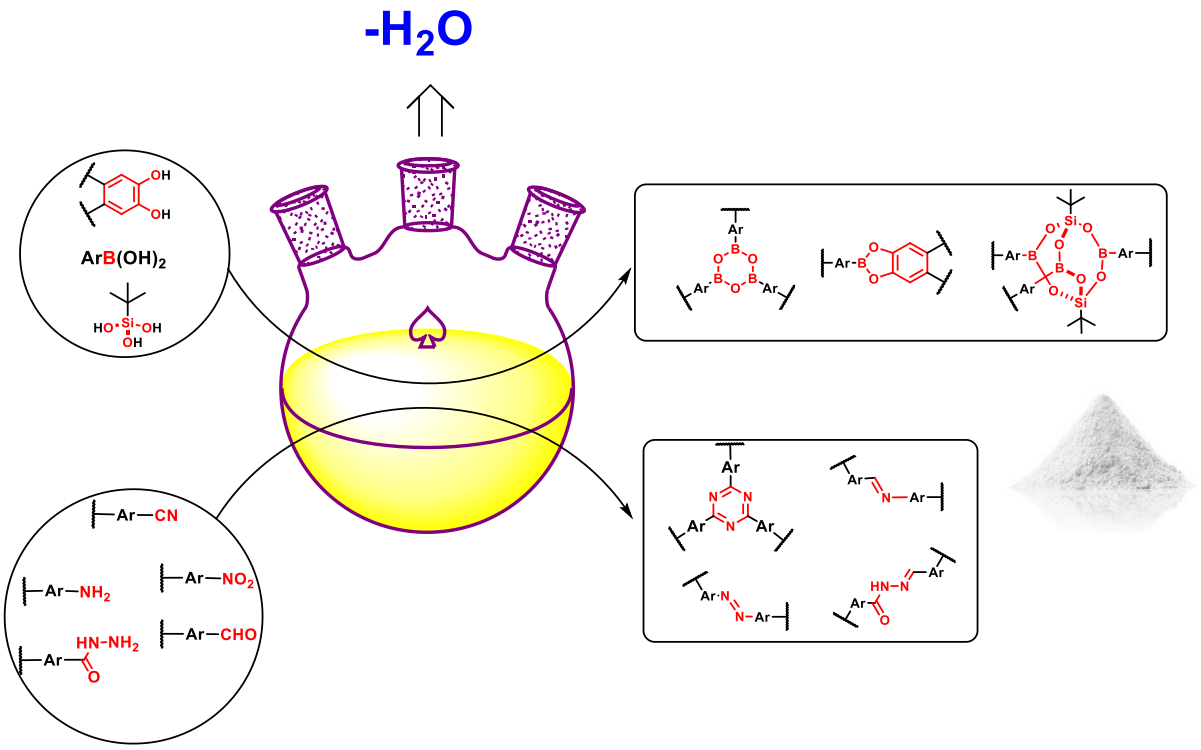

Figure 29 Graphical illustration of the most common organic bonds applied in the construction of COFs

Under water free conditions and a temperature oscillating around 85-120 ^{o}C, different solvents mixtures were utilized ranging from DMAc-*o*-dichlorobenzene, THF-methanol ending up on dioxane-toluene (mesitylene) dedicated for boron or imine mediated COFs respectively. [247] Microwave irradiation is also an alternative for upscaling synthesis. Nonetheless, as a major part of 2D drafted materials, based on the strong π-π interaction triggered by overlapping electron rich layers, molecular sheets rather need to adopt considerably disparate techniques. Hereby, in the nitrile cyclotrimerization, zinc dichloride plays a twofold role, being simultaneously the solvent and catalyst (ionothermal synthesis). The following protocols assume surface assisted synthesis to hamper defects over monolayers. The nano-assemblies are manufactured onto an Ag (111) surface at UHV conditions, monitored by STM.

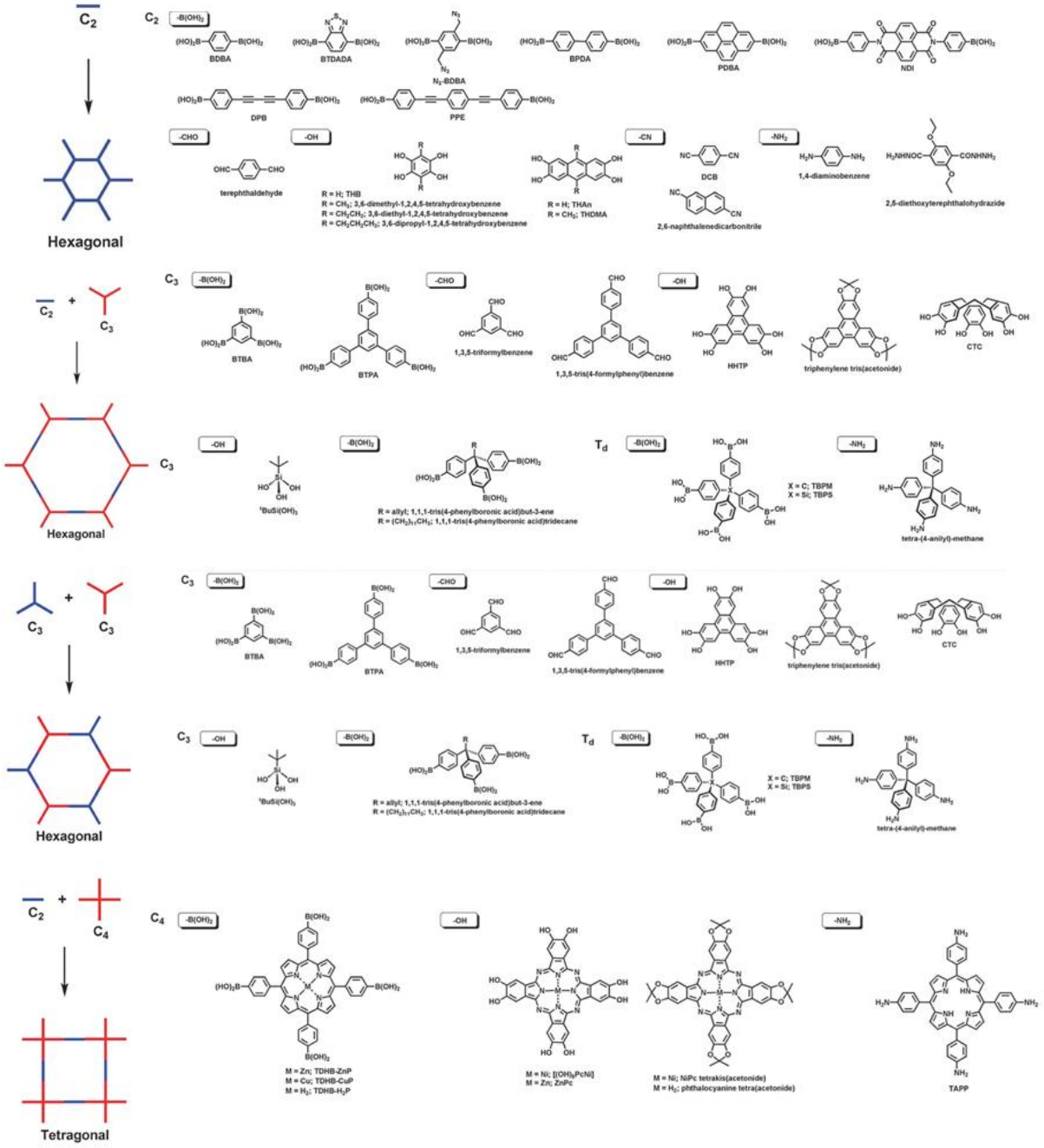

Figure 30 Illustrations show different class of the building blocks and their strong effect on the topology of newly constructed COFs.

Non-metallic surfaces as HOPG or neat graphene were exploited to form other stacked layers. In the first example powdered copper sulfate as a water trapping agent dramatically accelerates the reaction ratio enabling highly ordered COFs. In the second case, graphene under solvothermal conditions led to the desired boron subunits, creating films. A major part of obtained crystals or powders are insoluble in common organic solvents, thus there are

arrays of priceless analytical tools making their identification way easier like (powder) X-ray diffraction supported by theoretical simulations, MAS-NMR spectroscopy ranging from proton, carbon, boron nitrogen to oxygen isotopes, and SEM measurements to get more insight of COF morphology. [248]

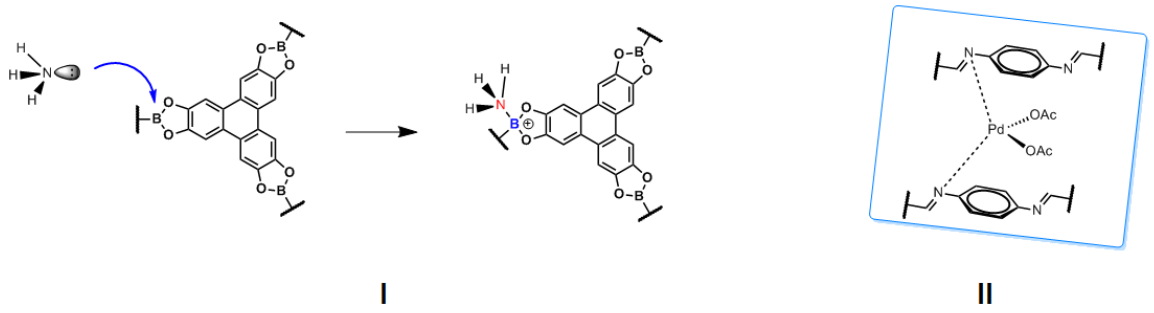

Figure 31 Applications of COF represented by selective ammonia uptake (**I**), cross-section of COF explained the possible catalytic center for Suzuki-Miyaura reaction.

The honeycomb structure typical for main 2D COF, built-up on highly conjugated backbones allows to discover beautiful applications as conductive materials in optoelectronics. Aromatic linkers embodied by pyrene, porphyrins, (metalo)phtalocyanine with maximal π-orbital overlap, among many others prove to be *p*-type semidcondactive materials with absorption bands reassemble the values near to the solar spectrum. Besides, abundance of the channels enhanced the whole transport realized with notably high mobility.[249] Whereas, the nanoporosity serves the opportunity to store gases (methane, hydrogen, carbon dioxide) and ammonia bringing new cavities addressed for heterogeneous catalysis.[250] The last two seem to be really outstanding because of the linkers and their accepting and donating character. Namely, the electron pure boron atom, when incorporated into the five-member-ring of a boronic ester affords bounding of the ammonia through common donor-acceptor interaction, with the total uptake approximately 15 mol/kg at room temperature and 1 bar (Figure **31**, **I**).[251] Secondly, a palladium complex of imine-bonded 1D COF is rendered useful in Suzuki-Miyaura or Sonogashira cross-coupling reactions, [252] giving exceptional yield values being recyclable for the further transformations (Figure **31**, **II**). Beyond that, a couple of the other catalytically active species accelerate conversion of following functional groups including thioethers oxidation, styrene epoxidation, reduction of Shiff-bases and amine oxidation. [253]

1.4.2.1 3D covalent organic framework based on tetraphenylmethane core structure.

As was demonstrated above, 2D organic building blocks may be easily extended by the selection of proper sub-components getting tailor-made 3D diamond frameworks, particularly keen to form highly porous and crystalline materials.[254] This strategy was applied by Yaghi in 2007, where boronic acid was subjected to self- and co-condensation resulting 3D COFs called COF 102, COF 105. Powder diffraction studies revealed the cubic space groups of both nets (*I*43*d*-**ctn**, *P*43*m*-**bor**), however the tetrahedral side view point 4=S_4/4m2= D_2 indicates lower structural strain of COF102 with respect to COF105. Taking advantage of Yaghi's invention, Dichtel reported boroxine linked frameworks with the post synthetic approach facing truncated mixed linkers (TML) what allows to functionalize additionally COF102.[255]

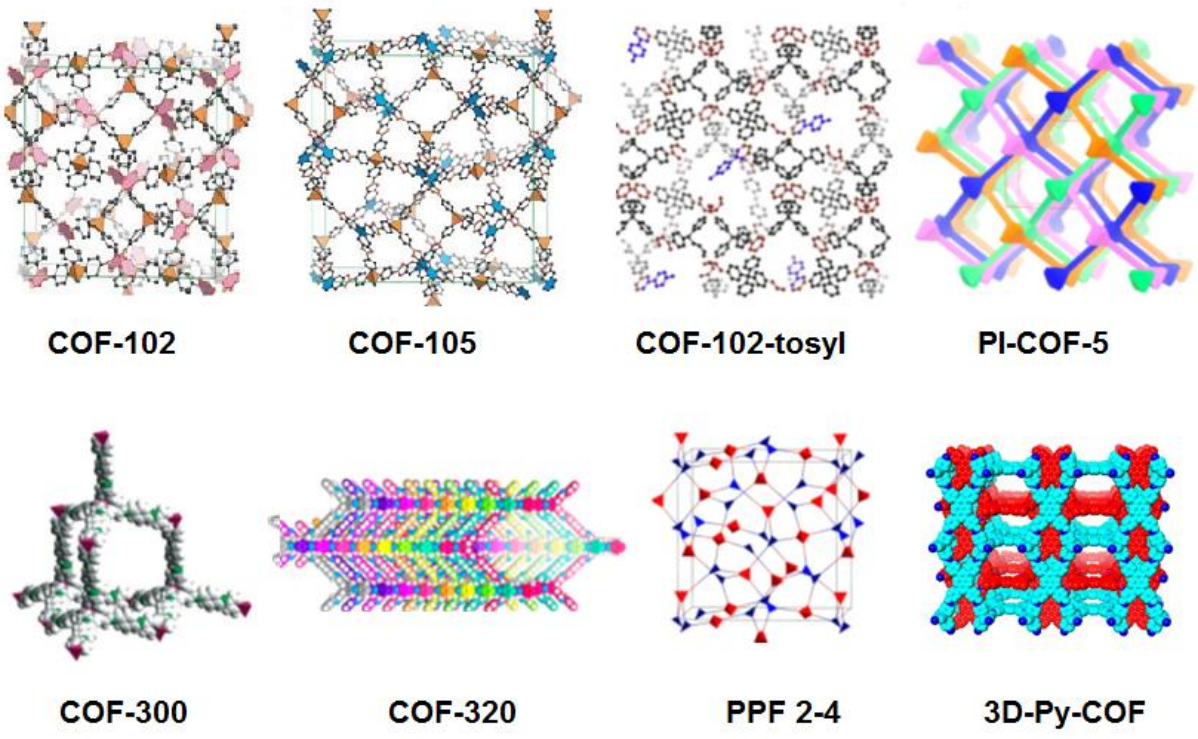

Figure 32 The evolution COFs made of TPM depicted in 3D projection, underscoring the diamond shape of polymers, ranging from boron-consisted porous structures (MOF102, 105, 102-tostyl), passing through imine-bridged ensembles (COF-300,320, PPF 2-4, 3D-Py-COF) ending up to imide-bonded (PI-COF-5).

Tetrakis aryl boronic acid underwent co-crystallization in presence of trigonal tris(boronic acid) with one head group substituted by the dangling octyl, dodecyl and allyl terminus, owing to the rapid framework increment with respect to the boroxine hydrolysis. The

percentage content of doped materials was judged quantitatively by NMR revealing one-third of the inoculated moieties into the COF102 network. Moreover, OsO_4 driven epoxidation evidenced the alkene existence in the analog structure being finally decolorized resin. These trifunctional co-monomers were replaced by series of simple arylboronic acids ranging from *p*-tolyl to *4*-nonylphenyl, *4*-vinylphenyl, *4*-formyl boronic acids.[256] The huge excess of the loaded ingredients affected similar contributions to initial trigonal ingredients (independently 33-37% units were uptake) giving more insight into the upper limit of truncated defects of Yaghi's COF. Furthermore, vinyl chains gave a rise to the next transformation. Reaction with propanothiol provided corresponding thiol-ene product delineating the way to manipulate the morphology and crystallinity of 3D future materials (Figure **32**).[257] From the other hand [2+4] imine condensation accelerated by water sequestration let to obtain crystalline material made of ditopic aldehydes as an connection patterns (terephthaldehyde and 4,4'-biphenylaldehyde) and a tetratopic core structure embedded by tetra-(4-anilyl)methane producing rod-like linked diamond framework (its synthesis was also conducted by surface assisted method). [258,259,260] XPRD studies of the shortest arrangement showed remarkably high symmetry in the $P4_2/mm$ space group, while in the elongated adamantane-like cage with precise atomic system microcrystalline features facilitate the structural analysis owing to RED measurements. Temperature-dependent experiments affirmed possible space groups classified as $I4_1md$ or $I42d$ as well as *Imma* in room temperature with **dia** topology. Simplicity of applied molecular shoulders has prone to tune the properties of Shiff-bases getting highly ordered 3D nets accomplished by library of aldehydes. Theretoo, trifold star-shape intermediates with sizes oscillating between 4.99-12.37 Å were employed and coupled with the same tetrahedral component.[261] The size-depended study suggested strong relationship between growths of the pores with respect to the diameter of linkers. Very recently, rectangle geometry of pyrene aromatic bridging moiety was explored over [4+4] condensation as a crystalline material with *Cmmm* space group and **pts** interpenetrated net.[262] Emitting properties of pyrene units encompassed whole polymeric structure, bringing about intense green luminescence in solid state, which implies its potential usage in explosive detection. Moreover, tetraphenylmethane was incorporated as precursor of luminescence behavior yielding porous, dynamic covalent aerogel which emission was proportional to the degree of gelation.[263] Furthermore, covalent gel bridged by (*R*,*R*)-Mn-salen complex, fused onto silica capillary was capable of enantioselective kinetic resolution of secondary alcohol,[264] whereas catalytic activity of palladium-COF300 complex was examined against Suzuki and Sonogashira cross-coupling reaction as an efficient, alternative heterogeneous

catalyst.[265] In addition, some other works involving tetra-(4-anilyl)methane emerged, profiting mainly form easy *exo*-amine group functionalization. Consequently, covalently spanned dynamic systems have been reported as polyimide polymers with relatively high thermal stability, suitable for the drug delivery with perfectly supervised loading and discharging process.[266] Furthermore, azo-linked nets were constructed from the same components utilizing symmetric and asymmetric synthetic approach (one amino, second nitro TPM derivatives), serving it for CO_2 sequestration because of dipole-quadruple interaction bearing Lewis base/acid (azo and carbon dioxide respectively).[267,268,269,270,271] Last but not least, trimerisation of tetrakis(4-cyanophenyl)methane afforded synthesis of triangular triazene-connected nodes as an thermally robust product based on **ctn** net with determined *I*43*d* and *P*43*m* space groups, ensuring benzene sorption due to π-π interaction.[272] However, one of the most prominent examples of COF was issued by Wuest assuming reversible [2+2] dimerization of nitrososyls to azodioxides as novel linkage grafted to dynamic covalent frameworks. Thus, tetrakis-(4-nitrosophenyl)methane was transferred by Fetizon reagent spontaneously producing tetrahedral azodioxy-merged COF (Figure **33**, **II**) in the large, diffractable crystalline form (Figure **33**, **I**). This modification has permitted the growth of the defect-free crystals in *P*462 space group typical for isostructural adamantine-like networks (Figure **33**, **III**). Unfortunately, its thermal instability caused the pores to collapse under relatively mild conditions. Nevertheless, these tetragonal individuals fulfill perfectly criterion of the host-guest motif using intrinsic free space and specific chemical interaction. As was mentioned above the medium pore size of chemical stitches range from 9-19 Å and may be regulated by the volume of the linker. Therefore all exemplified materials contain modular pockets available for small molecules as gases, thanks to the microporous nature of described polymers that exhibit high storage capacity during their physical sorption. Indeed, tips typified the physical parameters of an ideal chemical storage have been well-defined for technological applications of future materials.

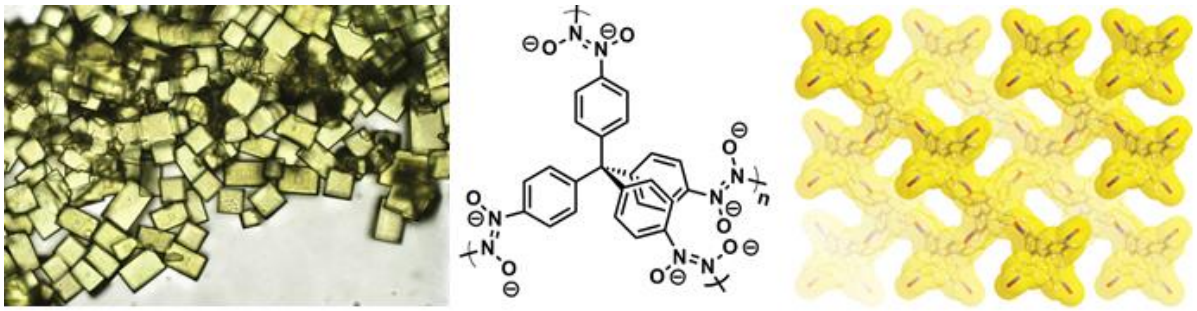

I II III

Figure 33 The photograph of COF crystals (**I**) ensued by nitrosyl polymerization (**II**) forming fourfold interpenetrated net (**III**).

Namely, great adsorption permeability, sufficient charge/discharge ratio, appropriate adsorption enthalpy and established heat capacity have reasoned the need of synthesized materials. Narrow pore distributions and extremely high surface area characteristic for COFs (founded for COF 103 value of 3620 m^2/g employing BET model) encouraged many research groups to investigate quantified and qualitative aspects of gas sorption and its storage inside the porous material. It has substantial meaning to address the realm of porous organic polymers to the uptake of environmentally harmful carbon dioxide that contributes annually more and more to global warming, and the prospective fuel components as hydrogen and methane, encapsulating them selectively and releasing their afterwards under full control. Relevant experiments estimated utility of demonstrated nodes towards gas saturation, putting an emphasis onto CO_2, H_2 and methane gating. Theoretical consideration helped to predict 2-3 times higher abilities of 3D COFs against gas squeezing comparably to the lower dimensionality, exceeding unsurpassed numbers of manufactured MOFs. [273,274,275] Taking into account their capacities as a function of pores, they afforded magnificent hydrogen uptake (70-82 mg/g), CH_4 above 20 wt% (178 mg/g), and about 1200 mg/g of carbon dioxide for COF 102, what was in total agreement to prior calculations.[276] Afterwards, in spite of excellent surface area values achieved for imine-bounded COF fluctuating in between 2400-1000 m^2/g and the others, the porous materials rather remain in scope of boron materials being often unable to conquer the score settled by boroxine nets. [277] The compromise between the rigid cores, size of the linker, and effective binding side have still remained a challenge.

2. Synthesis of tripodal architectures, from the basics to functionality

*Chapter **2** consists of tripodal, sulphur decorated modular platforms, their chemical design, synthetic strategies that were undertaken to pave the way to their successful preparation and subsequent modifications. Paramount importance of palladium-catalyzed reactions was magnified, particularly in terms to carbon-carbon bonds formation thanks to Suzuki cross-coupling, extremely precious in the synthesis of ''molecular towers''.*

2.1. Synthesis of modular assemblies[278]

2.1.1 Molecular Design

The rigid and well-defined tetrahedral geometry of tetraphenylmethane is suitable for tripodal foot architecture. Three phenyl rings can be decorated with the anchor group of interest (sulfanyl), and the fourth one is arranged perpendicular to the surface if all three anchor-group-decorated subunits interact equally with the surface. Owing to the nonconjugated character of the central sp^3 hybridized carbon, the molecular structures mounted on such foot architectures are expected to be arranged in a spatially well-controlled, but electronically decoupled, manner. To guarantee a tight contact of the foot structure and consequently good control over its spatial arrangement on the substrate, we decided to use aryl thiol anchor groups. The remaining question from a molecular design viewpoint is whether the *para* or the *meta* position is better suited to provide an efficient footing architecture. To address this question, we synthesized both structures (**33** and **50**), and studied their self-assembling behavior on gold substrates. The spacing of the anchoring group as well as the size of these specific nanostructures is a compromise between tightly packed mono- and dipodal systems and large multipodal platforms with low surface coverage. Even though functional groups allowing modular decoration of the structures (e. g., boronic acid derivatives or halides) would be very appealing from a synthetic strategy viewpoint, our initial focus was set on tripods decorated with nitrile group in *para* positions as spectroscopic marker for the study of their behavior in SAMs.

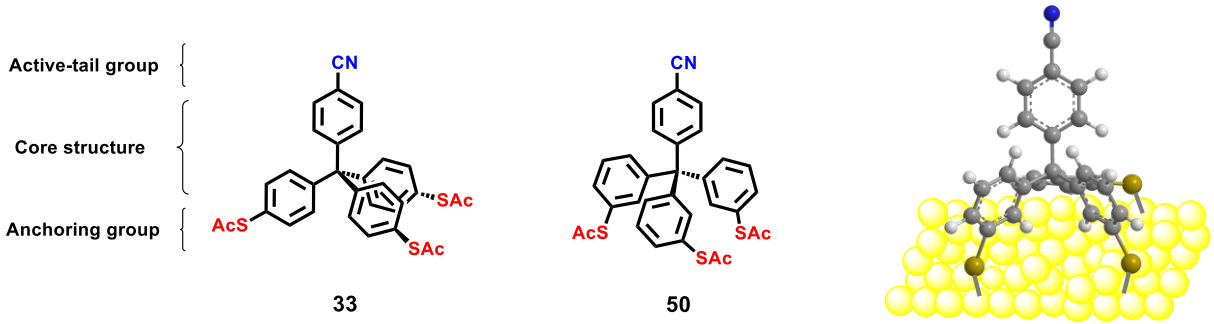

Figure 34 Structure of molecular tripods (**33**, **50**), and proposed arrangement of **50** on a gold substrate

2.1.2 Retrosynthetic analysis

Our retrosynthetic approach is displayed in Figure **35**, and consists of the assembly of the tetraphenylmethane structure in two steps. First, the three identical phenyl subunits decorated with the masked anchoring group (or a substituent enabling the later introduction of the anchoring group) are introduced by nucleophilic addition of the lithiated species to diethyl carbonate, providing the suitably substituted trityl alcohol. The second step is a Friedel-Crafts alkylation with aniline and/or phenol, providing the tetraphenylmethane derivatives with one phenyl ring substituted either with a primary amine or phenolic hydroxyl group in the *para* position. Functional group transformation chemistry subsequently allows both the establishment of the acetyl-protected thiol anchor groups and the transformation of the phenolic hydroxy group into the protruding functional group of choice. The same retrosynthetic strategy can be applied for both model compounds as the position of the anchor groups is selected by the choice of the starting materials. Interestingly, in spite of the self-evident molecular design and the straightforward synthesis, none of the subunits assembled here have been reported previously.

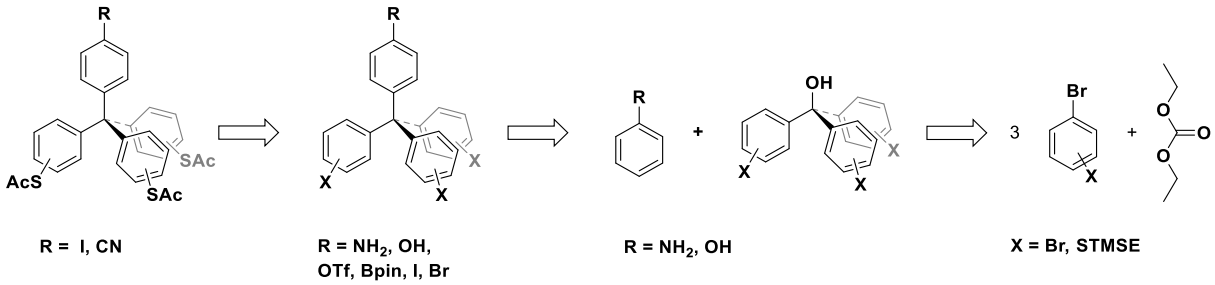

Figure 35 Retrosynthetic analysis of tetraphenylmethane platforms

2.1.3 Synthesis of short tripods library

The synthetic sequence yielding the *para*-substituted tetraphenylmethane derivative **33** was successfully accomplished in six steps and is outlined in Figure 35. The synthesis started with the thiol protection of commercially available 4-bromothiophenol with trimethyl(vinyl)silane through a radical reaction in the presence of 2,2'-azobis(2-methyl-propionitrile) (AIBN) as a radical initiator to provide 2-(trimethylsilyl)ethyl (TMSE) derivative **24** in 86% yield.[279,280] Subsequent addition of lithiated aryl bromide **24** to propylene carbonate gave the expected product in poor yield. The next attempt, involving less bulky carbonate (dimethyl carbonate) enables formation of TrOH **26** in modest 28% yield.

Scheme 2 Preparation of *para*-substituted tetraphenylmethane derivative **33**

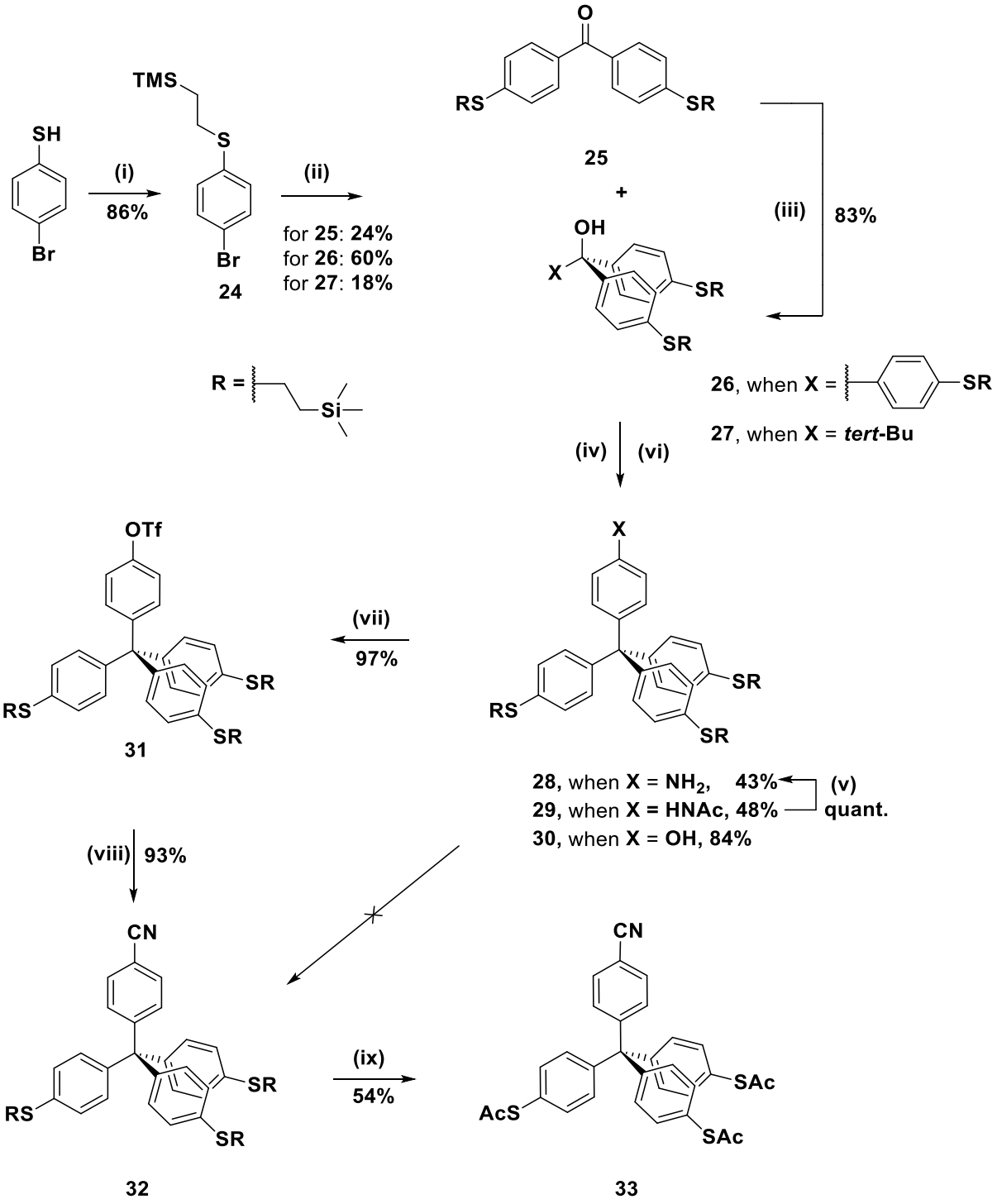

Reagents and conditions: (i) trimethyl(vinyl)silane, AIBN; (ii) **24,** *tert*-BuLi, $(EtO)_2CO$,THF; (iii) **24**, *tert*-BuLi, THF; (iv) $PhNH_2$, glacial AcOH, toluene; (v) $HCl_{(aq)}$, EtOH; (vi) PhOH, HCl, toluene; (vii) Tf_2O, Et_3N, CH_2Cl_2; (viii) $Zn(CN)_2$, CuCN, $Pd(PPh_3)_4$, DMF; (ix) $AgBF_4$, AcCl, CH_2Cl_2.

Hence, diethyl carbonate which exhibits the highest reactivity among so far applied carbonates was chosen to improve the yield of target triphenylmethanol **26**. The reaction with diethyl carbonate gave a mixture of benzophenone derivative **25** (24% yield) as well as the desired trityl alcohol **26** in 60% yield. Consequently, the isolated benzophenone derivative **25** was again reacted with an excess of lithiated aryl bromide **24** to obtain a second crop of trityl alcohol **26** in a yield of 83%. Then, trityl alcohol **26** was subjected to the acid-catalyzed Friedel-Crafts alkylation with freshly distilled aniline in the presence of glacial acetic acid to get the mixture of aniline **28** and acetanilide **29** terminated derivatives in 43%, 48% yield respectively. Acetanilide **29** was hydrolyzed quantitatively to aniline derivative **28**. Unfortunately, all attempts failed to prepare nitrile and iodo species (**32**, **35** respectively) by Sandmayer reaction due to the acidic reaction environment (mineral and Lewis acids at 0^oC-78^oC) that was applied over the course of Sandmayer reaction (Scheme **2** and **3**) that caused the partial cleavage of thiol protecting group.

Therefore, the strategy was slightly changed and phenol was used for the acid catalyzed Friedel-Crafts alkylation to provide tetraphenylmethane derivative **30** in 84% yield. The resulting phenol derivative **30** was esterified with triflic anhydride to afford triflate **31** in almost quantitative yield.

Scheme 3 Preparation of aryl halides **36**, **38**

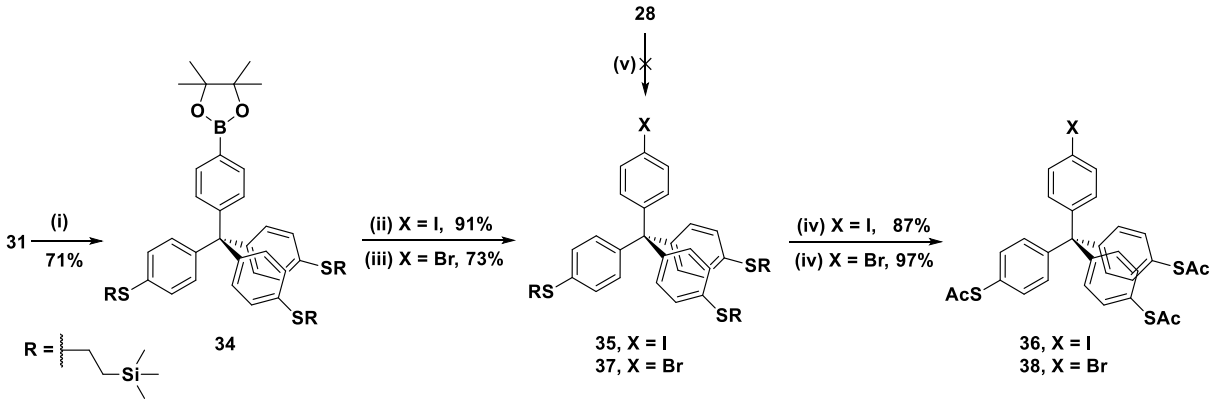

Reagents and conditions: (i) bis(pinacolato)diboron, $Pd(dppf)Cl_2$, KOAc, dioxane; (ii) CuI, NIS, toluene, DMF; (iii) CuBr, NBS, toluene, DMF; (iv) $AgBF_4$, AcCl, CH_2Cl_2; (v) H^+, $NaNO_2$, I_2, KI, water

Subsequently, the palladium-catalyzed cyanation of the triflate **31** with zinc and copper cyanide at 140°C provided the corresponding nitrile **32** in 93% yield. Final

transprotection of the thiols was performed successfully using $AgBF_4$ and acetyl chloride (AcCl) in dichloromethane to afford the desired thioacetate **33** in 54% yield. The acetyl protection group provides improved storing and handling features of the compound, as it prohibits polymerization through intermolecular disulfide formation. Its lability allows mild and efficient deprotection prior to or during the self-assembly process on gold substrates.

Triflate **31** was converted to the more reactive iodo derivative **36** (as outlined in Scheme **3**) to have in hand the modular tripodal platform bearing labile thioacetates for further functionalization through the Sonogashira cross-coupling reaction. The Miyaura borylation of aryl triflate **31** with bis(pinacolato)diboron in the presence of $Pd(dppf)Cl_2$ provided pinacol boronate **34** in 71% yield. This pinacol boron ester itself is an interesting building block, as it is suitable for the further functionalization of the tetraphenylmethane platform through Suzuki cross-coupling reactions. Then, the corresponding pinacol boronate **34** was treated with copper iodide and *N*-iodosuccinimide in anhydrous DMF and toluene (2:1, v/v) using the recently reported Osuka protocol[281] to afford the aryl iodide **35** in 91% yield. In parallel, *N*-bromosuccinimide was used as bromination reagent providing the aryl bromide **37** in 73% yield These aryl halides are ideal precursors to be explored for wide array of palladium catalyzed reactions, opening the doors to tune physical properties of the future nano objects deposited on gold surfaces. The transprotection of the thiols using $AgBF_4$ and acetyl chloride (AcCl) in dichloromethane provided the desired thioacetate **36** in 87% yield and its analogous bromide **38** in 97% yield. Both derivatives **36** and **38** were not only interesting synthetic precursors of more complex nano-objects, but were also envisaged to study the influence of the head group onto the self-assembly behavior and related surface phenomena of tripod derivatives.

The same synthetic strategy was applied for the preparation of the regioisomeric *meta*-substituted tetraphenylmethane derivative **43**, which is shown in Scheme **4**. The thiol of 3-bromothiophenol was protected as 2-(trimethylsilyl)ethyl derivative **39** in 73% yield. Subsequent lithiation of aryl bromide **39** with *tert*-BuLi and stepwise addition to diethyl carbonate provided the mixture of benzophenone **40** in 39% yield and trityl alcohol **41** in 44% yield. Isolated benzophenone **40** was again treated with lithiated species to obtain a second crop of trityl alcohol **41** in 76% yield. However, subsequent acid-catalyzed Friedel-Crafts alkylation of phenol with trityl alcohol **41** did not afford the pure single tetraphenylmethane product **43**. We used several Brønsted (HCl, CH_3SO_3H) and Lewis ($BF_3{\cdot}Et_2O$) acids in combination with co-solvents (toluene, xylenes) at different temperatures

(80-140°C), but all these attempts gave a complex mixture comprising regioisomers and side products, instead of the desired molecule. Even though NMR analysis indicated the presence of the desired tetraphenylmethane derivative **43**, its similarity with the side products did not allow its separation.

Scheme 4 Synthetic attempts toward the *meta*-substituted tetraphenylmethane **43**

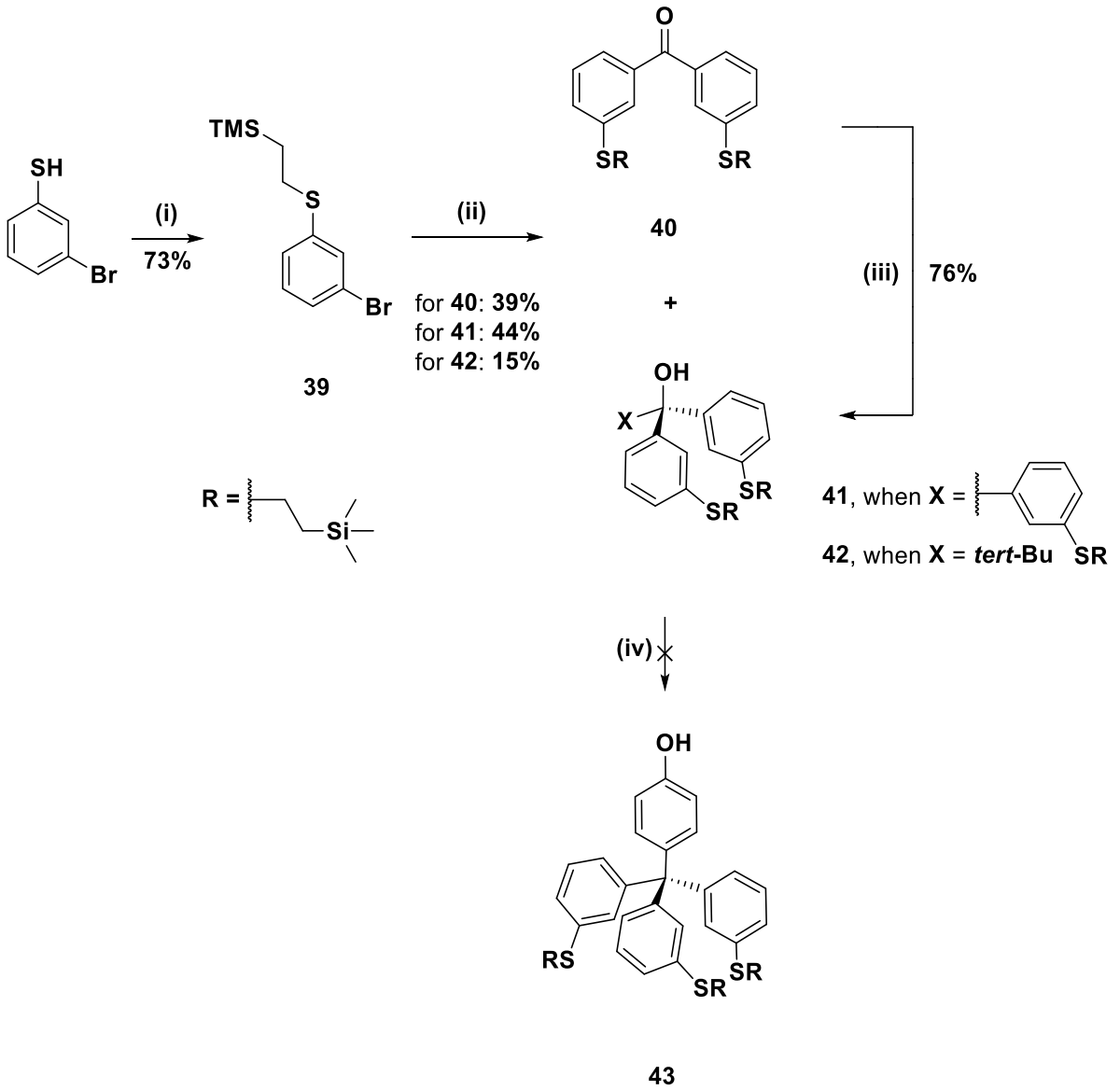

Reagents and conditions: (i) trimethyl(vinyl)silane, AIBN; (ii) *tert*-BuLi, $(EtO)_2CO$, THF; (iii) **39**, *tert*-BuLi, THF; (iv) PhOH, HCl, toluene.

We assumed that the increased proximity of the TMS-ethyl-protected sulfanyl group in the *meta* position of the trityl alcohol handicaps its reactivity sterically as well as electronically, and therefore, we decided to employ less sterically bulky substituents. The

new synthetic strategy leading to the *meta*-substituted tetraphenylmethane derivative **47** is outlined in Scheme **5**. The synthesis started with halogen-lithium exchange of five equivalents of 1,3-dibromobenzene and its subsequent addition to diethyl carbonate to provide the desired benzophenone **44** in 93% yield. It should be noted that in the case of 1,3-dibromobenzene, the formation of the trityl alcohol derivative **45** was not observed and the reaction mixture contained almost pure benzophenone derivative **44**. Additional lithiation of 1,3-dibromobenzene and subsequent addition to the benzophenone derivative **44** afforded tris(3-bromophenyl)methanol **45** in 82% yield. After Friedel-Crafts alkylation of **45** with phenol, the *meta*-brominated tetraphenylmethane derivative **46** was obtained in 88% yield. Subsequent protection of phenol as trimethylsilyl ether provided **47** in 89% yield, and allowed the further introduction of protected thiol moieties through the palladium-catalyzed reaction.

Scheme 5 Synthesis of the *meta*-brominated tetraphenylmethane **47**

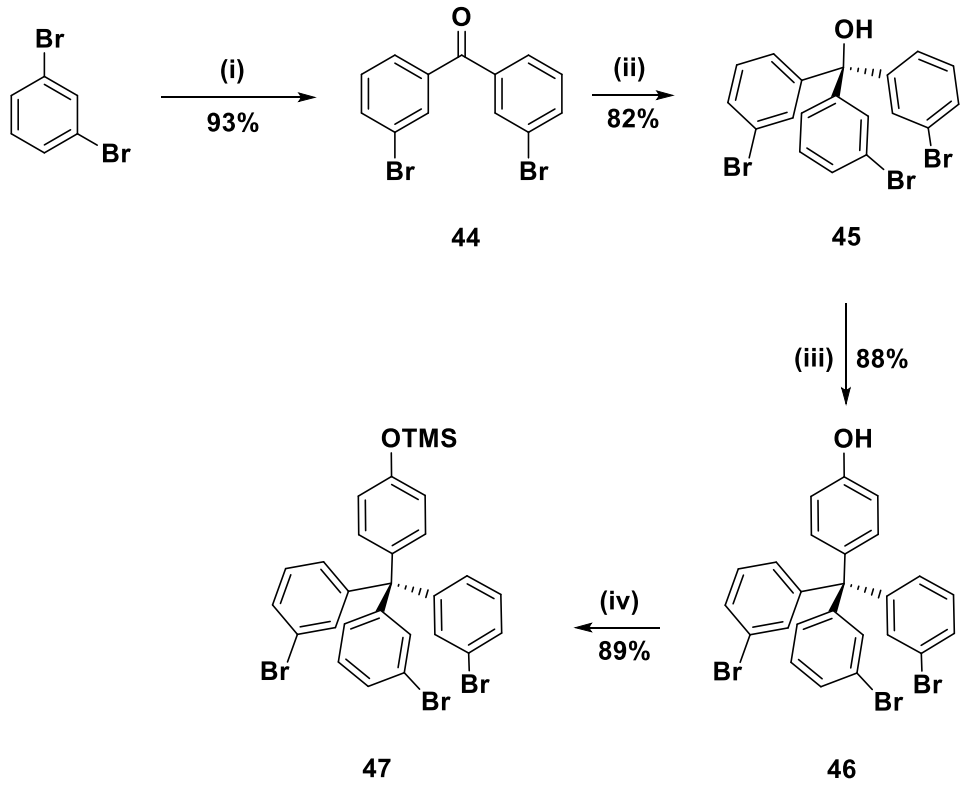

Reagents and conditions: (i) *n*-BuLi, $(EtO)_2CO$, THF; (ii) *1,3*-dibromobenzene, *n*-BuLi, THF; (iii) PhOH, HCl; (iv) Et_3N, TMSCl, Et_2O.

The thiol anchor groups were introduced in their TMS-ethyl-protected form. Therefore, the palladium-catalyzed reaction of the aryl bromide with the corresponding alkyl

thiol was considered.[282] The *meta*-brominated tetraphenylmethane derivative **47** was treated with 2-(trimethylsilyl)ethanethiol in the presence of $Pd_2(dba)_3$, Xantphos, and Hünig base to afford the deprotected phenolic species **43** in 92% yield upon acidic workup, as shown in Scheme **6**. After triflatation of **43** with triflic anhydride, the corresponding triflate **48** was isolated in 83% yield. The palladium-catalyzed cyanation of **48** yielded nitrile **49** in 74% yield and subsequent transprotection of the thiols provided the target thioacetate **50** in 77% yield.

Scheme 6 Synthesis of the *meta*-substituted tetraphenylmethane **50**

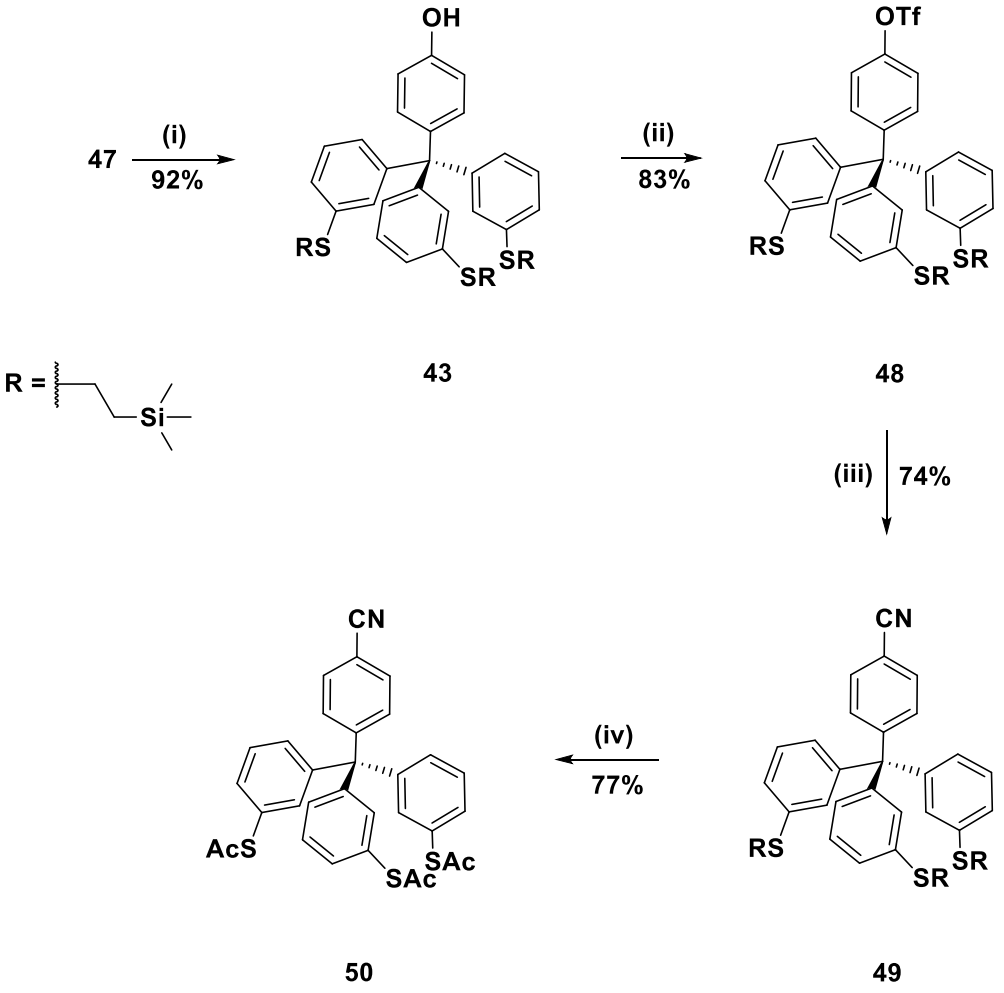

Reagents and conditions: (i) $Pd_2(dba)_3$, Xantphos, diisopropylethylamine, $TMSCH_2CH_2SH$, dioxane, H^+; (ii) Tf_2O, Et_3N, CH_2Cl_2; (iii) $Zn(CN)_2$, CuCN, $Pd(PPh_3)_4$, DMF; (iv) $AgBF_4$, AcCl, CH_2Cl_2.

Analogously to the isomeric *para*-substituted platform, triflate **48** was converted to the bromo and iodo derivatives **53, 55** (Scheme **6**), which is more reactive in palladium-catalyzed cross-coupling reactions than the triflate **48**. The Miyaura borylation of aryl triflate

48 provided the corresponding pinacol boronate **51** in 82% yield. With accordance to prior described synthesis of *para* terminated tripods, iodo and bromo functionalized derivatives were made. Therefore, the aryl boronate **51** was converted to the aryl iodide **52** and bromide **54** in 83% and 74% yield respectively. Finally, the previously mentioned transprotection of the thiols provided the desired thioacetates **53** (55% yield) and **54** (94% yield).

Scheme 7 Preparation of the aryl halides **53, 55**

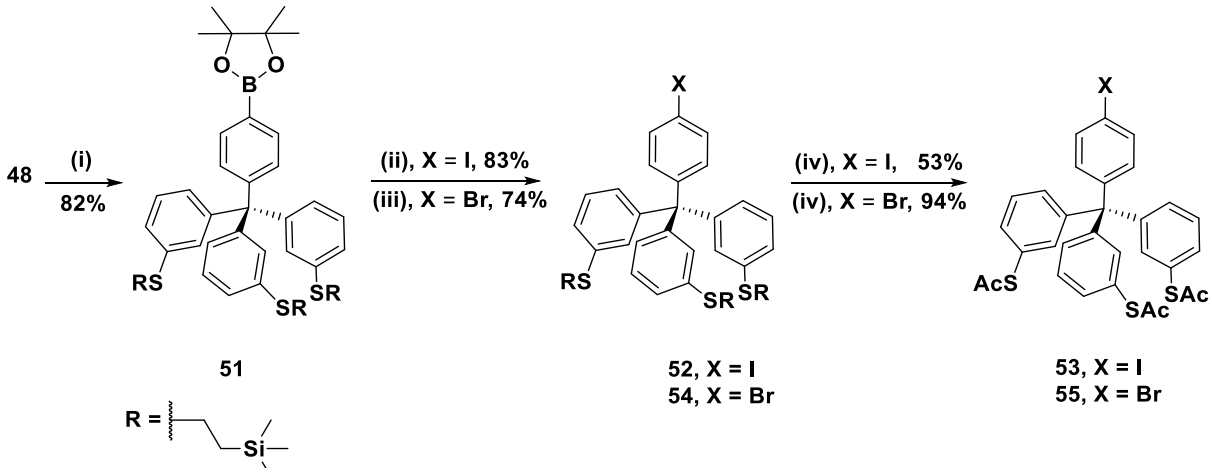

Reagents and conditions: (i) bis(pinacolato)diboron, Pd(dppf)Cl_2, KOAc, dioxane; (ii) CuI, NIS, toluene, DMF; (iv) CuI, NBS, toluene, DMF; (iii, v) $AgBF_4$, AcCl, CH_2Cl_2.

2.2 Synthesis of tower shaped molecules

2.1.1 Molecular Design

The rigid and well-defined geometry of tetraphenylmethane based tripodal unit suits perfectly to the role of molecular spacer laterally separating the subunits from each other when deposited on a surface and thus, the motive is also perfectly suited as modular platform. Based on these considerations, we decided to investigate the ability of the platform to arrange extended rigid-rod type structures perpendicular to the surface. For that purpose series of oligo-phenylenes of varying length comprising reactive termini were mounted on these platforms.

Of particular interest was the influence of the organic substituent mounted to the protruding aromatic ring on the structures that exhibit self-assembly behaviour. Using a more descriptive picture, we were interested in how big a mounted substituent is allowed to be maintaining an immobilization with all three anchor groups attached to the surface and thus showing an arrangement of the mounted substituent perpendicular to the surface. To the best of our knowledge, there are just a few studies in the literature dealing with stability of functionalized tripods on metal substrates. We thus became interested in the tripod functionalized molecular rods of various length displayed in Figure **36** as model compounds for STM-UHV experiments.

The tripodal building blocks developed in the previous chapter are ideally suited to mount suitably functionalized oligophenyl subunits by Suzuki coupling. Again, we first focused on nitrile terminated oligophenyls, mainly based on the experiences we recently made with alternative tripodal structures where the additional interactions of this group with the STM tip enabled the perfect localization of the molecule and its spatial arrangement on the substrate. However, the modular synthetic strategy allows for a large variety of functional groups terminating the oligophenylene rigid rod which is only limited by the stability of the protection groups masking the thiol- anchor groups. As second approach we also report the syntheses of oligophenylenes comprising a tetraphenylmethane foot and exposing a terminal acetyl protected thiol group. The motivation for this series is based in the mechanical strength of the bond formed to the counter electrode (e.g. a gold tip in a STM experiment) which makes these model compounds also suitable for STM-BJ experiments.

2.2.2 Retrosynthetic analysis

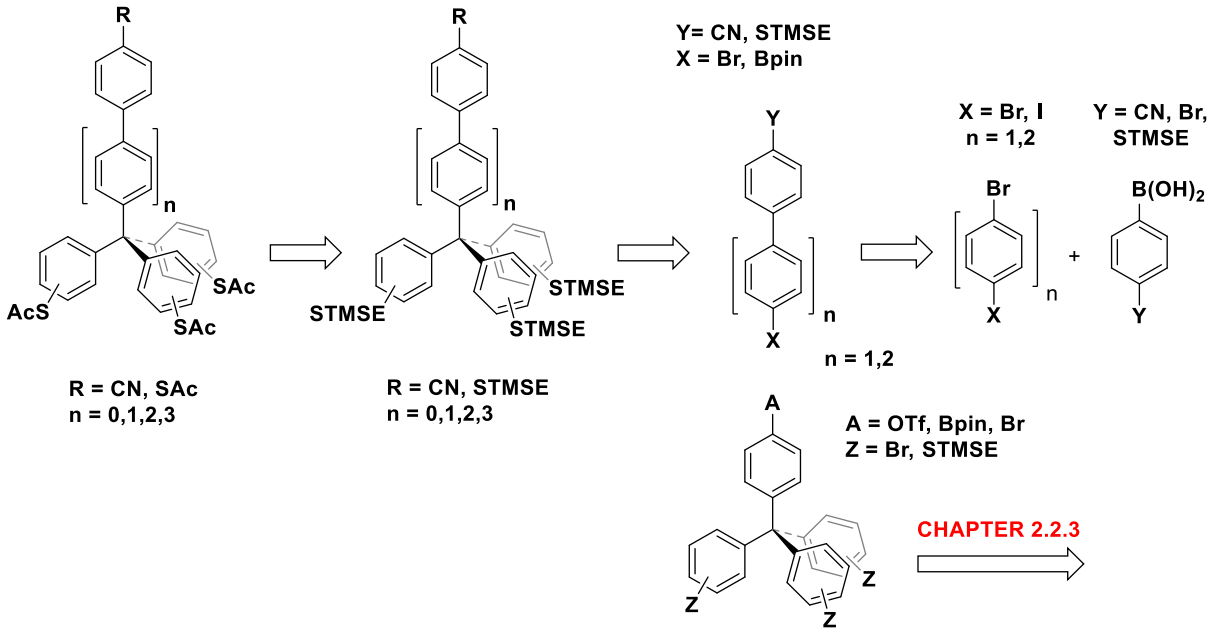

Figure 36 Retrosynthetic analysis of aromatic rods rooted to tetraphenylmethane modular platform

The retrosynthetic approach is outlined in Figure **36** showing two-steps assembly of desired tower shaped structures that are constructed from rod-like molecules and tripodal platforms. In the initial step molecular rods are synthesised by Suzuki cross-coupling reaction between aryl boronic acids and aryl bromides, providing biphenyl and terphenyl precursors with the desired *para* substitution pattern. Also the second step involves the Suzuki-type palladium-catalysed cross-coupling reaction between the tripodal platform and the molecular rods, providing the target tower shaped tripodal platforms.

The same strategy was applied for both regioisomeric tripodal platforms with the acetyl-protected thiol anchoring groups in *meta*- or *para*- position, with respect to the central carbon atom.

The shortest members of the second series, namely tetraphenylmethanes exposing an additional acetyl-protected thiol group in *para*-position of the fourth phenyl arm were synthesized via direct substitution either of the bromine atoms of tetrakis(4-bromo-phenyl)methane to provide tetrakis(4-acetylsulfanylphenyl) methane **74** after functional group transformations, or of the triflate of tris(3-bromophenyl)-4'-trifluroxyphenylmethane **75** to yield in tris(3-acetylsulfanylphenyl)-4-acetlysulfanylphenyl-methane **77** after

transprotection of the trimethylsilylethyl groups of **76**. The synthetic strategy is detailed in Scheme **10**.

2.2.3 Synthesis of nitrile terminated "tower-shaped" molecules.

Scheme 8 Applied synthetic pathway for the formation of the rod precursors **56**, **58**, **59**

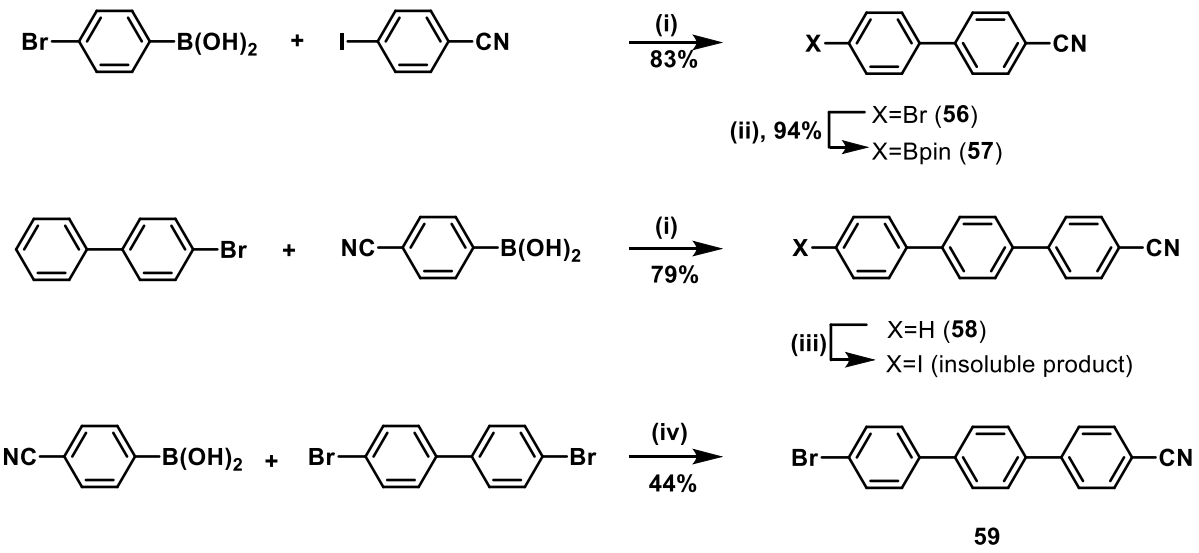

Reagents and conditions: (i) $[Pd(PPh_3)_4]$, K_2CO_3, dioxane, water (ii) bis(pinacolato)diboron, $Pd(dppf)Cl_2$, KOAc, dioxane; (iii) KIO_3, I_2, AcOH, $H_2SO_{4(conc.)}$; (iv) $[Pd(PPh_3)_4]$, K_2CO_3, toluene, THF, water.

The synthetic strategy to the molecular rods **56**-**59**, required for the assembly of molecular towers, comprising tetraphenylmethane foots exposing thioacetate anchoring group is outlined in Scheme **8**. The shortest biphenyl derivative **56** was prepared according to a slightly modified procedure of Farahat[283] et al., where 4-bromophenyllboronic acid was reacted with an excess of 4-iodobenzonitrile in the presence of a palladium catalyst to obtain 4'-bromo-(1,1'-biphenyl)-4-carbonitrile in 83% yield. Subsequent classical Miyaura borylation afforded pinacol boronic ester **57** in 94% yield.[284] Thanks to the versatility of π-conjugated oligo-*p*-phenylenes, several protocols dealing with various terphenylenes were reported.[285] Bearing in mind that suitably halide substituted bi- and terphenylenes can be obtained by selective iodination in *para* position, it is tempting to create these highly reactive iodinated species for their subsequent transformation in palladium catalyzed coupling reactions. Guided by this rational, 4-bromobiphenyl and 4-cyanophenylboronic acid were coupled via Suzuki reaction giving **58** in 79% yield.[286] The obtained terphenyl **58** was found to be an ideal candidate for the subsequent iodination. Adapting a procedure reported by the Michl group,[287] **58** was exposed to iodination conditions. Unfortunately the obtained crude

iodinated material refused to dissolve in common organic solvents disabling it further purification, analysis and further processing by wet chemistry. To circumvent this obstacle, an alternative pathway was applied based on comprehensive studies by Guillen and co-workers,[286] dealing with the synthesis of *p*-bromophenylenes. The authors examined the influence of functional groups onto the efficiency of C-C biaryl bonds formation by Pd catalyzed coupling reaction ranging from mild (exploiting Ag_2CO_3 as a base in RT) to the typical reaction conditions. Adaptation of the above procedure let to the successful synthesis of **59**, though longer reaction time was required. Hence, 4,4'-dibromobiphenyl and 2 equivalents of the boronic acid were refluxed under inert atmosphere providing the 4''-bromo-[1,1':4', 1''-terphenyl]-4-carbonitrile skeleton **59** in reasonable 44% yield considering the statistical nature of the Suzuki reaction. The assembly of the "molecular towers" comprising a tetraphenylmethane footing structure was mainly based on Suzuki cross-coupling reactions. Thus prepared rod precursors enabled the synthesis of designed tower shaped molecular platforms from the moderate to high yield, what is displayed in both variants in Scheme **9**.

Scheme 9 Synthesis of *para* (left column, **61**, **63, 65**) and *meta* (right column, **67**, **69**, **71**) nitrile terminated molecular towers.

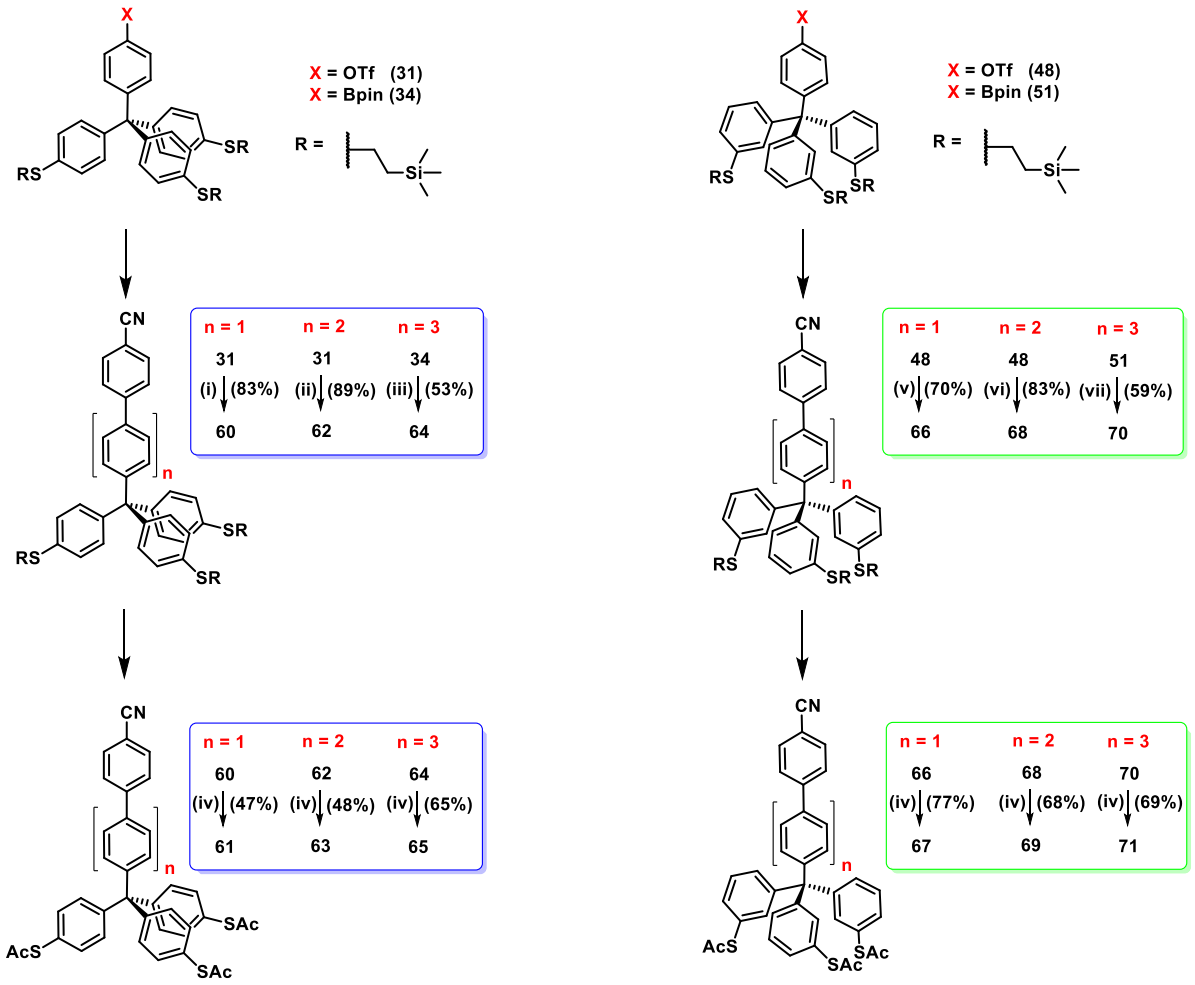

Reagents and conditions: (i) 4-cyanophenylboronic acid, $[Pd(PPh_3)_4]$, K_2CO_3, THF, water; (ii) **57**, $[Pd(PPh_3)_4]$, K_2CO_3, dioxane, water; (iii) **59**, $[Pd(PPh_3)_4]$, K_2CO_3, dioxane, water; (iv) $AgBF_4$, AcCl, 0^oC-RT; (v) 4-cyanophenylboronic acid, $[Pd(PPh_3)_4]$, Cs_2CO_3, dioxane, water; (vi) **57**, $[Pd(PPh_3)_4]$, Cs_2CO_3, dioxane, water; (vii) **59**, $[Pd(PPh_3)_4]$, Cs_2CO_3, dioxane, water.

Notably, biphenyl, terphenyl and quarterphenyl towers comprising trimethylsilylethyl masked anchoring groups were obtained in yields between moderate and very good, pointing at the chemical robustness of the masking group. The required key intermediates, namely the tetraphenylmethane building blocks with either a triflate or pinacol boronic ester were already discusses in the previous chapter. Triflates of both foot structures, the *meta*- and *para*-regioisomers were reacted with 4-cyanophenylboronic acid affording the "biphenyl-towers" (n=1) **60** and **66** in 83% and 70% yield respectively. For the assembly of the "terphenyl-towers" (n=2), the pinacol boronic esters **34**, **51** underwent Suzuki coupling with aryl

bromide **56**. Very similar R_f values of the biphenyl starting material and the freshly formed tetraphenylmethane products made their separation quite challenging. As alternative approach the positions of the functional groups involved in the Suzuki coupling were exchanged. Thus, bromide **56** was converted into pinacol boronic ester **57** via Miyaura coupling and subsequently reacted with both triflates **31**, **48**, leading to the "terphenyl-towers" (n=2) **62** and **68** in 89% and 83% yield respectively. This conversion constitutes a significant improvement in comparison with the initially implemented approach (Scheme **9**). In order to check the influence of used base on the efficiency of Suzuki cross-coupling reaction, we firstly reacted *para*-terminated tripods with potassium carbonate, while for the *meta*-substituted analogues stronger base was employed - caesium carbonate. Nevertheless, we did not notice considerable difference in the yield of conducted reactions. Therefore all further couplings were done with commonly exploited potassium carbonate. The last member of the series, the "quarterphenyl-towers" (n=3) were made by the palladium-catalysed coupling reaction between terphenyl **59** and the pinacol boronic esters **34** or **51**, providing the compounds **64** and **70** (53%, 59% yield). Readily synthesized derivatives were subjected to transprotection of thiol protected anchoring groups with $AgBF_4$ and AcCl in CH_2Cl_2, converting the *S*-trimethylsilylethyl moiety into thioacetals in moderate to good yields, providing *para* (**61**, **63**, **65** in 47%, 48% and 65% respectively) and *meta* analogous (**67**, **69**, **71** in 77%, 68% and 69% respectively).

2.2.4 Synthesis of Acetylsulfanyl *(-SAc)* terminated tower-shaped molecules.

Synthesis of fully acetylsulfanylated tripods started from tetraphenylmethane assemblies as the key building blocks and is outlined on the Scheme **10**. The first proposed strategy is based on palladium-catalyzed substitution of aryl halides by thioacetate moiety under the microwave conditions published by Lai and Backes.[288] Therefore, potassium thioacetate was employed as an inexpensive and robust reagent, which was supposed to form the desired *S*-aryl thioacetate derivatives (**74**, **77**) within one synthetic step. For the synthesis of *para* substituted analogue **74**, commercially available tetrakis(4-bromophenyl)methane was used, whereas the second precursor which is necessary for the synthesis of the asymmetric (*meta*) building block in a form of aryl triflate (**75**) was readily synthesized from phenol **46** (as was shown and discussed in the previous chapter). Thus, phenol **46** was converted to triflate **75** in 85% yield. Both required building blocks were subsequently reacted with potassium thioacetate under microwave conditions, always leading to an inseparable mixture of products. Chromatographic separation on silica provided the anticipated thioacetates **74**, **77** in a low few percent yield. Due to unsatisfying results of the previous method, we searched for another thiol to yield the final thioacetate with better efficiency. We had to change our synthetic approach, implementing thiol protected group with two synthetic steps. The question was which kind of protecting group would be one hand stable, but on the other hand would allow us the transprotection step to the desired *S*-acetyl moiety. We examined cheap and robust 1-butanethiol, which was firstly coupled with tetrakis-(4-bromophenyl)methane, thus providing tetrakis[(4-buthylsulfanyl)phenyl]methane **72** in excellent 95% yield. Unfortunately, the transprotection of butyl protected thiol to thioacetates using procedure published by Pijper[289] with $TiCl_4$ as a Lewis acid and acetyl chloride failed (reactants proved to be too weak to enable cleavage of thioethers) and starting material was recovered. Therefore, thiols had to be introduced in a more labile form, thus were masked with 2-(trimethylsilyl)ethyl groups as we demonstrated in the previous paragraphs. Accordingly, palladium catalyzed substitution of tetrakis(4-bromophenyl)methane and triflate **75** with 2-(trimethylsilyl)ethanethiol led to protected compound **73**, and **76** in a very good 94% and 71% yield respectively. These compounds were finally transprotected to acetyl protected moieties **74** and **77** in 85% and 80% yield respectively.

Scheme 10 Synthesis of thioacetate compounds **74, 77**

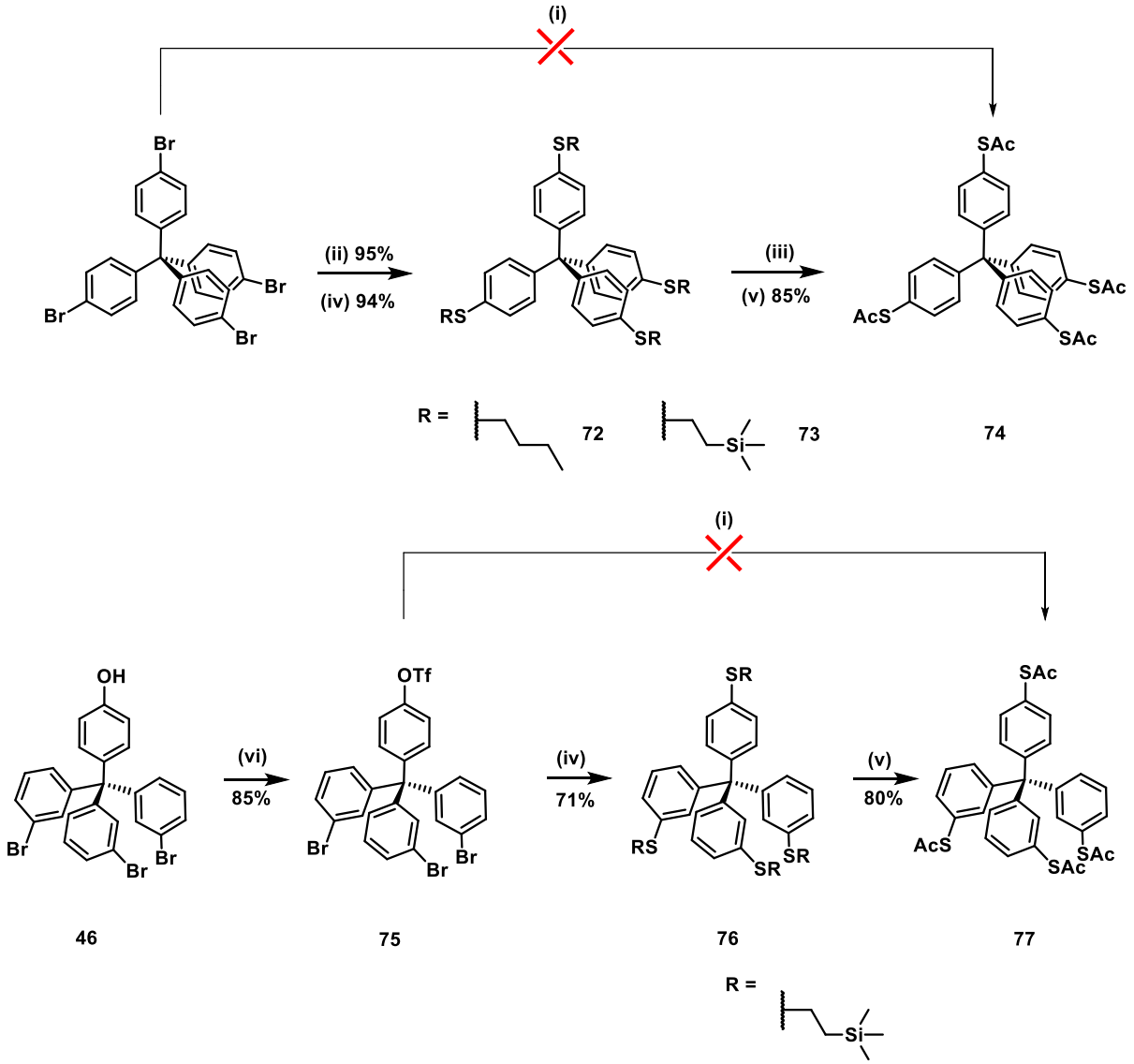

Reagents and conditions: (i) $Pd_2(dba)_3$, Xantphos, diisopropylethylamine, CH_3COSK, dioxane; (ii) $Pd_2(dba)_3$, Xantphos, diisopropylethylamine, *n*-Butylthiol, dioxane; (iii) $TiCl_4$, AcCl, toluene; (iv) $Pd_2(dba)_3$, Xantphos, diisopropylethylamine, $TMSCH_2CH_2SH$, dioxane; (v) $AgBF_4$, AcCl, CH_2Cl_2; (vi) Tf_2O, Et_3N, CH_2Cl_2.

The approach to the synthesis of molecular rods **78-81**, which are necessary to complete preparation of the second family of molecular towers is shown in Scheme **11**. The shortest building block (**78**) that comprises masked thiol was synthesized according to the procedure reported by Grunder.[215] Previously shown aryl bromide **24** was lithiated with *tert*-BuLi in metal-halogen exchange reaction. Lithiated species was quenched with tris(isopropyl) borate, giving boronic acid **78** in 40% yield.

Scheme 11 Synthesis of molecular rods **78**-**81** served for the construction of elongated tripods

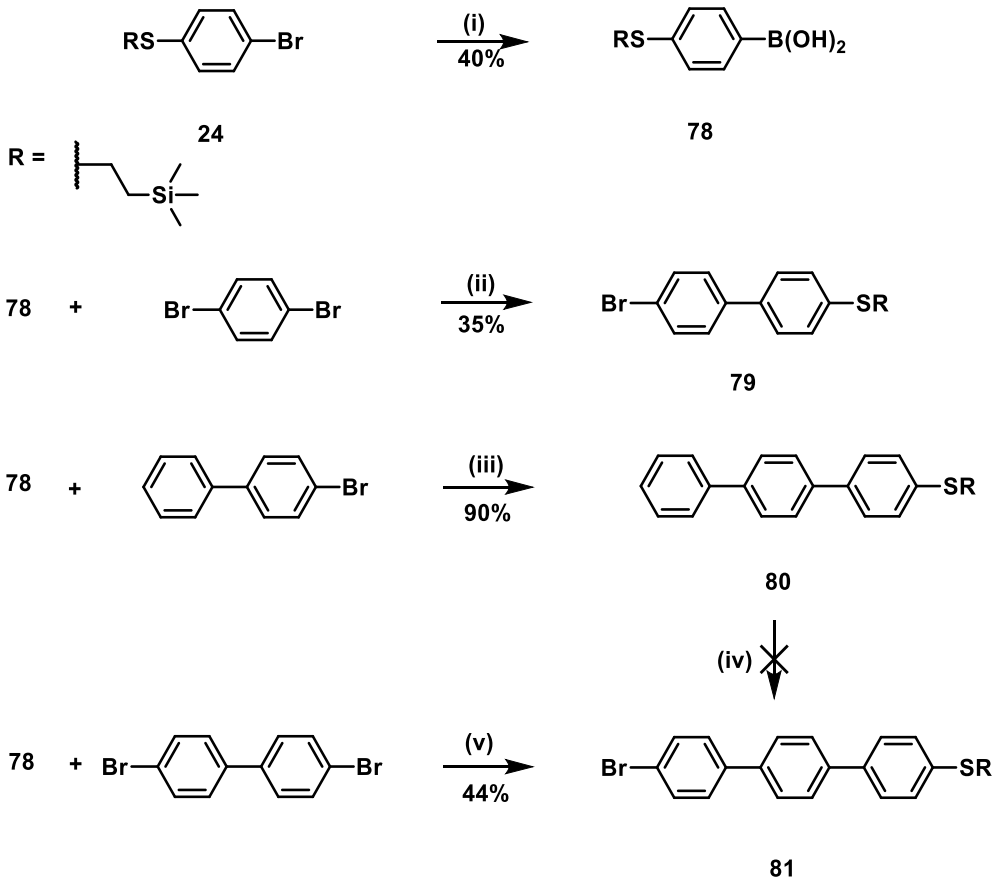

Reagents and conditions: (i) *tert*-BuLi, B(O-*i*Pr)$_3$, Et_2O; (ii) [$Pd(PPh_3)_4$], K_2CO_3, toluene, methanol, water; (iii) [$Pd(PPh_3)_4$], K_2CO_3, THF, water; (iv) bromine, chloroform; (v) [$Pd(PPh_3)_4$], K_2CO_3, toluene, THF, water.

Subsequently boronic acid **78** was considered to react with 1,4-dihalo benzene to obtain bipenyl precursor **79,** since it was reported by Sinclair and co-workers that it is possible to perform Suzuki reaction with diiodinated and dibrominated aryls in the chemoselective manner.[285] Herein however, independently from the applied conditions diiodo species underwent solely double coupling contrary to dibrominated derivative where selectivity was found to be controllable, thus the decision was made to utilize 1,4-dibromobenzene. Regarding this report, Suzuki reaction with boronic acid **78** with large excess (10 fold) of 1,4-dibromobenzene let to successful synthesis of biphenyl component **79**, getting it in 35% yield, acceptable for statistical Suzuki reaction. As was discussed before (see the synthesis of compound **58**), terphenylenes can be synthesized by applying selective halogenation.

Scheme 12 Synthetic strategy towards thiol terminated *para*- **83**, **85**, **87** (left column) and *meta*-molecules **89**, **91**, **93** (right column) tower-shaped tripods.

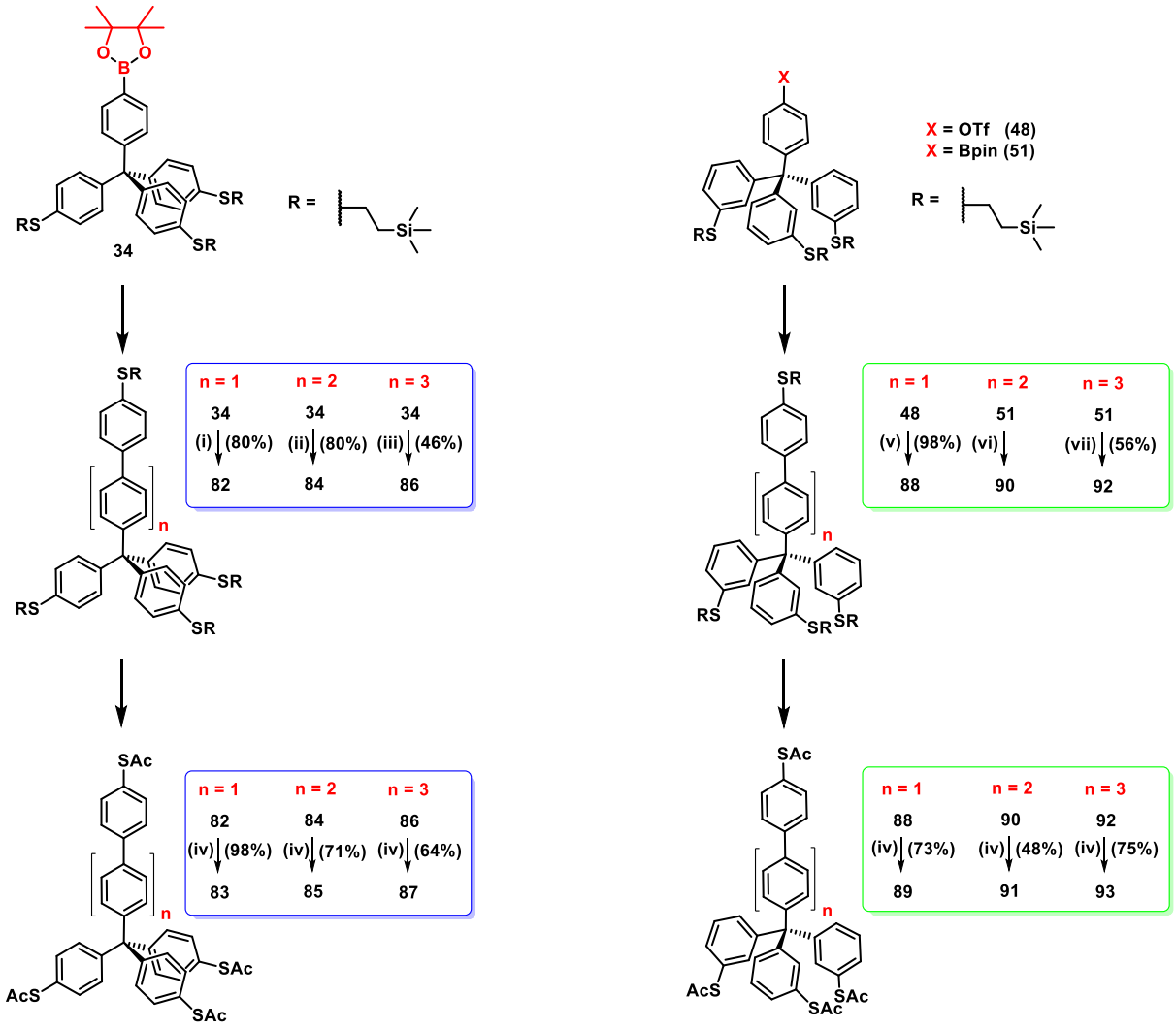

Reagents and conditions: (i) **24,** [$Pd(PPh_3)_4$], K_2CO_3, toluene, ethanol, water; (ii) **79**, [$Pd(PPh_3)_4$], K_2CO_3, toluene, ethanol, water; (iii) **81**, [$Pd(PPh_3)_4$], K_2CO_3, dioxane, water; (iv) $AgBF_4$, AcCl, 0 ^oC-RT; (v) **78**, [$Pd(PPh_3)_4$], K_2CO_3, toluene, ethanol, water; (vi) **79**, [$Pd(PPh_3)_4$], K_2CO_3, toluene, ethanol, water; (vii) **81**, [$Pd(PPh_3)_4$], K_2CO_3, dioxane, water.

In spite of above findings, we had to discard iodination protocol due to being non-selective. This reaction is made under acid conditions, which are not compatible with applied thiol-protecting group, rendering it deprotected. To overcome this problem, the attempt of bromination was made, therefore boronic acid **78** was subjected to the reaction with 4-bromobiphenyl providing terphenyl unit **80** in good yield (90%).

Prepared terphenyl **80** was subjected to the following published protocol, with the aim of synthesizing **81**.[290] Unfortunately, proposed straightforward attempt of halogenation was unsuccessful showing plenty of side products, as manifested by TLC, thus making the separation difficult. Terphenyl rod-like molecule **81** had to be obtained in an alternative way. By adapting the method, which was discussed in a previous paragraph, **81** was prepared in similar fashion to that described for analogues **59**. Thus, boronic acid **78** was coupled with 4,4'-dibromobiphenyl and after SiO_2 purification and recrystallization from hot toluene gave target terphenyl **81** in sufficient 44% yield. As was already mentioned formation of the "molecular towers" built on tripodal skeleton was carried out by using palladium catalyzed cross-coupling reaction. Owing to prior synthesized molecular rods, synthesis of all envisaged thioacetate decorated molecules can be performed, providing all variants in a good yield and is presented in Scheme **12**. Hereby, target "tower shaped" molecules were formed within two synthetic steps. For the synthesis of all regioisomeric analogues we exploited known building blocks. Namely, triflate and pinacol boronic ester were employed (both precursors were described detail in paragraph **2.3**). The *para*- terminated "biphenyl tower" was assembled starting from pinacol boronic ester **34** and aryl bromide **24**, providing the desired product **82** in moderate 80% yield. The *meta*- substituted triflate **48** was coupled with **78** to give biphenyl tower **88** in excellent 98% yield. For the latter one we did not apply boronic ester **51** (as we presented for *para* derivative), because we observed a very little difference in a polarity of applied rod and anticipated product, what did not allow for effective isolation of the desired compound. Please note that was the same problem was encountered for derivatives **62** and **68** (Scheme **9**). In order to reach "terphenyl towers", pinacol boronic ester **34** and **51** were utilized and subjected to the Suzuki reaction with aryl bromide **79** affording expected product **84** in good 80% yield, while separation of **90** proved to be troublesome, and the crude product was used directly in to the next step. Considering this problem for future actions, triflate has to be coupled with the biphenyl rod functionalized with pinacol boronic ester, what can significantly improve purification of the desired product. The last and the longest batch of "molecular towers" was synthesized in the same fashion, starting from corresponding pinacol boronic ester **34** and **48** providing compounds **86** and **92** in acceptable 65% and 75% yield. To convert all synthesized molecular towers into thioacetate terminated derivatives, capable of binding to a gold surface, commonly exploited transprotection protocol was used. Therefore, "biphenyl towers" (n=1) **83**, **89** were obtained in a very good 98% and 73% yield. Moreover, "quarterphenyl and terphenyl towers" (n=2

and 3 respectively) were synthesized in similar way, providing expected products **84**, **86** (*para*) and **90**, **92** (*meta*) in acceptable 71%, 64%, yield and 48%, 75% yield respectively.

2.3 Solid state analysis

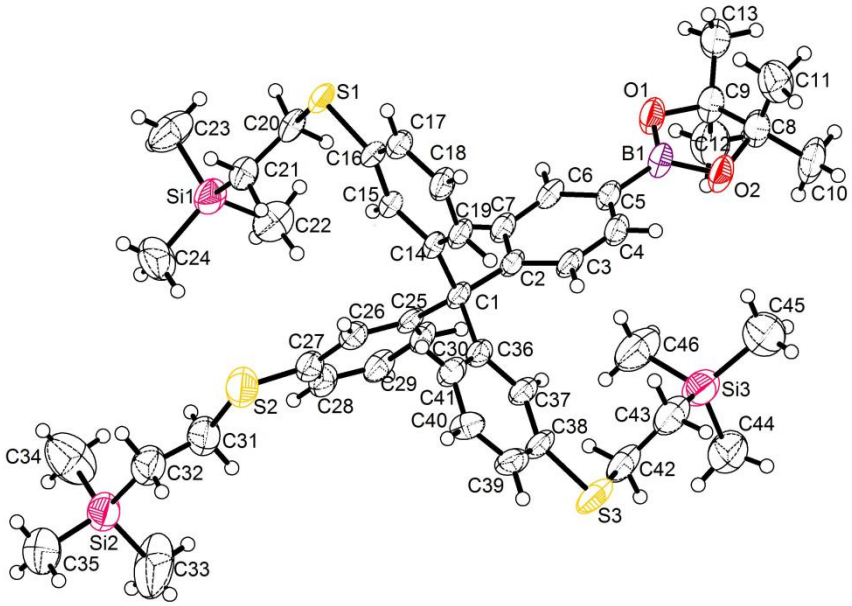

51

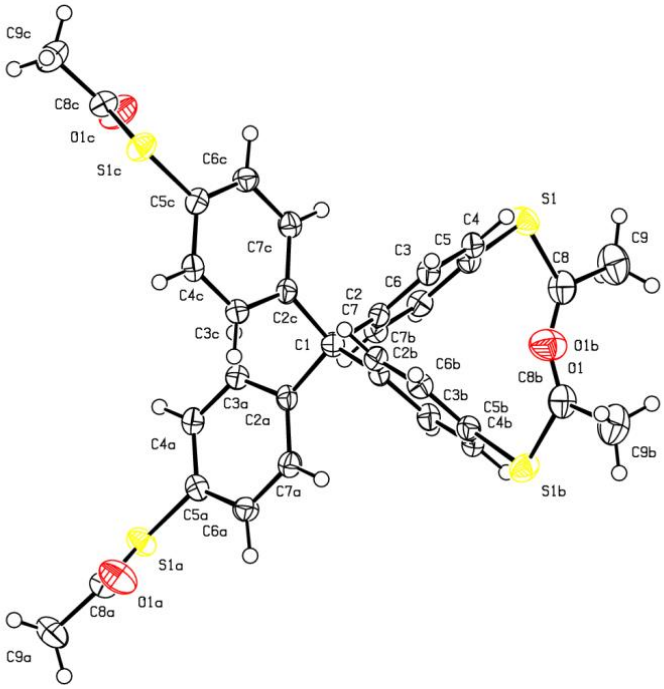

74

Figure 37 Solid-state structures of **51** (top), **74** (down) intermediates obtained from library of tripodal molecules.

Table 1 Data extracted from X-ray analysis of **51,** and **74.**

Identification code	**51**	**74**
Empirical formula	$C_{46}H_{67}BO_2S_3Si_3$	$C_{33}H_{28}O_4S_4$
Formula weight	843.25	616.79
Temperature/K	150.15	180.15
Crystal system	triclinic	tetragonal
Space group	$P\bar{1}$	$I4_1/a$
***a*/Å**	13.4071(13)	20.2681(16)
***b*/Å**	13.8537(15)	20.2681(16)
***c*/Å**	14.6265(13)	7.1102(8)
α/°	82.533(8)	90
β/°	83.494(8)	90
γ/°	68.612(8)	90
Volume/Å^3	2501.8(4)	2920.8(6)
Z	2	4
ρ_{calc}g/cm^3	1.119	1.403
μ/mm^{-1}	0.253	0.364
F(000)	908.0	1288.0
Crystal size/mm^3	0.38 × 0.31 × 0.16	0.37 × 0.09 × 0.08
Radiation	MoKα (λ = 0.71073)	MoKα (λ = 0.71073)
2Θ range for data collection/°	3.66 to 49.998	4.02 to 51.324
Reflections collected	20059	13369
Independent reflections	8302	1375
Goodness-of-fit on F^2	0.859	1.066
Largest diff. peak/hole / e Å^{-3}	1.55-0.57	0.26-0.15

The growth of all presented crystals suitable for X-ray diffraction analysis was initiated by evaporation from dichloromethane solution. All single crystal X-ray diffraction data are combined and specified in Table **1**. We initially hoped to crystalize both thiol protected compounds (2-(trimethylsilyl)ethyl, SAc), however their crystallization turned out to be

troublesome - presumably due to alkyl-silicon mediated PGs and non-favorable π-stacking mismatching . Thus, the first building block **51** tends to crystalize in *triclinic* crystal system in *P-1* space group. Presumably, presence of the entire molecule in asymmetric unit and merely 2 molecules per unit cell results in broken symmetry of **51,** where all C_1-C_2 bonds are not uniform ranging from 1.547-1562 Å. Two different short contacts formed between thioether and one of the proton from the methyl group ($S_1 \cdots H_{44}$ and $S \cdots H_{43}$ d = 2.976, 2.881 Å were found respectively), as well as weak interaction from $S_1 \cdots C_{39}$ was recognized (d = 3.352 Å). Major part of tetraphenylmethane structures show propeller conformation, being energetically more favored than opposite to *V*-shaped one, which occurs immensely rare (Δ = 4.5 kcal/mol). Nevertheless, contribution of hydrogen bonding may stabilize the structure and thus favor the latter conformation (Figure **37**). Solid state studies of **74** shows that this specific tetraphenylmethane structure crystalized in *V*-shaped conformation in tetragonal crystal system in $I4_1/a$ space group. Despite that the unit cell is occupied by 6 molecules, asymmetric unit is filled with ¼ of **74** which has simultaneously equal length of C_1-A_2 bond (d = 1.550 Å). These arguments match perfectly with high symmetry of perpendicularly assembled tetraphenylmethane **74**. Deeper analysis allows to typify hydrogen bonds. These are affected through interactions with the so called *para* and *meta* aromatic protons giving C_5-$H \cdots O_1$ and C_4-$H \cdots O_1 \cdots C_4$ contact (d = 2.566, 2.881 Å respectively). Noteworthy, the angle between C_5 atom of the protruding ring of derivative **51** decorated by pinacol boronic acid, central sp^3 C_1 atom and S_1 atom is found to be 93.85º, whereas analogous value for *para* terminated species **74** was determined as 113.76 º. These findings suggest that fourth aromatic ring of *meta* species **51** exhibits tilted conformation, while *para*'s one (**74**) is perpendicularly oriented. In a crystal structure of the *meta* isomer **51** one of the sulfur anchored ring is twisted, therefore we had to make an approximation that H_{40} reflects the location of anchor group upon surface deposition. Distances calculated between sulfur atoms S_1-S_2 (d = 6.7 Å) as well as S_1-H_{40} (d = 8.464 Å) and S_2-H_{40} (d = 5.944) match very well with the value found over the sequence of physical measurements (vide chapter **3**). The length between sulfur atoms for *para* species **74** was found as 9.459 Å (S_1-S_2) and 10.252 Å (S_2-S_3, S_1-S_3), being considerably larger than for asymmetric *meta* regioisomer, what is reflected in results of the surface-confined deposition studies.

2.4 Conclusions and outlook

In summary, two regioisomeric tripodal model compounds consisted of a tetraphenylmethane backbone and three acetyl-protected thiol substituents directly mounted on the phenyl ring in either *para*- (**33**) or *meta*- position (**50**) have been synthesized and fully characterized. However in order to obtain both modular platforms, diverse synthetic pathways had to be employed due to unexpected hindrance in the key synthetic step for the preparation of *meta*-substituted tripods, so the reaction conditions were varied considerably. Furthermore, the modular syntheses, introducing the protruding functionality in the *para* position of the fourth phenyl ring late in the sequence, enabled the provision not only of the model compounds **33** and **50** exposing a nitrile group, but also tripodal derivatives exposing other functional groups, like for instance aryl bromides, iodides or esters of boronic acid. These are eligible to perform manifold transition-metal-catalyzed coupling reactions leading to a library of functional molecules. Therefore, profiting from available building blocks, we designed and constructed the library of new 14 derivatives to study their charge transport properties. We were interested to compare the conductivity of the basic unit, comprised tetraphenylmethane foots regarding to the length and pendant head group. Hence, apart from the family of nitrile terminated "molecular towers" (**61**-**71**), we found the thioacetate decorated "molecular towers" (**74**-**93**) to be an ideal candidate for charge transport studies. We are able to synthesize all designed molecules from moderate to very good yield.

Indeed, halogen-terminated platforms seem to be an ideal candidate dedicated for the synthesis of other tailor-made molecules. It would be particularly tempting to have in a hand holder linked with electro-active tail groups, sensitive against light pulse that can play a role of molecular machine on the surface.

3 Characterization of tripods on gold surface

*In Chapter **3** were shown all, so far chemisorbed and investigated molecular tripods on gold surfaces and their surface behavior. Results of self-assembly were evaluated upon their deposition on the Au(111). Full characterization of molecular platform on surfaces is presented and discussed with respect to measurements done by means of X-ray based techniques, STM-UHV spectroscopy and surface electrochemistry. Conductive measurements of some of these molecules were examined using STM-BJ experiment.*

3.1 SAMs analysis based on X-ray techniques

Self-assembled monolayers (SAMs) formed by tunable molecular tripods, based on tripodal organic ligand, capable of multiple contact with the metal surfaces can be thus employed as molecular spacer, which prevents an interaction between active-tail group, mounted to the top of the tripod and surface. Therefore, in this subchapter physical measurements based on the surface spectroscopy are described in details in order to compare the anchoring behavior of *meta*- and *para*-tripodal platforms (**50**, **33**). Target molecules were immobilized onto gold coated silicon wafers to form their SAMs, in order to determine the quality of SAMs formed by **33** and **50** as well as to get more insight into their molecular arrangement on the surface. Applied XPS and NEXEFAS methods were used to determine the percentage population of both tripodal species so as to prove their capability of surface confinement via all three legs (or fewer than is assumed). The measurement of films of **33** and **50** were developed at the University of Heidelberg in group of Prof, Michail Zharnikov and done by Tobias Wächter together with profound interpretation of results.

3.1.1 Preparation of SAMs of 33 and 50

The samples for the spectroscopic characterization were prepared on freshly annealed gold-coated Si(100) wafers (typically 10 × 5 mm) with 5 nm Ti and 100 nm Au. These substrates were purchased from Georg-Albert-PVD, Germany. The substrates were immersed in 0.25 mM solution of *meta*- (**50**) or *para*- (**33**) tripodal molecules in the mixture of methanol/THF (3:1, v/v) containing 30% of 1M solution of ammonia in methanol as cleaving agent, at room temperature for 48 h. Consequently, samples were used for the further HRXPS and NEXAFS experiments at the synchrotron. Along with the SAMs of the tripodal molecules **33** and **50**, monolayers of hexadecanethiol (HDT) and 4′-(pyridin-4-yl)biphenyl-4-yl)methanethiol (PyPP1) were prepared on Au(111) substrate using the literature procedures.[291,292] These monolayers were used as references to calculate the effective thickness (HDT) and packing density (HDT and PyPP1) of the triad films. Significantly, the PyPP1 monolayer has a nitrogen atom in the terminal position, similar to the triad films in the proper adsorption geometry. The structure of this monolayer is similar to the basic $\sqrt{3} \times \sqrt{3}$ arrangement in the alkanethiolate SAMs,[291] with a packing density close to 4.63×10^{14} molecules/cm^2, corresponding to 0.216 nm^2/molecule.[301] The SAMs of the *meta*- (**50**) and *para*- (**33**) tripodal molecules were characterized by laboratory X-ray photoelectron spectroscopy (XPS), high-resolution X-ray photoelectron spectroscopy (HRXPS) and near-edge X-ray absorption fine structure (NEXAFS) spectroscopy.

3.1.2 High-resolution X-ray photoelectron spectroscopy

The laboratory XPS measurements were used for a preliminary screening only to optimize the preparation procedure. All experiments were performed at room temperature. The spectroscopic measurements were conducted under UHV conditions at a base pressure $<1.5 \times 10^{-9}$ mbar. Special care was taken to avoid damage induced by X-rays.[293,299] Laboratory XPS measurements were performed using a Mg Kα X-ray source (1253.6 eV) and a dedicated spectrometer (MAX200, Leybold-Heraeus). The acquisition of spectra was carried out in normal emission geometry with an energy resolution of ~0.9 eV. The X-ray source was operated at a power of 200 W and positioned ~1.5 cm away from the samples. The recorded spectra were normalized to the transmissions function of the spectrometer, and the binding energy scale was referenced to the Au $4f_{7/2}$ peak of clean gold at 84.0 eV.[294]The HRXPS experiments were performed at the D1011 beamline (bending magnet) at the MAX II storage ring of the MAX-IV synchrotron radiation facility in Lund, Sweden. The spectra were acquired in normal emission geometry at photon energies of 350 and 580 eV, depending on the acquisition range. The energy resolution was better than 100 meV allowing a clear separation of individual spectral components. The binding energy scale was referenced to the Au $4f_{7/2}$ peak of clean gold at 84.0 eV.[294] XP and HRXP spectra were fitted by symmetric Voigt functions and a Shirley-type background. To fit the S $2p_{3/2,1/2}$ doublet we used two peaks with the same full width at half-maximum (fwhm), the standard[294] spin-orbit splitting of ~1.18 eV (verified by fit), and a branching ratio of 2 ($S2p_{3/2}/S2p_{1/2}$). The fits were performed self-consistently: the same fit parameters were used for identical spectral regions.

HRXPS data were used to calculate the effective thickness of the triad films. A standard procedure was used,[295] based on the C 1s/Au 4f intensity ratio und a SAM (HDT/Au) with the well-defined thickness (1.84 nm) as a reference. Attenuation length values characteristic of densely packed alkanethiolate SAMs on Au(111) were used.[296]

The Au $4f_{7/2}$, C 1s, S 2p, and N 1s HRXP spectra of the *meta*- (**50**) and *para*- (**33**) films are presented in Figure **38**, along with fitting and decomposition of these spectra by characteristic emissions and doublets. The Au $4f_{7/2}$ spectrum in Figure **38(a)** shows noticeably lower intensity for **33**/Au as compared to **50**/Au, suggesting a higher film thickness in the former case. Indeed, according to the evaluation of the HRXPS data, the effective thicknesses of the *para*- (**33**) and *meta*- (**50**) films were estimated at 2.68 and 1.83 nm, respectively. Note that the above thickness difference is much less pronounced in

the C 1s spectra of the tripods' films in Figure **38(b)** due to the strong self-attenuation of the photoemission signal at the given kinetic energy.[297] These spectra are dominated by an intense emission at a binding energy of ~284.7 eV accompanied by a weak shoulder at ~286.5 eV. The dominant emission stems from the aromatic backbone while the shoulder can be assigned to the nitrile carbon.[298] It cannot be excluded however that the shoulder contains a small contribution from CO, at least in the case of **33**/Au, where a small signal at ~288.9 eV (COO) is observed as well.

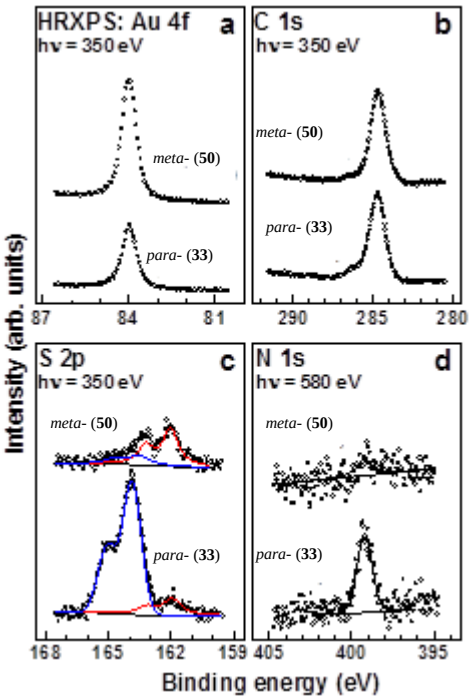

Figure 38 Au $4f_{7/2}$ **(a)**, C 1s **(b)**, S 2p **(c)**, and N 1s **(d)** HRXP spectra of the *meta*- (**50**) and *para*- (**33**) films acquired at photon energies of either 350 or 580 eV as marked in the panels (open circles). The fitting and decomposition of the spectra is shown (thin red and blue solid lines and thick black solid line), including the respective background (thin black solid lines).

The S 2p XP spectra of the tripod films in Figure **38(c)** exhibit two doublets at ~162.0 eV and 163.6-163.9 eV (S $2p_{3/2}$) assigned to the thiolate species bound to noble metal surfaces and disulfide or unbound sulfur, respectively.[299,300] The relative weights of the both components are distinctly different for **50**/Au and **33**/Au. Whereas the spectrum of **50**/Au is dominated by the thiolate-related doublet (75%), the opposite is the case for **33**/Au, where the disulfide/unbound sulfur doublet is the dominant feature (85%).

This suggests that the *meta*- (**50**) film represents a monolayer, with most of the terminal -SAc moieties being deprotected and bound to the substrate as the thiolates. The respective signal

is then strongly attenuated by the hydrocarbon overlayer, resulting in its comparably low intensity. In contrast, the *para*- (**33**) film represents presumably a multilayer, with some unbound sulfur moieties buried not deep in the matrix or even close to the film-ambience interface. Accordingly, the total intensity of the S 2p signal is significantly higher than in the **50**/Au case. These findings support the hypothesis of dimer formation in the case of the *para*-(**33**) submonolayer film prepared on a Au(111) single crystal studied by low temperature UHV STM (see Figures **41 (e)/(f)**).

The N 1s XP spectra of the tripod films in Figure **38(d)** exhibit a single emission at ~399.1 eV assigned to the nitrile nitrogen. The intensity of this emission is much lower in the case of **50**/Au as compared to **33**/Au suggesting much higher molecular coverage in the latter case, in agreement with the analysis of the S 2p spectra. Significantly, in the case of SAM, the nitrile group is located at the film-ambience interface in the upright adsorption geometry, so that the respective signal is not affected by the attenuation and can be taken as a measure of the surface coverage. With respect to 4′-(pyridin-4-yl)biphenyl-4-yl)methanethiol (PyPP1)/Au, which also has nitrogen in the terminal position (see the Experimental Part), the intensity of the N 1s signal in **50**/Au and **33**/Au was estimated at ~14% and 59%, respectively. Accordingly, in view of the known parameters of PyPP1/Au, viz. a packing density of 4.63 $\times 10^{14}$ molecules/cm^2 corresponding to a molecular footprint of 0.216 nm^2,[301,292] the effective packing density of **50**/Au and **33**/Au could be estimated at ~0.65×10^{14} and ~2.75×10^{14} molecules/cm^2, corresponding to a molecular footprint of ~1.5 nm^2 for **50**/Au (due to the multilayer character of the sample, an estimation of the molecular footprint for **33**/Au is not possible). An alternative evaluation of the effective packing density of **50**/Au, based on the S 2p/Au4f intensity ratio and using the well-defined hexadecanethiolate (HDT) SAM on Au(111) as a reference,[302,303] resulted in an effective packing density of ~1.1×10^{14} molecules/cm^2 corresponding to a molecular footprint of 0.9 nm^2. These values are somewhat different from the N 1s derived ones which is presumably related to the limitations of both evaluation procedures. But, on the other side, the values are not that far from each other, giving a reasonable estimate of the packing density in the SAM-like **50**/Au.

3.1.3 NEXAFS spectroscopy

The NEXAFS measurements were performed at same beamline as the HRXPS experiments. The spectral acquisition was carried out at the carbon and nitrogen K-edges in the partial electron yield mode with retarding voltages of −150 and −300 V, respectively. Linear polarized synchrotron light with a polarization factor of ~95% was used. The energy resolution was better than 100 meV. The incidence angle of the primary X-rays was varied from 90° (**E**-vector in the surface plane) to 20° (**E**-vector nearly normal to the surface) in steps of 10°-20° to monitor the orientational order within the tripod films. This approach is based on the linear dichroism in X-ray absorption, i.e., the strong dependence of the cross-section of the resonant photoexcitation process on the orientation of the electric field vector of the linearly polarized light with respect to the molecular orbital of interest.[305] The raw NEXAFS spectra were normalized to the incident photon flux by division through a spectrum of a clean, freshly sputtered gold sample. The energy scale was referenced to the most intense π* resonance of highly oriented pyrolytic graphite (HOPG) at 285.38 eV.[304,]

NEXAFS spectroscopy provides complementary information about the tripod films, in addition to HRXPS. C and N K-edge NEXAFS spectra of the *meta*- (**50**) and *para*- (**33**) films acquired at an X-ray incident angle of 55° are presented in Figures **39** and **40**, respectively. At this particular orientation, denoted as the "magic angle", the spectra are unaffected by orientational effects and are, therefore, exclusively representative of the electronic structure of unoccupied molecular orbitals.[305]

The C K-edge spectra of the tripod films in Figure **39** exhibit the characteristic absorption structure of the phenyl rings. They are dominated by a pronounced absorption resonance at ~285.1 eV (π_1*), accompanied by several weaker and broader resonances at ~287.6 eV (mixture of R* and C–H*), ~288.4 eV (π_2*), ~292.5 eV ($\sigma_{C\text{-}C}$*), ~297.0 eV ($\sigma_{C\text{-}C}$*), and ~305.0 eV ($\sigma_{C\text{-}C}$*).[305,306,307] The characteristic π* resonance of the nitrile moiety at ~286.7 eV[298,308] can only be traced in the spectrum of **33**/Au, as a shoulder at the absorption edge. The resonance at ~288.4 eV can also contain some contributions from the π* feature of COOH.[305]

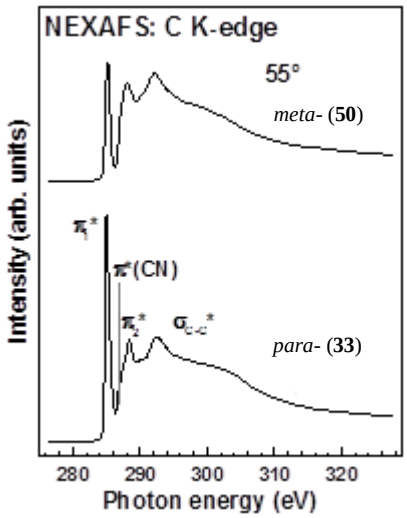

Figure 39 C K-edge NEXAFS spectra of the *meta*- (**50**) and *para*- (**33**) films acquired at an X-ray incident angle of 55°. The characteristic absorption resonances are marked.

The C K-edge spectra of the *meta*- (**50**) and *para*- (**33**) films differ to some extent regarding the intensity and exact shape of the absorption resonances. This difference is not surprising in view of the different coverage and distinctly different character of these films. In particular, a spectrum similar to that of benzene[305,306] or long-chain thiooligophenyl SAMs[307] can be expected for the multilayer *para*- (**33**) film, as indeed observed in Figure **39**. In contrast, the π* resonances can be quenched to some extent in the monolayer-like *meta*- (**50**) films, as observed in the respective spectrum, similar to the SAMs of phenylthiol on Au(111).[307] In addition, there can be a featureless-like absorption edge contribution from contamination which is presumably present to some extent in the *meta*- (**50**) and *para*- (**33**) films but is more pronounced in the former case, because of the lower coverage of the target molecules. Note that, at the ambient conditions, contamination is always present on the surface of Au substrate but is mostly removed upon the efficient self-assembly. The respective "self-cleaning" is, however, presumably less efficient in the case of tripod precursors, due to the comparably weak interaction between the molecular backbones, so that contamination cannot be avoided completely.

Whereas the features associated with the nitrile group are hardly visible in the C K-edge NEXAFS spectra of the tripod films, they are well perceptible in the N K-edge spectra of these films in Figure **40**, evidencing the intact character of the adsorbed molecules. Indeed, these spectra are dominated by the characteristic double resonance of benzonitrile at ~398.8 eV and ~399.75 eV. The same feature is observed in the spectra of molecular

benzonitrile in gas phase,[309] adsorbed benzonitrile,[310] and well-defined benzonitrile-terminated SAMs.[298,308,311,312] The appearance of the double resonance stems from the conjugation between the π* orbitals of the nitrile group and the adjacent phenyl ring. The degeneracy of the former orbital is consequently lifted and it splits into two states with different energies, oriented either perpendicular (π_1*) or parallel (π_3*) to the plane of the adjacent ring.[309,310] The delocalization of the π_1* orbital over the entire benzonitrile moiety leads to the lower intensity of the respective resonance as compared to π_3*, corresponding to the orbital localized at the nitrile group.

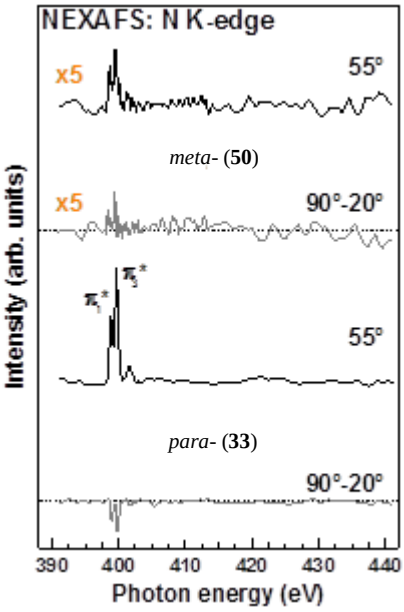

Figure 40 N K-edge NEXAFS spectra of the *meta*- (**50**) and *para*- (**33**) films acquired at an X-ray incident angle of 55° (black solid curves), along with the respective difference between the spectra collected under the normal (90°) and grazing (20°) incidence geometry (gray solid curves). The spectra of the *meta*- (**50**) films are zoomed by a factor of 5. The characteristic absorption resonances are marked. The horizontal dashed lines correspond to zero.

Along with the identification of the adsorbed species, NEXAFS data provide information of their orientation, based on the linear dichroism in X-ray absorption. The intensity of an absorption resonance is maximal if the orientation of the electric field vector of the linearly polarized light coincides with the transition dipole moment (TDM) of a molecular orbital of interest and is zero if the electric field vector is perpendicular to the TDM.[305] The TDMs of the π_1* and π_3* orbitals are perpendicular to the axis of the benzonitrile moiety[308] and should be directed parallel to the substrate at the upright orientation of the tripod molecules. This is indeed the case for **50**/Au, where the difference between the NEXAFS spectra collected

under the normal (90°) and grazing (20°) incidence geometry exhibit positive peaks at the positions of the π_1* and π_3* resonances (Figure **40**), corresponding to the higher intensity at 90° (**E** || to the surface). In contrast, these peaks are negative in the difference spectrum of **50**/Au, corresponding to the higher intensity at 20° (**E** almost ⊥ to the surface). This suggests a strong molecular inclination in the multilayer *para*- (**33**) film (on the average), having probably a certain supramolecular arrangement involving such an inclination.

3.2 STM analysis of spray-deposited tripods

Potential of tetraphenylmethane as a core structure featured with thiol-based anchoring moiety resulted in better control of the spatial arrangement. Stability of molecular platform on the metal surfaces and its specific foot imprint can be determined by UHV-STM experiments. Hence, comprehensive studies dealing with deposition of *S*-acetyl terminated tripodal architectures, appropriated for Au(111) surface were broadly described and discussed in the current chapter. Indeed, direct deposition methods involving single gold crystals Au (111) allow to gain insight into properties and the binding affinity of the tripods to the gold surface at low temperature. We have strived to deeply analyze all discovered effects even at the single molecule level. All of the STM, low temperature experiments were performed at Karlsruhe Institute of Technology, in the group of Prof. Wulf Wulfhekel emphasizing the way of the samples preparation prior to the deposition technique and their surface behavior under UHV conditions. The experiments were handled by Dr. Lukas Gerhald and master student Jan Homberg. Apart from the profound characterization of the shortest analogues **33**, **50** and their surface phenomena on the gold surface, preliminary results upon adsorption of **63**, **65** and **67** on metal surfaces are showed and discussed hereafter.

3.2.1 Experiments performed at 77K

Films of the tripodal platforms **33** and **50** for the STM investigation were prepared by immersing a sample of freshly prepared gold on mica in a solution of either *meta*- (**50**) or *para*- (**33**) tetraphenylmethane derivatives in a mixture of methanol/THF (3:1, v/v) containing 30 % of 1 M solution of ammonia in methanol as a cleaving agent, at room temperature for 48 h. After rinsing, the roughness of the prepared films was measured by STM at 77K in UHV. In the case of the *para* derivative **33**, no signal of the tunneling current could be detected, pointing to an insulating multilayer of molecules. In contrast, in the case of the *meta* derivative **50**, STM imaging could be performed, albeit without molecular resolution. Figure **41**(a) shows a large-scale STM image of the *meta* derivative **50** obtained at 77K in UHV. Here, atomic steps of the Au(111) surface can be seen, separating flat terraces of about 150 nm in width. The inset shows a cross section of a monoatomic step with a measured height of 229 pm, close to the expected step value of 235 pm. This clearly indicates 2 D growth of the molecular layer. This is in perfect agreement with the HRXPS and CV data, which indicated multilayer adsorption in the case of the *para* derivative **33** and a well-

ordered monolayer in the case of the *meta*- derivative **50**. However, molecular resolution could not be achieved, presumably owing to contamination on top of the relatively open surface of the tripod layer.

3.2.2 Experiments performed at 5.3 K

Hereby, in order to get insight in the adsorption geometry of the tripods on a well-defined surface, the low-coverage samples of *meta*- and *para*- molecules on a clean Au(111) single crystal were prepared. The tripods were deposited by spraying the dissolved molecules through a pulsed valve onto the Au(111) surface and, after an annealing procedure, the sample was cooled to 5.3 K for the UHV STM investigations. The advantage of this method described in detail in our recent publication over the deposition of a droplet lies in the reduced total amount of solution that is deposited. Using higher concentrations of molecules in the deposition solution allows to further reduce the influence of possible contamination of the solvent. We used 0.16 mM (for **50**, *meta*-) and 0.20 mM (for **33**, *para*-) solution in dichloromethane. After deposition, the surface was transferred into the UHV chamber ($p < 5 \times 10^{-10}$ mbar) and mildly heated to about 400 K for 60 min in order to remove remnants of the solvent and to promote the deprotection of the acetyl groups masking the three thiol anchor groups, in order to promote the immobilization of the tripodal molecules on the surface. Subsequently low-temperature STM investigations at about 5.3 K were performed in order to characterize the *meta*- and *para*- molecules on the Au(111) surface deposited by this method.

As can be seen in Figure **41(b)**, deposition of a submonolayer amount of *para*-molecules **33** leads to islands with long-range order and an apparent height of about 500 pm (see Figure **41(c)**). The hexagonal order agrees both with the threefold symmetry of the molecule and the underlying lattice. Figure **41(d)** shows an enlarged view of a unit cell (marked in black) with a lattice parameter of 3.25 nm and an area of $(¾)^{0.5} \times (3.25\ \text{nm})^2 = 9.16\ \text{nm}^2$. Assuming that each bright blob corresponds to one molecule, the unit cell of this hexagonal superstructure comprises six molecules, corresponding to a molecular footprint of 1.53 nm^2. The precise adsorption configuration, however, cannot be inferred from the STM measurements. As will be revealed in the discussion of the HRXPS results, for the film of the *para*- **33** derivative the disulfide/unbound sulfur doublet in the S 2p XP spectrum is the dominant signal. This indicates the possible formation of dimers (among other adsorbed species) and thus leads to the interpretation of two molecules forming one bright blob in the

STM image and thus to a molecular footprint of 0.77 nm² for one molecule. After further annealing at 450 K for another 60 min, the molecular islands rearrange and form a slightly more densely packed film (see Figures **41(e)/(f)**). Here, the lattice parameter of the unit cell amounts to 3.12 nm corresponding to an area of 8.43 nm², with the unit cell comprising dimers. Thus, the area occupied per molecule is 0.71 nm². The precise adsorption configuration, however, cannot be inferred from the STM measurements. In contrast to the *para*- derivative **33**, spray deposition of the *meta*- derivative **50** never led to ordered molecular films or islands. Instead, these molecules preferably adsorb along the step edges of the gold substrate as can be seen in Figure **41(g)**. We propose an array of identically adsorbed *meta*- derivatives equally spaced with a periodicity of 1.15 nm (see enlarged view Figure **41(h)**). From the periodicity of 1.15 nm, we can estimate the molecular footprint as the area of an equilateral triangle to ¼ × $(1.15\ nm)^2 \times (3)^{0.5} = 0.57\ nm^2$. This model is supported by the high resolution image of a single molecule shown in Figure **41(i)** and intuitively agrees with the assumption of dimer formation and a slightly larger footprint of 0.77 nm^2 in the case of the *para*- derivative **33**. Here the molecule can be identified by two brighter lobes directed towards the gold step edge and a third lobe that is slightly darker. The head group appears as a brighter protrusion in the center that jumps from the left to the right during the scan with the tip close to the sample.

In summary, the low temperature UHV studies demonstrate that both tetraphenylmethane derivatives **33** and **50** can be deposited in sub-monolayer concentration by "spraying" techniques, and after an annealing procedure, both derivatives form considerably different ordered molecular assemblies, with large islands for the *para*-derivative **33**, and rows at the step edges for the *meta*-molecule **50**. While the dimensions of the structures' subunits match with the molecules' sizes and corroborate the molecular origin of the structures, the investigations do not allow conclusions about the precise arrangement of the individual molecule on the substrate. While the observed patterns match with tripodal structures immobilized with all three anchor groups, the experiments are not able to proof this hypothesis as the tetrahedral shape of the model compounds allows for various arrangements which is beyond the resolution of the experiment.

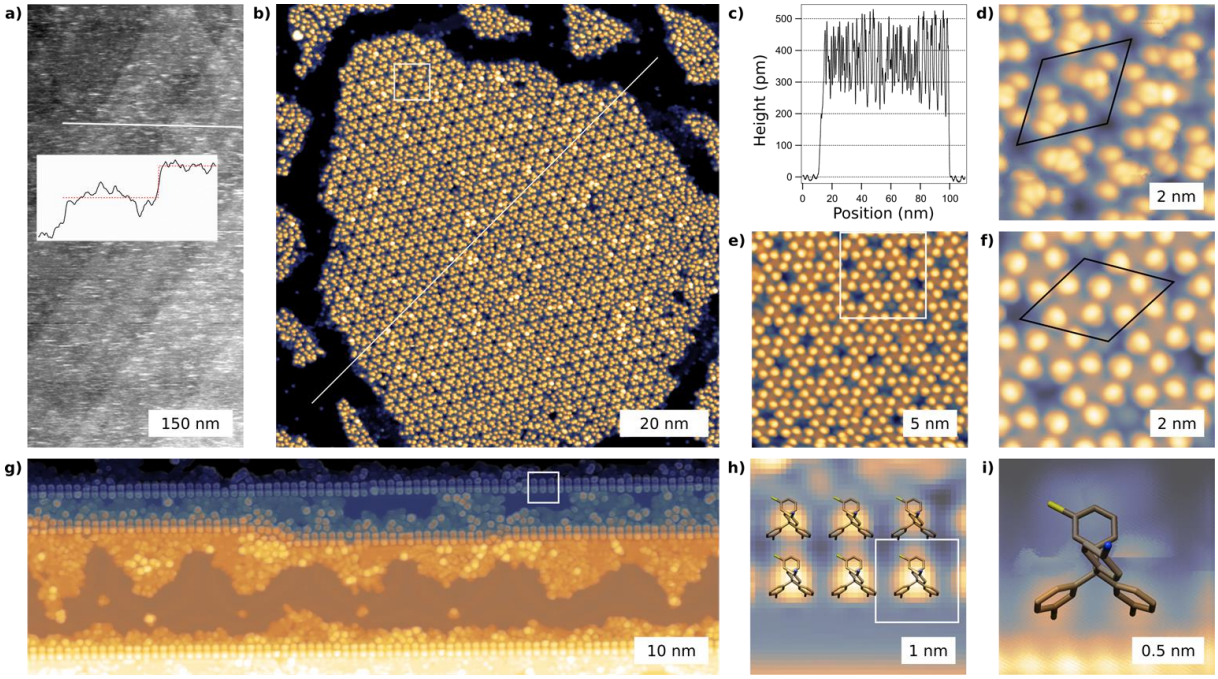

Figure 41 (a) Large scale overview of the SAM of *meta*- molecule **50** (77 K). The inset shows the cross section along the white dashed line with a step height of 230 pm. **(b)** Ordered island of *para*- molecules **33** deposited on clean Au(111) by spray deposition. **(c)** Cross section along the white line in **(b)**. **(d)** Enlarged view of the area marked in (b) with the unit cell marked in black. (e) Well-ordered arrangement of *para*- molecules **33** after prolonged heating. **(f)** Enlarged view of the area marked in **(e)** with the unit cell marked in black. (g) *Meta*- molecules **50** lined-up at the step edges of the Au(111) substrate. **(h)**/**(i)** Enlarged view of the area marked in **(g)**/**(h)** with the proposed adsorption model of the *meta*- molecule superimposed to scale. Tunneling parameters: **(b)**/**(d)**: 2 V, 5 pA, **(e)**/**(f)**: 2 V, 10 pA, **(g)**/**(h)**: 2 V, 20 pA, (i): 0.05 V, Feedback off.

3.2.3 Switchable molecules of the *para*- decorated tripodal 33 on the surface

Reversible switching of a molecule between two or more stable states is a phenomenon that is particularly interesting with regard to possible future applications in molecular electronics. In this work tetraphenylmethane molecules deposited on a Au(111) surface were studied at a low temperature. By using the tip of our scanning tunneling microscope, we were able to induce transitions between six different metastable conformational states noticed for **33**. An elaborate analysis of this switching behavior allows us to propose a well-founded model of the adsorption geometry and the conformational switching mechanism.

Here we present a low-temperature scanning tunneling microscopy (STM) study of tetraphenylmethane derivative **33** deposited on an Au(111) surface. These molecules intrinsically have a high number of degrees of freedom due to their four C-C single bonds. Adsorbed on the surface, six different metastable conformers were found and we managed to induce fully reversible transition between these states. On the basis of a detailed study of adsorption configuration and the observed switching behavior, we developed a model that explains the transitions between the six different conformational states. We were able to identify different critical parameters that influence the energy of the different states, which emphasizes the importance of the local environment of the molecule on its behavior.

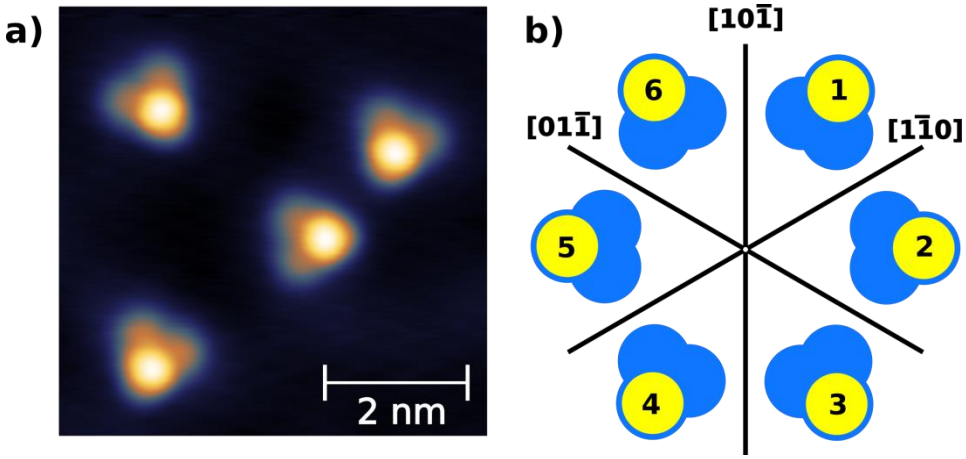

Figure 42 (a) Constant current STM of single tetraphenylmethane molecules adsorbed on a Au (111) surface**. (b)** Scheme showing the six existing different orientations

We deposited a tetraphenylmethane-based molecule **33** shown in Figure **42(a)** onto a clean Au(111) single crystal using a spray deposition method.[320] The sample was then transferred into our ultra-high vacuum chamber and annealed to 150ºC for about 60 min in order to promote deprotection of the thiol legs and proper adsorption of the molecules. Besides, the amount of possible contamination or solvent remnants is reduced. All STM experiments presented were carried out at 5 K. Figure **42(b)** shows a typical STM of four isolated molecules apparently adsorbed in different orientations but having the identical triangular shape with one edge being brighter than the other two. For all molecules observed in our experiments, only six different orientations with respect to the Au(111) lattice were found as is depicted in Figure **42(b)**. The probability to find a molecule in one of the six different states depends on the adsorption site. While on the fcc areas of the reconstructed Au(111) surface[313,314] the orientation with the molecular triangle pointing to the right (states 2, 4, 6 in Figure. **42(b)**) is more likely (N(246)/N(135) = 172/42 = 4.1), on the hcp domains the molecular triangle is found more often (N(246)/N(135) = 30/68 = 0.44) to point to the left

(states 1, 3, 5 in Figure **42(b)**). As fcc and hcp areas only differ in their subsurface layer, this indicates that the molecule interacts with the second layer of the substrate. Together with the fact that the molecules are isolated and randomly distributed even after the annealing process, this indicates that there is only one well-defined strongly bonded adsorption configuration of the molecule. We therefore assume that the molecule is bonded to the Au(111) surface with all its three thiol groups. Before we can discuss possible adsorption scenarios in detail, we shall present the switching behavior. In the presence of the STM tip and at sufficiently high bias voltage and set point current, the molecules show transitions between the different orientations. One typical series of images of the same two molecules is shown in Figure. **49(a)**. These images were recorded at a voltage of 120 mV and set point current of 50 pA. In between two images one scan at a voltage of 700 mV was performed in order to induce transitions. It can be seen that both molecules seem to rotate by 120^{o} around the center of the triangle, which is equivalent to the bright protrusion switching from one edge to another. Rarely, rotations of 60^{o} or 180^{o} can be observed. A displacement of the molecule with respect to the surface in the sense of classical diffusion has never been observed. Therefore, a real rotation of the molecule **33** including breaking of all three thiol-gold (S-Au) bonds at the same time can safely be excluded. Further, a rotation around one or two of its thiol-gold (S-Au) can be excluded as this would also involve a certain displacement of the molecular triangle which would have easily been seen in STM. This switching can not only be induced by scanning above the molecule but also with the STM tip held at a fixed position. The corresponding time trace of the tunneling current shown in Figure **49(b)** exhibits six different plateaus which represent the six different orientations of the molecule. Altogether, this leads us to the assumption that the observed transitions are based on an internal reconfiguration of the molecule and all three thiol-gold (S-Au) bonds remain fixed to the substrate.

The threefold switching that occurs more frequently and does not change the perimeter of the molecular triangle is obviously related to a rotation by 120^{o} of the molecular head group that is pointing upwards at an angle of about 80^{o} The three metastable states are then defined by the positions of the three phenyl groups attached to the substrate. The explanation of the apparent rotation by 60^{o} or 180^{o} is less obvious: we assume a chiral configuration of the three phenyl rings pointing to the surface that is induced by steric hindrance of neighboring phenyl groups. There are two possibilities for this configuration, corresponding to right and left-handed helicity. Then there are for each ring two carbon atoms that are closer to the surface and two that are farther away. In this picture, the three bright protrusions that form the molecular triangle are then constituted by the upper parts of

the phenyl rings rather than by the centers of the phenyl rings as might intuitively be expected. This scenario is depicted in Figure **43(a)**. Then an apparent rotation by 60° can straightforwardly be explained by a tilt of the phenyl rings around their single bonds towards the sulfur and towards the central sp^3-hybridized carbon atom, thereby switching the chirality of the adsorbed tetraphenylmethane.

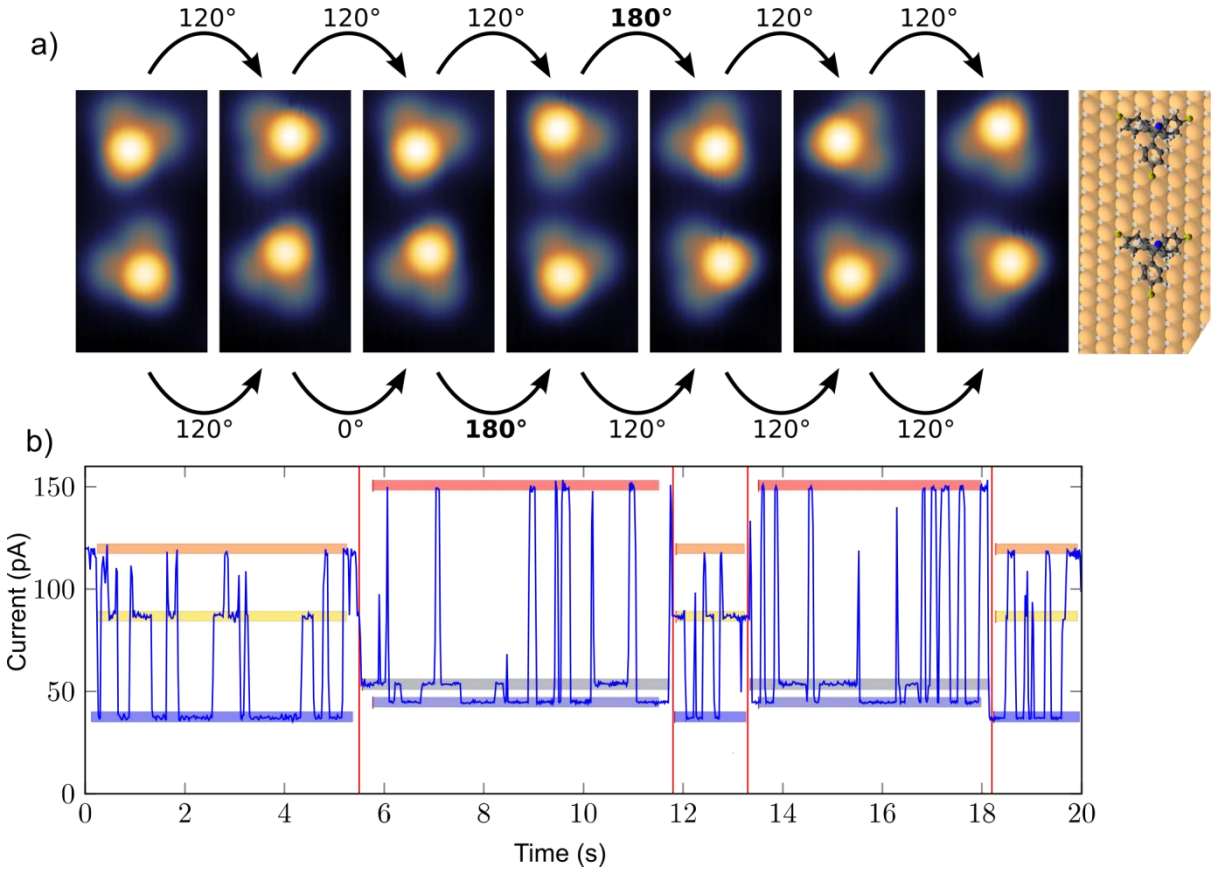

Figure 43 (a) constant current images recorded at U = 120 mV and I = pA, with a scan at 700 mV in between two images. **(b)** Current trace at fixed tip position with the six different current levels shown in color.

The six different states, in particular the two different chiralities, are not equal in energy, and a clear difference between the molecules **33** adsorbed on fcc domains and those adsorbed on hcp domains can be observed. This is represented in the switching statistics of individual molecules, (see Figure **43**) and is also seen in the statistics of the initial adsorption configuration mentioned above. Besides, it can be seen that molecules adsorbed on elbow sites of the herringbone reconstruction do not show any transitions (see red crosses in Figure **43**). Boltzmann statistics allows to relate the measured population ratios to thermal energy

$$k_B T = 0.42 meV \ @ \ 5K$$

$$\Delta E = k_B T \cdot ln \frac{N(2,4,6)}{N(1,3,5)}$$

With this, we get energy differences of

$$\Delta E_{fcc} = E_{fcc}^{1,3,5} - E_{fcc}^{2,4,6} = 0.11 \ to \ 0.68 \ meV$$

and

$$\Delta E_{hcp} = E_{hcp}^{1,3,5} - E_{hcp}^{2,4,6} = -0.22 \ to \ -0.48 \ meV$$

This makes the adsorption configuration of the molecules **33** a sensitive indicator of the stacking order of the underlying substrate. Interestingly, the chirality also depends on neighboring molecules. After analyzing a series of about 2000 scans of the two molecules presented in Figure **42(a)**, we found ratios of N(246):N(135) = 85:15, 86:14 and 87:13 for the second molecule when the first molecule is in state 1, 3, and 5, respectively. Ratios of 80:20, 80:20, and 78:22 are found for the second molecule with the first molecule being in state 2, 4, and 6, respectively.

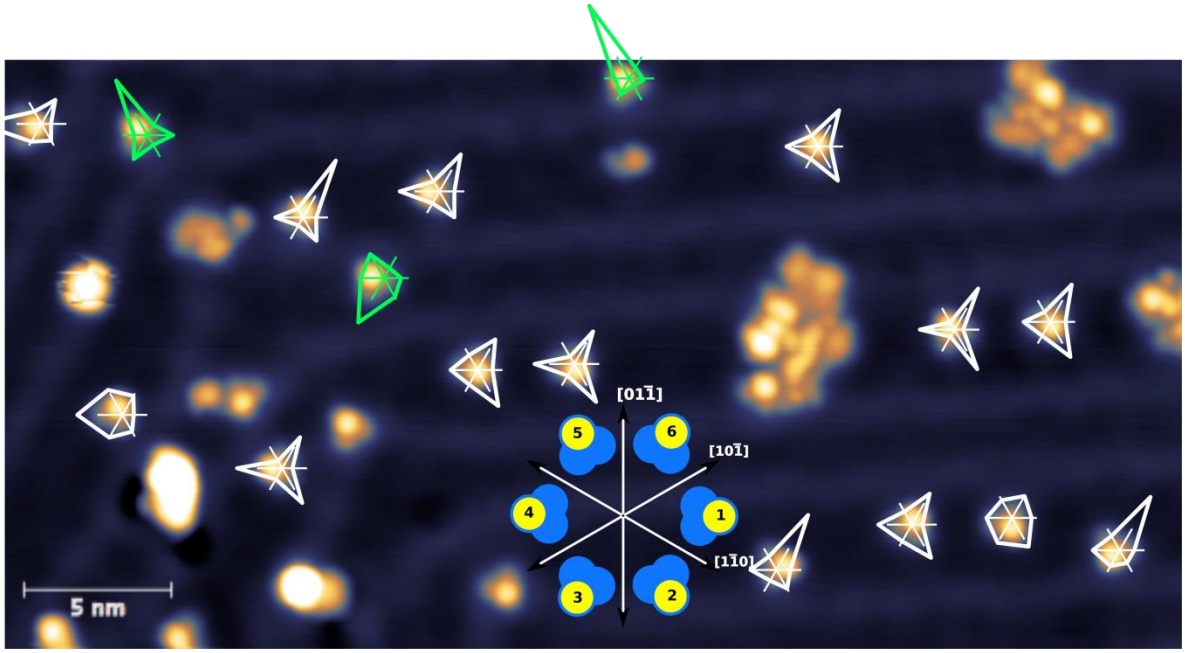

Figure 44 Polar graphs representing the population of the six different states of each molecules from a series of 420 scans at U = 120 mV and I = 50 pA, a can at 700 mV in between two images. Molecules adsorbed on fcc areas are shown in white, those adsorbed on hcp areas shown in green. The image is rotated by 60o for convenience

This is equivalent to an increase of the energy difference $\Delta E_{mol1} = E_{mol1}^{1,3,5} - E_{mol1}^{2,4,6}$ by 35% from 0.56 to 0.75 meV. Although this effect is superimposed by the dominant influence of the stacking of the underlying substrate, this experiment shows that the chiralities of neighboring molecules (**33**) are coupled and underlines the importance of the local environment of a molecule on its behavior.[315]

Considering these findings, we can discuss the adsorption configuration in detail. Six apparent orientations of the adsorbed molecules **33** can be observed. Each molecule can be switched between the same six orientations without diffusion as discussed above.

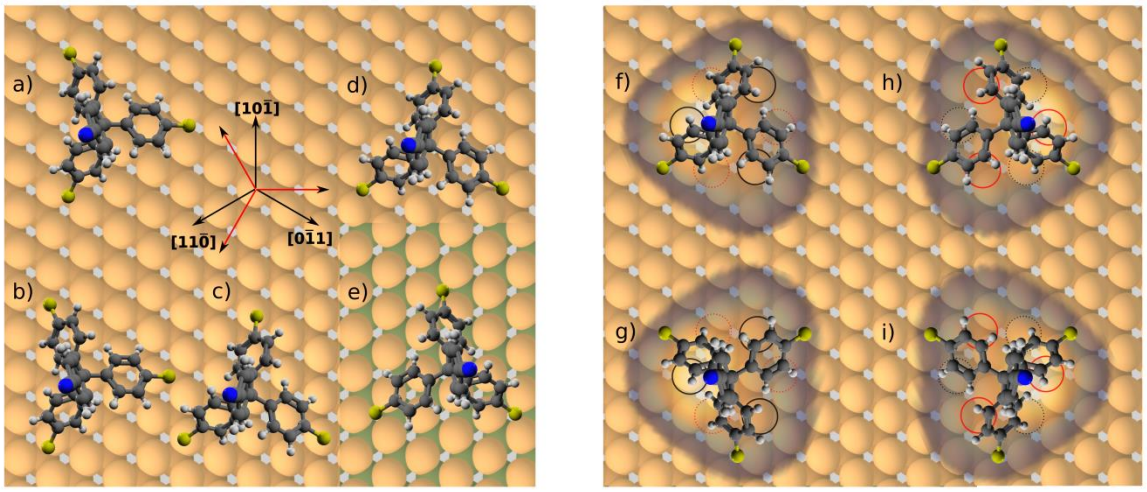

Figure 45 (a) Supposed adsorption configuration with semitransparent STM topography superimposed to scale **(b-f)** Possible orientations of the molecule with respect to the Au(111) lattice as discussed in the text

This suggests that the molecule **33** has only one adsorption configuration with lowest energy and is centered on a high-symmetry position of the Au(111) lattice (see Figure **45(a)** and **(b)**). Then, the three legs of the molecule were aligned with the mirror planes of the substrate lattice and the two helicities of a particular molecule would have same energy, which is in contradiction to our observations that three of the six states are preferred over the other three. Furthermore, in this case the edges of the triangle would correspond to the centers of the phenyl rings in order to fit to the apparent orientations and the observed switching by angles of 60° or 180° could not be explained. Therefore we exclude the models depicted in Figure **45 (a**) and **(b)** and suppose an alignment of the legs of the molecule with the [110] directions of the surface depicted in Figure **45 (c)** and **(d)**. In general, sulfur adsorbs preferentially on threefold hollow sites[316,317] although it might depend on the bond angle.[318] Thus, we focus on the possible configuration depicted in (d) where the sulfur atoms bind to fcc sites. Then, our

findings described above can be explained as follows: The two helicities of a particular molecule differ in energy as the three phenyl rings touch the surface at two different lattice sites depending on the helicity.

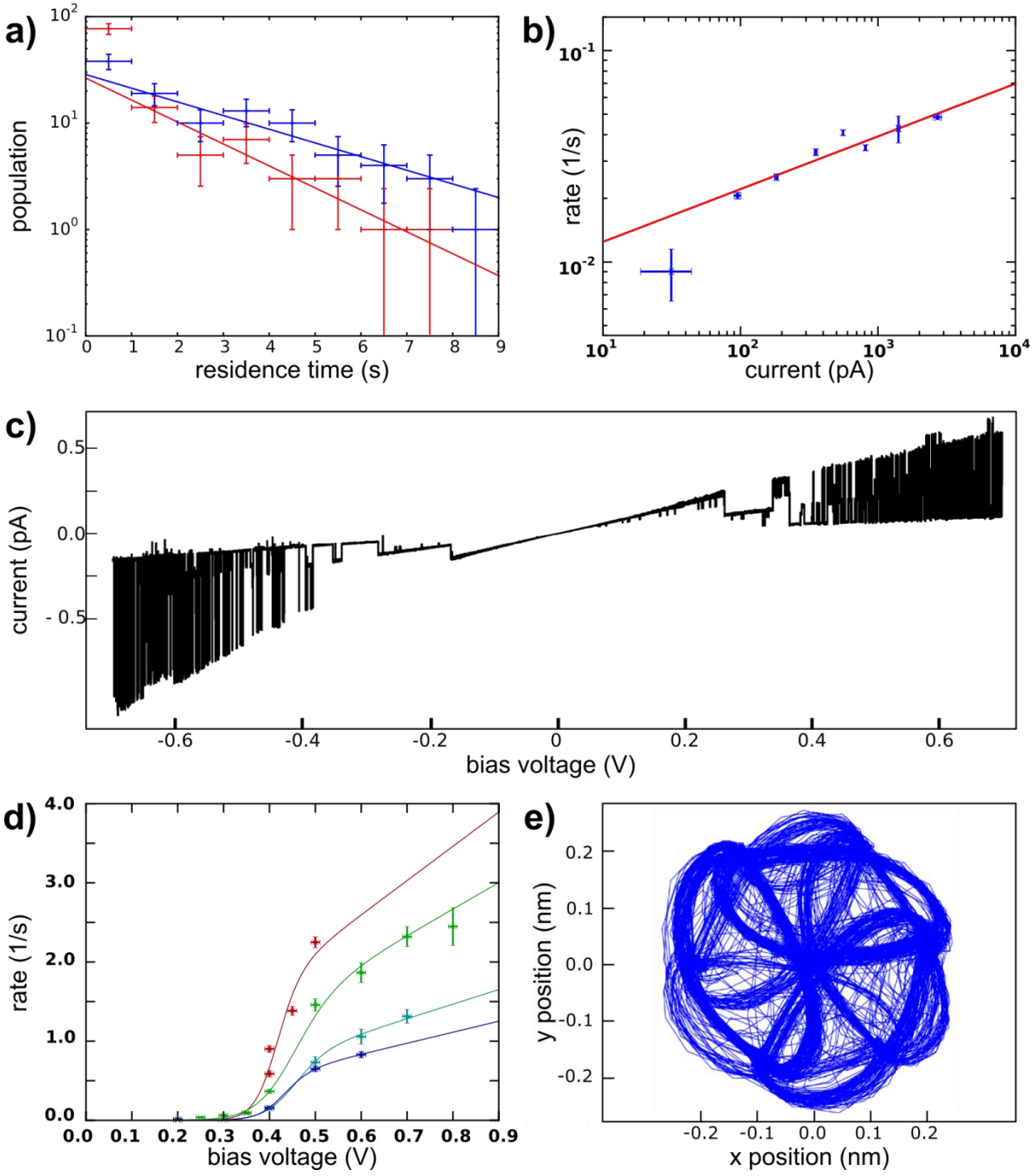

Figure 46 (a) Distribution of the measured residence time of the statistic switching. **(b)** Statistic switching as a function of the setpoint current at the voltage of 400 mV. **(c)** Current time traces as a function of the applied bias voltage at fixed z position. **(d)** Switching rate as a function of the applied voltage. **(e)** Tracking curve of the STM tip following the molecular head group

For the molecule depicted in Figure **45 (d)** that is adsorbed on an fcc domain of the surface a configuration with the phenyl rings touching the hollow sides forms a left-handed thread. The same adsorption configuration (that is the sulfur atoms are sitting on fcc sites and the phenyl rings are touching the surface on hollow sites) but on a hcp domain of the substrate, the molecule forms a ride-handed thread (see Fig. **45 e**)). Figure 45 (f) shows the molecular configuration overlaid with the corresponding STM image. The three possible states that can be accessed by rotation of 120^{o} of the molecular head group are indicated by solid (dotted) black circles in f (h), the three states that result from a change in helicity by a collective flip of the phenyl rings are indicated as dotted (solid) red circles. The mirrored adsorption orientations of f) and h) are energetically equivalent and result in the same apparent orientation but the opposite helicity as is depicted in Figure **45 (g)** and **(i)**. This means that the observed imbalance in the distribution of the apparent orientation for fcc and hcp domains of the substrate does not comprise an imbalance of the helicities of the adsorbed molecules. However, an apparent rotation of 60^{o} or 180^{o} of a particular molecule implies a change in helicity.

In the following, we further analyze the switching process. To this end, the residence times of the molecule **33** in one of the states were plotted as is shown in Figure **46(a)** and fitted with an exponential decay. From this, the mean lifetime of a state and its inverse, the transition rate, can be determined. This transition rate was then determined as a function of the tunneling current with the bias voltage set at 0.4 V. This dependency is shown in Figure **46(b)** in double logarithmic plot. The transition rate increases with the increasing current, and a fit to a power law (red line in Figure **46b**)) gives an exponent of 0.25. An inelastic single electron process would be characterized by an exponent close to 1.[319] The voltage dependence of the switching is shown in Figure **46** as a single current time trace. Obviously, at low voltages no switching takes place and higher voltages of both positive and negative polarity lead to higher transition rates. The value of the threshold voltage above which switching occurs is determined from a fit to the switching rate measured as a function of the voltage (see Figure **46d**)). We chose a logistic growth function multiplied by a linear term which reproduces the observed onset of the switching rate and the further increase for even higher voltages. With this we get a threshold voltage of 430 mV. So far, our discussion focused on the switching frequency, but it neglected the switching direction although this system with its rotational transitions suggests itself as molecular motor. Therefore we recorded the sense of rotation of the switching by making use of a built-in function of our

scanning electronics named atom tracking. In doing so, the tip oscillates laterally above the molecule following the position of maximum apparent height, which allows to track the rotational-like switching and to distinguish the six different states as is shown in Figure **46(e)**. We indeed find a slightly preferred direction of rotation which, however, does not depend on the chirality or the polarity of the applied bias. Therefore, we think that it is simply related to the circular modulation of the tip in the atom tracking mode.

3.2.4 Surface deposition of towers-shaped molecules 61, 63, 65

Hereafter, surface properties of the first batch of elongated, symmetric tripods, decorated by nitrile on the top of each nanostructure are revealed (**33**, **61**, **63**, and **65** respectively). Thus, a self-assembled template of tetraphenylmethane-based variants on a Au(111) surface which feature an acetyl protected thiol anchoring group that sticks out of the molecular film are presented. Using the tip of a scanning tunneling microscope, this acetyl group can be removed in a controlled way without destroying the remaining molecule. The modified molecule can readily be distinguished from the original ones such that information can be engraved in the molecular film. We show that the mesh size of this molecular graph paper can be tuned by varying the length of the molecular spacer group so that writing and reading information on the nanoscale with variable letter size is possible.

Here, low-temperature STM study of specifically designed tetraphenylmethane-based molecules **33**, **61**, **63**, **65** deposited on a Au(111) surface which arrange in regular patterns where the mesh size is controlled by the length of the molecular spacer group. This spacer group consists of a *n*-phenyl rod (where *n* is represented by bi-, ter-, and quarterphenyl) with a terminal nitrile group as specific marker dedicated for the tip of STM. We show that one of thioacetate-based anchoring groups of the tripod is protruding perpendicular to the surface. It can be thus cleaved by application of voltage pulses with the STM tip positioned above the acetyl protected thiol group. The molecules upon thiol deprotection appear darker in STM which allows an easy identification and opens up the possibility of writing information on the nanoscale with a predefined spacing of the mesh. The contrast of this molecular graph paper is based on the cleavage of bond between thiol and acetyl protecting group and thus it is very likely to persist up at room temperature conditions.

Four derivatives of tetraphenylmethane-based molecular tripods **33**, **61**, **63**, **65** were deposited from a dichloromethane solution that was sprayed onto clean Au(111) surfaces as described previously.[320] In order to promote proper arrangement in regular patterns, the samples were then transferred into the ultra-high vacuum (UHV) chamber, mildly annealed to

165 °C and transferred in situ to the STM chamber. All experiments were carried out at 5.3 K. All four variants arrange in regular islands with almost square-like unit cells (see Figure **47 (a)**) and an apparent height of 520 pm. As can be seen in close-up STM images (column a2-e2 in Figure **47**), the appearance of this brightest spot in the unit cell can take three different basic motifs (and their mirrored counterparts) while all four variants show the very same three motifs. The size of the unit cell varies with the number of phenyl rings in the spacer and is indicated by a black rhomboid in the columns a3/b3 and a4/b4 in Figure **47**. One side of the unit cell is aligned parallel to a closed-packed direction of the Au(111) lattice in all four cases (Figure **47** a3-d3). We propose the following adsorption model which is supported by superposition of our STM measurement with the molecular models and which assumes a molecular film that is commensurate with the Au(111) lattice (see Figure **47**, column a4-e4): The brightest spot within the unit cell can be identified with the protruding acetyl group. More precisely, it is formed by two acetyl groups of two molecules aligned back to back (see Figure **47**, columns a3-e3, a4-e4). The spacing between two bright blobs is then given by the length of the spacer group.

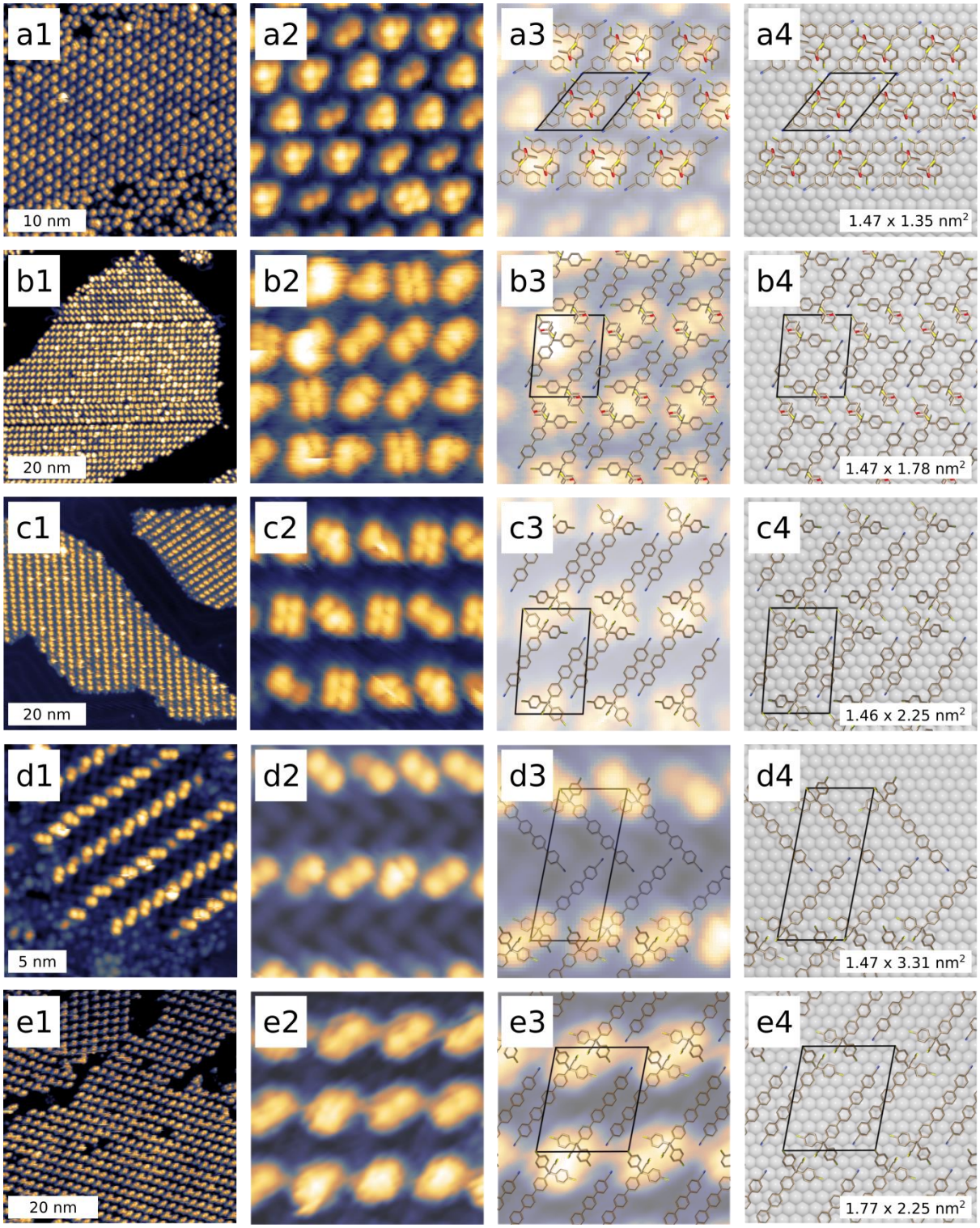

Figure 47 Configuration of adsorption of the tetraphenylmethane variants with different spacer groups: **(a)** monophenyl **33**, **(b)** biphenyl **61**, **(c)** terphenyl **63**, **(d-e)** quaterphenyl **65**. The first column shows a large scale overview image, column 2 shows 7x7 nm images with the motifs of individual acetyl groups of the corresponding variant, column 3 and 4 show 5x5 nm STM images with the molecular models superimposed to scale and the corresponding model of the Au(111). The size of the unit cell is given in fourth column a4-e4.

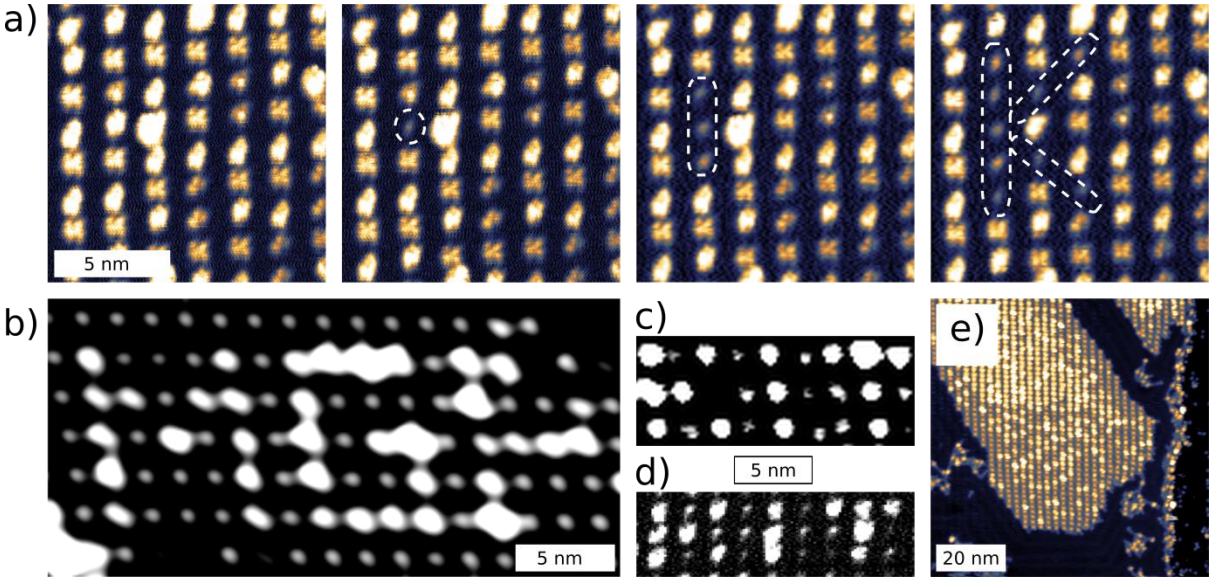

Figure 48 (a) Writing "K" in negative contrast on a 12 x 12 nm extract of tetraphenylmethane molecules **61** with a biphenyl spacer group. **(b)** Molecular Graph Paper (MGP), written on quaterphenyl derivatives **65**. (c), (d) "KIT" written on an array of the quaterphenyl/biphenyl variants (**65**/**61**). The width of both images is 17 nm. e) Island of terphenyl derivatives after heating to 200°C.

As the acetyl groups are pointing away from the surface, they can be freely addressed with the STM tip. Because this part of the molecule is decoupled from the metal surface, it is particularly suited for electron-induced single molecule chemistry. It is known that in thiol-based molecules which are lying flat on a metal substrate, voltage pulses from the STM tip can trigger breaking of the bond between the thiol and it acetyl protecting group.[321] We show that also freestanding acetyl groups can be removed by selective bond dissociation with voltage pulses of -3 V applied to the STM tip. This process is highly reproducible such that the self-assembled molecular layers can be modified molecule by molecule. Figure **48(a)** shows a sequence of four images of the very same area of a layer of the tetraphenylmethane variant **61** with a biphenyl spacer group. Step by step, acetyl groups are removed in order to print a negative of the letter "K". Clearly, the effect is highly localized such that indeed individual molecules can be addressed without influencing their neighbors. The self-assembled template functions as a molecular graph paper (MGP) that allows us to write information on the nanoscale in a well-controlled manner as is shown in Figure **48(b)** writing "MGP". The grid spacing of the molecular graph paper depends on the length of the spacer group of the involved tetraphenylmethane variant. Figure **48(c**,**d)** show the initials of our university KIT, written on quaterphenyl derivative **65** (Figure **48(c)**, grid

spacing 1.77 x 2.25 nm²) and on biphenyl derivative **61** (Figure **48(d)**, grid spacing 1.47 x 1.78 nm²). This chemical modification of the molecular pattern is highly stable and heating of the sample to temperatures of 200°C removes the acetyl groups only at the borders of the extended islands (see Figure **48(e)**). Within the islands, the acetyl groups still remain, which indicates that the chemical contrast that we rely on to write on the molecular graph paper is likely to withstand room temperature without degradation.

3.3 Surface electrochemistry

Self-assembled monolayers (SAMs) consisted of the redox-active molecular platform, with well-defined geometry and the distance between active-tail group as well as gold surface serves a great opportunity to be explored by electrochemical techniques. Therefore, characteristic of regioisomeric tripods **33** and **50** can be carried out. Rate of determined electron transfer is directly attributed to the number of molecular feet, which are fixed to the gold surface. It can be thus proven whether tripods are adsorbed via all three either less contacts than expected. Cyclic voltammetry experiments were done by Dr. Viliam Kolivoška at the J. Heyrovský Institute of Physical Chemistry, Czech Academy of Science.

For electrochemical desorption studies, the monolayers of *meta*- **50** and *para*-derivative **33** were prepared on gold bead electrodes (area 0.17 – 0.21 cm^2) by deposition from 0.2 mM solution in ethanol containing triethylamine (10% v/v ratio) at 60 °C for 16 hours. Subsequently, the electrodes were copiously rinsed by pure ethanol. Cyclic voltammograms were measured using Potenciostat/Galvanostat PGSTAT12 at v = 0.10 V/s. Desorption was performed in 0.5 M NaOH in ultrapure water in a three-electrode system containing bead gold working electrode in a hanging meniscus arrangement and pseudo-reference and auxiliary (both gold) electrodes.

Chemisorbed *meta*- (**50**) and *para*- (**33**) molecules were desorbed from gold substrate at negative applied potential during the cathodic voltammetric scan giving a corresponding desorption peak (see Figure **49**). Integration of the electric current gives the electric charge *Q*, which according to the Equation 1 provides information on the surface concentration of the adsorbed molecules Γ.[322]

$$\Gamma = (Q - Q_{dl})/nFA \qquad (1)$$

For the *meta*- (**50**) derivative, assuming negligible double-layer charging current (Q_{dl} = 0) and the number of transferred electrons *n* equal to three (one for each thiolate anchor), one obtains a value of (4.9 ± 0.2) × 10^{-10} mol/cm^2 for the surface concentration Γ. This represents (3.0 ± 0.2) × 10^{14} molecules/cm^2 and leads to the area occupied by one molecule equal to 3.4 × 10^{-15} cm^2/molecule. This value is in good agreement with that obtained from an STM image of individual molecules (5.7 × 10^{-15} cm^2/molecule) as well as with the area of a triangle made by three outer *para*- hydrogen atoms H17, H28, H39 (3.2 × 10^{-15} cm^2/molecule) of the similar *meta*- derivative **51** obtained from single-crystal X-ray diffraction (for more detail of X-ray data see paragraph **2.3**) and would provide even better agreement once the value of the double layer charge Q_{dl} is known and taken into account. In

any case, the above result unequivocally confirms that *meta*- (**50**) is anchored to the gold substrate via three thiolate bonds forming a chemisorbed compact monolayer (consistent with STM images in Figure **41(a)**). This finding is crucial if the well-ordered SAMs of *meta*- (**50**) tripods were to be used in further applications.

Integration of the total voltammetric response obtained upon the desorption of the *para*- (**33**) derivative led to the surface concentration value of $(5.9 \pm 0.4) \times 10^{-10}$ mol/cm^2 or $(3.6 \pm 0.3) \times 10^{14}$ molecules/cm^2, which is slightly higher than the value obtained for *meta*- (**50**) derivative $(3.0 \pm 0.2) \times 10^{14}$ molecules/cm^2) using the same assumptions for the Γ calculation. This value is in reasonable agreement with that obtained from the HRXPS measurements (~2.7×10^{14} molecules/cm^2). Moreover, a small voltammetric prewave at -0.85 V was reproducibly observed during desorption of the *para*- (**33**) derivative (Figure **49**). This could indicate the presence of an additional, physically adsorbed adlayer on the chemisorbed *para*- (**33**) monolayer, but more likely desorption of the disulfide dimers of the *para*- (**33**) bound to the gold surface by free thiol(s). At this point we cannot tell how many electrons are being transferred during desorption of the dimer and thus provide additional information on the composition of the film from the desorption data

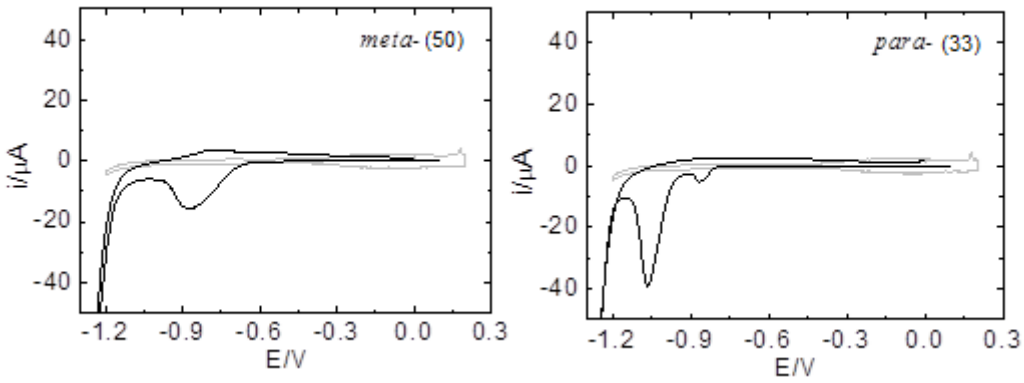

Figure 49 Cyclic voltammograms of *meta*- (**50**) (left) and *para*- (**33**) (right) self-assembled monolayer on gold electrode in 0.5 M NaOH aqueous electrolyte scan rate 0.10 V/s (black curves). Grey curves show the response of the bare gold electrode (i.e. with no adlayer) under otherwise the same conditions.

3.4 Preliminary results of STM-BJ measurements on the series of tower-shaped molecules.

As we have already mentioned, regarding to the position of anchoring groups, mounted to the skeleton of tetraphenylmethane platform and exposed tail group, tripods can exhibit variable values of one specific feature such as for instance charge transport (CT). Therefore, conductivity of molecular tripods can be studied by subjecting individual molecules between two metallic electrodes. It allows to form single molecular junctions to determine the impact of molecular structure (geometry, symmetry, nature of anchoring groups) on the charge transport mechanism and its value. Thus, STM-BJ experiments were performed investigating whole array of tripods terminated either by nitrile or thioacetate head groups on the top of each analyzed platform functionalized with anchoring groups in a *meta*- and *para*- positon as well. Measurements were successfully performed at the J. Heyrovský Institute of Physical Chemistry, Czech Academy of Science in the group of Dr. Magdaléna Hromadová, whereas all experiments were done by Dr. Viliam Kolivoška.

Single molecule conductance was measured using an original STM tubular scanner Agilent 5500 Scanning Probe Microscope with an in-house implemented current-to-voltage converter circuit with a wide dynamic range.[323] Current-time curves were converted to conductance-distance curves and corresponding histograms using a combination of an in-house developed software[324] and OriginPro were constructed. Logarithmic bin size of 0.005 was used for the construction of 1D histograms of $\log(G/G_0)$ values from the original data without any selection, where G is the conductance, presented in units of quantum conductance G_0 = 77.5 μS.[325] To get more insight into charge transport characteristic for whole library of synthesized tripods the solution of each molecules in mesitylene was prepared, ranging from 0.2 mM concentration for all nitrile terminated species, while for thioacetate terminated molecules the diluted solution for these molecules was done (0.01 mM), because of formed multilayers at the substrate/mesitylene interface (if c = 0.2 mM).

Hereafter, single molecule conductance measurements based on nitrile and -SAc decorated molecular platforms are presented. Demonstrated findings are taken up from STM-BJ accurate studies, involving 16 tetraphenylmethane derivatives differ from each other through the nature head groups (one batch contains nitrile, the second SAc featured terminus). Experimental results are assisted and exclusively corroborated by DFT calculations.

Figure **50** shows 1D, 2D and plateau length histogram of the junctions containing molecules **33**, **61**, **63**, **65**, serving as a representative example of nitrile terminated molecules. All nitrile terminated molecules showed two molecular conductance features (denoted as G_H - the highest conductance and G_L -the lowest conductance). In the 2D histogram, the G_H feature shows up as a highly inclined region of increased data density. It stems from the dominant contribution of the solvent through tunnelling in early stages of the molecular junction evolution, as already observed for other nitrile terminated molecules reported in the literature.[41] The G_H feature is followed by the G_L feature, being less inclined and considered as the true molecular conductance signature. In 1D histograms, the two features manifest themselves as regions with increased data density, allowing average molecular conductance values and distributions to be extracted. Quantized maxima appearing at $\log(G/G_0) \geq 0$ reflect the existence of gold-gold nanocontacts between the two electrodes, known to precede the molecular junction formation. Increased data density below $\log(G/G_0) = -6$ pertains to the noise level of the experimental setup. It is recorded upon breaking of the molecular junction in its G_L state. The data in the 2D histograms were further employed to investigate the stability of molecular junctions by means of the analysis based on molecular plateau length histograms. The latter are constructed by plotting the data density along the Δz scale at a certain conductance value between molecular conductance features and the noise level. The common value of $\log(G/G_0) = -5.5$ was chosen for all nitrile terminated compounds (see dashed line in the 2D histogram in Figure **50**, middle panel). For all para nitrile terminated molecules (*para*- **33**, **61**, **63**, **65**), found Δz distributions could be fitted by two maxima, denoted as Δz^0 and Δz^* in Figure **50**, right panel. The former maximum reflects the existence of measurement cycles, in which no molecules were trapped between the electrodes in the course of the junction evolution and is therefore not considered in further analysis. The latter maximum pertains to molecular junctions and is considered further. The determination of the absolute experimentally obtained molecular junction length Δz_{exp}, taken as a measure of the molecular junction stability, requires the snap-back correction of the distance scale to be performed. This correction is needed due to the plastic character of the junction deformation that occurs upon breaking of the last gold-gold atomic contact. In particular, the correction term $z_{corr} = 0.4$ nm needs to be added to the Δz^* value, obtaining the value of Δz_{exp}.

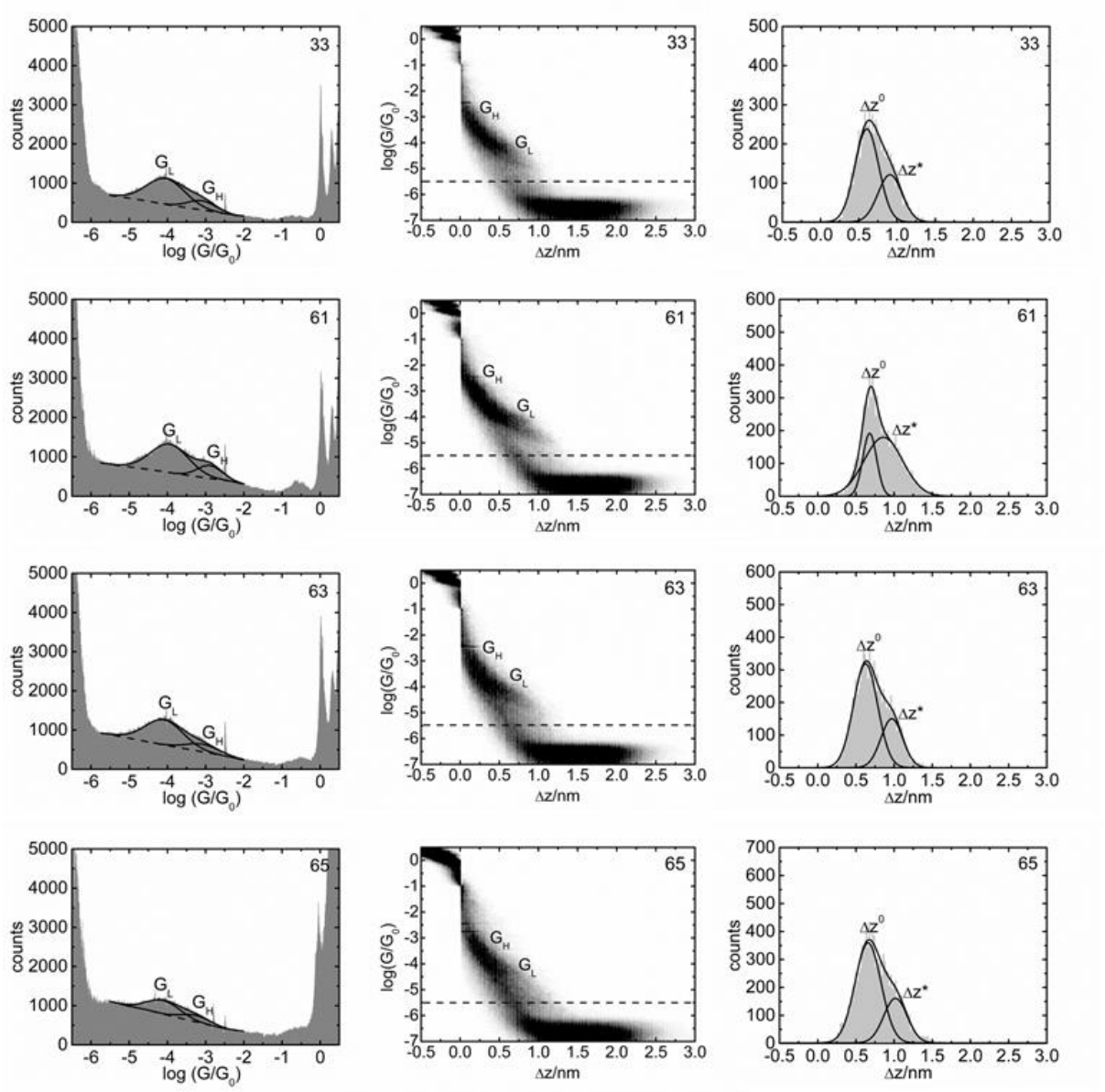

Figure 50 1D (left panel), 2D (middle panel) and molecular plateau length (right panel) histogram obtained for junctions containing the molecule of **33**, **61**, **63**, **65**.

While, Figure **51** shows the molecular junction length as a function of the number of repeating phenylenes units (*n*) constructed for *meta*- (left panel) and *para*- (middle panel) nitrile terminated molecules. For the shortest homolog of the *meta*- series, the G_L value is in a very good agreement with theoretically predicted junction conductance (G_T). The corresponding molecular junction configuration considered in the theoretical calculations is shown in the right panel of Figure **51**. G_T values of all molecules (both nitrile and thioacetate terminated) were obtained by density functional theory approach considering the electron tunnelling as the charge transport mechanism. The theoretical value obtained for the shortest member of the *para*- series is quite off trend set by G_T values of longer molecules.

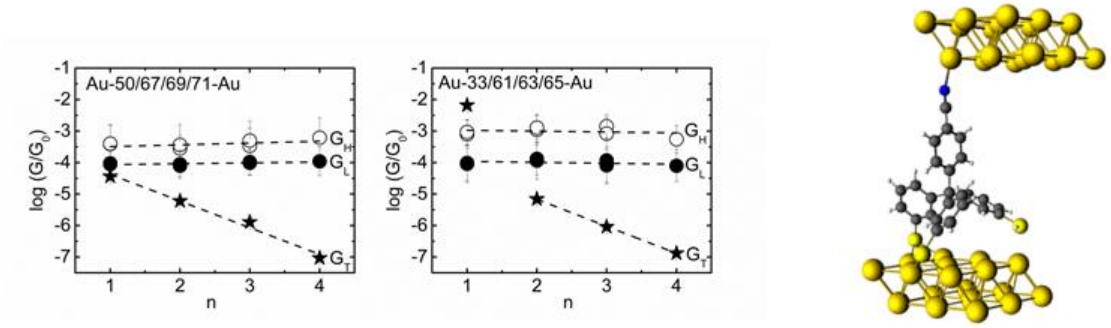

Figure 51 Molecular conductance as a function of *n* shown for *meta*- **50**, **67**, **69**, **71** (left panel) and *para*- **33**, **61**, **63**, **65** (middle panel) series of nitrile terminated molecules. Right panel shows molecular junction of meta- **50** as an example considered in the theoretical calculations.

This is most likely due to the proximity of molecular orbitals within theoretical calculation, causing an overestimation of the G_T value. Importantly, for $n \geq 2$ in both series, experimentally obtained molecular conductance values are systematically higher than theoretical predictions, which follow a clear exponential decay. The latter is a signature of electron tunnelling mechanism. Interestingly, the values of G_H and G_L are virtually independent of *n*. This independence indicates that the electron hopping might be the dominant mechanism of charge transport through the molecules. To confirm the latter, temperature resolved conductance measurements were carried out. However, they showed that the junction conductance is independent of temperature for both series of nitrile terminated molecules (see Figure 5**2**), ruling out the possibility of the electron hopping.

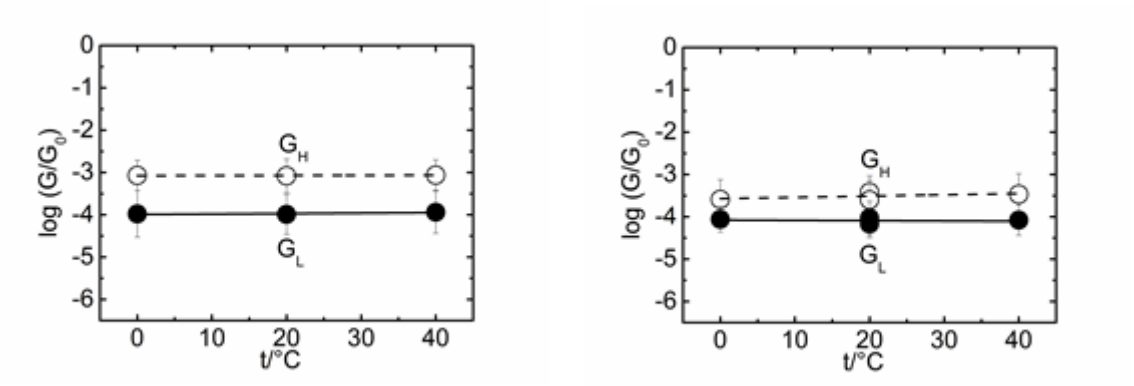

Figure 52 Molecular conductance as a function of temperature for *meta*- **69** (left panel) and *para*- **63** (right panel). For both molecules any relation between increasing of temperature and the increment of conductivity was found. This trend is common attribute of electron tunneling through the whole molecule.

The electron tunnelling is most likely the operative charge transport mechanism, despite the length independence of the molecular conductance. Molecular junctions attain only relatively high conductance states that break thermally and fully elongated molecular junctions are never reached.[326] This is corroborated by the fact that experimentally obtained molecular junction length values (Δz_{exp}) are (for $n \geq 2$) systematically lower than corresponding theoretical predictions (L_m) (Figure **53**). Nevertheless, Δz_{exp} values slightly increase with increasing *n* (the effect being more pronounced for *meta*- molecules), confirming that the principal molecular axis is involved in the charge transport through the molecule.

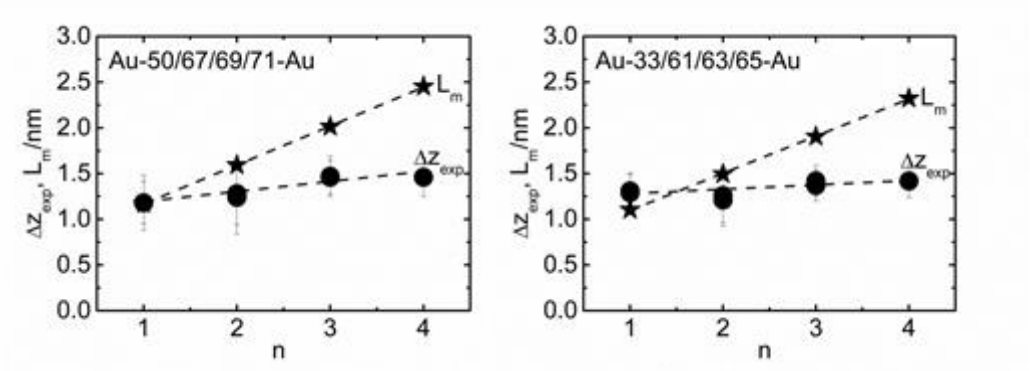

Figure 53 Theoretically predicted (L_m) and experimentally obtained (Δz_{exp}) molecular junction length as a function of *n* shown for *meta*- (left panel) and *para*- (right panel) series of nitrile terminated molecules **50**, **67**, **69**, **71** (meta) and **33**, **61**, **63**, **65** (para).

Figure **54** shows 1D (left panels), 2D (middle panels) and molecular plateau length (right

panels) histogram for the phenyl (n = 1, upper panels) and the quaterphenyl (n = 4, lower panels) member of the *meta*- molecules terminated by the thioacetate group at the top. The shortest member of the series shows only one conductance feature (G_H), while all longer three homologues (n = 2) show an additional feature at lower conductance values (G_L). The latter is assigned to the charge transport through the top thiol group. The G_H feature most likely stems from the charge transport via arms of the tripod. The same conclusions were drawn for the *para*- series of thiol terminated molecules (data not shown). For molecules possessing *meta*-tripodal platforms the experimentally obtained values of G_L are in a very good agreement with theoretical predictions (Figure. **55**, left panel). Both G_L and G_T values decrease exponentially with molecular length, confirming the operation of the electron tunneling through the molecule. For *para*- tripod based molecules, the G_L and G_T values differ by one to two orders of magnitude, but the same data trend may be noticed. While theoretically predicted junction conductance decreases strictly exponentially with the number of repeating units, certain scattering in the experimental data may be noticed. This is most likely caused by higher variation of geometric configurations of *para*- tripod attached to the gold electrode compared to the *meta*- tripod. Variation of configurations possibly decreases the electronic coupling between the molecule and the electrode, which may explain lower experimentally found conductance values compared to theoretical predictions.

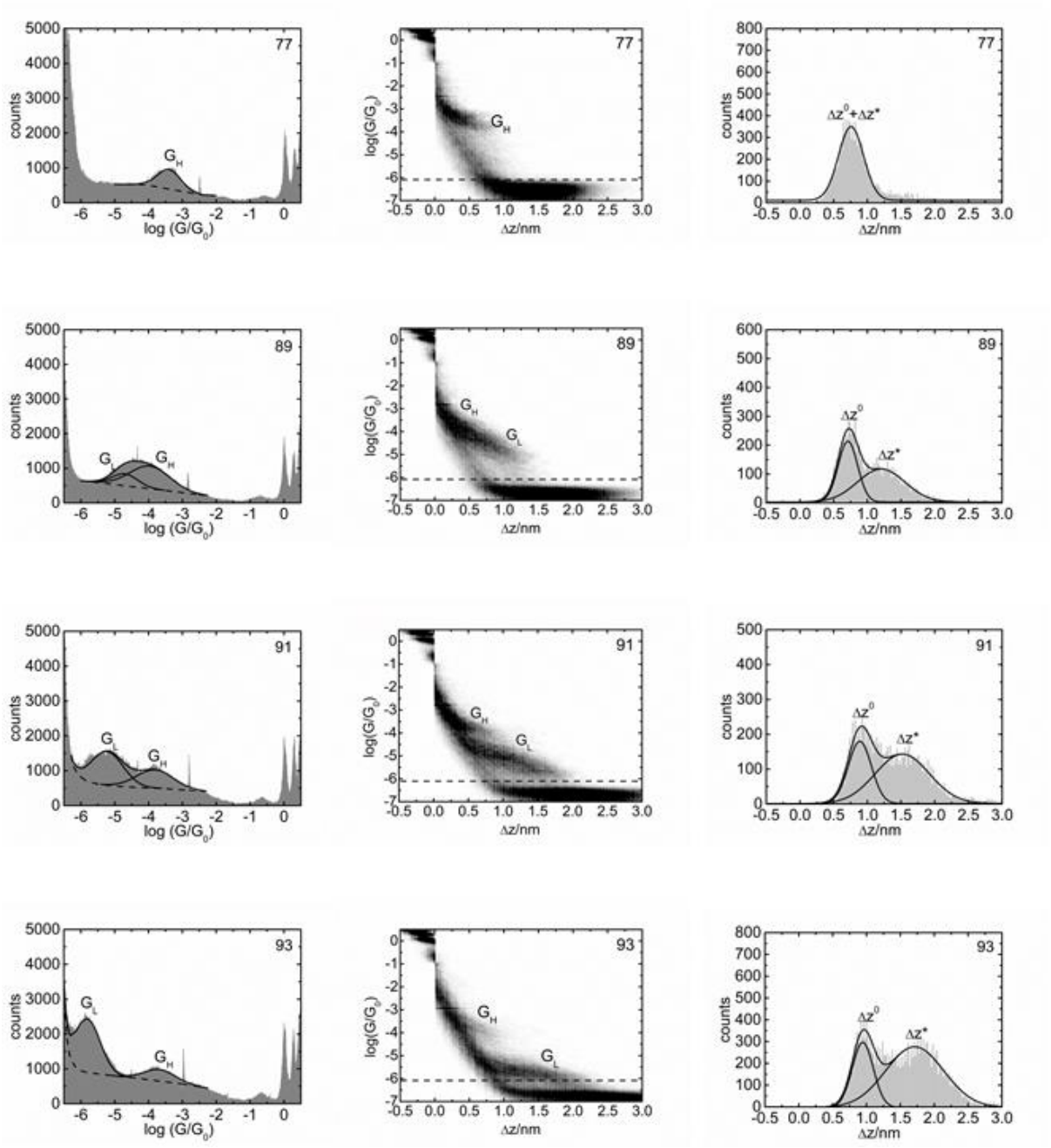

Figure 54 1D (left panels), 2D (middle panels) and molecular plateau length (right panels) histogram for the shortest phenyl (n = 1, first raw), biphenyl (n = 2, second raw), quaterphenyl (n = 3, first raw) and the quaterphenyl (n = 4, fourth raw) member of the *meta*-molecules terminated by the thiol group at the top.

The independence of G_H values on n indicates that this feature is indeed related to the charge transport through the arms of the tripod. Such molecular junction configurations were observed in early stages of their evolution (for molecules with $n \geq 2$) and were followed by configurations corresponding to the G_L region, where the charge transport through the top thiol group takes place.

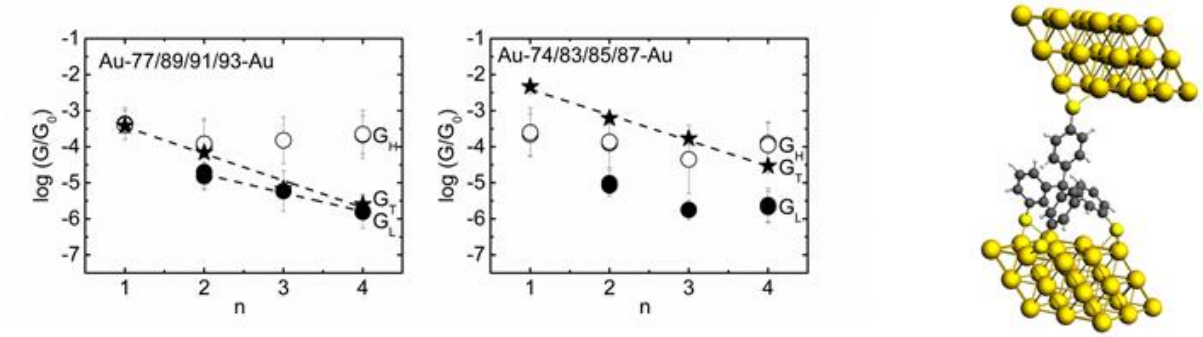

Figure 55 Molecular conductance as a function of n shown for *meta*- **77**, **89**, **91**, **93** (left panel) and *para*- **74**, **83**, **85**, **87**(right panel) series of thiol terminated molecules. Right panel shows molecular junction of meta-**77** as an example considered in the theoretical calculations.

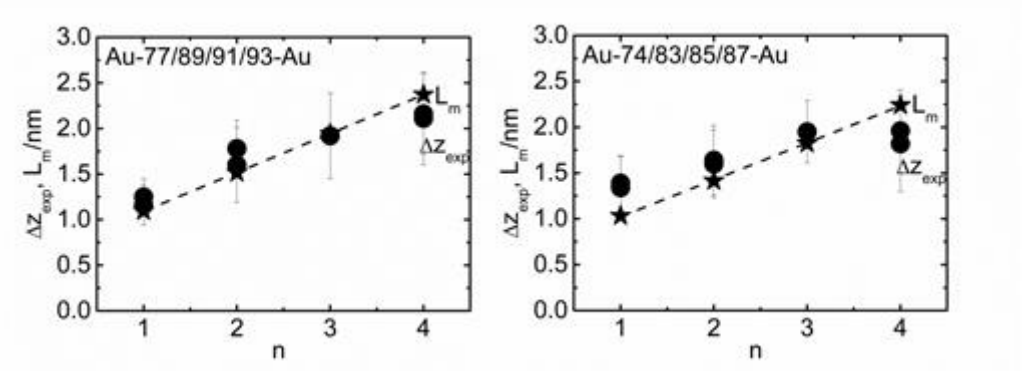

Figure 56 Theoretically predicted (L_m) and experimentally obtained (Δz_{exp}) molecular junction length as a function of *n* shown for meta- **77**, **89**, **91**, **93** (left panel) and *para*- **74**, **83**, **85**, **87** (right panel) series of thiol terminated molecules.

For both *meta*- and *para*- thiol terminated molecules, theoretically predicted and experimentally obtained molecular junction length values are in a very good agreement, as demonstrated in Figure **56**. This confirms that the top thiol group is involved in the charge transport through the molecule, in junction configurations corresponding to the G_L state. Unlike nitrile terminated molecules, fully elongated molecular junctions are formed and broken by force exerted by the tip during its retraction.

3.5 Conclusions

Self-assembly behavior of the modular platforms presented in the chapter **2**, namely **33** and **50** has been investigated in different coverage and preparation regimes through a variety of experimental techniques, including low temperature UHV-STM, HRXPS, NEXAFS spectroscopy, and reductive voltammetry desorption experiments. The experimental data obtained from the different techniques, and above all, the predominant thiolate signal in the S 2p XP spectra, suggest consistently that the adsorption of the *meta* substituted model compound **50** on Au(111) by the standard immersion procedure results in the formation of a well-defined SAM-like film with the majority of its constituents attached with all three legs to the gold surface. Other findings supporting a monolayer character for this compound are the intensity of the Au $4f_{7/2}$ HR XPS signal, the UHV-STM data, the N1s XP data, and the results of the electrochemical experiments. This interpretation was also supported by the N K-edge NEXAFS data, suggesting an upright orientation for the nitrile groups in **50**/Au. Sub-mono layer samples prepared by spraying solutions of the **50** into the UHV showed parallel rows of paired molecules at the gold step edges in the STM analysis, which allowed experiments of the dimensions of the deposited molecules. The observations for the regioisomer **33** with the thiol anchor groups in the *para* position suggest the formation of molecular multilayers, with a lower degree of orientational order, in comparison with **50**. The multilayer nature of these films is reflected in their thickness, as follows from the analysis of the intensity of the Au $4f_{7/2}$ HRXPS signal as well as from the insulated character of these films as observed in the UHV-STM experiments. A large fraction of the unbound docking groups was observed in the S2p XP spectrum, and no preferred orientation of the nitrile group was found in the NEXAFS data. However, deposited as a sub-monolayer in the UHV-STM experiment, large ordered domains consisting of molecules ordered in hexagonal tiles were observed. Although the experiment does not allow conclusions concerning the orientation of the molecule at the surface, the dimensions of the molecular footprint were obtained. Single- molecule conductance was measured for both tripodal molecules **33** and **50** through STM break junction experiments. Comparable values were obtained, which might point to the central sp^3-hybridized C atom as the structural feature controlling the electronic coupling irrespectively of the connection of the structure to the substrate.

Furthermore, over the course of the surface deposition investigated by low-T STM, we have shown that for tetraphenylmethane **33**, owing to four C_{sp3}-C_{Ar} bonds, six stable conformational isomers may exist in the adsorbed state. With the STM tip we are able to

induce a fully reversible switching. The population of these states, which is related to their energies via Boltzmann statistics, was found to minutely depend on the surface and subsurface atomic configuration of the substrate. Moreover, the chirality of the neighboring molecules has been shown to interact with each other, probably via 9 steric hindrances of the phenyl rings. This emphasizes the crucial role that is played by the local chemical and physical environment of a single molecule adsorbed on a surface. However, this phenomenon is still to be investigated.

To study the dimensionality of the deposited structure a first crop of nitrile terminated tower shape molecules (**61**, **63**, **65**) were deposited onto Au (111) surface and preliminary explored. Interestingly - with the currently used deposition method - all these tower-shaped structures are laying on the substrate exposing acetyl protected thiol groups. We have shown that we are able to remove locally the exposed acetyl-protection group by a voltage pulse applied by the STM tip. This STM based molecular manipulation is to the best of our knowledge the first reported room temperature stable "writing" at the nanoscale.

Various numbers of aromatic rings mounted to the core structure, decorated by nitrile and -thioacetate active-tail moieties were suitable for STM-BJ experiments. Therefore, all homologues of molecules containing *meta*- and *para*- regioisomeric tripods were found to form molecular junctions between two gold electrodes. Charge transport through the molecules was found to decisively depend on the character of the top anchoring group (nitrile or thioacetate). This clearly indicates that molecular junctions are broken at the top side of the molecule, confirming the chemical and mechanical robustness of the both *meta*- and *para*-tripods. While nitrile capped derivatives form highly conductive but not stable molecular junctions that break thermally, thiol terminated molecules are capable of forming fully elongated junctions that break mechanically by the probe retraction. Thiol terminated molecules were further found to show an additional molecular feature, the conductance of which is nearly independent of the molecular length. This feature was assigned to the charge transport through the legs of the tripod in the early stages of the molecular junction evolution. Importantly, thiol capped homologues of *meta*- and *para*- tripodal platforms were found to show junction characteristics that are in a very good agreement with theoretical predictions, pointing to the favourable attachment of this newly designed platform to the gold electrode. In all *meta*- and *para*-, nitrile and thioacetate – tailor-made molecules, electron tunnelling was found to be the dominant charge transport mechanism, corroborated by the observed temperature independence of the transport measurements.

4 Porous organic polymers

This Chapter described results on synthetic methodologies used for the preparation of imine-linked 3D porous organic frameworks comprised of tetraphenylmethane core and the most important analytical techniques employed for characterization of this new covalent organic framework. (COF)

4.1 Synthesis of monomer for polymerization

4.1.1 Molecular Design

The three dimensional topology of organic molecules with available internal cavities has gained particular attention due to the number of potential applications. Diamond-type network could be essentially obtained from tetrahedral components, thus affording porous material with well-defined tetragonal shape. Nevertheless, the design and selection of the right building block, which combines the required geometry with readily availability by utilization of modern tools of organic chemistry has still remained a challenge. Broadly discussed (in this thesis) a tetraphenylmethane node was adapted to the following project. A central sp^3-hybridized carbon atom decorated with four aromatic rings shall provide precise control of the geometry of synthesized material. Chemical modification at the *para*-position of each aromatic ring gives the opportunity to promote the assembly towards highly ordered, covalent material. We were particularly interested in monomers appropriate for further polymerization by reversible imine condensation reactions. [327]

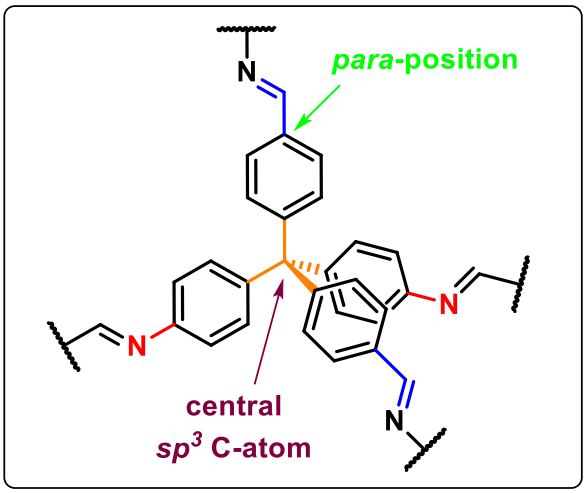

Figure 57 Molecular design of proposed 3D polymeric tetrahedral framework that comprises central sp^3 carbon atom (indicated by purple arrow). Green arrow pinpoints the *para* position of aromatic rings whereas tetraphenylmethane is terminated with amine and aldehyde groups.

Up to date, only homoleptic monomers have been reported, which showed formation of covalent organic frameworks (COFs) composed on four times terminated tetrakis(4-aminophenyl)methane and various aldehyde linkers.[248] This class of materials exhibit excellent permanent intrinsic porosity and narrow pore distribution which can be tuned by the length of linkers. Thus, the shorter connector is used, the better porosity may be expectably

reached. To the best of our knowledge, there is only one reported prominent example of molecular system based on tetraphenylmethane skeleton that forms COFs, profiting from boroxine condensation of (methanetetrayltetra-4,1-phenylene)tetraboronic acid.[125] Therefore, our novel approach is based on the synthesis of the first linker free, 3D Schiff base polymer that contains solely light elements (C, H, and N). This time, we designed monomer combining two amine FGs (red bond) and two formyl FGs (blue bond) attached symmetrically to tetraphenylmethane core (see Figure **57**). These should be prospectively an ideal candidate to undergo [2+2] self-polymerization toward imine-bonded material, reducing to the minimum the spacing among adjacent tetraphenylmethane components.

4.1.2 Retrosynthetic analysis

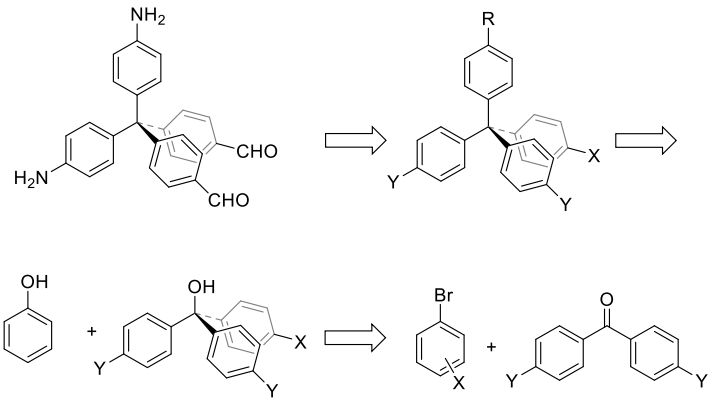

Figure 58 Retrosynthetic analysis of tetraphenylmethane monomer for the formation of COF.

Synthesis of tetraphenylmethane core structure runs smoothly in most cases irrespectively of the electronic nature of functional groups as well as position of the substituents located in each of aromatic rings attached to sp^3-hybridized central carbon atom. What is noteworthy, there was no advantage that could be taken up from the known literature procedures dealing with the synthesis of doubly substituted tetraphenylmethane entities. Thereupon, considerable efforts were developed to assemble synthetic protocols for the synthesis of tetragonal nodes featured with two different functional groups. Considering previously combined experience (see Chapter **2** dealing with chemistry of molecular tripods), synthetic pathways in all presented instances start from benzophenone (displayed on Figure **58**), which undergoes smooth addition of metalorganic species and consecutively leads to the construction of trityl alcohol. In the next step, Friedel-Crafts reaction delineates the path to obtain tetragonal building blocks. Synthetic transformations based on the broad scope of palladium-catalyzed reactions allow the synthesis of monomer that is capable of imine self-condensation.

4.1.3 Synthesis, results and discussion

In order to synthesize the target monomer **125** several approaches were proposed. In the first synthetic approach we assumed to start the synthesis from the building block, which contains masked amine group (in a form of imine). This would allow to introduce formyl groups within few transformations and gives the desired product in a simple manner. Therefore, the first synthetic strategy started from commercially available 4, 4'-diaminodiphenylmethane as outlined in Scheme **13**. The synthesis started with $TiCl_4$-DABCO mediated dehydration[328] of amine with benzophenone to form imine **94** in 90% yield. This bulky protecting group is stable enough against mild acidic conditions (therefore its purification onto silica gel becomes possible), oxidizing agents and, notably, is resistant against organometallic nucleophilic reagents. Therefore, oxidation of diphenylmethane derivative **94** proceeded cleanly in the presence of $KMnO_4$ and TBAB to form benzophenone **95** in 82% yield. Subsequent nucleophilic addition of monolithiated 1,4-dibromobenzene to carbonyl group provided trityl alcohol TrOH **96** in 86% yield.

Scheme 13 The first attempt to the synthesis of target **126** from symmetric amine precursor.

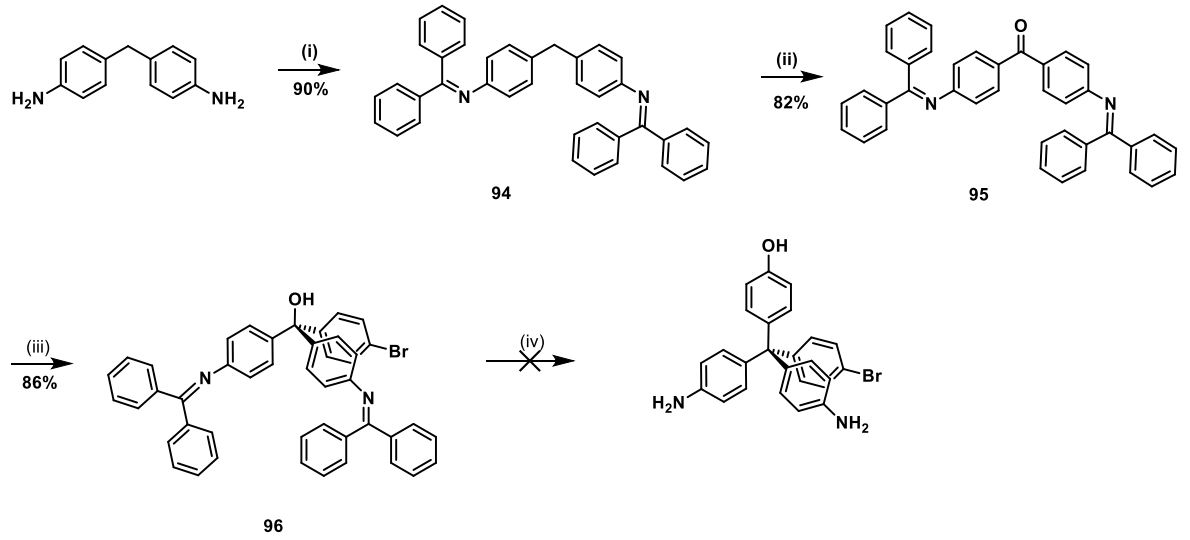

Reagents and conditions: (i) benzophenone, $TiCl_4$, DABCO, PhCl; (ii) $KMnO_4$, TBAB, 1,2-dichloroethane; (iii) 1,4-dibromobenzene, *n*-BuLi, THF; (iv) PhOH, HCl, toluene

Unfortunately, subsequent acid catalyzed Friedel-Crafts alkylation of phenol with trityl alcohol **96** did not afford the target tetraphenylmethane derivative compound - precursor of target monomer **126** - presumably due to acid-catalyzed deprotection of imines.

The results of the first failed approach, suggested to introduce the amine group rather in one of the final steps of the proposed synthetic strategy. Therefore, we decided to prepare symmetric intermediate that is initially functionalized with two formyl groups ready for further functionalization with two amine moieties, what is presented in Scheme **14**. Towards this strategy, 4,4'-dimethoxybenzophenone was acquired and subjected to the nucleophilic addition in a similar fashion as described above, thus giving trityl alcohol **97** (96% yield). Consecutive Friedel-Crafts alkylation with phenol in the molten state allows to attain tetragonal species **98** in 63% yield. Consecutively, synthesized phenol moiety **98** was esterified with triflic anhydride to afford triflate **99** in 93% yield. Both bromide and triflate leaving groups were transformed *via* the palladium-catalyzed cyanation to the corresponding nitrile **100** in 98% yield. Its reduction with DIBAL-H solution in THF at low temperature let to dialdehyde **101** in 46% yield. In the next synthetic step we intended to convert compound **101** into corresponding phenol. The cleavage of methyl ether is usually done with BBr_3, however the aldehyde is not compatible with this reagent and could be transformed to the undesired carboxylic acid.

Scheme 14 Alternative route to the target molecule via dialdehyde **101** scaffold.

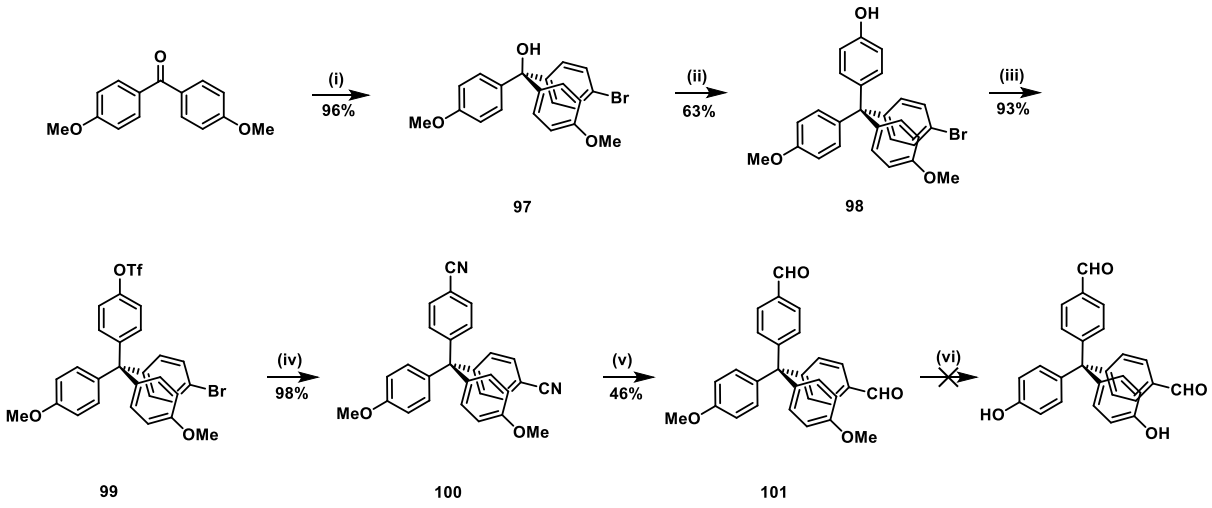

Reagents and conditions: (i) 1,4-dibromobenzene, *n*-BuLi, THF; (ii) PhOH, HCl; (iii) Et_3N, Tf_2O; CH_2Cl_2; (iv) $Zn(CN)_2$, CuCN, $Pd(PPh_3)_4$, DMF; (v) DIBAL-H, THF; (vi) *n*-octanthiol, NMP

Considering the application of an alternative cleavage agent that is capable of mild demethylation in the presence of aldehydes, we employed cleavage of methyl ether under reported conditions [329,330,331], where 1-octanethiol in NMP was used for demethylation of

broad array of examined molecules, successfully providing phenol derivatives from moderate up to excellent yields. Consequently, starting material **101** was heated overnight under inert atmosphere at 200°C. Nevertheless, inseparable mixture of products was obtained, thus described method did not cleanly afford to get the desired product and other synthetic approach had to be considered.

Scheme 15 Alternative strategy via dihalogeneted species **107**, **113**

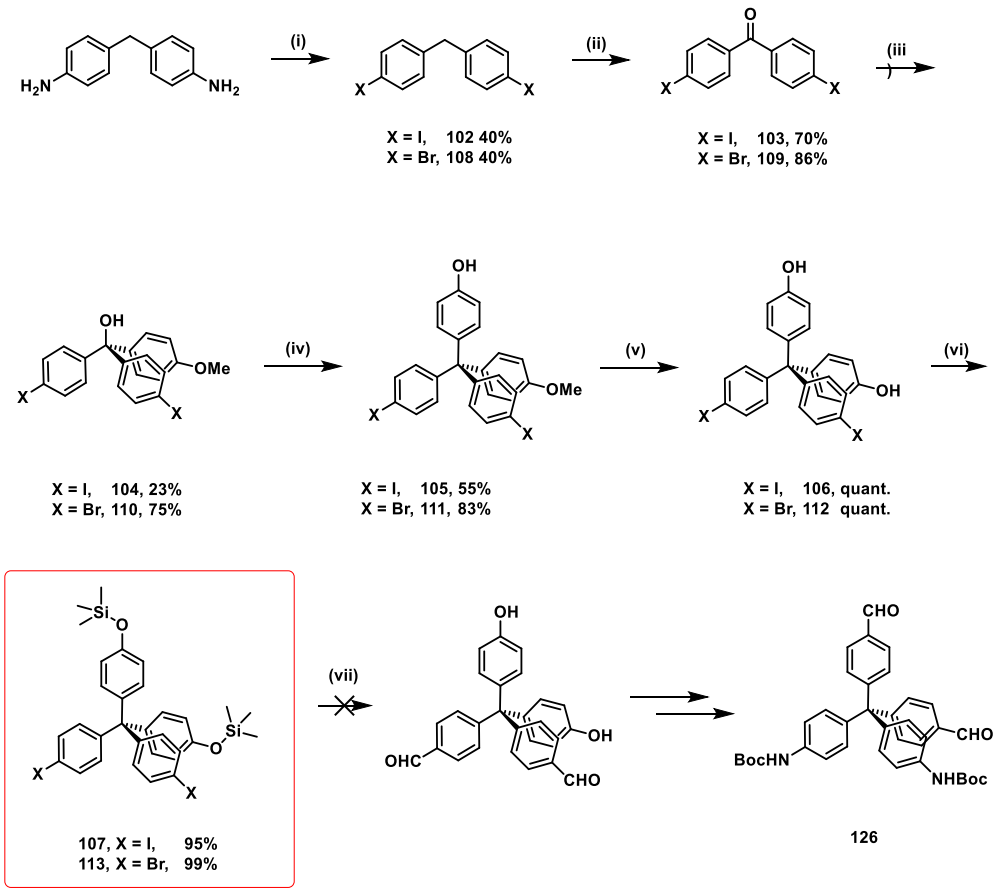

Reagents and conditions: For **X** = **I**: (i) $H_2SO_{4(conc).}$, $NaNO_2$, KI, I_2, H_2O; For **X** = **I**: $HBr_.$, $NaNO_2$, CuBr, H_2O; (ii) CrO_3, AcOH, H_2O; (iii) *p*-bromoanisole, *n*-BuLi, THF; (iv) PhOH, HCl; (v) BBr_3, CH_2Cl_2; (vi) TMSCl, Et_3N, Et_2O; (vii) *n*-BuLi, DMF, THF.

Alternative pathway for the synthesis of functionalized tetraphenylmethane, based on well-established halogen-metal exchange reaction of halogenated derivative followed by electrophilic quenching with DMF is outlined in Scheme **15**. New strategy employs diiodinated and dibrominated tetraphenylmethanes **107** and **113** as the main synthetic intermediates in the presence of protected phenolic groups that would allow the subsequent conversion to the *Boc*-protected amine derivative **125**. Regarding this, syntheses of

diiodinated and dibrominated species were initiated from the commercially available 4,4'-diaminodiphenylmethane building block and are shown on Scheme **15**. Diazotation with concentrated sulphuric acid and sodium nitrite as well as it further iodination with iodine and sodium iodide (Sandmayer reaction) lead to the crude product, which was purified on silica gel, giving 4 4'-diiododiphenylmethane **102** in 40% yield. Analogously, product **108** was obtained using Sandmayer reaction with the same efficiency.[332] Consequently, both iodinated and brominated species **102** and **109** were clearly oxidized by CrO_3 to corresponding benzophenones **103** and **109** (70% and 86% yield respectively).[333] Simplicity of this reaction allowed for up scalable synthesis of benzophenones even up to 5g. In the next step, commercially available *p*-bromoanisole was lithiated and further reacted with dry benzophenone **103** to give trityl alcohol **104**, unfortunately in a very poor yield (23%). The reason for this may be extremely low solubility of the benzophenone **103** in THF (great amounts of starting material were recovered) as well as the nature of carbon-iodine bond itself. It could be due to the high lability of the C_{Ar}-I bond, therefore *trans*-metalation might occur, being competitive against desired nucleophilic addition, what could sufficiently reduce the yield of obtained trityl alcohol **104**. We did not observe this problem during the synthesis of brominated analogue **110**. Halogen-metal exchange reaction led to obtain triphenylmethanol derivative **110** in 75% yield. Nonetheless, isolated amount of **104** was sufficient to employ Friedel-Crafts alkylation with phenol to get tetraphenylmethane derivative **105** in 55% yield. Similarly, bromo decorated species **111** was synthesized in 83% yield. The next reaction with the excess of BBr_3 in dry dichloromethane allows to reach diiodinated phenol **106** quantitatively. Dibrominated diol **112** was isolated quantitatively as well. Subsequently, phenol derivatives **106** and **112** were consequently protected as silyl ethers (TMS) providing **107** in 95% yield and **113** in 99% yield. Several reactions to perform lithiation of protected **107** and its reaction with DMF to the crucial aldehyde were made. Both halogen-decorated key building blocks **107** and **113** were reacted with an excess of *n*-BuLi or *tert*-BuLi and quenched with an excess of dry DMF. Nevertheless, independently from applied organometallic reagent, we observed a number of side products and this was noticed when we controlled the progress of reactions by means of TLC. These findings can be explained in the following manner. Under the applied reaction conditions aryl silyl ethers are prone to undergo directed *ortho* methalation,[334] which apparently runs faster than lithiation of aryl halides (**107** or **113**). As a result, selective synthesis of the desired product was not possible.

After many unsuccessful attempts to prepare the target monomer **125** for the final polymerization, we decided to change the synthetic strategy, which is now based on the synthesis of tetraphenylmethane derivative **117**. The latter bears two different leaving groups that allow us to control the regioselective introduction of the amino and aldehyde moieties in the final steps. Thus, the synthetic protocol outlined in Scheme **17**, has been developed to obtain the key intermediate **117** for the preparation of the target compound **125**. The synthesis started from 4,4‘-dichlorobenzophenone, which reacted with an excess of lithiated *p*-bromoanisole to afford trityl alcohol **114** in 99% yield. Consecutively, Friedel-Crafts alkylation with phenol provided tetraphenylmethane **115** in 74% yield. Subsequent demethylation with BBr_3 gave almost quantitatively diol **116**, which was then triflatated with triflic anhydride. The corresponding ditriflate **117** was isolated in 93% yield. The first approach to accomplish the synthesis of the desired compound **125** *via* chemoselective lithiation of **119** or **120** is described in Scheme **17**. The key intermediate **117** was subjected to Miyaura borylation providing selectively boronic ester **118** in 91% yield. Subsequent halogenation led to dichlorodihalo tetraphenylmethane scaffold **119** in 73% yield and **120** in 78% yield. Both derivatives **119** and **120** were thus reacted with organometallic agents (*n*-BuLi, to the next attempts we employed *tert*-BuLi and “Turbo Grignard” reagent[335]) to accomplish halogen-metal exchange reaction. Lithiated tetraphenylmethane was then quenched with DMF to introduce aldehyde to the skeleton of tetraphenylmethane. However, attempts of chromatographic purification of the crude material turned out to be unsuccessful (we think that for both derivatives, main products were scarcely soluble polymers, therefore we could not elute these materials from the chromatographic column). It was reasoned that newly formed aldehyde immediately reacted with lithiated species or, coupling of lithiated species occurred; both processes would lead to polymeric material.

Scheme 16 Synthesis of the key intermediate **117**.

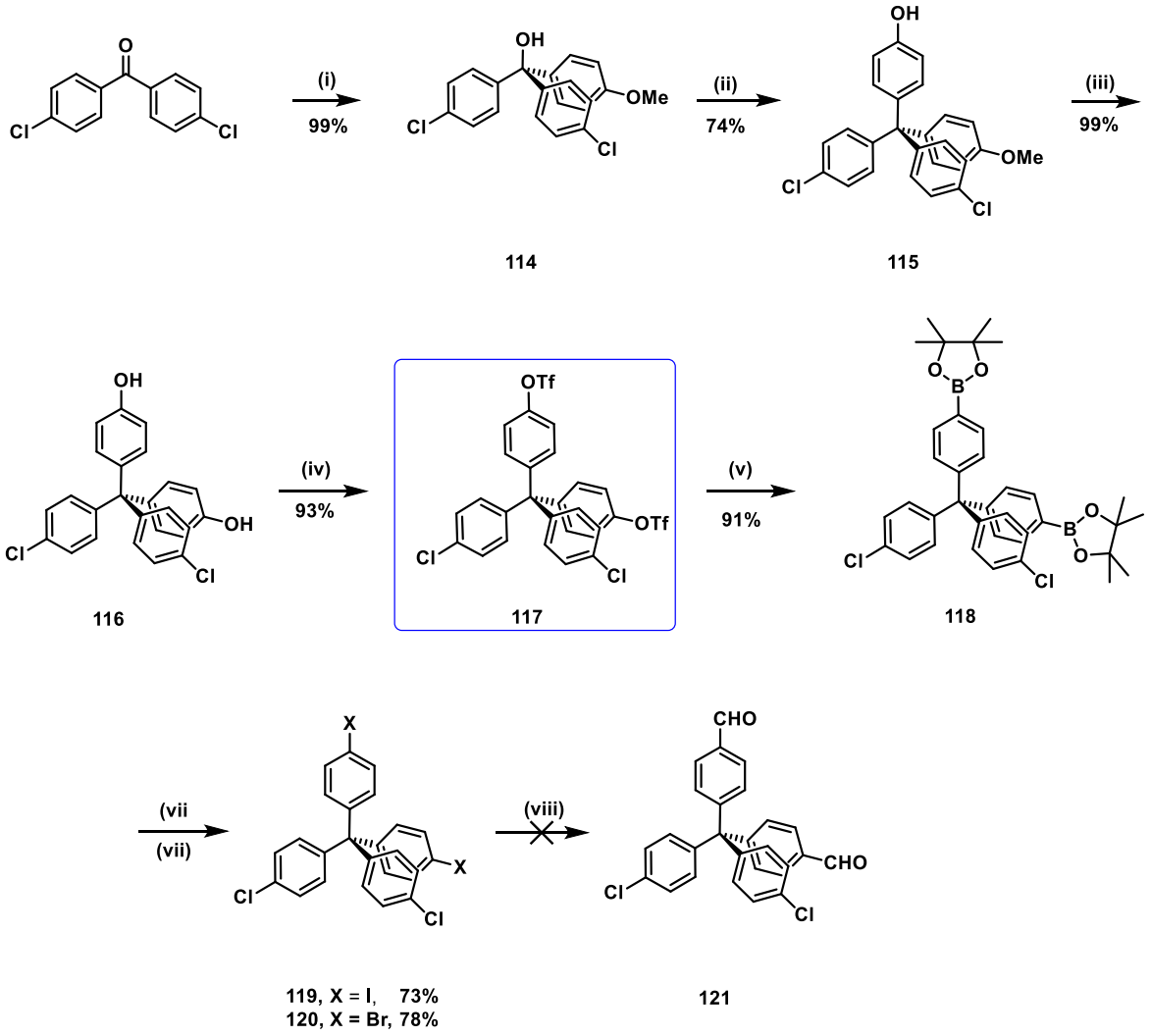

Reagents and conditions: (i) *p*-bromoanisole, *n*-BuLi, THF; (ii) PhOH, HCl; (iii) BBr_3, CH_2Cl_2; (iv) Et_3N, Tf_2O, CH_2Cl_2; (v) bis(pinacolato)diboron, $Pd(dppf)Cl_2$, KOAc, dioxane; (vi) CuI, NIS, toluene, DMF; (vii) CuBr, NBS, toluene, DMF; (vii) *n*-BuLi, DMF, THF.

When the synthetic methodology based on direct formylation of dichlorodihalo tetraphenylmethane derivatives **119** and **120** failed, we finally used the strategy outlined in Scheme **18**, which allowed us to successfully synthesize key component of the project: **125**. Crucial ditriflate **117** was converted to aldehyde terminated species **121**. This would afford insertion of *Boc*-protected amine in the one of the next synthetic steps and thus give the desired monomer **125** in a simple manner. First transformation that involved *palladium*-catalyzed cyanation of triflate **117** led to the synthesis of the nitrile terminated species **122** in 98% yield. In the next step nitrile **122** had to be reduced by DIBAL-H to enable formation of dialdehyde **121**. The tools of classic organic chemistry imply to carry out reduction of nitrile

by means of DIBAL-H at low temperature to avoid side products, stemming from post-reduction toward benzylic amine. Surprisingly, in THF and the temperature ranging from -78°C up to -20°C the nitrile derivative **122** did not interact with reducing agent and it was mainly the starting material that was recovered. Only when the reaction was conducted at 0°C, application of DIBAL-H allowed to obtain compound **121** in 65% yield.

Scheme 17 Successful synthesis of the monomer **125**.

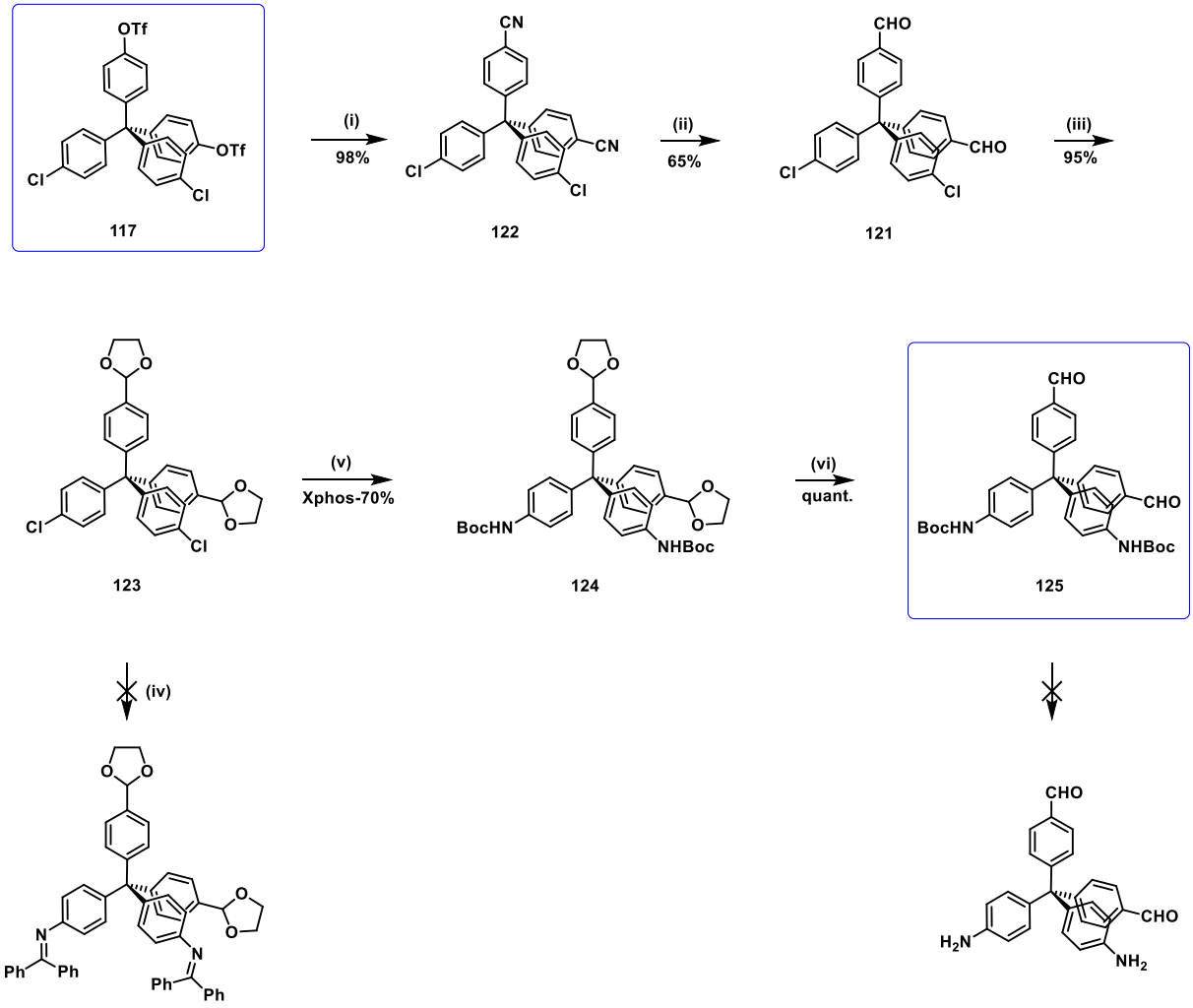

Reagents and conditions: (i) $Zn(CN)_2$, CuCN, $Pd(PPh_3)_4$, DMF; (ii) DIBAL-H, THF; (iii) ethylene glycol, *p*-TSA, toluene; (iv) benzophenone aldimine, $Ni(cod)_2$, BINAP, Cs_2CO_3, dioxane; (v) NHBoc, $Pd(OAc)_2$, SPhos or XPhos, Cs_2CO_3, dioxane; (vi) EtOAc, HCl.

Subsequently, the protection of aldehydes was carried out with ethylene glycol over the course of three days and gave 1,3-dioxalan derivative **123** almost quantitatively (95% yield). Such masked aldehyde **123** was subjected to catalytic amination. This key synthetic step was

carried out initially using *SPhos* (structure of used ligands are shown in Figure **59**) as a phosphine ligand (yield = 50%), nonetheless it was reported that utilization of *XPhos* can improve the yield of the reaction considerably. Therefore, upon applying *XPhos* we observed formation of product **126** in 70% yield.[336] (it should be noted as well, that we performed Buchwald amination under reported condition for aryl chlorides and we did not observed any progress of the reaction, isolating solely starting material **125**).[337]

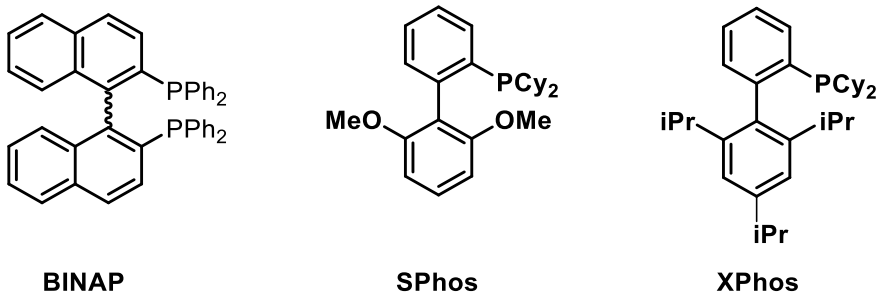

Figure 59 Phosphine ligands applied for catalytic amination.

In the last two synthetic steps, we planned to selectively deprotect acetal and carbamate groups, thus leading to the aldehyde and amine functionalized tetraphenylmethane that is suitable for *self*-condensation. The deprotection of 1,3-dioxalan terminated derivative **124** provided compound **125** quantitatively (the *Boc* protected amine stayed intact). As we discussed before, *Boc*-protected amine should be deprotected before polymerization. In order to employ relatively mild method for the cleavage of Boc, which would selectively provide monomer (bis(4-aminophenyl)-bis(4'-formylphenyl)methane), we decided to use method which is commonly utilized in protein chemistry and involves TFA as the cleaving agent. Therefore, TFA in dry dichloromethane was employed to hydrolyze carbamate **125**.[338] However we did not observe formation of the desired monomer, yielding flake-like material that was insoluble in common organic solvents. This can be explained in the following manner. First of the amine group is deprotected, but it forms the imine bond faster than deprotection of the second Boc-protected amine takes place, thus disfavoring isolation of bis(4-aminophenyl)-bis(4'-formylphenyl)methane as intermediate suitable for it direct polymerization. In view of the above results, we decided to apply acid free conditions, which can afford the synthesis of the desired monomer and its further polymerization in controllable way. A very few methods dealing with inorganic bases, which are able to catalyze deprotection of *Boc*-protected amine were reported. Therefore, sodium *tert*-butoxide in anhydrous THF[339], potassium phosphate in dry MeOH[340] or sodium carbonate in DME[341]

were employed but unfortunately all above-mentioned reaction failed. First one did not bring any progress with the Boc deprotection and starting **125** was recycled. In the second instance we applied microwave irradiation with K_3PO_4 as cleavage agent. Unfortunately, this protocol provided mono-deprotected species, as monitored by TLC of crude reaction mixture. When the time of the reaction was prolonged the insoluble material was again isolated, which we considered to be a polymer. This outcome may again confirm our speculation that compound **127** exhibits a large inclination to undergo spontaneous polymerization, affording once again material, which is not well-defined.

Based on previous unsuccessful attempts to perform selective deprotection of compound **125** toward synthesis of bis(4-aminophenyl)-bis(4'-formylphenyl)methane, we prepared set of model, easily accessible *Boc*-protected amines (**126**, **127**). This strategy was used in order to optimize reaction conditions for thermally driven *Boc*-cleavage, which can be prospectively applied for our target, more sophisticated system. The synthesis started from commercially available *p*-phenylenediamine where mono- (**126**) or di- (**127**) protected amines were obtained, and formation of products was controlled with the stoichiometry of used di-*tert*-butyl dicarbonate. When twofold excess of starting amine was applied, *mono*-protected amine intermediate **126** was exclusively obtained in 90% yield.[342] While, utilizing of an excess of Boc_2O resulted in the synthesis of *di*-protected amine **127** in 97% yield.[343]

Scheme 18 Synthesis of short molecules **126**-**129**.

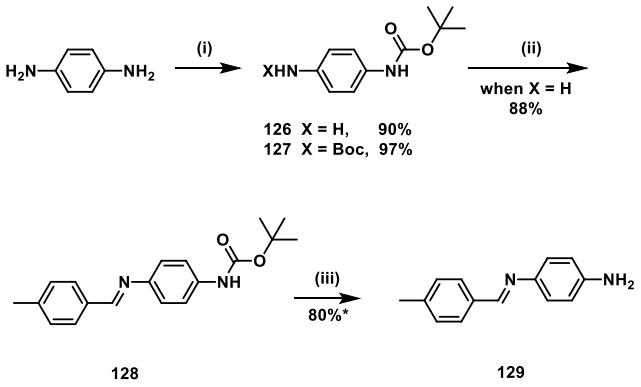

Reagents and conditions: (i) Boc_2O, CH_2Cl_2; (ii) LiCl, *p*-tolyl aldehyde, toluene; (iii) AcCl, MeOH

Compound **127** was thus used to examine thermal stability of Boc protecting group. As can be easily noticed, tested molecule **127** contains two *Boc*-protected amines, similar to previously shown **127**. The experiment in NMR tube seems to be the most effective to

determine the limiting temperature at which both *Boc*-protected amines are decarboxylated. The tube was loaded with 10 mg of **127**. It was dissolved in 0.6 mL of the deuterated DMSO (d_6). The tube was sealed and put into an oil bath to reach the required temperature. The solution was gradually heated up, starting from 155°C, increasing the temperature every hour about 10°C and the ^{1}H-NMR spectrum was measured straightforward. The progress of the reaction controlled by ^{1}H-NMR as function of temperature is presented on Figure **60**, where all spectra are stacked. It is shown that starting material **127** is stable up to 165°C, whereas at 175°C formation of mono-protected species **126** is observed. By elevating the temperature up to 185°C, we reasoned that applied protecting group was cleft providing solely *p*-phenylenediamine. This is evidenced by the lack of *tert*-Bu moiety (marked as violent dot) and the presence of broad amine protons (pink dot).

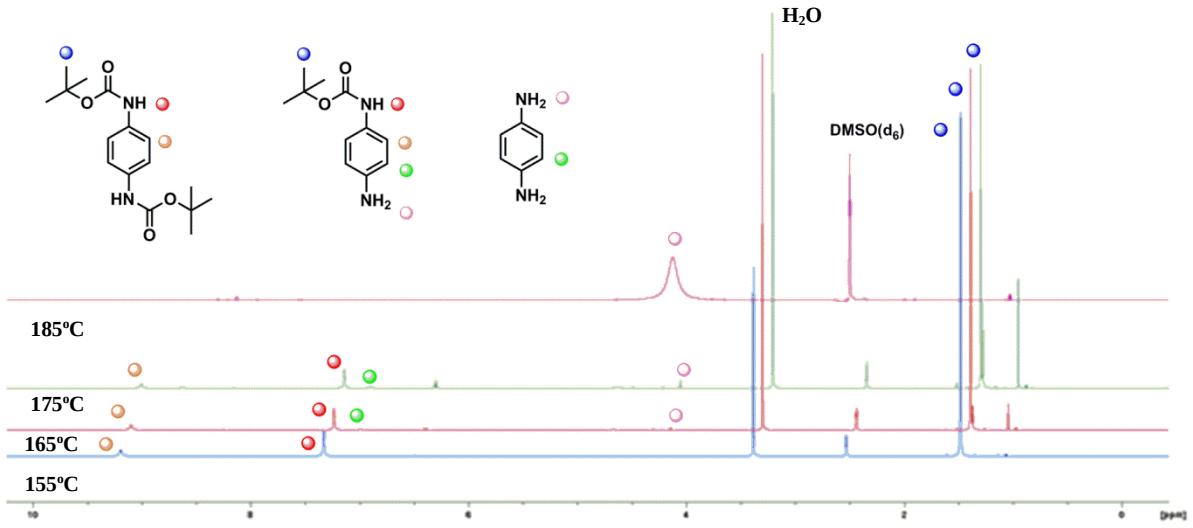

Figure 60 ^{1}H-NMR study of Boc cleavage under elevated temperature.

Considering results of NMR controlled experiment, we tried to scale up examined procedure by charging 50 mL pressure tube with our template **127**. Nonetheless, we used toluene instead of dimethyl sulfoxide as a solvent to ensure its brief removal (DMSO is unfortunately highly boiling solvent, hence to remove this solvent higher temperature has to be applied than the one needed for deprotection of Boc, what can favor rapid polymerization of compound **125**). Despite the fact that we applied the required temperature, we could not achieve the same effect as in NMR experiment, recycling every time compound **129**. These findings also suggested to modify the structure of the model compound in such a way to examine the stability of imine bond and *Boc*-protecting group under *in situ* formed HCl (this might happen during polymerization of the target system, once imine bond is formed, the second amine is

deprotected etc.) and are demonstrated on Scheme **19**. The synthesis was carried out starting from mono-protected compound **126**, which was reacted with *p*-tolyl aldehyde (LiCl was exploited as a water trapping agent) leading to imine **128** in 88% yield. Subsequently, this imine was dissolved in dry MeOH and AcCl and dropwise added to generate HCl *in situ*. This reaction afforded anticipated compound **128** in 80% yield, however the presence of the starting material was detected as well (according to the ^{1}H, ^{13}C NMR of the crude product, the **128**:**129** ratio was assessed by the integration of imine protons). Therefore we decided to reflect described strategy into our target molecule **125**. The molecule **125** was thus dissolved in a mixture of anhydrous methanol and dichloromethane (used as co-solvent) and addition of AcCl resulted in formation of HCl *in situ.* As a result of this reaction, *Boc* protecting group was removed from **125**, as expected. Indeed, applied methanol interacted with aldehydes, causing their conversion to diacetal **130**. ^{1}H-NMR spectrum of crude product **130** was compared with spectrum of the starting material **125** and is shown on Figure **61**. It is clear, that both formyl groups of the compound **125** were fully transformed to diacetal terminated species **130** and it can be explained as following. Cleavage of carbamate is recognized by the absence of methyl groups, which were marked as green spot on spectrum of compound **125** (formyl groups were marked as red dot on this spectrum). While existence of acetals is manifested by singlet that was marked as a brown dot on spectrum of the product **130** (in this case singlet of aldehydes obviously was not observed). The attempt of chromatographic purification of obtained crude material **130** resulted in its rapid polymerization. The same happened when deacetylation toward controlled synthesis of bis(4-aminophenyl)-bis(4'-formylphenyl)methane was performed, even though diluted acid was applied.

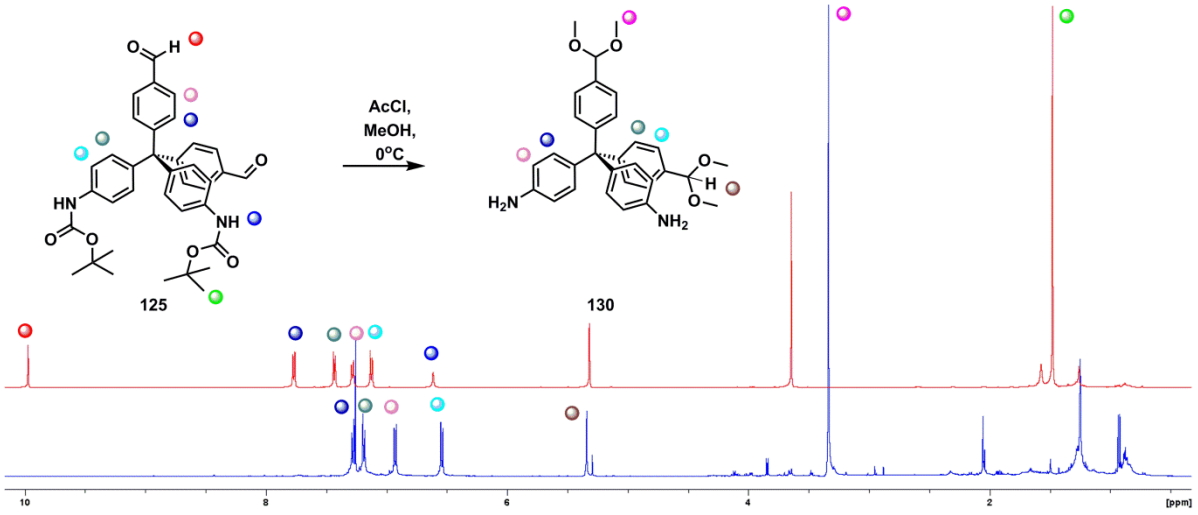

Figure 61 ^{1}H-NMR spectrum of **125** and **130**, which were measured in deuterated dichloromethane (d_2).

Profiting from so far conducted reactions and experiments we realized that compound **125** is the best candidate to be subjected to imine poly-condensation. Moreover, in order to find and optimize reaction conditions suitable for polymerization of target monomer **125**, we designed short molecular analogues of **125**. For this reason we used biphenyl skeleton tailored with *Boc*-protected amine, which is placed into *para* position of one ring as well as formyl group that is mounted on the second ring. The synthesis was accomplished in the following manner, starting from 4-iodoaniline which was protected by Boc, providing the desired carbamate **131** in moderate 60% yield (Scheme **19**).[344] Subsequently, iodinated species **131** was reacted with commercially available 4-formylbenzboronic acid leading to **132** in 64% yield.[345] Consecutively, obtained biphenyl **134,** exploited as pattern of tetraphenylmethane **125**, was subjected to the self-polymerization and this is shown in Scheme **19**. We examined three different conditions under which the formation of linear polymer became possible. Therefore, microwave driven reaction was heated up to 230°C over 1h for each sample of **132** in a mixture of *o*-1,2-dichlorobenzene/decanol (10/1), with addition of 1% AcOH/H_2O or only 1% of pure water (v/v). Upon irradiation process of all three samples, formation of yellowish gel was observed only in the first reaction setup. Thus, newly formed material was filtered, sonicated at first with hexane, afterwards with ethyl acetate to get rid of the remaining solvents. The new powder was readily analyzed by IR spectroscopy, which shows vibrations characteristic for Schiff base **133**, so the isolated

product was thus confirmed to be an imine-bonded polymer (all IR spectra will be discussed in detail in the next paragraph).

Scheme 19 Synthesis of molecular analogue **132**

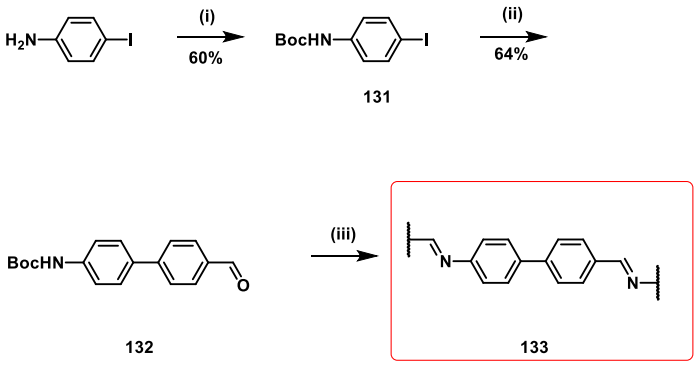

Reagents and conditions: (i) Boc_2O, Et_3N, MeOH; (ii) *p*-formylbenzboronic acid, K_2CO_3 $Pd(PPh_3)_4$, toluene, EtOH, H_2O; (iii) *o*-1,2-dichlorobenzene/decanol (10/1), 230°C.

As we discussed and proved in a previous paragraph, the conditions employed to reach linear polymer **133** can be exploited to synthesize 3D polymer (**134**), based on tetraphenylmethane core structure. The synthesis of the desired polymer was performed in an analogous manner in microwave reactor, utilizing molecule **125** as a monomer and is presented in Scheme **20**. Starting material was dissolved in a mixture of *o*-1,2-dichlorobenzene/decanol (10/1), loaded to the microwave and heated over 2h.

Scheme 20 Imine condensation of monomer **125** accelerated by microwave irradiation.

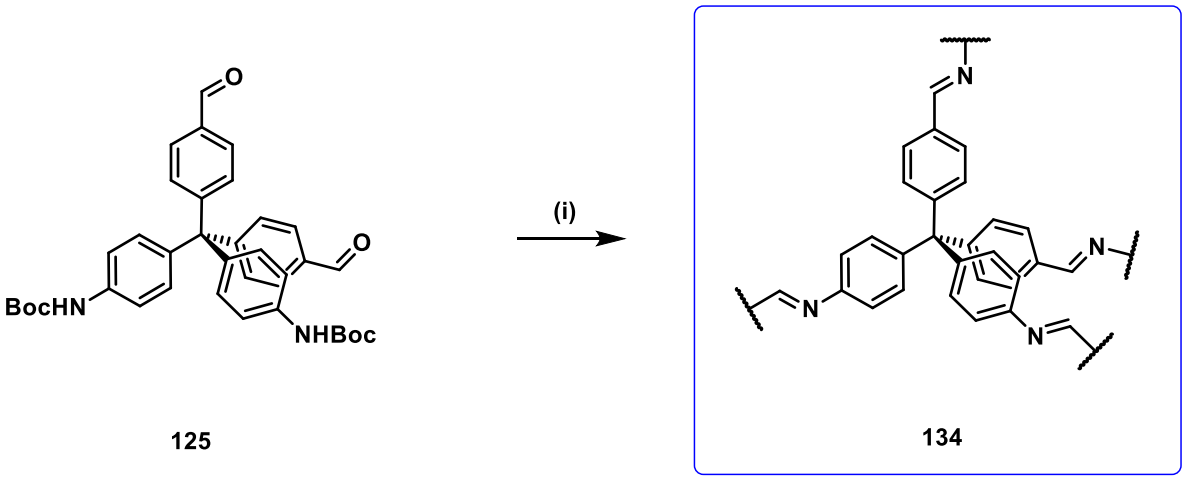

Reagents and conditions: (i) *o*-1,2-dichlorobenzene/decanol (10/1), 230°C, 2h

The yellow gel was filtered and washed well with diethyl ether, ethyl acetate and hexane. Subsequently, solid material was sonicated with diethyl ether and ethyl acetate and dried afterwards. Isolated powder was subjected to all possible and available analyses to corroborate formation of 3D polymeric structure and to get more insight in the properties of the material **134**.

4.2.1 Identification and analysis of obtained materials (133, 134)

As was aforementioned, both polymers **133** and **134** are insoluble in common organic solvents including acetone, methanol, DMF, dichloromethane or DMSO, so the X-ray powder diffraction (XPRD) is the first method of choice to confirm the nature of synthesized materials. In both instances no features of crystallinity of **133** and **134** were detected. It may be explained that presumably due to the nature of the polymerization process, which herein undergoes rapidly rather without kinetic control (contrary to solvothermal reaction) giving structurally disordered material. Next we checked the thermal stability of polymeric materials **133** and **134**. Thermogravimetric analysis TGA was made under argon atmosphere and it revealed that linear polymer **133** is stable up to 333ºC, while 3D polymer **134** exhibits thermal stability up to 517ºC, which is common for this class of polymers.[259, 261, 262]

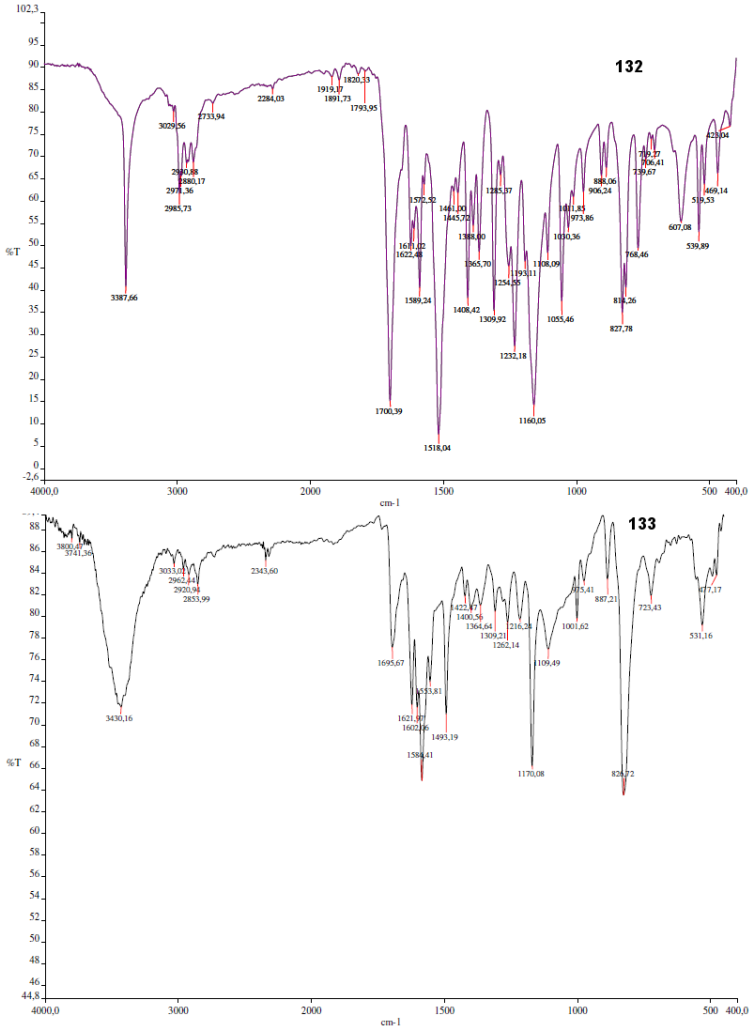

Figure 62 FT-IR spectra of monomer **132** and linear polymer **133**.

Due to insolubility of both obtained materials (**133**, **134**), powders were as well subjected to the FT-IR analysis. Owing to well-defined vibrations in organic compounds and their characteristic absorption frequencies, both monomers (**132**, **125**) and solid polymer (**133**, **134**) may be characterized profoundly with particular emphasis put on imine C=N stretching vibrations. Notably, before polymerization of target monomer **125** was made, we ensured that applied protocol could be reflected for the synthesis of 3D polymer **134**, determining at first the structure of obtained yellowish powder, which prospectively was converted to the desired model linear polymer **133**. In order to do so, the IR spectrum (in KBr) of the linear polymer **133** was stacked with spectrum of biphenyl monomer **132**, pointing out the most characteristic vibrations that allow for recognition of the imine-bridged polymer. Major evidence of the linear polymer formation **133** is manifested by the C=N imine vibration and the absence of vibrations characteristic for *Boc* protected amine and aldehyde. Table **4** shows all paramount bands which were accurately assigned as vibrations of bonds in a skeleton of analyzed molecules. Therefore, the most informative bands are indicated with vibration maxima screening structural features of carbamate. Thus, apart from the bands of tertiary butyl (for the detail see Table **4**), the most informative bands were found as vibration of carbonyl group with maximum at 1700 cm^{-1}, secondary and primary amide band at 1602 and 1422 cm^{-1}. Moreover, features of the aldehyde were reflected in maxima at 2734 cm^{-1} (Fermi's vibration) and aforementioned carbonyl stretching vibrations at 1700 cm^{-1} (in this instance it is overlapped by υ(C=O) stemming from carbonyl group of the carbamate). Furthermore, beyond several bands arising from vibrations of biphenyl aromatic backbone, the most critical ones that are a fingerprint for amine and aldehyde were emphasized. Therefore, striking difference in both spectra was manifested by decline of all pinpointed bands. In addition, appearance of typical bands characteristic for –C=N- and –C-C=N-C- is disclosed by stretching vibrations with maxima at 1621 and 1170 cm^{-1}. These are considered as representative and indicative of a polymeric Schiff-base material. Analogous analytical path confirms the existence of three dimensional, tetraphenylmethane based polymer, determining the nature of substitution on tetraphenylmethane rings. Due to the absence of -NHBoc and formyl group vibrations and formation of –C=N- and -C-C=N-C- moieties, stretching vibrations occurred with maxima at 1622 and 1210 cm^{-1} respectively. One may notice that in this type of covalent polymer, we may discriminate two different imines that are manifested by two neighboring vibrations on the spectrum of **134** (see Table **4**). In spite of the applied drying procedure as in case of **134**, the other vibrations indicate remaining solvents (weak vibrations, minor contribution of solvents), which both most likely play a role

of host molecules being strongly trapped along the channels of this 3D cavity, that may also suggest porous character of described material.

Table 2 Summary of peaks extracted from FT-IR spectra with overall interpretation, emphasizing structural differences in between monomers and polymers

Bands (cm^{-1})				Assignments
132	**133**	**125**	**134**	
3355 (s)	3430 (b)	3342 (b)	3438 (b)	υ (-NH), υ (=NH),
3059 (w)		3035 (w)	3027 (w)	υ ($-CH_{Ar}$)
2997 (w)				υ_{as} ($-CH_3$) *t*-Bu
2975 (m)		2976 (m)	2923 (s)	υ_{as} ($-CH_3$) *t*-Bu
2925 (m)		2930 (m)		υ_s ($-CH_3$) *t*-Bu
2840 (w)		2854 (w)		υ_s ($-CH_3$) *t*-Bu
			2852 (m)	υ (-H-C=N)
2743 (w)		2736 (w)		υ (CHO)
1700 (s) (overlapped)	1695 (m)	1725, 1702 (s)	1700 (w)	υ (C=O)
	1621 (m)		1622, 1620 (m)	υ (C=N)
1602 (s)		1600 (s)		υ_2^o (HNC=OR)
1588 (m)	1584 (s)	1573 (w)		υ (C_{Ar}=C_{Ar})
1532 (m)		1523 (s)		υ (C_{Ar}=C_{Ar})
1508 (s)				υ (C_{Ar}=C_{Ar})
	1493 (b)		1495 (m)	υ (C=C-C)
1455 (w)		1454 (w)		δ_s ($-CH_3$) *t*-Bu
1422 (m)		1408 (m)		υ_1^o (HNC=OR)
1399 (m)		1391 (m)		δ (HC=O)
1368 (m)		1367 (m)		δ_{as} ($-CH_3$) *t*-Bu
1326 (m)		1320 (m)		υ (C-N)
1237 (w)		1237 (s)		υ_s (C-O)
	1170 (s)		1210, 1173 (m)	υ (-C-C=N-C)
1190 (w)		1190 (s)	1171 (m)	υ (C-N)
1159 (m)		1052 (m)		υ_{as} (C-O)
1059 (m)		1016 (m)	1014 (m)	*overtones*
844 (m)				υ_{as} ($-CH_3$)
816 (s)	826 (s)	814 (s)	809 (s)	υ (para)
773 (m)		770 (m)		ρ (HNC=OR)

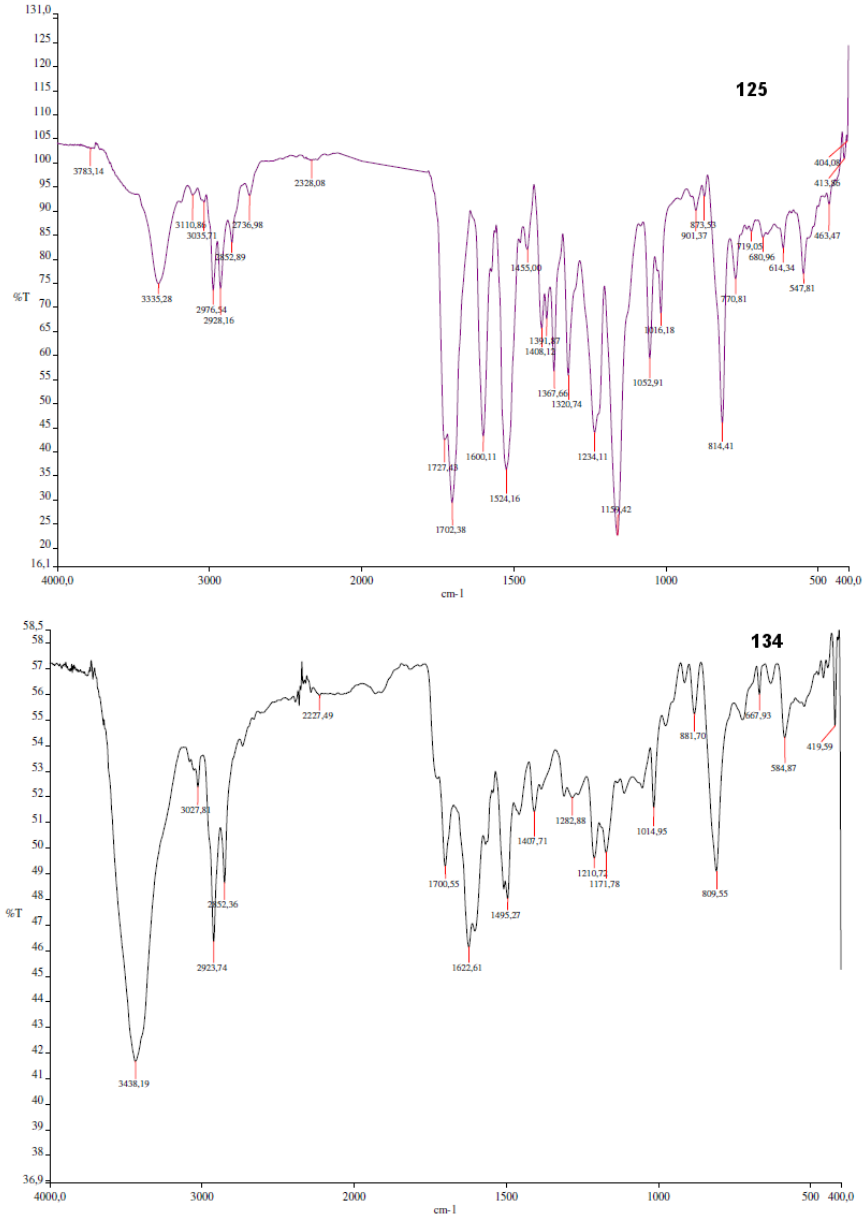

Figure 63 IR spectra of 3D precursor **125** and target polymer **134**

Compounds **125** and **134** were subjected to Raman spectroscopy as well. Spectra of both materials are depicted on Figure **66**. Typically in this technique, the presence of carbonyl stretching vibrations can be identified in the 1680-1800 cm^{-1} range, what is marked in the spectrum of the monomer **125**. Apart from carbonyl vibration at 1695 cm^{-1}, vibrations of aromatic rings of tetraphenylmethane core structure were found at 1601 cm^{-1}. The second spectrum recorded for **134** reveals the presence of vibrations common for aromatic rings (~1590 cm^{-1}). However, considerable difference is noted due to the specific imprint of imine bond, manifested by its stretching vibration. It can be demonstrated in range of 1610-80 cm^{-1} (υ(C=N)).[346] The Raman spectrum evidences anticipated stretching vibration, which stems

from imine bond of analyzed species and may be found at 1611 cm^{-1} (υ(C=N)). Moreover, we did not notice vibration of carbonyl group in referred spectrum of **134**. For the sake of clarity, the rest of indicated bands correspond to aromatic ring vibrations and the residual hexane with varied intensity.

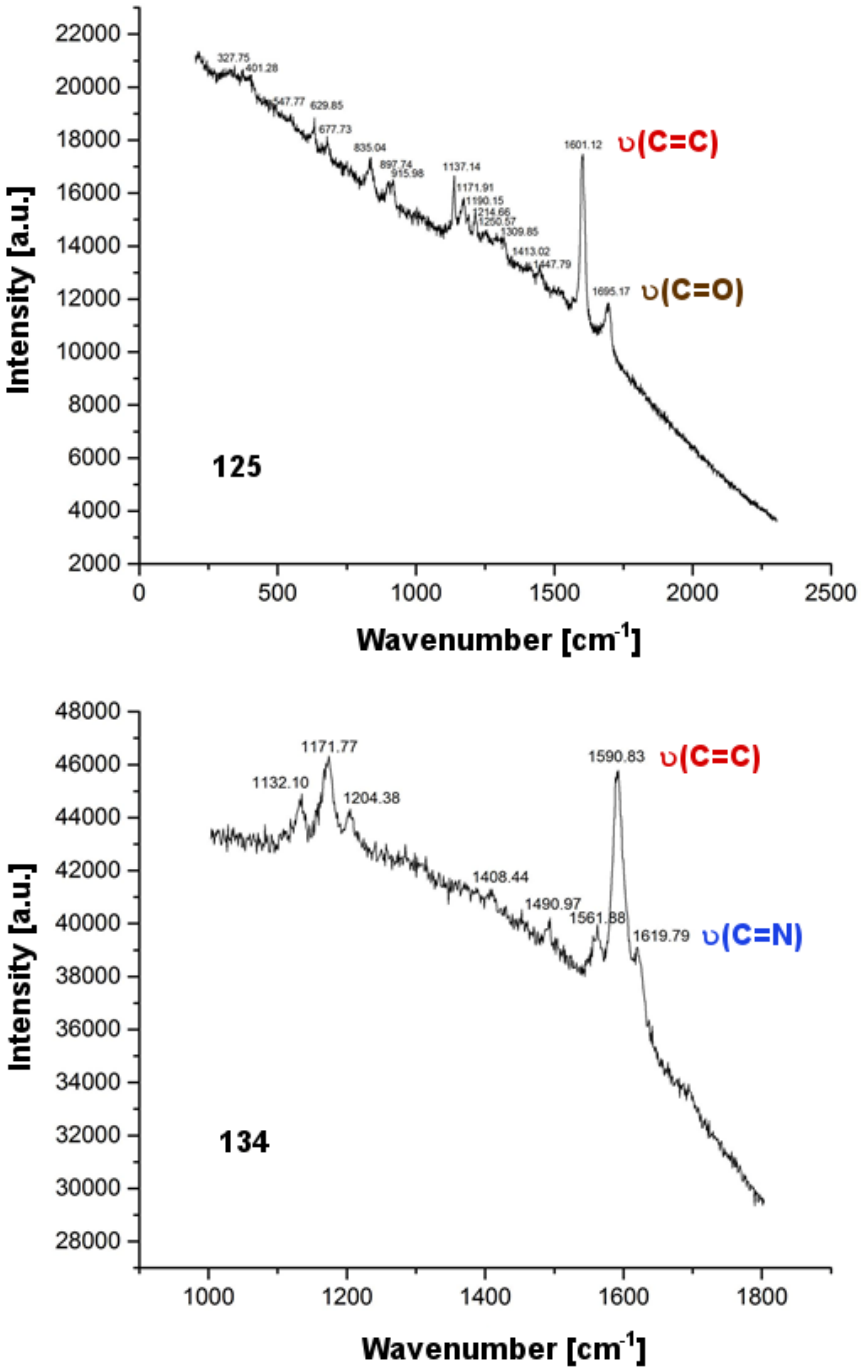

Figure 64 Raman spectra of monomer **125** and target polymer **134**, specific vibrations are marked in red color (aromatic ring) and blue one (imine bond), brown one (carbonyl).

Furthermore, characterization of the novel, linker-free material **134** was followed with NMR study in the solid-state. The MAS ^{13}C-NMR is a valuable method for identification of insoluble materials. Among many signals displayed on Figure **67**, which were attributed to resonance of aromatic rings and central carbon atom (these are showed and assigned in detail in Table **5**), the vital signal is recognized as a resonance of an imine bond at 159 ppm (see Figure **67**). Beyond signals defined as peaks of the target polymer **134** residual signal of hexane was found (13-29 ppm), in spite of long-term drying of a representative sample. Surprisingly, signal of the aldehyde group was found as well (192.28 ppm, HC=O, no vibrations of such were detected on IR and Raman spectra) which may be assigned to the terminal polymer groups.

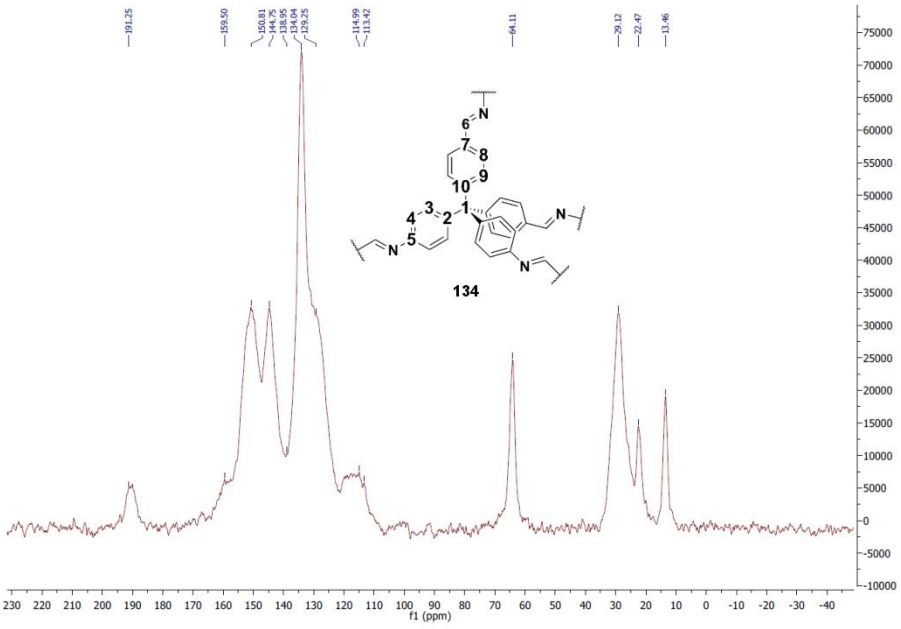

Figure 65 Solid-state ^{13}C CP-MAS spectrum of synthesized polymer **134**

Table 3 Description of signals founded in NMR spectrum of **134**. Picks are assigned in accordance to ^{13}C chemical shits.

Signal (ppm)	Assignment	Signal description
64.11	**1**	Aliphatic quaternary (alpha-aromatic)
113.42	**3**	Aromatic (beta-aliphatic, gamma-imine)
114.99	**8**	Aromatic (gamma -aliphatic, gamma-imine)
129.25	**9**	Aromatic (beta C_{Ar}=)
134.04	**2, 10**	Aromatic (alpha-aliphatic)
138.95	**7**	Aromatic (alpha C_{Ar}=)
144.75	**4**	Aromatic (beta-imine, gamma-aliphatic)
150.81	**5**	Aromatic (alpha-imine)
159.50	**6**	Alkene (alpha-imine, alpha-aromatic)

4.2.2 Morphology of 3D polymer

In order to get more insight into surface morphology of obtained polymeric material **134** and utilize available analytical tools, we chose to find an additional method to detect diamondoic character of tetraphenylmethane based material, manifested by its intrinsic porosity. Therefore, powder was probed and inspected by transmission electron microscopy (TEM), operated by Dr. Di Wang from Institute of Nanotechnology (KIT, Germany). The TEM sample of the polymeric material **134** was prepared by focused ion beam (FIB) and the experiment was performed at a FEI Titan 80-300 in TEM and STEM mode(STEM contrary to TEM is more sensitive to the scattering of the sample, therefore better contrast can be obtained). Energy dispersive X-ray spectroscopy (EDX) was used to detect the elements in the polymer.

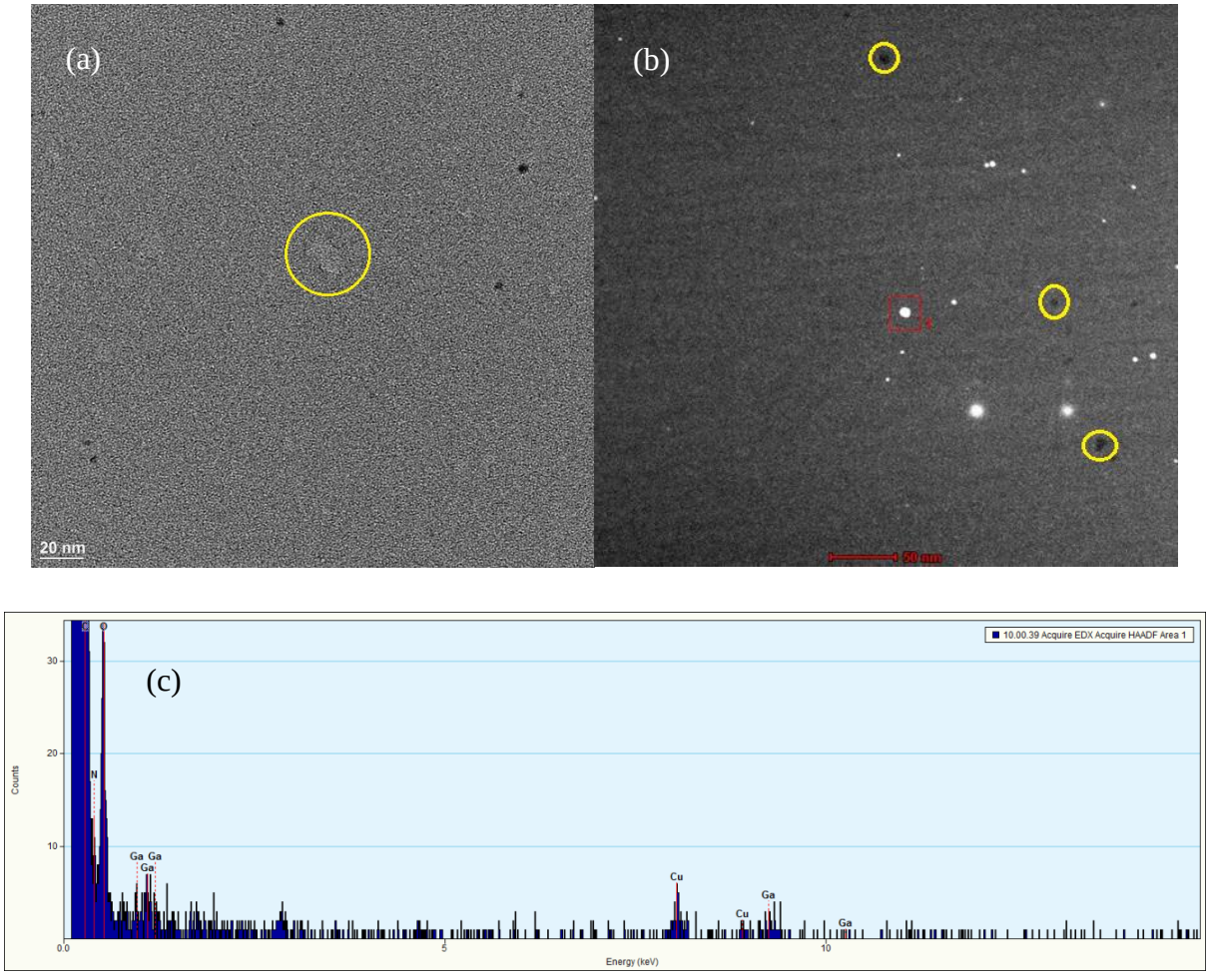

Figure 66 (a) Left image corresponds to TEM while the right one (b) to the STEM measurement (c) lower chart affirms Ga and Cu contribution

Previously developed X-ray powder diffraction of analyzed material **134** showed the amorphous character of the polymer **134**. This feature was additionally corroborated in results of the TEM experiment. The first analysis, which was conducted by TEM is presented in Figure **68(a)** and this measurement proved non crystalline character of investigated structure. It resembles the view of charcoal, therefore we switched the mode from TEM to STEM so as to evidence the existence of porosity. Hence, we figured out that the area indicated by the circle has brighter contrast than the surrounding one, which could be attributed to the pores (Figure **68 (a)**).

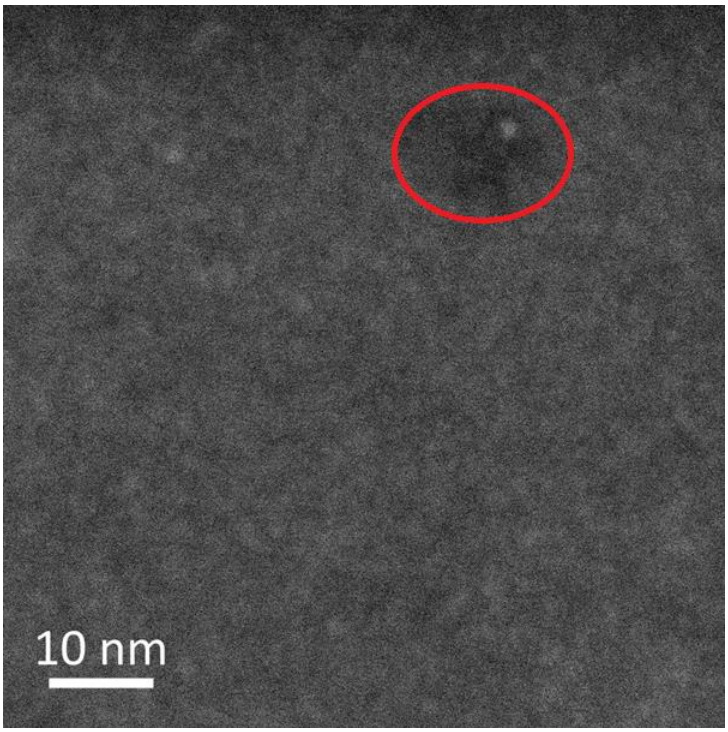

Figure 67 Zoom into the look of the surface, emphasizing its porous character

Therefore, porous morphology was indeed confirmed by STEM images (Figure **68 (b)**). Black spots were found out to be Ga particles, which were introduced during FIB process, so they are not the attribute of investigated material (Figure **68 (c)**). Moreover, in a STEM image at higher magnification shown in Figure **69**, it can be seen that in addition to the pores of size from a few nm to about 10 nm, the image also shows certain brightness variations (pores are shown as a darker area and pointed by the red circle). It indicates that the material forms nano-structures. Nevertheless, due to contamination and possible decomposition of the polymer under electron beam, it is difficult to characterize the fine structure further.

4.2.3 Gas sorption experiment

In terms to the previously discussed morphology of obtained material **134** where bright spots were defined as channels responsible for porosity of **134**, we searched for the other analysis that may confirm the attributes of obtained material, which we found and discussed after TEM and STEM experiments. In order to get more insight in the porosity of **135**, the gas sorption experiment was conducted to determine specific surface areas (SSA) of 3D polymer. The experiment was done by Dr. Peter Weidler at the Institute of Functional Interfaces (KIT, Germany). Prior to measurements, representative sample was dried overnight at 95^{o}C to get rid of remaining solvents or adsorbed water and to make a whole process clear. Note that after the process of drying, the mass declined by about 13.2% in contrast to the initial state. Thus, measurements of sorption of the argon were performed at 87 K using a Quantachrome Autosorb1 MP. The samples were degassed at 368 K in vacuum for 24 h before measurements. SSAs were calculated by using the Brunauer Emmett Teller (BET) method.[347] Alternatively, the SSA was estimated by applying a NLDFT equilibrium model with mixture of cylindrical and spherical shaped pores based on the DFT/Monte Carlo method.[348] Whereby, the BET surface area was determined only by single-point BET at 0.3 p/p_o and it oscillated around 1 m^2/g, while multi point BET was unfortunately not applicable. A fit of the isotherm, which exhibited positive adsorption values with DFT models yielded 1.9 m^2/g. These results overtly showed the poor character of the porosity (so far reported 3D COFs based on imine bonds showed the surface area in a 1000-3800 m^2/g range)[247] which is related directly to non-crystalline feature of obtained polymer and its extremely weak assembly. Therefore, more efforts have to be addressed to the polymerization process, which may give a boost to reach crystalline material with well-defined surface area.

4.3 Solid state analysis

Single crystal X-ray analysis of x-ray quality crystals obtained through the slow evaporation from the neat dichloromethane showed the molecules to be a series of tetraphenylmethane derivatives. The molecules in a solid state exhibit varied packing in the crystal lattice regarding on the FGs nature built on the tetraphenylmethane skeleton. Their structures are illustrated in Figures **62** and **63**, while all data are summed up in the Table **2** and **3**. Compounds **119** and **122** crystalized in tetrahedral crystal system in *I-4* space group with 16 molecules per units cell, creating hexagonal motif along *ab* plane, and $I4_1/a$ with 6 molecules per units cell respectively. High symmetry of **119** is reasoned by ¼ molecule in the asymmetric unit cell, contrary to **122**, where the entire molecule is presented. Moreover, the length of the bond constituted by central carbon atom C_1 and aromatic carbon C_2 with uniform length of all four contacts ~1.545 Å (**119**) and distances oscillated between 1.543-1.552 Å for **122**. The functional groups mounted to tetraphenylmethane core cause mutual interactions that may be exemplified as long halogen contacts I···Cl (d = 3.984Å), Cl-Cl (d = 3.814Å), Cl-Cl (d = 3.905 Å) disclosed for **119**, while **122** exhibit intermolecular N-C···N interactions (d = 3.225 Å), as well as H_3···Cl···H_3 (d = 2.437 Å, d = 2.395 Å, 44º). Furthermore, two other derivatives **120**, **121** (see Figure **62** and Table **3**) crystalized in *monoclinic* crystal system of lower symmetry being assigned to *C2/c* space group (**120**, **122**). Both are packed with 6, whereas boronic ester derivatives with 4 molecules per unit cell. Homogeneous length of C_1-C_2 bonds corroborate high structural order of compounds **120** and **122**, with identical length of 1.547 Å. Indeed, weak hydrogen bonding emerged in the tetraphenylmethane crystal structure and is detected in **121** involving formyl group as a acceptor and hydrogen donor from the aromatic ring. (C_4-H···O_1 (d = 2.357Å)). Considering the isostructural **120**, halogen was involved in an interaction between bromide and two aromatic carbon atoms C_4···Br_1···C_5 (d = 3.527 Å, d = 3.435 Å, 82º). The greatest amount of structural information was subtracted from crystallographic studies of single crystals of **116**, which grow in orthorhombic crystal system and *Pbcn* space group. Likewise **119,** diol **122** forms 3D crystal lattice bearing 16 molecules per unit cell and two molecules in asymmetric unit cell. Distances of C_1-C_2 range from 1.538-1.562 Å. With respect to the phenol as a feature of this FG, hydrogen bonds are formed between two hydroxyls of the adjacent tetraphenylmethane moieties, showing contrasted length of C_4-O···H bond 1.933 and 2.664 Å respectively. Analogously to the arrangement of bromides discussed above, aromatic

chlorides exerts halogen bonding in similar fashion $C_4 \cdots Cl \cdots C_5$ (d = 3.431Å, d = 3.362 Å, 77°).

Table 4 Data extracted from X-ray analysis of **116**, **119**, **122**.

Number	**116**	**119**	**122**
Empirical formula	$C_{25}H_{18}Cl_2O_2$	$C_{25}H_{16}Cl_2I_2$	$C_{27}H_{16}Cl_2N_2$
Formula weight	421.29	641.08	439.32
Temperature/K	180.15	180.15	150.15
Crystal system	orthorhombic	tetragonal	tetragonal
Space group	Pbcn	I-4	$I4_1/a$
a/Å	33.811(2)	12.7349(14)	17.4170(7)
b/Å	7.4978(4)	12.7349(14)	17.4170(7)
c/Å	32.666(2)	7.1256(9)	28.5647(13)
α/° β/° γ/°	90	90	90
Volume/Å^3	8281.1(9)	1155.6(3)	8665.2(8)
Z	16	2	16
ρ_{calc}g/cm^3	1.352	1.842	1.347
μ/mm^{-1}	2.965	2.962	0.317
F(000)	3488.0	612.0	3616.0
Crystal size /mm^3	0.41 × 0.11 × 0.03	0.28 × 0.09 × 0.08	0.35 × 0.18 × 0.08
Radiation	CuKα (λ = 1.54186)	MoKα (λ = 0.71073)	MoKα (λ = 0.71073)
2Θ range for data collection/°	5.41 to 125.874	4.524 to 51.086	2.738 to 52.258
Reflections collected	27495	1706	14919
Independent reflections	6450	1046	4261
Data/restraints/ parameters	6450/0/528	1046/6/77	4261/6/307
Goodness-of-fit on F^2	0.908	1.104	0.949
Largest diff. peak/hole / e Å^{-3}	0.47/-0.45	1.02/-0.95	0.32/-0.44

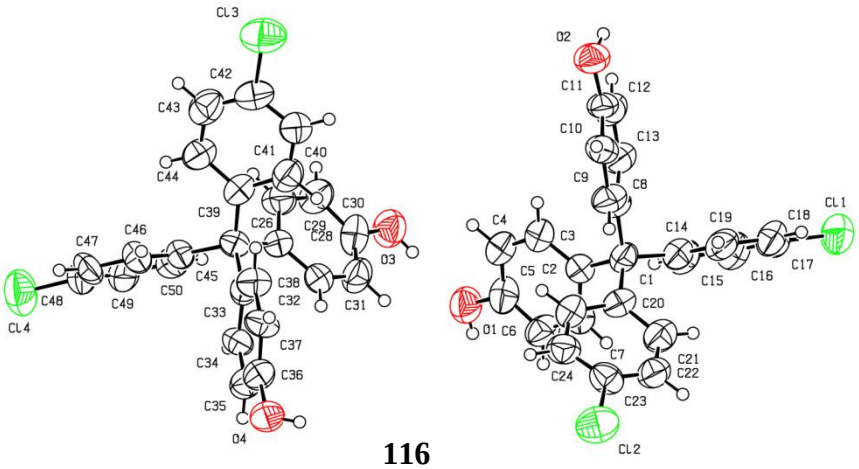

116

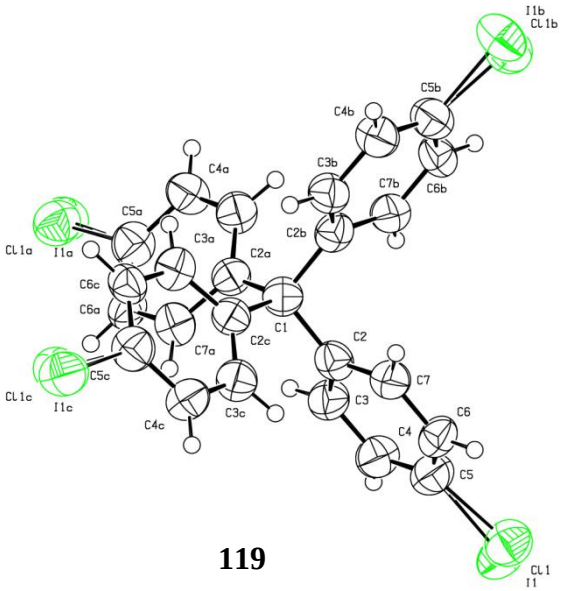

119

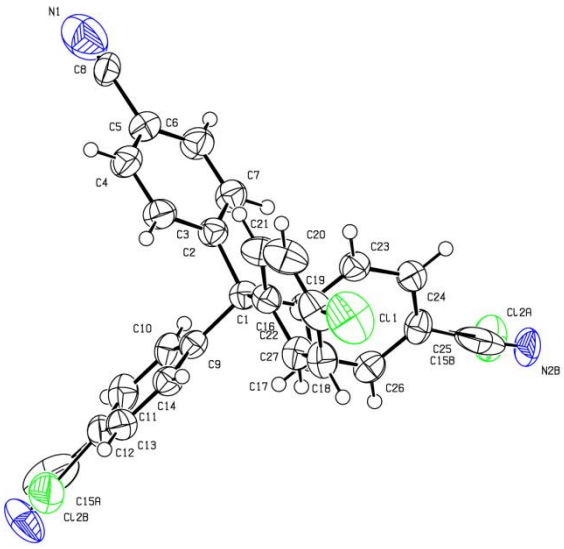

122

Figure 68 Solid-state structures of tetraphenylmethane derivatives **116**, **119, 122**.

Table 5 Data extracted from X-ray analysis of **120, 121**.

Number	**120**	**121**
Empirical formula	$C_{25}H_{16}Br_2Cl_2$	$C_{27}H_{18}Cl_2O_2$
Formula weight	547.10	445.31
Temperature/K	180.15	180.15
Crystal system	monoclinic	monoclinic
Space group	C2/c	C2/c
a/Å	19.0239(12)	19.190(4)
b/Å	7.6754(3)	7.4542(15)
c/Å	19.1893(13)	16.959(3)
α/° β/° γ/°	90/128.683(4) /90	90/115.84(3) /90
Volume/Å^3	2187.2(2)	2183.3(9)
Z	4	4
ρ_{calc}g/cm^3	1.661	1.355
μ/mm^{-1}	3.960	0.319
F(000)	1080.0	920.0
Crystal size /mm^3	0.48 × 0.21 × 0.12	0.28 × 0.22 × 0.18
Radiation	MoKα (λ = 0.71073)	MoKα (λ = 0.71073)
2Θ range for data collection/°	4.73 to 51.356	4.716 to 54.682
Reflections collected	5370	5088
Independent reflections	2013	2433
Data/restraints/ parameters	2013/0/139	2433/0/169
Goodness-of-fit on F^2	1.058	0.971
Largest diff. peak/hole / e Å^{-3}	0.44/-0.71	0.16/-0.24

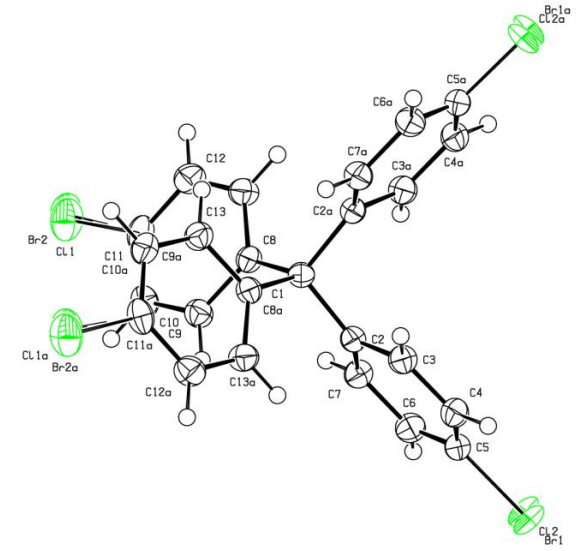

120

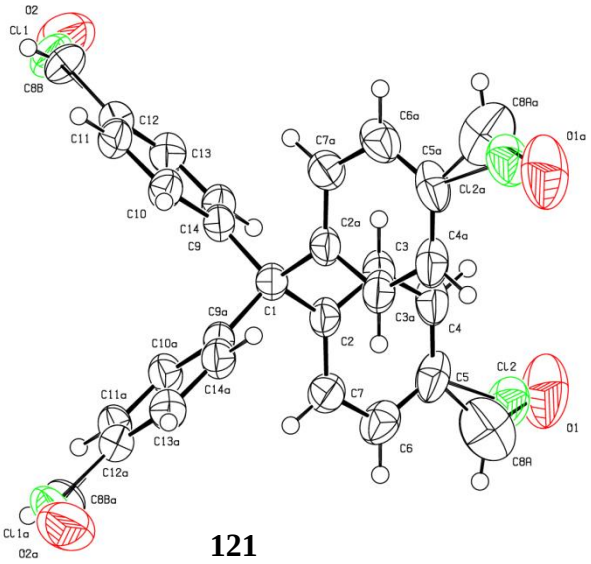

121

Figure 69 Solid-state structures of tetraphenylmethane derivatives **120**, **121**.

4.4 Conclusions and outlooks

We presented and discussed various approaches of the double functionalization of tetraphenylmethane core structure that was supposed to function as precursor of COF material. We examined four different synthetic strategies, however only the last one, which involved ditriflate **117** lead to successful synthesis of the desired monomer **125**. By using molecular analogs (**126**, **127**, **128**), we carried out complementary studies to get more insight in the *Boc* cleavage that is vital to obtain the monomer, which contains deprotected amine and aldehyde within the same molecule, appropriate for classical imine-condensation. Therefore, a number of molecular analogues were synthesized and investigated as well, and the obtained results were applied for target tetraphenylmethane system. Since we considered that deprotection of *Boc* with *in situ* formed HCl unexpectably leads to diacetal **130**, instead of the desired compound, we decided to conduct final polymerization by utilizing monomer **125**. In order to optimize the polymerization conditions, the complexity of the model system was reduced by studying the biphenyl **132** as functional proxy of tetraphenylmethane **125**, with the advantage of forming a processable linear polymer instead of an insoluble 3D network. We decided to investigate microwave driven polymerization. This allowed us to synthesized linear polymer **133** based on imine bonds. Is it thus clearly shown that established procedure can be effectively imitated for polymerization of target monomer **125**. Hence, reflection of previous conditions gives the opportunity to synthesize and then identify 3D polymeric structure **134**. Unfortunately, the obtained material was found to be non-crystalline with poor porosity, presumably due to the nature of microwave accelerated poly-condensation which, contrary to the solvothermal synthesis, does not ensure reversible equilibrium conditions probably required to form crystalline material.

Scheme 21 Imine condensation initiated from acetal **130.**

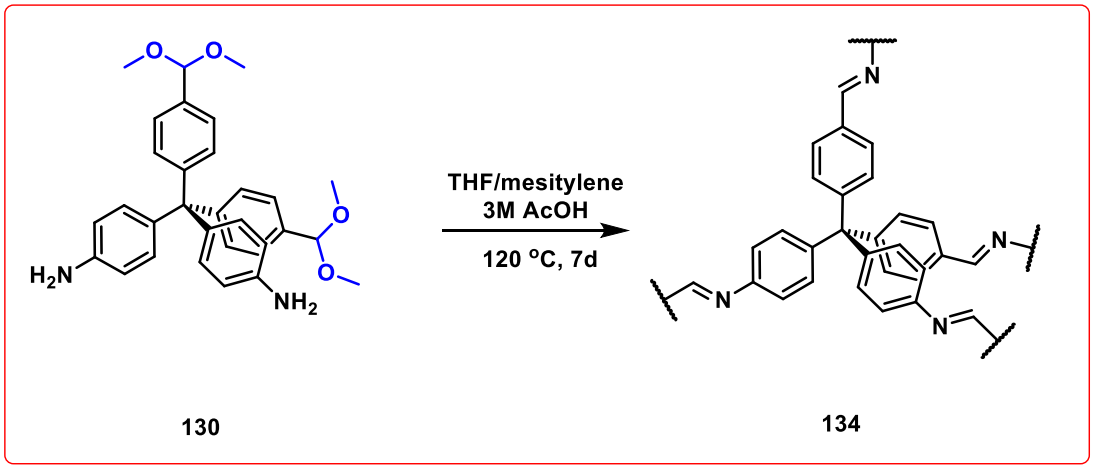

Thus, in order to considerably improve properties of expected material in terms of its crystallinity and porosity, more attention shall be paid to acetal comprising tetraphenylmethane monomer **125** (see Scheme **22**). As was recently reported, 2D COF can be reached from diacetal terminated rod and diamine, which were successfully subjected to imine condensation, and this reaction was developed by applying solvothermal synthesis. Therefore, diacetal **130** may be analogously used to synthesize 3D polymeric material according to the recently published protocol.[349]

5 General conclusions and outlooks

In this thesis, first part concerns the library of molecular architectures based on tetraphenylmethane building block which were synthesized and handled for nanotechnology, thus exploiting their pivotal areas with the potential of conferring additional knowledge to the general understanding of this domain. The second part was addressed to dynamic covalent chemistry, which demonstrates linker-free approach and was embodied in the synthesis of 3D COFs, which are supposed to act as a new generation of functional porous materials.

In the chapter **2** we demonstrated extensive synthetic pathways for the preparation of both regioisomeric molecular holders within 6 steps for *para* and 7 synthetic steps for *meta* decorated platforms. The modular character of newly prepared platforms is emphasized by the contribution of versatile leaving groups, attached to each of the presented tripods. This manipulation allowed us to construct full array of size-dependent tower-shaped molecules with the sequence of Suzuki-cross coupling reaction getting 12 elongated, target molecules from moderate to excellent yield.

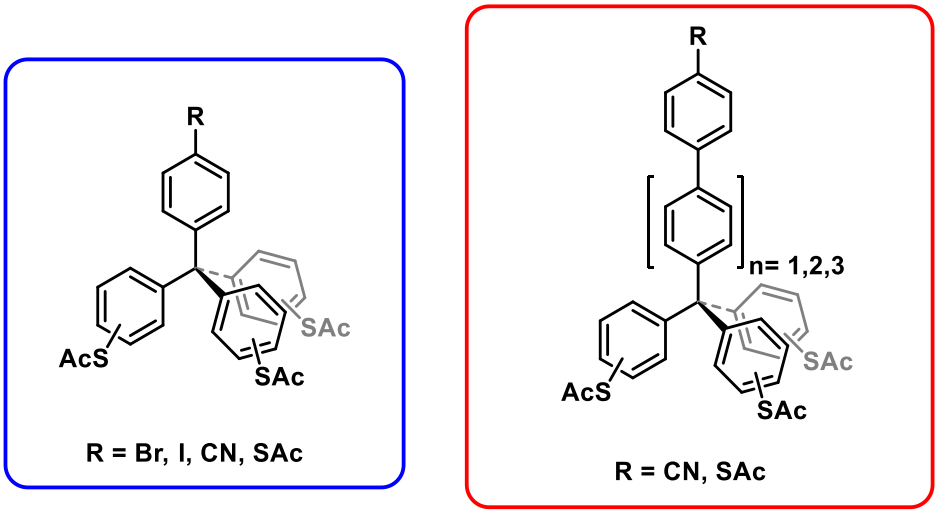

Figure 70 Illustration of successfully synthesized surface addressable molecular tripods

In the chapter **3** we prove the concept of molecular platforms constituted on tetraphenylmethane tetragonal skeleton by immobilization of the tripods on the gold interface. Created films of tripods and their direct deposition on single gold Au(111) allowed

to gain more insight into the self-assembly features of conceptual tetraphenylmethane motifs, recognizing their surface properties as switching phenomena attributed to the head group. While having in hand a series of oligoarylenes embedded to the tripodal core structure (**33**, **61**, **63**, **65**), molecular grafting capability was shown. Moreover, STM-BJ experiments helped to elucidate and understand charge-transport mechanism for the whole bunch of designed and successfully synthesized molecules, showing that thioacetate tripods (**74**, **77**, **83**, **85**, **87**, **89**, **91**, **93**) exhibit significantly higher conductivity, contrary to nitrile decorate platforms (**33**, **50**, **61**, **63**, **65**, **67**, **69**, **71**).

In the chapter **4** several of tetraphenylmethane synthetic modifications were performed in order to reach innovative, highly functionalized monomer **125** capable of imine self- condensation, providing to novel 3D COF material. We applied tools of modern organic chemistry, aided by *Pd*-catalyzed transformations to feature tetraphenylmethane core simultaneously substituted with carbamates and aldehydes. It must be noted that such bis-substituted tetraphenylmethane building blocks are reported for the first time. These are prone to form 3D polymer linked by dynamic imine bond. Formation of polymeric Shiff-base **134** was corroborated by accessible tools including IR, Raman Spectroscopy, MAS-NMR, and TEM characteristics. Analysis of obtained material **134** revealed its amorphous character and low porosity what may be right away reasoned by the lack of crystallinity.

Taking into account tunable properties and robustness of protecting groups applied over the course of presented synthetic transformations, molecular tripods may be decorated with unlimited numbers of active tail-groups profiting from chemistry of transition metal-complexes which improved considerably insertion of functional moieties via for instance widely exploited Suzuki reaction. Therefore functional, molecular machines based on tripods may be design and produced, exploring it properties on metal surfaces. Moreover, we have already suggested, that polymerization initiated from diacetal terminated tetraphenylmethane derivatives could promote the formation of crystalline polymer with higher intrinsic porosity.

6 Experimental Section

6.1 General Remarks

Reagents and Solvents

All starting materials were obtained from commercial suppliers (Acros Chemicals (Geel, Belgium), Merck (Darmstadt, Germany), ABCR (Karlsruhe, Germany), Alfa Aesar (Karlsruhe, Germany), Sigma-Aldrich (Schnelldorf, Germany), Synchem OHG, (Felsberg, Germany), TCI Europe (Zwijndrecht, Belgium), VWR (Karlsruhe, Germany), Fluorochem (Hadfield, United Kingdom)) and used without further purification if nothing else is explicitly remarked. Degassed solvents were obtained by three cycles of the freeze-pump-than or purged with argon or nitrogen for at least 15min. Dry DMF and dioxane were purchased from Acros Chemicals and Sigma-Aldrich, these are stored over 4 Å molecular sieves, and handled under inert atmosphere, while the others as diethyl ether, THF, toluene (Na/benzophenone), CH_2Cl_2 (CaH_2) were distilled under nitrogen atmosphere prior to use. Normal phase column chromatography (CC) was performed on silica gel 60 (230-240 mesh) obtained from Merck. Thin Layer Chromatography (TLC) was performed using Silica gel 60 F_{254} aluminium plates with a thickness of 0.25 mm purchased from Merck and spots were detected by fluorescence quenching under UV0light at 256 or 366 nm.

^{1}H-Nuclear Magnetic Resonance (^{1}H-NMR)

Bruker Avance NMR (500 MHz) spectrometer was used to record the spectra. Chemical shifts (δ) are quoted in parts per million (ppm) relative to residual solvent peaks ($CDCl_3$: 7.26 ppm, CD_2Cl_2: 5.32 ppm, MeOD: 3.30 ppm) or trimethylsilane (TMS: 0.00 ppm), and coupling constants (J) are reported in Hertz (Hz). The bond distance of the coupling constant is stated with a superscript number (^nJ). The measurements were performed at room temperature. The multiplicities are denoted as s = singlet, d = doublet, dd = doublet of the doublets t = triplet, q = quartet, m = multiplet.

^{13}C-Nuclear Magnetic Resonance (^{13}C-NMR)

Bruker Avance-NMR (126 MHz) spectrometer was used to record the spectra. Chemical shifts (δ) are quoted in parts per million (ppm) relative to residual solvent peaks ($CDCl_3$: 77.16 ppm, CD_2Cl_2: 53.84 ppm, MeOD: 40.84 ppm, either TMS: 0.00 ppm), and coupling constants (J) are reported in Hertz (Hz). The measurements were carried out at room temperature.

Mass Spectrometry (MS)

High-resolution mass spectra were recorded with a Bruker Daltonics (ESI microoTOF0-QII) mass spectrometer , Electron impact (EI) mass spectra were recorded with a Termo Scientific Trace 1300 GC/MS instrument with single quadrupole ISQ

Fourier Transfer Infrared Spectrometry (FT-IR)

Infrared spectra were recorded with a Perkin Elmer GX spectrometer in KBr pallets. The intensities of bands are denoted as w = weak, m = medium, s = strong and br = broad.

Elemental Analysis (EA)

Elemental analyses were obtained using a Vario MicroCube GHNS analyzer and measured by S. Stahl. The values are presented in mass percentage values.

Ultraviolet Spectroscopy (UV-Vis)

UV-Vis-spectra were recorded with a Varian Cary 500 Scan spectrophotometer in optical quartz 114-QS Hellma cuvettes (10 mm light path) at room temperature.

Microwave Reactions

Microwave reactions were carried out in a CEM Discover SP microwave system in capped vials.

Melting Points

Melting points (m.p.) were measured with a Büchi Melting Point B-540 and Opti Melt, Stanford Research System apparatus and are not corrected.

Thermogravimetric Analysis

Thermogravimetric Analysis (**TGA**) was carried out in a Thermobalance STA 409 with the dynamic helium gas flow (25 mL/min) as well as TGA 209 F1 LIBRA Netzsch with the dynamic nitrogen gas flow (20 mL/min) and done by S. Stahl and S. Leuthner.

6.2 Synthetic Procedures

4-Bromo-1-[2-(trimethylsilyl)ethylsulfanyl]benzene (24)

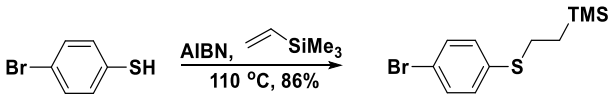

24

Compound **24** was synthesized adapting the published procedure.[280] Commercially available 4-bromothiophenol (10.30 g, 54.5 mmol), vinyltrimethylsilane (10.30 g, 109 mmol), and azobisisobutyronitrile (AIBN) (0.45 g, 2.73 mmol) were charged to 50 mL pressure tube under inert atmosphere. Afterwards, the tube was sealed and vigorously stirred overnight at 100 °C. The reaction was cooled down, the crude mixture was mixed with 8% solution of $NaOH_{aq}$ over 1 h and then extracted with Et_2O (2 x 200 mL). Organic layers were combined, dried over $MgSO_4$, filtrated and solvents were removed. Obtained yellow oil was purified by column chromatography on silica gel (700 g) in pure hexane providing 13.54 g of **24** in 86% yield as a clear oil. (R_f = 0.33, hexane); ^{1}H NMR (500 MHz, $CDCl_3$) δ ppm, 0.07 (s, 9H, CH_3), 0.92-0.96 (m, 2H, CH_2), 2.94-2.98 (m, 2H, CH_2), 7.17-7.20 (m, 2H, Ar-H), 7.40-7.43 (m, 2H, Ar-H); ^{13}C NMR (125.8 MHz, $CDCl_3$) δ ppm -0.6, 17.9, 30.8, 120.5, 130.8, 131.6, 132.9, 137.6

Tris{4-[2-(trimethylsilyl)ethylsulfanyl]phenyl}methanol (3)

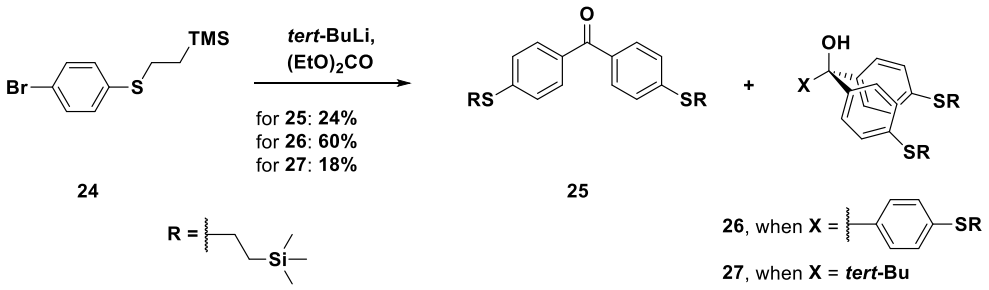

24 25

Method A: A dry and argon-flushed 100 mL Schlenk flask was charged with **24** (3.76 g, 13 mmol) and anhydrous THF (35 mL) was added. The solution was cooled to -78 °C and *tert*-BuLi (17.8 mL, 26 mmol, 15% in pentane) was added dropwise over 20 min. The reaction mixture was stirred at -78 °C for 2 h under argon. In a second 100 mL Schlenk flask, diethyl carbonate (0.44 mL, 3.71 mmol) was diluted with anhydrous THF (5 mL) under inert atmosphere and cooled to -78 °C. The solution of lithiated species was slowly added via a

cannula into the flask containing diethyl carbonate solution, after 1 h, the reaction mixture was allowed to warm to room temperature and stirred for an additional 16 h. The reaction mixture was quenched with saturated NH_4Cl solution (100 mL). The aqueous layer was washed with CH_2Cl_2 (2 x 100 mL). The combined organic layer was washed with brine (100 mL), dried over $MgSO_4$, and filtered. All volatiles were removed under reduced pressure and the residue was purified by column chromatography on silica gel (300 g) in hexane/EtOAc (9:1) to afford pure **26** (1.46 g) as a yellowish solid in 60% yield (R_f = 0.45, hexane/EtOAc = 9:1) and pure **25** (0.4 g) as a white solid in 24% yield (R_f = 0.54, hexane/EtOAc = 9:1);

For **26**: m.p. 121-131 °C; ^{1}H NMR (500 MHz, $CDCl_3$) δ ppm, 0.04 (s, 27H, CH_3), 0.92-0.96 (m, 6H, CH_2), 2.71 (s, OH), 2.94-2.96 (m, 6H, CH_2), 7.16-7.18 (m, 6H, Ar-H), 7.22-7.23 (m, 6H, Ar-H); ^{13}C NMR (125.8 MHz, $CDCl_3$) δ ppm -1.5, 17.0, 29.4, 81.6, 128.0, 128.5, 136.9, 144.1; IR (KBr) ν cm^{-1} 3446 (s, υ(OH)), 3025 (w, υ(=CH)), 2952 (s, υ_{as}(CH_2, CH_3)), 1594 (m, υ_{as}(C=C)), 1490 (s), 1417 (m, δ_{as}(CH_2, CH_3)), 1249 (s, δ_s(CH_3, TMS)), 1161 (m), 838 (s, δ_{as}(CH_3, TMS)), 693 (w, υ_{as}(SiC_3)); UV-Vis (λ_{max}[nm], ε, CH_2Cl_2) 269 (43 186); ESI(+) MS Calcd for $C_{34}H_{52}OS_3Si_3Na$ ([M+Na]$^+$, 679.2289), found *m/z* 679.2380; elemental analysis calcd (%) for $C_{34}H_{52}OS_3Si_3$ (656.25): C, 62.14; H, 7.98; found: C, 62.23; H, 8.05.

For **25**: m.p. 71-74 °C; ^{1}H NMR (500 MHz, $CDCl_3$) δ ppm 0.02 (s, 18H, CH_3), 0.97-1.00 (m, 4H, CH_2), 3.02-3.06 (m, 4H, CH_2), 7.29-7.31 (m, 4H, Ar-H), 7.70-7.71 (m, 4H, Ar-H); ^{13}C NMR (125.8 MHz, $CDCl_3$) δ ppm -1.5, 16.7, 28.4, 126.5. 130.7, 134.4, 144.5, 195.1; IR (KBr) ν cm^{-1} 3037 (w, s υ(C=CH)), 2958 (s, υ_{as}(CH_2, CH_3), 2952 (s, υ_s(CH_2, CH_3), 1657 (s, υ(C=O)), 1553 (s, υ(C=C)), 1401 (m, δ_s(CH_2, CH_3)), 1288 (m, CH_3, TMS)), 1088 (s), 830 (s), 692 (w, υ_{as}(SiC_3)); UV-vis (λ_{max}[nm], ε, CH_2Cl_2) 329 (29245); ESI(+) MS Calcd for $C_{23}H_{34}OS_2Si_2Na$ ([M+Na]$^+$, 469.1378), found *m/z* 469.1482; elemental analysis calcd (%) for $C_{23}H_{34}OS_2Si_2$ (446.16): C, 61.83; H, 7.67; found: C, 61.59; H, 7.88.

For **27**: m.p. 123-124^{o}C; ^{1}H NMR (500 MHz, $CDCl_3$) δ ppm, 0.03 (s, 18H, CH_3), 0.91-0.93 (m, 4H, CH_2), 0.95 (s, 9H, CH_3), 2.21 (s, 1H, OH), 2.92-2.96 (m, 4H, CH_2), 7.15-7.19 (m, 4H, Ar-H), 7.28-7.30 (m, 2H, Ar-H), 7.50 (s, 2H, Ar-H); ^{13}C NMR (125.8 MHz, $CDCl_3$) δ ppm -1.6, 17, 27.6, 29.3, 39.4, 82.7, 127.3, 129.1, 135.7, 143.4; IR (KBr) ν cm^{-1}: 3415 (υ(*OH*)), 3028 (w, υ(=CH)), 2953 (s, υ_{as}(CH_2, CH_3)), 2922 (s, υ_s(CH_2, CH_3)), 2854 (m), 1590 (m, υ(C=C)), 1488 (m, δ_{as}(CH_2, CH_3)), 1421 (w, δ_s(CH_2, CH_3)), 1269(m), 1250 (s, δ_s(CH_3,

TMS)), 1161 (m), 1096(m), 1010 (m), 893 (m), 860 (s), 841 (s, $\delta_{as}(CH_3$, TMS)), 828(s), 791(m), 696 (w, $\upsilon_{as}(SiC_3)$); UV-Vis (λ_{max}[nm], ε, CH_2Cl_2) 267 (22553); ESI(+) MS Calcd for $C_{27}H_{44}OS_2Si_2Na$ ($[M+Na]^+$, 527.2270), found *m/z* 527.2131; elemental analysis calcd (%) for $C_{27}H4_{44}OS_2Si_2$ (504.24); C 64.24 H 8.78, S 12.70; found: C 65.11, H 8.62.

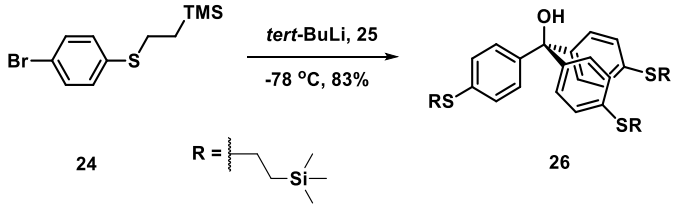

Method B: In a 100 mL Schlenk flask, **24** (1.16 g, 4.01 mmol) was dissolved in anhydrous THF (12 mL) under argon, cooled to -78 °C and degassed. Then *tert*-BuLi (5.6 mL, 8.24 mmol, 15% in pentane) was added dropwise over 25 min and the resulting mixture was stirred at -78 °C for 2 h. In a second 100 mL Schlenk flask, **24** (0.9 g, 2.02 mmol) was dissolved in THF (8 mL) under argon, and cooled to -78 °C. The solution of lithiated species was slowly added via a cannula into the flask containing solution of **25**. The yellow solution was stirred at -78 °C for 2 h, then allowed to warm to the room temperature and stirred for an additional 12 h. The reaction mixture was quenched with saturated NH_4Cl solution (100 mL). The aqueous layer was washed with CH_2Cl_2 (2 x 150 mL). The combined organic layer was washed with brine (100 mL), dried over $MgSO_4$, and filtered. The volatiles were removed under reduced pressure and the residue was purified by column chromatography on silica gel (200 g) in hexane/EtOAc (9:1) to yield 1.1 g (83%) of **26** as a yellowish solid.

4-(tris{4-[2-(trimethylsilyl)ethylsulfanyl]phenyl}methyl)aniline (**28**)**,**
4-(tris{4-[2-(trimethylsilyl)ethylsulfanyl]phenyl}methyl)acetanilide (**29**)

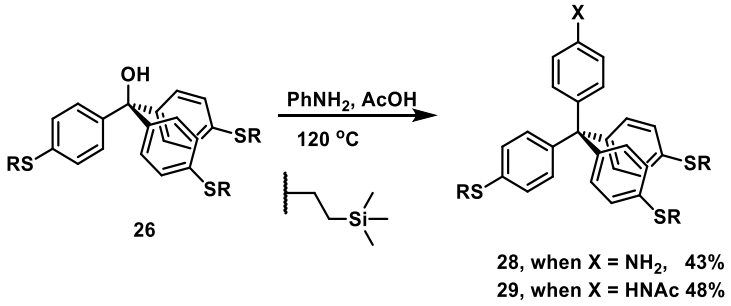

Method A Trityl alcohol **26** (1 g, 1.22 mmol) was placed to a 250 mL three-neck round bottom flask, equipped with a refluxed condenser and dissolved in 12 mL of glacial acetic acid. Subsequently a catalytic amount of concentrated hydrochloric acid was added, forming a violent solution. Afterwards freshly distilled aniline (0.56 g, 6.1 mmol) was loaded at once. Reaction mixture was than vigorously stirred and heated at 140 ^{o}C overnight. After cooling to room temperature, the reaction mixture was neutralized with sodium carbonate (100 mL); aqueous layer was washed with dichloromethane (3 x 200 mL). The combined organic layer was dried over magnesium sulfate and filtered. All volatiles were removed under reduced pressure and the residue was purified by column chromatography on silica gel (400 g) in hexane/EtOAc (7:3) to obtain 0.48 g of aniline **28** (43%) as orange oil. (R_f = 0.25, hexane/EtOAc 7:3); and 0.57 g of acetanilide **29** as an creamy oil in 48% yield. (R_f = 0. 77, hexane/EtOAc 7:3).

For 28: ^{1}H NMR (500 MHz, $CDCl_3$) δ ppm 0.04 (s, 27H, CH_3), 0.93-0.96 (m, 6H, CH_2), 2.93-2.97 (m, 6H, CH_2), 3.62 (s, 2H, NH_2) 6.57 (d, $J_{H,H}$ = 8.65 Hz, 2H, Ar-H), 6.92 (d, $J_{H,H}$ = 8.6 Hz, 2H, Ar-H), 7.09 (d, $J_{H,H}$ = 6.8 Hz, 1.75 Hz, 2H, Ar-H) 7.15 (d, $J_{H,H}$ = 8.6 Hz, 2H, Ar-H); ^{13}C NMR (125.8 MHz, $CDCl_3$) δ ppm -1.6, 16.9, 29.3, 63.3, 114.3, 127.4, 132, 135, 136.6, 144.4, 144.5, IR (KBr) ν cm^{-1}: 3374 (m, υ(NH_2)), 3028 (w, υ(=CH)), 2950 (s, υ_{as}(CH_2, CH_3)), 2918 (s, υ_s(CH_2, CH_3)), 2854 (w), 1621 (s, υ(C=C)), 1592 (w), 1511 (s, δ(NH)), 1487 (s), 1419 (w, δ_{as}(CH_2, CH_3)), 1399 (w, δ_s(CH_2, CH_3)), 1248 (s, δ_s(CH_3, TMS)), 1182 (m), 1162 (m), 1093 (m), 1013 (m), 858 (s), 839 (s, δ_{as}(CH_3, TMS)) 810 (s), 753 (m), 692 (w, υ_{as}(SiC_3)); UV-Vis (λ_{max}[nm], ε, CH_2Cl_2) 270 (41711); ESI(+) HRMS Calcd for

$C_{40}H_{57}S_3Si_3NH$ ([M+H]$^+$, 732.3039), found *m/z* 732.3007; elemental analysis calcd (%) for $C_{40}H_{57}S_3Si_3N$ (731.30) C 65.50; H 7.85, N 1.91; found: C 65.96, H 7.63, N 1.88.

For 29: ^{1}H NMR (500 MHz, CD_2Cl_2) δ ppm 0.03 (s, 27H, CH_3), 0.92-0.96 (m, 6H, CH_2), 2.16 (s, 3H, CH_3), 2.93-2.96 (m, 6H, CH_2), 7.07 (dd, $J_{H,H}$ = 6.8, 1.75 Hz, 6H, Ar-H), 7.11 (s, 2H, Ar-H), 7.15 (d, $J_{H,H}$ = 8.5 Hz, 6H, Ar-H), 7.24 (s, 1H, NH), 7.37 (d, $J_{H,H}$ = 8.6 Hz, 2H, Ar-H); ^{13}C NMR (125.8 MHz, $CDCl_3$) δ ppm -1.6, 16.9, 24.7, 29.2, 63.6, 119, 127.4, 131.5, 131.6, 135.3, 135.9, 142.5, 143.9, 168.4; IR (KBr) *ν* cm^{-1}: 3303 (m, *υ*(NH)), 3055 (w, *υ*(=CH)) 2951(s, $\upsilon_{as}(CH_2, CH_3)$), 2921(s, $\upsilon_s(CH_2, CH_3)$), 2852 (w), 1669 (m, *υ*(C=O)), 1601 (s, *υ*(C=C)), 1553 (s, *δ*(NH)), 1510 (s), 1489(s), 1405 (w, $\delta_{as}(CH_2, CH_3)$), 1371 (w, $\delta_s(CH_2, CH_3)$), 1320 (m), 1249 (s, $\delta_s(CH_3, TMS)$), 1190 (w), 1162 (w), 1094 (m), 1013 (m), 853(s), 840 (s, $\delta_{as}(CH_3, TMS)$) 754 (m), 693 (w, $\upsilon_{as}(SiC_3)$); UV-Vis (λ_{max}[nm], ε, CH_2Cl_2) 268 (28264); ESI(+) HRMS Calcd for $C_{42}H_{59}S_3Si_3NK$ ([M+K]$^+$, 812.2704), found *m/z* 812.2726; elemental analysis calcd (%) for $C_{42}H_{59}S_3Si_3N$ (773.31); C 65.14; H 7.68, N 1.81; found: C 62.84, H 7.16, N 1.68.

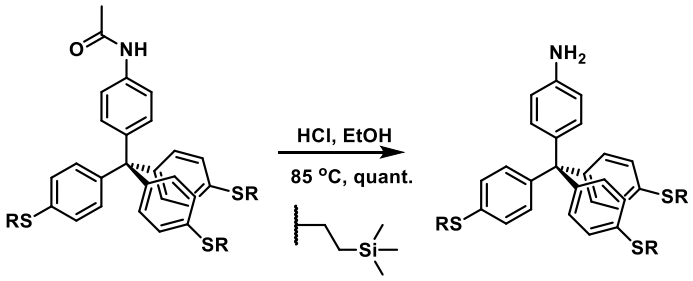

28 **29**

Method B **(**hydrolysis) Tetraphenylmethane derivatives **28** (0. 57 g, 0.67 mmol) was dissolved in a 5 mL of hot ethanol and transferred to the 100 mL two-neck round bottom flask equipped with a reflux condenser. Resulted solution was treated with 0.1 mL of concentrated hydrochloric acid and then refluxed overnight under an inert atmosphere. The reaction mixture was cooled down to room temperature, neutralized by saturated solution of sodium carbonate (50 mL), ethanol was removed and crude slurry was extracted with dichloromethane (3 x 100 mL). The combined organic layer were dried over magnesium sulfate and filtered, solvents were removed under vacuum providing the pure aniline **29** in an almost quantitative yield as a creamy oil.

4-(Tris{4-[2-(trimethylsilyl)ethylsulfanyl]phenyl}methyl)phenol (**30**)

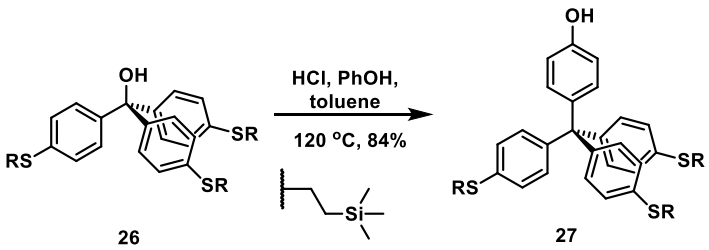

A 100 mL two-neck round bottom flask was charged with **26** (0.69 g, 1.05 mmol), phenol (1.97 g, 21 mmol), toluene (10 mL) under argon, and a few drops of concentrated HCl were added. The reaction mixture was heated at 120 °C for 14 h under argon. After cooling to room temperature, the navy-blue reaction mixture was diluted with toluene (120 mL) and quenched with solution of NaOH (2 M, 160 mL). The combined organic layer was washed with water (150 mL), dried over $MgSO_4$ and filtered. All volatiles were removed under reduced pressure and the residue was purified by column chromatography on silica gel (150 g) in hexane/EtOAc (5:1) to afford **30** (0.65 g) as an orange solid in 84% yield (R_f = 0.26, hexane/EtOAc = 9:1); m.p. 98-101 °C; ^{1}H NMR (500 MHz, $CDCl_3$) δ ppm 0.03 (s, 27H, CH_3), 0.92-0.95 (m, 6H, CH_2), 2.93-2.96 (m, 6H, CH_3), 4.79 (s. OH), 6.70 (d, $J_{H,H}$ = 8.6 Hz, 2H, Ar-H), 7.01 (d, $J_{H,H}$ = 8.65 Hz, 2H, Ar-H), 7.06-7.08 (m, 6H, Ar-H), 7.14-7.15 (m, 6H, Ar-H); ^{13}C NMR (125.8 MHz, $CDCl_3$) δ ppm -1.6, 17.0, 29.3, 63.4, 114.5, 127.4, 131.6, 132.4, 135.3, 139.0, 144.3, 153.8; IR (KBr) ν cm^{-1}: 3403 (s, υ(OH)), 3022 (w, υ(=CH)), 2951 (s, υ_{as}(CH_2, CH_3)), 2921 (s, υ_s(CH_2, CH_3)), 2852 (m), 1591 (m, υ(C=C)), 1488 (s), 1428 (m, δ_s(CH_2, CH_3)), 1352 (δ_{as}(CH_2, CH_3)), 1248 (s, (CH_3, TMS)), 837 (s), 692 (w, υ_{as}(SiC_3)); UV-Vis (λ_{max}[nm], ε, CH_2Cl_2) 271 (74485); ESI(+) MS Calcd for $C_{40}H_{56}OS_3Si_3Na$ ([M+Na]$^+$, 771.2698), found *m/z* 771.2609; elemental analysis calcd (%) for $C_{40}H_{56}OS_3Si_3$ (732.28): C, 65.52; H, 7.70; found: C, 65.30; H, 7.76.

4-(Tris{4-[2-(trimethylsilyl)ethylsulfanyl]phenyl}methyl)phenyl trifluoromethanesulfonate (31)

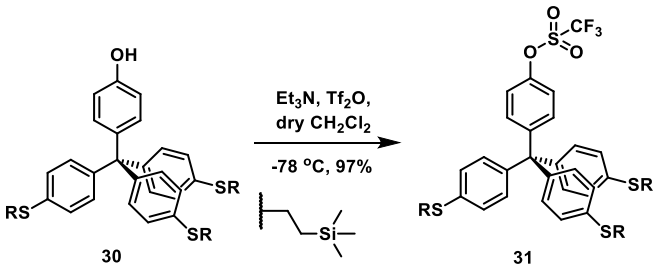

Trifluoromethanesulfonic anhydride (0.22 mL, 1.3 mmol) was added dropwise to the solution of **30** (0.56 g, 0.76 mmol) in dry triethylamine (0.2 mL, 1.4 mmol) and CH_2Cl_2 (20 mL) at -78 °C under argon atmosphere. The solution was stirred for 6 h at -78 °C, and then allowed to warm to room temperature and stirred for an additional 10 h, before quenching with water (100 mL). The aqueous layer was washed with CH_2Cl_2 (2 x 150 mL). The combined organic layer was washed with brine (100 mL), dried over $MgSO_4$ and filtered. The volatiles were removed under reduced pressure and the residue was purified by column chromatography on silica gel (130 g) with hexane/EtOAc (9:1) as an eluent to yield 0.64 g (97%) of **31** (R_f = 0.88, hexane/EtOAc = 9:1); m.p. 98-101 °C; ^{1}H NMR (500 MHz, $CDCl_3$) δ ppm 0.05 (s, 27H, CH_3), 0.93-0.96 (m, 6H, CH_2), 2.94-2.98 (m, 6H, CH_2) 7.04-7.05 (m, 6H, Ar-H) 7.14-7.17 (m, 8H, Ar-H), 7.28 (d, $J_{H,H}$ = 8.85 Hz, 2H, Ar-H); ^{13}C NMR (125.8 MHz, $CDCl_3$) δ ppm -1.6, 16.9, 29.1, 63.7, 120.5, 127.4, 131.4, 132.9, 136.1, 143.1, 147.2, 147.8; ^{19}F NMR (470.57 MHz, $CDCl_3$) -72.92; IR (KBr) ν cm^{-1}: 3025 (w, υ(=CH)), 2956 (s, υ_{as}(CH_2, CH_3)), 2922 (s, υ_s(CH_2, CH_3)), 2853 (m), 1557 (w, υ(C=C)), 1490 (s), 1429 (s, δ_s(CH_2, CH_3)), 1363 (m, δ_{as}(CH_2, CH_3)), 1250 (s, (CH_3, TMS)), 1214 (s), 1141 (m), 812 (s), 694 (w, υ_{as}(SiC_3)) UV-Vis (λ_{max}[nm], ε, CH_2Cl_2) 273 (33589); ESI(+) MS Calcd for $C_{41}H_{55}O_3S_4Si_3FNa$ ([M+Na]$^+$, 887.2186), found *m/z* 887.2121; elemental analysis calcd (%) for $C_{41}H_{55}O_3S_4Si_3F$ (864.23): C, 56.91; H, 6.41; found: C, 56.97; H, 6.55.

4-(Tris{4-[2-(trimethylsilyl)ethylsulfanyl]phenyl}methyl)benzonitrile (**32**)

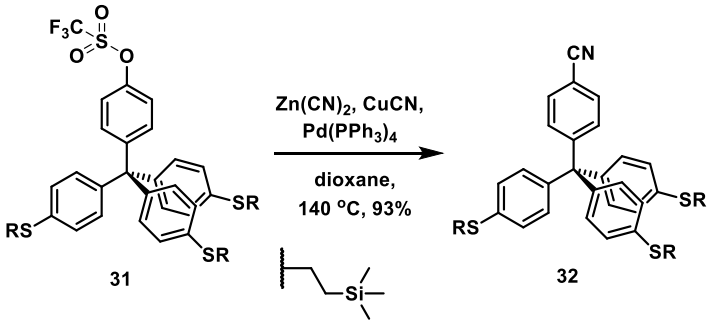

Caution! Inorganic cyanides are highly toxic compounds.

A 50 mL pressure tube was charged with triflate **31** (0.25 g, 0.29 mmol), zinc cyanide (0.14 g, 1.19 mmol), copper (I) cyanide (0.026 g, 0.29 mmol), $Pd(PPh_3)_4$ (0.034 g, 0.029 mmol) and anhydrous DMF (8 mL) under argon. The tube was sealed and stirred at 140 °C for 16 h. After cooling to room temperature, the resulting solution was quenched with Na_2CO_3 (60 mL). The aqueous layer was washed with CH_2Cl_2 (2 x 150 mL). The combined organic layer was washed with brine (100 mL), dried over $MgSO_4$ and filtered. All volatiles were removed under reduced pressure and the residue was purified by column chromatography on silica gel (70 g) in the mixture of hexane/EtOAc (9:1) to get 0.2 g of **32** as a white powder in 93% yield (R_f = 0.44, hexane/EtOAc = 9:1); m.p. 156-158 °C; ^{1}H NMR (500 MHz, $CDCl_3$) δ ppm 0.04 (s, 27H, CH_3), 0.92-0.96 (m, 6H, CH_2), 2.93-2.97 (m, 6H, CH_2), 7.03-7.05 (m, 6H, Ar-H), 7.15-7.17 (m, 6H, Ar-H), 7.33 (d, $J_{H,H}$ = 8.85 Hz, 2H, Ar-H), 7.54 (d, $J_{H,H}$ = 8.5 Hz, 2H, Ar-H); ^{13}C NMR (125.8 MHz, $CDCl_3$) δ ppm -1.5, 16.9, 29.1, 64.3, 110.2, 119.0, 127.4, 131.4, 131.6, 131.8, 136.3, 142.7, 152.2; IR (KBr) ν cm^{-1}: 3024 (w, υ(=CH)), 2953 (s, υ_{as}(CH_2, CH_3)), 2927 (s, υ_s(CH_2, CH_3)), 2854 (m), 2231 (m, υ(C≡N)), 1605 (w, υ(C=C)), 1489 (s), 1401 (s, δ_s(CH_2, CH_3)), 1343 (m, δ_{as}(CH_2, CH_3)), 1248 (s, (CH_3, TMS)), 1214 (s), 1141 (m), 1094 (s), 859 (s), 694 (w, υ_{as}(SiC_3)); UV-Vis (λ_{max}[nm], ε, CH_2Cl_2) 224 (13100), 270 (23 341); ESI(+) MS Calcd for $C_{41}H_{55}OS_3Si_3NNa$ ([M+Na]$^+$, 764.2697), found *m/z* 764.2548; elemental analysis calcd (%) for $C_{41}H_{55}OS_3Si_3N$ (741.28): C, 66.34; H, 7.47; N, 1.89; found: C, 66.56; H, 7.61; N, 1.92.

***S*,*S*′,*S*′′-{4,4',4''-[(4-cyanophenyl)methanetriyl)]tris(benzene-4,1-diyl)} tris(thioacetate)** (**33**)

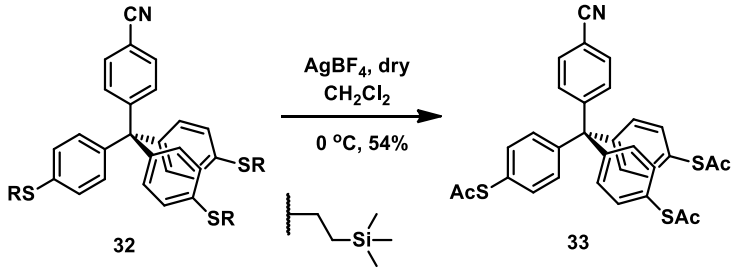

In a 50 mL oven-flamed Schlenk flask, tetraphenylmethane **32** (150 mg, 0.20 mmol) was dissolved in a mixture of dry CH_2Cl_2 (16 mL) and acetyl chloride (1.6 mL) under argon. The solution was treated with $AgBF_4$ (0.2 g, 1.02 mmol) and a green suspension was stirred at room temperature for 12 h. The completion of the reaction was checked by TLC (Hexane/EtOAc = 3:1). The reaction mixture was diluted with dichloromethane (100 mL) and slowly poured into the saturated solution of $NaHCO_3$ (60 mL). The precipitate was filtered through a pad of Celite, washed with CH_2Cl_2, and concentrated in a vacuo. The crude product was purified by column chromatography on silica gel (150 g) with hexane/EtOAc (3:1) to yield 62 mg (54%) of **33** as a white powder (R_f = 0.11, hexane/EtOAc = 3:1); m.p. 202-204 °C; ^{1}H NMR (500 MHz, $CDCl_3$) δ ppm 2.42 (s, 9H, CH_3), 7.21-7.22 (m, 6H, Ar-H), 7.32-7.34 (m, 6H, Ar-H), 7.37 (d, $J_{H,H}$ = 8.5 Hz, 2H, Ar-H), 7.57 (d, $J_{H,H}$ = 8.5 Hz, 2H, Ar-H); ^{13}C NMR (125.8 MHz, $CDCl_3$) δ ppm 30.47, 65.05, 110.7, 118.7, 126.9, 128.63, 128.69, 131.6, 131.7, 131.9, 134.05, 146.1, 150.9, 193.7; IR (KBr) ν cm^{-1}: 3029 (w, υ(=CH)), 2920 (s, υ_{as}(CH_3)), 2931 (m, υ_s(CH_3)), 2854 (m), 2227 (m, υ(C≡N)), 1704 (s, υ(C=O)), 1603 (w, υ(C=C)), 1486 (m), 1396 (w, δ_{as}(CH_3)), 1343 (w, δ_s(CH_3)), 1194 (s), 1117 (m), 820 (s), 618 (s); UV-Vis (λ_{max}[nm], ε, CH_3CN) 223 (31640), 250 (27521); ESI(+) HRMS Calcd for $C_{32}H_{25}NO_3S_3Na$ ([M+Na]$^+$, 590.0889), found *m/z* 590.0883; elemental analysis calcd (%) for $C_{32}H_{25}NO_3S_3$ (567.10): C, 67.70; H, 4.44; N, 4.47; N, 2.47; found: C, 67.89; H, 4.53; N, 2.58.

4-(Tris{4-[2-(trimethylsilyl)ethylsulfanyl]phenyl}methyl)phenylboronic acid pinacol ester (**34**)

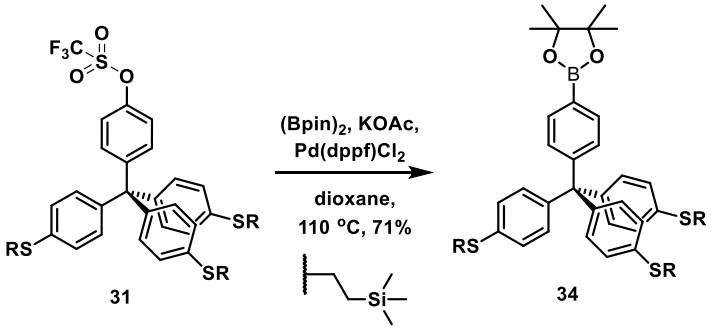

A 50 mL oven-flamed pressure tube was charged with triflate **31** (0.65 g, 0.75 mmol), anhydrous potassium acetate (0.22 g, 2.24 mmol), bis(pinacolato)diboron (0.29 g, 1.14 mmol), Pd(dppf)Cl_2 (0.061 g, 0.075 mmol) and dry dioxane (15 mL) under argon. The tube was sealed and stirred under at 120 °C for 16 h. After cooling, the reaction mixture was diluted with dichloromethane (200 mL) and washed with water (100 mL). The combined organic layer was washed with brine (100 mL), dried over $MgSO_4$ and filtered. The volatiles were removed under reduced pressure and the residue was purified by column chromatography on silica gel (130 g) with hexane/EtOAc (9:1) to provide 0.45 g of **34** as a yellow powder in 71% yield (R_f = 0.6, hexane/EtOAc = 9:1); m.p. 174-175 °C; ^{1}H NMR (500 MHz, $CDCl_3$) δ ppm 0.03 (s, 27 H, CH_3), 0.91-0.95 (m, 6H, CH_2), 1.32 (s, 12H, CH_3), 2.92-2.96 (m, 6H, CH_2), 7.08-7.09 (m, 6H, Ar-H), 7.13-7.15 (m, 6H, Ar-H), 7.20 (d, $J_{H,H}$ = 7.8 Hz, 2H, Ar-H), 7.68 (d, $J_{H,H}$ = 8 Hz, 2H, Ar-H); ^{13}C NMR (125.8 MHz, $CDCl_3$) δ ppm -1.5, 17.0, 25.1., 29.3, 64.3, 84.0, 127.5, 130.5, 131.5, 131.6, 134.2, 135.3, 143.9, 149.7; IR (KBr) ν cm^{-1}: 3059 (w, υ(=CH)), 2952 (s, υ_{as}(CH_2, CH_3)), 2924 (s., υ_s(CH_2, CH_3)), 2855 (m), 1730 (w), 1608 (w, υ(C=C)), 1486 (s), 1398 (s, δ_s(CH_2, CH_3)), 1361 (s, δ_{as}(CH_2, CH_3)), 1248 (s, CH_3, TMS)), 1214 (w), 1145 (m), 1091 (s), 860 (s), 837 (s), 808 (m), 751 (w), 695 (w, υ_{as}(SiC_3)); UV-Vis (λ_{max}[nm], ε, CH_2Cl_2) 271 (36961); ESI(+) MS Calcd for $C_{46}H_{67}BO_2S_3Si_3Na$ ([M+Na]$^+$, 865.3365), found *m/z* 865.3076; elemental analysis calcd (%) for $C_{46}H_{67}BO_2S_3Si_3$ (842.37): C, 65.52; H, 8.01; found: C, 65.74; H, 8.06.

1-Iodo-4-(tris{4-[2-(trimethylsilyl)ethylsulfanyl]phenyl}methyl)benzene (**35**)

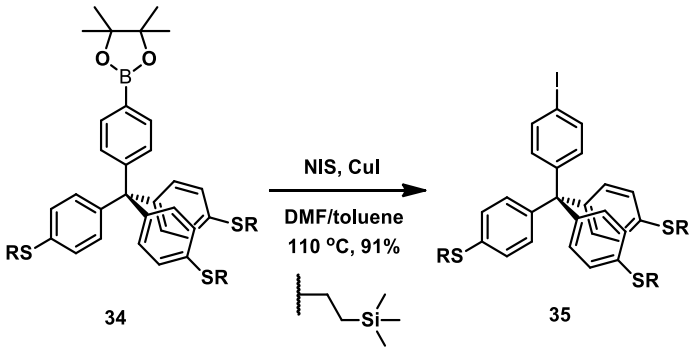

A 50 mL, two neck round-bottom flask was charged with pinacol ester **34** (0.15 g, 0.18 mmol), copper iodide (0.051 g, 0.27 mmol), *N*-iodosuccinimide (0.06 g, 0.27 mmol), anhydrous DMF (8 mL), and toluene (4 mL) under argon. The reaction mixture was stirred and heated at 110 °C for 24 h under argon atmosphere. After cooling, the reaction mixture was diluted with dichloromethane (200 mL) and washed with Na_2SO_3 solution (10%, 100 mL). The combined organic layer was washed with brine (100 mL), dried over $MgSO_4$ and filtered. All volatiles were removed under reduced pressure and the residue was purified by column chromatography on silica gel (100 g) with hexane/EtOAc (10:1) to obtain 0.14 g of **35** as a yellow powder in 91% yield (R_f = 0.92, hexane/EtOAc = 9:1); m.p. 70-71 °C; ^{1}H NMR (500 MHz, $CDCl_3$) δ ppm 0.04 (s, 27 H, CH_3), 0.92-0.95 (m, 6H, CH_2), 2.93-2.96 (m, 6H, CH_2), 6.92-6.93 (d, $J_{H,H}$ = 9 Hz, 2H, Ar-H), 7.04-7.06 (m, 6H, Ar-H), 7.14-7.16 (m, 6H, Ar-H), 7.56 (d, $J_{H,H}$ = 8 Hz, 2H); ^{13}C NMR (125.8 MHz, $CDCl_3$) δ ppm -1.5, 16.9, 29.2, 63.8, 92.1, 127.4, 131.5, 131.6, 133.2, 135.7, 136.9, 143.4, 146.5; IR (KBr) ν cm^{-1}: 3023 (w, υ(=CH)), 2952 (s, υ_{as}(CH_2, CH_3)), 2923 (s, υ_s(CH_2, CH_3)), 2853 (m), 1739 (w), 1590 (w, υ(C=C)), 1484 (s), 1399 (s, δ_s(CH_2, CH_3)), 1248 (s, CH_3, TMS)), 1194 (w), 1163 (m), 1093 (s), 1006 (m), 858 (s), 838 (s), 809 (m), 753 (w), 693 (w, υ_{as}(SiC_3)); UV-Vis (λ_{max}[nm], ε, CH_2Cl_2) 271 (38610); ESI(+) HRMS Calcd for $C_{40}H_{55}IS_3Si_3Na$ ([M+Na]$^+$, 865.1711, found *m/z* 865.1716; elemental analysis calcd (%) for $C_{40}H_{55}IS_3Si_3$ (842.18): C, 56.98; H, 6.57; found: C, 57.09; H, 6.65.

***S*,*S′*,*S′′*-{4,4',4''-[(4-Iodophenyl)methanetriyl)]tris(benzene-4,1-diyl)} tris(thioacetate) (36)**

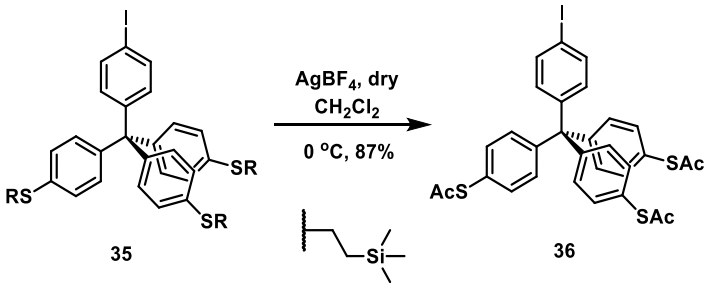

The desired product was prepared according to the method described for the preparation of **33**, starting from **35** (0.11 g, 0.13 mmol), $AgBF_4$ (0.2 g, 1.05 mmol) in a mixture of dry dichloromethane (12 mL) and acetyl chloride (1.2 mL) under argon. The suspension was stirred at room temperature for 12 h. The crude product was purified by column chromatography on silica gel (150 g) in hexane/EtOAc (5:1) to provide 0.076 g of **36** as a white powder in 87% yield (R_f = 0.41 hexane/EtOAc = 3:1); m.p. 272-273 °C; ^{1}H NMR (500 MHz, $CDCl_3$) δ ppm 2.42 (s. 9H, CH_3), 6.97 (d, $J_{H,H}$ = 9.5 Hz, 2H, Ar-H), 7.22-7.24 (m, 6H, Ar-H), 7.30-7.32 (m, 6H, Ar-H), 7.59 (d, $J_{H,H}$ = 8 Hz, 2H, Ar-H); ^{13}C NMR (125.8 MHz, $CDCl_3$) δ ppm 30.5, 64.6, 92.7, 126.4, 131.8, 131.9, 133.1, 133.9, 137.2, 145.5, 146.9, 194.0; IR (KBr) ν cm^{-1}: 3039 (w, υ(=CH)), 2954 (s, $\upsilon_{as}(CH_3)$), 2924 (m, $\upsilon_s(CH_3)$), 2854 (m), 1741 (s, υ(C=O)), 1590 (w, υ(C=C)), 1485 (m), 1467 (w, $\delta_{as}(CH_3)$), 1390 (w, $\delta_s(CH_3)$), 1261 (m), 1092 (w), 817 (m), 616 (s); UV-vis (λ_{max}[nm], ε, CH_2Cl_2) 251 (18696); ESI(+) MS Calcd for $C_{31}H_{25}IO_3S_3Na$ ([M+Na]$^+$, 690.9903), found *m/z* 690.9890; elemental analysis calcd (%) for $C_{40}H_{55}IS_3Si_3$ (668.00): C, 55.69; H, 3.77; found: C, 55.52; H, 3.68.

1-(4-Bromo)-4-(tris{4-[2-(trimethylsilyl)ethylsulfanyl]phenyl}methyl)benzene (**37**)

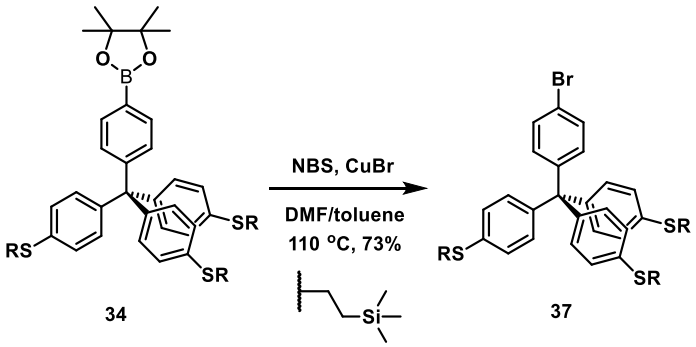

Following the procedure reported for the synthesis of **35**. Oven-flamed 100 mL single neck round bottom flask was charged with pinacol boronic ester **34** (0.19 g, 0.22 mmol) *N*-bromosuccinimide (0.06 g, 0.33 mmol), and copper bromide (0.095 g, 0.66 mmol) dissolved in the mixture of toluene (4 mL) and dimethylformamide (8 mL). The reaction mixture was purged by argon over 30 min, and then heated at 110 °C overnight. Upon cooling to room temperature solvents were evaporated. The residue was diluted with dichloromethane (150 mL) and washed with sodium sulfite solution (150 mL). Aqueous layer was separated and additionally extracted with dichloromethane (2 x100 mL). The combined organic layer was dried over magnesium sulfate and filtered. All volatiles were removed under reduced pressure and the crude product was purified by column chromatography on silica gel (100 g) in hexane/ CH_2Cl_2 (2:1) to obtain 0.13 g of **37** (73%) as a yellow solid. (R_f = 0.23, hexane/ CH_2Cl_2 2:1); m.p. 227-229 °C; ^{1}H NMR (500 MHz, $CDCl_3$) δ ppm 0.04 (s, 27H, CH_3), 0.92-0.95 (m, 6H, CH_2), 2.94-2.98 (m, 6H, CH_2), 7.07-7.10 (m, 8H, Ar-H), 7.14-7.17 (m, 6H, Ar-H), 7.39 (d, $J_{H,H}$ = 8 Hz, 2H, Ar-H); ^{13}C NMR (125.8 MHz, $CDCl_3$) δ ppm -1.8, 17.1, 29.3, 63.9, 120.4, 127.5, 131, 131.6, 133.1, 136.1, 143.7 146.2; IR (KBr) ν cm^{-1}: 3020 (w, υ(=CH)) 2949 (s, υ_{as}(CH_2, CH_3)), 2918 (s, υ_s(CH_2, CH_3)), 2851 (w), 1588 (s, υ(C=C)), 1484 (s), 1398 (m, δ_{as}(CH_2, CH_3)), 1248 (s, δ_s(CH_2, CH_3)), 1322 (w), 1248 (s, δ_s(CH_3, TMS)), 1195 (w), 1163 (w), 1145 (m), 1196 (m), 1164 (m), 1093 (s), 1010 (s) 859 (s), 839 (s, δ_{as}(CH_3, TMS)) 810 (m), 692 (w, υ_{as}(SiC_3)); UV-Vis (λ_{max}[nm], ε, CH_2Cl_2) 272 (29317); ESI(+) HRMS Calcd for $C_{40}H_{51}S_3Si_3BrK$ ($[M+K]^+$, 831.1262), found *m/z* 831.0907; elemental analysis calcd (%) for $C_{40}H_{51}S_3Si_3Br$ (794.20): C 60.34; H 6.96; found: C 60.49, H 7.58.

***S*,*S′*,*S′′*-{4,4',4''-[(4-Bromophenyl)methanetriyl)]tris(benzene-4,1-diyl)} tris(thioacetate)** (**38**)

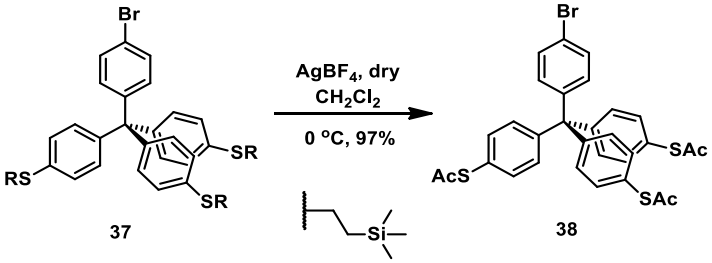

A procedure for transprotection of **36** was adopted as follows. Compound **37** (0.09 g, 0.11 mmol) was loaded to an oven-flamed and argon flashed Schlenk flask and dissolved in dry dichloromethane (21 mL). Subsequently acetyl chloride (2.1 mL) was dropwise added under argon at 0 ^{o}C. The solution was treated with silver tetrafluoroborate (0.18 g, 0.91 mmol) and suspension was stirred overnight at room temperature. Afterward, the reaction was quenched with saturated solution of sodium hydrocarbonate (50 mL) and washed with dichloromethane (3 x 100 mL). The combined organic layers were dried over magnesium sulfate, passed through pad of Celite, and the residues were removed under vacuum. The crude product was purified by column chromatography on silica gel (120 g), with Hex/EtOAc 3:1) providing 0.068 g (97%) of **38** as a white powder. (R_f = 0.56, hexane/EtOAc 3:1); m.p. 215-218 ^{o}C; ^{1}H NMR (500 MHz, CD_2Cl_2) δ ppm 2.40 (s, 9H, CH_3), 7.15 (d, $J_{H,H}$ = 8.75 Hz, 2H, Ar-H), 7.29 (d, $J_{H,H}$ = 8.75 Hz, 6H, Ar-H), 7.34 (d, $J_{H,H}$ = 8.7 Hz, 6H, Ar-H), 7.44 (d, $J_{H,H}$ = 8.8 Hz, 2H, Ar-H); ^{13}C NMR (125.8 MHz, CD_2Cl_2) δ ppm 30.5, 64.8, 121, 126.9, 131.5, 131.8, 132.9, 132.9, 134.2, 145.1, 147.2, 193.9; IR (KBr) ν cm^{-1}:3060 (w, υ(=CH)), 2924 (s, υ_{as}(CH_3)), 2854 (m, υ_s(CH_3)), 1705 (s, υ(C=O)), 1584 (w, υ(C=C)), 1486 (m), 1393 (m, δ_{as}(CH_3)), 1347 (m, δ_s(CH_3)), 1122 (m), 1092 (m), 1011 (m), 954 (m), 819 (s), 617 (s, υ(C-Br)), UV-Vis (λ_{max}[nm], ε, acetone) 212 (62093); ESI(+) MS Calcd for $C_{31}H_{25}BrO_3S_3Na$ ([M+Na]$^+$, 645.0027), found *m/z* 644.9997; elemental analysis calcd (%) for $C_{31}H_{25}BrO_3S_3$ (620.01): C 59.90; H 4.05; found: C 60.79; H 4.71.

3-Bromo-1-[2-(trimethylsilyl)ethylsulfanyl]benzene (**39**)

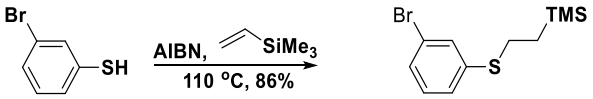

39

Compound **39** was synthesized according to the published procedure.[279] 3-Bromothiophenol (5 g, 26.4 mmol), vinyltrimethylsilane (5.55 g, 55.4 mmol), and azobisisobutyronitrile (AIBN) (0.22 g, 1.32 mmol) were charged to 50 mL pressure tube under inert atmosphere. Afterwards, the tube was sealed and vigorously stirred overnight at 100 °C. The reaction was cooled down, the crude mixture was mixed with 8% solution of $NaOH_{aq}$ over 1 h and then extracted with Et_2O (2 x 120 mL). Organic layers were combined, dried over $MgSO_4$, filtrated and solvents were removed. Obtained yellow oil was purified by column chromatography on silica gel (700 g) in pure hexane providing 6.59 g of **39** in 86% yield. (R_f = 0.29, hexane); ^{1}H NMR (500 MHz, $CDCl_3$) δ ppm, 0.12 (s, 9H, CH_3), 0.98-1.01 (m, 2H, CH_2), 3-3.04 (m, 2H, CH_2), 7.17-7.20 (t, 1H, Ar-H), 7.25-7.27 (m, 1H, Ar-H), 7.32-7.34 (m, 1H, Ar-H), 7.47-7.48 (m, 1H, Ar-H); ^{13}C NMR (125.8 MHz, $CDCl_3$) δ ppm -0.7, 17.7, 30.3 123.8, 128.0, 129.5, 131.1, 131.8, 132.9, 141.0

Tris{3-[2-(trimethylsilyl)ethylsulfanyl]phenyl}methanol (**41**)

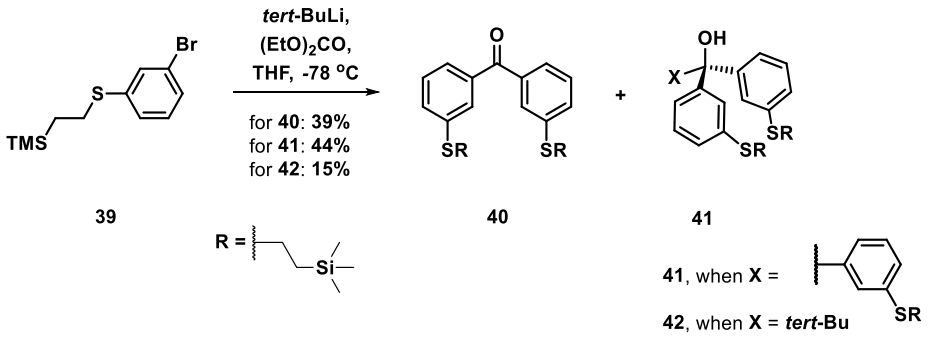

Method A: The desired product was prepared according to the method described for the preparation of **26**, starting from **39** (3 g, 10.4 mol) in anhydrous THF (30 mL), *tert*-BuLi (14 mL, 21 mmol, 15% in pentane), and diethyl carbonate (0.36 mL, 2.97 mmol) in anhydrous THF (6 mL) under argon. After 16 h, the reaction mixture was quenched, and the crude product was purified by column chromatography on silica gel (350 g) with hexane/EtOAc

(9:1) to get 0.85 g of **41** as yellow oil in 44% yield and 0.52 g of **40** as a yellowish solid in 39% yield and side product **41** as an creamy oil in 15% yield.

For **41**: (R_f = 0.43, hexane/EtOAc = 9:1); m.p. 92-94 °C; ^{1}H NMR (500 MHz, $CDCl_3$) δ ppm 0.01 (s, 27H, CH_3), 0.85-0.89 (m, 6H, CH_2), 2.75 (s, OH), 2.86-2.89 (m, 6H, CH_2), 7.01-7.03 (m, 3H, Ar-H), 7.19-7.20 (m, 5H, Ar-H); 7.20-7.23 (m, 5H, Ar-H); ^{13}C NMR (125.8 MHz, $CDCl_3$) δ ppm -1.6, 16.9, 29.4, 81.9, 125.4, 127.6, 127.9, 128.6, 137.5, 147.2; IR (KBr) ν cm^{-1}: 3460 (s, υ(OH)), 3029 (w, υ(=CH)), 2950 (s, υ_{as}(CH_2, CH_3)), 2922 (s, υ_s(CH_2, CH_3)), 2854 (m), 1584 (w, υ(C=C)), 1467 (s), 1411 (s, δ_s(CH_2, CH_3)), 1370 (s, δ_{as}(CH_2, CH_3)), 1247(s, CH_3, TMS)), 1114 (m), 1095 (s), 857 (s), 841 (s), 695 (w, υ_{as}(SiC_3)); UV-Vis (λ_{max}[nm], ε, CH_2Cl_2) 257 (25970); ESI(+) MS Calcd for $C_{34}H_{52}OS_3Si_3Na$ ([M+Na]$^+$, 679.2380), found *m/z* 697.2307; elemental analysis calcd (%) for $C_{34}H_{52}OS_3Si_3$ (656.25): C, 62.14; H, 7.98; found: C, 62.29; H, 8.08.

For **40**: (R_f = 0.5, hexane/EtOAc = 9:1); m.p. 123-125 °C; ^{1}H NMR (500 MHz, $CDCl_3$) δ ppm 0.04 (s, 18H, CH_3), 0.93-0.96 (m, 4H, CH_2), 2.97-3.01 (m, 4H, CH_2), 7.36-7.39 (m, 2H, Ar-H), 7.49-7.50 (m, 2H, Ar-H), 7.52-7.54 (m, 2H, Ar-H), 7.69 (s, 2H, Ar-H), 7.70 (s, 1H), ^{13}C NMR (125.8 MHz, $CDCl_3$) δ ppm -1.6, 16.9, 29.4, 128.8, 129.5, 132.5, 138.2, 138.6, 196.1; IR (KBr) ν cm^{-1}: 3055 (w, υ(=CH)), 2951 (s, υ_{as}(CH_2, CH_3)), 2927 (s, υ_s(CH_2, CH_3)), 2853 (m), 1658 (s, υ(C=O)), 1561 (w, υ(C=C)), 1431 (m, δ_s(CH_2, CH_3)), 1414 (m, δ_{as}(CH_2, CH_3)), 1260 (s, CH_3, TMS)), 1145 (m), 1091 (s), 847 (s), 840 (s), 695 (w, υ_{as}(SiC_3)); UV-Vis (λ_{max}[nm], ε, CH_2Cl_2) 265 (23085); ESI(+) HRMS Calcd for $C_{23}H_{34}OS_2Si_2K$ ([M+K]$^+$, 485.1221), found *m/z* 485.1247; elemental analysis calcd (%) for $C_{23}H_{34}OS_2Si_2$ (446.16): C, 61.83; H, 7.67; found: C, 61.67; H, 7.90.

For **42**: m.p. 89-91 °C; ^{1}H NMR (500 MHz, $CDCl_3$) δ ppm 0.01 (s, 18H, CH_3), 0.86-0.88 (m, 4H, CH_2), 0.90 (s, 9H, CH_3), 2.25 (s, 1H, OH), 2.89-2.92 (m, 4H, CH_2), 7.18 (dd, $J_{H,H}$ = 6.75, 1.85 Hz, 4H, Ar-H), 7.42 (dd, $J_{H,H}$ = 6.65, 1.9 Hz, 4H, Ar-H), ^{13}C NMR (125.8 MHz, $CDCl_3$) δ ppm -1.6, 17.1, 27.7, 29.8, 39.4, 82.9, 126.2, 127.4, 127.8, 129.2, 136.2, 146.6; IR (KBr) ν cm^{-1}:3415 (υ(OH)), 3028 (w, υ(=CH)) 2953 (s, υ_{as}(CH_2, CH_3)), 2922 (s, υ_s(CH_2, CH_3)), 2854 (m), 1590 (m, υ(C=C)), 1470 (m, δ_{as}(CH_2, CH_3)), 1404 (w, δ_s(CH_2, CH_3)), 1249 (m, δ_s(CH_3, TMS)), 1162 (m), 1105 (w), 1047 (m), 893 (m), 862 (s), 840 (s, δ_{as}(CH_3, TMS)) 828 (s), 749 (m), 696 (w, υ_{as}(SiC_3)); UV-Vis (λ_{max}[nm], ε, CH_2Cl_2) 267 (22553); ESI(+) HRMS Calcd for

$C_{27}H_{44}OS_2Si_2K$ ([M+K]$^+$, 543.2009), found *m/z* 543.2089; elemental analysis calcd (%) for $C_{27}H4_{44}OS_2Si_2$ (504.24); C 64.24 H 8.78; found: C 64.20, H 8.36.

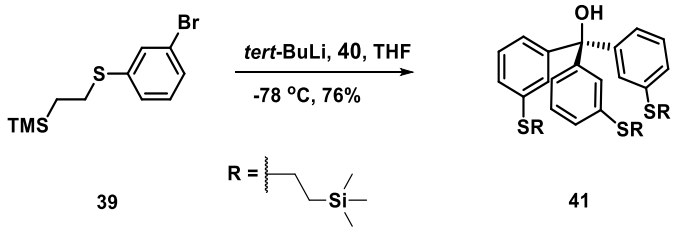

Method B: The desired product was prepared according to the method described for the preparation of **26**, starting from **39** (0.97 g, 3.35 mmol) in anhydrous THF (15 mL), *tert*-BuLi (4.55 mL, 6.71 mmol, 15% in pentane), and **40** (0.75 g, 1.6 mmol) in anhydrous THF (10 mL) under argon. After 12 h, the reaction mixture was quenched, and the crude product was purified by column chromatography on silica gel (200 g) in hexane/EtOAc (9:1) to yield 1 g (76%) of **41** as yellowish oil.

3,3'-dibromobenzophenone (**44**)

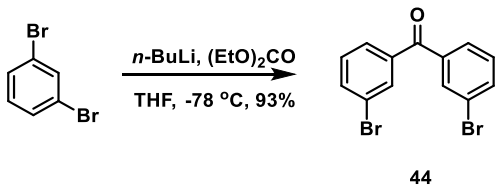

A flame-dried, argon-flushed 100 mL Schlenk flask was charged with 1,3-dibromobenzene (2 g, 8.47 mmol) and anhydrous THF (30 mL). The solution was cooled to -78 °C and *n*-BuLi (1.6 M in hexane, 5.3 mL, 8.48 mmol) was added dropwise over 20 min. The reaction mixture was stirred at -78 °C for 2 h under argon. In a second 100 mL Schlenk flask, diethyl carbonate (0.21 mL, 1.7 mmol) was diluted in anhydrous THF (10 mL) under an inert atmosphere and cooled to -78 °C. The solution of lithiated species was slowly added via a cannula into the flask containing carbonate solution, after 1 h, the reaction mixture was allowed to warm to room temperature and stirred for an additional 15 h. The reaction mixture was quenched with saturated NH_4Cl solution (100 mL). The aqueous layer was washed with CH_2Cl_2 (3 × 100 mL). The combined organic layer was washed with brine (100 mL), dried

over $MgSO_4$ and filtered. The volatiles were removed under reduced pressure and the residue was purified by column chromatography on silica gel (200 g) in hexane/EtOAc (20:1) to afford 0.53 g of **44** as a white solid in 93% yield (R_f = 0.4, hexane/EtOAc = 20:1); m.p. 123-125 °C; ^{1}H NMR (500 MHz, CD_2Cl_2) δ ppm 7.38-7.41 (m, 2H, Ar-H), 7.68-7.69 (m, 2H, Ar-H), 7.75-7.77 (m, 2H, Ar-H), 7.91-7.92 (m, 2H, Ar-H); ^{13}C NMR (125.8 MHz, CD_2Cl_2) δ ppm 123.0, 128.9, 130.5, 133.0, 136.0, 139.3, 193.8; IR (KBr) ν cm^{-1}: 3061 (w, υ(=CH)), 2922 (s), 1651 (s, υ(C=O), 1563 (w, υ(C=C)), 1470 (m), 1417 (m); UV-Vis (λ_{max}[nm], ε, CH_2Cl_2) 265 (9490); ESI(+) HRMS Calcd for $C_{13}H_8Br_2ONa$ ([M+Na]$^+$, 362.8814), found *m/z* 362.8802; elemental analysis calcd (%) for $C_{13}H_8Br_2O$ (337.89): C, 45.92; H, 2.37; found: C, 45.97; H, 2.34.

Tris(3-bromophenyl)methanol (**45**)

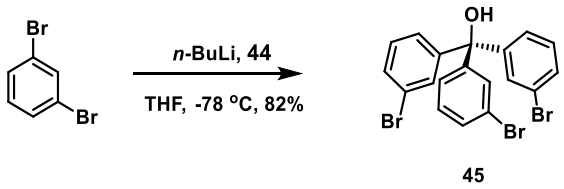

45

In a 100 mL Schlenk flask, 1,3-dibromobenzene (1.9 g, 8.1 mmol) was dissolved in anhydrous THF (30 mL) under argon, cooled to -78 °C and degassed. Then *n*-BuLi (1.6 M. in hexane, 5.3 mL, 8.4 mmol) was added dropwise over 20 min and the resulting mixture was stirred at -78 °C for 2 h. In a second 100 mL Schlenk flask, **44** (1.8 g, 5.33 mmol) was dissolved in THF (10 mL) under argon, and cooled to -78 °C. The solution of lithiated species was slowly added via a cannula into the flask containing the solution of **44**. The yellow solution was stirred at -78 °C for 2 h, then allowed to warm to room temperature and stirred for an additional 12 h. The reaction mixture was quenched with saturated NH_4Cl solution (100 mL). The aqueous layer was washed with CH_2Cl_2 (3 x 100 mL). The combined organic layer was washed with brine (100 mL), dried over $MgSO_4$ and filtered. The volatiles were removed under reduced pressure and the residue was purified by column chromatography (300 g) in hexane/EtOAc (10:1) to provide 2.15 g of **45** as a yellow oil in 82% yield (R_f = 0.29, hexane/EtOAc = 10:1): ^{1}H NMR (500 MHz, $CDCl_3$) δ ppm 3.07 (s, OH), 7.14 (d, $J_{H,H}$ = 7.9 Hz, 3H, Ar-H), 7.19-7.22 (m, 3H, Ar-H), 7.45 (d, $J_{H,H}$ = 7.85 Hz, 3H, Ar-H), 7.48 (s, 3H, Ar-H); ^{13}C NMR (125.8 MHz, $CDCl_3$) δ ppm 68.1, 122.9, 126.8

130.0, 130.8, 131.2, 148.1; IR (KBr) ν cm^{-1}: 3442(s, υ(OH)), 3061 (w, υ(=CH)), 2926 (s), 1564 (w, υ(C=C)), 1509 (s), 1470 (s), 1416 (m), 1416 (m), 1200 (m), 785 (w); UV-Vis (λ_{max}[nm], ε, CH_2Cl_2) 267 (5540); ESI(+) HRMS Calcd for $C_{19}H_{13}Br_3ONa$ ([M+Na]$^+$, 518.8389), found *m/z* 518.8376; elemental analysis calcd (%) for $C_{19}H_{13}Br_3O$ (493.25): C, 45.92; H, 2.64; found: C, 45.99; H, 2.56.

4-[Tris(3-bromophenyl)methyl]phenol (**46**)

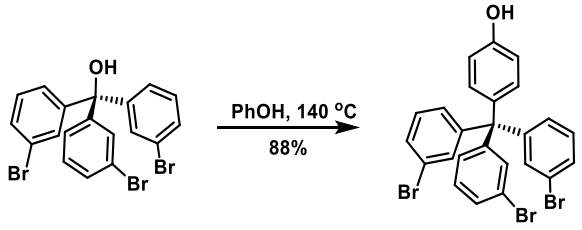

45 46

The desired product was prepared according to the method described for the preparation of **30**, starting from **45** (2.13 g, 4.32 mmol), phenol (4.81 g, 51 mmol), and a few drops of concentrated HCl. The reaction mixture was heated at 140 °C for 14 h under argon. The residue was purified by column chromatography on silica gel (300 g) in hexane/EtOAc (10:1) to afford 2.17 g of **46** as a white solid in 88% yield (R_f = 0.35, hexane/EtOAc = 10:1): m.p. 178-180 °C; ^{1}H NMR (500 MHz, $CDCl_3$) δ ppm 5.17 (s, OH), 6.76 (d, $J_{H,H}$ = 8.8 Hz, 2H, Ar-H), 6.98 (d, $J_{H,H}$ = 8.8 Hz, 2H, Ar-H), 7.07 (d, $J_{H,H}$ = 8.05 Hz, 3H, Ar-H), 7.13-7.16 (m, 3H, Ar-H), 7.32 (s, 3H, Ar-H), 7.36 (d, $J_{H,H}$ = 9.25 Hz, 3H, Ar-H); ^{13}C NMR (125.8 MHz, $CDCl_3$) δ ppm 64.1, 115.1, 122.4, 129.5, 129.9, 130.0, 132.3, 133.5, 137.3, 148.4, 154.3; IR (KBr) ν cm^{-1}: 3422 (s, υ(OH)), 3058 (w, υ(=CH)), 2922 (s), 1590 (w, υ(C=C)), 1468 (s), 1404 (m), 1215 (m), 832 (s), 782 (s); UV-Vis (λ_{max}[nm], ε, CH_2Cl_2) 280 (4420); ESI(+) HRMS Calcd for $C_{25}H_{17}Br_3ONa$ ([M+Na]$^+$, 594.8682), found *m/z* 596.8680; elemental analysis calcd (%) for $C_{25}H_{17}Br_3O$ (569.88): C, 52.39; H, 2.99; found: C, 52.42; H, 2.88.

Trimethyl{4-[tris(3-bromophenyl)methyl]phenoxy}silane (**47**)

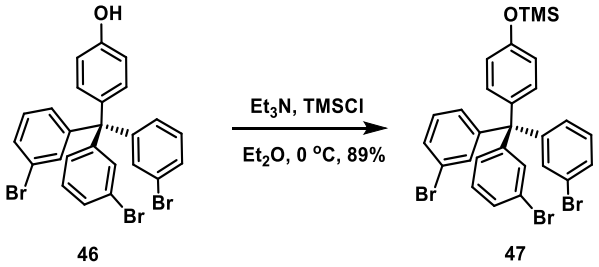

Trimethylsilyl chloride (0.50 g, 4.17 mmol) was added dropwise to a solution of **46** (1.32 g, 2.32 mmol) in the mixture of anhydrous triethylamine (0.43 g, 4.17 mmol) and diethyl ether (11 mL) at 0 °C under argon atmosphere. The reaction mixture was stirred for 3 h, and then allowed to warm to room temperature and stirred for an additional 12 h. The resulting solution was quenched with water (100 mL). The aqueous layer was washed with diethyl ether (2 x 150 mL). The combined organic layer was washed with brine (100 mL), dried over $MgSO_4$ and filtered. The volatiles were removed under reduced pressure and the residue was purified by column chromatography on silica gel (130 g) with hexane/EtOAc (9:1) to get 1.32 g of **47** as a white powder in 89% yield (R_f = 0.84, hexane/EtOAc = 9:1); m.p. 42-45 °C; ^{1}H NMR (500 MHz, $CDCl_3$) δ ppm 0.28 (s, 9H, CH_3), 6.76 (d, $J_{H,H}$ = 8.8 Hz, 2H, Ar-H), 6.97 (d, $J_{H,H}$ = 8.8 Hz, 2H, Ar-H), 7.08 (d, $J_{H,H}$ = 8.05 Hz, 3H, Ar-H), 7.13-7.17 (m, 3H, Ar-H), 7.32 (s, 3H, Ar-H), 7.37 (d, $J_{H,H}$ = 7.8 Hz, 3H, Ar-H); ^{13}C NMR (125.8 MHz, $CDCl_3$) δ ppm 0.5, 64.1, 119.4, 122.3, 129.4, 129.8, 130.0, 132.1,133.6, 137.7, 148.4, 153.9; IR (KBr) ν cm^{-1}: 3034 (w, υ(=CH)), 2956 (s, $\upsilon_{as}(CH_3)$), 2922 (s, $\upsilon_s(CH_3)$), 2852 (m), 1585 (w, υ(C=C)), 1470 (s), 1406 (s, $\delta_s(CH_3)$), 1352 (s, $\delta_{as}(CH_3)$), 1248 (s, CH_3, TMS)), 1215 (s), 832 (s), 782 (s), 683(w, $\upsilon_{as}(SiC_3)$); UV-Vis (λ_{max}[nm], ε, CH_2Cl_2) 274 (9059); ESI(+) HRMS Calcd for $C_{25}H_{17}Br_3ONa$ ([M+Na, - TMS]$^+$, 596.8682), found *m/z* 594.8690; elemental analysis calcd (%) for $C_{28}H_{25}Br_3OSi$ (641.92): C, 52.12; H, 3.91; found: C, 52.34; H, 3.97.

4-(Tris{3-[2-(trimethylsilyl)ethylsulfanyl]phenyl}methyl)phenol (**43**)

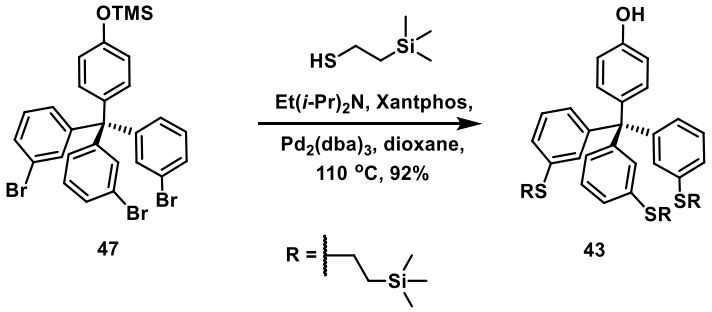

A 25 mL pressure tube was charged with **47** (1.3 g, 2.03 mmol), Xantphos (0.094 g, 0.016 mmol), $Pd_2(dba)_3$ (0.093 g, 0.0089 mmol) and anhydrous dioxane (14 mL). The tube was evacuated and refilled with argon three times. Then *N*,*N*-diisopropylethylamine (2.3 g, 18 mmol) and 2-(trimethylsilyl)ethanethiol (2.5 g, 12 mmol) were added under argon and the tube was quickly sealed. The reaction mixture was heated at 120 °C for 24 h. After cooling, the reaction mixture was diluted with dichloromethane (200 mL) and washed with solution of HCl (1 M, 100 mL). The combined organic layer was washed with brine (100 mL), dried over $MgSO_4$ and filtered. The volatiles were removed under reduced pressure and the residue was purified by column chromatography on silica gel (300 g) in hexane/EtOAc (10:1) to provide the title compound **43** (1.36 g) as a yellow oil in 92% yield (R_f = 0.2, hexane/EtOAc = 10:1): ^{1}H NMR (500 MHz, $CDCl_3$) δ ppm -0.02 (s, 27H, CH_3), 0.80-0.84 (m, 6H, CH_2), 2.77-2.81 (m, 6H, CH_2), 5.04 (s, OH), 6.70 (d, $J_{H,H}$ = 8.75 Hz, 2H, Ar-H), 6.97 (d, $J_{H,H}$ = 8.54 Hz, 3H, Ar-H), 7.03 (d, $J_{H,H}$ = 8.75 Hz, 2H, Ar-H) 7.11-7.12 (m, 6H, Ar-H), 7.13-7.17 (m, 3H, Ar-H); ^{13}C NMR (125.8 MHz, $CDCl_3$) δ ppm -1.6, 16.9, 29.5, 68.2, 114.6, 126.6, 128.1, 128.8, 131.2, 132.5, 136.7, 138.4, 147.4, 154.0; IR (KBr) ν cm^{-1}: 3435 (s, υ(OH)), 3055 (w, υ(=CH)), 2951 (s, υ_{as}(CH_2, CH_3)), 2924 (s., υ_s(CH_2, CH_3)), 2852 (m), 1609 (w, υ(C=C)), 1509 (s), 1471 (s), 1430 (s, δ_s(CH_2, CH_3)), 1368 (s, δ_{as}(CH_2, CH_3)), 1248 (s, CH_3, TMS)), 1214 (s), 1145 (m), 1091 (s), 857 (s), 840(s), 687 (w, υ_{as}(SiC_3)); UV-Vis (λ_{max}[nm], ε, CH_2Cl_2) 275 (51292); ESI(+) MS Calcd for $C_{40}H_{56}OS_3Si_3Na$ ([M+Na]$^+$, 755.2693), found *m/z* 755.2515; elemental analysis calcd (%) for $C_{40}H_{56}OS_3Si_3$ (732.28): C, 65.52; H, 7.70; found: C, 66.15; H, 7.81.

4-(Tris{3-[2-(trimethylsilyl)ethylsulfanyl]phenyl}methyl)phenyl trifluoromethanesulfonate (**48**)

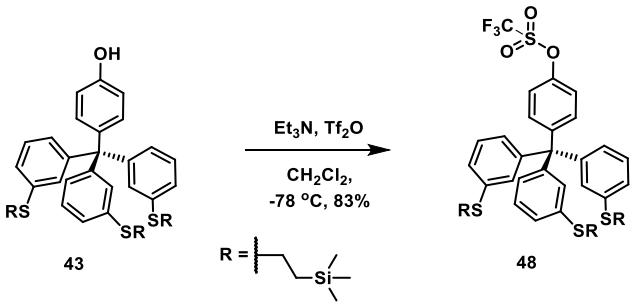

he desired product was prepared according to the method described for the preparation of **31**, starting from **43** (0.3 g, 0.41 mmol), triflic anhydride (0.2 g, 0.71 mmol) in the mixture of anhydrous triethylamine (0.12 mL, 0.82 mmol), dichloromethane (25 mL) at -78 °C under argon. The reaction mixture was stirred for 6 h, and then allowed to warm to room temperature and stirred for an additional 10 h. The residue was purified by column chromatography on silica gel (150 g) in hexane/EtOAc (9:1) to provide to the title compound **48** (0.29 g) as an yellowish oil in 83% yield (R_f = 0.81, hexane/EtOAc = 9:1): ^{1}H NMR (500 MHz, $CDCl_3$) δ ppm -0.01 (s, 27H, CH_3), 0.81-0.84 (m, 6H, CH_2), 2.78-2.82 (m, 6H, CH_2), 6.92-6.93 (m, 3H, Ar-H), 7.07-7.08 (m, 3H, Ar-H), 7.13-7.17 (m, 6H, Ar-H), 7.17-7.20 (m, 2H, Ar-H), 7.29 (d, $J_{H,H}$ = 3 Hz, 2H, Ar-H); ^{13}C NMR (125.8 MHz, $CDCl_3$) δ ppm -1.6, 17.2, 29.7, 65.2, 120.9, 127.0, 128.7, 128.8, 131.2, 133.4, 137.9, 146.9, 147.3, 148.3; ^{19} F NMR (470.57 MHz, $CDCl_3$) δ ppm -73.30; IR (KBr) ν cm^{-1}: 3060 (w, υ(=CH)), 2953 (s, υ_{as}(CH_2, CH_3)), 2927 (s, υ_s(CH_2, CH_3)), 2854 (m), 1582 (m, υ(C=C)), 1497 (w), 1427 (s, δ_s(CH_2, CH_3)), 1380 (s, δ_{as}(CH_2, CH_3)), 1247 (s, CH_3, TMS)), 1250 (s), 1213 (s), 1142 (s), 858 (s), 840 (s), 697 (w, υ_{as}(SiC_3)); UV-Vis (λ_{max}[nm], ε, CH_2Cl_2) 268 (25 170); ESI(+) MS Calcd for $C_{41}H_{55}O_3S_4FSi_3Na$ ([M+Na]$^+$, 887.2186), found *m/z* 887.2126; elemental analysis calcd (%) for $C_{41}H_{55}O_3S_4Si_3F$ (864.23): C, 56.91; H, 6.41; found: C, 57.03; H, 6.59.

4-(Tris{3-[2-(trimethylsilyl)ethylsulfanyl]phenyl}methyl)benzonitrile (**49**)

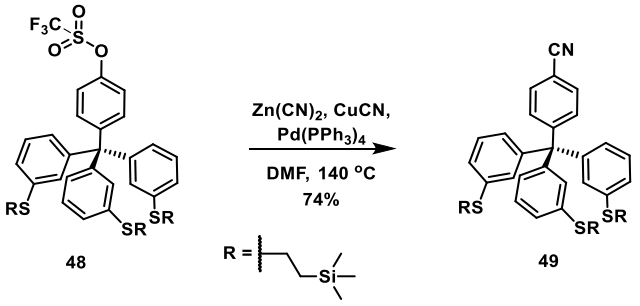

The desired product was prepared according to the method described for the preparation of **32**, starting from triflate **48** (0.15 g, 0.17 mmol), zinc cyanide (0.049 g, 0.42 mmol), copper (I) cyanide (0.015 g, 0.17 mmol), $Pd(PPh_3)_4$ (0.029 g, 0.025 mmol) in anhydrous DMF (10 mL) under argon. After 16 h at 140 °C, the reaction mixture was purified by column chromatography on silica gel (100 g) in the mixture of hexane/EtOAc (9:1) to obtain 0.13 g of **49** as an yellow oil in 74% yield (R_f = 0.67, hexane/EtOAc = 9:1): ^{1}H NMR (500 MHz, $CDCl_3$) δ ppm -0.01 (s, 27H, CH_3), 0.80-0.84 (m, 6H, CH_2), 2.78-2.81 (m, 6H, CH_2), 6.91-6.93 (m, 3H, Ar-H), 7.07 (s, 3H, Ar-H), 7.14 (d, $J_{H,H}$ = 7.8 Hz, 2H, Ar-H), 7.17-7.20 (m, 3H, Ar-H), 7.35 (d, $J_{H,H}$ = 8.55 Hz, 2H, Ar-H), 7.55 (d, $J_{H,H}$ = 8.6 Hz, 2H, Ar-H); ^{13}C NMR (125.8 MHz, $CDCl_3$) δ ppm -1.57, 16.84, 29.45, 65.29, 110.39, 118.87, 126.79, 128.43, 128.47, 130.83, 131.65, 131.87, 137.49, 154.96, 151.72; IR (KBr) ν cm^{-1}: 3059 (w, υ(=CH)), 2951 (s, υ_{as}(CH_2, CH_3)), 2924 (s, υ_s(CH_2, CH_3)), 2856 (m), 2228 (m, υ(C≡N)), 1582 (s, υ(C=C)), 1509 (s), 1471 (s), 1407 (s, δ_s(CH_2, CH_3)), 1344 (s, δ_{as}(CH_2, CH_3)), 1248 (m, CH_3, TMS)), 1261 (s), 1145 (m), 1091 (s), 875(s), 860 (s), 696 (w, υ_{as}(SiC_3)); UV-Vis (λ_{max}[nm], ε, CH_3CN) 224 (19670); ESI(+) MS Calcd for $C_{41}H_{55}S_3Si_3NK$ ($[M+K]^+$, 780.2436), found *m/z* 780.2485; elemental analysis calcd (%) for $C_{41}H_{55}OS_3Si_3N$ (741.28): C, 66.34; H, 7.47; N, 1.89; found: C, 66.49; H, 7.65; N, 1.91.

***S*,*S*′,*S*′′-{3,3',3''-[4-(cyanophenyl)methanetriyl]tris(benzene-3,1-diyl)} tris(thioacetate)** (**50**)

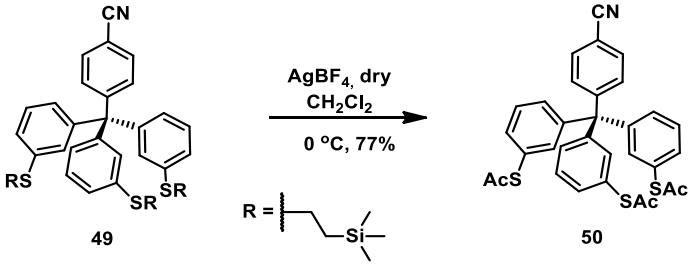

The desired product was prepared according to the method described for **33**, starting from **49** (0.12 g, 0.16 mmol), $AgBF_4$ (0.22 g, 1.12 mmol), acetyl chloride (1.2 mL) in anhydrous dichloromethane (12 mL) under argon. After 12 h at room temperature, the reaction mixture was quenched and purified by column chromatography on silica gel (150 g) in hexane/EtOAc (3:1) to give 0.07 g of **50** as an orange powder in 77% yield (R_f = 0.11, hexane/EtOAc = 3:1); m.p. 151-154 °C; ^{1}H NMR (500 MHz, $CDCl_3$) δ ppm 2.35 (s. 9H, CH_3), 7.26 (s, 3H, Ar-H), 7.29 (dd, $J_{H,H}$ = 4.25 Hz, 1.75 Hz, 3H, Ar-H), 7.35-7.38 (m, 6H, Ar-H), 7.44 (d, $J_{H,H}$ = 8.35 Hz, 2H, Ar-H), 7.60 (d, $J_{H,H}$ = 8.4 Hz, 2H, Ar-H); ^{13} C NMR (125.8 MHz, $CDCl_3$) δ ppm 30.4, 65.1, 110.6, 118.8, 128.2, 129.1, 131.6, 131.8, 132.0, 132.7, 137.2, 146.1, 151.0, 193.7; IR (KBr) ν cm^{-1}: 3060 (w, υ(=CH)), 2923 (s, υ_{as}(CH_3)), 2853 (m, υ_s(CH_3)), 2228 (m, υ(C≡N)), 1705 (s, υ(C=O)), 1584 (w, υ(C=C)), 1470, 1416 (m), 1408 (w, δ_{as}(CH_3)), 1341 (w, δ_s(CH_3)), 1243 (m), 1098 (m), 1119 (s), 886 (w), 613(s); UV-Vis (λ_{max}[nm], ε, CH_3CN) 223 (48219); ESI(+) HRMS Calcd for $C_{32}H_{25}NO_3S_3Na$ ([M+Na]$^+$, 590.0889), found *m/z* 590.0872; elemental analysis calcd (%) for $C_{32}H_{25}NO_3S_3$ (567.10): C, 67.70; H, 4.44; N, 2.47; found: C, 67.82; H, 4.49; N, 2.52.

4-(Tris{3-[2-(trimethylsilyl)ethylsulfanyl]phenyl}methyl)phenylboronic acid pinacol ester (**51**)

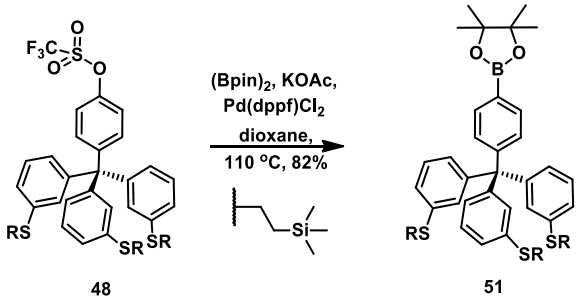

The desired product was prepared according to the method described for **34**, starting from triflate **48** (0.29 g, 0.34 mmol), anhydrous potassium acetate (0.14 g, 1.36 mmol), bis(pinacolato)diboron (0.13 g, 0.51 mmol), $Pd(dppf)Cl_2$ (0.028 g, 0.034 mmol) in anhydrous dioxane (15 mL) under argon. After 16 h at 120 °C, the residue was purified by column chromatography on silica gel (130 g) in hexane/EtOAc (10:1) to provide 0.23 g of **51** as a yellow powder in 82% yield (R_f = 0.48, hexane/EtOAc = 10:1); m.p. 129-130 °C; ^{1}H NMR (500 MHz, $CDCl_3$) δ ppm -0.02 (s, 27H, CH_3), 0.79-0.83 (m, 6H, CH_2), 1.32 (s, 12H, CH_3), 2.76-2.80 (m, 6H, CH_3), 6.97-6.99 (m, 3H, Ar-H), 7.10-7.11 (m, 3H, Ar-H), 7.13-7.16 (m, 6H, Ar-H), 7.22 (d, $J_{H,H}$ = 8.25 Hz, 2H, Ar-H), 7.68 (d, $J_{H,H}$ = 8.4 Hz, 2H, Ar-H), ^{13}C NMR (125.8 MHz, $CDCl_3$) δ ppm -1.6; 16.9, 25.1, 29.5, 65.3, 83.9, 126.6, 127.8, 128.1, 128.7, 130.6, 131.2, 134.3, 136.8, 147.0, 149.3; IR (KBr) ν cm^{-1}: 3059 (w, υ(=CH)), 2950 (s, υ_{as}(CH_2, CH_3)), 2921 (s, υ_s(CH_2, CH_3)), 2852 (m), 1733 (m), 1609 (m), 1580 (s, υ(C=C)), 1470 (s), 1402 (s, δ_s(CH_2, CH_3)), 1364(s, δ_{as}(CH_2, CH_3)), 1247 (m, CH_3, TMS)), 1162 (s), 1143 (m), 1091 (s), 1017 (m), 860 (s), 838 (s), 693 (w, υ_{as}(SiC_3)); UV-Vis (λ_{max}[nm], ε, CH_2Cl_2) 265 (27425); ESI(+) MS Calcd for $C_{46}H_{67}BO_2S_3Si_3Na$ ([M+Na]$^+$, 865.3605), found *m/z* 865.3226; elemental analysis calcd (%) for $C_{46}H_{67}BO_2S_3Si_3$ (842.37): C, 65.52; H, 8.01; found: C, 65.73; H, 8.12.

1-Iodo-4-(tris{3-[2-(trimethylsilyl)ethylsulfanyl]phenyl}methyl)benzene (**52**)

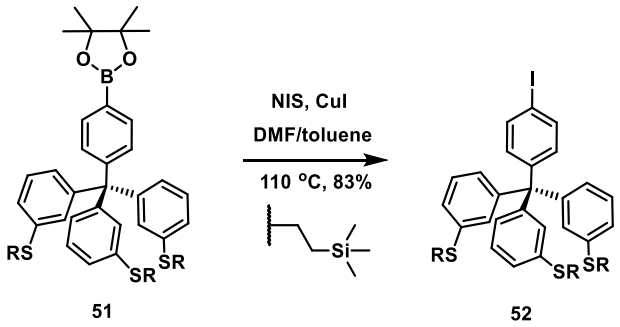

The desired product was prepared according to the method described for **35**, starting from pinacol ester **51** (0.36 g, 0.43 mmol), copper iodide (0.12 g, 0.64 mmol), *N*-Iodosuccinimide (0.14 g, 0.64 mmol) in anhydrous DMF (13 mL) and toluene (6.5 mL) under argon. After 24 h at 110 °C, the residue was purified by column chromatography on silica gel (120 g) in hexane/EtOAc (10:1) to get 0.3 g of **52** as a yellow powder in 83% yield (R_f = 0.75, hexane/EtOAc = 10:1); m.p. 136-137 °C; ^{1}H NMR (500 MHz, $CDCl_3$) δ ppm 0.0 (s, 27 H, CH_3), 0.81-0.85 (m, 6 H, CH_2), 2.80-2.84 (m, 6 H, CH_2), 6.98-7.00 (m, 5 H, Ar-H), 7.11-7.14 (m, 6H, Ar-H), 7.17-7.20 (m, 3 H, Ar-H), 7.60 (d, $J_{H,H}$ = 7.8 Hz, 2H, Ar-H); ^{13}C NMR (125.8 MHz, CD_2Cl_2) δ ppm -1.55, 17.27, 29.73, 65.27, 92.49, 126.86, 128,66, 128.72, 131.13, 133.55, 137.33, 137.77, 146.63; 147.12; IR (KBr) ν cm^{-1}: 3058 (w, υ(=CH)), 2952 (s, υ_{as}(CH_2, CH_3)), 2921 (s, υ_s(CH_2, CH_3)), 2853 (m), 1581 (s, υ(C=C)), 1473 (s), 1403 (s, δ_s(CH_2, CH_3)), 1248 (s, CH_3, TMS)), 1162 (s), 1104 (m), 1089 (s), 1006 (m), 862 (s), 840 (s), 695 (w, υ_{as}(SiC_3)); UV-Vis (λ_{max}[nm], ε, CH_2Cl_2) 267 (24704); ESI(+) MS Calcd for $C_{40}H_{55}S_3Si_3INa$ ([M+Na]$^+$, 865.1711), found *m/z* 887.1564; elemental analysis calcd (%) for $C_{40}H_{55}S_3Si_3I$ (842.18): C, 56.98; H, 6.57; found: C, 57.11; H, 6.70.

***S*,*S*′,*S*′′-{3,3',3''-[(4-Iodophenyl)methanetriyl)]tris(benzene-3,1-diyl)} tris(thioacetate) (53).**

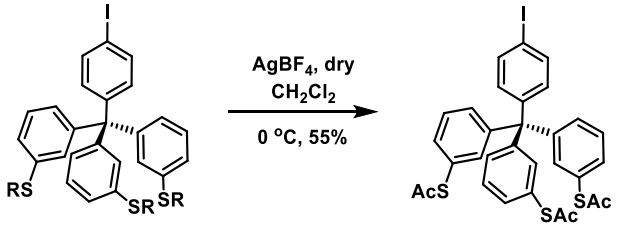

52 53

The desired product was prepared according to the method described for **33**, starting from **52** (0.29 g, 0.43 mmol), with $AgBF_4$ (0.4 g, 2.06 mmol) in the mixture of anhydrous dichloromethane (18 mL) and acetyl chloride (1.8 mL) under argon. The suspension was stirred at room temperature for 12 h. The crude product was purified by column chromatography on silica gel (150 g) in hexane/EtOAc (5:1) to provide 0.13 g of **53** as a yellow powder in 55% yield (R_f = 0.31, hexane/EtOAc = 5:1); m.p. 122-125 °C; ^{1}H NMR (500 MHz, $CDCl_3$) δ ppm 2.37 (s. 9H, CH_3), 7.04 (d, $J_{H,H}$ = 8.6 Hz 3H, Ar-H), 7.26-7.27 (m, 6H, Ar-H), 7.27-7.29 (m, 3H, Ar-H), 7.32-7.35 (m, 3H, Ar-H), 7.62 (d, $J_{H,H}$ = 8.6 Hz, 2H, Ar-H); ^{13} C NMR (125.8 MHz, $CDCl_3$) δ ppm 30.4, 64.7, 92.7, 127.9, 129.0, 131.8, 132.6, 133.1, 137.2, 137.3, 145.5,146.7, 193.9; IR (KBr) ν cm^{-1}: 3056 (w, υ(=CH)), 2924 (s, $\upsilon_{as}(CH_3)$), 2853 (m, $\upsilon_s(CH_3)$), 1702 (s, υ(C=O)), 1583 (w, υ(C=C)), 1467 (m, δ_{as}(CH_3)), 1402 (w, δ_s(CH_3)), 1344 (w), 1120 (m), 1098 (m), 1119 (s), 947 (m), 888 (w), 613 (s); UV-Vis (λ_{max}[nm], ε, CH_3CN) 209 (39207); ESI(+) HRMS Calcd for $C_{31}H_{25}IO_3S_3Na$ ([M+Na]$^+$, 690.9903), found *m/z* 690.9909; elemental analysis calcd (%) for $C_{31}H_{25}IO_3S_3$ (668.00): C, 55.69; H, 3.77; found: C, 55.58; H, 3.72.

1-Bromo-4-(tris{3-[2-(trimethylsilyl)ethylsulfanyl]phenyl}methyl)benzene (**54**)

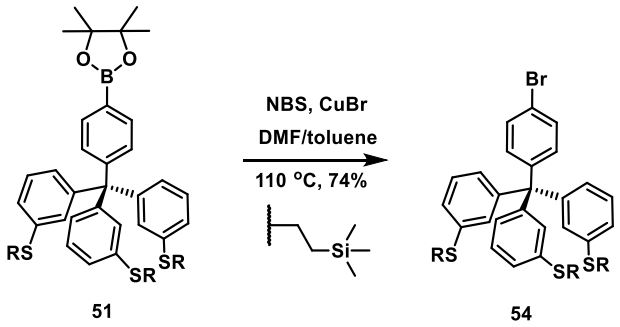

The desired product was prepared according to the procedure reported for **37**. Oven-flamed 100 mL two neck round bottom flask was charged with pinacol boronic ester **51** (0.13 g, 0.15 mmol) *N*-bromosuccinimide (0.042 g, 0.23 mmol), copper bromide (0.66 g, 0.46 mmol) and dissolved in in the mixture of toluene (3 mL) and dimethylformamide (6 mL). The mixture was purged with argon over 30 min, and consecutively heated at 110 ^{o}C overnight. Upon cooling to room temperature solvents were evaporated. Remaining solution was diluted with dichloromethane (150 mL) and washed with saturated solution of sodium sulfite (150 mL). Aqueous layer was separated and additionally extracted with dichloromethane (2 x100 mL). The combined organic layer was dried over magnesium sulfate and filtered. Volatiles were removed under reduced pressure and purified by column chromatography on silica gel (200 g) in hexane/EtOAc (9:1) to obtain 0.09 g of **54** (74%) as a brown solid. (R_f = 0.87, hexane/EtOAc 9:1); m.p. 241-242 ^{o}C; ^{1}H NMR (500 MHz, $CDCl_3$) δ ppm 0.01 (s, 27H, CH_3), 0.80-0.84 (m, 6H, CH_2), 2.77-2.81 (m, 6H, CH_2), 6.93-6.95 (m, 3H, Ar-H), 7.06-7.08 (m, 2H, Ar-H), 7.09 (s, 3H, Ar-H), 7.12-7.13 (m, 3H, Ar-H) 7.15-7.18 (m, 3H, Ar-H), 7.37 (d, $J_{H,H}$ = 6.8 Hz, 2H, Ar-H); ^{13}C NMR (125.8 MHz, $CDCl_3$) δ ppm -2.43, 16.01, 28.62, 63.89, 119.75, 125.79, 127.39, 127.73, 130.07, 130.10, 132.08, 136.27, 144.47, 145.78; IR (KBr) ν cm^{-1}: 3024 (w, υ(=CH)) 2952 (s, υ_{as}(CH_2, CH_3)), 2924 (s, υ_s(CH_2, CH_3)), 2854 (w), 1608 (s, υ(C=C)), 1583 (m), 1486 (s), 1399 (m, δ_{as}(CH_2, CH_3)), 1362 (s, δ_s(CH_2, CH_3)), 1322 (w), 1248 (s, δ_s(CH_3, TMS)), 1195 (w), 1163 (w), 1145 (m), 1092 (m), 1013 (m), 859 (s), 839 (s, δ_{as}(CH_3, TMS)) 809 (m), 694 (w, υ_{as}(SiC_3)), 660 (w, υ(C-Br)); UV-Vis (λ_{max}[nm], ε, CH_2Cl_2) 270 (19496); ESI(+) MS Calcd for $C_{40}H_{55}S_3Si_3BrNa$ ([M+Na,]$^+$, 819.1836), found *m/z* 819.1786; elemental analysis calcd (%) for $C_{40}H_{55}S_3Si_3Br$ (794.20): C 60.34; H 6.96; found: C 60.81, H 7.15.

***S*,*S*′,*S*′′-{3,3',3''-[(4-Bromophenyl)methanetriyl)]tris(benzene-3,1-diyl)} tris(thioacetate) (55)**

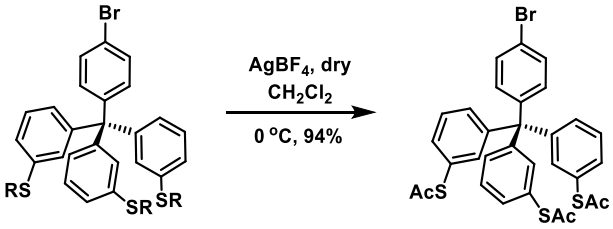

54 55

Compound **54** (0.08 g, 0.1 mmol) was loaded to an oven-flamed and argon flashed Schlenk flask and dissolved in dry dichloromethane (12 mL). Subsequently acetyl chloride (1.2 mL) was dropwise added under argon at 0 °C. The solution was treated with silver tetrafluoroborate (0.16 g, 0.81 mmol) and suspension was stirred overnight at room temperature. Afterwards, the reaction mixture was quenched with saturated solution of sodium hydrocarbonate (50 mL) and washed with dichloromethane (3 x 100 mL). The combined organic layer was dried over magnesium sulfate, passed through a pad of Celite, and all volatiles were removed under vacuum. The crude product was purified by column chromatography on silica gel (120 g), with Hexane/EtOAc 3:1) getting 0.065 g (94%) of **55** as a brown powder. (R_f = 0.44, hexane/EtOAc 3:1); m.p. 160-161 °C; ^{1}H NMR (500 MHz, CD_2Cl_2) δ ppm 2.34 (s, 9H, CH_3), 7.13 (d, $J_{H,H}$ = 8.6 Hz, 2H, Ar-H), 7.23-7.26 (m, 9H, Ar-H), 7.29-7.32 (m, 3H, Ar-H), 7.39 (d, $J_{H,H}$ = 8.6 Hz, 2H, Ar-H); ^{13}C NMR (125.8 MHz, CD_2Cl_2) δ ppm 30.4, 64.5, 120.8, 127.9, 128.9, 131.2, 131.8, 132.5, 132.8, 137.2, 144.7, 146.7, 193.8; IR (KBr) ν cm^{-1}: 3058 (w, υ(=CH)), 2924 (s, υ_{as}(CH_3)), 2853 (m, υ_s(CH_3)), 2225 (m, υ(C≡N)), 1703 (s, υ(C=O)), 1583 (w, υ(C=C)), 1468 (m), 1401 (w, δ_{as}(CH_3)), 1350 (w, δ_s(CH_3)), 1120 (m), 1098 (m), 1009 (m), 948 (m), 888 (w), 796 (m), 612 (s, υ(C-Br)), UV-Vis (λ_{max}[nm], ε, acetone) 227 (15369); ESI(+) MS Calcd for $C_{31}H_{25}BrO_3S_3Na$ ([M + Na]$^+$, 645.0027), found *m/z* 644.9972; elemental analysis calcd (%) for $C_{31}H_{25}BrO_3S_3$ (620.01): C 59.90; H 4.05; found: C 60.05; H 4.19.

4-bromobiphenyl-4'-carbonitrile (**56**)[283]

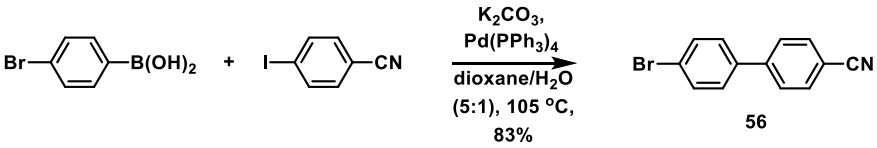

Biphenyl **56** was synthesized by using similar method described in the literature.[283] 4-Bromophenylboronic acid (0.4 g, 1.99 mmol), 4-iodobenzonitrile (0.91 g, 3.98 mmol), potassium carbonate (0.55 g, 3.98 mmol) was loaded to a 100 mL two-neck round bottom flask and dissolved in dioxane (50 mL) and water (10 mL). Solution was flushed with argon (30 min) and tetrakis(triphenylphosphine)palladium(0) (0.023 g, 0.2 mmol) was added at once. The reaction mixture was refluxed overnight under argon atmosphere. Afterwards dioxane was removed in vacuo. Crude product was diluted with dichloromethane (200 mL) and extracted with brine (100 mL). Aqueous layer was separated and washed with dichloromethane (2 x 100 mL). Organic layers were combined, dried over magnesium sulfate and filtered. Solvents were evaporated and the crude product was purified on silica gel (250 g) in hexane/EtOAc (10:1) yielding the product **56** as a white solid (0.42 g, 83%). (R_f = 0.46, hexane/EtOAc 10:1); ^{1}H NMR (500 MHz, $CDCl_3$) δ ppm, 7.43-7.46 (m, 2H, Ar-H) 7.59-7.63 (m, 2H, Ar-H), 7.63-7.66 (m, 2H, Ar-H), 7.71-7.74 (m. 2H, Ar-H); ^{13}C NMR (125.8 MHz, $CDCl_3$) δ ppm 111.5, 118.9, 123.3, 127.7, 128.9, 132.4, 132.9, 138.2, 144.6.

4'-cyano-biphenyl-4-boronic acid pinacol ester (**57**)[284]

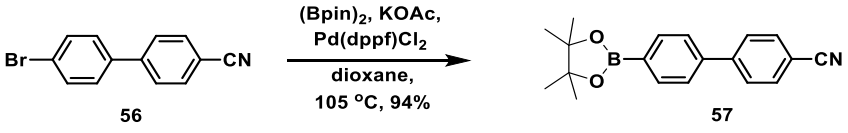

Pinacol boronic ester **57** was synthesized according to a modified literature procedure.[284] 4-Bromobiphenyl-4'-carbonitrile (0.45 g, 1.75 mmol), bis(pinacolato)diboron (0.67 g, 2.63 mmol), potassium acetate (0.52 g, 5.25 mmol) was loaded to an oven-flamed pressure tube and dissolved in 50 mL of dry dioxane. A solution was flushed with argon for 30 min and bis(diphenylphosphino)ferrocene palladium(II) dichloride (0.09 g, 0.13 mmol) was added at once. The reaction mixture was refluxed overnight under argon atmosphere. Then dioxane was removed. The crude product was diluted with dichloromethane (200 mL) and extracted

with brine (100 mL). Aqueous layer was separated and washed with dichloromethane (2 x 150 mL). Organic layers were combined, dried over magnesium sulfate and filtered. Solvents were evaporated and crude product was purified on silica gel (100 g) in hexane/EtOAc (9:1) yielding the product **57** as a white solid (0.5 g, 94%). (R_f = 0.51, hexane/EtOAc 9:1); m.p. 189-191ºC; ^{1}H NMR (500 MHz, $CDCl_3$) δ ppm, 1.37 (s, 12H, CH_3), 7.58-7.61 (m, 2H, Ar-H) 7.68-7.75 (m, 4H, Ar-H), 7.90-7.93 (m, 2H, Ar-H), ^{13}C NMR (125.8 MHz, $CDCl_3$) δ ppm 25.2, 111.3, 119.1, 123.3, 126.7, 128, 132.8, 135.7, 141.8, 145.7.

1,1':4',1''-Terphenyl-4-carbonitrile (**58**)[286]

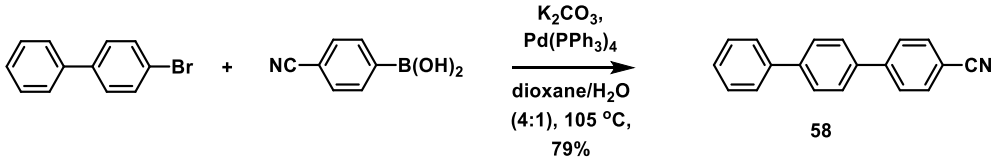

To an argon flushed 100 mL two-neck round bottom flask 4-bromobiphenyl (0.37 g, 1.59 mmol), 4-cyanophenyl boronic acid (0.28 g, 1.9 mmol), potassium carbonate (1 g, 7.6 mmol) were added and dissolved in dioxane (40 mL), water (10 mL). The reaction mixture was purged with argon for 40 min. Subsequently, tetrakis(triphenylphosphine)palladium(0) (0.15 g, 0.13 mmol) was added at once and the reaction mixture was refluxed overnight. Afterwards the reaction mixture was cooled down and the solvents were removed. The residue was diluted with dichloromethane and washed with brine (100 mL). Aqueous layer was separated and extracted with dichloromethane (2 x 100 mL). Organic layers were combined, dried over magnesium sulfate and filtered. Solvents were evaporated and the crude product was purified on silica gel (150 g) in hexane/CH_2Cl_2 (1:2) affording product **58** as a white powder (0.32 g, 79%). (R_f = 0.58, hexane/CH_2Cl_2 1:2), ^{1}H NMR (500 MHz, CD_2Cl_2) δ ppm, 7.39-7.40 (m, 1H. Ar-H), 7.46-7.49 (m, 2H, Ar-H), 7.66-7.68 (m, 2H, Ar-H), 7.71-7.77 (m, 8H, Ar-H), ^{13}C NMR (125.8 MHz, CD_2Cl_2) δ ppm 110.86, 118.81, 126.89, 127.43, 127.52, 127.60, 127.65, 128.83, 132.59, 137.88, 140.03, 141.28, 144.88.

4’’-Iodo-1,1’:4’,1’’-terphenyl-4-carbonitrile

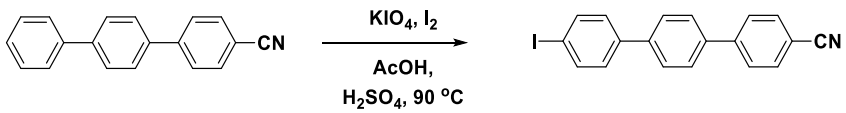

The iodination was carried out according to a modified literature procedure.[287] A round bottom flask was charged **58** (1 g, 0.39 mmol), potassium iodate (0.021 g, 0.098 mmol), iodine (0.043 g, 0.17 mmol), glacial acetic acid (15 mL), water (1.25 mL) and concentrated sulfuric acid (0.7 mL). The resulted solution was heated overnight and vigorously stirred at 90 ^{o}C. The crude mixture was cooled down to room temperature, precipitated solid was filtered and subsequently washed with 25 mL of AcOH, 20 mL of $Na_2SO_{3\ (aq)}$ and 50 mL of water. The obtained white powder was then treated with 100 mL of toluene to remove organic residues. The isolated white solid is insoluble in common organic solvents.

4’’-Bromo-1,1’:4’,1’’-terphenyl-4-carbonitrile (**59**)[286]

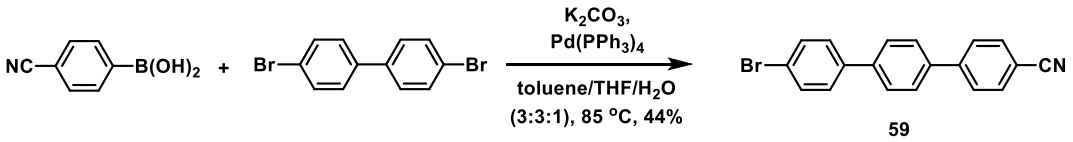

In a 100 mL argon flushed two-neck round bottom flask 4,4’-dibromobiphenyl (1 g, 3.21 mmol), 4-cyanophenyl boronic acid (0.24 g, 1.6 mmol), potassium carbonate (0.44 g, 3.21 mmol) were added and dissolved in toluene (30 mL), tetrahydrofuran (10 mL) and water (10 mL). The solution was purged with argon for 40 min. Subsequently tetrakis(triphenylphosphine)palladium(0) (0.13 g, 0.12 mmol) was added at once and the reaction mixture was heated overnight at 85 ^{o}C. The reaction mixture was cooled down and solvents were removed. The residue was diluted with dichloromethane and washed with brine (100 mL). Aqueous layer was separated and extracted with dichloromethane (2 x 150 mL). Organic layers were combined, dried over magnesium sulfate and filtered. Solvents were evaporated and crude product was at first purified on silica gel (200 g) in hexane/CH_2Cl_2 (1:2) and then recrystallized from hot toluene providing the desired product **59** as a white powder (0.24 g, 44%). (R_f = 0.57, hexane/CH_2Cl_2 1:2); ^{1}H NMR (500 MHz, CD_2Cl_2) δ ppm,

7.54-7.56 (d, 2H, Ar-H) 7.60-7.62 (m, 2H, Ar-H), 7.71 (m, 4H, Ar-H), 7.76 (m, 4H, Ar-H); ^{13}C NMR (125.8 MHz, CD_2Cl_2) δ ppm 111.41, 119.2, 122.22, 127.85, 127.88, 128.08, 128.99, 132.34, 133.04, 138.72, 139.48, 140.43, 145.9.

4-(Tris{4-[2-(trimethylsilyl)ethylsulfanyl]phenyl}methyl)biphenyl-4'-carbonitrile (**60**)

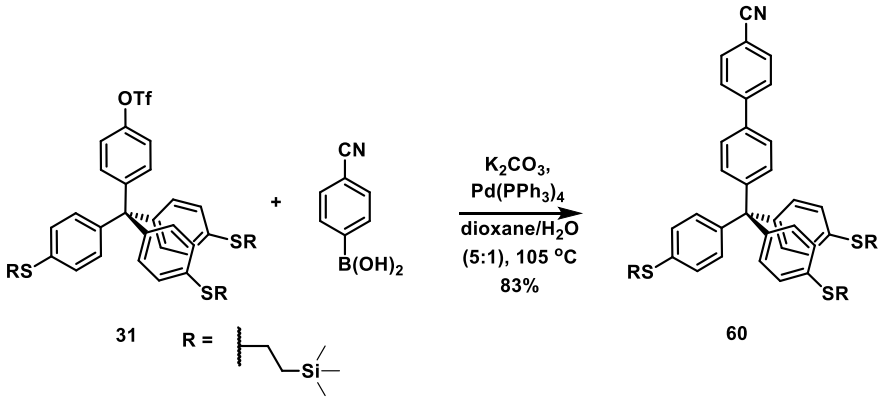

A 100 mL two neck round bottom flask was charged with **31** (0.19 g, 0.22 mmol), 4-cyanobenzenbornic acid (0.082 g, 0.36 mmol), potassium carbonate (0.099 g, 0.72 mmol), tetrakis(triphenylphosphine)palladium(0) (0.03 g, 0.0023 mmol). The reagents were dissolved in dioxane (50 mL) and water (10 mL), and the solution was purged with argon. The reaction mixture was refluxed for 24 h under argon atmosphere. After cooling down to room temperature, the crude mixture was diluted with dichloromethane (150 mL) and washed with brine (100 mL), aqueous layer was additionally extracted with dichloromethane (2 x 150 mL). The combined organic layer were dried over magnesium sulfate and filtered. All volatiles were removed under reduced pressure and the residue was purified by column chromatography on silica gel (300 g) in hexane/EtOAc (9:1) to obtain 0.15 g of **60** (83%) as a white powder. (R_f = 0.55, hexane/EtOAc 9:1); m.p. 184-185 °C; ^{1}H NMR (500 MHz, CD_2Cl_2) δ ppm 0.04 (s, 27H, CH_3), 0.92-0.96 (m, 6 H, CH_2), 2.95-2.98 (m, 6 H, CH_2), 7.14-7.15 (m, 6 H, Ar-H), 7.15-7.18 (m, 6 H, Ar-H), 7.33 (d, $J_{H,H}$ = 7.5 Hz, 2H, Ar-H) 7.53 (d, $J_{H,H}$ = 8.5 Hz, 2H, Ar-H), 7.71-7.72 (m, 4H, Ar-H); ^{13}C NMR (125.8 MHz, CD_2Cl_2) δ ppm -2.2, 16.7, 28.9, 63.7, 110.9, 118.9, 126.4, 127.1, 127.5, 131.3, 131.5, 132.6, 135.7, 136.7, 143.5, 144.8, 147.3; IR (KBr) ν cm^{-1}: 3028 (w, υ(=CH)), 2951 (s, υ_{as}(CH_2, CH_3)), 2921 (s, υ_s(CH_2, CH_3)), 2853 (m), 2227 (m, υ(C≡N)), 1606 (m, υ(C=C)), 1590 (w), 1489 (s), 1439 (w, δ_{as}(CH_2, CH_3)), 1399 (w, δ_s(CH_2, CH_3)), 1271 (w), 1248 (s, δ_s(CH_3, TMS)), 1094 (m), 1013 (m), 856 (s), 841 (s, δ_{as}(CH_3, TMS)) 813 (s), 756 (m), 694 (w, υ_{as}(SiC_3)); UV-Vis (λ_{max}[nm],

ε, CH_2Cl_2) 273 (49183); ESI(+) MS Calcd for $C_{47}H_{59}S_3Si_3NNa$ ($[M+Na]^+$, 840.3015, found *m/z* 840.3275; elemental analysis calcd (%) for $C_{47}H_{59}S_3Si_3N$ (817.31): C 68.97; H 7.27, N 1.71; found: C 69.48, H 7.48, N 1.80.

***S,S′,S′′*-{4,4',4''-[(4-cyanobiphenyl)methanetriyl)]tris(benzene-4,1-diyl)} tris(thioacetate)** (**61**)

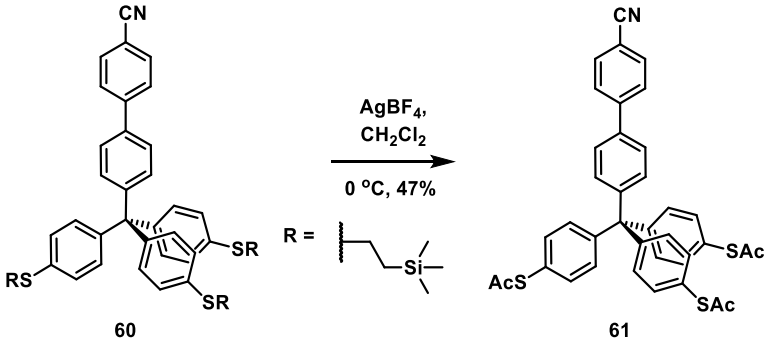

Compound **60** (0.15 g, 0.18 mmol) was added to an oven-flamed and argon flushed 50 mL Schlenk flask and dissolved in dry dichloromethane (20 mL). Subsequently acetyl chloride (2 mL) was dropwise added under argon at 0 °C. The solution was treated with silver tetrafluoroborate (0.28 g, 1.46 mmol) and the suspension was stirred overnight at room temperature. Afterwards the reaction was quenched with saturated solution of sodium hydrocarbonate (70 mL) and washed with dichloromethane (3 x 100 mL). The combined organic layer was dried over magnesium sulfate, passed through a pad of Celite, and the volatiles were removed under vacuum. The crude product was purified by column chromatography on silica gel (120 g), with hexane/EtOAc 3:1) providing 0.056 g (47%) of **61** as a white powder. (R_f = 0.33, hexane/EtOAc 3:1); m.p. 160-161 °C; ^{1}H NMR (500 MHz, CD_2Cl_2) δ ppm 2.40 (s, 9H, CH_3), 7.33-7.36 (m, 12H, Ar-H), 7.40 (d, $J_{H,H}$ = 8.55 Hz, 2H, Ar-H), 7.58 (d, $J_{H,H}$ = 8.55 Hz, 2H, Ar-H), 7.72 (m, 4H, Ar-H); ^{13}C NMR (125.8 MHz, CD_2Cl_2) δ ppm 30.07, 64.60, 111.0, 118.83, 126.46, 126.79, 127.57, 131.42, 131.46, 132.63, 133.81, 137.15, 144.67, 146.15, 147.07, 193.57; IR (KBr) ν cm^{-1}: 3061 (w, υ(=CH)), 2924 (s, $\upsilon_{as}(CH_3)$), 2854 (m, $\upsilon_s(CH_3)$), 2225 (m, υ(C≡N)), 1710 (s, υ(C=O)), 1605 (w, υ(C=C)), 1395 (w, $\delta_{as}(CH_3)$), 1349 (w, $\delta_s(CH_3)$), 1117 (m), 1092 (m), 1014 (m), 953 (m), 817 (m), 617 (s); UV-Vis (λ_{max}[nm], ε, CH_2Cl_2) 271 (31342); ESI(+) HRMS Calcd for $C_{38}H_{29}NO_3S_3Na$

([M+Na]$^+$, 666.1207, found *m/z* 666.1199; elemental analysis calcd (%) for $C_{38}H_{29}NO_3S_3$ (643.13): C 70.89; H 4.54, N 2.18; found: C 71.08; H 4.68, N 2.28.

4''-(Tris{4-[2-trimethylsilyl)-ethylsulfanyl]phenyl}methyl)-1,1':4',1''-(4-cyano)-4-(terphenyl-4-carbonitrile (**62**)

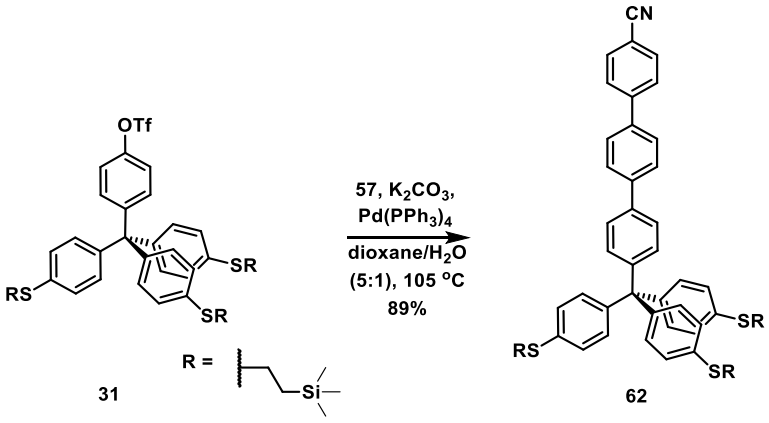

The product **62** was synthesized according to the method reported for **60**. Namely, triflate **31** (0.25 g, 0.29 mmol), biphenyl **57** (0.12 g, 0.5 mmol), potassium carbonate (0.12 g, 0.88 mmol), tetrakis(triphenylphosphine)palladium(0) (0.003 mmol, 0.034 g) were added to the argon flushed 100 mL two-neck round bottom flask equipped with attached refluxed condenser and dissolved in the mixture of dioxane (40 mL) and water (8 mL). The reaction mixture was stirred under argon overnight and heated at 105 °C. The crude product was purified by column chromatography on silica gel (200 g) in hexane/EtOAc (9:1) to yield 0.23 g of **62** as a white powder in 89% yield. (R_f = 0.47, hexane/EtOAc 9:1); m.p. 168-171 °C; ^{1}H NMR (500 MHz, CD_2Cl_2) δ ppm 0.043 (s, 27H, CH_3), 0.93-0.96 (m, 6H, CH_2), 2.95-2.99 (m, 6H, CH_2), 7.16-7.19 (m, 12H, Ar-H), 7.32 (d, $J_{H,H}$ = 8.5 Hz, 2H, Ar-H), 7.57 (d, $J_{H,H}$ = 8.5 Hz, 2H, Ar-H), 7.69-7.75 (m, 8H, Ar-H); ^{13}C NMR (125.8 MHz, CD_2Cl_2) δ ppm 2.14, 16.74, 28.9, 63.71, 110.94, 118.86, 126.11, 127.15, 127.48, 127.51, 127.61, 131.30, 131.38, 132.66, 135.56, 137.63, 137.94, 140.67, 143.72, 144.92, 146.24; IR (KBr) ν cm^{-1}: 3032 (w, υ(=CH)), 2950 (s, υ_{as}(CH_2, CH_3)), 2923 (s, υ_s(CH_2, CH_3)), 2853 (w), 2229 (m, υ(C≡N)), 1606 (m, υ(C=C)), 1591 (w), 1488 (s), 1439 (w, δ_{as}(CH_2, CH_3)), 1398 (w, δ_s(CH_2, CH_3)), 1248 (s, δ_s(CH_3, TMS)), 1094 (m), 1012 (m), 859 (s), 840 (s, δ_{as}(CH_3, TMS)), 811 (s), 692 (w, υ_{as}(SiC_3)); UV-Vis (λ_{max}[nm], ε, CH_2Cl_2) 275 (45372); ESI(+) HRMS Calcd for

$C_{53}H_{63}S_3Si_3NNa$ ([M+Na]$^+$, 916.3328, found *m/z* 916.3697; elemental analysis calcd (%) for $C_{53}H_{63}S_3Si_3N$ (893.34): C 71.16, H 7.10, N 1.57; found: C 71.12, H 7.46, N 1.69.

***S,S′,S′′*-{4,4',4''-[(4-Cyano-1,1':4',1''-terphenyl-4''-yl)methanetriyl)]tris(benzene-4,1-diyl)} tris(thioacetate)** (**63**)

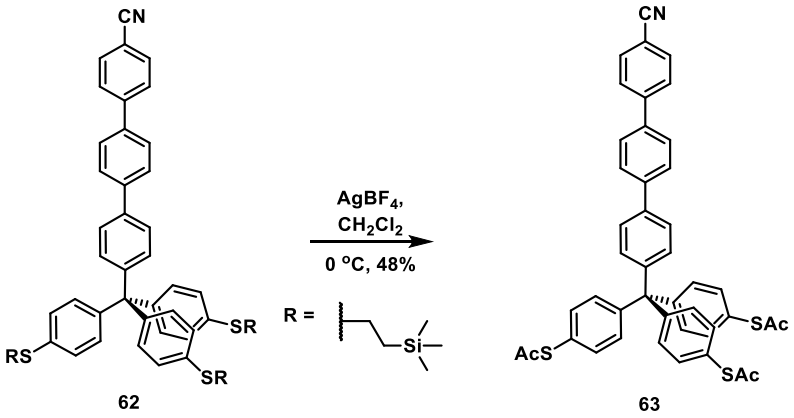

The desired product **63** was obtained according to the method described for the preparation of **60**, Oven-flamed 50 mL Schlenk flask was charged with **62** (0.18 g, 0.2 mmol), silver tetrafluoroborate (0.32 g, 1.62 mmol), and acetyl chloride (3.5 mL). All reagents were suspended in anhydrous dichloromethane (35 mL) under argon and stirred overnight at room temperature. The reaction mixture was quenched with $NaHCO_3$ (100 mL) and purified by column chromatography on silica gel (100 g) in hexane/EtOAc (5:1) to provide 0.07 g of **63** as a white powder in 48% yield. (R_f = 0.25, hexane/EtOAc 5:1); m.p. 261-262 °C; ^{1}H NMR (500 MHz, $CDCl_3$) δ ppm 2.40 (s, 9H, CH_3), 7.35-7.39 (m, 14H, Ar-H), 7.62 (d, $J_{H,H}$ = 8.45 Hz, 2H, Ar-H) 7.73 (d, $J_{H,H}$ = 8.45 Hz, 2H, Ar-H), 7.77-7.78 (m, 6H, Ar-H); ^{13}C NMR (125.8 MHz, $CDCl_3$) δ ppm 30.84, 64.99, 111.35, 119.28, 126.78, 126.92, 127.90, 127.98, 128.04, 131.69, 131.91, 133.07, 134.20, 138.46, 138.50, 140.90, 145.32, 145.33, 147.67, 194.03, IR (KBr) *v* cm^{-1}: 3029 (w, υ(=CH)), 2924 (m, $\upsilon_{as}(CH_3)$), 2854 (w, $\upsilon_s(CH_3)$), 2226 (m, υ(C≡N)), 1711 (w, υ(C=O)), 1606 (m, υ(C=C)), 1487 (s), 1394 (w, $\delta_{as}(CH_3)$), 1351 (w, $\delta_s(CH_3)$), 1119 (m), 1092 (m), 1015 (m), 948 (m), 813 (m), 616 (m); UV-Vis (λ_{max}[nm], ε, CH_2Cl_2) 305 (38135); 258 (26508); ESI(+) MS Calcd for $C_{44}H_{33}NO_3S_3Na$ ([M+Na]$^+$, 742.1520, found *m/z* 742.1418; elemental analysis calcd (%) for $C_{44}H_{33}NO_3S_3$ (719.16): 73.41, H 4.62, N 1.95; found: C 73.37, H 4.71, N 2.01.

4’’’-(Tris{4-[2-trimethylsilyl)-ethylsulfanyl]phenyl}methyl)-1,1’:4’,1’’,4’’:1’’’-quarterphenyl-4-carbonitrile (**64**)

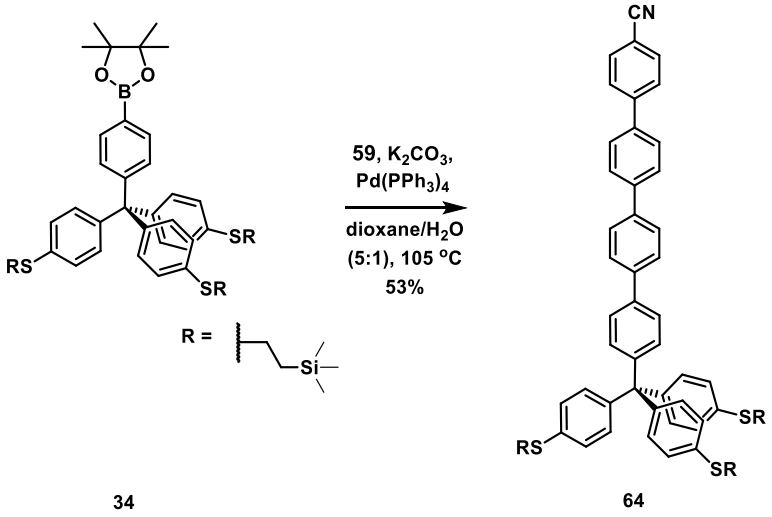

34 64

An argon-flushed two-neck round bottom flask was charged with pinacol boronic ester **34** (0.2 g, 0.24 mmol), **59** (0.1 g, 0.31 mmol), potassium carbonate (0.082 g, 0.59 mmol), and dissolved in the mixture of dioxane (55 mL) and water (12 mL). Then, the solution was purged with argon for 20 min., tetrakis(triphenylphosphine)palladium(0) (0.023 g, 0.0024 mmol) was added at once and the reaction mixture was stirred under argon overnight and at 105 °C. After cooling, dioxane was removed and slurry was diluted with dichloromethane (3 x 150 mL). Organic layers were combined, dried over $MgSO_4$, filtered and volatiles were evaporated. The crude product was purified by column chromatography on silica gel (150 g) in hexane/CH_2Cl_2 (2:1) to obtain 0.12 g of **64** as a white powder in 53% yield. (R_f = 0.15, hexane/CH_2Cl_2 2:1); m.p. 173-178 °C; ^{1}H NMR (500 MHz, CD_2Cl_2) δ ppm 0.05 (s, 27H, CH_3), 0.89-0.93 (m, 6H, CH_2), 2.88-2.92 (m, 6H, CH_2), 7.17-7.18 (m, 12H, Ar-H), 7.32 (d, $J_{H,H}$ = 8.35 Hz, 2H, Ar-H), 7.58 (d, $J_{H,H}$ = 8.45 Hz, 2H, Ar-H), 7.71-7.78 (m. 12H, Ar-H); ^{13}C NMR (125.8 MHz, CD_2Cl_2) δ ppm -1.74, 17.14, 29.31, 64.11, 111.36, 119.28, 126.45, 127.56, 127.76, 127.77, 127.91, 128.06, 129.77, 131.72, 133.75, 133.08, 135.93, 138.32, 138.44, 139.36, 140.15, 141.16, 144.17, 145.44, 146.40; IR (KBr) ν cm^{-1}: 3030 (w, υ(=CH)), 2952 (m, υ_{as}(CH_2, CH_3)), 2924 (s, υ_s(CH_2, CH_3)), 2853 (m), 2226 (m, υ(C≡N)), 1724 (w), 1604 (w, υ(C=C)), 1486 (m), 1398 (w, δ_s(CH_2, CH_3)), 1248 (m, δ_s(CH_3, TMS)), 1094 (m), 1014 (m), 858 (m), 838 (m, δ_{as}(CH_3, TMS)) 809 (s), 692 (w, υ_{as}(SiC_3)); UV-Vis (λ_{max}[nm], ε, CH_2Cl_2) 315 (32257); 274 (22095); ESI(+) MS Calcd for

$C_{59}H_{67}S_3Si_3NNa$ ([M+Na]$^+$, 992.3641), found *m/z* 992.3597; elemental analysis calcd (%) for $C_{59}H_{67}S_3Si_3N$ (970.62): C 73.01, H 6.96, N 1.44; found: C 73.14, H 7.28, N 1.56.

_S,S′,S′′_-{4,4',4''-[(4-Cyano-1,1’:4’,1’’:4’’,1’’’-quaterphenyl(-4’’’-yl) methanetriyl)]tris(benzene-4,1-diyl)} tris(thioacetate) (**65**)

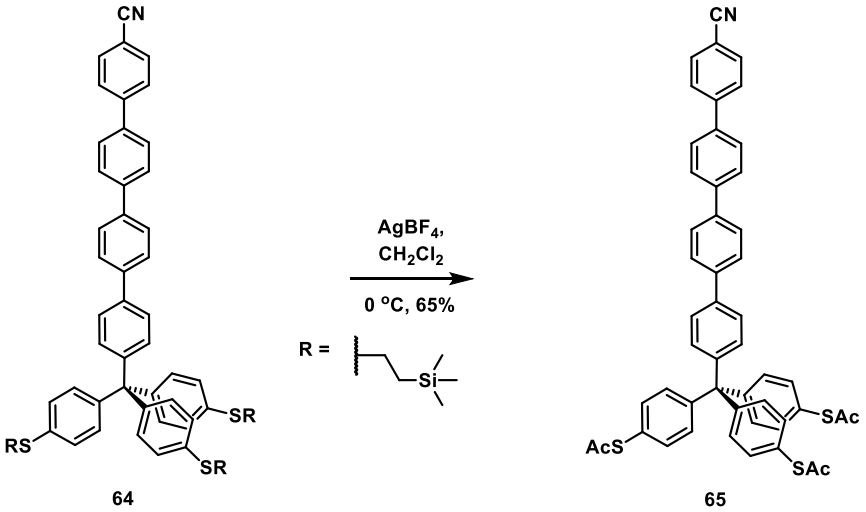

The trans-protection was procced according to the method described for the preparation of **61**. Starting material **64** (0.12 g, 0.12 mmol), silver tetrafluoroborate (0.19 g, 0.96 mmol), and acetyl chloride (1.8 mL) were suspended in anhydrous dichloromethane (18 mL) and stirred under argon overnight at room temperature. The reaction mixture was quenched and purified by column chromatography on silica gel (150 g) in hexane/CH_2Cl_2 (1:4) to obtain 0.064 g of **65** as a yellow powder in 65% yield. (R_f = 0.26, hexane/CH_2Cl_2 1:4); m.p. 299-300 ^oC; ^1H NMR (500 MHz, CD_2Cl_2) δ ppm 2.40 (s, 9H, CH_3), 7.37-7.39 (m, 14H, Ar-H), 7.62 (d, $J_{H,H}$ = 8.5 Hz, 2H, Ar-H), 7.72-7.74 (m, 6H, Ar-H), 7.77-7.78 (m, 6H, Ar-H); ^{13}C NMR (125.8 MHz, CD_2Cl_2) δ ppm 30.07, 64.58, 110.95, 118.87, 126.35, 126.44, 127.36, 127.43, 127.50, 127.51, 127.65, 129.36, 131.25, 131.51 132.67, 133.78, 138.05, 138.37, 139.07, 139.57, 140.74, 144.88, 144.93, 193.64; IR (KBr) ν cm^{-1} 3030 (w. υ(=CH)), 2956 (m, υ_{as}(CH_3)), 2925 (s, υ_s(CH_3)), 2854 (w), 2226 (m, υ(C≡N)), 1711 (s, υ(C=O)), 1605 (m, υ(C=C)), 1486 (s), 1394 (w, δ_{as}(CH_3)), 1351 (w, δ_s(CH_3)), 1267 (w), 1117 (s), 1092 (m), 1015 (w), 811 (s), 616 (s); UV-Vis (λ_{max}[nm], ε, CH_2Cl_2) 316 (23003); 316 (11872); ESI(+) MS Calcd for $C_{50}H_{37}NO_3S_3Na$ ([M+Na]$^+$, 818.1833), found *m/z* 818.1772; elemental analysis calcd (%) for $C_{50}H_{37}NO_3S_3$ (796.03): C 75.44, H 4.68, N 1.76; found: C 74.58, H 4.79, N 1.85.

4'-(Tris{3-[2-(trimethylsilyl)ethylsulfanyl]phenyl}methyl)-biphenyl-4'-carbonitrile (**66**)

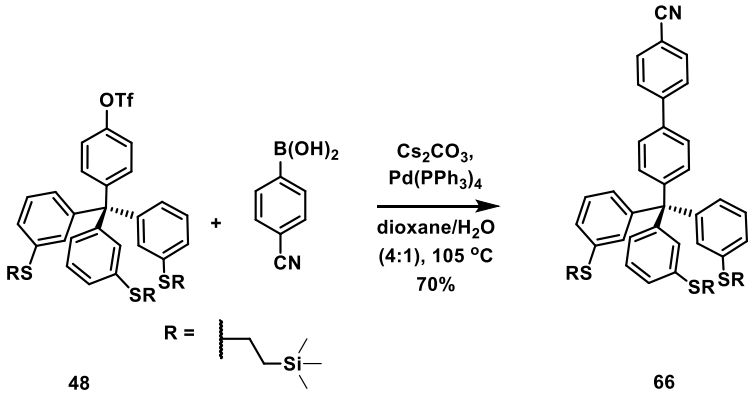

The desired product **66** was synthesized according the method reported for the preparation of **60**. A 100 mL two neck round bottom flask equipped with a reflux condenser was charged with triflate **48** (0.15 g, 0.18 mmol), 4-cyanobenzenboronic acid (0.082 g, 0.35 mmol), cesium carbonate (0.18 g, 0.53 mmol), tetrakis(triphenylphosphine)palladium(0) (0.021 g, 0.0018 mmol). The reagents were dissolved in dioxane (8 mL) and water (2 mL), and the solution was purged with argon for 20min. The reaction mixture was heated at 105 ^{o}C for 24 h under argon atmosphere. After cooling to room temperature, dioxane was removed. The residue was diluted with dichloromethane (250 mL) and washed with brine (100 mL). The combined organic layer was dried over $MgSO_4$ and filtered. All volatiles were removed under reduced pressure and the residue was purified by column chromatography on silica gel (100 g) in hexane/EtOAc (9:1) to obtain 0.1 g of **66** (70%) as pale yellow oil. (R_f = 0.56, hexane/EtOAc 9:1); ^{1}H NMR (500 MHz, $CDCl_3$) δ ppm -0.03 (s, 27H, CH_3), 0.81-0.84 (m, 6H, CH_2), 2.79-2.82 (m, 6H, CH_2), 6.99-7.00 (m, 3H, Ar-H), 7.13-7.26 (m, 9H, Ar-H), 7.32 (d, $J_{H,H}$ = 8.5 Hz, 2H, Ar-H), 7.49 (d, $J_{H,H}$ = 8.5 Hz, 2H, Ar-H), 7.67 (d, $J_{H,H}$ = 8.45 Hz, 2H, Ar-H), 7.71 (d, $J_{H,H}$ = 8.45 Hz, 2H, Ar-H); ^{13}C NMR (125.8 MHz, $CDCl_3$) δ ppm -1.6, 16.80, 29.43, 64.89, 110.99, 119.11, 126.49, 126.54, 127.63, 128.20, 128.62, 131.00, 131.89, 132.74, 136.99, 145.02, 146.76, 146.90; IR (KBr) ν cm^{-1}: 3030 (w, υ(=CH)), 2952 (s, υ_{as}(CH_2, CH_3)), 2924 (s, υ_s(CH_2, CH_3)), 2853 (m), 2226 (m, υ(C≡N)), 1733 (w), 1606 (m), 1581 (m, υ(C=C)), 1488 (m), 1471 (m, δ_{as}(CH_2, CH_3)), 1401 (w, δ_s(CH_2, CH_3)), 1260 (s), 1248 (s), 1088 (m), 1005 (m), 839 (s, δ_s(CH_3, TMS)), 816 (s), 698 (w, υ_{as}(SiC_3)) UV-Vis (λ_{max}[nm], ε, CH_2Cl_2) 271 (35395); ESI(+) MS Calcd for $C_{47}H_{59}NSi_3S_3K$ ([M+K]$^+$, 856.2749), found *m/z* 856.2865; elemental analysis calcd (%) $C_{47}H_{59}S_3Si_3N$ (817.31): C, 68.97; H, 7.27; N 1.71; found: C, 69.20; H, 7.36; N 1.95.

***S*,*S*′,*S*′′-{3,3',3''-[(4-Cyanobiphenyl)methanetriyl]tris(benzene-3,1-diyl)} tris(thioacetate)** (**67**)

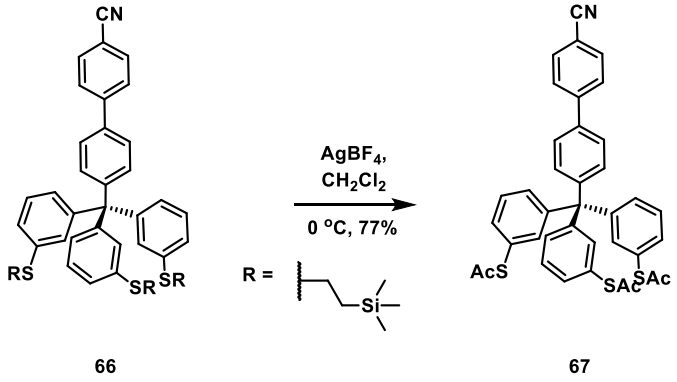

The desired product **67** was obtained according to a method described for the preparation of **61.** Thus, in a 25 mL Schlenk flask, compound **66** (0.084 g, 0.1 mmol) was dissolved in dry dichloromethane (12 mL), and subsequently acetyl chloride (1.2 mL) was added under argon at 0 ^{o}C. The solution was treated with silver tetrafluoroborate (0.16 g, 0.82 mmol) and suspension was stirred overnight at room temperature. Afterwards, the reaction mixture was quenched with saturated solution of $NaHCO_3$ (70 mL) and washed with dichloromethane (3 x 100 mL). The combined organic layer was dried over $MgSO_4$, passed through a pad of Celite, and all volitiles were removed under vacuum. The crude product was purified by column chromatography on silica gel (120 g), with Hexane/EtOAc 3:1) providing 0.051 g (77%) of **67** as a yellow powder. (R_f = 0.31, hexane/EtOAc 3:1); m.p. 129-130 ^{o}C; ^{1}H NMR (500 MHz, $CDCl_3$) δ ppm 2.37 (s, 9H, CH_3), 7.27-7.28 (m, 3H, Ar-H), 7.28-7.29 (m, 3H, Ar-H), 7.32-7.35 (m, 6H, Ar-H), 7.40 (d, $J_{H,H}$ = 8.45 Hz, 2H, Ar-H), 7.53 (d, $J_{H,H}$ = 8.4 Hz, 2H, Ar-H), 7.68 (d, $J_{H,H}$ = 8.45 Hz, 2H, Ar-H), 7.71 (d, $J_{H,H}$ = 8.5 Hz, 2H, Ar-H); ^{13}C NMR (125.8 MHz, $CDCl_3$) δ ppm - 29.85, 64.73, 111.02, 119.10, 126.88, 127.70, 127.85, 128.90, 131.78, 131.84, 132.47, 132.74, 137.24, 145.0, 146.32, 146.91, 193.91; IR (KBr) ν cm^{-1}: 3059 (w, υ(=CH)), 2956 (s, $\upsilon_{as}(CH_3)$), 2929 (s, $\upsilon_s(CH_3)$), 2854 (m), 2225 (m, υ(C≡N)), 1702 (s, υ(C=O)), 1605 (w), 1583 (w, υ(C=C)), 1491 (m), 1466 (m), 1400 (w, $\delta_s(CH_3)$), 1378 (w), 1351 (w, $\delta_s(CH_3)$) 1261 (w), 1121 (m), 1099 (m), 947 (m), 823 (m), 791 (m), 614 (m); UV-Vis (λ_{max}[nm], ε, CH_2Cl_2) 283 (26206), 390 (3798); ESI(+) HRMS Calcd for $C_{38}H_{29}NO_3S_3Na$ ([M+Na]$^{+}$, 666.1207), found *m/z* 666.1203; elemental analysis calcd (%) for $C_{38}H_{29}NO_3S_3$ (643.13): C, 70.89; H, 4.54; N, 2.18; found: C; 71.08; H, 4.68; N, 2.50.

4’’-(Tris{3-[2-(trimethylsilyl)ethylsulfanyl]phenyl}methyl)-1,1’:4’,1’’-terphenyl-4-carbonitrile (**68**)

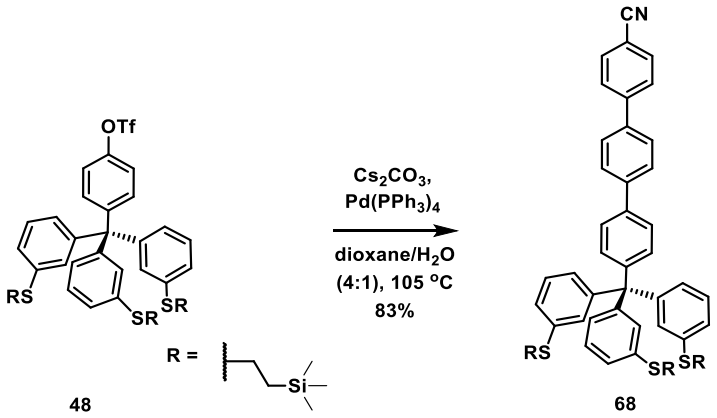

The product **68** was synthesized according to a method reported for the preparation of **62**. Triflate **48** (0.17 g, 0.2 mmol), boronic ester **57** (0.078 g, 0.36 mmol), cesium carbonate (0.19 g, 0.61 mmol), tetrakis(triphenylphosphine)palladium(0) (0.021 g, 0.002 mmol) were charged to an argon-flushed two-neck round bottom flask and dissolved in the mixture of dioxane/water (12/3 mL). The reaction mixture was stirred under argon overnight and heated at 105 ^{o}C. The crude product was purified by column chromatography on silica gel (120 g) in hexane/EtOAc (9:1) to yield 0.15 g of **68** as an orange waxy oil in 83% yield. (R_f = 0.55, hexane/EtOAc 9:1); ^{1}H NMR (500 MHz, $CDCl_3$) δ ppm -0.02 (s, 27H, CH_3), 0.83-0.87 (m, 6H, CH_2), 2.79-2.85 (m, 6H, CH_2), 7.01-7.03 (m, 3H, Ar-H), 7.13-7.22 (m, 9H, Ar-H), 7.29-7.31 (m, 2H, Ar-H), 7.52-7.55 (m, 2H, Ar-H), 7.68-7.69 (m, 4H, Ar-H), 7.72-7.74 (m. 4H, Ar-H); ^{13}C NMR (125.8 MHz, $CDCl_3$) δ ppm -1.56, 16.94, 29.5, 64.95, 111.10, 119.17, 126.34, 126.63, 127.74, 127.78, 127.80, 127.95, 128.21, 128.78, 131.20, 131.78, 132.85, 136.95, 138.07, 141.0, 145.33, 145.83, 147.05; IR (KBr) ν cm^{-1}: 3030 (w, υ(=CH)), 2952 (s, υ_{as}(CH_2, CH_3)), 2924 (s, υ_s(CH_2, CH_3)), 2853 (m), 2226 (m, υ(C≡N)), 1606 (m), 1581 (m, υ(C= C)), 1488 (m), 1470 (m, δ_{as}(CH_2, CH_3)), 1401 (m, δ_s(CH_2, CH_3)), 1260 (s, δ_s(CH_3, TMS)), 1248 (s), 1102 (w), 1088 (w), 1005 (m), 859 (s), 839 (s, δ_{as}(CH_3, TMS)), 816 (s), 698 (m, υ_{as}(SiC_3)); UV-Vis (λ_{max}[nm], ε, CH_2Cl_2) 271 (31516); 303 (36844); ESI(+) MS Calcd for $C_{53}H_{63}S_3Si_3NNa$ ([M+Na]$^+$, 916.3328), found *m/z* 916.3219; elemental analysis calcd (%) for $C_{53}H_{63}S_3Si_3N$ (893.34): C, 71.16; H, 7.10; N. 1.57; found: C, 71.12; H, 7.46; N. 1.52.

***S*,*S*′,*S*′′-{3,3',3''-[(4-Cyano-1,1':4',1''-terphenyl-4''-yl)methanetriyl)]tris(benzene-3,1-diyl)} tris(thioacetate)** (**69**)

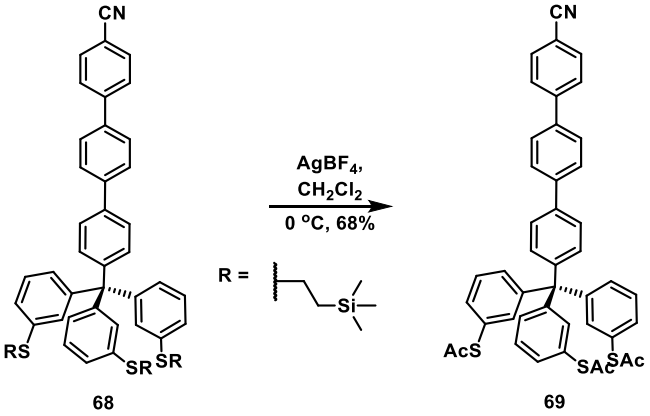

The desired product **69** was obtained according to a method described for the preparation of **63**. Starting material **68** (0.11 g, 0.13 mmol), silver tetrafluoroborate (0.25 g, 1.25 mmol), acetyl chloride (1.5 mL) were loaded to an oven-flamed 50 mL Schlenk flask, suspended in anhydrous dichloromethane (15 mL) under argon and stirred overnight at room temperature. The reaction was quenched and purified by column chromatography on silica gel (100 g) in hexane/EtOAc (5:1) to provide 0.06 g of **69** as a yellow waxy oil in 68% yield. (R_f = 0.18, hexane/EtOAc 5:1); ^{1}H NMR (500 MHz, $CDCl_3$) δ ppm 2.37 (s, 9H), 7.28-7.29 (m, 3H), 7.34-7.38 (m, 11H, Ar-H), 7.58 (d, $J_{H,H}$ = 8.4 Hz, 2H, Ar-H), 7.70 (d, $J_{H,H}$ = 8.3 Hz, 2H, Ar-H), 7.71-7.74 (m, 6H, Ar-H); ^{13}C NMR (125.8 MHz, $CDCl_3$) δ ppm 29.91, 64.79, 111.10, 119.18, 126.7, 127.75, 127.80, 127.86, 128.92, 131.68, 132.0, 132.50, 132.86, 137.34, 138.11, 138.14, 140.92, 145.28, 145.32, 147.18, 194.05; IR (KBr) ν cm^{-1}: 3059 (υ(=CH)), 2957 (m, $\upsilon_{as}(CH_3)$), 2929 (s, $\upsilon_s(CH_3)$), 2854 (m), 2225 (m, υ(C≡N)), 1702 (s, υ(C=O)), 1605 (w), 1584 (w), 1488 (w), 1466 (m), 1400 (w, $\delta_s(CH_3)$), 1351 (w, $\delta_{as}(CH_3)$), 1261 (w), 1099 (m), 1022 (w), 947 (m), 817 (m), 800 (m), 613 (m); UV-Vis (λ_{max}[nm], ε, CH_2Cl_2) 305 (23456); ESI(+) MS Calcd for $C_{44}H_{33}S_3O_3NNa$ ([M+Na]$^+$, 742.1520), found *m/z* 742.1508; elemental analysis calcd (%) for $C_{44}H_{33}NO_3S_3$ (719.16): C, 73.41; H, 4.62; N, 1.95; found: C, 73.37; H, 4.71; N. 2.08.

4’’’-(Tris{3-[2-(trimethylsilyl)ethylsulfanyl]phenyl}methyl)-1,1’:4’,1’’:4’’,1’’’-quaterterphenyl-4-carbonitrile (70)

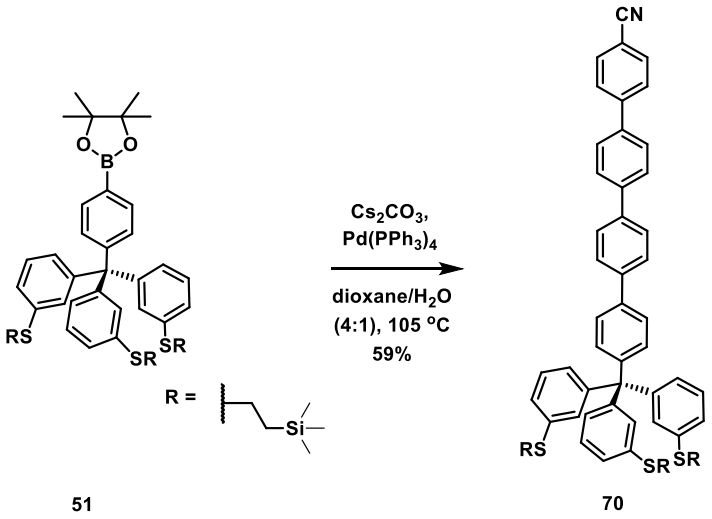

51 70

Envisaged product **70** was synthesized according to a method reported for the preparation of **64**. Pinacol boronic ester **51** (0.18 g, 0.21 mmol), terphenyl **59** (0.13 g, 0.4 mmol), cesium carbonate (0.28 g, 0.86 mmol), tetrakis(triphenylphosphine)palladium(0) (0.025 g, 0.0021 mmol) were charged to a argon-flushed two-neck round bottom flask, and dissolved in the mixture of dioxane/water (50/10 mL). The reaction mixture was stirred under argon overnight and heated at 105 °C. The crude product was purified by column chromatography on silica gel (150 g) in hexane/CH_2Cl_2 (2:1) to obtain 0.12 g of **70** as yellow oil in 59% yield. (R_f = 0.88, hexane/CH_2Cl_2 2:1); ^{1}H NMR (500 MHz, $CDCl_3$) δ ppm 0.05 (s, 27H, CH_3), 0.89-0.93 (m, 6H, CH_2), 2.88-2.92 (m, 6H, CH_2), 7.12-7.13 (m, 3H), 7.20-7.22 (m, 3H), 7.26-7.29 (m, 6H, Ar-H), 7.40 (d, $J_{H,H}$ = 8.4 Hz, 2H, Ar-H), 7.66 (d, $J_{H,H}$ = 8.4 Hz, 2H, Ar-H), 7.78-7.84 (m, 12H, Ar-H); ^{13}C NMR (125.8 MHz, CD_2Cl_2) δ ppm -1.76, 17.09, 29.55, 65.14, 111.32, 119.26, 126.45, 126.55, 127.67, 127.76, 127.87, 128.02, 128.42, 128.65, 129.74, 131.07, 131.78, 133.05, 137.43, 138.40, 139.31, 140.03, 141.13, 145.31, 145.85, 147.39; IR (KBr) ν cm^{-1}: 3029 (w, υ(=CH)), 2957 (m, υ_{as}(CH_2, CH_3)), 2924 (υ_s(CH_2, CH_3)), 2226 (w, υ(C≡N)), 1698 (w), 1635 (w), 1652 (w), 1457 (w), 1398 (w, δ_s(CH_2, CH_3)), 1352 (δ_{as}(CH_2, CH_3)), 1262 (m, δ_s(CH_3, TMS)), 1117 (m), 1003 (m), 951 (w), 829 (w, δ_{as}(CH_3, TMS)) 816 (m), 611 (w, υ_{as}(SiC_3)); UV-Vis (λ_{max}[nm], ε, CH_2Cl_2) 269 (31686); 316 (44199); ESI(+) MS Calcd for $C_{59}H_{67}S_3Si_3NNa$ ([M+Na]$^+$, 992.3641), found *m/z* 992.3564;

elemental analysis calcd (%) for $C_{59}H_{67}S_3Si_3N$ (969.37): C, 73.01; H, 6.96; N. 1.44; found: C, 73.90; H, 7.56; N, 1.68.

_S,S′,S′′_-{3,3',3''-[(4-Cyano-1,1':4',1'':4'',1'''-quaterphenyle-4-yl)methanetriyl)]tris(benzene-3,1-diyl)} tris(thioacetate) (**71**)

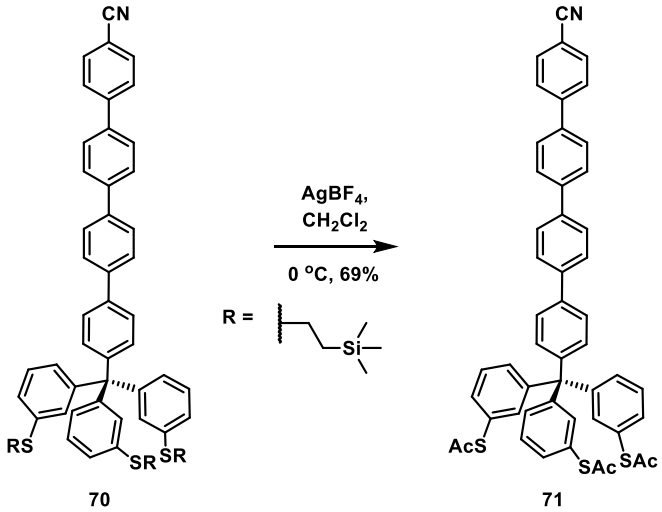

The transprotection was developed according to a method described for the preparation of **65**. Starting material **70** (0.095 g, 0.098 mmol), silver tetrafluoroborate (0.15 g, 0.78 mmol), acetyl chloride (1.5 mL) were charged to an oven-flamed 50 mL Schlenk flask and dissolved in anhydrous dichloromethane (15 mL). The reaction mixture was stirred under argon overnight at room temperature. The reaction mixture was quenched and purified by column chromatography on silica gel (100 g) in hexane/CH_2Cl_2 (1:2) to obtain 0.055 g of **71** as a white solid in 69% yield. (R_f = 0.24, hexane/ CH_2Cl_2 5:1); m.p. 173-175 °C; ^{1}H NMR (500 MHz, CD_2Cl_2) δ ppm 2.37 (s, 9H, CH_3), 7.31-7.32 (m, 3H, Ar-H), 7.38-7.40 (m, 11H, Ar-H), 7.57-7.59 (m, 2H, Ar-H), 7.64 (d, $J_{H,H}$ = 8.5 Hz, 2H, Ar-H), 7.74-7.76 (m, 6H, Ar-H), 7.78-7.81 (m, 6H, Ar-H); ^{13}C NMR (125.8 MHz, CD_2Cl_2) δ ppm 30.42, 64.99, 111.33, 119.27, 126.78, 127.74, 127.77, 127.90, 128.04, 128.40, 129.03, 129.75, 131.07, 131.72, 132.07, 132.65, 133.06, 137.47, 138.42, 138.61, 139.42, 139.94, 141.12, 145.31, 147.47, 194.03; IR (KBr) ν cm^{-1}: 3430 (w, υ(=CH)), 2924 (m, $\upsilon_{as}(CH_3)$), 2854 (w), 2227 (w, υ(C≡N)), 1698 (m, υ(C=O)), 1635 (m), 1558 (w), 1457 (m), 1398 (w, $\delta_s(CH_3)$), 1352 (w, $\delta_{as}(CH_3)$), 1266 (w), 1117 (m), 951 (w), 829 (w), 816 (m), 611 (m); UV-Vis (λ_{max}[nm], ε, CH_2Cl_2) 315 (55161); ESI(+) MS Calcd for $C_{50}H_{37}NO_3S_3Na$ ([M+Na]$^+$, 818.1833), found *m/z* 818.1794; elemental

analysis calcd (%) for $C_{50}H_{37}NO_3S_3$ (796.03): C, 75.44; H, 4.68; N, 1.76; found: C, 74.87; H, 4.71; N, 2.01.

Tetrakis[4-(*n*-butylsulfanyl)phenyl]methane (**72**)

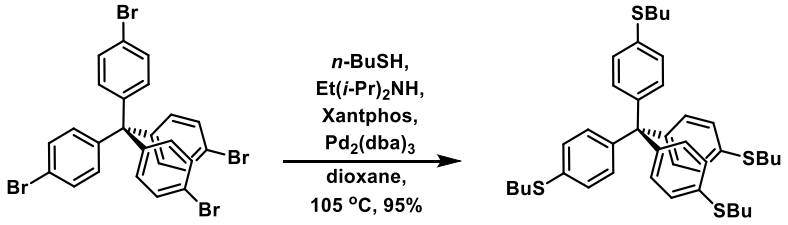

72

Tetrakis(4-bromophenyl)methane (0.2 g, 0.31 mmol), Xantphos (0.027 g, 0.047 mmol), tris(dibenzylideneacetone)dipalladium(0) (0.029 g, 0.047 mmol), anhydrous dioxane (14 mL), *N*,*N*-diisopropylethylamine (0.49 g, 3.77 mmol) were loaded to an oven-flamed 50 mL pressure tube and purged with argon, subsequently *n*-butylthiol (0.23 g, 2.51 mmol) was added. The tube was sealed and the reaction mixture was heated at 120 °C for 24 h. After cooling, dioxane was removed, crude product was diluted with dichloromethane and water and extracted with CH_2Cl_2 (3 x 150 mL). Organic layers were combined, dried over $MgSO_4$, filtrated and the volatiles were removed under vacuum. The crude product was purified by column chromatography on silica gel (150 g) in hexane/EtOAc (20:1) to provide 0.2 g of **72** as a yellow powder in 95% yield. (R_f = 0.56, hexane/ EtOAc 20:1); m.p. 272-273 °C; ^{1}H NMR (500 MHz, CD_2Cl_2) δ ppm 0.91-0.94 (m, 12H, CH_3), 1.42-1.48 (q, 8H, CH_2), 1.61-1.67 (m, 8H, CH_2), 2.89-2.92 (m, 8H, CH_2), 7.07 (d, $J_{H,H}$ = 8.55 Hz, 2H, Ar-H), 7.16 (d, $J_{H,H}$ = 8.55 Hz, 2H, Ar-H); ^{13}C NMR (125.8 MHz, CD_2Cl_2) δ ppm 13.8, 22.1, 31.3, 33.0, 63.6, 127.4, 131.5, 135.1, 143.8; IR (KBr) ν cm^{-1}: 3073 (w, υ(=CH)), 2956 (s, υ_{as}(CH_2, CH_3)), 2926 (m, υ_s(CH_2, CH_3)), 2857 (m), 1626 (w, υ(C=C)), 1590 (w), 1487 (m), 1434 (w, δ_s(CH_2, CH_3)), 1400 (w, δ_s(CH_2, CH_3,)), 1095 (m), 1013 (m), 811 (m), UV-Vis (λ_{max}[nm], ε, CH_2Cl_2) 270 (30995); ESI(+) MS Calcd for $C_{41}H_{52}S_4Na$ ([M+Na]$^+$, 695.2850), found *m/z* 695.2767; elemental analysis calcd (%) for $C_{41}H_{52}S_4$ (672.30): C 73.16, H 7.79;. found: C 73.30, H 7.91.

Tetrakis{4-[2-(trimethylsilyl)ethylsulfanyl]phenyl}methane (**73**)

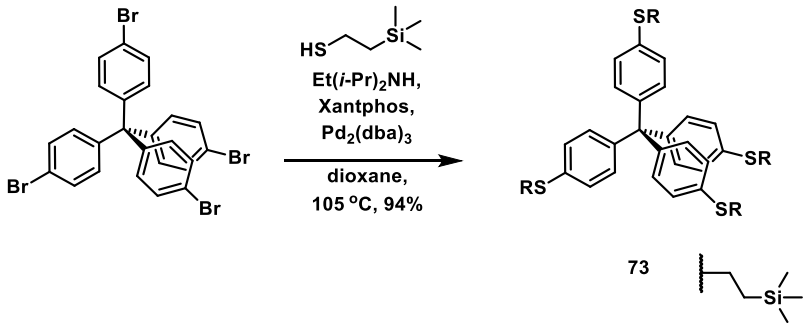

The product **73** was synthesized according to a method reported for the preparation of **72**. Tetrakis(4-bromophenyl)methane (0.12 g, 0.19 mmol), Xantphos (0.016 g, 0.028 mmol), tris(dibenzylideneacetone)dipalladium(0) (0.02 g, 0.028 mmol), anhydrous dioxane (10 mL), *N*,*N*-diisopropylethylamine (0.26 g, 1.98 mmol) and 2-(trimethylsilyl)ethanethiol (0.24 g, 1.89 mmol) were heated at 105 °C for 24 h under argon atmosphere. The crude product was purified by column chromatography on silica gel (150 g) in hexane/EtOAc (20:1) to obtain 0.15 g of **73** as a white powder in 94% yield. (R_f = 0.58, hexane/EtOAc 20:1); m.p. 183-185 ^{o}C; ^{1}H NMR (500 MHz, CD_2Cl_2) δ ppm 0.04 (s, 27H, CH_3), 0.92-0.95 (m, 8H, CH_2), 2.93-2.96 (m, 8H, CH_2), 7.07 (d, $J_{H,H}$ = 8.35 Hz, 8H, Ar-H), 7.15 (d, $J_{H,H}$ = 8.55 Hz, 8H, Ar-H); ^{13}C NMR (125.8 MHz, CD_2Cl_2) δ ppm -1.5, 17, 29.3, 63.7, 127.5, 131.6, 135.5, 143.9; IR (KBr) ν cm^{-1}: 3078 (w, υ(=CH)), 2952 (s, υ_{as}(CH_2, CH_3)), 2924 (m, υ_s(CH_2, CH_3)), 2854 (m), 1635 (w), 1590 (w, υ(C= C)), 1486 (m), 1417 (w, δ_s(CH_2, CH_3)), 1378 (w, δ_s(CH_3, TMS)), 1248 (s), 1093 (m), 1013 (m), 859 (s), 838 (m, δ_{as}(CH_3, TMS)), 810 (s), 693 (w, υ_{as}(SiC_3)); UV-Vis (λ_{max}[nm], ε, CH_2Cl_2) 271 (31876); ESI(+) HRMS Calcd for $C_{45}H_{68}S_4Si_4Na$ ([M+Na]$^+$, 871.3179), found *m/z* 871.3186; elemental analysis calcd (%) for $C_{45}H_{68}S_4Si_4$ (848.33): C 63.62, H 8.07; found: C 64.02, H 7.88.

***S,S′,S′′,S′′′*-[4,4',4'',4'''-(Methanetetrayl)tetrakis(benzene-4,1-diyl)] tetrakis(thioacetate)** (**74**)

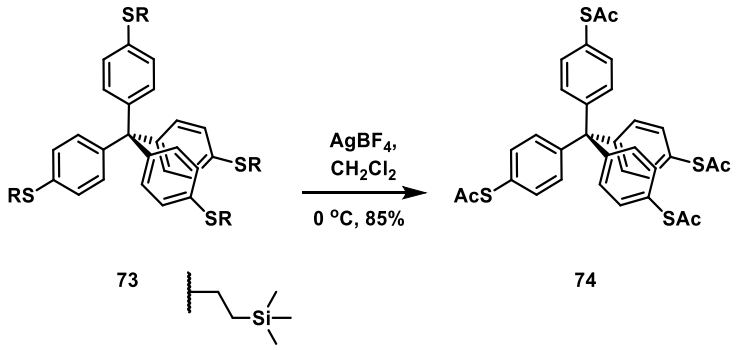

The trans-protection was developed according to a method described for the preparation of **50**. Starting material **73** (0.16 g, 0.19 mmol), $AgBF_4$ (0.37 g, 1.93 mmol), acetyl chloride (3 mL) were loaded to an oven-flamed 50 mL Schlenk flask and suspended in anhydrous dichloromethane (30 mL). The reaction mixture was stirred under argon overnight at room temperature. The reaction mixture was quenched and purified by column chromatography on silica gel (100 g) in hexane/CH_2Cl_2 (1:2) to obtain 0.1 g of **74** as white solid in 85% yield. (R_f = 0.12, hexane/ CH_2Cl_2 1:2); m.p. 175-177 °C; ^{1}H NMR (500 MHz, CD_2Cl_2) δ ppm 2.39 (s, 12H, CH_3), 7.32 (d, $J_{H,H}$ = 8.6 Hz, 8H, Ar-H), 7.35 (d, $J_{H,H}$ = 8.6 Hz, 8H, Ar-H); ^{13}C NMR (125.8 MHz, CD_2Cl_2) δ ppm 30.5, 65.1, 126.9, 131.8, 134.2, 147.3, 194; IR (KBr) ν cm^{-1} 3030 (w, υ(=CH)), 2957 (m, $\upsilon_{as}(CH_3)$), 2924 (m, $\upsilon_s(CH_3)$), 2854 (w), 1710 (s, υ(C=O)), 1486 (s), 1394 (m, $\delta_{as}(CH_3)$), 1346 (m, $\delta_s(CH_3)$), 1111 (m), 1092 (s), 1014 (m) 957 (m), 821 (s), 617 (s); UV-Vis (λ_{max}[nm], ε, CH_2Cl_2) 255 (21459); ESI(+) HRMS Calcd for $C_{33}H_{28}O_4S_4Na$ ($[M+Na]^+$, 639.0768), found *m/z* 639.0667; elemental analysis calcd (%) for $C_{33}H_{28}O_4S_4$ (616.09): C 64.26, H 4.58; found: C 64.80, H 4.83.

4-[Tris(3-bromophenyl)methyl]phenyl trifluoromethanesulfonate (**75**)

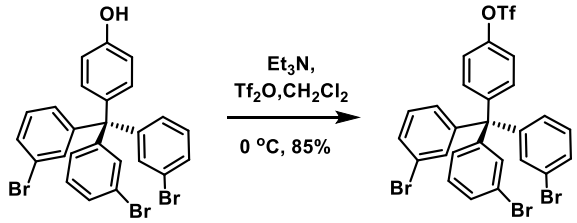

46 75

The previously reported derivative **46** (0.3 g, 0.53 mmol) was loaded to oven-flame Schlenk flask under argon atmosphere and dissolved in freshly distilled dichloromethane (40 mL). Afterwards triethylamine (0.11 mL, 0.79 mmol) was added at once and stirred over 2 h at room temperature. Subsequently the reaction mixture was cooled down to 0 ^{o}C and triflic anhydride (0.13 mL, 0.76 mmol) was dropwise added. The reaction mixture was vigorously stirred overnight under argon atmosphere. The reaction mixture was quenched with water (100 mL). Resulted solution was extracted with CH_2Cl_2 (3 x 100 mL). Organic layers were combined, dried over magnesium sulfate and filtrated. Filtrate was concentrated under vacuum. The residue was passed through a short silica pad providing desired product **75** in 85% yield (0.36 g) as a white powder. (R_f = 0.62, hexane/ EtOAc 10:1); m.p. 146-147 ^{o}C; ^{1}H NMR (500 MHz, CD_2Cl_2) δ ppm 7.05-7.06 (m, 3H, Ar-H), 7.17-7.24 (m, 7H Ar-H), 7.27-7.28 (m, 3H, Ar-H), 7.39-7.41 (m, 3H, Ar-H); ^{13}C NMR (125.8 MHz, CD_2Cl_2) δ ppm 64.5, 121.2, 122.8, 128.5, 130, 130.5, 132.9, 133.6, 145.8, 147.5, 148.3; ^{19}F NMR (470.57 MHz, $CDCl_3$) -72.80; IR (KBr) ν cm^{-1}: 3063 (w, υ(=CH)), 2925 (m, υ_{as}(CH_2, CH_3)), 2854 (m, υ_s(CH_2, CH_3)), 1588 (m, υ(C=C)), 1561 (m), 1497 (w, δ_{as}(CH_2, CH_3)), 1470 (s), 1424 (s, δ_s(CH_2, CH_3)), 1304 (w), 1250 (m, δ_s(CH_3, TMS)), 1222 (s), 1139 (s), 1016 (m), 996 (m), 893 (m), 837 (m), 786 (s), 726 (m), 604 (s, υ(C-Br)); UV-Vis (λ_{max}[nm], ε, acetone) 212 (57404); ESI(-) MS Calcd for $C_{26}H_{16}Br_3F_3O_3SK$ ([M+K]$^{+}$, 742.7763), found *m/z* 742.7346; elemental analysis calcd (%) for $C_{26}H_{16}Br_3F_3O_3S$ (701.83): C 44.28, H 2.29; found: C 44.81, H 2.65.

1-Tris[2-(trimethylsilyl)ethylsulfanyl]-4-(tris{3-[2-(trimethylsilyl)ethylsulfanyl phenyl]phenyl}methyl) benzene (**76**)

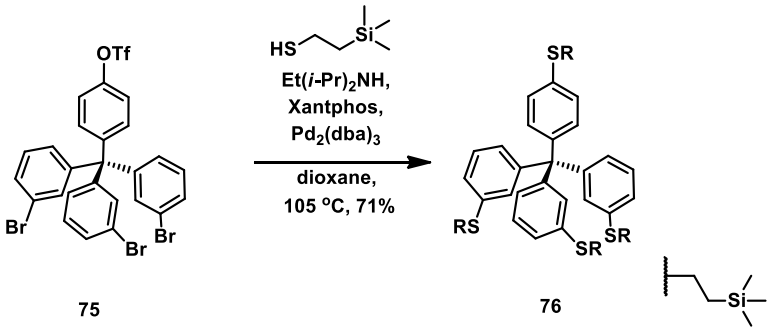

75 76

The reaction was developed according to a method described for the preparation of **73** An oven-flamed 25 mL pressure tube was charged with **75** (0.14 g, 0.2 mmol), Xantphos (0.017 g, 0.029 mmol), tris(dibenzylideneacetone)dipalladium(0) (0.018 g, 0.02 mmol) and anhydrous dioxane (10 mL). The tube was evacuated and refilled with argon three times. Then *N*,*N*-diisopropylethylamine (0.26 g, 1.98 mmol) and 2-(trimethylsilyl)ethane thiol (0.16 g, 1.2 mmol) were added under argon and the tube was quickly sealed. The reaction mixture was heated at 105 °C for 24 h. After cooling, the reaction mixture was diluted with dichloromethane (150 mL) and washed with water (100 mL). The combined organic layers were washed with brine (100 mL), dried over $MgSO_4$ and filtered. The volatiles were removed under reduced pressure and the residue was purified by column chromatography on silica gel (200 g) in hexane/CH_2Cl_2 (2:1) to provide the title compound **76** (0.12 g) as a yellow oil in 71% yield (R_f = 0.48, hexane/CH_2Cl_2 2:1); m.p. 294-297 ^oC; ^1H NMR (500 MHz, CD_2Cl_2) δ ppm 0.82 (s, 27H, CH_3), 0.83 (s, 9H, CH_3), 0.84-0.92 (m, 6H, CH_2), 0.93-0.95 (m, 2H, CH_2), 2.78-2.94 (m, 6H, CH_2), 2.94-2.96 (m, 2H, CH_2), 6.95-6.97 (m, 3H, Ar-H), 7.09 (d, $J_{H,H}$ = 8.6 Hz, 2H, Ar-H), 7.11-7.17 (m. 11H, Ar-H); ^{13}C NMR (125.8 MHz, CD_2Cl_2) δ ppm -1.74, 16.8, 29, 39.4, 64.6, 126.5, 127.2, 128, 128.6, 131.1, 131.5, 135.6, 136.7, 143.2, 146.9; IR (KBr) ν cm^{-1}: 3058 (w, υ(=CH)), 2953 (s, υ_{as}(CH_2, CH_3)), 2924 (m, υ_s(CH_2, CH_3)), 2854 (m), 1628 (w), 1582 (m), 1466 (s), 1414 (w, δ_s(CH_2, CH_3)), 1377 (w, δ_s(CH_3, TMS)), 1249 (m, δ_s(CH_3, TMS)),), 1091 (w), 1013 (w), 858 (s), 840 (m, δ_{as}(CH_3, TMS)) 694 (w, υ_{as}(SiC_3)); UV-Vis (λ_{max}[nm], ε, CH_2Cl_2) 268 (13106); ESI(+) HRMS Calcd for $C_{45}H_{68}S_4Si_4Na$ ($[M+Na]^+$, 871.3179), found *m/z* 871.3196; elemental analysis calcd (%) for $C_{45}H_{68}S_4Si_4$ (848.33): C 63.61, H 8.07; found: C 63.14, H 8.62.

S,S',S''-{4-Acetylsulfanylphenyl-[3,3',3''-(methanetriyl)tris(benzene-3,1-diyl)]} tris(thioacetate) (**77**)

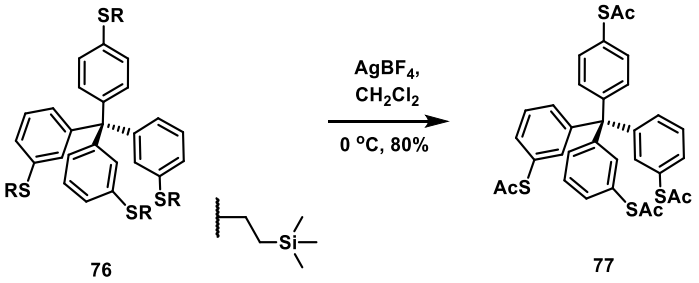

The transprotection was developed according to a method described for the preparation of **74**. Starting material **76** (0.095 g, 0.11 mmol), silver tetrafluoroborate (0.22 g, 1.12 mmol), acetyl chloride (2 mL) were charged to an oven-flamed 50 mL Schlenk flask and suspended in anhydrous dichloromethane (20 mL). The reaction mixture was stirred under argon overnight at room temperature. The reaction mixture was quenched and purified by column chromatography on silica gel (100 g) in hexane/CH_2Cl_2 (1:4) to obtain 0.055 g of **77** as a white solid in 80% yield. (R_f = 0.29, hexane/CH_2Cl_2 1:4); m.p. 264-266 ^oC; ^1H NMR (500 MHz, CD_2Cl_2) δ ppm 2.35 (s, 9H, CH_3), 2.40 (s, 3H, CH_3), 7.28-7.31 (m, 6H, Ar-H), 7.34-7.46 (m, 10H, Ar-H); ^{13}C NMR (125.8 MHz, CD_2Cl_2) δ ppm 30.5, 30.5, 65.1, 126.9, 128.5, 129.1, 132, 132.8, 134.2, 137.5, 147.1, 147.3, 194, 194; IR (KBr) ν cm^{-1} 3028 (w, υ(=CH)), 2956 (m, υ_{as}(CH_3)), 2924 (s, υ_s(CH_3)), 2854 (w), 1704 (s, υ(C=O)), 1584 (w), 1480 (s), 1405 (w, δ_{as}(CH_3)), 1351 (w, δ_s(CH_3)), 1269 (w), 1122 (s), 1100 (m), 948 (m), 812 (s), 793 (w), 615 (s); UV-Vis (λ_{max}[nm], ε, CH_2Cl_2) 312 (26278); ESI(+) HRMS Calcd for $C_{33}H_{28}O_4S_4Na$ ($[M+Na]^+$, 639.0768), found *m/z* 639.0665; elemental analysis calcd (%) for $C_{33}H_{28}O_4S_4$ (616.09): C 64.26, H 4.58; found: C 64.71, H 4.91.

4-[2-(Trimethylsilyl)ethylsulfanyl]phenylboronic acid (78)[215]

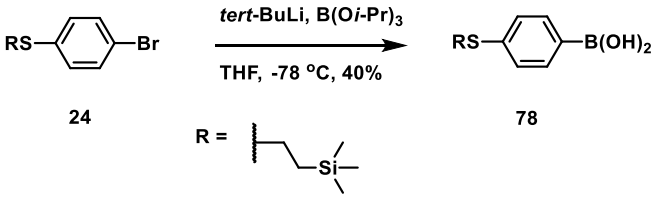

Compound **78** was prepared according to a procedure reported by Grunder. [215] A dry and argon-flushed 250 mL oven-flamed Schlenk flask was charged with **24** (2 g, 6.91 mmol) and dissolved in a freshly distilled tetrahydrofuran (35 mL). The solution was cooled to -78 °C and *tert*-BuLi (10.6 mL, 18 mmol, 15% in pentane) was added dropwise over 20 min. The reaction mixture was stirred at -78 °C for 2 h under argon. In a second 100 mL oven-flamed Schlenk flask, triisopropylborate (8 mL, 34.51 mmol) was diluted with tetrahydrofuran (5 mL) under an inert atmosphere and cooled to -78 °C. The solution of lithiated species was slowly added via a cannula into the flask containing borate solution, after 1 h, the reaction mixture was allowed to warm to room temperature and stirred for an additional 16 h. The reaction mixture was quenched with saturated NH_4Cl solution (100 mL). The aqueous layer was washed with *tert*-butyl methyl ether (2 x 100 mL). The combined organic layer was washed with brine (100 mL), dried over $MgSO_4$, and filtered. All volatiles were removed under reduced pressure and the solid was recrystallized from hot hexane giving **78** as a white powder in 40% yield (1.09 g). ^{1}H NMR (500 MHz, CD_3OD) δ ppm 0.04 (s, 9H, CH_3), 0.89-0.93 (m, 2H, CH_2), 2.96-3.30 (m, 2H, CH_2), 7.20-7.21 (m, 2H, Ar-H), 7.63-7.65 (m, 2H, Ar-H); ^{13}C NMR (125.8 MHz, CD_3OD) δ ppm -1.7, 17.7, 29.4, 102.3, 128.0, 135.4, 141.4.

4-Bromo-4'-[2-(trimethylsilyl)ethylsulfanyl]biphenyl (**79**)

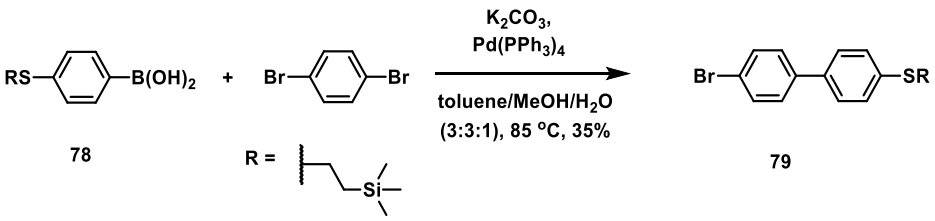

A 100 mL round bottom flask equipped with a refluxed condenser was charged with boronic acid **78** (0.48 g, 1.9 mmol), 1,4-dibromobenzene (4.84 g, 19.05 mmol), potassium carbonate

(0.4 g, 2.8 mmol), tetrakis(triphenylphosphine)palladium(0) (0.11 g, 0.095 mmol) and dissolved in a mixture of toluene, methanol and water (30/30/10 mL). Resulted mixture was flushed with argon and heated to 70 ^{o}C overnight. After cooling to room temperature solvents were removed, the residue was dissolved in dichloromethane (200 mL) and washed with water (100 mL). Aqueous layer was separated and washed again with dichloromethane (2 x 150 mL). Combined organic fraction was dried over magnesium sulfate, filtered and concentrated under vacuum. The residue was purified by column chromatography on silica gel (150 g, hexane) providing 0.24 g of **79** as a white powder in 35% yield. (R_f = 0.43, hexane); m.p. 198-199 ^{o}C; ^{1}H NMR (500 MHz, CD_2Cl_2) δ ppm 0.06 (s, 9H, CH_3), 0.94-0.98 (m, 2H, CH_2), 2.99-3.03 (m, 2H, CH_2), 7.35 (d, $J_{H,H}$ = 8.45 Hz, 2H, Ar-H), 7.46-7.48 (m, 2H, Ar-H), 7.49-7.51 (m, 2H, Ar-H), 7.56 (d, $J_{H,H}$ = 8.6 Hz, 2H, Ar-H); ^{13}C NMR (125.8 MHz, CD_2Cl_2) δ ppm -1.72, 17.16, 29.53, 121,69, 127.56, 127.80, 129.13, 132.27, 137.30, 137.80, 139.84; IR (KBr) ν cm^{-1}: 2952 (w, υ(=CH)), 2924 (m, υ_{as}(CH_2, CH_3)), 2854 (m, υ_s(CH_2, CH_3)), 1634 (w), 1591 (w), 1474 (s), 1387 (w, δ_s(CH_2, CH_3)), 1248 (s, δ_s(CH_3, TMS)), 1100 (m), 1079 (m), 1006 (m), 859 (m), 839 (m, δ_{as}(CH_3, TMS)) 804 (s), 688 (w, υ_{as}(SiC_3)); UV-Vis (λ_{max}[nm], ε, CH_2Cl_2) 296 (12813); ESI(+) MS Calcd for $C_{17}H_{22}SSiNa$ ([M+Na +H, -Br]$^{+}$, 309.1109), found *m/z* 309.1999; elemental analysis calcd (%) for $C_{17}H_{21}SSiBr$ (364.03): C 55.88; H 5.79; found: C 56.16, H 5.95.

4-[2-(Trimethylsilyl)ethylsulfanyl]-1,1':4',1''-terphenyl (**80**)

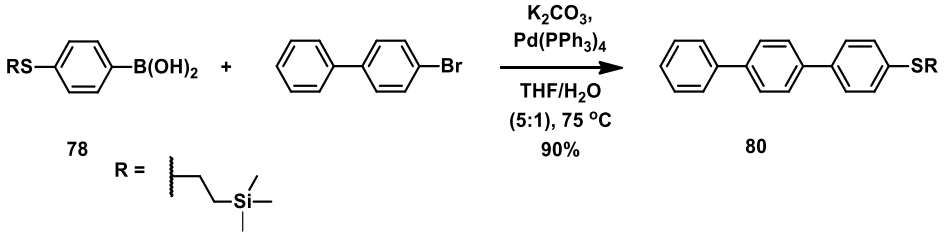

A 100 mL round bottom flask was charged with boronic acid **78** (0.14 g, 0.56 mmol), 4-bromobiphenyl (0.1 g, 0.43 mmol), potassium carbonate (0.18 g, 0.11 mmol), tetrakis(triphenylphosphine)palladium(0) (0.043 g, 0.049 mmol) and dissolved in a mixture of tetrahydrofuran and water (50/10 mL). Resulted mixture was flushed with argon, and then heated at 75 ^{o}C overnight under an inert atmosphere. After cooling to room temperature the solvents were removed, the residues was extracted with dichloromethane and washed with

water (100 mL). Aqueous layer was separated and washed again with dichloromethane (2x 150 mL) Combined organic fraction was dried over magnesium sulfate, filtrated and concentrated in vacuum. The residue was purified by column chromatography on silica gel (150 g, hexane/CH_2Cl_2 (1:2) proving 0.14 g of **80** as a white powder in 90% yield. (R_f = 0.52, hexane/ CH_2Cl_2 1:2), m.p. 184-187 ^oC; ^1H NMR (500 MHz, CD_2Cl_2) δ ppm 0.07 (s, 9H, CH_3), 0.96-0.99 (m, 2H, CH_2), 3.01-3.04 (m, 2H, CH_2), 7.36-7.39 (m, 3H, Ar-H), 7.45-7.48 (m, 2H, Ar-H), 7.51-7.54 (m, 1H, Ar-H), 7.59 (dd, $J_{H,H}$ = 6.6, 1.9 Hz, 2H, Ar-H), 7.65-7.69 (m, 3H, Ar-H); ^{13}C NMR (125.8 MHz, CD_2Cl_2) δ ppm 0.26, 19.19, 31.64, 129,28, 129.45, 129.60, 129.78, 129.82, 131.23 139.27 140.05, 141.69, 142.34, 142.89; IR (KBr) ν cm^{-1}: 3031 (w, υ(=CH)), 2951 (m), 2923 (m, $\upsilon_{as}(CH_2, CH_3)$), 2854 (w, $\upsilon_s(CH_2, CH_3)$), 1593 (m, υ(C=C)), 1481 (s), 1447 (m), 1396 (m, $\delta_s(CH_2, CH_3)$), 1248 (w, $\delta_s(CH_3$, TMS)), 1162 (m), 1098 (m), 1005 (m), 844 (m), 816 (m, $\delta_{as}(CH_3$, TMS)) 761 (s), 691 (w, $\upsilon_{as}(SiC_3)$); UV-Vis (λ_{max}[nm], ε, CH_2Cl_2) 320 (30012); ESI(+) MS Calcd for $C_{23}H_{26}SSiNNa$ ($[M+Na]^+$, 385.1422), found *m/z* 385.1389; elemental analysis calcd (%) for $C_{23}H_{26}SSi$:(362.15): C 76.18, H 7.23; found: C 76.53, H 7.61.

4’’’-Bromo-4-[2-(trimethylsilyl)ethylsulfanyl]-1,1’:4’,1’’-terphenyl (**81**)

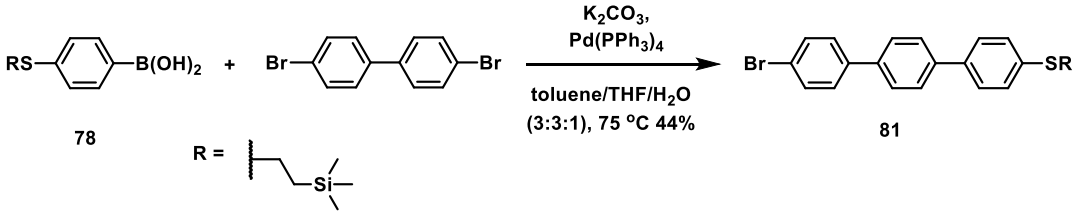

Compound **81** was prepared in a similar way as **79**. A 100 mL round bottom flask was charged with boronic acid **78** (0.53 g, 0.21 mmol), 4,4’-dibromobiphenyl (1.3 g, 4.17 mmol), potassium carbonate (0.57 g, 4.17 mmol), tetrakis(triphenylphosphine)palladium(0) (0.12 g, 0.011 mmol) and dissolved in a mixture of toluene, tetrahydrofuran and water (30/30/10 mL). Resulted mixture was flushed with argon, and then heated at 70 ^oC overnight under inert atmosphere. After cooling to room temperature solvents were removed, the residue was extracted with dichloromethane and washed with water (100 mL). Aqueous layer was separated and washed again with dichloromethane (2 x 100 mL). Combined organic fraction was dried over magnesium sulfate, filtrated and concentrated in vacuo. The residue was purified by column chromatography on silica gel (300 g, hexane/CH_2Cl_2 5:1). Afterwards

white powder was recrystallized from hot toluene getting 0.4 g of **81** as a white solid in 44% yield. (R_f = 0.44, hexane/CH_2Cl_2 5:1); m.p. 294-297 ^oC; ^1H NMR (500 MHz, CD_2Cl_2) δ ppm 0.06 (s, 9H, CH_3), 0.96-0.99 (m, 2H, CH_2), 2.99-3.03 (m, 2H, CH_2), 7.39 (d, $J_{H,H}$ = 8.25 Hz, 2H, Ar-H), 7.50 (d, $J_{H,H}$ = 8.5 Hz, 2H, Ar-H), 7.57 (t, $J_{H,H}$ = 8.45 Hz, 2H, Ar-H), 7.62 (d, $J_{H,H}$ = 8.45 Hz, 2H, Ar-H), 7.66 (d, $J_{H,H}$ = 8.55 Hz, 2H, Ar-H); ^{13}C NMR (125.8 MHz, CD_2Cl_2) δ ppm -1.61, 17.0, 29.61, 121,74, 127.56, 127.43, 127.45, 128.70, 129.22, 132.06, 136.89, 137.89, 138.94, 139.68, 139.35; IR (KBr) ν cm^{-1}: 3027 (w, υ(=CH)), 2920 (m, $\upsilon_{as}(CH_2, CH_3)$), 2853 (m, $\upsilon_s(CH_2, CH_3)$), 1906 (w), 1724 (w), 1649 (w), 1479 (s), 1383 (w, $\delta_s(CH_2, CH_3)$), 1349 (w, $\delta_s(CH_3$, TMS)), 1071 (m), 999 (m), 827 (m, $\delta_{as}(CH_3$, TMS)), 807 (s), 688 (w, $\upsilon_{as}(SiC_3)$); UV-Vis (λ_{max}[nm], ε, CH_2Cl_2) 290 (35150); EI MS *m/z* (%) 333.08 (100), 253.15 (29), 226.14 (17), 163.01 (9), 133.07 (19), 119 (8), 103.03 (14); elemental analysis calcd (%) for $C_{23}H_{25}SSi$ (385.14): C 62.57, H 5.71; found: C 62.74, H 5.89.

4-[2-(trimethylsilyl)ethylsulfanyl]-4'-(tris{4-[2-(trimethylsilyl)ethylsulfanyl]phenyl}methyl) biphenyl (**82**)

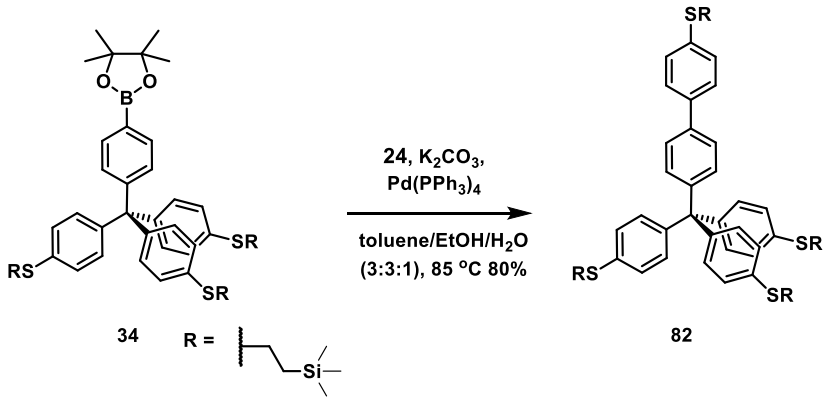

Compound **82** was prepared according to a procedure described for the synthesis of **60**. Pinacol boronic ester **34** (0.17 g, 0.2 mmol), aryl bromide **24** (0.065g, 0.26 mmol), potassium carbonate (0.068 g, 0.49 mmol), and tetrakis(triphenylphosphine)palladium(0) (0.023 g, 0.019 mmol) were placed in 100 mL round bottom flask. Reagents were dissolved in the mixture of toluene (30 mL), ethanol (30 mL), water (10 mL) and degassed with argon. Subsequently, the reaction mixture was heated at 85 ^oC overnight under an inert atmosphere. After cooling, dioxane was removed. The crude product was diluted with water (100 mL) and dichloromethane (150 mL) and then extracted with dichloromethane (2 x 100 mL). Combined organic fraction was dried over magnesium sulfate, filtrated and concentrated in vacuo. The residue was purified by column chromatography on silica gel (200 g, hexane/EtOAc 40:1)

providing 0.15 g of **82** as a yellow powder in 80% yield. (R_f = 0.39, hexane/EtOAc 40:1); m.p. 84-86 °C; ^{1}H NMR (500 MHz, CD_2Cl_2) δ ppm 0.04 (s, 27H, CH_3), 0.05 (s, 9 H, CH_3), 0.93-0.97 (m, 8H, CH_2), 2.95-3.02 (m, 8H, CH_2), 7.15-7.19 (m, 12H, Ar-H), 7.27 (d, $J_{H,H}$ = 8.6 Hz, 2H, Ar-H), 7.34 (d, $J_{H,H}$ = 8.5 Hz, 2H, Ar-H), 7.50 (d, $J_{H,H}$ = 8.6 Hz, 2H, Ar-H), 7.53 (d, $J_{H,H}$ = 8.5 Hz, 2H, Ar-H); ^{13}C NMR (125.8 MHz, CD_2Cl_2) δ ppm -1.73, 17.15, 17.18, 29.32, 29.62, 64.08, 125.82, 126.23, 127.56, 127.57, 129.19, 131.72, 135.90, 137.18, 137.93, 138.33, 144.19, 146.10; IR (KBr) ν cm^{-1}: 3075 (w, υ(=CH)), 3024 (w, υ(=CH)), 2950 (s), 2918 (m, υ_{as}(CH_2, CH_3)), 2852 (w, υ_s(CH_2, CH_3)), 1591 (m), 1485 (s, δ_{as}(CH_2, CH_3)), 1399 (m, δ_s(CH_2, CH_3)), 1247 (m, δ_s(CH_3, TMS)), 1163 (m), 1094 (m), 1012 (m) 859 (s), 837 (s, δ_{as}(CH_3, TMS)), 691 (w, υ_{as}(SiC_3)); UV-Vis (λ_{max}[nm], ε, CH_2Cl_2) 276 (26474); ESI(+) MS Calcd for $C_{51}H_{72}S_4Si_4Na$ ([M+Na]$^+$, 947.3492), found *m/z* 947.3330; elemental analysis calcd (%) for $C_{51}H_{72}S_4Si_4$ (924.36): C 66.17, H 7.84; found: C 66.47, H 8.01.

***S,S′,S′′*-{4-Acetylsulfanylbiphenyl-4'-yl)-[4,4',4''-(methanetriyl)tris(benzene-4,1-diyl)} tris(thioacetate)** (**83**)

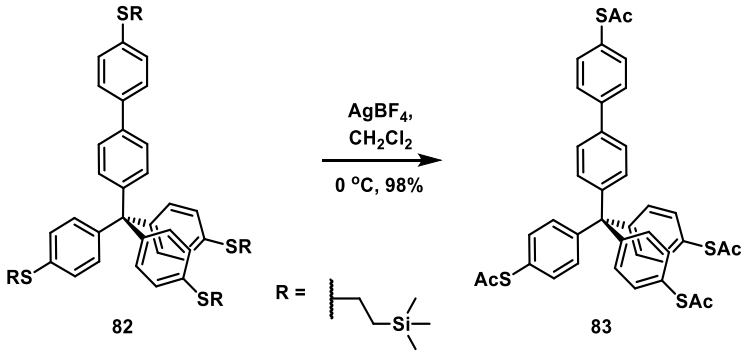

The transprotection was conducted according to a method described for the preparation of **74**. Starting material **82** (0.094 g, 0.01 mmol), silver tetrafluoroborate (0.2 g, 1.02 mmol) and acetyl chloride (2.5 mL) were placed to an oven-flamed 50 mL Schlenk flask and suspended in anhydrous dichloromethane (25 mL). The reaction mixture was stirred under argon overnight at room temperature. The reaction mixture was quenched and purified by column chromatography on silica gel (100 g) in hexane/EtOAc (1:5) to obtain 0.07 g of **83** as a white solid in 98% yield. (R_f = 0.22, hexane/CH_2Cl_2 1:4); m.p. 262-263 °C; ^{1}H NMR (500 MHz, CD_2Cl_2) δ ppm 2.40 (s, 9H, CH_3), 2.42 (s, 3H, CH_3), 7.34-7.37 (m, 14H, Ar-H), 7.46-7.48 (d, $J_{H,H}$ = 8.35 Hz, 2H, Ar-H), 7.58 (d, $J_{H,H}$ = 8.5 Hz, 2H, Ar-H), 7.66 (d, $J_{H,H}$ = 8.4 Hz, 2H, Ar-H); ^{13}C NMR (125.8 MHz, CD_2Cl_2) δ ppm 30.10, 30.47, 64.97, 126.77, 127.08, 127.64, 128.06, 131.66, 131.90, 134.18, 135.30, 138.41, 141.80, 145.65, 147.64; (KBr) ν cm^{-1} 3025 (w. υ(=CH)), 2952 (w, υ_{as}(CH_3)), 2924 (s, υ_s(CH_3)), 2854 (w), 1703 (s, υ(C=O)), 1587 (w),

1484 (s), 1490 (m, $\delta_{as}(CH_3)$), 1348 (m, $\delta_s(CH_3)$), 1117 (s), 1092 (w), 1014 (m), 1004 (m), 949 (s), 814 (s), 616 (s); UV-Vis (λ_{max}[nm], ε, acetone) 212 (26485); ESI(+) MS Calcd for $C_{39}H_{32}O_4S_4Na$ ($[M+Na]^+$, 715.1081), found *m/z* 715.0923; elemental analysis calcd (%) for $C_{39}H_{32}O_4S_4$ (692.12): C 67.60, H 4.65; found: C 67.95, H 4.77.

4-[2-(trimethylsilyl)ethylsulfanyl])-4''-(tris{4-[2-(trimethylsilyl)ethylsulfanyl]phenyl}methyl)-1,1':4'1''-terphenyl (**84**)

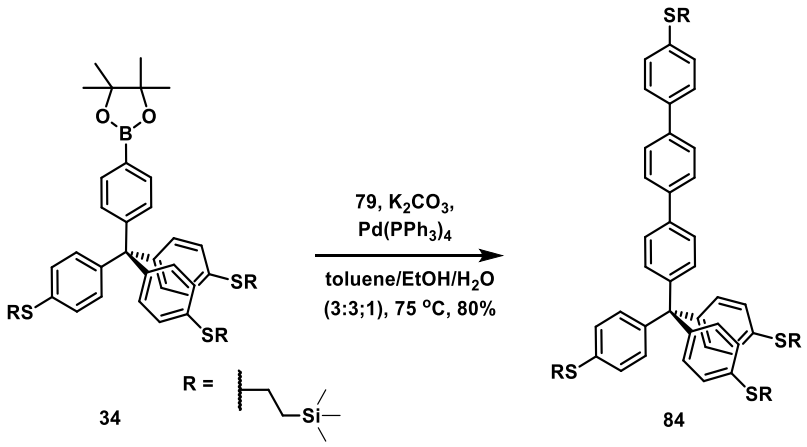

Pinacol boronic acid **34** (0.18 g, 0.21 mmol), biphenyl precursor **79** (0.093 g, 0.26 mmol), potassium carbonate (0.71 g, 0.51 mmol) and tetrakis(triphenylphosphine)palladium(0) (0.025 g, 0.021 mmol) were placed in 100 mL round bottom flask, dissolved in a mixture of toluene, ethanol, water (30/30/10 mL) and degassed with argon. Subsequently, the reaction mixture was heated at 75 °C overnight under an inert atmosphere. After cooling, solvents were evaporated and the residue was diluted with water (100 mL) and dichloromethane (150 mL). The crude product was extracted with dichloromethane (2 x 100 mL). Combined organic fraction was dried over magnesium sulfate, filtrated and concentrated in vacuo. Crude product was purified by column chromatography on silica gel (250 g, hexane/EtOAc (1:40) providing 0.17 g of **84** as white powder in 80% yield. (R_f = 0.43, hexane/ EtOAc 1:40); m.p. 151-153 °C; ^{1}H NMR (500 MHz, CD_2Cl_2) δ ppm 0.04 (s, 27H, CH_3), 0.06 (s, 9H, CH_3), 0.93-0.99 (m, 8H, CH_2), 2.96-3.01 (m, 6H, CH_2), 3.02-3.04 (m, 2H, CH_2), 7.18 (dd, $J_{H,H}$ = 8.4, 1.9 Hz, 2H, Ar-H), 7.38 (dd, $J_{H,H}$ = 8.8, 1.9 Hz, 2H, Ar-H), 7.57 (d, $J_{H,H}$ = 8.75 Hz, 2H, Ar-H), 7.59 (d, $J_{H,H}$ = 6.65 Hz, 2H, Ar-H), 7.67-7.68 (m, 2H, Ar-H); ^{13}C NMR (125.8 MHz, CD_2Cl_2) δ ppm -1.77, 17.11, 17.16, 29.28, 30.07, 64.07, 126.37, 127.44, 127.52, 127.54, 127.54, 129.19, 131.69, 135.88, 137.26, 137.98, 138.38, 139.60, 139.65, 144.16, 146.22; IR (KBr) *v* cm^{-1}: 3077 (w, υ(=CH)), 3027 (w, υ(=CH)), 2950 (s), 2922 (m, $\upsilon_{as}(CH_2, CH_3)$), 2853 (s, $\upsilon_s(CH_2, CH_3)$), 1591 (w, υ(C=C)), 1484 (s, $\delta_{as}(CH_2, CH_3)$), 1421 (w, $\delta_s(CH_2, CH_3)$), 1248

(s, $\delta_s(CH_3$, TMS)), 1196 (m), 1163 (m), 1094 (s), 1013 (m), 859 (s), 837 (s, $\delta_{as}(CH_3$, TMS)), 807 (s), 693 (w, $\upsilon_{as}(SiC_3)$); UV-Vis (λ_{max}[nm], ε, CH_2Cl_2) 307 (39655); 274 (38000); ESI(+) MS Calcd for $C_{57}H_{76}S_4Si_4Na$ ([M+Na]$^+$, 1023.3805), found *m/z* 1023.3719; elemental analysis calcd (%) for $C_{57}H_{76}S_4Si_4$ (1000.39): C 68.34, H 7.84; found: C 68.89, H 7.98.

_S,S'',S''_-{4-Acetylsulfanyl-1,1':4',1''-terphenyl-4''-yl)-[4,4',4''-(methanetriyl) tris(benzene-4,1-diyl)} tris(thioacetate) (**85**)

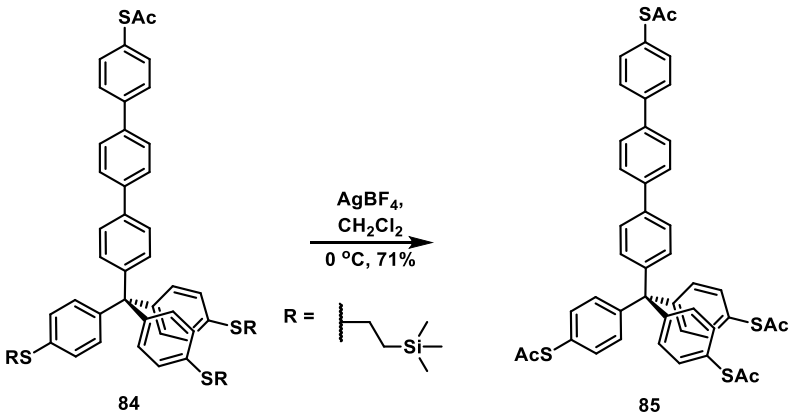

The transprotection was developed according to a method described for the preparation of **74**. Starting material **84** (0.15 g, 0.15 mmol), silver tetrafluoroborate (0.29 g, 1.5 mmol), acetyl chloride (2.5 mL) were charged to an oven-flamed 50 mL Schlenk flask and treated with anhydrous dichloromethane (25 mL). The reaction mixture was stirred under argon overnight at room temperature. The reaction mixture was quenched and purified by column chromatography on silica gel (150 g) in hexane/EtOAc (1:5) to obtain 0.082 g of **85** as a yellow solid in 71% yield. (R_f = 0.29, hexane/ EtOAc 1:5); m.p. 265-278 °C; ^{1}H NMR (500 MHz, CD_2Cl_2) δ ppm 2.41 (s, 9H, CH_3), 2.43 (s, 3H, CH_3), 7.35-7.39 (m, 14H, Ar-H), 7.50 (d, $J_{H,H}$ = 8.3 Hz, 2H, Ar-H), 7.62 (d, $J_{H,H}$ = 8.5 Hz, 2H, Ar-H), 7.70-7.71 (m, 6H, Ar-H); ^{13}C NMR (125.8 MHz, CD_2Cl_2) δ ppm 30.10, 30.47, 64.97, 126.74, 126.87, 127.59, 127.82, 127.93, 128.00, 131.64, 131.92, 134.18, 135.37, 138.76, 139.37, 140.11, 142.04, 145.28, 147.71, 194.06, 194.38; IR (KBr) *v* cm^{-1} 3028 (w, υ(=CH)), 2954 (m, $\upsilon_{as}(CH_3)$), 2923 (s, $\upsilon_s(CH_3)$), 2853 (w), 1704 (s, υ(C=O)), 1588 (w), 1483 (s), 1391 (w, δ_{as}(CH_3)), 1347 (m, δ_s(CH_3)), 1116 (s), 1092 (s), 1014 (m), 949 (s), 810 (s), 616 (s); UV-Vis (λ_{max}[nm], ε, CH_2Cl_2) 213 (24531); ESI(+) HRMS Calcd for $C_{45}H_{36}O_4S_4Na$ ([M+Na]$^+$, 791.1394), found *m/z* 791.1317; elemental analysis calcd (%) for $C_{45}H_{36}O_4S_4$ (768.15): C 70.28, H 4.72; found: C 70.88, H 4.91.

4-[2-(trimethylsilyl)ethylsulfanyl])-4’’’-(tris{4-[2-(trimethylsilyl)ethylsulfanyl]phenyl}methyl)-1,1’:4’1’’:4’’,1’’’-quaterphenyl (**86**)

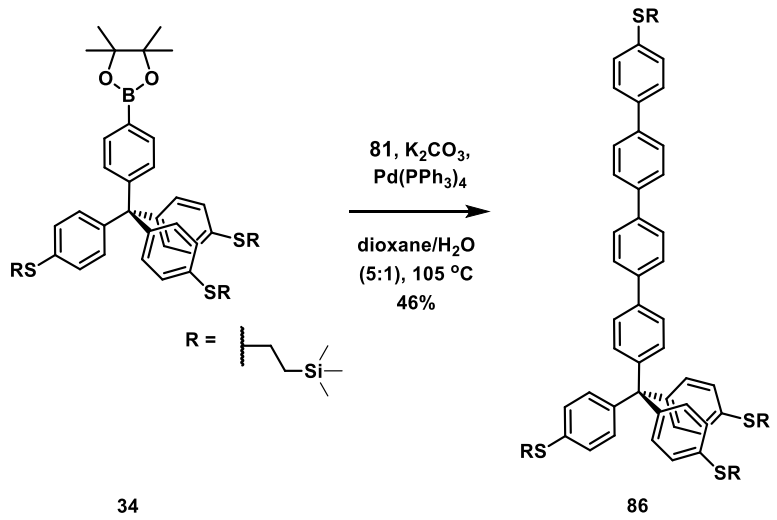

The product **86** was synthesized according the method reported for the preparation of **82**. Pinacol boronic ester **34** (0.25 g, 0.3 mmol), terphenyl precursor **81** (0.14 g, 0.31 mmol), potassium carbonate (0.82 g, 0.59 mmol) and tetrakis(triphenylphosphine)palladium(0) (0.034 g, 0.03 mmol) were loaded to a two-neck, argon-flushed round bottom flask and dissolved in a mixture of dioxane/water (80/15 mL). The reaction mixture was stirred under argon overnight and heated at 105 ^{o}C. The crude product was purified by column chromatography on silica gel (150 g) in hexane/CH_2Cl_2 (2:1) to provide 0.15 g of **86** as a white powder in 46% yield. (R_f = 0.22, hexane/CH_2Cl_2 2:1); m.p. 292-293 ^{o}C; ^{1}H NMR (500 MHz, CD_2Cl_2) δ ppm 0.04 (s, 27 H, CH_3), 0.07 (s, 9H, CH_3), 0.93-0.99 (m, 8H, CH_2), 2.95-3.05 (m, 6H, CH_2), 7.17-7.18 (m, 13H, Ar-H), 7.31 (d, $J_{H,H}$ = 8.4 Hz, 2H, Ar-H), 7.39 (d, $J_{H,H}$ = 8.3 Hz, 2H, Ar-H), 7.59-7.61 (m, 4H, Ar-H), 7.69-7.75 (m, 6H, Ar-H); ^{13}C NMR (125.8 MHz, CD_2Cl_2) δ ppm -1.75, 17.14, 17.20, 29.31, 39.63, 64.10, 126.42, 126.53, 127.27, 127.51, 127.56, 127.58, 127.64, 127.66, 127.69, 129.17, 129.23, 131.64, 131.90, 135.90, 138.41, 139.71, 139.76, 139.78, 144.19; IR (KBr) ν cm^{-1}: 3028 (w, υ(=CH)), 2950 (m), 2922 (m, υ_{as}(CH_2, CH_3)), 2852 (s, υ_s(CH_2, CH_3)), 1591 (w), 1483 (w, δ_{as}(CH_2, CH_3)), 1398(w, δ_s(CH_2, CH_3)), 1248 (m, δ_s(CH_3, TMS)), 1194 (w), 1164 (w), 1094 (m), 1012 (m), 858 (m), 839 (m, δ_{as}(CH_3, TMS)) 807 (s), 692 (w, υ_{as}(SiC_3)); UV-Vis (λ_{max}[nm], ε, CH_2Cl_2) 340 (87246); 275 (74121); ESI(+) HRMS Calcd for $C_{63}H_{80}Si_4S_4K$ ([M+K]$^+$, 1115.3857), found *m/z* 1115.3866; elemental analysis calcd (%) for $C_{63}H_{80}Si_4S_4$ (1076.42): C 70.70, H 7.48; found: C 70.96, H 7.69.

***S,S′,S′′*-{4-Acetylsulfanyl-1,1’:4’,1’’:4’’,1’’’-quaterterphenyl-4’’’-yl)-[4,4',4''-(methanetriyl) tris(benzene-4,1-diyl)} tris(thioacetate)** (**87**)

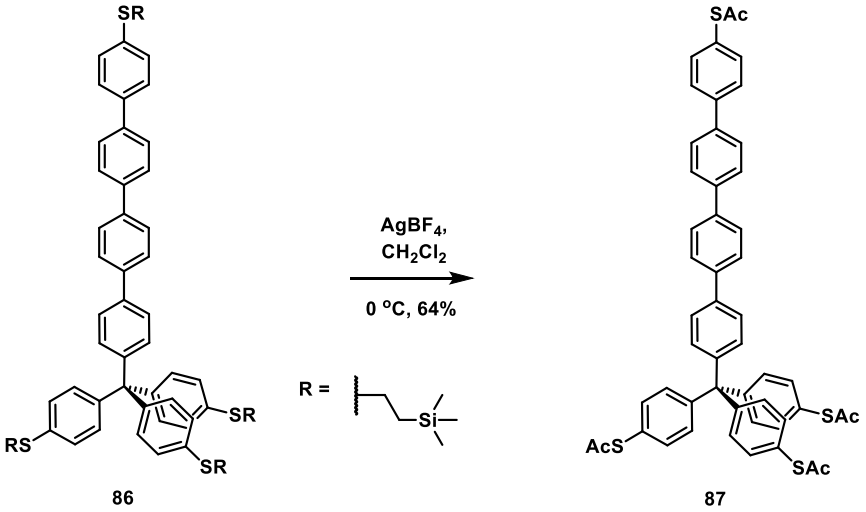

The transprotection was developed according to a method described for the preparation of **74**. Starting material **86** (0.11 g, 0.1 mmol), silver tetrafluoroborate (0.2 g, 1.02 mmol) and acetyl chloride (2.5 mL) in anhydrous dichloromethane (25 mL) were stirred under argon overnight at room temperature. The reaction mixture was quenched and purified by column chromatography on silica gel (100 g) in hexane/CH_2Cl_2 (1:4) to obtain 0.055 g of **87** as a white solid in 64% yield. (R_f = 0.38, hexane/CH_2Cl_2 1:4); m.p. 289-291 ^oC; ^1H NMR (500 MHz, CD_2Cl_2) δ ppm 2.40 (s, 9H, CH_3), 2.43 (s, 3H, CH_3), 7.34-7.39 (m, 14H, Ar-H), 7.51 (d, $J_{H,H}$ = 8.35 Hz, 2H, Ar-H), 7.62 (d, $J_{H,H}$ = 8.45 Hz, 2H, Ar-H), 7.71-7.77 (m, 10H, Ar-H); ^{13}C NMR (125.8 MHz, CD_2Cl_2) δ ppm 30.07, 30.47, 64.98, 126.75, 126.83, 127.61, 127.73, 127.76, 127.78, 128.01, 131.63, 131.92, 134.17, 135.18, 139.37, 139.75, 140.35, 142.06, 145.20, 145.72, 194.04, 194.36; IR (KBr) ν cm^{-1} 3028 (w, υ(=CH)), 2957 (m, $\upsilon_{as}(CH_3)$), 2925 (s, $\upsilon_s(CH_3)$), 2855 (w), 1711 (s, υ(C=O)), 1483 (s), 1463 (w, $\delta_{as}(CH_3)$), 1351 (w, $\delta_s(CH_3)$), 1270 (w), 1119 (s), 1093 (w) 1015 (w), 950 (m), 810 (s), 732 (w), 616 (s); UV-Vis (λ_{max}[nm], ε, CH_2Cl_2) 312 (38515); ESI(+) MS Calcd for $C_{51}H_{40}O_4S_4Na$ ($[M+Na]^+$, 867.1707), found *m/z* 867.1539; elemental analysis calcd (%) for $C_{51}H_{40}O_4S_4$ (845.12): C 72.48, H 4.77; found: C 72.88 4, H 4.94.

4-[2-(trimethylsilyl)ethylsulfanyl]-4'-(tris{3-[2-(trimethylsilyl)ethylsulfanyl]phenyl}methyl) biphenyl (**88**)

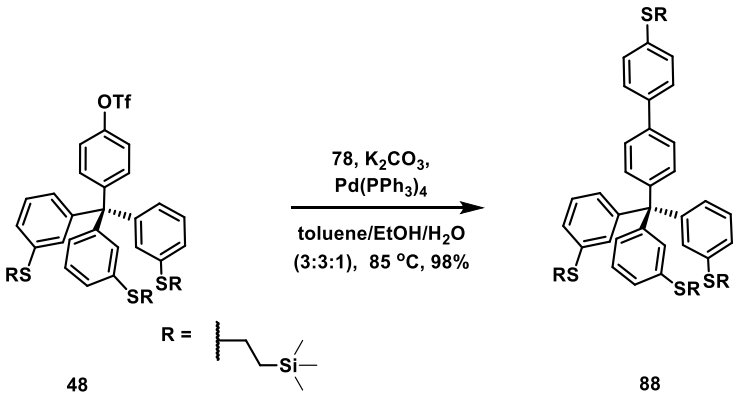

Triflate **48** (0.2 g, 0.23 mmol), boronic acid **78** (0.065g, 0.25 mmol), potassium carbonate (0.096 g, 0.069 mmol) and tetrakis(triphenylphosphine)palladium(0) (0.027 g, 0.023 mmol) were placed to 100 mL round bottom flask and dissolved in a mixture of toluene, ethanol, water (30/30/10 mL respect). The solution was degassed with argon, and then heated at 85 ^{o}C overnight under an inert atmosphere. After cooling, solvents were removed, the residue was diluted with water (100 mL) and dichloromethane (150 mL), the crude product was extracted with dichloromethane (2 x 100 mL). Combined organic fractions were dried over magnesium sulfate, filtrated concentrated in vacuo. The crude product was purified by column chromatography on silica gel (200 g, hexane/EtOAc (40:1) providing 0.21 g of **88** as a colorless oil in 98% yield. (R_f = 0.37, hexane/EtOAc 40:1), ^{1}H NMR (500 MHz, CD_2Cl_2) δ ppm 0.02 (s, 27H, CH_3), 0.05 (s, 9H, CH_3), 0.82-0.85 (m, 6H, CH_2), 0.95-0.97 (m, 2H, CH_2), 2.80-2.85 (m, 6H, CH_2), 2.99-3.03 (m, 2H, CH_2), 7.04-7.06 (m, 2H, Ar-H), 7.14-7.15 (m, 4H, Ar-H), 7.19-7.20 (m, 6H, Ar-H), 7.30 (d, $J_{H,H}$ = 8.5 Hz, 2H, Ar-H), 7.34 (d, $J_{H,H}$ = 8.4 Hz, 2H, Ar-H), 7.52 (d, $J_{H,H}$ = 8.6 Hz 2H, Ar-H), 7.54 (d, $J_{H,H}$ = 8.45 Hz, 2H, Ar-H); ^{13}C NMR (125.8 MHz, CD_2Cl_2) δ ppm -1.75, 17.10, 17.16, 29.56, 29.62, 65.13, 126.24, 126.57, 127.58, 128.41, 128.66, 129.20, 131.08, 131.76, 137.11, 137.42, 137.84, 138.42, 145.58, 147.41; IR (KBr) ν cm^{-1}: 3058 (w, υ(=CH)), 3028 (w, υ(=CH)), 2951 (s), 2922 (m, υ_{as}(CH_2, CH_3)), 2853 (s, υ_s(CH_2, CH_3)), 1581 (s, υ(C=C)), 1483 (s, δ_{as}(CH_2, CH_3)), 1412 (m, δ_s(CH_2, CH_3)), 1248 (m, δ_s(CH_3, TMS)), 1162 (m), 1096 (m), 1006 (m) 858 (s), 840 (s, δ_{as}(CH_3, TMS)), 700 (w, υ_{as}(SiC_3)); UV-Vis (λ_{max}[nm], ε, CH_2Cl_2) 295 (28717); 270 (32756); ESI(+) HRMS Calcd for $C_{51}H_{72}S_4Si_4Na$ ([M+Na]$^+$, 947.3492), found *m/z* 947.4314; elemental analysis calcd (%) for $C_{51}H_{72}S_4Si_4$ (924.36): C 66.17; H 7.84; found: C 66.64, H 7.98.

***S*,*S*′,*S*′′-{3,3',3''-[(4-Acetylsulfanylbiphenyl-4'-yl)-[3,3',3''-(methanetriyl)tris(benzene-3,1-diyl)]}tris(thioacetate) (89)**

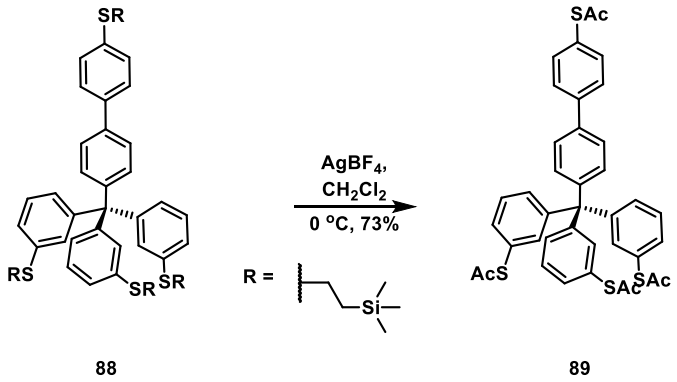

88 89

The transprotection was conducted according to a method described for the preparation of **74**. Starting material **88** (0.16 g, 0.18 mmol), silver tetrafluoroborate (0.34 g, 1.76 mmol) and acetyl chloride (3.2 mL) in anhydrous dichloromethane (32 mL) were stirred under argon overnight at room temperature. The reaction mixture was quenched and purified by column chromatography on silica gel (100 g) in hexane/EtOAc (1:5) to obtain 0.088 g of **89** as a white powder in 73% yield. (R_f = 0.3, hexane/EtOAc 1:5); m.p. 235-236 °C; ^{1}H NMR (500 MHz, CD_2Cl_2) δ ppm 2.35 (s, 9H, CH_3), 2.42 (s, 3H, CH_3), 7.29-7.30 (m, 3H, Ar-H), 7.35-7.38 (m, 11H, Ar-H), 7.47 (dd, $J_{H,H}$ = 4.45, 1.7 Hz, 2H, Ar-H), 7.58 (dd, $J_{H,H}$ = 6.6, 1.8 Hz, 2H, Ar-H), 7.66 (dd, $J_{H,H}$ = 8.4 Hz, 2H, Ar-H); ^{13}C NMR (125.8 MHz, CD_2Cl_2) δ ppm 30.42, 30.45, 64.99, 127.01, 127.60, 128.01, 128.42, 129.03, 131.74, 132.07, 132.66, 135.29, 139.46, 138.27, 141.78, 145.67, 147.41, 194.00, 194.33; IR (KBr) ν cm^{-1} 3057 (w, υ(=CH)), 3027 (w, υ(=CH)), 2954 (m, $\upsilon_{as}(CH_3)$), 2923 (s, $\upsilon_s(CH_3)$), 2854 (w), 1702 (s, υ(C=O)), 1583 (s), 1469 (s), 1408 (m, $\delta_{as}(CH_3)$), 1351 (m, $\delta_s(CH_3)$), 1120 (s), 1002 (w), 947 (s), 818 (s), 791 (w), 614 (s); UV-Vis (λ_{max}[nm], ε, CH_2Cl_2) 213 (24531); ESI(+) HRMS Calcd for $C_{39}H_{32}O_4S_4Na$ ([M+Na]$^+$, 715.1081), found *m/z* 715.0966; elemental analysis calcd (%) for $C_{39}H_{32}O_4S_4$ (692.12): C 67.60, H 4.65; found: C 67.92, H 4.84.

4-[2-(trimethylsilyl)ethylsulfanyl]-4''-(tris{3-[2-(trimethylsilyl)ethylsulfanyl]phenyl}methyl)-1,1':4',1'' terphenyl (90)

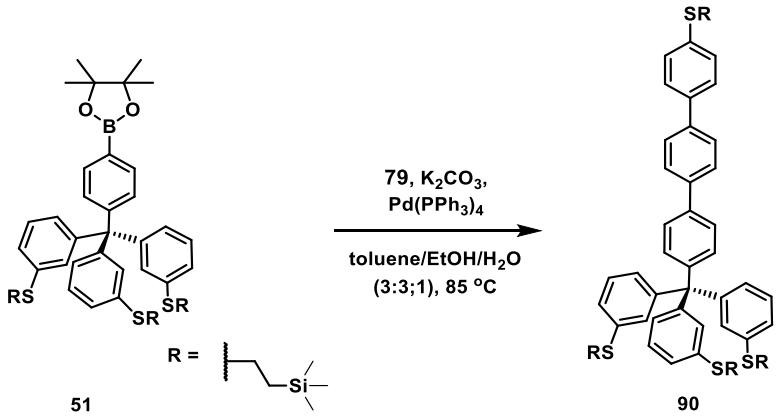

Pinacol boronic ester **51** (0.18 g, 0.21 mmol), biphenyl **79** (0.083 g, 0.23 mmol), potassium carbonate (0.086 g, 0.063 mmol), tetrakis(triphenylphosphine)palladium(0) (0.024 g, 0.021 mmol) were placed in 100 mL round bottom flask and dissolved in a mixture of toluene, ethanol, water (30/30/10 mL respectively). Resulting solution was deoxygenated for 30 min with argon, and subsequently heated at 85 °C overnight under an inert atmosphere. After cooling, solvents were removed under reduce pressure and the residue was diluted with water (100 mL) and dichloromethane (150 mL). Crude product was extracted with dichloromethane (2 x 100 mL). Combined organic fraction was dried over magnesium sulfate, filtrated and concentrated in vacuo. The crude product was purified by column chromatography on silica gel (200 g, hexane/EtOAc 1:20) providing 0.14 g of a colorless oil, however the obtained material was always contaminated with starting rod **79**, so the crude material was used for the next step without further purification (R_f = 0.31, hexane/ EtOAc 1:20).

***S,S′,S′′*-{3,3',3''-[(4-Acetylsulfanylbiphenyl-1,1':4',1''terphenyl-4''-yl)-[3,3',3''-(methanetriyl)tris(benzene-3,1-diyl)]}tris(thioacetate) (91)**

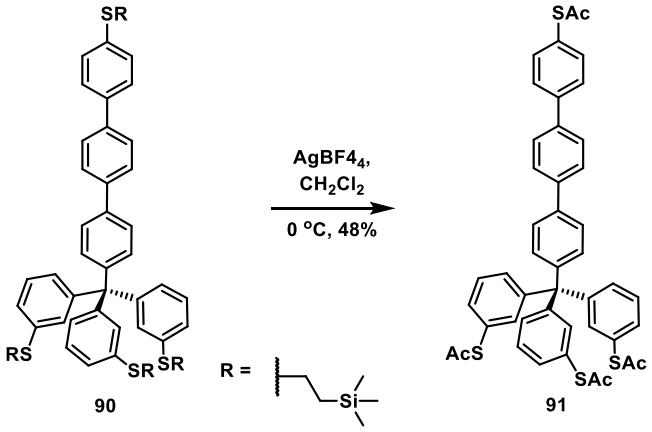

The transprotection was conducted according to a method described for the preparation of **74**. The crude material **90** (0.12 g, 0.12 mmol), silver tetrafluoroborate (0.24 g, 1.12 mmol), and acetyl chloride (3.5 mL) in anhydrous dichloromethane (35 mL) were stirred under argon overnight at room temperature. The reaction was quenched and purified by column chromatography on silica gel (100 g) in hexane/CH_2Cl_2 1:4) to obtain 0.07 g of **91** as a yellow solid in 48% yield after two steps. (R_f = 0.3, hexane/CH_2Cl_2 1:4); m.p. 136-139 °C; ^{1}H NMR (500 MHz, CD_2Cl_2) δ ppm 2.35 (s, 9H, CH_3), 2.43 (s, 3H, CH_3), 7.29-7.31 (m, 3H, Ar-H), 7.35-7.38 (m, 11H, Ar-H), 7.37 (d, $J_{H,H}$ = 8.25 Hz, 2H, Ar-H), 7.50 (d, $J_{H,H}$ = 8.45 Hz, 2H, Ar-H), 7.70-7.72 (m, 6H, Ar-H); ^{13}C NMR (125.8 MHz, CD_2Cl_2) δ ppm 30.43, 30.47, 65.01, 126.71, 127.58, 127.58, 127.78, 127.92, 128.00, 128.42, 129.04, 131.73, 132.09, 132.67, 135.37, 137.49, 138.62, 139.34, 140.10, 142.05, 145.31, 147.49, 194.04, 194.38; IR (KBr) ν cm^{-1} 3057 (w, υ(=CH)), 3027 (w, υ(=CH)), 2954 (w, $\upsilon_{as}(CH_3)$), 2924 (m, $\upsilon_s(CH_3)$), 2852 (w), 1703 (s, υ(C=O)), 1583 (m), 1480 (s), 1403 (m, $\delta_{as}(CH_3)$), 1351 (m, $\delta_s(CH_3)$), 1120 (s), 1002 (w), 948 (s), 814 (s), 791 (w), 614 (s); UV-Vis (λ_{max}[nm], ε, acetone) 212 (73591); ESI(+) HRMS Calcd for $C_{51}H_{36}O_4S_4Na$ ([M+Na]$^+$, 791.1394), found *m/z* 791.1340; elemental analysis calcd (%) for $C_{51}H_{36}O_4S_4$ (768.15): C 70.28, H 4.72; found: C 70.55, H 4.94.

4-[2-(trimethylsilyl)ethylsulfanyl]-4’’’-(tris{3-[2-(trimethylsilyl)ethylsulfanyl]phenyl}methyl)-1,1’:4’,1’’:4’’,1’’’-quaterphenyl (**92**)

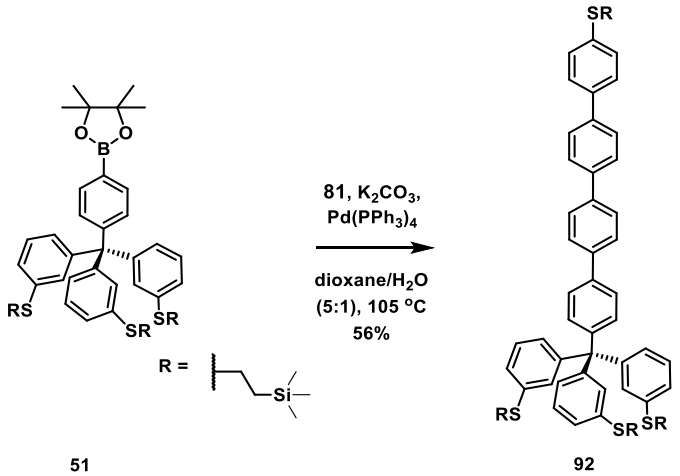

Pinacol boronic ester **51** (0.21 g, 0.25 mmol), terphenyl rod **81** (0.11g, 0.26 mmol), potassium carbonate (0.086 g, 0.063 mmol)and tetrakis(triphenylphosphine)palladium(0) (0.14 g, 0.12 mmol) were placed to a 100 mL two-neck round bottom flask and treated with the mixture of dioxane (50 mL), water (10 mL) and degassed for 30 min with argon. Subsequently the reaction mixture was refluxed overnight under an inert atmosphere. After cooling, solvents were evaporated. The crude product was diluted with water (100 mL) and dichloromethane (150 mL) and extracted with dichloromethane (2 x 100 mL). Combined organic fraction was dried over magnesium sulfate, filtrated and concentrated in vacuum. Crude product was purified by column chromatography on silica gel (200 g, hexane/CH_2Cl_2 (2:1) providing 0.15 g of **92** as orange oil in 56% yield. (R_f = 0.31, hexane/ CH_2Cl_2 2:1), ^{1}H NMR (500 MHz, CD_2Cl_2) δ ppm 0.02 (s, 27H, CH_3), 0.062 (s, 9H, CH_3), 0.82-0.85 (m, 6H, CH_2), 0.85-0.99 (m, 2H, CH_2), 2.79-2.82 (m, 6H, CH_2), 2.83-3.03 (m, 2H, CH_2), 7.01-7.03 (m, 3H, Ar-H), 7.17-7.19 (m, 3H, Ar-H), 7.28 (d, $J_{H,H}$ = 8.5 Hz, 2H, Ar-H), 7.38 (d, $J_{H,H}$ = 8.45 Hz, 2H, Ar-H), 7.54 (d, $J_{H,H}$ = 8.55 Hz, 2H, Ar-H), 7.58 (d, $J_{H,H}$ = 8.66 Hz, 2H, Ar-H), 7.70-7.73 (m. 4H, Ar-H); ^{13}C NMR (125.8 MHz, CD_2Cl_2) δ ppm -1.59, -1.63, 16.84, 17.03, 29.68, 29.84, 64.87, 126.19, 126.56, 127.56, 127.36, 127.41, 127.47, 127.49, 128.10, 128.75, 129.29, 131.15, 131.63, 136.69, 136.82, 138.12, 138.31, 139.54, 139.63, 145.30, 147.06; IR (KBr) υ cm^{-1}: 3028 (w, υ(=CH)), 2923 (m, υ_{as}(CH_2, CH_3)), 2853 (s, υ_s(CH_2, CH_3)), 1634 (w, υ(C=C)), 1582 (w), 1486 (w, δ_{as}(CH_2, CH_3)), 1403 (w, δ_s(CH_2, CH_3)), 1248 (m, δ_s(CH_3, TMS)), 1097 (m), 1005(m), 858 (m), 840 (m, δ_{as}(CH_3, TMS)) 810 (s), 694 (w, υ_{as}(SiC_3)); UV-Vis (λ_{max}[nm], ε, CH_2Cl_2) 318 (51578), 270 (27102); ESI(+) MS Calcd for $C_{63}H_{80}Si_4S_4K$

([M+K]$^+$, 1115.3857), found *m/z* 1115.3824), found *m/z* 1023.2446; elemental analysis calcd (%) for $C_{63}H_{80}S_4Si_4$ (1076.42): C 70.70, H 7.48; found: C 70.99, H 7.83.

_S,S',S''_-{3,3',3''-[(4-Acetylsulfanylbiphenyl-1,1':4',1'':4'',1'''-quaterphenyl-4'''-yl)-[3,3',3''-(methanetriyl)tris(benzene-3,1-diyl)]}tris(thioacetate) (93)

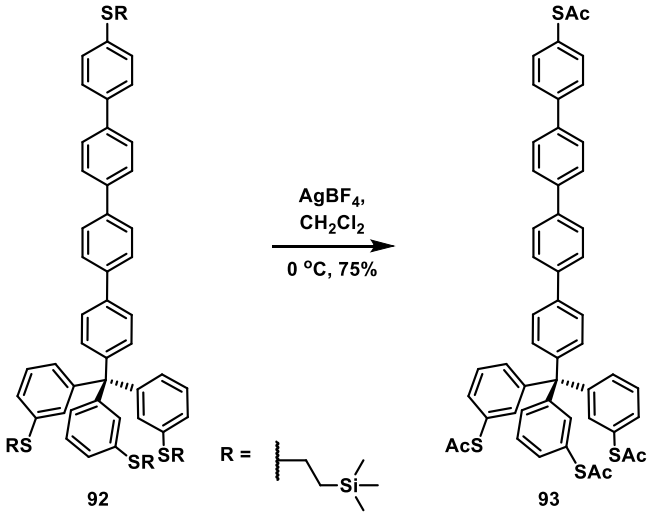

The transprotection was conducted according to a method described for the preparation of **74**. Starting material **92** (0.095 g, 0.088 mmol), $AgBF_4$ (0.17 g, 0.88 mmol) and acetyl chloride (2.5 mL) were suspended in anhydrous dichloromethane (25 mL). The reaction mixture was stirred under argon overnight at room temperature. The reaction mixture was quenched and purified by column chromatography on silica gel (100 g) in hexane/CH_2Cl_2 (1:4) to obtain 0.056 g of **93** as a white solid in 75% yield. (R_f = 0.32, hexane/CH_2Cl_2 1:4), m.p. 259-261 ^{o}C; ^{1}H NMR (500 MHz, CD_2Cl_2) δ ppm 2.36 (s, 9H, CH_3), 2.44 (s, 3H, CH_3), 7.30-7.31 (m, 3H, Ar-H), 7.36-7.39 (m, 11H, Ar-H), 7.51 (d, $J_{H,H}$ = 8.3 Hz, 2H, Ar-H), 7.63 (d, $J_{H,H}$ = 8.5 Hz, 2H, Ar-H), 7.72-7.76 (m, 10H, Ar-H); ^{13}C NMR (125.8 MHz, CD_2Cl_2) δ ppm 30.11, 30.44, 65.02, 125.64, 126.79, 127.73, 127.76, 127.77, 127.97, 128.03, 128.44, 128.57, 129.05, 129.38, 131.74, 132.11, 132.68, 135.40, 137.51, 138.73, 139.76, 140.37, 142.08, 145.24, 147.52, 194.03, 194.37; IR (KBr) ν cm^{-1} 3028 (w. υ(=CH)), 2956 (m, $\upsilon_{as}(CH_3)$), 2924 (s, $\upsilon_s(CH_3)$), 2853 (w), 1703 (s, υ(C=O)), 1584 (w), 1479 (s), 1403 (w, $\delta_{as}(CH_3)$), 1350 (w, $\delta_s(CH_3)$), 1264 (w), 1120 (s), 1001 (m) 947 (m), 811 (s), 792 (m), 694 (m); UV-Vis (λ_{max}[nm], ε, CH_2Cl_2) 312 (38515); ESI(+) MS Calcd for $C_{51}H_{40}O_4S_4Na$ ([M+Na]$^+$, 867.1707), found *m/z* 867.1581; elemental analysis calcd (%) for $C_{51}H_{40}O_4S_4$ (845.12): C 72.48, H 4.77; found: C 72.86, H 5.01.

4,4'-Methylenebis[*N*-(diphenylmethylene)-benzeneamine (94) [328]

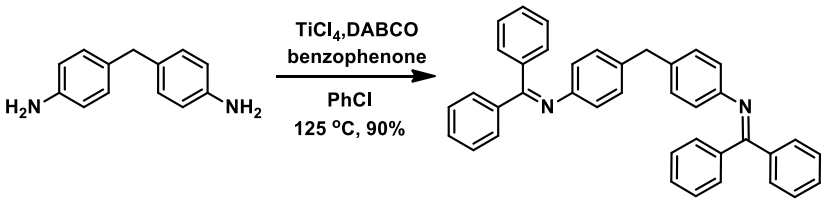

94

Compound **94** was synthesized according to a reported protocol.[328] An oven-flamed, 500 mL three neck round bottom flask, equipped with refluxed condenser and dropping funnel was charged with 4,4'-diaminodiphenylmethane (1 g, 5.04 mmol), benzophenone (1.94 g, 10.6 mmol), and DABCO (1.44 g, 7.56 mmol). Reagents were dissolved in 15 mL of chlorobenzene under argon and $TiCl_4$ (0.84 mL, 1.73 mmol) was dropwise added. Afterwards, the reaction mixture was vigorously stirred under an inert atmosphere overnight at 125 °C. Upon cooling to room temperature, precipitated solid was filtered and washed with chlorobenzene (100 mL). The combined organic layer was dried over $MgSO_4$, and filtered. All volatiles were removed under reduced pressure and the residual yellowish residue was purified by column chromatography on silica gel (500 g) in hexane/EtOAc (10:1) to afford pure **94** (2.40 g) as a yellowish solid in 90% yield (R_f = 0.77, hexane/EtOAc = 10:1); ^{1}H NMR (500 MHz, CD_2Cl_2) δ ppm, 3.78 (s, 2H, CH_2), 6.66 (d, $J_{H,H}$ = 8 Hz, 4H, Ar-H), 6.89 (d, $J_{H,H}$ = 8.5 Hz, 4H, Ar-H), 7.14 (d, $J_{H,H}$ = 7.55 Hz, 4H, Ar-H), 7.27-7.31 (m, 6H, Ar-H), 7.42 (t, $J_{H,H}$ = 8.55 Hz, 4H, Ar-H), 7.49 (t, $J_{H,H}$ = 8.55 Hz, 2H, Ar-H), 7.57 (d, $J_{H,H}$ = 7.75 Hz, 4H, Ar-H); ^{13}C NMR (125.8 MHz, CD_2Cl_2) δ ppm 19.2, 40.0, 122.9, 125.5, 128.4, 129, 130.2, 140.4, 141.9, 142.0.

Bis{4-[(diphenylmethylene)amino]phenyl} methanone (95)[328]

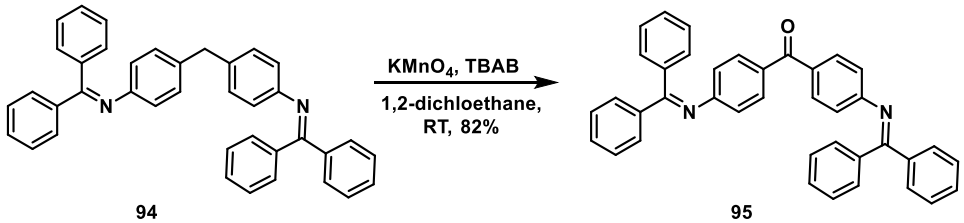

94 95

A single neck, 100 mL round bottom flask was loaded with starting material **94** (0.35 g, 0.66 mmol), potassium permanganate (0. 32 g, 2 mmol), TBAB (0.32 g, 0.99 mmol) and dissolved in 15 mL of 1,2-dichloroethane. The reaction mixture was stirred for 24 h at room temperature. Subsequently, the reaction mixture was quenched with saturated solution of

$NaHSO_3$ (120 mL) and washed with dichloromethane (3 x 150 mL). The organic layers were combined, dried over $MgSO_4$, and filtered. All volatiles were removed under reduced pressure and the residue was purified by column chromatography on silica gel (300 g) in hexane/EtOAc (10:1) to afford pure **95** (0.29 g) as a yellow solid in 82% yield (R_f = 0.43, hexane/EtOAc = 10:1). ^{1}H NMR (500 MHz, $CDCl_3$) δ ppm, 6.79 (d, $J_{H,H}$ = 8.45 Hz, 4H, Ar-H), 7.14 (d, $J_{H,H}$ = 6.9 Hz, 4H, Ar-H), 7.27-7.31 (m, 6H, Ar-H), 7.44 (t, $J_{H,H}$ = 7.55 Hz, 4H, Ar-H) 7.49 (t, $J_{H,H}$ = 7.15 Hz, 2H, Ar-H), 7.60 (d, $J_{H,H}$ = 8.45 Hz, 4H, Ar-H), 7.78 (d, $J_{H,H}$ = 7.5 Hz, 4H, Ar-H); ^{13}C NMR (125.8 MHz, CD_2Cl_2) δ ppm, 120.5, 128.2, 129.5, 131.2 135.8, 139.2, 155.3, 169.0, 195.5.

4-Bromophenyl-bis{4-[(diphenylmethylene)amino]phenyl} methanol (96)

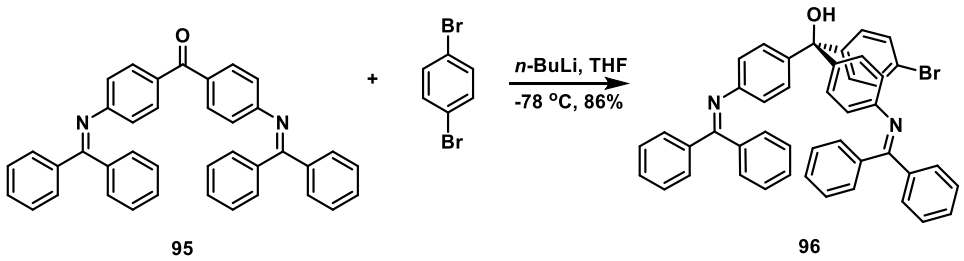

A dry and argon-flushed 50 mL Schlenk flask was charged with 1,4-dibromobenzene (0.29 g, 0.54 mmol) and anhydrous THF (8 mL) was added. The solution was cooled to -78 °C and *n*-BuLi (0.37 mL, 0.59 mmol, 1.6 M in hexane) was added dropwise over 20 min. The reaction mixture was stirred at -78 °C for 2 h under argon. In a second 50 mL Schlenk flask, benzophenone **95** (0.28 g, 0.52 mmol) was dissolved in anhydrous THF (7 mL) under inert atmosphere and cooled to -78 °C. The solution of lithiated species was slowly added via a cannula into the flask containing diethyl carbonate solution, after 1 h, the reaction mixture was allowed to warm to room temperature and stirred for an additional 16 h. The reaction mixture was quenched with saturated NH_4Cl solution (100 mL). The aqueous layer was washed with CH_2Cl_2 (2 x 100 mL). The combined organic layer was washed with brine (100 mL), dried over $MgSO_4$, and filtered. All volatiles were removed under reduced pressure and the residue was purified by column chromatography on silica gel (200 g) in hexane/EtOAc (10:1) to afford pure **96** (0.29 g) as a dark-blue solid in 86% yield (R_f = 0.33, hexane/EtOAc = 10:1); m.p. 127-129 ºC; ^{1}H NMR (500 MHz, $CDCl_3$) δ ppm 2.80 (s, 1H, OH), 6.66 (d, $J_{H,H}$ = 8.45 Hz, 4H, Ar-H), 6.91 (d, $J_{H,H}$ = 8.5 Hz, 4H, Ar-H), 6.99 (d, $J_{H,H}$ = 8.6 Hz, 2H, Ar-H), 7.13 (dd, $J_{H,H}$ = 6.9 Hz, 1.9 Hz, 4H, Ar-H), 7.27-7.29 (m, 4H, Ar-H), 7.39 (d, $J_{H,H}$ = 8.55 Hz, 2H, Ar-H), 7.43-7.44 (m, 4H, Ar-H), 7.51 (t, $J_{H,H}$ = 7.6 Hz, 2H, Ar-H), 7.78 (d, $J_{H,H}$ = 7.75

Hz, 4H, Ar-H); ^{13}C NMR (125.8 MHz, $CDCl_3$) δ ppm 81.4, 120.6, 127.9, 128.1, 128.3, 128.8, 129.5, 129.7, 130.8, 136.2, 139.6, 141.3, 146.3, 150.7, 168.9; IR (KBr) ν cm^{-1} 3367 (s υ(OH)), 3027 (w, υ(=CH)), 2952 (w, υ_{as}(, CH_3)), 2934 (w, $\upsilon_s(CH_3)$), 2853 (s, $\upsilon(CH_3\text{-}O)$), 1655 (s, (s, υ(C=N)), 1598 (s), 1577 (s), 1510 (s), 1393 (m, $\delta_s(CH_3)$), 1362 ($\delta_{as}(CH_3)$), 1301 (m), 1277 (s, υ(C-N)), 1178 (s, $\upsilon(3^o\text{-}OH)$), 1072 (w), 1007 (m), 917 (m), 822 (s), 763 (m), 700 (s), 637 (s, υ(C-Br)); UV-Vis (λ_{max}[nm], ε, CH_2Cl_2) 269 (43186); ESI(+) MS Calcd for $C_{45}H_{33}BrN_2ONa$ ($[M+Na]^+$, 721.1716), found *m/z* 721.1657; elemental analysis calcd (%) for $C_{45}H_{33}BrN_2O$ (696.18): C, 77.47; H, 4.77; N, 4.02; found: C, 77.56; H, 4.79; N, 4.23.

4-Bromophenyl-bis(4'-methoxyphenyl) methanol (**97**)

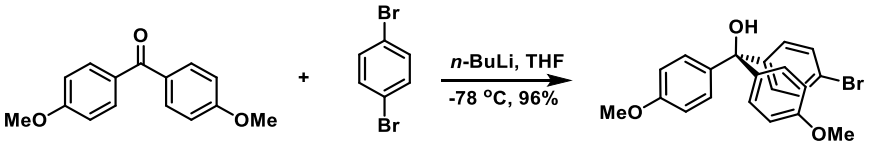

97

A dry and argon-flushed 100 mL Schlenk flask was charged with 1,4-dibromobenzene (4.38 g, 18 mmol) and anhydrous THF (35 mL) was added. The solution was cooled to -78 °C and *n*-BuLi (12 mL, 19.1 mmol, 1.6 M in hexane) was added dropwise over 30 min. The reaction mixture was stirred at -78 °C for 2 h under argon. In a second 100 mL Schlenk flask, 4,4'-dimethoxybenzophenone (1.5 g, 6.18 mmol) was dissolved in anhydrous THF (30 mL) under inert atmosphere and cooled to -78 °C. The solution of lithiated species was slowly added via a cannula into the flask containing solution of benzophenone, after 1 h, the reaction mixture was allowed to warm to room temperature and stirred for an additional 16 h. The reaction mixture was quenched with saturated NH_4Cl solution (200 mL). The aqueous layer was washed with CH_2Cl_2 (3 × 200 mL). The combined organic layer was washed with brine (100 mL), dried over $MgSO_4$, and filtered. All volatiles were removed under reduced pressure and the residue was purified by column chromatography on silica gel (300 g) in hexane/EtOAc (6:1) to afford pure **97** (2.38 g) as a reddish oil in 96% yield (R_f = 0.33, hexane/EtOAc = 6:1); ^{1}H NMR (500 MHz, $CDCl_3$) δ ppm, 2.86 (s, 1H, OH), 3.79 (m, 6H, CH_3), 6.83 (d, $J_{H,H}$ = 8.85 Hz, 2H, Ar-H), 7.15 (dd, $J_{H,H}$ = 6.8, 2.05 Hz, 2H, Ar-H), 7.42 (d, $J_{H,H}$ = 8.6 Hz, 2H, Ar-H); ^{13}C NMR (125.8 MHz, $CDCl_3$) δ ppm 55.4, 81.2, 113.4, 117.3, 121.3, 129.2, 129.7, 131, 146.5, 158.9; IR (KBr) ν cm^{-1} 3477 (s, υ(OH)), 3000 (w, υ(=CH)), 2954 (m, $\upsilon_{as}(CH_3)$), 2932 (m, $\upsilon_s(CH_3)$), 2835 (s, $\upsilon(CH_3\text{-}O)$), 1606 (s, (w, υ(C=C)), 1509 (s), 1393 (m, $\delta_s(CH_3)$), 1301 ($\delta_{as}(CH_3)$), 1250 (s, $\upsilon(C_{Ar}\text{-}O\text{-}C)$), 1154 (s, $\upsilon(3^o\text{-}OH)$), 1071 (s), 1033

(s), 1008 (s), 826 (s), 583 (s, υ(C-Br)); UV-vis (λ_{max}[nm], ε, CH_2Cl_2) 269 (43186); ESI(+) HRMS Calcd for $C_{21}H_{19}BrO_3Na$ ($[M+Na]^+$ 421.0415), found *m/z* 421.0405; elemental analysis calcd (%) for $C_{21}H_{19}BrO_3$ (398.05): C, 63.17; H, 4.80; found: C, 62.70; H, 4.93.

4-{[4-Bromophenyl-bis(4-methoxyphenyl)]methyl} phenol (**98)**

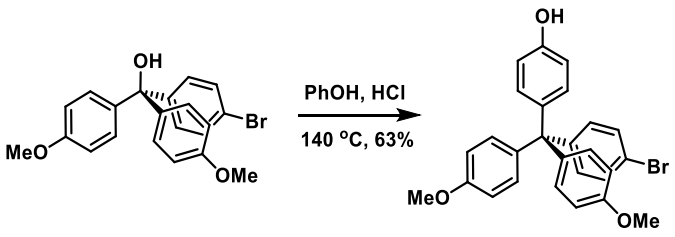

97 98

A 100 mL two-neck round bottom flask was charged with **97** (0.5 g, 1.26 mmol), phenol (1.77 g, 18.84 mmol), and a few drops of concentrated HCl were added. The reaction mixture was heated at 140 °C for 14 h under argon. After cooling to room temperature, the dark-red reaction mixture was diluted with toluene (200 mL) and quenched with NaOH solution (2 M, 160 mL). The combined organic layer was washed with water (150 mL), dried over $MgSO_4$ and filtered. All volatiles were removed under reduced pressure and the residue was purified by column chromatography on silica gel (450 g) in hexane/EtOAc (3:1) to afford **98** (0.38 g) as a pale-yellow powder in 63% yield (R_f = 0.46, hexane/EtOAc = 3:1); m.p. 122-123 °C; ^{1}H NMR (500 MHz, $CDCl_3$) δ ppm 3.80 (s, 6H, CH_3), 5.51 (s, 2H, OH), 6.72 (d, $J_{H,H}$ = 9.1 Hz, 2H, Ar-H), 6.80 (d, $J_{H,H}$ = 8.75 Hz, 4H, Ar-H), 7.02 (d, $J_{H,H}$ = 8.6 Hz, 2H, Ar-H), 7.06-7.08 (m, 6H, Ar-H), 7.36 (d, $J_{H,H}$ = 8.55 Hz, 2H, Ar-H); ^{13}C NMR (125.8 MHz, $CDCl_3$) δ ppm 55.5, 62.8, 113.1, 114.6, 120.1, 127.7, 130.7, 132.2, 132.4, 133.0, 139.2, 147, 153.9, 157.7; IR (KBr) ν cm^{-1} 3392 (s, υ(OH)), 3032 (w, υ(=CH)), 2952 (m, υ_{as}(CH_3)), 2932 (m, υ_s(CH_3)), 2834 (s, υ(CH_3-O)), 1607 (s, (w), 1507 (s), 1441 (m, δ_s(CH_3)), 1373 (w, δ_{as}(CH_3)), 1249 (s, υ(C_{Ar}-O-C)), 1179 (s, υ(C_{Ar}-OH)), 1075 (m), 1034 (s), 1009 (s), 823 (s), 581 (s, υ(C-Br)); UV-vis (λ_{max}[nm], ε, CH_2Cl_2) 271 (74485); ESI(+) MS Calcd for $C_{27}H_{23}BrO_3Na$ ($[M+Na]^+$, 497.0620), found *m/z* 497.0728; elemental analysis calcd (%) for $C_{27}H_{23}BrO_3$ (474.08): C, 68.22; H, 4.88; found: C, 68.64; H, 4.87.

4-{[4-Bromophenyl-bis(4-methoxyphenyl)]methyl} phenyl trifluoromethanesulfonate (99)

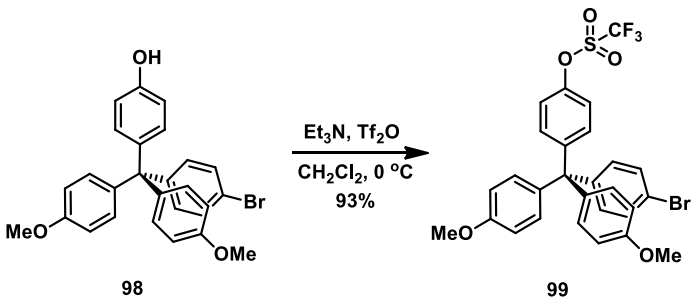

Trifluoromethanesulfonic anhydride (0.33 mL, 1.94 mmol) was added dropwise to the solution of **98** (0.65 g, 1.29 mmol) in dry triethylamine (0.34 mL, 2.46 mmol) and CH_2Cl_2 (20 mL) at 0 °C under argon atmosphere. The solution was stirred for 2 h at 0 °C, and then allowed to warm to room temperature and stirred for an additional 10 h, before quenching with water (100 mL). The aqueous layer was washed with CH_2Cl_2 (3 × 250 mL). The combined organic layers were washed with brine (100 mL), dried over $MgSO_4$ and filtered. The volatiles were removed under reduced pressure and the residue was purified by column chromatography on silica gel (130 g) with hexane/EtOAc (3:1) as an eluent to yield 0.77 g (93%) of **99** as a yellow oil (R_f = 0.68, hexane/EtOAc = 3:1); ^{1}H NMR (500 MHz, $CDCl_3$) δ ppm 4.01 (s, 6H, CH_3), 7.02 (d, $J_{H,H}$ = 8.9 Hz, 4H, Ar-H) 7.23-7.26 (m, 6H, Ar-H), 7.37 (d, $J_{H,H}$ = 8.95 Hz, 2H, Ar-H), 7.76 (d, $J_{H,H}$ = 8.85 Hz, 2H, Ar-H), 7.60 (d, $J_{H,H}$ = 8.65 Hz, 2H, Ar-H); ^{13}C NMR (125.8 MHz, $CDCl_3$) δ ppm 55.3, 63.1, 113.2, 117.6, 120.4, 120.5, 130.9, 131.9, 132.7, 132.8, 138.0, 145.8, 147.5, 147.7, 158.0; ^{19}F NMR (470.57 MHz, $CDCl_3$) -72.9; IR (KBr) ν cm^{-1} 3035 (w, υ(=CH)), 2957 (m, $\upsilon_{as}(CH_3)$), 2927 (m, $\upsilon_s(CH_3)$), 2856 (s, $\upsilon(CH_3$-O)), 1704 (s), 1607 (s), 1509 (s), 1462 (m, $\delta_s(CH_3)$), 1424 (s, υ_{as}(S=O)), 1252 (s, $\upsilon(C_{Ar}$-O-C)), 1208 (s, υ_s(S=O)) 1041 (m), 1036 (s, (υ(C-F)), 1012 (m), 889 (s), 824 (s), 607 (s, υ(C-Br)); UV-Vis (λ_{max}[nm], ε, CH_2Cl_2) 273 (33589); ESI(+) MS Calcd for $C_{28}H_{22}BrF_3O_5SNa$ ([M+Na]$^+$, 631.0202), found *m/z* 631.0176; elemental analysis calcd (%) for $C_{28}H_{22}BrF_3O_5S$ (606.03): C, 55.36; H, 3.65; found: C, 55.90; H, 5.03.

4,4'-[Bis(4-methoxyphenyl)methyl] dibenzonitrile (100)

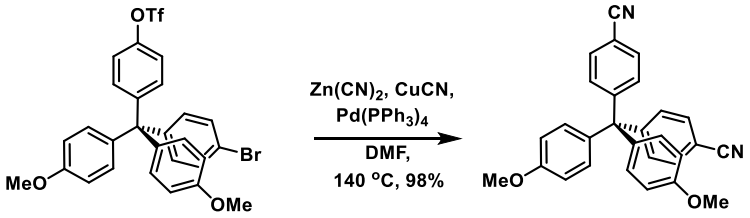

99 100

An oven-flamed, 50 mL pressure tube was charged with triflate **99** (0.75 g, 1.24 mmol), zinc cyanide (0.23 g, 1.92 mmol), copper (I) cyanide (0.17 g, 1.92 mmol), $Pd(PPh_3)_4$ (0.029 g, 0.025 mmol) and anhydrous DMF (10 mL) under argon. The tube was sealed and stirred at 140 °C for 16 h. After cooling to room temperature, the resulting solution was quenched with Na_2CO_3 (100 mL). The aqueous layer was washed with CH_2Cl_2 (3 × 100 mL). The combined organic layer was washed with brine (100 mL), dried over $MgSO_4$ and filtered. All volatiles were removed under reduced pressure and the residue was purified by column chromatography on silica gel (70 g) in the mixture of hexane/EtOAc (5:1) to get 0.52 g of **100** as a white powder in 98% yield (R_f = 0.17, hexane/EtOAc = 5:1); m.p. 149-150 °C; ^{1}H NMR (500 MHz, $CDCl_3$) δ ppm 3.79 (s, 6H, CH_3), 6.81 (d, $J_{H,H}$ = 8.85 Hz, 4H, Ar-H), 7.01 (d, $J_{H,H}$ = 8.85 Hz, 4H, Ar-H), 7.31 (d, $J_{H,H}$ = 8.5 Hz, 4H, Ar-H), 7.56 (d, $J_{H,H}$ = 8.45 Hz, 4H, Ar-H); ^{13}C NMR (125.8 MHz, $CDCl_3$) δ ppm 55.4, 64.2, 110.4, 113.6, 118.7, 131.5, 131.7, 131.8, 136.9, 151.8, 158.2; IR (KBr) ν cm^{-1} 3037 (w, υ(=CH)), 2954 (w, $\upsilon_{as}(CH_3)$), 2925 (m, $\upsilon_s(CH_3)$), 2853 (s, $\upsilon(CH_3\text{-}O)$), 2231 (s, υ(C≡N)), 1605 (s, υ(C=C)), 1508 (s), 1460 (m, $\delta_s(CH_3)$), 1405 (w, $\delta_{as}(CH_3)$), 1297 (m, υ(C-N)), 1252 (s, $\upsilon(C_{Ar}\text{-}O\text{-}C)$), 1182 (s), 1118 (m), 1032 (s), 825 (s); UV-Vis (λ_{max}[nm], ε, CH_2Cl_2) 224 (13100), 270 (23341); ESI(+) MS Calcd for $C_{29}H_{22}N_2O_2Na$ ($[M+Na]^+$, 453.1477), found *m/z* 453.1579; elemental analysis calcd (%) for $C_{29}H_{22}N_2O_2$ (430.17): C, 80.91; H, 5.15; N, 6.51; found: C, 80.12; H, 5.51; N, 6.42.

4,4'-[Bis(4-methoxyphenyl)methyl] dibenzaldehyde (**101)**

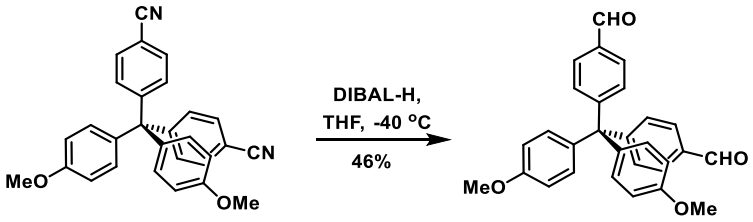

100 101

A dry and argon-flushed 100 mL Schlenk flask was charged with **100** (0.52 g, 1.21 mmol) and anhydrous THF (40 mL) was added. The solution was cooled to 0 °C and DIBAL-H (2.9 mL, 2.9 mmol, 1 M solution in toluene) was added dropwise over 30 min. The reaction mixture was stirred overnight at -40° C under argon. The reaction mixture was quenched with 2 M HCl solution (100 mL). The aqueous layer was washed with CH_2Cl_2 (3 x 100 mL). The combined organic layer was washed with brine (100 mL), dried over $MgSO_4$, and filtered. All volatiles were removed under reduced pressure and the residue was purified by column chromatography on silica gel (300 g) in hexane/EtOAc (3:1) to afford pure **101** (0.24 g) as a yellowish solid in 46% yield (R_f = 0.38, hexane/EtOAc = 3:1); m.p. 121-131 °C; ^{1}H NMR (500 MHz, $CDCl_3$) δ ppm 3.79 (s, 6H, CH_3), 6.81 (d, $J_{H,H}$ = 8.95 Hz, 4H, Ar-H) 7.08 (d, $J_{H,H}$ = 8.95 Hz, 4H, Ar-H), 7.40 (d, $J_{H,H}$ = 8.31 Hz, 4H, Ar-H), 7.78 (d, $J_{H,H}$ = 8.4 Hz, 4H, Ar-H), 9.99 (s, 2H, H-CO); ^{13}C NMR (125.8 MHz, $CDCl_3$) δ ppm 55.4, 64.5, 113.4, 129.2, 131.5, 132, 134.4, 137.6, 153.7, 157.1, 191.9; IR (KBr) ν cm^{-1} 3033 (w, υ(=CH)), 2952 (w, $\upsilon_{as}(CH_3)$), 2925 (m, $\upsilon_s(CH_3)$), 2853 (s, $\upsilon(CH_3\text{-}O)$), 2734 (w, υ(H-C=O)), 1699 (s, υ(C=O)), 1603 (s, υ(C=C)), 1508 (s), 1461 (m, $\delta_s(CH_3)$), 1382 (w, $\delta_{as}(CH_3)$), 1299 (w), 1251 (s, $\upsilon(C_{Ar}\text{-}O\text{-}C)$), 1214 (s, $\upsilon(C_{Ar}\text{-}C\text{-}O)$), 1182 (m), 1032 (s), 817 (s); UV-vis (λ_{max}[nm], ε, CH_2Cl_2) 269 (43186); ESI(+) MS Calcd for $C_{29}H_{42}O_4Na$ ($[M+Na]^+$, 459.1572), found *m/z* 459.1711; elemental analysis calcd (%) for $C_{29}H_{42}O_4$ (436.17): C, 79.80; H, 5.54; found: C, 79.83; H, 5.85.

4,4'-Diiododiphenylmethane (102)[332]

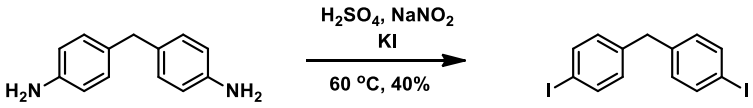

102

Compound **102** prepared according to a reported method.[332] A 500 mL three neck round bottom flask, equipped with refluxed condenser and a dropping funnel was charged with 4,4'-diaminodiphenylmethane (8 g, 40 mmol), concentrated sulfuric acid (32 mL) and cooled down to 0 °C. Separately, sodium nitrate (7.94 g, 115.2 mmol) was dissolved in 16 mL of water, cooled down to 0 °C. Afterwards, solution of nitrite was transferred to a dropping funnel and dropwise added over 30 min. to the same solution. Consecutively, aqueous solution of potassium iodide (42 g, 250 mmol) in 150 mL of H_2O was dropped to ice-cold solution diazonium salt. The reaction mixture was heated up to 60 °C over 2 h. Upon cooling, the reaction mixture was quenched with 500 mL of Na_2SO_3 and aqueous layer was washed with dichloromethane (3 x 500 mL). The combined organic layers were dried over $MgSO_4$, and filtered. All volatiles were removed under reduced pressure and the residual yellowish slurry was purified by column chromatography on silica gel (900 g) in hexane/EtOAc (10:1) to afford pure **102** (6.7 g) as a yellowish solid in 40% yield (R_f = 0.86, hexane/EtOAc = 10:1); ^{1}H NMR (500 MHz, CD_2Cl_2) δ ppm 3.78 (s, 2H, CH_2), 6.66 (d, $J_{H,H}$ = 8 Hz, 4H, Ar-H), 6.89 (d, $J_{H,H}$ = 8.5 Hz, 4H, Ar-H), 7.14 (d, $J_{H,H}$ = 7.55 Hz, 4H, Ar-H), 7.27-7.31 (m, 6H, Ar-H), 7.42 (d, $J_{H,H}$ = 8.55 Hz, 4H, Ar-H), 7.49 (d, $J_{H,H}$ = 8.55 Hz, 2H, Ar-H), 7.57 (d, $J_{H,H}$ = 7.75 Hz, 4H, Ar-H); ^{13}C NMR (125.8 MHz, CD_2Cl_2) δ ppm 41.0, 91.8, 131.0, 137.7, 140.1.

4,4'-Diiodobenzophenone (103)[332]

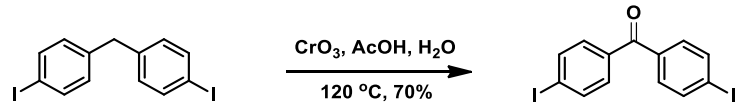

102 103

A single neck, 100 mL round bottom flask, equipped with a reflux condenser was loaded with starting material **102** (6.7 g, 15.95 mmol), chromium oxide (VI) (7.97 g, 79.75 mmol) and suspended in a mixture of glacial acetic (61 mL) acid and H_2O (24 mL). The reaction mixture was refluxed for 36 h. The crude mixture was cooled down to 0 °C and neutralized with NaOH (pellets). Subsequently, the precipitate was filtered through a fritted funnel, washed

with water and dried. White powder was recrystallized from hot toluene, affording 4.84 g of the product **103** as white needles in 70% yield. ^{1}H NMR (500 MHz, $CDCl_3$) δ ppm, 7.45 (bm, 4H, Ar-H), 7.85 (bm, 4H, Ar-H); ^{13}C NMR (125.8 MHz, $CDCl_3$) δ ppm, 100.6, 131.6, 136.5, 137.9, 195.6.

Bis(4-iodophenyl)-4-methoxyphenyl]methanol (104)

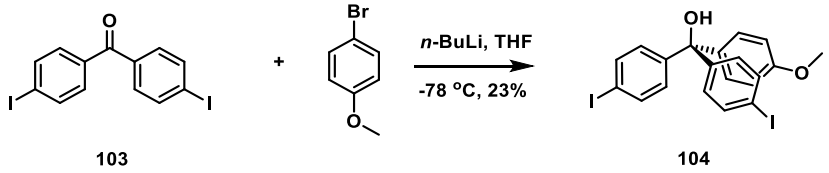

A dry and argon-flushed 50 mL Schlenk flask was charged with 4-bromoanisole (0.7 mL, 5.53 mmol) and anhydrous THF (20 mL) was added. The solution was cooled to -78 °C and *n*-BuLi (3.6 mL, 5.76 mmol, 1.6 M in hexane) was added dropwise over 20 min. The reaction mixture was stirred at -78 °C for 2 h under argon. In a second 250 mL Schlenk flask, benzophenone **103** (1.8 g, 4.15 mmol) was dissolved in anhydrous THF (80 mL) under an inert atmosphere and cooled to -78 °C. The solution of lithiated species was slowly added via a cannula into the flask containing solution of benzophenone. After 1 h, the reaction mixture was allowed to warm to room temperature and stirred for an additional 16 h. The reaction mixture was quenched with saturated NH_4Cl solution (100 mL). The aqueous layer was washed with CH_2Cl_2 (2 x 200 mL). The combined organic layer was washed with brine (100 mL), dried over $MgSO_4$, and filtered. All volatiles were removed under reduced pressure and the residue was purified by column chromatography on silica gel (500 g) in hexane/EtOAc (15:1) to afford pure **104** (0.52 g) as a yellow oil in 23% yield (R_f = 0.08, hexane/EtOAc = 15:1); ^{1}H NMR (500 MHz, $CDCl_3$) δ ppm 2.70 (s, 1H, OH), 6.82-6.85 (m, 2H, Ar-H), 7.01-7.04 (m, 4H, Ar-H), 7.09-7.12 (m, 2H, Ar-H), 7.62-7.65 (m, 4H, Ar-H); ^{13}C NMR (125.8 MHz, $CDCl_3$) δ ppm 55.5, 113.7, 129.2, 129.9, 137.3, 138.2, 146.4, 159.2; IR (KBr) ν cm^{-1} 3463 (s, υ(OH)), 3057 (w, υ(=CH)), 2967 (w, $\upsilon_{as}(CH_3)$), 2927 (w, $\upsilon_{s}(CH_3)$), 2834 (s, $\upsilon(CH_3$-O)), 1643 (s), 1606 (s), 1579 (s), 1509 (s), 1481 (s), 1461 (w, $\delta_{s}(CH_3)$), 1390 ($\delta_{as}(CH_3)$), 1301 (m), 1250 (s, $\upsilon(C_{Ar}$-O-C)), 1178 (s, $\upsilon(3^{o}$-OH)), 1064 (w), 1032 (m), 1003 (m), 915 (s), 814 (s), 579 (s, υ(C-I)); UV-Vis (λ_{max}[nm], ε, CH_2Cl_2) 238 (21345); ESI(+) MS Calcd for $C_{20}H_{16}O_2I_2Na$ ($[M+Na]^+$, 564.9212, found *m/z* 564.9171; elemental analysis calcd (%) for $C_{20}H_{16}I_2O_2$ (541. 92): C, 44.31; H, 2.97; found: C, 44.71; H, 3.15.

{[Bis(4-iodophenyl)]-(4-methoxyphenyl)methyl} phenol (**105**)

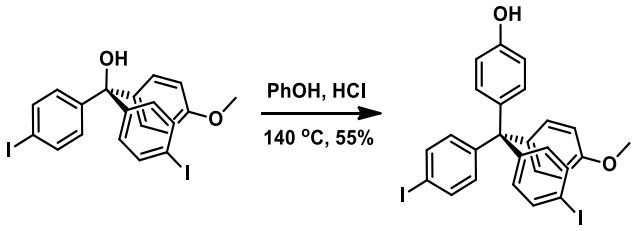

104 105

A 100 mL two-neck round bottom flask was charged with **104** (0.5 g, 0.92 mmol), phenol (0.9 g, 9.2 mmol), and a few drops of concentrated HCl were added. The reaction mixture was heated at 140 °C for 16 h under argon. After cooling to room temperature, the red reaction mixture was diluted with toluene (200 mL) and quenched with NaOH solution (2 M, 100 mL). The combined organic layer was washed with water (100 mL), dried over $MgSO_4$ and filtered. All volatiles were removed under reduced pressure and the residue was purified by column chromatography on silica gel (400 g) in hexane/EtOAc (9:1) to afford **105** (0.31 g) as a yellow oil in 55% yield (R_f = 0.11, hexane/EtOAc = 9:1); ^{1}H NMR (500 MHz, $CDCl_3$) δ ppm 3.78 (s, 3H, CH_3), 4.9 (s, 1H, OH), 6.70-6.72 (m, 2H, Ar-H), 6.77-6.79 (m, 2H, Ar-H), 6.91 (d, $J_{H,H}$ = 8.6 Hz, 2H, Ar-H), 6.98 (d, $J_{H,H}$ = 8.6 Hz, 2H, Ar-H), 7.01-7.03 (m, 2H, Ar-H), 7.05-7.13 (m, 2H, Ar-H), 7.19-7.24 (m, 2H, Ar-H), 7.54-7.57 (m, 2H, Ar-H); ^{13}C NMR (125.8 MHz, $CDCl_3$) δ ppm 55.4, 67.1, 92, 113.1, 114.6, 127.8, 131.9, 132.1, 132.3, 133.0, 136.7, 146.7, 153.8, 157.8; IR (KBr) ν cm^{-1} 3357 (b, υ(OH)), 3031 (w, υ(=CH)), 2934 (m, υ_s(CH_3)), 2853 (s, υ(CH_3-O)), 1606 (s), 1509 (s), 1484 (m), 1439 (w, δ_s(CH_3)), 1390 (w, δ_{as}(CH_3)), 1250 (s, υ(C_{Ar}-O-C)), 1179 (s, υ(C_{Ar}-OH)), 1094 (m), 1034 (m), 1004 (s), 816 (s); UV-vis (λ_{max}[nm], ε, CH_2Cl_2) 215 (53650); ESI(+) HRMS Calcd for $C_{26}H_{20}OI_2Na$ ([M+Na]$^+$, 640.9450, found *m/z* 640.9403; elemental analysis calcd (%) for $C_{26}H_{20}I_2O_2$ (617.96): C, 50.51.; H, 3.26; found: C, 50.88; H, 3.46.

4, 4'-[Bis(4-iodophenyl)methylene] diphenol (**106**)

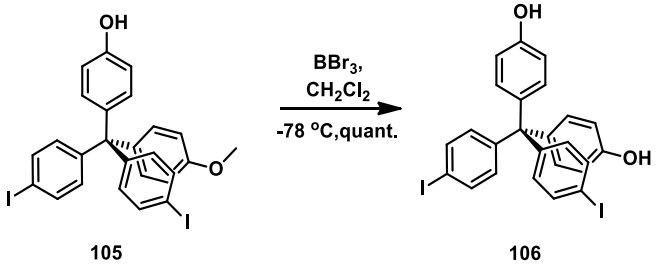

105 106

An oven-flamed, 100 mL, two-neck round bottom flask, equipped with a dropping funnel was charged with starting material **105** (0.31 g, 0.51 mmol) and freshly distilled dichloromethane (20 mL) under argon. The reaction mixture was than cooled to -78^{o}C and BBr_3 (1.5 mL, 1.5 mmol, 1 M solution in CH_2Cl_2) was dropwise added. Afterwards, the resulting mixture was stirred overnight under argon atmosphere. The reaction mixture was quenched with saturation solution of Na_2SO_3 (100 mL), the aqueous layer was washed with CH_2Cl_2 (3 × 100 mL). The combined organic layer was washed with brine (100 mL), dried over $MgSO_4$, and filtered. All volatiles were removed under reduced pressure and the residue was purified by flash column chromatography on silica gel (100 g) in hexane/EtOAc (3:1) to afford pure compound **106** (0.3 g) as a reddish oil in 99% yield (R_f = 0.26, hexane/EtOAc = 3:1); ^{1}H NMR (500 MHz, $CDCl_3$) δ ppm 5.16 (s, 2H, OH), 6.77-6.79 (m, 4H, Ar-H), 7.00 (d, $J_{H,H}$ = 8.6 Hz, 2H, Ar-H), 7.06 (d, $J_{H,H}$ = 8.65 Hz, 4H, Ar-H), 7.18 (d, $J_{H,H}$ = 8.6 Hz, 2H, Ar-H), 7.28-7.30 (m, 2H, Ar-H), 7.64 (d, $J_{H,H}$ = 8.7 Hz, 2H, Ar-H); ^{13}C NMR (125.8 MHz, $CDCl_3$) δ ppm 63.5, 92.0, 114.8, 132.2, 133.2, 136.8, 138.0, 147.1, 154.6; IR (KBr) υ cm^{-1} 3298 (b, υ(OH)), 2924 (m), 2853 (w), 1592 (m), 1509 (m), 1483 (s), 1453 (m), 1384 (w), 1235 (s, $\upsilon(C_{Ar}\text{-}O)$), 1179 (s, υ(C-OH)), 1004 (s), 823 (s); UV-vis (λ_{max}[nm], ε, CH_2Cl_2) 234 (10856); ESI(+) HRMS Calcd for $C_{25}H_{18}I_2O_2Na$ ([M+Na]$^{+}$, 626.9294), found *m/z* 626.9275; elemental analysis calcd (%) for $C_{25}H_{18}I_2O_2$ (603.94): C, 49.70; H, 3.00; found: C, 49.94; H, 3.05.

4, 4'-[Bis(4-iodophenyl)methylene]-bis(phenyl trimethylsilyl ether) (**107**)

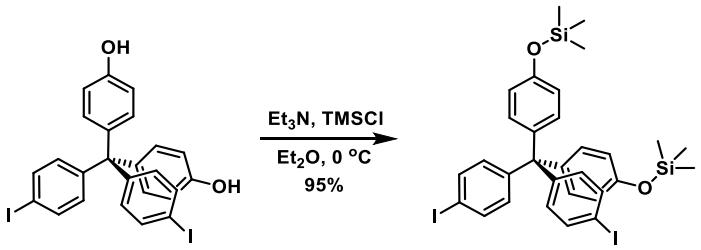

106 **107**

Trimethylsilyl chloride (0.1 mL, 0.65 mmol) was added dropwise to the solution of **106** (0.28 g, 0.46 mmol) in dry triethylamine (0.09 mL, 0.65 mmol) and freshly distilled Et_2O (20 mL) at 0 °C under argon atmosphere. The solution was stirred for 2 h at 0 °C, and then allowed to warm to room temperature and stirred for an additional 10 h, before quenching with water (100 mL). The aqueous layer was washed with Et_2O (3 x 100 mL). The combined organic layer was washed with brine (100 mL), dried over $MgSO_4$ and filtered. The volatiles were removed under reduced pressure affording the desired product **107** (0.33 g) in 95% yield as a white powder. (R_f = 0.91, hexane/EtOAc = 5:1); m.p. 240-241 °C; ^{1}H NMR (500 MHz, $CDCl_3$)

δ ppm 0.26 (s, 18H, CH_3), 6.70 (d, $J_{H,H}$ = 8.7 Hz, 4H, Ar-H), 6.89 (d, $J_{H,H}$ = 8.55 Hz, 4H, Ar-H), 6.95 (d, $J_{H,H}$ = 8.75 Hz, 4H, Ar-H), 7.55 (d, $J_{H,H}$ = 8.6 Hz, 4H, Ar-H); ^{13}C NMR (125.8 MHz, $CDCl_3$) δ ppm 0.04, 63.4, 92, 119, 132.1, 133.2, 136.7, 138.8, 146.8, 153.6; IR (KBr) ν cm^{-1} 3036 (w, υ(=CH)), 2969 (m, $\upsilon_{as}(CH_3)$), 2928 (m, $\upsilon_s(CH_3)$), 1610 (s), 1508 (s), 1482 (s), 1399 (w), 1453 (s, $\delta_s(CH_3)$), 1390 ($\delta_{as}(CH_3)$), 1245 (s), 1179 (s, υ(C-O)), 1004 (s, υ(C-O-Si)), 1013 (s), 578 (m, υ(C-I)); UV-Vis (λ_{max}[nm], ε, CH_2Cl_2) 234 (25011); ESI(+) HRMS Calcd for $C_{25}H_{18}I_2O_2Na$ ([M-TMS]$^+$, 626.9265, found *m/z* 626.9294; elemental analysis calcd (%) for $C_{31}H_{34}I_2O_2Si_2$ (748.02): C, 49.74; H, 4.58; found: C, 49.97; H, 4.75.

4,4'-Dibromodiphenylmethane (**108**)[333]

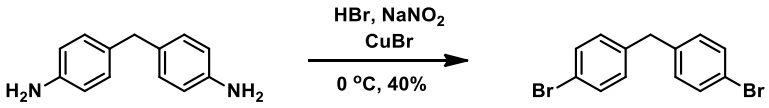

108

A 250 mL three-neck round bottom flask, equipped with a reflux condenser and dropping funnel was charged with 4,4'-diaminodiphenylmethane (10 g, 50 mmol), concentrated hydrobromic acid (90 mL) and cooled down to 0 °C. Separately, sodium nitrate (8.25 g, 120 mmol) was dissolved in 80 mL of water and cooled down to 0 °C. Afterwards, solution of nitrite was transferred to a dropping funnel and dropwise added over 40 min to the same solution. Consecutively, a 500 mL three-neck round bottom flask was charged with a solution of copper bromide (21.51 g, 150 mmol) in 80 mL of HBr and cooled down to 0 °C. Freshly formed diazonium salt was dropwise added to the CuBr solution. The reaction mixture was vigorously stirred at ambient conditions overnight. The reaction mixture was neutralized with 500 mL of saturated solution of Na_2CO_3 and aqueous layer was washed with dichloromethane (3 x 500 mL). The combined organic layers were dried over $MgSO_4$, and filtered. All volatiles were removed under reduced pressure and the residual yellowish slurries were purified by column chromatography on silica gel (1000 g) in hexane/EtOAc (20:1) to afford pure compound **108** (6.5 g) as a yellowish solid in 40% yield (R_f = 0.95, hexane/EtOAc = 20:1); ^{1}H NMR (500 MHz, CD_2Cl_2) δ ppm, 3.88 (s, 2H, CH_2), 7.03 (d, $J_{H,H}$ = 8.45 Hz, 4H, Ar-H), 7.41 (dd, $J_{H,H}$ = 6.5, 1.9 Hz, 4H, Ar-H); ^{13}C NMR (125.8 MHz, $CDCl_3$) δ ppm 40.9, 120.4, 130.8, 131.9, 139.6, 139.6.

4,4'-Dibromobenzophenone (**109**)[333]

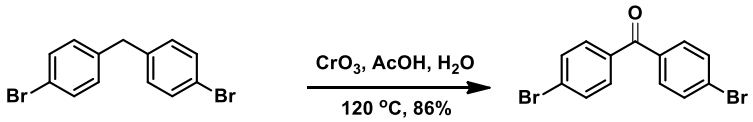

108 **109**

Compound **109** was prepared adopting the protocol for the synthesis of **103**. A single neck, 100 mL round bottom flask, equipped with a refluxed condenser was loaded with starting material **108** (6.45 g, 20 mmol), chromium oxide (9.8 g, 99 mmol), and suspended in a mixture of glacial acetic acid (90 mL) and H_2O (30 mL). The reaction mixture was refluxed for 36 h. The crude mixture was cooled down to 0 °C and neutralized with NaOH (pellets).

Subsequently, the precipitate was filtered through a fritted funnel and washed with an excess of water. White powder was recrystallized from hot toluene to afford 5.7 g of the product **109** as white needles in 86% yield. ^{1}H NMR (500 MHz, $CDCl_3$) δ ppm 7.64-7.69 (bm, 8H, Ar-H); ^{13}C NMR (125.8 MHz, $CDCl_3$) δ ppm 128, 131.6, 131.9, 136, 194.7.

[Bis(4-bromophenyl)-4-methoxyphenyl]methanol (**110**)

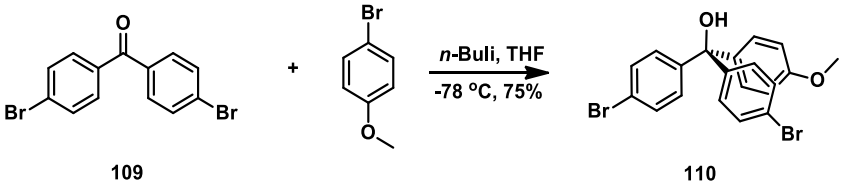

109 110

A dry and argon-flushed 100 mL Schlenk flask was charged with 4-bromoanisole (0.81 mL, 6.47 mmol) and anhydrous THF (40 mL) was added. The solution was cooled to -78 °C and *n*-BuLi (4.3 mL, 6.76 mmol, 1.6 M in hexane) was added dropwise over 20 min. The reaction mixture was stirred at -78 °C for 2 h under argon. In a second 250 mL Schlenk flask, benzophenone **109** (2 g, 5.91 mmol) was dissolved in anhydrous THF (35 mL) under an inert atmosphere and cooled to -78 °C. The solution of lithiated species was slowly added via a cannula into the flask containing solution of benzophenone. After 1 h, the reaction mixture was allowed to warm to room temperature and stirred for an additional 16 h. The reaction mixture was quenched with saturated NH_4Cl solution (100 mL). The aqueous layer was washed with CH_2Cl_2 (3 x 200 mL). The combined organic layer was washed with brine (100 mL), dried over $MgSO_4$, and filtered. All volatiles were removed under reduced pressure and the residue was purified by column chromatography on silica gel (700 g) in hexane/EtOAc (9:1) to afford pure **110** (1.96 g) as a dark-blue oil in 75% yield (R_f = 0.29, hexane/EtOAc = 9:1); ^{1}H NMR (500 MHz, $CDCl_3$) δ ppm 2.83 (s, 1H, OH), 3.80 (s, 3H, CH_3), 6.83-6.85 (d, $J_{H,H}$ = 8.85 Hz, 2H, Ar-H), 7.11 (d, $J_{H,H}$ = 8.85 Hz, 2H, Ar-H), 7.15 (d, $J_{H,H}$ = 8.6 Hz, 4H, Ar-H), 7.43 (d, $J_{H,H}$ = 8.65 Hz, 4H, Ar-H), ^{13}C NMR (125.8 MHz, $CDCl_3$) δ ppm 55.4, 81.2, 113.6, 121.7, 129.2, 129.7, 131.2, 138.3, 145.8, 159.1; IR (KBr) ν cm^{-1} 3468 (s, υ(OH)), 3000 (w, υ(=CH)), 2954 (w, $\upsilon_{as}(CH_3)$), 2928 (w, $\upsilon_{s}(CH_3)$), 2836 (s, $\upsilon(CH_3\text{-}O)$), 1607 (s, υ(C=C)), 1582 (s), 1509 (s),1485 (s), 1461 (m, $\delta_{s}(CH_3)$), 1394 (m, $\delta_{as}(CH_3)$), 1299 (s, $\upsilon(C_{Ar}\text{-}O)$), 1179 (s, $\upsilon(3^{o}\text{-}OH)$), 1154 (m), 1073 (m), 1008 (s), 906 (s), 819 (s), 599 (s, υ(C-Br)); UV-Vis (λ_{max}[nm], ε, CH_2Cl_2) 233 (22297); ESI(+) HRMS Calcd for $C_{20}H_{16}Br_2O_2Na$ ([M+Na]$^{+}$, 470.9340, found *m/z* 470.9395; elemental analysis calcd (%) for $C_{20}H_{16}Br_2O_2$ (445.95): C, 53.60; H, 3.60; found: C, 53.85; H, 3.91.

{[Bis(4-bromophenyl)]-(4-methoxyphenyl)methyl} phenol (**111**)

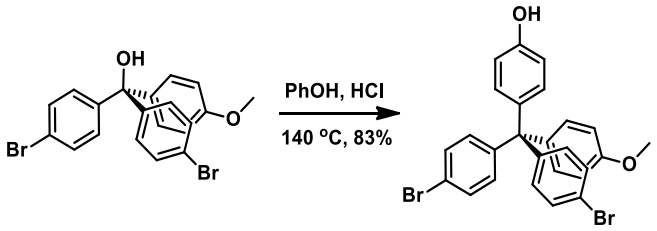

110 111

A 100 mL two-neck round bottom flask was charged with **110** (1.89 g, 4.24 mmol), phenol (5 g, 51 mmol), and a few drops of concentrated HCl were added. The reaction mixture was heated at 140 °C for 16 h under argon. After cooling to room temperature, the red reaction mixture was diluted with toluene (400 mL) and quenched with NaOH solution (2 M, 200 mL). The combined organic layer was washed with water (100 mL), dried over $MgSO_4$ and filtered. All volatiles were removed under reduced pressure and the residue was purified by column chromatography on silica gel (300 g) in hexane/EtOAc (5:1) to afford **111** (1.85 g) as a cream powder in 83% yield (R_f = 0.33, hexane/EtOAc = 5:1); m.p. 94-96 °C; ^{1}H NMR (500 MHz, $CDCl_3$) δ ppm 3.79 (s, 3H, CH_3), 4.77 (s, 1H, OH), 6.72 (d, $J_{H,H}$ = 8.75 Hz, 2H, Ar-H), 6.78 (d, $J_{H,H}$ = 8.9 Hz, 2H, Ar-H), 6.99 (d, $J_{H,H}$ = 8.7 Hz, 2H, Ar-H), 7.02-7.10 (m, 5H, Ar-H), 7.21 (d, $J_{H,H}$ = 8.7 Hz, 1H, Ar-H), 7.36 (d, $J_{H,H}$ = 8.7 Hz, 1H, Ar-H), 7.37 (d, $J_{H,H}$ = 8.7 Hz, 2H, Ar-H); ^{13}C NMR (125.8 MHz, $CDCl_3$) δ ppm 55.2, 63.0, 113.2, 114.7, 120.4, 127.9, 130.9, 132.0, 132.3, 132.4, 132.8, 146.1, 153.9, 157.9; IR (KBr) ν cm^{-1} 3339 (b, υ(OH)), 3031 (w, υ(=CH)), 2929 (m, $\upsilon_s(CH_3)$), 2835 (s, $\upsilon(CH_3\text{-}O)$), 1608 (m), 1509 (s), 1441 (m, $\delta_s(CH_3)$), 1374 (w, $\delta_{as}(CH_3)$), 1250 (s, $\upsilon(C_{Ar}\text{-}O\text{-}C)$), 1180 (s, $\upsilon(C_{Ar}\text{-}O)$), 1094 (w), 1009 (m), 819 (s); UV-vis (λ_{max}[nm], ε, CH_2Cl_2) 233 (22297); ESI(+) MS Calcd for $C_{26}H_{20}Br_2O_2Na$ ($[M+Na]^+$, 546.9670), found *m/z* 546.9709; elemental analysis calcd (%) for $C_{26}H_{20}Br_2O_2$ (521. 98): C, 59.57; H, 3.85; found: C, 59.85; H, 3.97.

4, 4'-[Bis(4-bromophenyl)methylene] diphenol (**112**)

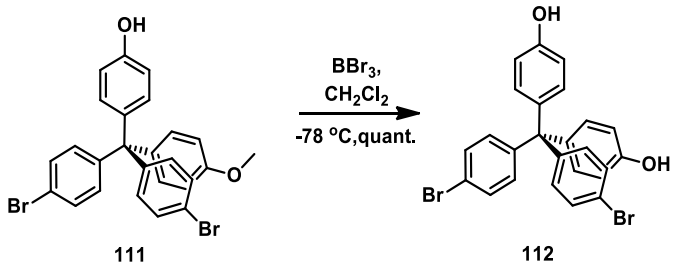

An oven-flamed, 100 mL, two-neck round bottom flask, equipped with a dropping funnel was charged with starting material **111** (1.8 g, 3.45 mmol) and freshly distilled dichloromethane (30 mL) under argon. The reaction mixture was than cooled to -78 ^{o}C and BBr_3 (10.3 mL, 11 mmol, 1 M solution in CH_2Cl_2) was dropwise added. Subsequently, the resulting mixture was stirred overnight under argon atmosphere. The reaction mixture was quenched with saturated solution of Na_2SO_3 (120 mL), the aqueous layer was washed with CH_2Cl_2 (3 x 200 mL). The combined organic layer was washed with brine (100 mL), dried over $MgSO_4$, and filtered. All volatiles were removed under reduced pressure and the residue was purified by flash column chromatography on silica gel (200 g) in hexane/EtOAc (2:1) to afford pure **112** (1.73 g) as a white powder in 97% yield (R_f = 0.5, hexane/EtOAc = 2:1); m.p. 180-182 ^{o}C; ^{1}H NMR (500 MHz, $CDCl_3$) δ ppm 5.34 (s, 2H, OH), 6.71 (d, $J_{H,H}$ = 9.3 Hz, 4H, Ar-H), 6.98 (d, $J_{H,H}$ = 8.8 Hz, 4H, Ar-H), 7. 09 (d, $J_{H,H}$ = 8.7 Hz, 4H, Ar-H), 7.21 (d, $J_{H,H}$ = 8.6 Hz, 2H, Ar-H), 7.25 (d, $J_{H,H}$ = 8.75 Hz, 2H, Ar-H), 7.31-7.33 (m, 2H, Ar-H), 7.63 (d, $J_{H,H}$ = 8.7 Hz, 4H, Ar-H); ^{13}C NMR (125.8 MHz, $CDCl_3$) δ ppm 68.2, 114.7, 120.4, 127.9, 130.8, 132.1, 132.2, 132.8, 146.1, 154; IR (KBr) ν cm^{-1} 3264 (b, υ(OH)), 2854 (w), 1612 (m), 1594 (m), 1509 (s), 1486 (m), 1444 (m), 1367 (w), 1241 (s, $\upsilon(C_{Ar}\text{-}O)$), 1179 (s, υ(C-OH)), 1009 (s), 823 (s); UV-vis (λ_{max}[nm], ε, CH_2Cl_2) 230 (13173); ESI(+) MS Calcd for $C_{25}H_{18}O_2Br_2Na$ ([M+Na]$^{+}$, 532.9572, found *m/z* 532.9742; elemental analysis calcd (%) for $C_{25}H_{18}Br_2O_2$ (507.97): C, 58.85; H, 3.56; found: C, 58.98; H, 3.71.

4, 4'-[Bis(4-bromophenyl)methylene]-bis(phenyl trimethylsilyl ether) (**113**)

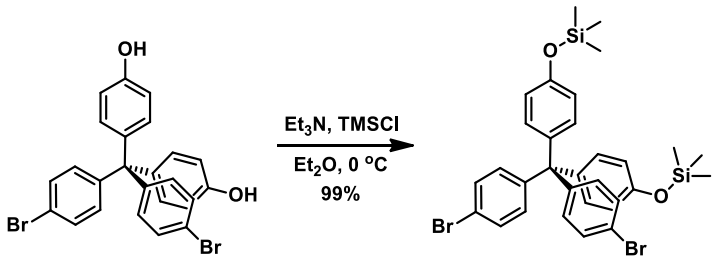

112 113

Trimethylsilyl chloride (0.21 mL, 1.65 mmol) was added dropwise to the solution of **112** (0.21 g, 0.41 mmol) in dry triethylamine (0.23 mL, 1.65 mmol) and freshly distilled Et_2O (20 mL) at 0 °C under argon atmosphere. The solution was stirred for 2 h at 0 °C, and then allowed to warm to room temperature and stirred for an additional 10 h, before quenching with water (150 mL). The aqueous layer was washed with Et_2O (3 x 100 mL). The combined organic layer was washed with brine (100 mL), dried over $MgSO_4$ and filtered. The volatiles were removed under reduced pressure and the residue was purified by column chromatography on silica gel (200 g) with hexane/EtOAc (5:1) as an eluent to yield 0.26 g (99%) of **113** as a white powder. (R_f = 0.93, hexane/EtOAc = 5:1); m.p. 102-103 °C; ^{1}H NMR (500 MHz, $CDCl_3$) δ ppm 0.26 (s, 18H, CH_3), 6.71 (d, $J_{H,H}$ = 8.75 Hz, 4H, Ar-H), 6.96 (d, $J_{H,H}$ = 8.75 Hz, 4H, Ar-H), 7.02-7.03 (m, 3H, Ar-H), 7.08 (d, $J_{H,H}$ = 8.7 Hz, 1H, Ar-H), 7.21 (d, $J_{H,H}$ = 8.7 Hz, 1H, Ar-H), 7.35-7.37 (m, 3H, Ar-H); ^{13}C NMR (125.8 MHz, $CDCl_3$) δ ppm 63.1, 118.9, 120.2, 127.6, 130.6, 132.0, 132.7, 138.8, 146, 153.5; IR (KBr) ν cm^{-1} 3034 (w, υ(C=CH)), 2959 (m, $\upsilon_{as}(CH_3)$), 2926 (w, $\upsilon_s(CH_3)$), 2854 (m), 1600 (m), 1503 (s), 1408 (w, $\delta_s(CH_3)$), 1395 ($\delta_{as}(CH_3)$), 1267 (s, $\upsilon(C_{Ar}\text{-}O)$, 1175 (s, υ(C-O)), 1010 (s, υ(C-O-Si)), 921 (s), 846 (s, $\upsilon(SiMe_3)$ 694 (w, υ(C-Br));UV-Vis (λ_{max}[nm], ε, CH_2Cl_2) 231 (12791); ESI(+) MS Calcd for $C_{31}H_{34}Br_2O_2Si_2Na$ ($[M+Na]^+$, 677.0344 found *m/z* 677.0220; elemental analysis calcd (%) for $C_{31}H_{34}Br_2O_2Si_2$ (652.05): C, 56.88; H, 5.24; found: C, 56.92; H, 5.43.

Bis(4-chlorophenyl)-4-methoxyphenyl]methanol (**114**)

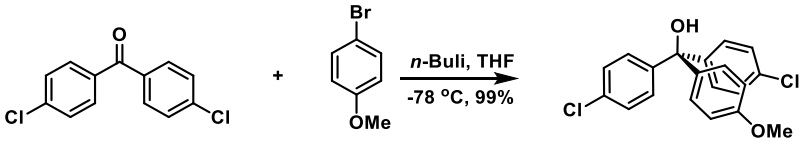

114

A dry and argon-flushed 100 mL Schlenk flask was charged with 4-bromoanisole (1.2 mL, 9.55 mmol) and anhydrous THF (20 mL). The solution was cooled to -78 °C and *n*-BuLi (6.2 mL, 9.95 mmol, 1.6 M in hexane) was added dropwise. The reaction mixture was stirred at -78 °C for 2 h under argon. In a second 100 mL Schlenk flask, 4,4'dichlorobenzophenone (2 g, 7.96 mmol) was dissolved in anhydrous THF (40 mL) under an inert atmosphere and cooled to -78 °C. The solution of lithiated species was slowly added via a cannula into the flask containing solution of benzophenone. After 1 h, the reaction mixture was allowed to warm to room temperature and stirred for an additional 16 h. The reaction mixture was quenched with saturated NH_4Cl solution (200 mL). The aqueous layer was washed with CH_2Cl_2 (3 x 200 mL). The combined organic layer was washed with brine (100 mL), dried over $MgSO_4$, and filtered. All volatiles were removed under reduced pressure and the residue was purified by column chromatography on silica gel (500 g) in hexane/EtOAc (20:1) to afford pure **114** (2.84 g) as a reddish oil in 99% yield (R_f = 0.08, hexane/EtOAc = 20:1); ^{1}H NMR (500 MHz, $CDCl_3$) δ ppm 2.80 (s, 1H, OH), 3.80 (m, 6H, CH_3), 6.84 (d, $J_{H,H}$ = 8.95 Hz, 2H, Ar-H), 7.12 (d, $J_{H,H}$ = 8.95 2H, Ar-H), 7.21 (d, $J_{H,H}$ = 8.75 Hz, 4H, Ar-H), 7.28 (d, $J_{H,H}$ = 8.7 Hz, 4H, Ar-H); ^{13}C NMR (125.8 MHz, $CDCl_3$) δ ppm 55.4, 81.1, 113.6, 128.2, 129.2, 129.3, 133.4, 138.4, 145.3, 159.1; IR (KBr) ν cm^{-1} 3464 (s, υ(OH)), 3036 (w, υ(=CH)), 2956 (m, $\upsilon_{as}(CH_3)$), 2930 (m, $\upsilon_s(CH_3)$), 2837 (w, $\upsilon(CH_3\text{-}O)$), 1608 (s), 1510 (s), 1489 (s), 1399 (m, $\delta_s(CH_3)$), 1301 (m, $\delta_{as}(CH_3)$), 1251 (s, $\upsilon(C_{Ar}\text{-}O\text{-}C)$), 1179 (s, $\upsilon(3^o\text{-}OH)$), 1093 (s), 1013 (s), 908 (s), 824 (s); UV-vis (λ_{max}[nm], ε, acetone) 207 (36762); ESI(+) HRMS Calcd for $C_{20}H_{16}Cl_2O_2Na$ ([M+Na]$^+$, 381.0425, found *m/z* 381.0400; elemental analysis calcd (%) for $C_{20}H_{16}Cl_2O_2$ (358.05): C, 66.87; H, 4.49; found: C, 67.01; H, 4.78.

{[Bis(4-chlorophenyl)]-(4-methoxyphenyl)methyl} phenol (**115**)

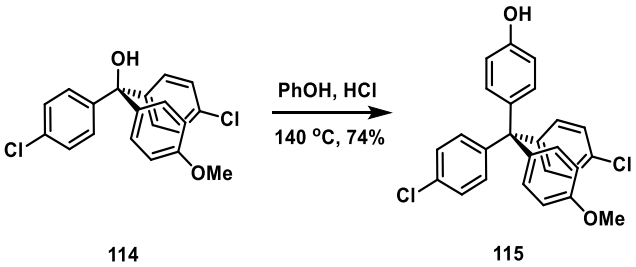

114 **115**

A 100 mL two-neck round bottom flask was charged with **114** (2.26 g, 6.3 mmol), phenol (7.11 g, 75.6 mmol), and a few drops of concentrated HCl were added. The reaction mixture was heated at 140 °C for 16 h under argon. After cooling to room temperature, the red reaction mixture was diluted with toluene (400 mL) and quenched with NaOH solution (2 M, 200 mL). The combined organic layer was washed with water (150 mL), dried over $MgSO_4$ and filtered. All volatiles were removed under reduced pressure and the residue was purified by column chromatography on silica gel (600 g) in hexane/EtOAc (5:1) to afford **115** (2.02 g) as a yellow powder in 74% yield (R_f = 0.26, hexane/EtOAc = 5:1); m.p. 122-123 °C; ^{1}H NMR (500 MHz, $CDCl_3$) δ ppm 3.79 (s, 6H, CH_3), 4.96 (s, 2H, OH), 6.72 (d, $J_{H,H}$ = 8.8 Hz, 2H, Ar-H), 6.80 (d, $J_{H,H}$ = 8.95 Hz, 2H, Ar-H), 6.99 (d, $J_{H,H}$ = 8.8 Hz, 2H, Ar-H), 7.04 (d, $J_{H,H}$ = 8.9 Hz, 2H, Ar-H), 7.10 (d, $J_{H,H}$ = 8.7 Hz, 2H, Ar-H), 7.24 (d, $J_{H,H}$ = 8.7 Hz, 2H, Ar-H); ^{13}C NMR (125.8 MHz, $CDCl_3$) δ ppm 55.6, 63.1, 113.3, 114.8, 128, 132.2, 132.3, 132.4, 132.6, 138.6, 138.9, 145.8, 154.1, 158.1; IR (KBr) ν cm^{-1} 3357 (b υ(OH)), 3031 (w, υ(=CH)), 2931 (m, $\upsilon_s(CH_3)$), 2836 (s, $\upsilon(CH_3\text{-}O)$), 1608 (s), 1507 (s), 1488 (m), 1441 (m, $\delta_s(CH_3)$), 1368 (w, $\delta_{as}(CH_3)$), 1251 (s, $\upsilon(C_{Ar}\text{-}O\text{-}C)$), 1180 (s, $\upsilon(C_{Ar}\text{-}OH)$), 1095 (m), 1035 (m), 1013 (s), 821 (s); UV-vis (λ_{max}[nm], ε, acetone) 208 (51635); ESI(-) MS Calcd for $C_{26}H_{19}O_2Cl_2$ ([M-H]$^-$, 433.0762), found *m/z* 433.0527; elemental analysis calcd (%) for $C_{20}H_{20}Cl_2O_2$ (438.04): C, 71.73; H, 4.63; found: C, 71.60; H, 4.71.

4,4‘-[Bis(4-chlorophenyl)methylene] diphenol (**116**)

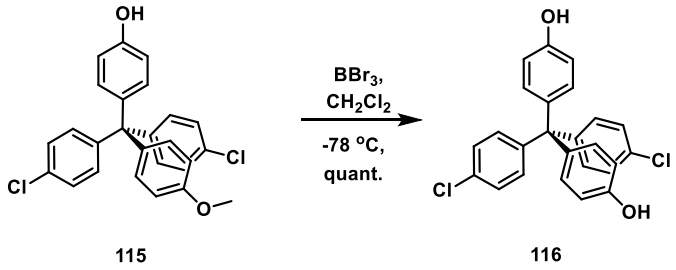

115 116

An oven-flamed, 100 mL, two-neck round bottom flask with attached dropping funnel was charged with starting material **115** (2.1 g, 4.79 mmol) and of freshly distilled dichloromethane (30 mL) under argon stream. The reaction mixture was than cooled to -78 ^{o}C and BBr_3 (22 mL, 22 mmol, 1 M solution in CH_2Cl_2) was dropwise added. Subsequently, the resulting mixture was stirred overnight under argon atmosphere. The reaction mixture was quenched with saturation solution of Na_2SO_3, the aqueous layer was washed with CH_2Cl_2 (3 x 200 mL). The combined organic layer was washed with brine (100 mL), dried over $MgSO_4$, and filtered. All volatiles were removed under reduced pressure and the residue was purified by column chromatography on silica gel (500 g) in hexane/EtOAc (3:1) to afford pure **116** (1.99 g) as a reddish oil in 99% yield (R_f = 0.14, hexane/EtOAc = 3:1); m.p. 206-209 ^{o}C; ^{1}H NMR (500 MHz, $CDCl_3$) δ ppm, 5.04 (s, 2H, OH), 6.72 (d, $J_{H,H}$ = 8.8 Hz, 4H, Ar-H), 6.98 (d, $J_{H,H}$ = 8.85 Hz, 4H, Ar-H), 7.42 (dd, $J_{H,H}$ = 4.7, 1.95 Hz, 4H, Ar-H), 7.21 (d, $J_{H,H}$ = 8.75 Hz, 4H, Ar-H); ^{13}C NMR (125.8 MHz, $CDCl_3$) δ ppm 62.9, 114.6, 127.8, 132.1, 132.2, 132.3, 138.6, 145.5, 153.9; IR (KBr) ν cm^{-1} 3494 (b, υ(OH)), 3027 (w, υ(=CH)), 2926 (m, $\upsilon_s(CH_3)$), 2854 (s, $\upsilon(CH_3\text{-}O)$), 1653 (w), 1611 (m), 1509 (s), 1488 (s), 1433 (m, $\delta_s(CH_3)$), 1378 (w, $\delta_{as}(CH_3)$), 1243 (s, $\upsilon(C_{Ar}\text{-}O)$), 1179 (s, υ(C-OH)), 1096 (s), 1013 (s), 1008 (s), 822 (s); UV-vis (λ_{max}[nm], ε, acetone) 209 (21475); ESI(+) HRMS Calcd for $C_{25}H_{18}O_2Cl_2Na$ ([M+Na]$^{+}$, 443.0518), found *m/z* 443.0582; elemental analysis calcd (%) for $C_{25}H_{18}Cl_2O_2$ (420.07): C, 71.27; H, 4.31; found: C, 71.52; H, 4.57.

4,4‘-[Bis(4-chlorophenyl)methylene]-bis(phenyl trifluoromethanesulfonate) (**117**)

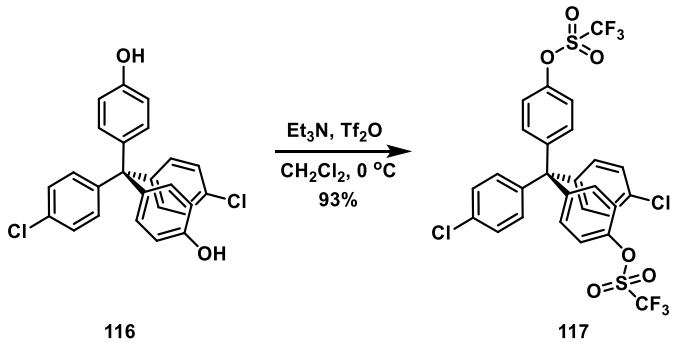

116 117

Trifluoromethanesulfonic anhydride (1.4 mL, 8.2 mmol) was added dropwise to the solution of **116** (2.1 g, 5 mmol) in dry triethylamine (1.15 mL, 8.26 mmol) and CH_2Cl_2 (20 mL) at 0 °C under argon atmosphere. The solution was stirred for 2 h at 0 °C, and then allowed to warm to room temperature and stirred for an additional 10 h, before quenching with water (150 mL). The aqueous layer was washed with CH_2Cl_2 (3 x 300 mL). The combined organic layer was washed with brine (100 mL), dried over $MgSO_4$ and filtered. The volatiles were removed under reduced pressure and the residue was purified by column chromatography on silica gel (200 g) with hexane/EtOAc (5:1) as an eluent to yield 3.17 g (93%) of **117** as a white powder. (R_f = 0.93, hexane/EtOAc = 5:1); m.p. 123-124 °C; ^{1}H NMR (500 MHz, $CDCl_3$) δ ppm 7.05 (d, $J_{H,H}$ = 8.6 Hz, 4H, Ar-H), 7.23 (m, 8H, Ar-H), 7.28 (d, $J_{H,H}$ = 8.6 Hz, 4H, Ar-H); ^{13}C NMR (125.8 MHz, $CDCl_3$) δ ppm 63.6, 117.6, 121.0, 128.5, 132.1, 132.6, 133.2, 143.5, 145.9, 148.1; ^{19}F NMR (470.57 MHz, $CDCl_3$) -72.9; IR (KBr) ν cm^{-1} 3036 (w, υ(=CH)), 1593 (w), 1494 (s), 1423 (s), 1424 (s), 1251 (s, υ(C_{Ar}-O)), 1216 (s, υ_s(S=O)) 1141 (m, υ(C-O-S)), 1015 (s, υ(C-F)), 1012 (m), 889 (s), 819 (s), 753 (m, υ(C-Cl)); UV-Vis (λ_{max}[nm], ε, CH_2Cl_2) 212 (30096); ESI(+) MS Calcd for $C_{27}H_{16}Cl_2F_6O_6S_2Na$ ([M+Na]$^+$, 706.9567), found *m/z* 706.9743; elemental analysis calcd (%) for $C_{27}H_{16}Cl_2F_6O_6S_2$ (683.97): C, 47.31; H, 2.35; found: C, 47.52; H, 2.61.

4,4‘-[Bis(4-chlorophenyl)methylene]-bis(phenyl boronic acid pinacol ester) (**118**)

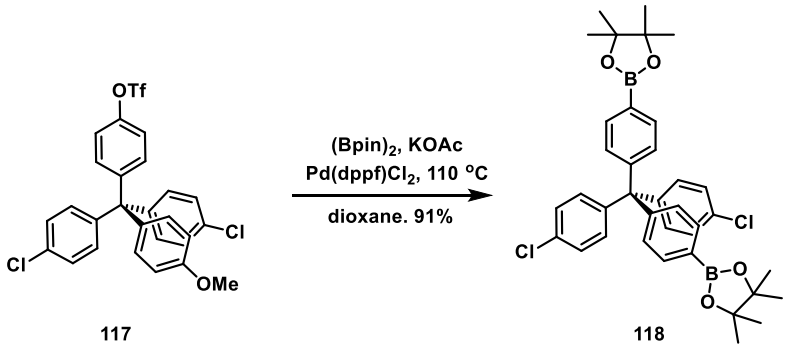

117 118

An oven-flamed 50 mL pressure tube was charged with triflate **117** (1 g, 1.46 mmol), anhydrous potassium acetate (1.15 g, 11.68 mmol), bis(pinacolato)diboron (1.11 g, 4.38 mmol), Pd(dppf)Cl_2 (0.012 g, 0.15 mmol) and dry dioxane (30 mL) under argon. The tube was sealed and stirred under at 110 °C for 48 h. After cooling, the reaction mixture was diluted with dichloromethane (300 mL) and washed with water (100 mL). The combined organic layer was washed with brine (100 mL), dried over $MgSO_4$ and filtered. The volatiles were removed under reduced pressure and the residue was purified by column chromatography on silica gel (500 g) with hexane/EtOAc (5:1) to provide 0.85 g of **118** as a yellow powder in 91% yield (R_f = 0.56, hexane/EtOAc = 5:1); m.p. 210-212 °C; ^{1}H NMR (500 MHz, $CDCl_3$) δ ppm 1.33 (s, 24 H, CH_3), 7.14 (d, $J_{H,H}$ = 8.75 Hz, 4H, Ar-H), 7.19 (d, $J_{H,H}$ = 8.8 Hz, 4H, Ar-H), 7.21 (dd, $J_{H,H}$ = 6.15, 1.95 Hz, 4H, Ar-H), 7.69 (d, $J_{H,H}$ = 8.25 Hz, 4H, Ar-H); ^{13}C NMR (125.8 MHz, $CDCl_3$) δ ppm 25.0, 64.7, 84.0, 128.0, 130.3, 132.3, 132.4 143.4, 144.8, 149.0; IR (KBr) ν cm^{-1}: 3028 (w, υ(=CH)), 2955 (w, $\upsilon_{as}(CH_3)$), 2923 (m, $\upsilon_s(CH_3)$), 2852 (s, $\upsilon(CH_3\text{-}O)$), 1701 (b), 1651 (s), 1603 (s), 1493(s), 1451 (m), 1406 (w, $\delta_s(CH_3)$), 1366 (w, $\delta_{as}(CH_3)$), 1321 (m), 1229 (m, υ(C-O)), 1157 (s, υ(C-O-B)), 1094 (s), 1014 (w), 1004 (m), 817 (m), 753 (m, υ(C-Cl)), 696 (υ, (C-B)); UV-vis (λ_{max}[nm], ε, CH_2Cl_2) 224 (19207), 229 (21995); ESI(+) MS Calcd for $C_{37}H_{40}B_2O_4Cl_2Na$ ([M+Na]$^+$, 663.2401, found *m/z* 663.2354; elemental analysis calcd (%) for $C_{37}H_{40}B_2O_4Cl_2$ (640.25): C, 69.30; H, 6.28; found: C, 69.18; H, 6.54.

4,4‘-[Bis(4-chlorophenyl)methylene] diiodobenzene (**119**).

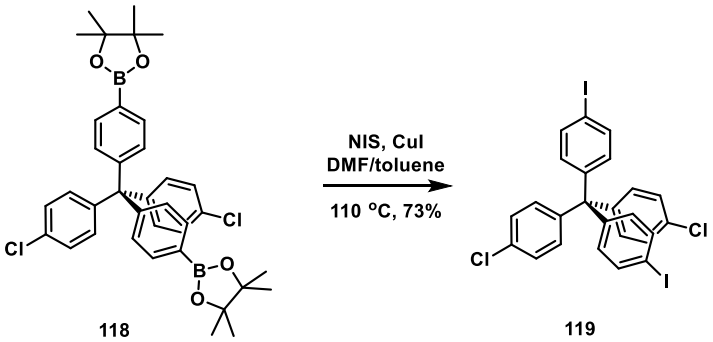

A 100 mL, two neck round-bottom flask was charged with pinacol ester **118** (0.84 g, 1.31 mmol), copper iodide (0.75 g, 3.94 mmol), *N*-iodosuccinimide (0.88 g, 3.94 mmol), anhydrous DMF (30 mL) and toluene (15 mL) under argon. The reaction mixture was stirred and heated at 110 °C for 48 h under argon atmosphere. After cooling, the reaction mixture was diluted with dichloromethane (300 mL) and washed with Na_2SO_3 solution (10%, 200 mL). The combined organic layer was washed with brine (100 mL), dried over $MgSO_4$ and filtered. All volatiles were removed under reduced pressure and the residue was purified by column chromatography on silica gel (200 g) with hexane/EtOAc (5:1) to obtain 0.61 g of **119** as a yellow powder in 73% yield (R_f = 0.63, hexane/EtOAc = 5:1): m.p. 243-245 °C; ^{1}H NMR (500 MHz, CD_2Cl_2) δ ppm 6.92 (d, $J_{H,H}$ = 8.45 Hz, 4H, Ar-H), 7.10 (d, $J_{H,H}$ = 8.6 Hz, 4H, Ar-H), 7.25 (d, $J_{H,H}$ = 8.6 Hz, 4H, Ar-H), 7.61 (d, $J_{H,H}$ = 8.5 Hz, 4H, Ar-H); ^{13}C NMR (125.8 MHz, CD_2Cl_2) δ ppm 64.7, 93.2, 129, 133.1, 133.3, 133.7, 138, 145, 146.4; IR (KBr) *v* cm^{-1} 3058 (w, *υ*(=CH)), 2958 (s), 2925 (m), 2854 (s), 1732 (w), 1640 (w, *υ*(C=C)), 1572 (w), 1481 (m), 1395 (w), 1261 (s), 1006 (m), 810 (s), 702 (w, *υ*(C-Cl)), 537 (w, *υ*(C-I)); UV-vis (λ_{max}[nm], *ε*, CH_2Cl_2) 212 (34771); ESI(-) HRMS Calcd for $C_{25}H_8I_2Cl_2Na$ ([M+Na]$^+$, 654.8042, found *m/z* 654.7990; elemental analysis calcd (%) for $C_{25}H_8I_2Cl_2Na$ (639.87): C, 46.84; H, 2.52; found: C, 47.95; H, 3.05.

4,4‘-[Bis(4-chlorophenyl)methylene] dibromobenzene (**120**).

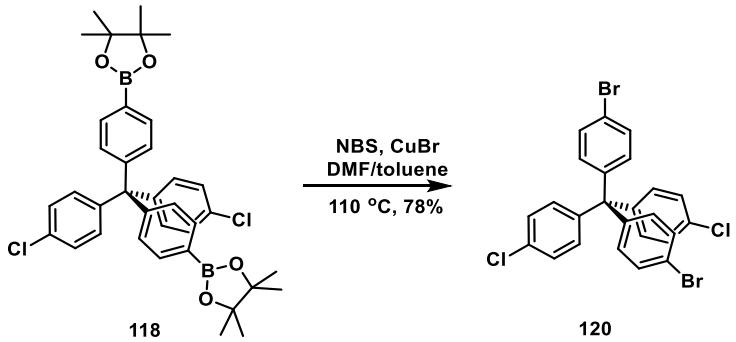

A 100 mL, two neck round-bottom flask was charged with pinacol ester **118** (0.5 g, 0.78 mmol), copper bromide (0.67 g, 4.68 mmol), *N*-bromosuccinimide (0.42 g, 2.34 mmol), anhydrous DMF (12 mL) and toluene (6 mL) under argon. The reaction mixture was stirred and heated at 110 °C for 48 h under argon atmosphere. After cooling, the reaction mixture was diluted with dichloromethane (300 mL) and washed with Na_2SO_3 solution (10 %, 200 mL). The combined organic layer was washed with brine (100 mL), dried over $MgSO_4$ and filtered. All volatiles were removed under reduced pressure and the residue was purified by column chromatography on silica gel (200 g) with hexane/EtOAc (5:1) to obtain 0. 33 g of **120** as a yellow powder in 78 % yield (R_f = 0.63, hexane/EtOAc = 5:1); m.p. 234-235 °C; ^{1}H NMR (500 MHz, $CDCl_3$) δ ppm.7.02 (d, $J_{H,H}$ = 8.7 Hz, 4H, Ar-H), 7.07 (d, $J_{H,H}$ = 8.7 Hz, 4H, Ar-H), 7.24 (d, $J_{H,H}$ = 8.7 Hz, 4H, Ar-H), 7.39 (d, $J_{H,H}$ = 8.65 Hz, 4H, Ar-H); ^{13}C NMR (125.8 MHz, $CDCl_3$) δ ppm 63.2, 121.0, 128.3, 131.2, 132.2, 132.5, 132.7, 144.1, 144.7; IR (KBr) *v* cm^{-1} 3026 (w, *υ*(=CH)), 2924 (s), 2853 (s), 1484 (s), 1399 (w), 1188 (m), 1095 (m), 1034 (s), 1009 (m), 812 (s), 732 (w, *υ*(C-Br)); 540 (s, *υ*(C-Br)); UV-vis (λ_{max}[nm], *ε*, CH_2Cl_2) 211 (26497); ESI(+) MS Calcd for $C_{25}H_{16}Br_2Cl_2Na$ ([M+Na]$^+$, 685.8514, found *m/z* 685.4587; elemental analysis calcd (%) for $C_{25}H_{16}Br_2Cl_2$ (842.18): C, 54.88; H, 2.95; found: C, 54.92; H, 3.07.

4,4‘-[Bis(4-chlorophenyl)methylene] dibenzonitrile (**122**)

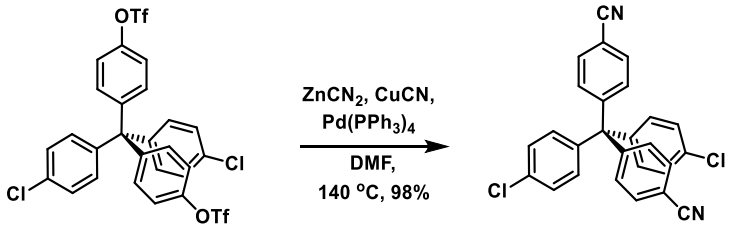

117 122

An oven-flamed, 50 mL pressure tube was charged with triflate **117** (1 g, 1.46 mmol), zinc cyanide (0.86 g, 7.3 mmol), copper (I) cyanide (0.4 g, 4.38 mmol), $Pd(PPh_3)_4$ (0.17 g, 0.17 mmol) and anhydrous DMF (15 mL) under argon. The tube was sealed and stirred at 140 °C for 16 h. After cooling to room temperature, the resulting reaction mixture was quenched with saturated solution of Na_2CO_3 (100 mL). The aqueous layer was washed with CH_2Cl_2 (3 x 150 mL). The combined organic layer was washed with brine (100 mL), dried over $MgSO_4$ and filtered. All volatiles were removed under reduced pressure and the residue was purified by column chromatography on silica gel (200 g) in the mixture of hexane/EtOAc (3:1) to get 0.63 g of **122** as an orange powder in 98 % yield (R_f = 0.64, hexane/EtOAc = 3:1); m.p. 156-158 °C; ^{1}H NMR (500 MHz, $CDCl_3$) δ ppm 7.05 (d, $J_{H,H}$ = 8.6 Hz, 4H, Ar-H), 7.28 (d, $J_{H,H}$ = 8.85 Hz, 4H, Ar-H), 7.30 (d, $J_{H,H}$ = 8.55 Hz, 4H, Ar-H), 7.60 (d, $J_{H,H}$ = 8.4 Hz, 4H, Ar-H); ^{13}C NMR (125.8 MHz, $CDCl_3$) δ ppm 64.7, 111.1, 118.4, 128.4, 131.4, 131.9, 132.1, 133.4, 142.8, 150.3; IR (KBr) ν cm^{-1} 3067 (w), 2923 (w), 2853 (s), 2233 (s, υ(C≡N)), 1603 (m), 1487 (s), 1402 (m), 1093 (m, υ(C-N)), 1012 (s), 817 (s), 739 (m, υ(C-Cl)); UV-Vis (λ_{max}[nm], ε, CH_2Cl_2) 224 (13100), 270 (23341); ESI(+) HRMS Calcd for $C_{27}H_{16}Cl_2N_2Na$ ([M+Na]$^+$, 461.0588), found *m/z* 461.0533; elemental analysis calcd (%) for $C_{27}H_{16}Cl_2N_2$ (439.34): C, 73.81; H, 3.67; N, 6.38; found: C, 73.20; H, 3.84; N, 3.69.

4,4‘-[Bis(4-chlorophenyl)methylene] dibenzaldehyde (**121**)

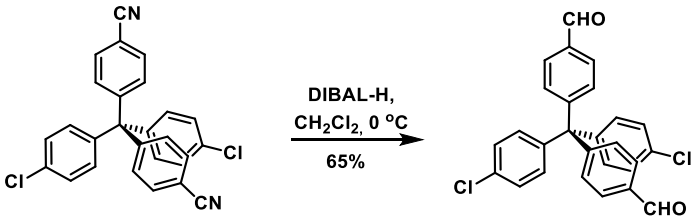

122 **121**

A dry and argon-flushed 100 mL Schlenk flask was charged with **122** (1.98 g, 4.51 mmol) and anhydrous CH_2Cl_2 (40 mL) was added. The solution was cooled to -78 °C and DIBAL-H (13.55 mL, 13.5 mmol, 1 M solution in toluene) was added dropwise over 30 min. The reaction mixture was stirred overnight at 0 °C under argon. The reaction mixture was quenched with 2 M HCl solution (100 mL). The aqueous layer was washed with CH_2Cl_2 (3 x 200 mL). The combined organic layer was washed with brine (100 mL), dried over $MgSO_4$, and filtered. All volatiles were removed under reduced pressure and the residue was purified by column chromatography on silica gel (300 g) in hexane/EtOAc (4:1) to afford pure **121** (1.3 g) as a yellowish solid in 65% yield (R_f = 0.47, hexane/EtOAc = 4:1); m.p. 221-223 °C; ^{1}H NMR (500 MHz, CD_2Cl_2) δ ppm 7.16 (dd, $J_{H,H}$ = 6.75, 2.05 Hz, 4H, Ar-H), 7.29 (dd, $J_{H,H}$ = 6.75, 1.75 Hz, 4H, Ar-H), 7.40 (d, $J_{H,H}$ = 8.7 Hz, 4H, Ar-H), 7.80 (dd, $J_{H,H}$ = 6.75, 1.9 Hz, 4H, Ar-H), 9.99 (s, 2H, H-CO); ^{13}C NMR (125.8 MHz, CD_2Cl_2) δ ppm 65.2, 128.7, 129.6, 131.7, 132.5, 133.1, 135.2, 144, 152.3, 191.9; IR (KBr) ν cm^{-1} 3030 (w), 2924 (m), 2852 (m), 2737 (w, υ(H-C=O)), 1702 (s, υ(C=O)), 1603 (s), 1487 (m), 1311 (w), 1216 (s, υ(C_{Ar}-C-O)), 1182 (m, υ(C-O)), 1094 (s), 1013 (m), 811 (s); UV-Vis (λ_{max}[nm], ε, CH_2Cl_2) 267 (11579); ESI(+) HRMS Calcd for $C_{27}H_{14}O_2Cl_2$ ([M-4H]$^+$, 440.0371, found *m/z* 440.0303; elemental analysis calcd (%) for $C_{27}H_{18}O_2Cl_2$ (445.34): C, 72.82; H, 4.07; found: C, 72.96; H, 4.09.

4,4‘-[Bis(4-chlorophenyl)methylene]-bis[1,3-dioxolane-(1-phenyl)-4’-diyl] (**123**)

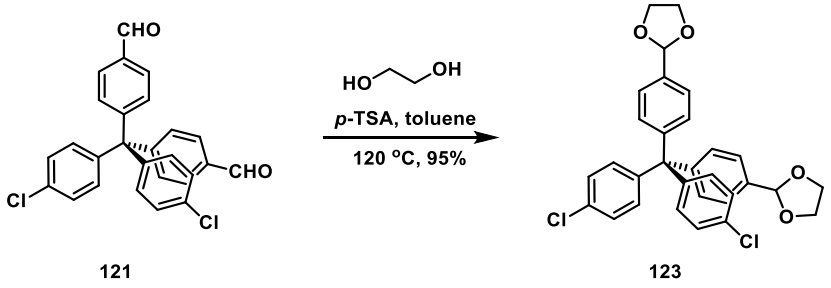

121 123

An oven-flamed two neck round bottom flask, equipped with reflux condenser and Dean-Stark trap was charged with starting material **121** (0.94 g, 2.1 mmol), ethylene glycol (0.7 mL, 12.6 mmol) *p*-TSA (0.05 g, 0, 011 mmol), and 100 mL of freshly distilled toluene under argon stream. Upon cooling, the reaction mixture was quenched with saturated solution of Na_2CO_3 (100 mL). The aqueous layer was washed with CH_2Cl_2 (3 x 200 mL). The combined organic layer was washed with brine (100 mL), dried over $MgSO_4$, and filtered. All volatiles were removed under reduced pressure giving pure **123** (1.1 g) as a white powder almost quantitatively (97%). (R_f = 0.28, hexane/EtOAc = 4:1); m.p. 256-258 °C; ^{1}H NMR (500 MHz, CD_2Cl_2) δ ppm 3.97-4.02 (m, 4H, CH_3), 4.06-4.10 (m, 4H, CH_3), 5.72 (s, 2H, CH), 7.16 (dd, $J_{H,H}$ = 8.75, 1.75 Hz, 4H, Ar-H) 7.22 (dd, $J_{H,H}$ = 6.75, 1.95 Hz, 4H, Ar-H), 7.24 (d, $J_{H,H}$ = 8.45 Hz, 4H, Ar-H), 7.36 (dd, $J_{H,H}$ = 8.75, 1.9 Hz, 4H, Ar-H); ^{13}C NMR (125.8 MHz, CD_2Cl_2) δ ppm 64.4, 65.8, 103.8, 126.5, 128.2, 131.1, 132.4, 132.7, 136.7, 145.3, 147.3; IR (KBr) ν cm^{-1} 3032 (w, υ(=CH)), 2951 (m, $\upsilon_{as}(CH_3)$), 2923 (m, $\upsilon_s(CH_3)$), 2877 (s, $\upsilon(CH_3\text{-O})$), 1702 (s), 1603 (s), 1507 (s), 1487 (m), 1401 (w, $\delta_s(CH_3)$), 1382 (w, $\delta_{as}(CH_3)$), 1221 (s, $\upsilon(C_{Ar}\text{-O-C})$), 1083 (s, $\upsilon(C_{Ar}\text{-O})$), 1012 (m), 945 (m), 818 (s) 722 (w, υ(C-Cl); UV-Vis (λ_{max}[nm], ε, CH_2Cl_2) 227 (18624), 272 (20516); ESI(+) MS Calcd for $C_{31}H_{26}O_4Cl_2Na$ ([M+Na]$^+$, 555.1106), found *m/z* 555.1064; elemental analysis calcd (%) for $C_{31}H_{26}O_4Cl_2$ (533.44): C, 69.80; H, 4.91; found: C, 69.94; H, 5.11.

4,4‘-{Bis[1,3-dioxolane-(1-phenyl)-4’-diyl]-bis[(carbamic acid-*N*-phenyl-1,1-dimethylethyl ester)-4’-diyl] (**124**)

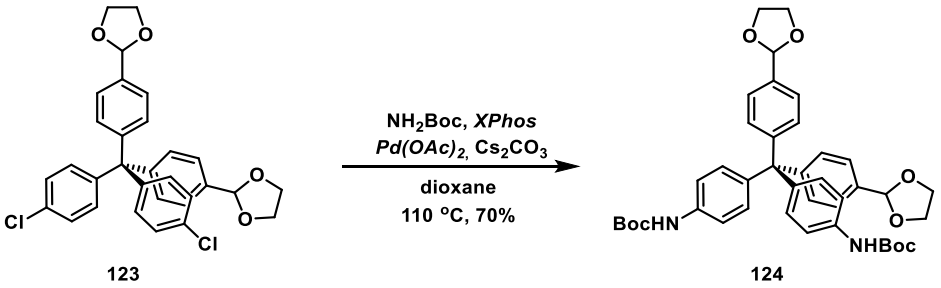

An oven-flamed, 50 mL pressure tube was charged with starting material **123** (0.5 g, 0.97 mmol), Cs_2CO_3 (0.91 g, 2.81 mmol), XPhos (0.11 g, 0.23mmol), NH_2Boc (0.28 g, 2.34 mmol) and30 mL of dry dioxane. Subsequently, solution was purged for 20min with argon and $Pd(OAc)_2$ (0.021 g, 0.0094 mmol) was added. The tube was sealed and stirred at 110 °C for 16 h. After cooling to room temperature, dioxane was removed and the residue was washed with water (100 mL) and CH_2Cl_2 (3 x 150 mL). The combined organic layer was washed with brine (100 mL), dried over $MgSO_4$ and filtered. All volatiles were removed under reduced pressure and the residue was purified by column chromatography on silica gel (200 g) in the mixture of hexane/EtOAc (7:3) to obtain 0.46 g of **124** as a yellow powder in 70% yield (R_f = 0.25, hexane/EtOAc = 7:3); m.p. 175-176 °C; ^{1}H NMR (500 MHz, CD_2Cl_2) δ ppm 1.48 (s, 18H, CH_3) 3.97-4.00 (m, 4H, CH_3), 4.06-4.11 (m, 4H, CH_3), 5.72 (s, 2H, CH), 6.57 (s, 2H, NH), 7.16 (d, $J_{H,H}$ = 8.75 Hz, 4H, Ar-H), 7.22 (dd, $J_{H,H}$ = 6.9, 1.95 Hz, 8H, Ar-H), 7.33 (d, $J_{H,H}$ = 8.4 Hz, 4H, Ar-H); ^{13}C NMR (125.8 MHz, CD_2Cl_2) δ ppm 28.4, 65.8, 80.7, 103.9, 117.9, 126.2, 131.2, 131.8, 135.2, 136.2, 136.9, 141.5, 148.4, 153.0; IR (KBr) ν cm^{-1} 3333 (b, υ(NH)), 3032 (w, υ(=CH)), 2977 (m, $\upsilon_{as}(CH_3)$), 2930 (m, $\upsilon_s(CH_3)$), 2877 (s, $\upsilon(CH_3\text{-}O)$), 1727 (s), 1594 (s), 1523 (s), 1487 (m), 1392 (m, $\delta_s(CH_3)$), 1367 (w, $\delta_{as}(CH_3)$), 1231 (s, $\upsilon(C_{Ar}\text{-}O\text{-}C)$), 1163 (s, $\upsilon(C_{Ar}\text{-}O)$), 1084 (m), 1052 (m), 1018 (m), 8198 (s); UV-Vis (λ_{max}[nm], ε, CH_2Cl_2) 254 (26961); ESI(+) HRMS Calcd for $C_{41}H_{46}N_2O_8Na$ ([M+Na]$^+$, 713.3152, found *m/z* 717.3147; elemental analysis calcd (%) for $C_{41}H_{46}O_8N_2$ (694.33): C, 70.87; H, 6.67; N, 4.03; found: C, 70.52; H, 6.61; N 3.93.

4,4'-{Bis[(carbamic acid-*N*-phenyl-1,1-dimethylethyl ester)-4'-diyl]} dibenzaldehyde (125)

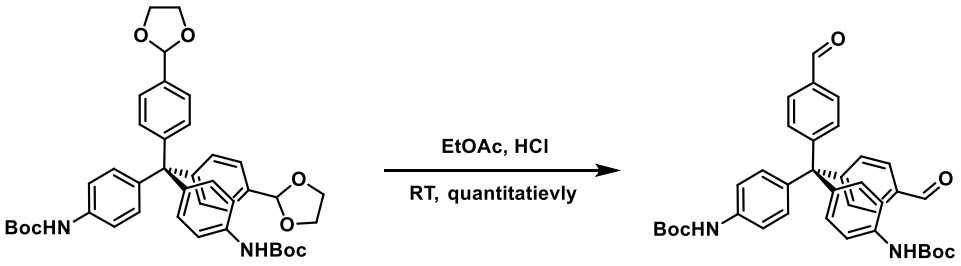

124 125

A two-neck, round bottom flask was charged with starting material **124** (0.7 g, 1 mmol), and 10 mL of ethyl acetate. Consecutively, catalytic amounts of 12 M HCl were added and the reaction mixture was vigorously stirred overnight in room temperature. Afterwards, the reaction mixture was carefully neutralized with saturated solution of $NaHCO_3$ (100 mL). The resulting two layer system was extracted with ethyl acetate (3 x 150 mL). The combined organic layer was washed with brine (100 mL), dried over $MgSO_4$ and filtered. All volatiles were removed under reduced pressure and the residue was purified by flash column chromatography on silica gel (100 g) in the mixture of hexane/EtOAc (1:1) to obtain 0.6 g of **125** as a yellow powder in 99% yield (R_f = 0.33, hexane/EtOAc = 1:1); m.p. 248-250 °C; ^{1}H NMR (500 MHz, CD_2Cl_2) δ ppm 1.40 (s, 18H, CH_3), 6.59 (s, 2H, NH), 7.13 (d, $J_{H,H}$ = 8.75 Hz, 4H, Ar-H), 7.28 (d, $J_{H,H}$ = 8.7 Hz, 4H, Ar-H), 7.43 (d, $J_{H,H}$ = 8.35 Hz, 4H, Ar-H), 7.77 (d, $J_{H,H}$ = 8.45 Hz, 4H, Ar-H); ^{13}C NMR (125.8 MHz, CD_2Cl_2) δ ppm 28.4, 65.1, 80.6, 118.2, 129.4, 131.7, 131.8, 134.9, 137.4, 140.1, 153.0, 154.5, 192.1; IR (KBr) ν cm^{-1} 3032 (w, υ(=CH)), 2951 (m, υ_{as}(CH_3)), 2923 (m, υ_s(CH_3)), 2877 (s, υ(CH_3-O)), 1702 (s), 1603 (s), 1507 (s), 1487 (m), 1401 (w, δ_s(CH_3)), 1382 (w, δ_{as}(CH_3)), 1221 (s, υ(C_{Ar}-O-C)), 1083 (s, υ(C_{Ar}-O)), 1012 (m), 945 (m), 818 (s) 722 (w, υ(C-Cl)); UV-vis (λ_{max}[nm], ε, CH_2Cl_2) 252 (31221); ESI(+) MS Calcd for $C_{37}H_{38}O_6N_2Na$ ([M+Na]$^+$, 629.2628), found *m/z* 629.2554; elemental analysis calcd (%) for $C_{37}H_{38}O_6N_2$ (606.27): C, 73.25; H, 6.31; N, 4.62; found: C, 73.33; H, 6.70; N, 4.69.

4,4'-{bis[4-(dimethoxymethylphenyl)-1,1-diyl]} dianiline (**130**)

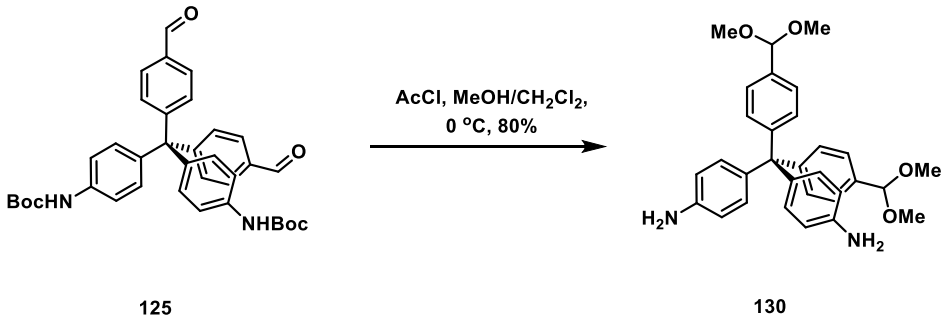

125 130

An oven flamed and argon flushed 25 mL Schlenk flask was charged with starting material **125** (0.03 g, 0.05 mmol), 2 mL of anhydrous MeOH and 5 mL of freshly distilled CH_2Cl_2 under argon stream. Solution was cooled down to 0 ^oC and AcCl (0.021 mL, 0.29 mmol) was dropwise added. The reaction mixture was stirred overnight under an inert atmosphere. Subsequently, the reaction was carefully neutralized with saturated solution of $NaHCO_3$ (50 mL) and extracted with CH_2Cl_2 (3 x 80 mL). The combined organic layer was washed with brine (500 mL), dried over $MgSO_4$ and filtered. All volatiles were removed under reduced pressure. Crude product **130** was subjected to NMR analysis. ^1H NMR (500 MHz, CD_2Cl_2) δ ppm 3.34 (s, 12H, CH_3), 5.34 (s, 2H, CH), 6.54 (d, $J_{H,H}$ = 6.6 Hz, 4H, Ar-H); 6.93 (d, $J_{H,H}$ = 8.6 Hz, 4H, Ar-H); 7.19 (d, $J_{H,H}$ = 8.4 Hz, 4H, Ar-H), 7.26-7.29 (m, 4H, Ar-H), (R_f = 0.07, hexane/EtOAc = 3:7), product unstable.

(4-Aminophenyl)carbamic acid 1,1-dimethylethyl ester (**126**)[342]

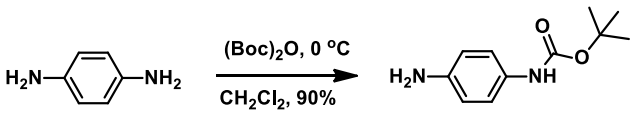

129

An oven-flamed, 250 mL two-neck round bottom flask, equipped with refluxed condenser was loaded with *p*-phenylenediamine (1 g, 9.25 mmol) and 60 mL of freshly distilled dichloromethane. The solution was purged with argon and cooled down to 0 ^oC. Precooled di-*tert*-butyl dicarbonate (0.91 g, 4.16 mmol) was dissolved in CH_2Cl_2 (5 mL) and dropwise added. Subsequently, the reaction mixture was stirred at room temperature overnight. Then, crude product was washed with water (200 mL) and extracted with CH_2Cl_2 (3 x 200 mL). The combined organic layer was washed with brine (100 mL), dried over $MgSO_4$ and filtered. All volatiles were removed under reduced pressure and the residue was purified by flash

column chromatography on silica gel (300 g) in the mixture of petroleum ether/EtOAc (2:1) to get 0.78 g of **126** as a white powder in 90% yield (R_f = 0.15, petroleum ether/EtOAc = 2:1); ^{1}H NMR (500 MHz, $CDCl_3$) δ ppm 1.51 (s, 9H, CH_3), 3.54 (s, 2H, NH_2), 6.27 (s, 1H, NH), 6.62-7.65 (b, 2H, Ar-H), 7.13 (d, $J_{H,H}$ = 8.7 Hz, 2H, Ar-H); ^{13}C NMR (125.8 MHz, $CDCl_3$) δ ppm 28.4, 78.6, 115.6, 120.9, 129.7, 142.4, 153.3.

[Bis(4-carbamic acid-*N*-phenyl-1, 1-dimethylethyl ester)] (**127**)[343]

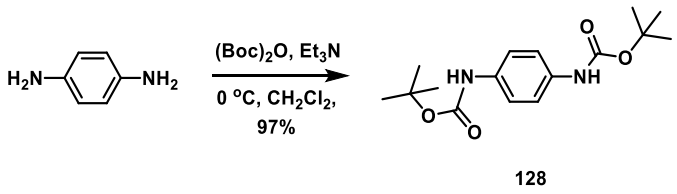

128

An oven-flamed, 250 mL two-neck round bottom flask, equipped with refluxed condenser was loaded with *p*-phenylenediamine (1 g, 9.25 mmol), dissolving it in 50 mL of freshly distilled dichloromethane and of Et_3N (2.8 mL, 20 mmol). The solution was purged with argon and cooled down to 0 ^{o}C. Precooled di-*tert*-butyl dicarbonate (4.03 g, 18.5 mmol) was dissolved in CH_2Cl_2 (10 mL) and dropwise added. Subsequently, the reaction mixture was stirred at room temperature overnight. Then, crude product was washed with water (200 mL) and extracted with CH_2Cl_2 (3 x 250 mL). The combined organic layer was washed with brine (100 mL), dried over $MgSO_4$ and filtered. All volatiles were removed under reduced pressure and the residue was purified by flash column chromatography on silica gel (500 g) in the mixture of petroleum ether/EtOAc (2:1) to get 2.78 g of **127** as a white powder in 97% yield (R_f = 0.58, petroleum ether/EtOAc = 2:1); ^{1}H NMR (500 MHz, DMSO (d_6) δ ppm 1.45 (s, 9H, CH_3), 7.29 (b, 4H, Ar-H), 7.29 (s, 2H, NH), 6.62-7.65 (b, 2H, Ar-H) 7; ^{13}C NMR (125.8 MHz, DMSO (d_6) δ ppm 28.2, 78.8, 118.6, 134.0, 152.9.

Carbamic acid, *N*-{[4-[[(4-methylphenyl)methylene]amino]phenyl]}-1,1-dimethylethyl ester(**128**)

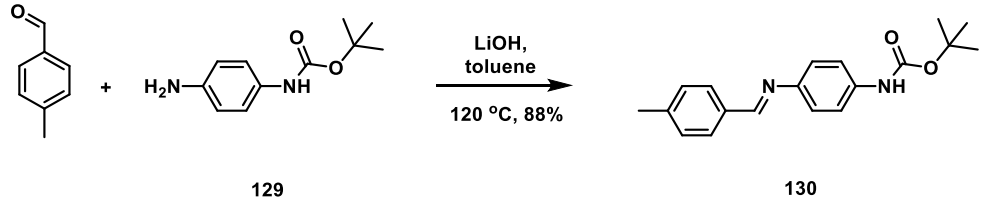

129 **130**

An oven flamed, 100 mL single neck round bottom flask, equipped with reflux condenser was charged with amine **127** (0.2 g, 0.96 mmol), *p*-tolylaldehyde (0.24 mL, 2 mmol) and

catalytic amount of anhydrous LiCl under argon atmosphere. Subsequently freshly distilled toluene (30 mL) was added. Reaction mixture was refluxed overnight under argon atmosphere. Upon cooling, yellow product precipitated, which filtrated, and obtained material was washed with additional 50 mL of toluene giving 0.26 g of **128** as a yellow powder in 88% yield. M.p. 113-114 °C; ^{1}H NMR (500 MHz, CD_2Cl_2) δ ppm 1.51 (s, 9H, CH_3), 2.44 (s, 3H, CH_3), 6.66 (s, 1H, NH), 7.19 (d, $J_{H,H}$ = 8.45 Hz, 2H, Ar-H), 7.29 (d, $J_{H,H}$ = 7.5 Hz, 2H, Ar-H), 7.39 (d, $J_{H,H}$ = 7.75 Hz, 2H, Ar-H), 7.78 (d, $J_{H,H}$ = 7.55 Hz, 4H, Ar-H); ^{13}C NMR (125.8 MHz, CD_2Cl_2) δ ppm 21.7, 28.4, 80.7, 119.5, 119.9, 129.0, 129.8, 134.3, 137.2, 142.2, 147.3, 153.1, 159, 191.2; IR (KBr) ν cm^{-1} 3387 (m, υ(NH)), 3029 (w, υ(=CH)), 2985 (m, $\upsilon_{as}(CH_3)$), 2930 (m, $\upsilon_s(CH_3)$), 2880 (s, υ(*t*-Bu-O)),1702 (s, υ(C=O)), 1622 (w, υ(C=N)), 1589 (m, υ_2^o(HNC=OR)), 1518 (s), 1408 (m, $\delta_s(CH_3)$), 1388 (m, $\delta_{as}(CH_3)$), 1309 (m), 1232 (s, υ(-C-C=N-C)), 1160 (s, υ(C-O)), 1012 (m, υ(C-O-N)), 945 (m), 814 (s) 768 (w, ρ(HNC=OR)); UV-Vis (λ_{max}[nm], ε, CH_2Cl_2) 275 (19969), 326 (15827); ESI(+) MS Calcd for $C_{19}H_{22}N_2O_2Na$ ($[M + Na]^+$, 333.1579), found *m/z* 333.1619; elemental analysis calcd (%) for $C_{19}H_{22}N_2O_2$ (310.17): C, 73.52; H, 7.14; N, 9.03: found: C, 73.66; H, 7.38; N, 9.25.

***N*^{1}-(Phenylmethylene)-1,4-benzenediamine** (**129**)

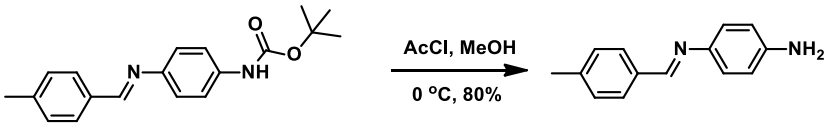

130 131

An oven flamed and argon flashed 50 mL Schlenk flask was charged with starting material **128** (0.33 g, 1.6 mmol), and anhydrous MeOH (30 mL) under argon stream. Solution was cooled down to 0 ^{o}C and AcCl (0.8 mL, 11 mmol) was dropwise added. The reaction mixture was stirred overnight under inert atmosphere. Subsequently, the reaction was carefully neutralized with 80 mL of saturated solution of $NaHCO_3$ and extracted with CH_2Cl_2 (3 x 100 mL). The combined organic layer was washed with brine (100 mL), dried over $MgSO_4$ and filtered. All volatiles were removed under reduced pressure. The yield of crude product was determined by NMR analysis and was found to be 80%, it was assessed according to the integration of the imine protons). ^{1}H NMR (500 MHz, CD_2Cl_2) δ ppm 2.39 (s, 3H, CH_3), 5.30 (s, 2H, NH), 7.26-7.40 (m, 5H, Ar-H), 7.80 (d, $J_{H,H}$ = 7.95 Hz, 2H, Ar-H)), 8.48 (s, 1H, =NH); ^{13}C NMR (125.8 MHz, CD_2Cl_2) δ ppm 21.2, 115.04, 121.6, 128.5, 129.3, 133.7, 141.8, 149.8, 156.2, 159.3.

[4-Iodo-(4'-carbamic acid-*N*-phenyl-1, 1-dimethylethyl ester)] (131)[344]

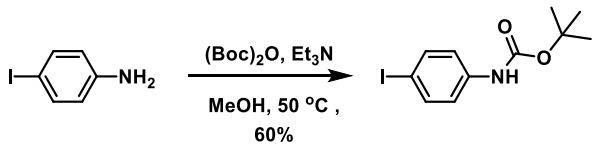

131

An oven flamed, two-neck round bottom flask, equipped with reflux condenser was loaded with 4-iodaniline (2 g, 9.13 mmol), di-*tert*-butyl dicarbonate (3.98 g, 18 mmol), dry triethyl amine (4 mL) and anhydrous methanol (18 mL) under argon. The reaction mixture was heated at 50 ^{o}C and stirred overnight. After cooling, solvents were removed and the crude product was extracted with EtOAc (3x 200 mL) and with water (150 mL). The combined organic layer was washed with brine (100 mL), dried over $MgSO_4$ and filtered. All volatiles were removed under reduced pressure and the residue was purified by column chromatography on silica gel (500 g) in the mixture of hexane/EtOAc (1:1) to get 1.75 g of **131** as a white powder in 60% yield (R_f = 0.42, hexane/EtOAc = 1:1); ^{1}H NMR (500 MHz, $CDCl_3$) δ ppm 1.51 (s, 9H, CH_3), 6.45 (s, 1H, NH), 7.14 (d, $J_{H,H}$ = 8.5 Hz, 2H, Ar-H) 7.57 (dd, $J_{H,H}$ = 6.9, 1.85 Hz, 2H, Ar-H); ^{13}C NMR (125.8 MHz, $CDCl_3$) δ ppm 28.4, 81.4, 85.9, 120.5, 138, 138.3, 152.6.

Carbamic acid, *N*-[4'-formyl(1,1'-biphenyl)-4-yl]-1,1-dimethylethyl ester (132)[345]

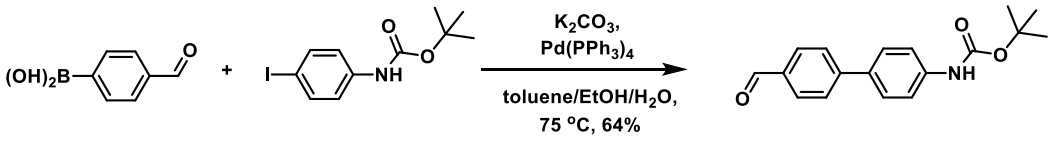

131 132

Biphenyl **133** was synthesized by using similar method to the published procedure.[345] 4-Formylphenylboronic acid (0.95 g, 6.34 mmol), Boc-protected amine **131** (1.35 g, 4.23 mmol), potassium carbonate (1.75 g, 12.66 mmol), toluene (21 mL), ethanol (7 mL) and water (7 mL) were loaded to the 250 mL two-neck round bottom flask, equipped with reflux condenser. The Solution was flushed with argon and tetrakis(triphenylphosphine)palladium(0) (0.034 g, 0. 29 mmol) was added. Reaction mixture was heated at 75 ^{o}C overnight under argon atmosphere. Afterwards solvents were removed. Crude product was diluted with dichloromethane (200 mL) and extracted with brine (100 mL). Aqueous layer was separated and washed with dichloromethane (2 x 200 mL). Organic layers were combined, dried over magnesium sulfate and filtered. Solvents were evaporated

and crude product was purified on silica gel (400 g) in hexane/CH_2Cl_2 (1:2) yielding product **132** as a yellow solid (0.19 g, 64%). (R_f = 0.19, hexane/CH_2Cl_2 1:2); ^{1}H NMR (500 MHz, $CDCl_3$) δ ppm 1.54 (s, 9H, CH_3), 6.61 (s, 1H, NH), 7.48 (d, $J_{H,H}$ = 8.5 Hz, 2H, Ar-H), 7.58 (d, $J_{H,H}$ = 8.65 Hz, 2H, Ar-H), 7.24 (d, $J_{H,H}$ = 8.25 Hz, 2H, Ar-H), 7.93 (d, $J_{H,H}$ = 8.35 Hz, 2H, Ar-H); ^{13}C NMR (125.8 MHz, $CDCl_3$) δ ppm 28.5, 81.0, 118.9, 127.3, 128.1, 130.5, 134.3, 135, 139, 146.7, 152.7, 192.1.

Polymer 133

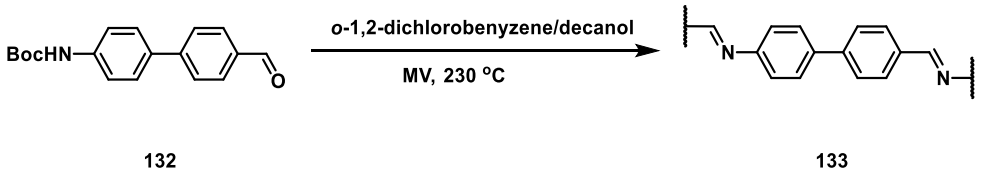

132 133

Oven-flamed and argon flushed 20 mL tube was charged with monomer **133** (0.18 g, 0.61 mmol), and mixture of *o*-1,2-dichlorobenzene/decanol (20/2 mL). The solution was purged with argon over 30 min, the tube was sealed and the reaction was carried out in microwave reactor over 1.5 h at 230 °C. Upon cooling, precipitated yellow solid was filtered and washed with 200 mL of Et_2O. Subsequently, crude product was sonicated 6h against EtOAc and the next 6 h against hexane. Orange powder was filtrated and dried under vacuum over 4 days providing 0.12 mg of polymer **133** in 71% yield. Elemental analysis calcd (%) for $(C_{13}H_9N)_n \cdot 3\ H_2O$ (179.07): C, 66.94; H, 6.48; N, 6.00: found: C, 67.65; H, 5.35; N, 5.35.

For the detail analysis see paragraph **4.3**

Polymer 134

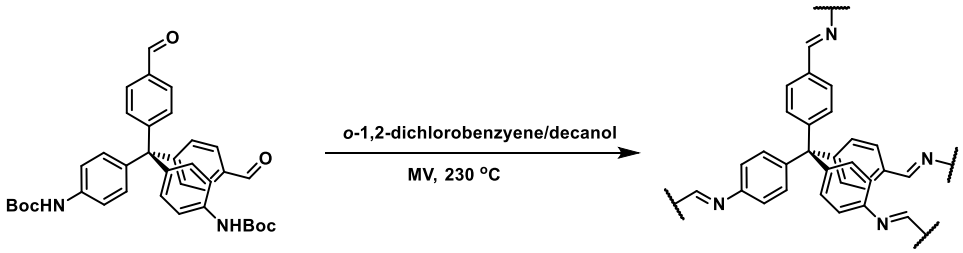

125 134

Oven-flamed and argon flushed 20 mL tube was charged with monomer **125** (0.15 g, 0.25 mmol) and the mixture of *o*-1,2-dichlorobenzene/decanol (4/0.4 mL). The solution was purged with argon over 30 min, the tube was sealed and the reaction was carried out in microwave reactor over 2 h at 230 ^{o}C. Upon cooling, precipitated yellow solid was filtered and washed with 200 mL of Et_2O. Subsequently, crude product was sonicated 6h against EtOAc and the next 6 h against hexane. Orange powder was filtrated and dried under vacuum over 4 days getting 0.091 mg of polymer **134** in 65% yield. Elemental analysis calcd (%) for $(C_{27}H_{12}N_2)_n \cdot 5\ H_2O$ (460.20): C, 70.42; H, 6.13; N, 6.08: found: C, 70.71; H, 5.41; N, 5.18.

For the detail analysis see paragraph **4.3**

7 References

1 R.M. Metzger, *Chem.Rev*. **2015**, *115*, 5056-5115

2 G.E. Moore, Cramming more components onto integrated circuits. *Electronics*, **1965**, *38* (8):114.

3 G.E. Moore, *IEEE Solid-State Circuits Soc. Newsl*. **2006**, *11*, 33-35.

4 N. Robertson, C.A. McGowan, *Chem. Soc. Rev*. **2003**, *32*, 96-103.

5 J.J.L. Morton, D. R. McCamey, M. A. Eriksson, S. A. Lyon, *Nature* **2011**, *479*, 345-353.

6 R.P. Feynman, "*Engineering and Science*, Volume *23*, 5, February **1960**," can be found at http://resolver.caltech.edu/CaltechES:23.5.0, 1960.

7 H. Choi, C.C.M Mody, *The Long History of Molecular Electronics, Microelectronics Origins of Nanotechnology*, **2009**, Social Studies of Science *39/11*, 11-50.

8 S.V. Aradhya, L. Venkataraman, *Nat. Nanotechnol.* **2013**, *8*, 399-410.

9 H. Kuhn, D. Möbius, *Angew. Chem. Int. Ed.* **1971**, *10*, 620-637.

10 A. Aviram, M.A. Ratner, *Chem. Phys. Lett.* **1974**, *29*, 277-283.

11 H. Song, M.A. Reed, T. Lee, *Adv. Mater.* **2011**, *23*, 1583-1608.

12 R.L. Carroll, Ch.B. Gorman, *Angew. Chem. Int. Ed.* **2002**, *41*, 4378-440.

13 N. Weibel, S Grunder, M. Mayor, *Org. Biomol. Chem.* **2007**, *5*, 2343-2353.

14 Z.J. Donhauser, B.A. Mantooth, K.F. Kelly, L.A. Bumm, J.D. Monell, J.J. Stapleton, J. Price, A.M. Rawlett, D.L. Allara, J.M. Tour, *Science* **2001**, *292*, 2303-2307.

15 B.Q. Xu, N.J. Tao, *Science* **2003**, *301*, 1221-1223.

16 W. Haiss, H. Van Zalinger, S.J. Higgins, D. Bethell, H. Hobenreich, D.J. Schiffrin, R.J. Nichols, *J. Am. Chem. Soc.* **2003**, *125*, 15294-15295.

17 T. Dadosh, Y. Gordin, R. Krahne, I. Khivrich, D. Mahalu, V. Frydman, J. Sperling, A. Yacoby, I. Bar-Joseph, *Nature* **2005**, *436*, 677-680.

18 R.L. McCreery, *Chem. Mater*. **2004**, *16*, 4477-4496.

19 C. Li, A. Mishchenko, T. Wandlowski, *Topp. Curr. Chem.* **2012**, *313*, 121-188.

20 N.J. Tao, *Nat. Nanotechnol.* **2006**, *1*, 173-181.

21 L. Venkataraman, J.E. Klare, C. Nuckolls, M.S. Hybertsen, M.L. Steigerwald, *Nature* **2006**, *442*, 904-907.

22 L.A. Bumm, J.J. Arnold, T.D. Dunbar, D.L. Allara, P.S. Weiss, *J. Phys. Chem. B* **1999**, *103*, 8122-8127.

23 S. Wu, M.T. González, R. Huber, S. Grunder, M. Mayor, C. Schönenberger, M. Calame, *Nat. Nanotechnol.* **2008**, *3*, 569-574.

24 G. Binnig, H. Rohrer, *Ibm J. Res. Dev*. **1986**, *30*, 355-369.

25 G. Binnig, H. Rohrer, *Angew. Chem. Int. Ed.* **1987**, *26*, 606-614.

26 B. Bushan, O. Marti, Nanotribology and Nanomechanics I, *Scanning Probe Microscopy – Principle of Operation, Instrumentation, and Probes*, 2011, 37-110, Springer.

27 N.A. Poggi, L.A. Bottomley, P.T. Lillehei, *Anal. Chem*. **2002**, *74*, 2851-2862.

28 S.N. Magonov, M.-H. Whangbo, Surface Analysis with STM and AFM: Experimental and Theoretical Aspects of Image Analysis; Weinheim: New York, 1996.

29 G.E. McGuire, P.S. Weiss, J.G. Kushmerick, J.A. Johnson, S.J. Simko, R.J. Nemanich, *Anal. Chem*. **1997**, *69*, 231-250.

30 G. Haugstad, Atomic Force Microscopy: Understanding Basic Modes and Advanced Applications, John Wiley & Sons, 2012.

31 C. J. Chen, Introduction to Scanning Tunneling Spectroscopy, 2nd Ed., Oxford University Press, 2008.

32 J. Moreland, J.W. Ekin, *Appl. Phys. Lett*. **1985**, *47*, 175-177.

33 J. Moreland, J.W. Ekin, *J. Appl. Phys*. **1985**, *58*, 3888-3895.

34 C.J. Muller, J.M. Vanruitenbeek, L. Dejongh, *J. Inst. Phys. Conf. Ser*. **1992**, 171-174.

35 C.J. Muller, J.M. Vanruitenbeek, L.J. Dejongh, *Phys. Rev. Lett*. **1992**, *69*, 140-143.

36 E. Scheer, N. Agraït, J.C. Cuevas, A.L. Yeyati, B. Ludoph, A. Martin-Rodero, G.R. Bollinger, J.M. van Ruitenbeek, C. Urbina, *Nature* **1998**, *394*, 154-157.

37 M. A Reed, C. Zhou, C.J. Muller, T.P. Burgin, J.M Tour, *Science* **1997**, *278*, 252-254.

38 C. Zhou, M.R. Desphande, M. A Reed, J.M Tour, *Appl. Phys. Lett*. **1997**, *71*, 611-613.

39 D. Xiang, H. Jeong, T. Lee, D. Mayer, *Adv. Mat. 2013*, *25*, 4845-4867.

40 D. Xiang, X. Wang, Ch. Jia, T. Lee, X. Guo. *Chem. Rev.* **2016**, *116*, 4318-4440.

41 C. Huang, A.V. Rudnev, W. Hong, Th. Wandlowski, *Chem. Soc. Rev*. **2015**, *44*, 889-901.

42 E. Leary, A. La Rosa, M.T. González, G. Rubio-Bollinger, N. Agrait, N. Martin, *Chem. Soc. Rev*. **2014**, *44*, 920-942 .

43 R.J. Nichols, S.J. Higgins, *Annu. Rev. Anal. Chem*. **2015**, *8*, 389-417.

44 X. Li, J. He, J. Hihath, B. Xu, S.M. Lindsay, N. Tao, *J. Am. Chem. Soc.* **2006**, *128*, 2135-2141.

45 J. Ulrich, D. Esreil, W. Pontius, L. Venkataraman, D. Millar, L.H. Doerrer, *J. Phys. Chem. B* **2006**, *110*, 2462-2466.

46 E.A. Osorio, T. Bjørnholm, J. -M. Lehn, M. Ruben, H.S. van der Zant, *J. Phys. Condens. Matter* **2008**, *20*, 374121.

47 A. Danilov, S. Kubatkin, S. Kafanov, P. Hedegård, N. Stuhr-Hansen, K. Moth-Poulsen, T. Bjørnholm, *Nano Lett.* **2008**, *8*, 323-327.

48 J.C. Love, L.A. Estroff, J.K. Kriebel, R.G. Nuzzo, G.M. Whitesides, *Chem. Rev.* **2005**, *105*, 1103-1170.

49 G. Roberts, *Langmuir-Blodgett Films;* Springer US: **1990**.

50 G. Decher, *Langmuir-Blodgett Films: An Introduction* Cambridge University Press: Cambridge, UK, **1996**.

51 F. Chen, X. Li, J. Hihath, Z. Huang, N. Tao, *J. Am. Chem. Soc.* **2006**, *128*, 15874-15881.

52 D. Dulić, F. Pump, S. Campidelli, P. Lavie, G. Cuniberti, A. Filoramo, *Angew. Chem. Int. Ed.* **2009**, *48*, 8273-8276.

53 I. Diez-Perez, Z. Li, J. Hihath, J.H. Li, C.Y. Zhang, X.M. Yang, L. Zang, Y.J. Dai, X.L. Feng, K. Müllen, *Nat. Commun.* **2010**, *1*, 1-5.

54 C. Li, I. Pobelov, T. Wandlowski, A. Bagrets, A. Arnold, F. Evers, *J. Am. Chem. Soc.* **2008**, *130*, 318-326.

55 L. Venkataraman, J.E. Klare, I.W. Tam, C. Nuckolls, M.S. Hybertsen, M.L. Steigerwald, *Nano Lett.* **2006**, *6*, 458-462.

56 Y.S. Park, A.C. Whalley, M. Kamenetska, M.L. Steigerwald, M.S. Hybertsen, C. Nuckolls, L. Venkataraman, *J. Am. Chem. Soc.* **2007**, *129*, 15768-15769.

57 M. Kamenetska, S.Y. Quek, A.C. Whalley, M.L. Steigerwald, H.J. Choi, S.G. Louie, C. Nuckolls, M.S. Hybertsen, J.B. Neaton, L. Venkataraman, *J. Am. Chem. Soc.* **2010**, *132*, 6817-6821.

58 W. Hong, D.Z. Manrique, P. Moreno-García, M. Gulcur, A. Mishchenko, C. Lambert, C. M.R. Bryce, T. Wandlowski, *J. Am. Chem. Soc.* **2012**, *134*, 2292-2304.

59 E.S. Tam, J.J. Parks, W.W. Shum, Y. W. Zhong, M.B. Santiago-Berrios, X. Zheng, W.T. Yang, G.K.L. Chan, H.D. Abruna, D.C. Ralph, *ACS Nano* **2011**, *5*, 5115-5123.

60 Y. Ie,T. Hirose, H. Nakamura, M. Kiguchi, N. Takagi, M. Kawai, Y. Aso, *J. Am. Chem. Soc.* **2011**, *133*, 3014-3022.

61 S. Yasuda, S. Yoshida, J. Sasaki, Y. Okutsu, T. Nakamura, A. Taninaka, O. Takeuchi, H. Shigekawa, *J. Am. Chem. Soc.* **2006**, *128*, 7746-7747.

62 B.M. Boardman, J.R. Widawsky, Y.S. Park, C.L Schenck, L.; Venkataraman, M.L. Steigerwald, C. Nuckolls, *J. Am. Chem. Soc.* **2011**, *133*, 8455-8457.

63 K. Yokota, M. Taniguchi, T. Kawai, *J. Am. Chem. Soc.* **2007**, *129*, 5818-5819.

64 Y. Ie, T. Hirose, A. Yao, T. Yamada, N. Takagi, M. Kawai, Y. Aso, *Phys. Chem. Chem Phys.* **2009**, *11*, 4949-4951

65 C.A. Martin, D. Ding, J.K. Sørensen, T. Bjørnholm, J.M. van Ruitenbeek, H.S. van der Zant, *J. Am. Chem. Soc.* **2008**, *130*, 13198-13199.

66 E. Leary, M.T. Gonzalez, C. van der Pol, M.R. Bryce, S. Filippone, N. Martin, G. Rubio-Bollinger, N. Agrait, *Nano Lett.* **2011**, *11*, 2236-2241.

67 E. Lörtscher, V. Geskin, B. Gotsmann, J. Fock, J.K. Sørensen, T. Bjørnholm, J. Cornil, H.S. van der Zant, H. Riel, *Small* **2013**, *9*, 209-214.

68 B. Kim, J.M. Beebe, Y. Jun, X.-Y. Zhu, C.D. Frisbie, *J. Am. Chem. Soc.* **2006**, *128*, 4970.

69 E. Lörtscher, C.J. Cho, M. Mayor, M. Tschudy, C. Rettner, H. Riel, *ChemPhysChem* **2011**, *12*, 1677-1682.

70 A. Mishchenko, L.A. Zotti, D. Vonlanthen, M. Bürkle, F. Pauly, J.C Cuevas, M. Mayor, T. Wandlowski, *J. Am. Chem. Soc.* **2011**, *133*, 184-187.

71 L.A. Zotti, T. Kirchner, J.C. Cuevas, F. Pauly, T. Huhn, E. Scheer, A. Erbe, *Small* **2010**, *6*, 1529-1535.

72 C.H. Ko, M.J. Huang, M. D. Fu, C.H. Chen, *J. Am. Chem. Soc.* **2010**, *132*, 756-764.

73 D. Gao, F. Scholz, H.-G. Nothofer, W.E. Ford, U. Scherf, J.M. Wessels, A. Yasuda, A., F. von Wrochem, *J. Am. Chem. Soc.* **2011**, *133*, 5921-5930.

74 Y.J. Xing, T.H. Park, R. Venkatramani, S. Keinan, D.N. Beratan, M.J. Therien, E. Borguet, *J. Am. Chem. Soc.* **2010**, *132*, 7946-7956.

75 A.V. Tivanski, Y.F He, E. Borguet, H.Y. Liu, G.C. Walker, D.H Waldeck, *J. Phys. Chem. B* **2005**, *109*, 5398-5402.

76 Z. Li, M. Smeu, M.A. Ratner, E. Borguet, *J. Phys. Chem. C* **2013**, *117*, 14890-14898.

77 A.V. Zhukhovitskiy, M.G. Mavros, T. van Voothis, J.A. Johnson, *J. Am. Chem. Soc.* **2013**, *135*, 7418-7421.

78 C.M. Crudden, J.H. Horton, I.I. Ebralidze, O.V. Zenkina, A.B. McLean, B. Drevniok, Z. She, H.-B. Kraatz, N.J. Mosey, T. Seki, E.C. Keske, J.D. Leake, A. Rousina-Webb, G. Wu, *Nat. Chem.* **2014**, *6*, 409-414.

79 M. Carrara, F. Nüesch, L. Zuppiroli, *Synthetic Metals* **2001**, *121*, 1633-1634.

80 V. Kaliginedi, A.V. Rudnev, P. Moreno-Garcia, M. Baghernejad, C. Huang, C.; Hong, T. Wandlowski, *Phys. Chem. Chem. Phys.* **2014**, *16*, 23529-23539.

81 C.R. Arroyo, E. Leary, A. Castellanos-Gomez, G. Rubio-Bollinger, M.T. Gonzalez, N. Agrait, *J. Am. Chem. Soc.* **2011**, *133*, 14313-14319.

82 W.B. Chen, J.R. Widawsky, H. Vazquez, S.T. Schneebeli, M.S. Hybertsen, R. Breslow, L. Venkataraman, *J. Am. Chem. Soc.* **2011**, *133*, 17160-17163.

83 M. Kiguchi, S. Kaneko, *Chem. Phys. Chem.* **2012**, *13*, 1116-1126.

84 M. Mayor, H.B. Weber, J. Reichert, M. Elbing, C. von Hänisch, D. Beckmann, M. Fischer, *Angew. Chem. Int. Ed.* **2003**, *42*, 5834-5838.

85 D. Vonlanthen, A. Mishchenko, M. Elbing, M. Neuburger, T. Wandlowski, M. Mayor, *Angew. Chem. Int. Ed.* **2009**, *48*, 8886-8890.

86 A. Mishchenko, D. Vonlanthen, V. Meded, M. Bürkle, C. Li, I.V. Pobelov, A. Bagrets, J.K Viljas, F. Pauly, F. Evers, M. Mayor, T. Wandlowski, *Nano Lett.* **2010**, *10*, 156-163.

87 M.L. Perrin, R. Frisenda, M. Koole, J.S. Seldenthuis, J.A.C. Gil, H. Valkanier, J.C. Hummelen, N. Renaud, F.C Grozema, J.M. Thijssen, D. Dulić, H.S. van der Zant, *Nat. Nanotechnol.* **2014**, *9*, 830-834.

88 D. McLachlan-Jr, H. T. Sumsion, *Acta Cryst*. **1950**, *3*, 217-219

89 M. Gomberg, *J. Am. Chem. Soc*. **1898**, *20*, 773-780.

90 F. Ulmann, A. Münzhauber, *Ber. Dtsch. Chem. Ges*. **1903**, *36*, 404.

91 Th. J. Zimmermann, Th. J. J. Müller, *Synthesis* **2002**, *9*, 1157-1162

92 M. Simard, D. Su, J.D. Wuest, *J. Am. Chem. Soc* **1991**, *113*, 4696-4698

93 D. Su, F.M. Menger, *Tetrahedron Lett.* **1999**, *40*, 9157-9161.

94 B. F. Hoskins, R. Robson, *J. Am. Chem. Soc*. **1990**, *112*, 1546-1554.

95 L.M. Wilson, A.C. Griffin, *J. Mat. Chem. C* **1993**, *3*, 991-994.

96 M. Grimm, B. Kirste, H. Kurreck, *Angew. Chem. Int. Ed. Engl.* **1986**, *25*, 1096-1097.

97 F.A. Neugebauer, H. Fischer, R. Bernhardt, *Chem. Ber*. **1976**, *109*, 2389-2394.

98 D. Su, F.M. Menger, *Tetrahedron Lett*. **1997**, *38*, 1485-1488.

99 O. Mongin, A. Gossauer, *Tetrahedron Lett*. **1996**, *22*, 3825-3828.

100 O. Mongin, A. Gossauer, *Tetrahedron Lett*. **1997**, *20*, 6835-3846.

101 Ch.I. Schilling, O. Plietzch, M. Nieger, T. Muller, S. Bräse, *Eur. J. Org. Chem*. **2011**, 1743-1754.

102 T.J. Zimmermann, O. Freudel, R. Gompper, T.J.J. Müller, *Eur. J. Org. Chem*. **2000**, 3305-3312.

103 J.-H. Fournier, X. Wang, J.D. Wuest, *Can. J. Chem*. **2003**, *81*, 376-380.

104 Ch.I. Schilling, S. Bräse, *Org. Biomol. Chem* **2007**, *5*, 3586-3588.

105 L. Monnerau, T. Muller, S. Bräse, Adv. Func. Mater. **2014**, *24*, 1054-1058.

106 For the recent Review articles: (a) Y. M. Chabre, R.Roy, *Chem. Soc. Rev*. **2013**, *42*, 4657-4708 (b) W. Wu, R. Tang, Q. Li, Z. Li, *Chem. Soc. Rev*. **2015**, *44*, 3997-4022 (c) B.A.G. Hammer, R. Moritz, R. Stangenberg, M. Baumgarten K. Müllen, *Chem. Soc.Rev*. **2015**, *44*, 4072-4090 (d) B.A.G. Hammer, K. Müllen, *Chem. Rev*. **2016**, *116*, 2103-2140

107 M. Valášek, M. Lindner, M. Mayor, *Beilstein J. Nanotechnol.* **2016**, *7*, 374-405.

108 T. Sakata, S. Murayama, A. Ueda, H. Otsuka, Y. Miyahara, *Langmuir* **2007**, *23*, 2269-2272.

109 D. Hirayama, K. Takimiya, Y. Aso, T. Otsubo, T. Hasobe, H. Yamada, H. Imahori, S. Fukuzumi, Y. Sakata, *J. Am. Chem. Soc*. **2002**, *124*, 532-533.

110 S. -E. Zhu, Y. -M. Kuang, F. Geng, J. -Z. Zhu, C. -Z. Wang, Y. -J. Yu, Y. Luo, Y. Xiao, K. -Q. Liu, Q. -S. Meng, L. Zhang, S. Jiang, Y. Zhang, G. -W. Wang, Z. -C. Dong, J. G. Hou, *J. Am. Chem. Soc*. **2013**, *135*, 15794-15800.

111 L. Wei, K. Padmaja, W. J. Youngblood, A. B. Lysenko, J.S. Lindsey, D. F. Bocian, *J. Org. Chem*. **2004**, *69*, 1461-1469.

112 Q. Li, A. V. Rukavishnikov, P. A. Petuhkov, T.O. Zaikova, C. Jin, J. F. W. Keana, *J. Org. Chem*. **2003**, *68*, 4862-4869.

113 K. -Y. Chen, O. Ivashenko, G. T. Carroll, J. Robertus, J. C. M. Kistemaker, G. London, W. R. Browne, P. Rudolf, B. L. Feringa, *J. Am. Chem. Soc.* **2014**, *136*, 3219-3224.

114 T. C. Pijper, O. Ivashenko, M. Walko, P. Rudolf, W. R. Browne, B. L. Feringa, *J. Phys. Chem. C* **2015**, *119*, 3648-3657.

115 E. Galoppini, W. Guo, W. Zhang, P. G. Hoertz, P. Qu, G. J. Meyer, *J. Am. Chem. Soc*. **2002**, *124*, 7801-7811.

116 B. Long, K. Nikitin, D. Fitzmaurice, *J. Am. Chem. Soc*. **2003**, *125*, 5152-5160.

117 Y. Kuramochi, A. Sandanayaka, A. Satake, Y. Araki, K. Ogawa, O. Ito, Y. Kobuke, *Chem. Eur. J*. **2009**, *15*, 2317-2327.

118 J. Hierrezuelo, E. Guillén, J. M. López-Romero, R. Rico, M. R. López-Ramírez, J. C. Otero, C. Cai, *Eur. J. Org. Chem.* **2010**, *29*, 5672-5680.

119 K. Nikitin, K.; Lestini, M. Lazzari, S. Altobello, D. Fitzmaurice, *Langmuir* **2007**, *23*, 12147-12153.

120 J.A. Hutchison, H. Uji-i, A. Deres, T. Vosch, S. Rocha, S. Müller, A.A. Bastian, J. Enderlein, H. Nourouzi, C. Li, A. Herrmann, K. Müllen, F. De Schryver, J. Hofkens, *Nat. Nanotechnol*. **2014**, *9*, 131-136.

121 J. Rodríguez-López, N.L. Ritzert, J.A. Mann, C. Tan, W.R. Dichtel, H.D. Abruña, *J. Am. Chem. Soc*. **2012**, *134*, 6224-6236.

122 J.A. Mann, W. R. Dichtel, *ACS Nano.* **2013**, *7*, 7193-7193.

123 S. Ramachandra, K. C. Schuermann, F. Edafe, B. Belser, C.A. Nijhuis, W.F. Reus, G.M. Whitesides, L. De Cola, *Inorg. Chem*. **2011**, *50*, 1581-1591.

124 J. Kim, B. Chen, T.M. Reineke, H.L. Li, M. Eddaoudi, D.B. Moler, M. O'Keeffe, O.M. Yaghi, *J. Am. Chem. Soc*. **2001**, *123*, 8239-8247

125 H.M. El-Kaderi, J.R. Hunt, J.L. Mendoza-Cortés, A.P. Côté, R.E. Taylor, M. O'Keeffe, Omar M. Yaghi, *Science* **2007**, *316*, 268-272.

126 W.J. Oldham-Jr, R.J. Lachiotte, G.C. Bazan, *J. Am. Chem. Soc*. **1998**, *120*, 2987-2988

127 S. Wang, W.J. Oldham-Jr, R.A. Hudack-Jr, G.C. Bazan, *J. Am. Chem. Soc*. **2000**, *122*, 5695-5709.

128 M.R. Robinson, S. Wang, G.C. Bazan, Y. Cao, *Adv. Mat.* **2000**, *12*, 1701-1704.

129 S. Sengupta, S.K. Sadhukhan, *Tetrahedron Lett.* **1999**, *40*, 9157-9161.

130 S. Sengupta, P. Purkayastha, *Org. Biomol. Chem.* **2003**, *1*, 436-440.

131 S. Sengupta, S.K. Sadhukhan, S. Muhuri, *Synthesis* **2003**, *15*, 2329-2332.

132 S. Sengupta, S. Muhuri, *Tetrahedron Lett.* **2004**, *45*, 2895-2898.

133 H.-Ch. Yeh, R.-H. Lee, L.-H. Chan, T.-Y.J. Lin, Ch.-T. Chen, E. Balasubramaniam, Y.-T. Tao, *Chem. Mat*. **2001**, *13*, 2788-2796.

134 X.-M. Liu, Ch. He, J. Huang, J. Xu, *Chem. Mat*. **2005**, *17*, 434-441.

135 H. Zhao, Ch. Tanjutco, S. Thayumanavan, *Tetrahedron Lett.* **2001**, *43*, 4421-4424.

136 S. Sengupta, S.K. Sadhukhan, S. Muhuri, *Tetrahedron Lett.* **2002**, *43*, 3521-3524.

137 Ch. Lambert, W. Gaschler, G. Nöll, M. Weber, E. Schmälzlin, Ch. Bräuchle, K. Meerholz, *J. Chem. Soc. Perkin Trans. 2* **2001**, 964-974.

138 T. Qin, G. Zhou, H. Sheiber, R. E. Bauer, M. Baumgarten, Ch.E. Anson, E.J.W. List, K. Müllen, *Angew. Chem. Int. Ed.* **2008**, *47*, 8292-8296.

139 R.E. Bauer, J.C.G. Clark, K. Müllen, *New J. Chem*. **2007**, *31*, 1275–1282.

140 D. Lubczyk, M. Grill, M. Baumgarten, S. R. Waldvogel, K. Müllen, *ChemPlusChem* **2012**, *77*, 102–105.

141 F. Köhn, J. Hofkens, U.-M. Wiesler, M. Cotlet, M. van der Auweraer, K. Müllen, F. C. De Schryver, *Chem. – Eur. J*. **2001**, *7*, 4126–4133.

142 K. Chiad, M. Grill, M. Baumgarten, M. Klapper, K. Müllen, *Macromolecules* **2013**, **46**, 3554–3560.

143 R. Bauer, D. Liu, A. Ver Heyen, F. De Schryver, S. De Feyter, K. Müllen, *Macromolecules* **2007**, *40*, 4753–4761.

144 R. Stangenberg, I. Saeed, S. L. Kuan, M. Baumgarten,T. Weil, M. Klapper, K. Müllen, *Macromol. Rapid Commun*. **2014**, *35*, 152–160.

145 C. Minard-Basquin, T. Weil, A. Hohner, J. O. Rädler, K. Müllen, *J. Am. Chem. Soc.* 2003, 125, 5832–5838.

146 A. Herrmann, G. Mihov, G. W. M. Vandermeulen, H.-A.Klok, K. Müllen, *Tetrahedron,* **2003**, *59*, 3925–3935.

147 G. Mihov, D. Grebel-Koehler, A. Lübbert, G. W. M.Vandermeulen, A. Herrmann, H.-A. Klok, K. Müllen, *Bioconjugate Chem*. **2005**, *16*, 283–293

148 M. Mondeshki, G. Mihov, R. Graf, H. W. Spiess, K. Müllen, P. Papadopoulos, A. Gitsas G. Floudas, *Macromolecules* **2006**, *39*, 9605–9613.

149 R. Stangenberg, Y. Wu, J. Hedrich, D. Kurzbach, D. Wehner,G. Weidinger, S. L. Kuan, M.I. Jansen, F. Jelezko, H. J. Luhmann, D. Hinderberger, T. Weil, K. Müllen, *Adv. Healthcare Mater*. **2014**, *4*, 377-384.

150 O. Enoki, H. Katoh, K. Yamamoto, *Org. Lett*. **2006**, *8*, 569-571.

151 K. Albrecht, R. Pernites, M.J. Felipe, R.C. Advicula, K. Yamamoto, *Macromolecules.* **2006**, *8*, 569-571.

152 F. Brunet, M. Simard, J.D. Wuest, *J. Am. Chem. Soc*. **1997**, *119*, 2737-2738.

153 D. Boils, M.-E. Perron, F. Monchamp, H. Duval, T. Maris, J.D. Wuest, *Macromolecules* **2004**, *37*, 7351-7357.

154 D. Laliberté, T. Maris, E. Demers, F. Helzy, M. Arseneault, D. Wuest, *Crystal Growth&Design* **2005**, *5*, 1451-1456.

155 J.-H. Fournier, T. Maris, J.D. Wuest, W. Guo, E. Galoppini, *J. Am. Chem. Soc*. **2003**, *125*, 1002-1006.

156 D. Laliberatė, T. Maris, J.D. Wuest, *Can. J. Chem* **2004**, *82*, 386-398.

157 J.-H. Fournier, T. Maris, J.D. Wuest, *J. Org. Chem*. **2003**, *69*, 1762-1775.

158 J.K. Zareba, M. J. Bialek, J. Janczak, J. Zon, A. Dobosz, *Crystal Growth&Design* **2014**, *14*, 6143-6153.

159 O. Plietzsch, Ch.I. Schilling, M. Nieger, T. Muller, S. Bräse, *Tetrahedron Asymmetry* **2010**, *21*, 1474-149.

160 T. Ben, H. Ren, S.Q. Ma, D. P. Cao, J.H. Lan, X.F. Jing, W. C. Wang, J. Xu, F. Deng, J.M. Simmons, S.L. Qiu, G.S. Zhu, *Angew. Chem. Int. Ed.* **2009**, *48*, 9457-9460.

161 A. Patra, J.-M. Koenen, U. Scherf, *Chem. Commun.* **2011**, *47*, 9612-9614.

162 E. Stöckl, X. Wu, A. Trewin, C.D. Wood, R. Clowes, N.L. Campbell, J.T.A. Jones, Y. Z. Khimyak, D.J. Adams, A.I. Cooper, *Chem. Commun*. **2009**, *45*, 212-214.

163 U.H.F. Bunz, K. Seehafer, F.L. Geyer, M. Bender, I. Braun, E. Smarsly, J. Freudenberg, *Macromol. Rapid. Commun.* **2014**, *35*, 1466-1496.

164 J.R. Holst, E. Stöckel, D.J. Adams, A.I. Cooper, *Macromolecules* **2010**, *43*, 8531-8538.

165 H.P. Ma, H. Ren, X.Q. Zou, S. Meng, F.X. Sun, G.S. Zhu, *Polym. Chem.* **2014**, *5*, 144-152.

166 H.P. Ma, H. Ren, X.Q. Zou, F.X. Sun, Z.J. Yan, K. Cai, D.Y. Wang, G.S. Zhu, *J. Mater. Chem. A* **2013**, *1*, 752-758.

167 H.C. Cho, H.S. Lee, J. Chun, S.M. Lee, H.J. Biog, S.U. Son, *Chem. Commun*. **2011**, *47*, 917-919.

168 J. Chun, J.H. Park, J. Biog, S.M. Lee, H.J. Biog, S.U. Son, *Chem. Mater*. **2012**, *24*, 3458-3463.

169 P. Ganesan, X. Yang, J. Loos, T.J. Savenije, R.D. Abellon, H. Zuilhof *J. Am. Chem. Soc.* **2005**, *127*, 14530-14531.

170 G. Li, Z. Wang, *Macromolecules* **2013**, *46*, 3058-3066.

171 O.K. Fara, A.M. Spokoyny, B.G. Hauser, Y.-S. Bae, S.E. Brown, R.Q. Snurr, Ch. A. Mirkin, J.T. Hupp, *Chem. Mat.* **2009**, 21, 3033-3035.

172 O.K. Fara, Y.-S. Bae, B.G. Hauser, S.E. Brown, A.M. Spokoyny, R.Q. Snurr, Ch. A. Mirkin, J.T. Hupp, *Chem. Commun.* **2010**, 46, 1056-1058.

173 K.V. Rao, R. Haldar, Ch. Kulkarni, T.K. Maji, S.J. George, *Chem. Mat*. **2012**, *24*, 969-971.

174 A. M. Shultz, O.K. Fara, J.T. Hupp, S. T. Nguyen, *Chem. Sci.* **2011**, *2*, 686-689

175 M.G. Rabbani, H. M. El-Kaderi, *Chem. Mat*. **2012**, *24*, 1511-1517.

176 W.Zhu, Ch. Tian, T. Jin, J. Wang, S.M. Mahurin, W. Mei, Y. Xiong, J. Hu, X. Feng, H. Liu, S. Dai, *Chem. Commun.* **2014**, *50*, 15055-15058.

177 Y.-Ch. Zhao, D. Zhou, Q. Chen, X.-J. Zhang, N. Bian, A.-D. Qi, B.-H. Han, *Macromolecules* **2011**, *44*, 6382-6388.

178 M.H. Weston, O.K. Fara, B.G. Hauser, J.T. Hupp, S.T. Nguyen *Chem. Mat.* **2012**, *24*, 1292-1296.

179 D.-P. Liu, Q. Chen, Y.Ch. Zhao, A.-D. Qi, B.-H. Han, *ACS Macro Lett.* **2013**, *2*, 522-526

180 Y. Han, L.-M. Zhang, Y.-Ch. Zhao, T. Wang, B.-H. Han, *ACS Appl. Mater. Interfaces.* **2013**, *2*, 522-526.

181 Z. Xie, Ch. Wang, K.E. deKrafft, W. Lin, *J. Am. Chem. Soc*. **2011**, *133*, 2056-2059

182 Ch.A. Wang, Z.K. Zhang, T.Yue, Y. Lei, L. Wang, W.D. Wang, Y. Zhang, Ch. Liu, W. Wang, Ch, *Chem. Eur. J*. **2012**, *18*, 6718-6723.

183 W.-K. An, M.-Y. Han, Ch.-A. Wang, S.-M. Yu, Y. Zhang, S. Bai, W. Wang, *Chem. Eur. J*. **2014**, *20*, 11019-11028.

184 X. Wang, J. Zhang, Y. Liu, Y. Cui, *Bull. Chem. Soc. Jpn*. **2014**, *87*, 435-440.

185 J. Dong, Y. Liu, Y. Cui, *Chem. Commun*. **2014**, *50*, 14949-14952.

186 J.M. Tour, L. Jones, D. L. Pearson, J.J.S. Lamba, T.P. Burgin, G.M. Whitesides, D. Allara, A.N. Parikh, A. Atre, *J. Am. Chem. Soc.* **1995**, *117*, 9529.

187 L. Kankate, L. Turchanin, A. Gölzhäuser, *Langmuir* **2009**, *25*, 10435-10438.

188 E. Delamarche, B. Michel, H. Kang, C. Gerber, *Langmuir* **1994**, *10*, 4103-4108.

189 Z. Huang, F. Chen, P. Bennett, N.J Tao, *J. Am. Chem. Soc.* **2007**, *129*, 13225-13231.

190 H.L. Tierney, J.W. Han, A.D. Jewell, E.V. Iski, A.E. Baber, D.S. Sholl, E. Sykes, H. *J. Phys. Chem. C* **2011**, *115*, 897-901.

191 H. Häkkinen, *Nat. Chem.* **2012**, *4*, 443-455.

192 W. Azzam, B.I. Wehner, R.A. Fischer, A. Terfort, C. Woll, C. *Langmuir* **2002**, *18*, 7766-7769.

193 H. Valkanier, E.H. Huisman, P. A. van Hal, D.M. de Leeuw, R.C. Chiechi, J.C. Hummelen, *J. Am. Chem. Soc.* **2011**, *133*, 4930-4939.

194 P. Chinwangso, C.A. Jamison, T.R. Lee, *Acc. Chem. Res.* **2011**, *44*, 511-519.

195 L. Wei, H. Tiznado, G. Liu, K. Padmaja, J.S. Lindsey, F. Zaera, D.F. Bocian, *J. Phys. Chem. B* **2005**, *109*, 23963-23971.

196 Y. Yao, J.M. Tour, *J. Org. Chem*. **1999**, *64*, 1968-1971.

197 H. Jian, J.M. Tour, *J. Org. Chem*. **2003**, *68*, 5091-5103.

198 L. Cheng, B. Cheng, J.M. Tour, *J. Am. Chem. Soc*. **2006**, *128*, 13479-13489.

199 Y. Shirai, J.M. Guerrero, T. Sasaki, T. He, H. Ding, G. Vives, B.-C. Yu, L. Cheng, A.K. Flatt, P.G. Taylor, Y. Gao, J.M. Tour, *J. Org. Chem*. **2009**, *74*, 7885-7897.

200 R. Sakamato, Y. Ohirabaru, R. Matsuoka, H. Maeda, S. Katagiri, H. Nishihara, *Chem. Comm*. **2013**, *49*, 7108-7110.

201 Q. Li, C. Jin, P.A. Petuhkov, A.V. Rukavishnikov, T.O. Zaikova, A. Phadke, D.H. LaMunyon, M.D. Lee, J.W.F. Keana, *J. Org. Chem*. **2004**, *69*, 1010-1019.

202 D. Takamatsu, Y. Yamakoshi, K. Fukui, *J. Phys. Chem. B* **2006**, *110*, 1968-1970.

203 K.W. Kittredge, M.A. Milton, M.A Fox, J.K. Whitesell, *Helv. Chim. Acta* **2002**, *85*, 788-798.

204 T. Kitagawa, Y. Idomoto, H. Matsubara, D. Hobara, T. Kakiuchi, T.; Okazaki, K. Komatsu, *J. Org. Chem.* **2006**, *71*, 1362-1369.

205 S. Katano, Y. Kim, H. Matsubara, T. Kitagawa, M. Kawai, *J. Am. Chem. Soc*. **2007**, *129*, 2511-2515.

206 T. Kitagawa, H. Matsubara, K. Komatsu, H. Katsuyuki, T. Okazaki, T. Hase, *Langmuir* **2013**, *29*, 4275-4282.

207 T. Weidner, N. Ballav, U. Siemeling, D. Troegel, T. Walter, R. Tacke, D.G. Castner, M. Zharnikov, *J. Phys. Chem. C* **2009**, *113*, 19609-19617.

208 T. Weidner, M. Zharnikov, J. Hoßbach, D.G. Castner, U. Siemeling, *J. Phys. Chem. C* **2010**, *114*, 14975-14892.

209 D. Takamatsu, K. Fukui, S. Aroua, Y. Yamakoshi, *Org. Biomol. Chem*. **2010**, *8*, 3655-3664.

210 A.V. Rukavishnikov, A. Phadke, M.D. Lee, D.H. LaMunyon, P.A. Petuhkov, F.J. Keana, *Tetrahedron Lett.* **1999**, *40*, 6353-6355.

211 U.G.E. Perera, F. Ample, H. Kersell, Y. Zhang, G. Vives, J. Echeverria, M. Grisolia, G. Rapenne, C. Joachim, S.-W. Hla, *Nat. Nanotechnol.* **2013**, *8*, 46-51.

212 X. Zheng, M.E. Mulcahy, D. Horinek, F. Galeotti, T.F. Magnera, J. Michl, *J. Am. Chem. Soc.* **2004**, *126*, 4540-4542.

213 B. Baisch, D. Raffa, U. Jung, O.M. Magnussen, C. Nicolas, J. Lacour, J. Kubitschke, R. Herges, *J. Am. Chem. Soc.* **2009**, *131*, 442-443.

214 L. Zhu, H. Tang, Y. Harima, K. Yamashita, Y. Aso, T. Otsubo, *J. Mater. Chem.* **2002,** *12*, 2250-2254.

215 S. Grunder, R. Huber, S. Wu, C. Schönenberger, M. Calame, M. Mayor, *Eur. J. Org. Chem*. **2010**, 833-845.

216 M. Mastalerz, *Angew. Chem. Int. Ed. Engl*. **2008**, *47*, 445-447.

217 S.L. James, *Chem. Soc. Rev*. **2003**, *43*, 276-288.

218 S.T. Meek, J.A. Greathouse, M.D. Allendorf, *Adv. Mat*. **2011**, *23*, 249-267.

219 N. Stock, S. Biswas, *Chem. Rev*. **2012**, *112*, 933-960.

220 T.R. Cook, Y.-R. Zheng, P.J. Stang, *Chem. Rev*. **2013**, *113*, 734-777.

221 S.M. Cohen, *Chem. Rev*. **2012**, *112*, 970-1000.

222 K.T. Tanabe, S.M. Cohen, *Chem. Soc. Rev*. **2011**, *40*, 498-819.

223 S. Chaemchue, N.A. Kabir, K. Zhou, F. Verpoort, *Chem. Soc. Rev*. **2013**, *42*, 9304-9332.

224 R.B. Getmann, Y.-S. Bae, Ch.E. Wilmer, R.Q. Snurr, *Chem. Rev*. **2012**, *112*, 703-723.

225 P. Suh, H.J. Park, T.K. Prasad, D.-W. Lim, *Chem. Rev*. **2012**, *112*, 782-835.

226 J.-R. Li, J. Sculley, H.-C. Zhou, *Chem. Rev*. **2012**, *112*, 869-932.

227 H. Wu, Q. Gong, D.H. Olson, J. Li, *Chem. Rev*. **2012**, *112*, 836-868.

228 Y. Xui, Y. Yue, G, Qin, B. Chen, *Chem. Rev*. **2012**, *112*, 1126-1162.

229 D. Bradshaw, A. Garai, J. Huo, *Chem. Soc. Rev*. **2012**, *112*, 2344-2381.

230 P. Horcajada, R. Gref, T. Baati, P.K. Allan, G. Maurin, P. Couvreur, G. Fèrey, R.E. Morris, Ch. Serre. *Chem. Rev*. **2012**, *112*, 1232-1268.

231 J. Liu, L. Chen, H. Cui, J. Zhang, L. Zhang, Ch.-Y. Su, *Chem. Soc. Rev*. **2014**, *43*, 6011-6061.

232 M. O'Keeffe, O.M. Yaghi, *J. Am. Chem. Soc*. **2012**, *112*, 678 -702.

233 W. Lu, Z. W. Z.-Y. Gu, T.-F. Liu, J. Park, J. Park, J. Tian, M. Zhang, Q. Zhang, Th. Gentle III, M. Bosch, H.C. Zhou, *Chem. Soc. Rev*, **2014**, *43*, 5561-5693.

234 B.F. Hoskins, R. Robson, *J. Am. Chem. Soc*. **1989**, *111*, 5692-5964.

235 J. Kim, B. Chen, T.M. Reineke, H. Li, M. Eeddaoudi, D.B. Moler, M. O'Keefe, O.M. Yaghi, *J. Am. Chem. Soc*. **2001**, *123*, 8239-8247.

236 L. Ma, A. Jin, Z. Xie, W. Lin, *Angew. Chem. Int. Ed.* **2009**, *48*, 9905-9908.

237 D. Liu, Z. Xie, L. Ma, W. Lin, *Inorg. Chem*. **2010**, *49*, 9107-9109.

238 K. Matsumoto, M. Kannami, D, Inokuchi, H. Kurata, T. Kawase, M. Oda, *Org. Lett*. **2007**, *9*, 2903-2906.

239 K. Matsumoto, D. Onokuchi, Y. Hirao, H. Kurata, T. Kubo, *Crystal Growth&Design*, **2010**, *10*, 2854-2856.

240 Ch.B. Caputo, V.N. Vukotic, N.M. Sirizzoti, S.J. Loeb, *Chem. Commun*. **2011**, *47*, 8545-8547.

241 X.-Y. Chen, H.-Y. Shi, R.-B. Huang, L.-S. Zheng, J. Tao, *Chem. Commun*, **2013**, *49*, 10977-10979.

242 M. Dincă, A. Dailly, J.R. Long, *Chem. Eur. J* **2008**, *14*, 10280-10285.

243 Z.B. Lim, H. Li, S. Sun, J.Y. Lek, A. Trewin, Y.M. Lam, A.C. Grimsdale, *J. Mat. Chem*. **2012**, *22*, 6218-6218.

244 Y. Yamanoi, Y, Yamamoto, M. Miyachi, M. Shimada, A. Minoda, S. Oshima, Y. Kobori, H. Nisihara, *Langmuir* **2013**, *29*, 8768-8772.

245 J.K. Zareba, M.J. Bialek, J. Janczak, M. Nyk, J. Zon, M. Samoc, *Inorg. Chem*. **2015**, *54*, 10568-10575.

246 X. Feng, X. Diang, D. Jiang, *Chem. Soc. Rev*. **2012**, *41*, 6010-6022.

247 Z. Xiang, D. Cao, *J. Mat. Chem. A*. **2013**, *1*, 2691-2718.

248 S.-Y. Ding, W. Wang, *Chem. Soc. Rev*. **2013**, *42*, 548-568.

249 M. Dogru, Th. Bein, *Chem. Commun*. **2014**, *50*, 5531-5546.

250 U. Diaz, A. Corma, *Coord. Chem. Rev*. **2016**, *311*, 85-124.

251 C.J. Doonan, D.J. Tranchemontagne, T.G. Glover, J.R. Hunt, O.M Yaghi, *Nat. Chem*. **2010**, *2*, 235-238.

252 W. Leng, Y. Peng, J. Zhang, H. Lu, X. Feng, R. Ge, B. Dong, B. Wang, X. Hu, Y. Gao, *Chem. Eur. J*. **2016**, *22*, 1-6.

253 Y. Zhang, J.Y. Ying, *ACS Catal*. **2015**, *5*, 2681-2691.

254 P.J. Waller, F. Gandara, O.M. Yaghi, *Acc. Chem. Res*. **2015**, *48*, 3053–3063.

255 D.N Bunck, W.R. Dichtel, *Angew. Chem. Int. Ed*. **2012**, *51*, 1885-1889.

256 S.B. Brucks, D.N Bunck, W.R. Dichtel, *Polymer* **2013**, 1-5.

257 D.N Bunck, W.R. Dichtel, Chem. Commun. **2013**, *49*, 2457-2459.

258 F.J. Uribe-Romo, J.R. Hunt, H. Furukawa, C. Klock, M. O'Keefe, O.M. Yaghi, *J. Am. Chem. Soc.* **2009**, *135*, 16336-16339.

259 Y-B. Zhang, J. Su, H. Furukawa, Y. Yun, F. Gandara, A. Duong, X. Zou, O.M. Yaghi, *J. Am. Chem. Soc* **2013**, *131*, 4570-4571.

260 H. Lu, Ch. Wang, J. Chen, J. Chen, R. Ge, W. Leng, B. Dong, J. Huang, Y. Gao, *Chem. Commun.* **2015**, *51*, 15562-15565.

261 Y. Zhu, H. Long, W. Zhang, *Chem. Mat*. **2013**, *25*, 1630-1635.

262 G. Lin, H. Ding, D. Yuan, B. Wang, Ch. Wang, *J. Am. Chem. Soc* **2016**, *138*, 3302–3305.

263 W. Luo, Y. Zhu, J. Zhang, J. He, Z. Chi, P.M. Miller, L. Chen, Ch-Y. Su, *Chem. Commun*. **2014**, *50*, 11942-11945.

264 H. Liu, J. Feng, J. Zhang, P. W. Miller, L. Chen, Ch-Y. Su, *Chem. Sci* **2015**, 6, 2292-2296.

265 R.S.B. Gonçalves, A.B.V. de Oliveira, H.C. Sindra, B.S. Archanjo, M.E. Mendoza, L.S.A. Carneiro, C.D. Buarque, P.M. Esteves, *ChemCatChem* **2016**, *8*, 743-750.

266 Q. Fang, J. Wang, S. Gu, R.B. Kaspar, Z. Zhuang, J. Zheng, H. Guo, S, Qiu, Y. Yan, *J. Am. Chem. Soc* **2015**, *137*, 8352–8355.

267 H.A. Patel, S.H. Je, J. Park, D.P. Chen, Y. Jung, C.T. Yavuz, A. Coskun, *Nat. Commun*. **2013**, *4*, 1357-1363.

268 H.A. Patel, S.H. Je, J. Park, Y. Jung, A. Coskun, C.T. Yavuz, *Chem. Eur. J.* **2014**, *20*, 772-780.

269 J. Lu, J. Zhang, *J. Mat. Chem. A*. **2014**, *2*, 13831-13834.

270 P. Arab, M.G. Rabbani, A;K. Sekizkardes, T. Islamoglu, H.M. El-Kaderi, *Chem. Mat.* **2014**, *26*, 1385-1392.

271 O. Buyukcakir, S.H. Je, J. Park, H.A. Patel, Y. Jung, C.T. Yavuz, A. Coskun, *Chem. Eur. J*. **2015**, *21*, 1-9.

272 H. Ren, T. Ben, E. Wang, X. Jing, M. Xue, B. Liu, Y. Cui, S. Qiu, G. Zhu, *Chem. Commun*. **2010**, *46*, 291-293.

273 E. Klontzas, E. Tylianakis, G.E. Froudakis, *J. Phys. Chem. B* **2008**, *112*, 9095-9098.

274 S.S. Han, H. Furukawa, O.M. Yaghi, W.A Goddard III, *J.Am. Chem. Soc* **2008,** *130*, 11580-11581.

275 D. Cao, J. Lan, W. Wang, B. Smit, *Angew. Chem. Int. Ed. Engl*. **2009**, *48*, 4730-4733

276 H. Furukawa, O.M. Yaghi, *J.Am. Chem. Soc* **2009**, *131*, 8875-8883.

277 H. Ma, H. Ren, S. Meng, Z. Yan, H. Zhao, F. Sun, G. Zhu, *Chem. Commun* **2013**, *49*. 9773-9775.

278 M. Lindner, M. Valášek, J. Homberg, K. Edelmann, L. Gerhard, W. Wulfhekel, O. Fuhr, T. Wächter, M. Zharnikov, V. Kolivoška, L. Pospíšil, G. Mészáros, M. Hromadová, M. Mayor, *Chem. Eur.J* **2016**, *22*, 13218-13235.

279 V. Kolivoška, M. Mohos, I. V. Pobelov, S. Rohrbach, K. Yoshida, W. J. Hong, Y. C. Fu, P. Moreno-Garcia, G. Mészáros, P. Broekmann, M. Hromadová, R. Sokolová, M. Valášek, T. Wandlowski, *Chem Commun*. **2014**, *50*, 11757-11759.

280 C. J. Yu, Y. Chong, J. F. Kayem, M. Gozin, *J. Org. Chem*. **1999**, *64* 2070-2079.

281 K. Fujimoto, H. Yorimitsu, A. Osuka, *Org. Lett.* **2014**, *16*, 972-975.

282 T. Itoh, T. Mase, *Org. Lett*. **2004**, *6*, 4587-4590.

283 A.A. Farahat, A. Kumar, M. Say A. El-Din M. Barghash, F.E. Goda, H.M. Eisa, T. Wenzler, R. Brun, Y. Liu, L. Mickelson, W.D. Wilson, D.W. Boykin, *Bioorg. Med. Chem*. **2010**, *18*, 557-566.

284 D. Oesch, N.W. Luedtke, *Chem. Commun* **2015**, *51*, 12641-12644.

285 (a) D.J. Sinclair, M.S. Sherburn, *J.Org.Chem*. **2005**, *70*, 3730-3733(b) Ch. Honda, K. Takimiya, Y. Aso, *Mol. Cryst. Liq.Cryst*. **2006**, *455*, 373-379 (c) M. Schiek, K. al-Shamery, A. Lützen, Synthesis, **2007**, *4*, 613-621.

286 E. Guillen, J. Hierrezuelo, R. Martinez-Mallorquin, J.M. Lopez-Romero, R. Rico, *Tetrahedron* **2011**, *67*, 2555-5261.

287 L. Kobr, K. Zhao, Y. Shen, R.K. Shoemaker, Ch.T. Rogers, J. Michl, *Adv. Mat*. **2013**, *25*, 443-448.

288 Ch. Lai, B.J. Backes, *Tetrahedron Lett* **2007**, *48*, 3033-3037.

289 Th. C. Pijper, J. Robertus, W.R. Browne, B.L. Feringa, *Org.Biomol.Chem*. **2015**, *13*, 265-268.

290 L.O. Pèrs, F.G. Guillet, G. Froyer, *Org.Biomol.Chem.***2004**, *2*, 452-454.

291 J. Liu, B. Schüpbach, A. Bashir, O. Shekhah, A. Nefedov, M. Kind, A. Terfort, C. Wöll, *Phys. Chem. Chem. Phys.* **2010**, *12*, 4459-4472.

292 F. Chesneau, J. Zhao, C. Shen, M. Buck, M. Zharnikov, *J. Phys. Chem. C* **2010**, *114*, 7112-7119.

293 K. Heister, M. Zharnikov, M. Grunze, L. S. O. Johansson, A. Ulman, *Langmuir* **2001**, *17*, 2541-2544.

294 J. F. Moulder, W. E. Stickle, P. E. Sobol, K. D Bomben, *in Handbook of X-ray Photoelectron Spectroscopy*; (Eds.: J. Chastian), Perkin-Elmer Corp., Eden Prairie, MN, **1992**.

295 J. Thome, M. Himmelhaus, M. Zharnikov, M. Grunze, *Langmuir* **1998**, *14*, 7435-7449.

296 C. L. A. Lamont, J. Wilkes, *Langmuir* **1999**, *15*, 2037-2042.

297 B. D. Ratner, D. G. Castner, *Electron Spectroscopy for Chemical Analysis.* (Eds.: J. C. Vickerman), Surface Analysis - The Principle Techniques, Wiley & Sons, Chichester, **1997**.

298 N. Ballav, B. Schüpbach, S Neppl, P. Feulner, A. Terfort, M. Zharnikov, *J. Phys. Chem. C* **2010**, *114*, 12719-12727.

299 M. Zharnikov, *J. Electron. Spectr. Relat. Phenom.* **2010**, *178-179*, 380.

300 F. Sander, T. Peterle, N. Ballav, F. von Wrochem, M. Zharnikov, M. Mayor, *J. Phys. Chem. C* **2010**, *114,* 4118-4125.

301 F. Schreiber, *Prog. Surf. Sci.* **2000**, *65*, 151-256.

302 F. Chesneau, B. Schüpbach, K Szelągowska-Kunstman, N. Ballav, P. Cyganik, A. Terfort, M. Zharnikov, *Phys. Chem. Chem. Phys.* **2010**, *12*, 12123-12137.

303 P. Waske, T. Wächter, A. Terfort, M. Zharnikov, *J. Phys. Chem. C* **2014**, *118*, 26049-26060.

304 P. E. Batson, *Phys. Rev. B* **1993**, *48*, 2608.

305 J. Stöhr, *NEXAFS Spectroscopy*; Springer Series in Surface Science 25; Springer-Verlag, Berlin, **1992**.

306 J. Horsley, J. Stöhr, A. P. Hitchcock, D. C. Newbury, A. L. Johnson, F. Sette, *J. Chem. Phys.* **1985**, *83*, 6099-6107.

307 S. Frey, V. Stadler, K. Heister, W. Eck, M. Zharnikov, M. Grunze, B. Zeysing, A. Terfort, *Langmuir* **2001**, *17*, 2408-2415.

308 N. Ballav, B. Schüpbach, O. Dethloff, P. Feulner, A. Terfort, M. Zharnikov, *J. Am. Chem. Soc.* **2007**, *129*, 15416-15117.

309 S. Carniato, V. Ilakovac, V. J.-J. Gallet, E. Kukk, Y. Luo, *Phys. Rev. A* **2005**, *71*, 022511.

310 S. Rangan, J. -J. Gallet, F. Bournel, S. Kubsky, K. Le Guen, G. Dufour, F. Rochet, F. Sirotti, S. Carniato, V. Ilakovac, *Phys. Rev. B* **2005**, *71*, 165318.

311 L. Hallmann, A. Bashir, T. Strunskus, R. Adelung, V. Staemmler, C. Wöll, F. Tuczek, *Langmuir* **2008**, *24*, 5726-5733.

312 H. Hamoudi, S. Neppl, P. Kao, B. Schüpbach, P. Feulner, A. Terfort, D. Allara, M. Zharnikov, *Phys. Rev. Lett.* **2011**, *107*, 027801.

313 J. V. Barth, H. Brune, G. Ertl, R. J. Behm, *Phys. Rev. B* **1990**, *42*, 9307

314 V. Repain, J. M. Berroir, S. Rousset, and J. Lecoeur, *Appl. Surf. Science* **2000**,*30*, 162163

315 T. Kumagai, F. Hanke, S. Gawinkowski, J. Sharp, K. Kotsis, J. Waluk, M. Persson, L. Grill, *Nat. Chem*. **2014**, *6*, 41-46.

316 J. Gottschalck, B. Hammer, *J. Chem. Phys*. **2002**, *116*, 784-790.

317 N. A. Rogozhnikov, *Russian J. Electrochem*. **2013**, *49*, 1150-1158.

318 E. Fertitta, E. Voloshina, B. Paulus, *J. Comp. Chem*. **2014** *35*, 204-213.

319 F. Elste, G. Weick, C. Timm, F. V. Oppen, *Appl. Phys. A* **2008**, *93*, 345-354.

320 M. Valášek, K. Edelmann, L. Gerhard, O. Fuhr; M. Lukas, M. Mayor, *J. Org. Chem*. **2014**, *79*, 7342-7357.

321 T. Huan, L. Fabris, G.C. Bazan, W. Ho, *Nat. Chem*. **2013**, *5* 36-41.

322 V. Kolivoška, R. Sokolová, J. Kocábová, C. Loukou, J. M. Mallet, M. Hromadová, *Monatsh. Chem.* **2016**, *147*, 45-51.

323 G. Mészáros, C. Li, I. Pobelov, T. Wandlowski, *Nanotechnology* **2007**, *18*, 424004.

324 J. Gasior, program STMconductivity.exe

325 P. Moreno-García, A. La Rosa, V. Kolivoška, D. Bermejo, W. Hong, K. Yoshida, M. Baghernejad, S. Filippone, P. Broekmann, T. Wandlowski, N. Martin, *J. Am. Chem. Soc.* **2015**, *137*, 2318-2327.

326 P. Moreno-Garcia, M. Gulcar, D.Z. Manrique, T. Pope, W. Hong, V. Kaliginedi, C. Huang, A.S. Batsanov, M.R. Bryce, C.J. Lambert, T. Wandlowski, *J. Am. Chem. Soc*. **2013**, *135*, 12228-12240.

327 M.E. Belowich, J.F. Stoddart, *Chem. Soc. Rev*. **2012**, *41*, 2003-2024.

328 K. Takanashi, H. Chiba, M. Higuchi, K. Yamamoto, *Org. Lett*. **2004**, *6*, 1709-1712.

329 A.K. Chakraborti, L. Sharma, M.K. Nayak, *J. Org. Chem*. **2002**, *67*, 6406-6414.

330 N.S. Gavande, S. Kundu, N.S. Badgujur, G.Kaur, A.K. Chakraborti, *Tetrahedron*, **2006**, *62*, 4201-4204.

331 J. Chae, *Arch. Pharm. Res*. **2008**, *31*, 305-309.

332 P.O' Sullivan, I. Rozas, *ChemMedChem*. **2014**, *9*, 2065-2073.

333 J. He, L. Hongmei, D. Yanfeng, O. Xuemei, W. Jing. T. Silu, Z. Xiahong, W. Pangfei, M. Dongee, *J. Phys. Chem C*. **2009**, *113*, 6761-6767.

334 R. Manetsch, L. Zheng, M.T. Reymond, W.-D. Woggon, J.-L. Reymond., *Chem Eur. J.* **2004**, *10*, 2487-2506.

335 P. Knochel, W. Dohle, N.Gommermann, F.F. Kneisel, F. Koppem, T. Korn, I. Sapountzis, V.A. Vu, *Angew. Chem. Int. Ed*. **2003**, *42*, 4302-4320.

336 L. Qin, H. Cui, D. Zou, J. Li, Y. Wu, Z. Zhu, Y. Wu, *Tetrahedron Lett*. **2010**, *51*, 4445-4448.

337 J.P. Wolfe, J. Åhman, J.P. Sadighi, R. A. Singer, S.L. Buchwald, *Tetrahedron Lett*. **2010**, *51*, 4445-4448.

338 R.A.T.M. van Benthem, H. Hiemstra, W.M. Speckamp, *J. Org. Chem.* **1992**, *57*, 6083-6085.

339 N.J. Tom, W.M. Simon, H.N. Frost, M. Ewing, *Tetrahedron Lett* **2004**, *45*, 905-906

340 S.R. Dandepally, A.L. Williams, *Tetrahedron Lett*. **2009**, *50*, 1071-1074.

341 S.El. Kazzouli, J. Koubachi, S. Barteina-Raboin, A. Mouaddib, G. Guillamaumet, *Tetrahedron Lett.* **2006**, *47*, 8575-8577.

342 D.M. Mofford, G.R. Reddy, S.C. Miller, *J. Am. Chem. Soc*. **2014**, *136*, 13277–13282.

343 J.K. Sørensen, J. Fock, A.H. Pedersen, A.B. Petersen, K. Jennum, K. Bechgaard, K. Kilså, V. Geskin, J. Cornil, T. Bjørnholm, M. B. Nielsen, *J. Org. Chem*. **2011**, *76*, 245–263.

344 D.K. Maiti, A. Banerjee, *Chem. Commun*. **2013**, *49*, 6909-6911.

345 H. Qingzhong, M. Negri, K. Jahn-Hoffmann, Y. Zhuang, S. Olgen, M. Bartels, U. Mueller-Vieira, Th. Lauterbach, R.W. Hartmann, Bioorg. Med. Chem. 2008,16, 7715-7727

346 M. vom Lee, H. Kim, H. Rhee, J. Choo, *Bull. Korean. Chem. Soc*. **2003**, *24*, 205-208

347 S. Brunauer, P. H. Emmett , E. Teller, *J. Am. Chem. Soc*. **1938**, *60*, 309-319.

348 S. Lowell, J.E. Shields, M.A. Thomas, M. Thommes, Characterization of Porous Solids and Powders: Surface Area, Pore Size and Density, Springer Verlag, 2006, 347.

349 Zh-J. Li, S-Y. Ding, H-D. Xue, W. Cao, W. Wang, *Chem. Commun*. **2016**,*52*, 7217-7220

8 Appendix

8.1 TGA charts of synthesized polymers.

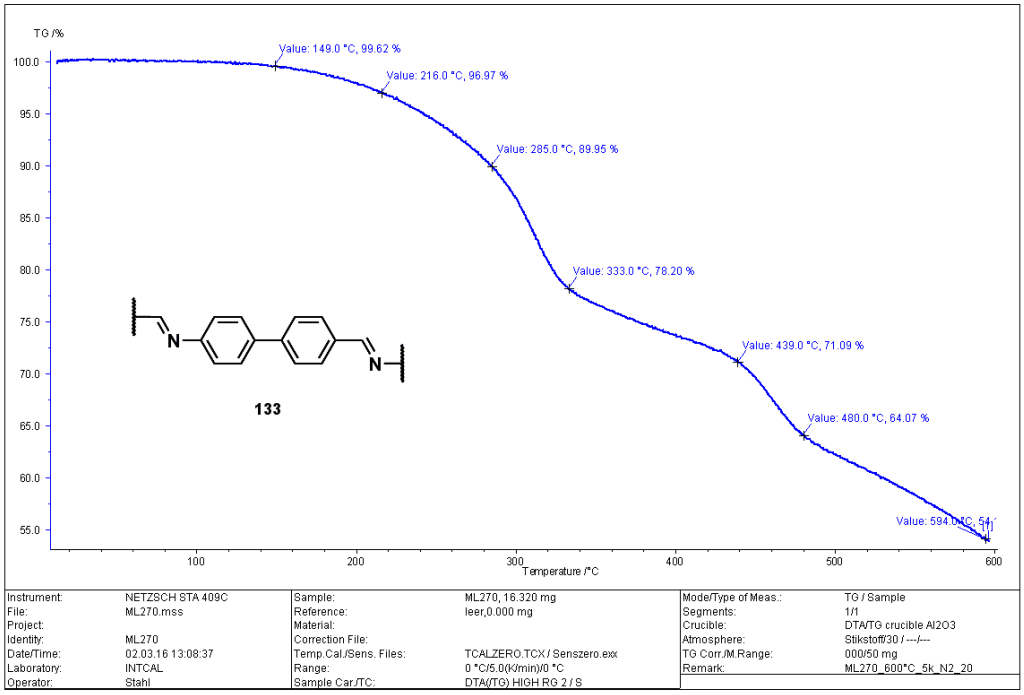

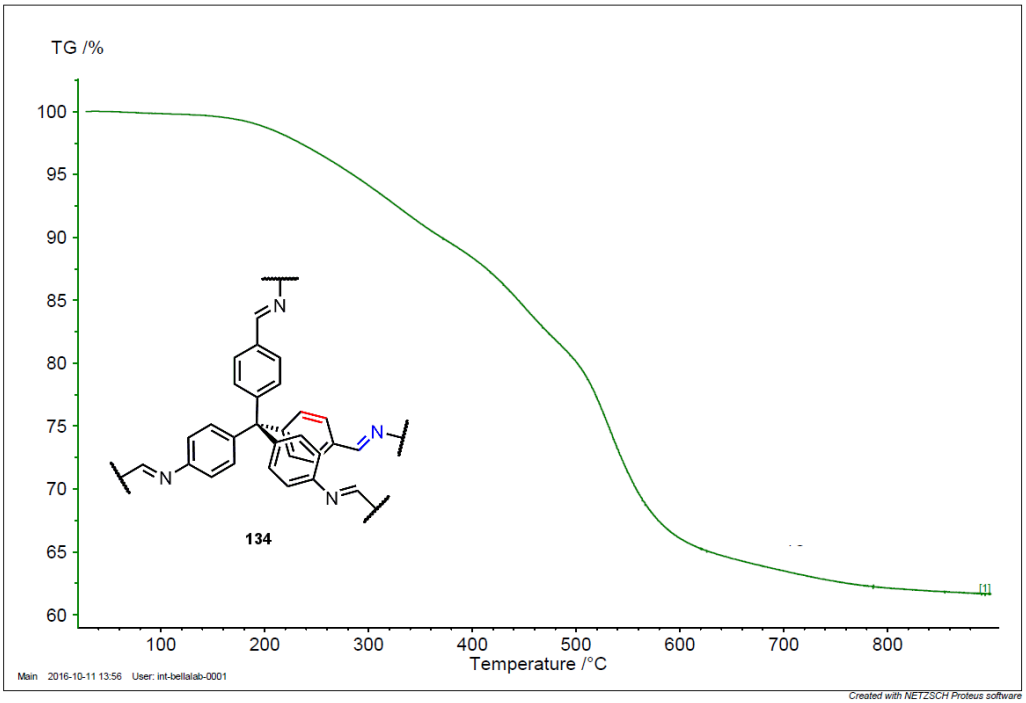

Figure 71 Stability of obtained polymer determined with TG analysis for **133** (upper chart), **134** (lower chart)

8.2 Contributions

All molecules presented in this work were synthesized and analyzed by Marcin Lindner in a Group of Prof. Dr. Marcel Mayor at the Institute of Nanotechnology (Karlsruhe Institute of Technology, Germany). Showed and discussed results of chemical and physical measurements were carried out in the following groups:

- Prof. Dr. Wulf Wulfhekel at the Institute of Nanotechnology (UHV-STM experiments, KIT, Germany),
- Prof. Dr. Michail Zharnikov at Institute of Physical Chemistry (University of Heidelberg, Germany)
- Dr. Magdalena Hromadová at the J. Heyrovsky Institute of Physical Chemistry (Cyclic Voltammetry and STM-BJ experiments, Czech Academy of Science, Prague, Czech Republic)
- Dr. Olaf Fuhr at the Institute of Nanotechnology (X-ray single crystal, XPRD analysis, KIT, Germany)
- Dr. Sylvio Indris at the Institute of Applied Materials (MAS-NMR, KIT, Germany)
- Dr. Di Wang, at the Institute of Nanotechnology (TEM and STEM, KIT, Germany)
- Dr. Peter Weidler at the Institute of Functional Interfaces (Gas sorption, KIT, Germany)

8.3 Publications

Part of the results presented in this work were already published in the following articles:

Valášek, Michal; Lindner, Marcin; Mayor, Marcel

Rigid multipodal platforms for metal surfaces

Beilstein Journal of Nanotechnology. **2016**, *7*, 374-405.

Lindner, Marcin; Valášek, Michal; Homberg, Jan; Edelmann, Kevin; Gerhard, Lukas; Wulfhekel, Wulf; Fuhr, Olaf; Wächter, Tobias; Zharnikov, Michael; Kolivoška, Viliam; Pospíšil, Lubomír; Mészáros, Gábor; Hromadová, Magdaléna; Mayor, Marcel

Importance of the Anchor Group Position (*Para* versus *Meta*) in Tetraphenylmethane Tripods: Synthesis and Self-Assembly Features

Chemistry – A European Journal **2016**, *22*, 13218-13235

8.4 Curriculum Vitae

Personal details

Surname: Lindner

Name: Marcin

Date of birth: 15.11.1988

Place of birth: Gostyń

Nationality: Polish

Personal Skills and Competences

Experienced and trained with techniques applied in organic chemistry, including Schlenk-line techniques, microwave conducted reactions, multistep reactions, purification and characterization of organic compounds. Good knowledge and experience in following analytical techniques: NMR spectroscopy (Bruker), ESI-MS Micro-ToF (Bruker, Waters), MALDI-Tof (Waters), GC/MS (Theremo Scientific), HPLC chromatography, LC-MS mass spectrometry (Waters), infrared spectroscopy. Well-familiarized with scientific data bases as Reaxy's and SciFinder.

Languages: English – fluent (C1), German-communicative (B1)

Experienced in co-operation in international team

Professional experience, Hands-on-chemistry experience – 4 years.

Since 09.2012 – 12.2016 – Researcher at Institute of Nanotechnology (Karlsruhe Institute of Technology, Germany) and PhD candidate at Faculty of Science (University of Basel – Switzerland).

Key responsibilities: The design and synthesis of organic compounds served toward application in molecular electronics (nanotechnology), monomers and precursors for *3D* covalent/metal organic frameworks, an isolation, purification and characterization of synthesized compounds.

09.2010 – Internship at the Quality Department, Phase and Chemicals Lab at the Glaxo Smith Kline (Poznań, Poland).

Key responsibilities: Mobile phases and chemicals preparation support of the quality control department manifested by buffer and solution preparation according *ISO 9001* requirements.

Education and Trainings

2012-2016 – PhD (graduated with "***magna cum laude***") under supervision of Prof. Dr. Marcel Mayor, University of Basel (Faculty of Science, "*Tailor – Made Tetraphenylmethanes: From Surface Decoration to 3D Organic Polymers*")

2010-2012 – M.Sc. under supervision of Prof. Dr. hab. Jacek Gawroński, Adam Mickiewicz University in Poznań (Department of Chemistry, Organic Stereochemistry Group)

2007-2010 – B.Sc. under supervision of Prof. Dr. hab. Bogdan Marciniec, Adam Mickiewicz University in Poznań (Department of Chemistry, Organometallic Chemistry Group)

2004-2007, High School, Zespół Szkół Ogólnokształcących Zawodowych im. Ziemi Pogorzelskiej *w* Pogorzeli (Poland)

Conference, Meetings, Posters, Presentations, Awards

Scholarship Financed by European Union, in the frame of European Social Fund (2010-2012)
Scholarship of the President of the University (2011-2012)
Scholarship of Mother Universities (2010-2011)
Scholarship of Polish Prime Minister (2006-2007)
13th European Conference on Molecular Electronics, Strasbourg (France), 2015 (poster presentation**, POSTER AWARDED by the Journal of Material Chemistry C**)
7th International Conference of Molecular Electronics, Strasbourg (France), 2014 (poster presentation)
Surface-Confined Synthesis of Nanostructures, Winter School, Baden-Baden (Germany) 2013 (poster presentation)
School of Physical Organic Chemistry "Self-organization and interaction behind", Przesieka (Poland) 2012 (poster presentation)
Marie Skłodowska-Curie Symposium on the Foundations of Physical Chemistry, Warsaw (Poland) 2012
Participation in organizing of "17th International Symposium on Homogeneous Catalysis" in Poznan (Poland) 2010

Publication List:

1. Valášek Michal, Lindner Marcin., Mayor Marcel., "Rigid multipodal platforms for metal surfaces" *Beilstein. J. Nanotechnol***, 2016,** 7, 374-405

2. Lindner, Marcin; Valášek, Michal; Homberg, Jan; Edelmann, Kevin; Gerhard, Lukas; Wulfhekel, Wulf; Fuhr, Olaf; Wächter, Tobias; Zharnikov, Michael; Kolivoška, Viliam; Pospíšil, Lubomír; Mészáros, Gábor; Hromadová, Magdaléna; Mayor, Marcel, "Importance of the Anchor Group Position (*Para* versus *Meta*) in Tetraphenylmethane Tripods: Synthesis and Self-Assembly Features", *Chem. Eur. J.* **2016**, *22*, 13218-13235